frontiers | Research Topics

Genetic adaption and metabolic response of aquatic animals to diverse water environment parameters

Edited by
Qingchao Wang, Cristian Araneda, Yu-Hung Lin and Jianlong Ge

Published in
Frontiers in Physiology
Frontiers in Marine Science

ISSN 1664-8714
ISBN 978-2-83250-932-6
DOI 10.3389/978-2-83250-932-6

About Frontiers

Frontiers is more than just an open access publisher of scholarly articles: it is a pioneering approach to the world of academia, radically improving the way scholarly research is managed. The grand vision of Frontiers is a world where all people have an equal opportunity to seek, share and generate knowledge. Frontiers provides immediate and permanent online open access to all its publications, but this alone is not enough to realize our grand goals.

Frontiers journal series

The Frontiers journal series is a multi-tier and interdisciplinary set of open-access, online journals, promising a paradigm shift from the current review, selection and dissemination processes in academic publishing. All Frontiers journals are driven by researchers for researchers; therefore, they constitute a service to the scholarly community. At the same time, the *Frontiers journal series* operates on a revolutionary invention, the tiered publishing system, initially addressing specific communities of scholars, and gradually climbing up to broader public understanding, thus serving the interests of the lay society, too.

Dedication to quality

Each Frontiers article is a landmark of the highest quality, thanks to genuinely collaborative interactions between authors and review editors, who include some of the world's best academicians. Research must be certified by peers before entering a stream of knowledge that may eventually reach the public - and shape society; therefore, Frontiers only applies the most rigorous and unbiased reviews. Frontiers revolutionizes research publishing by freely delivering the most outstanding research, evaluated with no bias from both the academic and social point of view. By applying the most advanced information technologies, Frontiers is catapulting scholarly publishing into a new generation.

What are Frontiers Research Topics?

Frontiers Research Topics are very popular trademarks of the *Frontiers journals series*: they are collections of at least ten articles, all centered on a particular subject. With their unique mix of varied contributions from Original Research to Review Articles, Frontiers Research Topics unify the most influential researchers, the latest key findings and historical advances in a hot research area.

Find out more on how to host your own Frontiers Research Topic or contribute to one as an author by contacting the Frontiers editorial office: frontiersin.org/about/contact

Genetic adaption and metabolic response of aquatic animals to diverse water environment parameters

Topic editors

Qingchao Wang — Huazhong Agricultural University, China
Cristian Araneda — University of Chile, Chile
Yu-Hung Lin — National Pingtung University of Science and Technology, Taiwan
Jianlong Ge — Yellow Sea Fisheries Research Institute, Chinese Academy of Fishery Sciences (CAFS), China

Citation

Wang, Q., Araneda, C., Lin, Y.-H., Ge, J., eds. (2022). *Genetic adaption and metabolic response of aquatic animals to diverse water environment parameters*. Lausanne: Frontiers Media SA. doi: 10.3389/978-2-83250-932-6

Table of contents

frontiers | Frontiers in Physiology

TYPE Editorial
PUBLISHED 18 November 2022
DOI 10.3389/fphys.2022.1092413

OPEN ACCESS

EDITED AND REVIEWED BY
Pung Pung Hwang,
Academia Sinica, Taiwan

*CORRESPONDENCE
Qingchao Wang,
qcwang@mail.hzau.edu.cn

SPECIALTY SECTION
This article was submitted to Aquatic Physiology,
a section of the journal
Frontiers in Physiology

RECEIVED 08 November 2022
ACCEPTED 10 November 2022
PUBLISHED 18 November 2022

CITATION
Ge J, Lin Y-H, Araneda C and Wang Q (2022), Editorial: Genetic adaption and metabolic response of aquatic animals to diverse water
environment parameters.
Front. Physiol. 13:1092413.
doi: 10.3389/fphys.2022.1092413

Editorial: Genetic adaption and metabolic response of aquatic animals to diverse water environment parameters

Jianlong Ge[1], Yu-Hung Lin[2], Cristian Araneda[3] and Qingchao Wang[4]*

[1]Key Laboratory of Sustainable and Development of Marine Fisheries, Ministry of Agriculture and Rural Affairs, Yellow Sea Fisheries Research Institute, Chinese Academy of Fishery Sciences, Qingdao, China, [2]Department of Aquaculture, National Pingtung University of Science and Technology, Pingtung, Taiwan, [3]Departamento de Producción Animal, Facultad de Ciencias Agronómicas, Universidad de Chile, Santiago, Chile, [4]Department of Aquatic Animal Medicine, College of Fisheries, Huazhong Agricultural University, Wuhan, China

KEYWORDS

aquatic animals, genetic adaptation, metabolic response, water parameters, temperature stress, hypoxia

Editorial on the Research Topic
Genetic Adaption and Metabolic Response of Aquatic Animals to Diverse Water Environment Parameters

Aquatic animals are continuously exposed to complex water environmental conditions including dynamic temperature range, low dissolved oxygen levels, high ammonia levels, varying salinity levels, enriched pathogenic bacteria and unbalanced food resources. Promising research has revealed that aquatic animals evolved to adapt to the extremely changeable aquatic environments for survival. The Research Topic "Genetic adaption and metabolic response of aquatic animals to diverse water environment parameters" has been conceived to set out such knowledge. Here, we offer an overview of the contents of this Research Topic, which collects 10 original research articles, one brief research report and one data report article.

Water temperature plays an essential role in the growth, survival, and reproduction of aquatic animals, and wide temperature fluctuations often put aquatic animals under either cold stress or heat stress. Due to the specific characteristics, zebrafish has been widely applied as an experimental model. In this Research Topic, cold stress and heat stress were both applied in zebrafish both *in vivo* and *in vitro*. Wang et al. indicated a close connection between oxidative stress and the cold tolerance ability of zebrafish using ZF4 cells, which could be helpful for better understanding the cold tolerance mechanism of fish. The study by Aguilar et al. revealed the explicit redistribution of energy stores and protein catabolism in zebrafish during heat stress *via* metabolomics profiling. Another study by Chang et al. was conducted on sea cucumber *Apostichopus japonicas*, which

constructed a miRNA-mRNA regulatory network in the body wall of sea cucumber during heat stress.

Dissolved oxygen and ammonia are also key physical and chemical factors in aquatic ecological environment. Hypoxia stress has always been a thorny problem in aquaculture, and here authors evaluated the influence of hypoxia stress on both rainbow trout (*in vivo*) and ZFL cells (*in vitro*). Han et al. showed that triploid rainbow trout are in a defensive state under hypoxic stress caused by actual production operations (i.e., catching, gathering, transferring, or weighting). Using ZFL cells, Hu et al. also demonstrated the iron loss in cytoplasm and mitochondria during hypoxia, which leads to mitochondrial damage and ultimately cell death. Besides dissolved oxygen, ammonia has also been recognized one of the major limiting factors in intensive aquaculture systems, and aquatic animals have evolved specific ammonia detoxification strategies to cope with environmental ammonia. Wang et al. identified the differentially expressed neuropeptides in the eyestalk and cerebral ganglia of swimming crab (*Portunus trituberculatus*) under ammonia exposure, which provides a fundamental support for unraveling the regulatory roles of the neuropeptides in ammonia toxification process.

Additionally, salinity is one of the main physical properties that govern the distribution of fishes across aquatic habitats. Recently, salinization of freshwater has been one of the main causes of biological degradation of global river ecosystems. Harshini et al. reported the transcriptomic responses of kidney in *Labeo rohita* (rohu) during salinization stress, which helps to the understanding of osmoregulatory process in *L. rohita* during adaptation to salinity changes. Ranasinghe et al. identified the key regulatory role of SREBP-1 in cholesterol accumulation in livers of *Oryzias dancena* during acclimatization to fresh water and seawater.

Besides the water physicochemical factors, the water-borne pathogenic bacteria and feed resources also pose great risks to aquatic organisms. Especially, the phenotypic and genetic complexity of pathogenic bacteria significantly increase the challenges of aquatic organisms. Kang et al. reported the interspecific genetic and antibiotic resistance diversity of 192 isolates of *Vibrio Harveyi* clade collected from 2000 to 2020 from China coastal areas. In another study, Yu et al. pointed out the potential risk for the storage and transmission of resistance genes existing in antimicrobial susceptibility isolates among 33 *Vibrio scophthalmi* isolates collected from diseased marine fish intestines between 2002 and 2020. Additionally, nutrition also significantly affected the metabolism and health of fish. Cao et al. indicated that dietary hydroxyproline supplementation significantly enhanced growth performance, collagen synthesis and muscle quality of juvenile *Carassius auratus* Triploid. Wang et al. also evaluated the programming of antioxidant capacity, immunity, and lipid metabolism in *Misgurnus anguillicaudatus* larvae linked to sodium chloride and hydrogen peroxide pre-treatment during egg hatching.

In summary, this Research Topic delivers new ideas for future research in revealing genetic adaption and metabolic response of aquatic animals to diverse water environmental parameters including temperature, oxygen, ammonia, salinity, bacteria and nutrition. All the research articles in this Research Topic show that aquatic animals have evolved multiple adaptive mechanisms to deal with diverse aquatic environmental conditions. Both genetic adaptation and metabolic responses are involved in these processes, on which researchers are working from different viewpoints. We thank all the authors for their contributions and hope that this Research Topic will encourage more scientists to deepen knowledge about the relationship between aquatic animal behavior and diverse water environmental parameters.

Author contributions

QW and JG was responsible for the idea of this special volume, wrote, and reviewed this editorial topic. CA and YL reviewed this editorial topic. All authors contributed to the article and approved the submitted version.

Funding

This work was funded by the China Scholarship Council [CSC (2021) 109] and National Key R&D Program of China (2018YFD0901604).

Conflict of interest

The authors declare that the research was conducted in the absence of any commercial or financial relationships that could be construed as a potential conflict of interest.

Publisher's note

frontiers in Physiology

ORIGINAL RESEARCH
published: 28 October 2021
doi: 10.3389/fphys.2021.768907

The Programming of Antioxidant Capacity, Immunity, and Lipid Metabolism in Dojo Loach (*Misgurnus anguillicaudatus*) Larvae Linked to Sodium Chloride and Hydrogen Peroxide Pre-treatment During Egg Hatching

*Mengya Wang[1], Wenyu Xu[2], Jiahong Zou[1], Shuaitong Li[1], Zixi Song[1], Feifei Zheng[1], Wei Ji[1], Zhen Xu[1] and Qingchao Wang[1]**

[1]*Department of Aquatic Animal Medicine, College of Fisheries, Huazhong Agricultural University, Wuhan, China,* [2]*Ocean University of China, Qingdao, China*

OPEN ACCESS

Edited by:
Youji Wang,
Shanghai Ocean University, China

Reviewed by:
Kang-le Lu,
Jimei University, China
Xiaodan Wang,
East China Normal University, China

***Correspondence:**
Qingchao Wang
qcwang@mail.hzau.edu.cn

Specialty section:
This article was submitted to Aquatic Physiology, a section of the journal Frontiers in Physiology

Received: *01 September 2021*
Accepted: *11 October 2021*
Published: *28 October 2021*

Citation:
Wang M, Xu W, Zou J, Li S, Song Z, Zheng F, Ji W, Xu Z and Wang Q (2021) The Programming of Antioxidant Capacity, Immunity, and Lipid Metabolism in Dojo Loach (Misgurnus anguillicaudatus) Larvae Linked to Sodium Chloride and Hydrogen Peroxide Pre-treatment During Egg Hatching. Front. Physiol. 12:768907. doi: 10.3389/fphys.2021.768907

Non-nutritional stress during early life period has been reported to promote the metabolic programming in fish induced by nutritional stimulus. Sodium chloride (NaCl) and hydrogen peroxide (H_2O_2) have been widely applied during fish egg hatching, but the influences on health and metabolism of fish in their later life remain unknown. In the present study, H_2O_2 treatment at 400 mg/L but not 200 mg/L significantly increased the loach hatchability and decreased the egg mortality, while NaCl treatment at 1,000 and 3,000 mg/L showed no significant influences on the loach hatchability nor egg mortality. Further studies indicated that 400 mg/L H_2O_2 pre-treatment significantly enhanced the antioxidant capacity and the mRNA expression of genes involved in immune response of loach larvae, accompanied by the increased expression of genes involved in fish early development. However, the expression of most genes involved in lipid metabolism, including catabolism and anabolism of loach larvae, was significantly upregulated after 200 mg/L H_2O_2 pre-treatment. NaCl pre-treatment also increased the expression of antioxidant enzymes; however, only the expression of C1q within the detected immune-related genes was upregulated in loach larvae. One thousand milligram per liter NaCl pre-treatment significantly increased the expression of LPL and genes involved in fish early development. Thus, our results suggested the programming roles of 400 mg/L H_2O_2 pre-treatment during egg hatching in enhancing antioxidant capacity and immune response of fish larvae *via* promoting fish early development.

Keywords: fish egg hatching, hydrogen peroxide, sodium chloride, programming, antioxidant capacity

INTRODUCTION

The environmental and trophic conditions encountered at the early developmental period of animals have been confirmed to perform profound effects on the metabolism and physiology of individuals later in life, which is termed metabolic programming (when modifying metabolism; Lucas, 1998). Long-lasting modification in gene expression patterns is one of the most important biological mechanisms described in such case of adaptions, and it may persist later in life in the absence of the environmental stimulus that initiated them (George et al., 2012; Kongsted et al., 2014). In aquatic animals, including fish and shrimp, the concept of metabolic programming has been tested as well. Preliminary study in rainbow trout (*Oncorhynchus mykiss*) showed that only a strict nutritional stimulus had a minor programming effect on hepatic glucose metabolism (Geurden et al., 2007, 2014). Later studies indicated that an acute exposure to hypoxia alone (Liu et al., 2017a) or combined with an early nutritional stimulus, such as high-carbohydrate diet (Liu et al., 2017b), high dietary carbohydrate:protein ratios (Hu et al., 2018) induced obvious programming in the liver of juvenile rainbow trout. The hypoxic conditions resulted in the higher expression of *HIF-1α* which has been reported to modulate the nutrient metabolism (Menendez-Montes et al., 2021), antioxidant capacity (Lacher et al., 2018), and immune responses (Ni et al., 2020). However, the hypoxia may easily result in high mortality, and it is important to explore other non-nutritional stress. Due to the safety and friendly to human health and environment ecology, sodium chloride (NaCl) and hydrogen peroxide (H_2O_2) have been tested in the fry hatch of many fish species (Magondu et al., 2011). NaCl has been used effectively in aquaculture as antiparasitic agent (Schelkle et al., 2011; Dewi et al., 2018), growth-promoting agent in *Carassius auratus* (Imanpoor et al., 2012) and *Mugil liza* (Lisboa et al., 2015), and survival enhancing agent in *Pelecus cultratus* larvae (Kujawa et al., 2017), *Ictalurus punctatus*, *C. auratus*, *Morone saxatilis*, and *Acipenser oxyrinchus* (Altinok and Grizzle, 2001). Moreover, NaCl affects the embryonic development and larval vigor of *Epinephelus akaara* (Wang et al., 2002) and *Rhombosolea tapirina* (Hart and Purser, 1995). In one plateau species of loach, *Triplophysa (Hedinichthys) yarkandensis*, NaCl application with salinity at 4% resulted in the lowest deformity rate (Chen et al., 2016). H_2O_2 has received attention for its control of several fish pathogens and is recommended as a general disinfectant in aquaculture for treating aquaculture water and surface of tanks before introduction of fish (Avendaño-Herrera et al., 2006). H_2O_2 has been shown to promote the egg hatching rate of rainbow trout (Schreier et al., 1996; Barnes et al., 1998), channel catfish (*I. punctatus*; Small and Wolters, 2003), and *C. gariepinus* (Rasowo et al., 2007).

During multiple environmental challenges, free radical would be released, but the over-production of O_2^- would cause oxidative damage to proteins, nucleic acids, and lipids (Kurien and Scofield, 2003). Thus, cellular antioxidant defenses system in fish and other animals are developed to scavenge the excessive reactive oxygen species (*ROS*; Pisoschi and Pop, 2015; Klein et al., 2017). Like hypoxia, H_2O_2 and NaCl treatment have also been proved to affect antioxidant capacity. Salinity or NaCl treatment significantly affected the mRNA expression and activity of antioxidant enzymes, including superoxide dismutase (*SOD*), glutathione S-transferase (*GST*), and glutathione (*GSH*) in multiple tissues of olive flounder (*Paralichthys olivaceus*; Kim et al., 2021), European seabass (*Dicentrarchus labrax*; Islam et al., 2020), *D. labrax,* and *Chanos Chanos* (Chang et al., 2021). Similarly, H_2O_2 exposure has also been reported to affect antioxidant capacity in common carp (*Cyprinus carpio*; Jia et al., 2020) and largemouth bass (*Micropterus salmoides*; Sinha et al., 2020). Besides antioxidant system, fish remains the first bony vertebrate to develop both innate and adaptive immunity which help themselves to defend against infected pathogens or other environmental challenges (Wang et al., 2019). The immune responses of European seabass and common carp (*C. carpio*) were significantly affected by different salinities (Islam et al., 2020) and H_2O_2 exposure (Jia et al., 2021), respectively. The programming effects on individuals of later life by environmental treatment or nutritional stimulus at early life stage mainly result from an alteration of the functional development of crucial organs (Pittman et al., 2013). It is well known that fish larvae along with the fertilized eggs grow very fast and experience significant changes in physiology; thus, they are very fragile and most susceptible to environmental stressors during fish ontogeny (Fuiman, 1983; Alvarez et al., 2021). The organs in the newly hatched fish larva are not well developed, and thus, it is not easy to do histological evaluation in fish larvae (Fuiman et al., 1999). The molecular methods *via* evaluating the relative mRNA expression levels of early development-related genes are useful and effective to systematically evaluate the influences of pre-treatment on the fry (Hu et al., 2018).

Dojo loach *Misgurnus anguillicaudatus* (Cantor 1842) is one of the important freshwater aquaculture species in China whose production has reached 367,428 tons by 2020 (Ministry of Agriculture and Rural Affairs of the People's Republic of China, 2021) and can be used as a Chinese medicine for the treatment of hepatitis, carbuncles, inflammations, and cancers (Qin et al., 2002). The sustainable development of loach aquaculture industry relies on the stable loach fry supply, whose artificial breeding has been successfully overcome in recent years (Gao et al., 2014; Huang et al., 2015). However, the diseases resulting from microorganism infection or other environmental factors during fish hatchery have threatened the production of larval loach (Shamsi et al., 2021). The applications of antibiotics and insecticides have been seriously restricted in many countries (Holmström et al., 2003; Cabello, 2006; Shao et al., 2021), while no specific fish vaccine nor mature vaccination route is available for fish fry (Rojo-Cebreros et al., 2018; Wang et al., 2020), which seriously restricts the stable fish fry stocks. In the present study, NaCl and H_2O_2 were applied during loach egg hatching and the effects on the antioxidant capacity, immunity and lipid metabolism of fish larvae were evaluated as well as monitoring the early development-related genes.

MATERIALS AND METHODS

Fish Stock and Egg Fertilization

Mature broodstock fish (average weight 18 ± 2.1 g), obtained from broodstock ponds, were selected and transferred to the hatchery. All fish were then acclimated in hatching tanks for 1 day without feeding. To induce spawning, the selected female fish were injected with DOM (4 mg/kg fish) and LRH-A2 (35 μg/kg fish), and the male fish were injected with same reagents but half dosage. After 12 h, the eggs were stripped into a dry bowl and fertilized with milt from a ripe male. After fertilization, the fertilized eggs were randomly counted into bottles with 100 eggs each. The individual hatching bottles were randomly assigned in triplicate to static bath treatments of given concentrations of either NaCl (1,000 and 3,000 mg/L), H_2O_2 (200 and 400 mg/L), and a control (nothing added) for 60-min exposure before being transferred to randomized compartments of the incubation tank for further incubation. The water temperature was controlled at 24–26°C and dissolved oxygen (DO) controlled at 7.5–7.8 mg/L, which were monitored using an oxygen-temperature meter (model 55, YSI, Yellow Springs Ohio, United States).

Egg Hatching and Hatchability Calculation

Loach larvae came out of the membrane after 24-h fertilization. Then, the hatching bottles were removed from the incubation tank. The numbers of live hatched larvae, dead hatched larvae, total dead eggs, and fungi-infected dead eggs were counted for the calculation of following parameters and then sent back to the incubation tank.

Hatchability (%) = The number of live hatched larvae/the total number of eggs * 100.

Fry mortality (%) = The number of dead hatched larvae/the total number of eggs * 100.

Egg mortality (%) = The number of total dead egg/the total number of eggs * 100.

Fungi-induced egg mortality (%) = The number of fungi-infected dead egg/the total number of eggs * 100.

Other factor-induced egg mortality (%) = The number of (total dead eggs excluding fungi-infected ones)/ the total number of eggs * 100.

Larviculture, RNA Extraction, and cDNA Synthesis

Loach larvae showed feed-hunting behavior at 4 days after rupture, and then, larvae in all groups were fed with artemia for another 7 days. At the end of feeding, all the loach larvae were collected and immediately frozen in liquid nitrogen and stored at −80°C before analysis.

The whole loach larvae were homogenized in TRIzol reagent (Invitrogen, Carlsbad, CA, United States) for RNA extraction according to the manufacturer's recommendations. After RNA extraction procedures, the purity and concentration of RNA were monitored by NanoDrop 2000 spectrophotometer (Thermo scientific, United States), with their 260:280 ratios between 1.8 and 2.0. Additionally, 1.0% agarose gel electrophoresis was adopted to determine the integrity of RNA. The quantified RNA samples were then used for cDNA synthesis (Invitrogen, Carlsbad, CA, United States). Briefly, the potential existing genomic DNA was removed from the RNA samples with same amount using DNase. Then, 1 μg of treated RNA was used for the synthesis of cDNA using the reverse transcriptase kit with oligo dT primers following manufacturer's instructions.

Quantitative RT-PCR

The synthesized cDNA was used for the quantitative real-time PCR (qPCR) analysis using the Eva Green 2 × qPCR Master mix (ABM, Canada). qPCR was conducted on 7500 Real-time PCR system (Applied Biosystems, United States), with each PCR performed with triplicate samples and the cycling conditions set with 30 s at 95°C, 1 s at 95°C, and 10 s at 58°C for 40 cycles. In addition, a melt curve analysis was performed after amplification to verify the accuracy of each amplicon.

The relative quantification of the target genes involved in the antioxidant system [*SOD*, catalase (*CAT*), glutathione peroxidase (*GPx*), and metallothionein (*Mt*)], genes related to immune responses [*C1q*, *C3-1*, *C8b*, mannose-binding lectin-associated serine protease-1 (*MASP-1*), interleukin 15 receptor subunit alpha (*IL15Rα*), and heat shock protein 70 (*Hsp70*)], genes involved in lipid metabolism [carnitine palmitoyltransferase 1alpha (*Cpt1α*), lipoprotein lipase (*LPL*), fatty acid desaturase 2 (*Fads2*), and proliferator-activated receptor gamma (*PPARγ*)] and early development-related genes [spondin 1b (*spon1b*), intraflagellar transport protein 22 (*IFT22*), vascular endothelial growth factor Aa (*VEGFAa*), glutamate dehydrogenase (*gdh*), annexin A1a (*anxa1a*), vasoactive intestinal peptide (*VIP*), protein phosphatase 1 (*PP1*), and protein phosphatase 2A catalytic subunit beta isoform (*PP2AB*)] were determined *via* normalized against elongation factor 1-alpha (*EF1α*). Then, relative abundance of target genes was calculated by using the $2^{-\Delta\Delta Ct}$ method. All primers used in the present study are shown in **Table 1**.

Statistical Analysis

All statistical analyses were performed using SPSS 17.0. Data were analyzed by one-way analysis of variance (ANOVA) followed by Tukey's multiple range tests to determine the effects of NaCl and H_2O_2 on egg hatching and gene expression. Differences were considered significant when $p < 0.05$. All data were expressed as mean ± standard deviation of the mean (SD), except the specific statement.

RESULTS

Effects of H_2O_2 and NaCl Treatment on Hatching Performances of Loach Larvae

The hatching performances including hatchability, larval mortality, egg mortality including fungi-induced mortality

TABLE 1 | Primers used in the present study.

Gene	Forward sequence	Reverse sequence
Spon1b	GTCGGACGGTTTCTGTAGGA	GAGGGTAAATCCACGAAAGTAAG
IFT22	TGGGATTGTGGAGGAGATTTC	AGTTTGCTCAGTTTTGGGGC
VEGFAa	TCTGCTCTATAACCCTCACCGC	GTCATTTTTGCTCTTCCCTCCT
gdh	TGCCTGTGTGACTGGTAAGCC	CCATAACGGTGAAGATAACGCA
anxa1a	TGCTGTGGTGAAATGTGCTG	AGTCTCCTTTGGTGTCGTCCT
VIP	GTCTCTTCACAAGCGGATACAG	TGGTCCTCCATCAAATCATCAC
PP1	GAGGACGGTTATGAGTTTTTTGC	GCTTTCTTCTCTGACGGCTTG
PP2AB	ACAGTCACACTTCTTGTTGCCCT	ATTTCCTCAAGCACTCGTCGTA
SOD	GACCATGCTGTGCAGAGTCGGATA	GGGCTGAAGGGACACTTGGGTAATA
CAT	GTGCTAAACCGAAACCCTGT	GCTGTTGGGGTAGTAGTTAGGAG
GPx	TCTAAATGAGGCAAGACCCCAGTA	CTCCCTTTAGGCTGTTCCTTCATC
Mt	GAAACGATACAGCAAAGGAACC	CTTACAAACGCATCCAGAGGC
C1q	TGCGTATGGTTGGCTTGTGGG	GAATAGGCGGTGAAGGAGAAAGAGTAGA
C3-1	TTTTCTATGATGCTGGTCTGATGTTTG	CGATGTACGTGGCTCGTCGTT
C8b	CCATGCCAGGGTTTCCGTTGT	CACCAGCATAGTAGCGGTTATCAAGC
MASP-1	ATAACTACATAGGTGGCTTCTACTGT	CCTCCTCTTGCTCAATGCGATACA
IL15Rα	GGAGCACAAGCAGACAAAAT	CTATGATTGATGTACTAGCTGGTTT
Hsp70	GGTCCTTCCAAGTCATCAG	GCAATCTCCTTCATCTTCAC
Cpt1α	CCATCTCTTCTGCCTCTAC	GCCACACCATAACCATCA
LPL	ACCTGGCTGTAACCTTCA	AACGGCATCATATCTCTGG
Fads2	CACAGGTTCGGCACTTACAC	TCGCATCTTCTCCAGCATAATG
PPARγ	TGGCTTTCACTATGGCGTTCA	GCATTTGTTGCGACTCTTCTTG
EF1α	TCAGCGCCTACATCAAGAAG	TTACGCTCAACCTTCCATCC

Spon1b, spondin 1b; IFT22, intraflagellar transport protein 22 homolog; VEGFAa, vascular endothelial growth factor Aa; gdh, glutamate dehydrogenase; anxa1a, annexin A1a; VIP, vasoactive intestinal peptide; PP1, protein phosphatase 1; PP2AB, protein phosphatase 2A catalytic subunit beta isoform; SOD, superoxide dismutase; CAT, catalase; GPx, glutathione peroxidase; Mt, metallothionein; MASP-1, mannose-binding lectin-associated serine protease-1; IL15Rα, interleukin 15 receptor subunit alpha; Hsp70, heat shock protein 70; Cpt1α, carnitine palmitoyltransferase 1alpha; LPL, lipoprotein lipase; Fads2, fatty acid desaturase 2; PPARγ, proliferator-activated receptor gamma; and EF1α, elongation factor 1-alpha.

and other-induced mortality of loach after H_2O_2 and NaCl treatment are shown in **Figure 1**. Four hundred milligram per liter H_2O_2 treatment significantly increased larvae hatchability, while the larvae mortality showed no significant differences after H_2O_2 treatment. Additionally, the egg mortality was also significantly decreased after 400 mg/L H_2O_2 treatment. However, the decreased egg mortality after 400 mg/L H_2O_2 treatment was not due to fungi, but by other factors, as the fungi-induced egg mortality was even higher in 400 mg/L H_2O_2 treatment group.

NaCl treatment showed no significant effects on larval hatchability nor fry mortality. Similarly, the total egg mortality along with the fungi-induced egg mortality was not affected by NaCl treatment. However, the other factor-induced egg mortality was decreased during 1,000 mg/L NaCl treatment.

Effects of H_2O_2 and NaCl Pre-treatment During Egg Hatching on the Expression of Genes Involved in Development of Loach Larvae

Figure 2 indicated the influences of H_2O_2 and NaCl pre-treatment during egg hatching on the expression of early development-related genes of loach larvae. The expression of *spon1b*, *IFT22*, *VEGFAa*, and *PP2AB* was significantly upregulated after 400 mg/L H_2O_2 pre-treatment. The expression of *gdh*, *VIP*, and *PP1* was significantly upregulated with the increased dosage of H_2O_2, and highest expression level was detected at 400 mg/L H_2O_2 pre-treatment. No significant effects of H_2O_2 pre-treatment were detected on the expression of *anxa1a*.

The expression of *spon1b*, *IFT22*, *gdh*, *VIP*, *VEGFAa*, *PP1*, and *PP2AB* in loach larvae was significantly upregulated after NaCl pre-treatment; however, their expression levels were significantly higher at 1,000 mg/L NaCl pre-treatment than those at 3,000 mg/L NaCl pre-treatment. The expression of *anxa1a* was also significantly upregulated after 1,000 mg/L NaCl pre-treatment but back to normal after 3,000 mg/L NaCl pre-treatment.

Effects of H_2O_2 and NaCl Pre-treatment During Egg Hatching on the Expression of Genes Involved in Antioxidant Capacity of Loach Larvae

The mRNA expression levels of genes involved in the antioxidant capacity of loach larvae after H_2O_2 and NaCl pre-treatment are shown in **Figure 3**. The expression levels of *SOD* and *Mt* were significantly upregulated with the increased dosage of H_2O_2, and the highest expression levels were both detected at 400 mg/L H_2O_2 pre-treatment. The expression of *GPx* was also significantly upregulated after H_2O_2 pre-treatment; however, no significant differences were detected between two dosages. Additionally, the expression of *CAT* was not significantly affected by H_2O_2 pre-treatment.

The expression of *SOD* was significantly upregulated with the increased dosage of NaCl, and highest expression level was detected at 3,000 mg/L NaCl pre-treatment. The expression

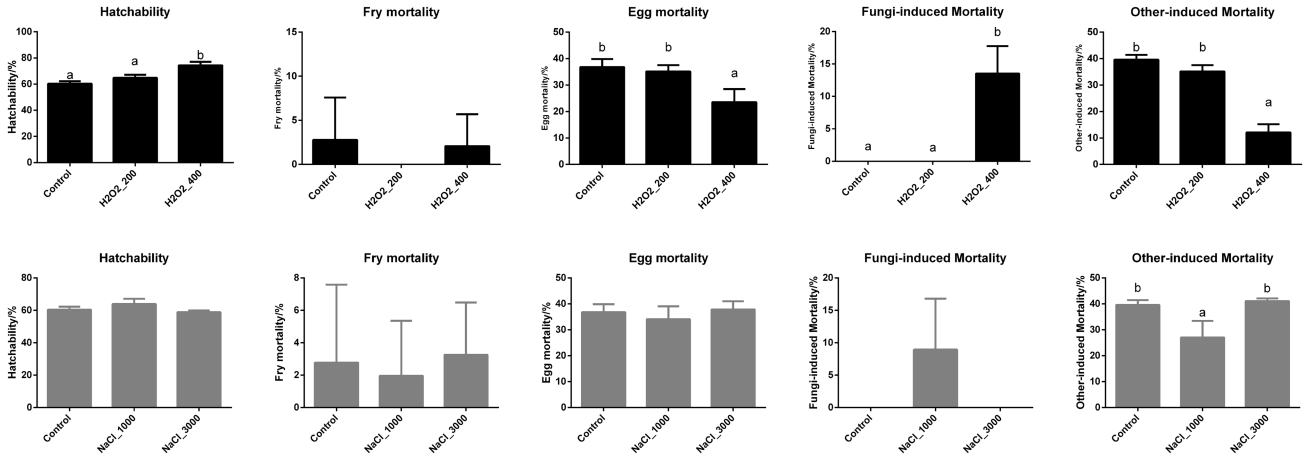

FIGURE 1 | Effects of H_2O_2 (200, 400 mg/ml) and NaCl (1,000, 3,000 mg/ml) pre-treatment during egg hatching on the hatchability, fry mortality, egg mortality including fungi-induced mortality and other factor-induced mortality of loach.

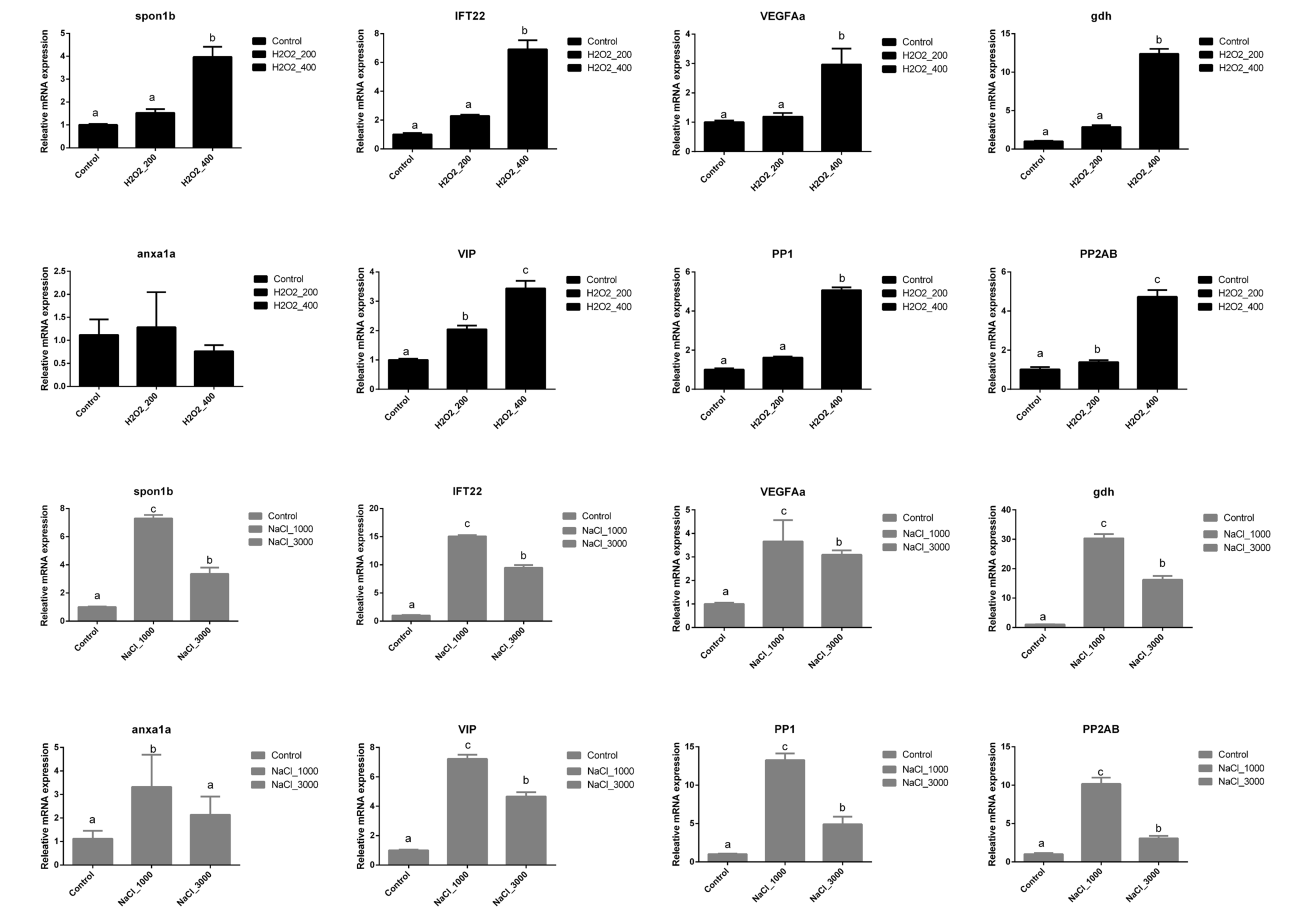

FIGURE 2 | Effects of H_2O_2 (200, 400 mg/ml) and NaCl (1,000, 3,000 mg/ml) pre-treatment during egg hatching on the relative expression levels of genes involving early development including *spon1b, IFT22, VEGFAa, gdh, anxa1a, VIP, PP1,* and *PP2AB* in loach larvae.

of *GPx* was only significantly upregulated after 3,000 mg/L NaCl pre-treatment. The expression of *Mt* was significantly upregulated by H_2O_2 pre-treatment, but the highest expression level was detected at 1,000 mg/L NaCl pre-treatment. Additionally, 1,000 mg/L NaCl pre-treatment significantly decreased the expression of *CAT*.

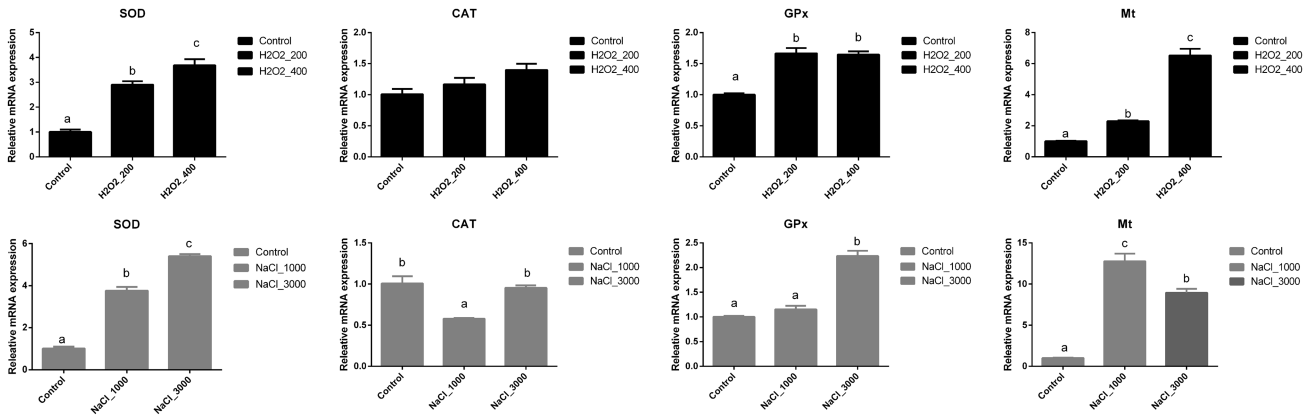

FIGURE 3 | Effects of H_2O_2 (200, 400 mg/ml) and NaCl (1,000, 3,000 mg/ml) pre-treatment during egg hatching on the relative expression levels of genes involving antioxidant capacity, including *SOD, CAT, GPx,* and *Mt* in loach larvae.

Effects of H_2O_2 and NaCl Pre-treatment During Egg Hatching on the Expression of Genes Involved in Immune Response of Loach Larvae

Figure 4 indicated the different expression levels of genes involved in the immune response of loach larvae after H_2O_2 and NaCl pre-treatment during egg hatching. The expression of *C1q* was also significantly upregulated after H_2O_2 pre-treatment; however, no significant differences were detected between two dosages. The expression of *C3-1* and *Hsp70* was significantly upregulated after 400 mg/L H_2O_2 pre-treatment. The expression of *IL15Rα* was significantly higher in loach larvae after 200 mg/L H_2O_2 pre-treatment than that after 400 mg/L H_2O_2 pre-treatment. No significant influences of H_2O_2 pre-treatment were detected on the expression of *C8b* nor *MASP-1*.

The expression of *C1q* was also significantly upregulated after 1,000 mg/L NaCl pre-treatment but back to normal after 3,000 mg/L NaCl pre-treatment. The expression of *C8b* was significantly downregulated after 3,000 mg/L NaCl pre-treatment. The expression of *MASP-1* was significantly downregulated after NaCl pre-treatment but no significant differences were detected between two dosages. The expression of *Hsp70* was significantly downregulated after NaCl pre-treatment, and the lowest expression level was detected after 1,000 mg/L NaCl pre-treatment. No significant influences were detected on the expression of *C3-1* nor *IL15Rα* in loach larvae after NaCl pre-treatment.

Effects of H_2O_2 and NaCl Pre-treatment During Egg Hatching on the Expression of Genes Involved in Lipid Metabolism of Loach Larvae

H_2O_2 and NaCl pre-treatment during egg hatching also significantly affected the expression of genes involved in the lipid metabolism of loach larvae (**Figure 5**). The expression of *Cpt1α*, *LPL*, and *Fads2* was significantly upregulated after 200 mg/L H_2O_2 pre-treatment. The mRNA expression levels of *Cpt1α* and *LPL* went back to normal after 400 mg/L H_2O_2 pre-treatment, while the expression of *Fads2* was even decreased after 400 mg/L H_2O_2 pre-treatment. The expression of *PPARγ* was significantly higher in loach larvae after 200 mg/L H_2O_2 pre-treatment than that after 400 mg/L H_2O_2 pre-treatment.

The expression of *Cpt1α* and *PPARγ* was significantly downregulated after 1,000 mg/L NaCl pre-treatment, but back to normal after 3,000 mg/L NaCl pre-treatment. The genes expression level of *LPL* was significantly upregulated after 3,000 mg/L NaCl pre-treatment. The expression of *Fads2* was significantly downregulated after NaCl pre-treatment, while no significant differences were detected between two NaCl dosages.

DISCUSSION

The disease prevention or control is of great importance to keep the healthy fish fry stocks (Subasinghe et al., 2000), so antibiotics and insecticides were traditionally applied during fish fry breeding. However, the applications of antibiotics and insecticides have been seriously restricted in many countries, including China, because they are not only highly toxic to humans and fish and not easy to be degraded in the environment, but also lead to the potential development of antibiotic resistance (Holmström et al., 2003; Cabello, 2006; Zhou et al., 2019; Shao et al., 2021). Fish vaccine is of great potential in the prevention of disease outbreaks; however, only eight fish vaccines have been licensed in China, which is far more from enough to main the continual development of aquaculture production in China (Wang et al., 2020). Especially in fish fry, there is no available fish vaccine nor mature vaccination route, which seriously restricts the stable fish fry stocks (Rojo-Cebreros et al., 2018). The safe and environmental-friendly drugs, including H_2O_2 and NaCl, have been tested in the fry hatching of many fish species (Magondu et al., 2011). H_2O_2 has been proved to promote the hatching rate of eggs in multiple fish species. For example, H_2O_2 treatment at 500–1,000 ppm significantly increased hatching rates and controlled fungi in rainbow trout eggs (Schreier et al., 1996; Barnes et al., 1998). In channel catfish (*I. punctatus*), H_2O_2 treatment at low concentrations of 70–250 mg/L significantly increased percent hatching of fish

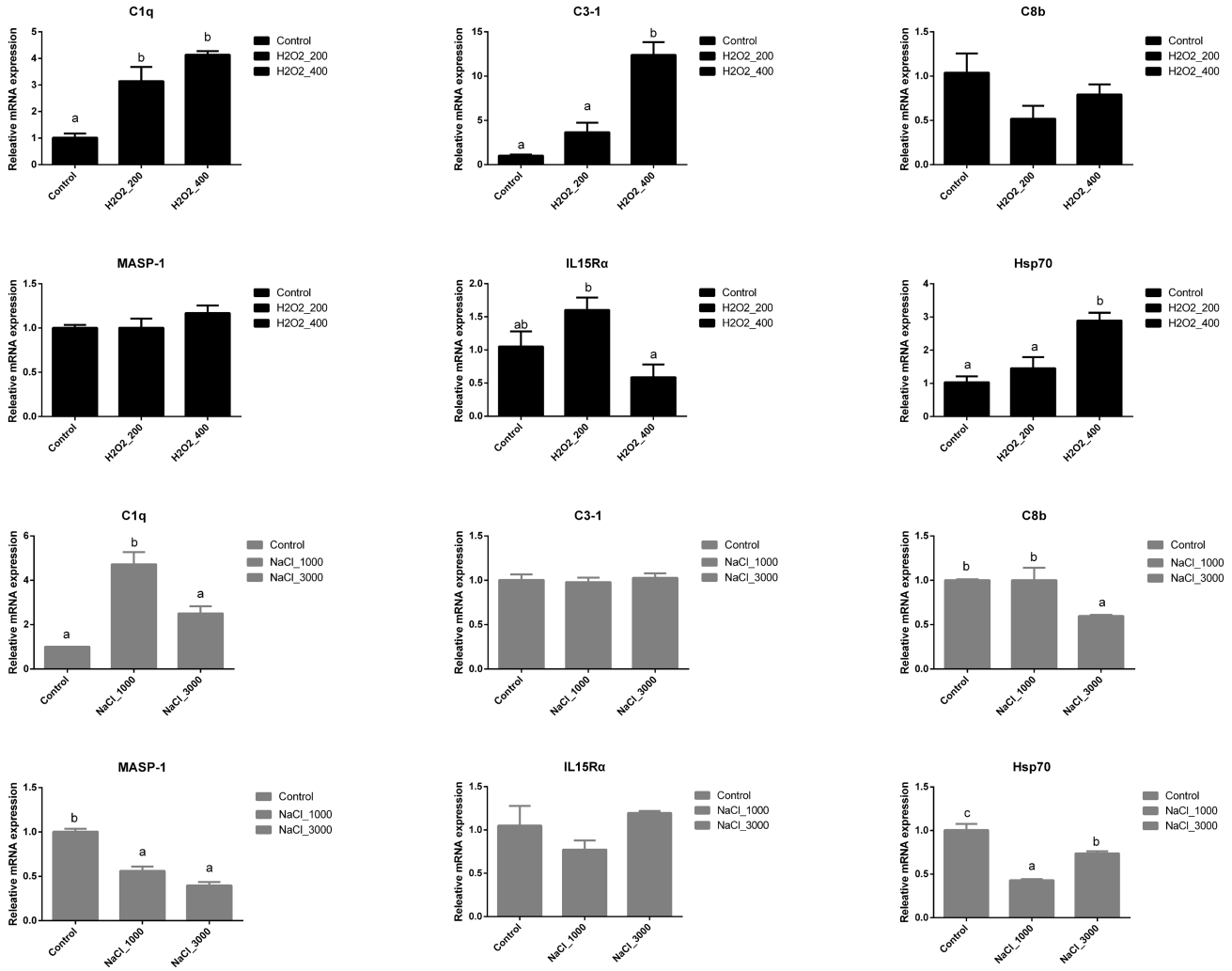

FIGURE 4 | Effects of H_2O_2 (200, 400 mg/ml) and NaCl (1,000, 3,000 mg/ml) pre-treatment during egg hatching on the relative expression levels of genes involving immunity, including *C1q, C3-1, C8b, MASP-1, IL15Rα,* and *Hsp70* in loach larvae.

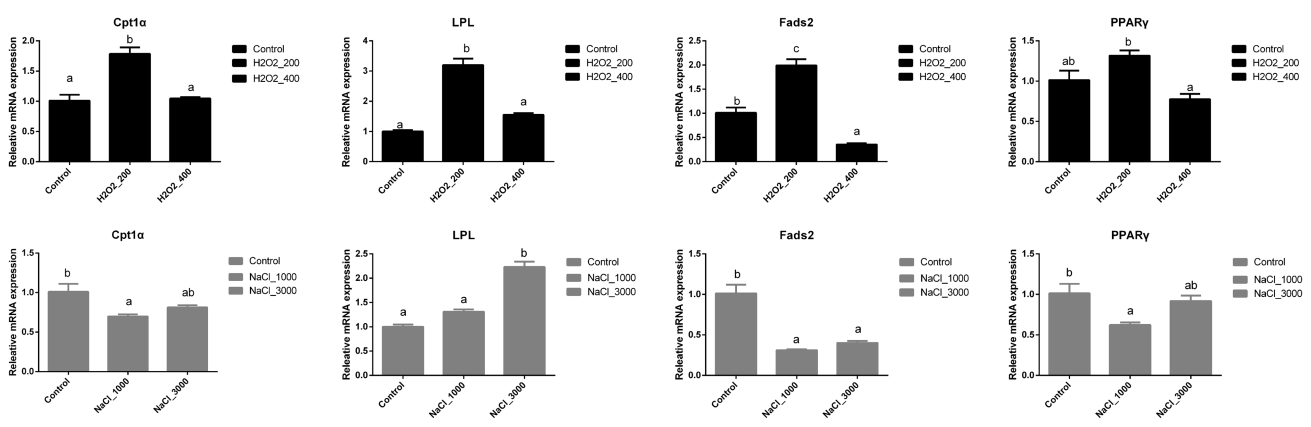

FIGURE 5 | Effects of H_2O_2 (200, 400 mg/ml) and NaCl (1,000, 3,000 mg/ml) pre-treatment during egg hatching on the relative expression levels of genes involving lipid metabolism, including *Cpt1α, LPL, Fads2,* and *PPARγ* in loach larvae.

eggs (Small and Wolters, 2003), and later studies indicated that higher dosage of H_2O_2 (500 or 750 mg/L) could also improve the percent hatching of channel catfish eggs (Rach et al., 2004). One study also compared the effects of H_2O_2 on eight species of warm- and cool-water fish eggs which identified the concentration of 1,000 mg/L to be most effective in improving hatching rate (Rach et al., 1998). The unfertilized fish eggs are especially vulnerable to fungal infection from the family *Saprolegniaceae* (Post, 1987), which produces mycelia to facilitate spreading from the nonviable to the healthy eggs and cause egg mortality (Teresa Vega-Ramírez et al., 2013). In the present study, H_2O_2 treatment at 400 mg/L significantly improved the hatchability and also decreased the egg mortality. However, the decreased egg mortality after 400 mg/L treatment was not due to the inhibition of fungi as the fungi-induced egg mortality was even increased in 400 mg/L H_2O_2 treatment. Four hundred milligram per liter H_2O_2 treatment might contribute to the other factors, including bacterial inhibition or water parameters protection. This was in accordance with studies in salmon (*Salmo salar*) as H_2O_2 concentration strongly affected salmon mortality, but did not alter mucous cell area or density, pre-adult lice removal efficiency, or the re-infection success of lice copepodids (Overton et al., 2018). Besides H_2O_2, NaCl has also been reported to affect the hatching rate of fish eggs; however, the effects varied depending on the dosage of NaCl and the fish species. Schnick (1988) reported that the 3,000 ppm NaCl dip effectively removed protozoa from fish egg surfaces and limited any mycelial production that may lower egg hatching. Salt treatment at 0–5,000 mg/L significantly improved egg hatching in channel catfish (Froelich and Engelhardt, 1996), and NaCl significantly improved the hatching rate of koi carp (*C. carpio haematopterus*) at 1,000 and 2,500 mg/L for a 60 min exposure duration but even toxic to the eggs at 5,000 mg/L (Phelps and Walser, 1993). In the present study, NaCl treatment at 1,000 and 3,000 mg/L did not significantly affect fish egg hatching rate nor the fry mortality. Moreover, the total mortality and fungi-induced mortality of loach eggs were also not significantly affected after NaCl treatment. However, 1,000 mg/L NaCl treatment significantly inhibited the other factor-induced egg mortality excepting fungi. NaCl treatment showing no effects on the hatching performance of loach in the present study may be due to the test dosages of NaCl and the fish species. A much wider dosage range of NaCl during loach hatching could be tested in the future study.

Although plenty of studies have evaluated the influences of NaCl and H_2O_2 pre-treatment on the egg hatching of many fish species, little information is known about the influences of these pre-treatments on fish larvae health and nutrient metabolism. Recent studies have indicated that nutritional stimuli (quantity or quality of nutrients) and non-nutritional environmental stress experienced at critical periods of an organism's life can result in permanent changes in postnatal growth potential, health, and metabolic status in animals including fish and shrimp (Burdge and Lillycrop, 2010; Hu et al., 2018). Moreover, temperature has also been reported to affect the liver transcriptome response of spotted seabass (*Lateolabrax maculatus*) induced by dietary protein level (Cai et al., 2020). Thus, the effects of NaCl and H_2O_2 during egg hatching on antioxidant capacity, immune responses, and lipid metabolism of loach larvae were systematically evaluated. In previous studies, the metabolic programming in aquatic has been mainly focused on carbohydrate metabolism due to the desired protein-sparing effects (Hu et al., 2018); however, lipid metabolism is also important and also serves the protein-sparing effect (Peng et al., 2019). Especially, fish larvae require much higher energy consumption for the rapid growth (Abi-Ayad and Kestemont, 1994; Gaon et al., 2021) and lipid serves as the most efficient nutrient for energy supply (Kupriyanova et al., 2021). In the present study, both the genes involved in lipid catabolism, such as *Cpt1α* and *LPL,* and genes involved in lipid anabolism, such as *Fads2,* along with the regulatory factor, *PPARγ*, were significantly upregulated in 200 mg/L H_2O_2 pre-treatment group, but back to normal level at 400 mg/L. However, most genes were downregulated by NaCl pre-treatment excepting *LPL* which was significantly upregulated after 3,000 mg/L NaCl pre-treatment. This phenomenon has been reported in earlier studies which suggested that nutritional programming by dietary carbohydrates in European seabass larvae may not always be as expected (Zambonino-Infante et al., 2019). These differential results may result from different fish species, different stimulus patterns, and/or dosages.

In animals, the *ROS* play important roles in tissue homeostasis, cellular signaling, differentiation (Harris and DeNicola, 2020), and their levels are tightly regulated by cellular antioxidant system to prevent unwanted consequences (Pérez-Jiménez et al., 2017). However, oxidative stress will be generated when the balance between the production and neutralization of *ROS* is broken to favor the former, thus causing oxidative damage to proteins, nucleic acids and lipids, destroying important cellular processes and increasing mutations (Loro et al., 2012). Like in mammals, the cellular antioxidant defenses system in fish has been identified and proven to be functional during multiple situations which include *ROS* scavenging, oxidative stress protection, and attenuation of membrane lipid peroxidation (Hermans et al., 2007). Consequently, the major front-line antioxidant enzymes, such as *SOD* (neutralizes superoxide radicals to H_2O_2), *CAT,* and *GPx* (neutralizes H_2O_2 to water), and small non-protein antioxidants (scavenges all active oxygen species directly) work in a cascade to protect cells from oxidative stress (Ighodaro and Akinloye, 2018). Oxidative responses of both invertebrates and vertebrates under salinity challenges have been emphatically discussed. In juvenile olive flounders, the activities of *SOD*, *GST*, and *GSH* in the liver and gill were significantly affected by salinity (Kim et al., 2021). The activities of serum antioxidants, including *SOD, GPx, CAT,* and glutathione reductase (*GR*) in the spleen of European seabass after cold stress, were affected by salinity (Islam et al., 2020). Early studies have indicated the influences of environmental parameters including seawater acidification and cadmium on the antioxidant defense of flounder *P. olivaceus* larvae (Cui et al., 2020). In the present study, NaCl pre-treatment significantly induced the higher expression levels of *SOD*, *GPx*, and *Mt*, which is similar to previous studies in other juvenile fish and fish larvae. However, the expression level of *CAT* was not significantly upregulated

but even decreased after 1,000 mg/L NaCl pre-treatment. This is similar to earlier reports that, unlike *SOD*, no significant changes were observed in the mRNA expression or activity of *CAT* in the livers of *D. labrax* and *Chanos Chanos* under different salinity (Chang et al., 2021). H_2O_2, as a strong oxidant, can increase the intracellular *ROS* level and induce oxidative stress. However, the effects of H_2O_2 on fish antioxidant defense, including the levels of antioxidant enzymes (e.g., *SOD* and *CAT*) and nonenzymatic antioxidants (e.g., *GSH*), varied depending on the duration and dosage of H_2O_2 treatment. It has been reported that short and moderate H_2O_2 treatment stimulated the levels of the antioxidant enzymes, while chronic and severe H_2O_2 treatment impaired antioxidant defense system (Jia et al., 2021). In common carp (*C. carpio*), the oxidative stress-related genes, including *nrf2, gstα, sod, cat,* and/or *gpx1,* were upregulated in liver, gills, muscle, intestines, and/or kidney, but downregulated in heart after H_2O_2 exposure (Jia et al., 2020). In the brain and liver tissue of largemouth bass, 2.5 mg/L sodium carbonate peroxyhydrate containing H_2O_2 as the active ingredient resulted in an increase of *SOD*, *CAT*, *GPX*, *GR*, and *GST* activity (Sinha et al., 2020). In the present study, the expression of *SOD*, *GPx,* and *Mt* in loach larvae was significantly increased after H_2O_2 pre-treatment. However, like the unaffected *CAT* expression during NaCl treatment, no significant changes were found on the expression of *CAT* in loach larvae after H_2O_2 pre-treatment. Thus, H_2O_2 (200 and 400 mg/L) and NaCl (1,000 and 3,000 mg/L) pre-treatment during egg hatching significantly stimulated the antioxidant defense system in loach larvae.

Besides antioxidant defense system, the immune system also protects fish against environmental stress and teleost is the first bony vertebrate to develop both innate and adaptive immunity. Salinity and H_2O_2 have been shown to affect the fish immune responses, for example, the immune responses of European seabass acclimatized after extreme ambient cold stress were significantly affected by different salinities (Islam et al., 2020) and transcriptome analysis also identified 100 differentially expressed genes involved in the immune system of common carp (*C. carpio*) after H_2O_2 exposure (Jia et al., 2021). Especially, the complement system, which is composed of more than 35 soluble plasma proteins, plays an essential role in alerting and clearing of potential pathogens and also contributes to the development of an acquired immune response (Ferreira and Cortes, 2021). The complement system of teleost fish, like that of higher vertebrates, can be activated through all three pathways of complement (Nakao et al., 2011). Complement 3 (*C3*), the key component in teleost, is present in several isoforms that are the products of different genes (Sunyer et al., 1996). The lectin pathway is initiated through the interaction of *MBL* (like *C1q*) and ficolins with sugar moieties expressed on the surface of many microorganisms. *C1q* has been cloned in multiple fish species, such as channel catfish *I. punctatus* (Li et al., 2012) and killifish *F. heteroclitus* (Kocabas et al., 2002). Moreover, *MASP1* has such a broad specificity and has significant substrates other than complement proteins (Hajela et al., 2002). Besides, *C8* is responsible for the formation of membrane attack complex (Liyanage et al., 2018). In the present study, H_2O_2 pre-treatment during egg hatching significantly induced the higher mRNA expression level of *C3-1* and *C1q* in loach larvae, but did not affect the mRNA expression level of *C8b* nor *MASP-1*. This was similar to previous study that the expression levels of complement *C3, C4*, and *C7* in the Atlantic salmon skin were significantly upregulated by 24-h exposure to H_2O_2 (Karlsen et al., 2021). NaCl pre-treatment only increased the mRNA expression level of *C1q*, but decreased the mRNA expression levels of *C8b* and *MASP-1*. The mRNA expression level of *C3-1* was not significantly affected during NaCl pre-treatment. Under the stimulation of inflammatory mediators, activation signals, and pathogenic infection, interleukin 15 (*IL15*) could transfer from the endoplasmic reticulum to cell membrane after binding with its receptor (*IL15R*) and control multiple process, including cell proliferation and inhibition of apoptosis (Chen et al., 2018). Additionally, *Hsps* has been shown to be an integral part of the cellular stress response pathways in fishes (Metzger et al., 2016) and widely used as biomarkers of exposure to environmental stressors (Mitra et al., 2018). In the present study, H_2O_2 pre-treatment induced the mRNA expression of *IL15Rα* at 200 mg/L and *Hsp70* at 400 mg/L, while NaCl pre-treatment decreased *Hsp70* expression at two dosages but did not affect the expression of *IL15Rα*.

Fish fry is rather fragile at the early development period and can be easily affected by the surrounding environment. As reported earlier, the newly hatched loach larva had a long straight intestinal tube with a very simple structure (Luo et al., 2016), and the effectiveness of drug pre-treatment on the fry could be monitored by evaluating the relative mRNA expression levels of early development-related genes. *Spon1b* was originally isolated from the developing embryonic floor plate of vertebrates and performs a positive function in nervous system development. A study in Japanese flounder showed that *spon1b* was maternally expressed with transcripts present from one-cell stage to hatching stage, peaking at tailbud stage (Hu et al., 2016). *IFT* sculpts the proteome of cilia and flagella and plays critical roles in cilia biogenesis, quality control, and signal transduction by delivering proteins to the growing ciliary tip and selectively transporting signaling molecules (Webb et al., 2020). *VEGFA* is required for the differentiation of endothelial cells (vasculogenesis) and for the sprouting of new capillaries (angiogenesis), and duplicated *VEGFA* in the zebrafish has been reported to mediate vascular development (Bahary et al., 2007). *Gdh* in the Antarctic fish *Chaenocephalus aceratus* has been reported to have relationship with cold adaptation (Ciardiello et al., 2000). *Anxa1a* also play a significant role in epimorphic regeneration of zebrafish caudal fin tissue (Quoseena et al., 2020). In zebrafish, *VIP*-like immunoreactive cells exist in the olfactory pit, the retina, and several regions of the brain at 24 h post-fertilization (hpf) embryos (Mathieu et al., 2001). *PP1* and *PP2A* are proteins with major *Ser/Thr* protein phosphatase activity in eukaryotic cells and always interact with multiple proteins of diverse structure (regulatory subunits) with little substrate specificity; thus, they are a key regulator of cell development and oncogenic transformation (Dzulko et al., 2020). In the present study, excepting *anxa1a*, the expression levels of early development-related genes, including

spon1b, IFT22, VEGFAa, gdh, VIP, PP1, and *PP2AB,* were significantly increased after 400 mg/L H_2O_2 pre-treatment, which agrees well with the higher hatching rate in this group. However, although NaCl treatment increased their expression in loach larvae especially at 1,000 mg/L, the hatching rate of loach was not significantly affected.

In all, our study indicated the long-time effects of H_2O_2 and NaCl pre-treatment during fish egg hatching on the health and metabolism of fish larvae. Besides the role in promoting egg hatchability, H_2O_2 pre-treatment at appropriate dosage also stimulated the antioxidant system and immune system of fish larvae, which could be linked to the good performance in fish early development.

DATA AVAILABILITY STATEMENT

The original contributions presented in the study are included in the article/supplementary material, further inquiries can be directed to the corresponding author.

ETHICS STATEMENT

The animal study was reviewed and approved by Animal Experiment Committee of Huazhong Agricultural University.

AUTHOR CONTRIBUTIONS

QW designed and wrote the main context. MW conducted most experimental protocol. WX wrote the manuscript. JZ, SL, and ZS conducted the experimental analysis. FZ, WJ, and ZX supplied the relevant materials. All authors contributed to the article and approved the submitted version.

FUNDING

This article was funded by National Natural Science Foundation of China (Grant Nos. 31802317 and 32172996).

REFERENCES

Abi-Ayad, A., and Kestemont, P. (1994). Comparison of the nutritional status of goldfish (*Carassius auratus*) larvae fed with live, mixed or dry diet. *Aquaculture* 128, 163–176. doi: 10.1016/0044-8486(94)90111-2

Altinok, I., and Grizzle, J. M. (2001). Effects of low salinities on *Flavobacterium columnare* infection of euryhaline and freshwater stenohaline fish. *J. Fish Dis.* 24, 361–367. doi: 10.1046/j.1365-2761.2001.00306.x

Alvarez, P., Cotano, U., Estensoro, I., Etxebeste, E., and Irigoien, X. (2021). Assessment of larval growth patterns: a comparison across five fish species in the Bay of Biscay. *Reg. Stud. Mar. Sci.* 47:101958. doi: 10.1016/j.rsma.2021.101958

Avendaño-Herrera, R., Magariños, B., Irgang, R., and Toranzo, A. E. (2006). Use of hydrogen peroxide against the fish pathogen *Tenacibaculum maritimum* and its effect on infected turbot (*Scophthalmus maximus*). *Aquaculture* 257, 104–110. doi: 10.1016/j.aquaculture.2006.02.043

Bahary, N., Goishi, K., Stuckenholz, C., Weber, G., Leblanc, J., Schafer, C. A., et al. (2007). Duplicate VegfA genes and orthologues of the KDR receptor tyrosine kinase family mediate vascular development in the zebrafish. *Blood* 110, 3627–3636. doi: 10.1182/blood-2006-04-016378

Barnes, M. E., Ewing, D. E., Cordes, R. J., and Young, G. L. (1998). Observations on hydrogen peroxide control of *Saprolegnia* spp. during rainbow trout eggs incubation. *Prog. Fish Cult.* 60, 67–70. doi: 10.1577/1548-8640(1998)060<0067:OOHPCO>2.0.CO;2

Burdge, G. C., and Lillycrop, K. A. (2010). Nutrition, epigenetics, and developmental plasticity: implications for understanding human disease. *Annu. Rev. Nutr.* 30, 315–339. doi: 10.1146/annurev.nutr.012809.104751

Cabello, F. C. (2006). Heavy use of prophylactic antibiotics in aquaculture: a growing problem for human and animal health and for the environment. *Environ. Microbiol.* 8, 1137–1144. doi: 10.1111/j.1462-2920.2006.01054.x

Cai, L. S., Wang, L., Song, K., Lu, K. L., Zhang, C. X., and Rahimnejad, S. (2020). Evaluation of protein requirement of spotted seabass (*Lateolabrax maculatus*) under two temperatures, and the liver transcriptome response to thermal stress. *Aquaculture* 516:734615. doi: 10.1016/j.aquaculture.2019.734615

Chang, C. H., Mayer, M., Rivera-Ingraham, G., Blondeau-Bidet, E., Wu, W. Y., Lorin-Nebel, C., et al. (2021). Effects of temperature and salinity on antioxidant responses in livers of temperate (*Dicentrarchus labrax*) and tropical (*Chanos Chanos*) marine euryhaline fish. *J. Therm. Biol.* 99:103016. doi: 10.1016/j.jtherbio.2021.103016

Chen, X., Kong, W., Yu, Y., Dong, S., Huang, Z., Yu, W., et al. (2018). Molecular characterization and expression analysis of interleukin 15 (IL15) and interleukin-15 receptor subunit alpha (IL15Rα) in Dojo loach (*Misgurnus anguillicaudatus*): their salient roles during bacterial, parasitic and fungal infection. *Mol. Immunol.* 103, 293–305. doi: 10.1016/j.molimm.2018.10.012

Chen, S. G., Li, D. P., Xie, C. X., Yao, N., Wang, S., and Ren, D. Q. (2016). "Influence of salinity on hatching rate and larval vitality in *Triplophysa (Hedinichthys) yarkandensis* (Day)." in *The Annual Conference of Chinese Fisheries Association;* November 2–4, 2016.

Ciardiello, M. A., Camardella, L., Carratore, V., and Prisco, G. D. (2000). L-glutamate dehydrogenase from the Antarctic fish *Chaenocephalus aceratus*: primary structure, function and thermodynamic characterisation: relationship with cold adaptation. *Biochim. Biophys. Acta* 1543, 11–23. doi: 10.1016/s0167-4838(00)00186-2

Cui, W., Cao, L., Liu, J., Ren, Z., Zhao, B., and Dou, S. (2020). Effects of seawater acidification and cadmium on the antioxidant defense of flounder *Paralichthys olivaceus* larvae. *Sci. Total Environ.* 718:137234. doi: 10.1016/j.scitotenv.2020.137234

Dewi, R. R., Siallagan, W., and Suryanto, D. (2018). The efficacy of sodium chloride application in the control of fish lice (*Argulus* sp.) infection on tilapia (*Oreochromis niloticus*). *Acta Aquat. Sci. J.* 5, 4–7. doi: 10.29103/aa.v5i1.584

Dzulko, M., Pons, M., Henke, A., Schneider, G., and Krämer, O. H. (2020). The PP2A subunit PR130 is a key regulator of cell development and oncogenic transformation. *Biochim. Biophys. Acta Rev. Cancer* 1874:188453. doi: 10.1016/j.bbcan.2020.188453

Ferreira, V. P., and Cortes, C. (2021). *The Complement System, Reference Module in Biomedical Sciences*. Main St. Salt Lake City, UT 84111, USA: Elsevier.

Froelich, S. L., and Engelhardt, T. (1996). Comparative effects of formalin and salt treatments on hatch rate of koi carp eggs. *Prog. Fish Cult.* 58, 209–211. doi: 10.1577/1548-8640(1996)058<0209:CEOFAS>2.3.CO;2

Fuiman, L. A. (1983). Growth gradients in fish larvae. *J. Fish Biol.* 23, 117–123. doi: 10.1111/j.1095-8649.1983.tb02886.x

Fuiman, L. A., Smith, M. E., and Malley, V. N. (1999). Ontogeny of routine swimming speed and startle responses in red drum, with a comparison of responses to acoustic and visual stimuli. *J. Fish Biol.* 55, 215–226. doi: 10.1111/j.1095-8649.1999.tb01057.x

Gao, J., Koshio, S., Wang, W., Li, Y., Huang, S., and Cao, X. (2014). Effects of dietary phospholipid levels on growth performance, fatty acid composition and antioxidant responses of Dojo loach *Misgurnus anguillicaudatus* larvae. *Aquaculture* 426–427, 304–309. doi: 10.1016/j.aquaculture.2014.02.022

Gaon, A., Tandler, A., Nixon, O., El Sadin, S., Allon, G., and Koven, W. (2021). The combined DHA and taurine effect on vision, prey capture and growth

in different age larvae of gilthead sea bream (*Sparus aurata*). *Aquaculture* 545:737181. doi: 10.1016/j.aquaculture.2021.737181

George, L. A., Zhang, L., Tuersunjiang, N., Ma, Y., Long, N. M., Uthlaut, A. B., et al. (2012). Early maternal undernutrition programs increased feed intake, altered glucose metabolism and insulin secretion, and liver function in aged female offspring. *Am. J. Physiol. Regul. Integr. Comp. Physiol.* 302, R795–R804. doi: 10.1152/ajpregu.00241.2011

Geurden, I., Aramendi, M., Zambonino-Infante, J., and Panserat, S. (2007). Early feeding of carnivorous rainbow trout (*Oncorhynchus mykiss*) with a hyperglucidic diet during a short period: effect on dietary glucose utilization in juveniles. *Am. J. Physiol. Regul. Integr. Comp. Physiol.* 292, R2275–R2283. doi: 10.1152/ajpregu.00444.2006

Geurden, I., Mennigen, J., Plagnes-Juan, E., Veron, V., Cerezo, T., Mazurais, D., et al. (2014). High or low dietary carbohydrate:protein ratios during first-feeding affect glucose metabolism and intestinal microbiota in juvenile rainbow trout. *J. Exp. Biol.* 217, 3396–3406. doi: 10.1242/jeb.106062

Hajela, K., Kojima, M., Ambrus, G., Wong, K. H., Moffatt, B. E., Ferluga, J., et al. (2002). The biological functions of MBL-associated serine proteases (MASPs). *Immunobiology* 205, 467–475. doi: 10.1078/0171-2985-00147

Harris, I. S., and DeNicola, G. M. (2020). The complex interplay between antioxidants and ROS in cancer. *Trends Cell Biol.* 30, 440–451. doi: 10.1016/j.tcb.2020.03.002

Hart, P. R., and Purser, G. J. (1995). Effects of salinity and temperature on eggs and yolk sac larvae of the greenback flounder (*Rhombosolea tapirina* Günther, 1862). *Aquaculture* 136, 221–230. doi: 10.1016/0044-8486(95)01061-0

Hermans, N., Cos, P., Maes, L., De Bruyne, T., Vanden Berghe, D., Vlietinck, A. J., et al. (2007). Challenges and pitfalls in antioxidant research. *Curr. Med. Chem.* 14, 417–430. doi: 10.2174/092986707779941005

Holmström, K., Gräslund, S., Wahlström, A., Poungshompoo, S., Bengtsson, B. E., and Kautsky, N. (2003). Antibiotic use in shrimp farming and implications for environmental impacts and human health. *Int. J. Food Sci. Technol.* 38, 255–266. doi: 10.1046/j.1365-2621.2003.00671.x

Hu, H., Liu, J., Plagnes-Juan, E., Herman, A., Leguen, I., Goardon, L., et al. (2018). Programming of the glucose metabolism in rainbow trout juveniles after chronic hypoxia at hatching stage combined with a high dietary carbohydrate: protein ratios intake at first-feeding. *Aquaculture* 488, 1–8. doi: 10.1016/j.aquaculture.2018.01.015

Hu, H., Xin, N., Liu, J., Liu, M., Wang, Z., Wang, W., et al. (2016). Characterization of F-spondin in Japanese flounder (*Paralichthys olivaceus*) and its role in the nervous system development of teleosts. *Gene* 575, 623–631. doi: 10.1016/j.gene.2015.09.037

Huang, S., Cao, X., Tian, X., Luo, W., and Wang, W. (2015). Production of tetraploid gynogenetic loach using diploid eggs of natural tetraploid loach, *Misgurnus anguillicaudatus*, fertilized with UV-irradiated sperm of *Megalobrama amblycephala* without treatments for chromosome doubling. *Cytogenet. Genome Res.* 147, 260–267. doi: 10.1159/000444384

Ighodaro, O. M., and Akinloye, O. A. (2018). First line defence antioxidants-superoxide dismutase (SOD), catalase (CAT) and glutathione peroxidase (GPX): their fundamental role in the entire antioxidant defence grid. *Alex. J. Med.* 54, 287–293. doi: 10.1016/j.ajme.2017.09.001

Imanpoor, M. R., Najafi, E., and Kabir, M. (2012). Effects of different salinity and temperatures on the growth, survival, haematocrit and blood biochemistry of goldfish (*Carassius auratus*). *Aquac. Res.* 43, 332–338. doi: 10.1111/j.1365-2109.2011.02832.x

Islam, M. J., Kunzmann, A., Bögner, M., Meyer, A., Thiele, R., and James Slater, M. (2020). Metabolic and molecular stress responses of European seabass, *Dicentrarchus labrax* at low and high temperature extremes. *Ecol. Indic.* 112:106118. doi: 10.1016/j.ecolind.2020.106118

Jia, R., Du, J., Cao, L., Feng, W., He, Q., Xu, P., et al. (2020). Chronic exposure of hydrogen peroxide alters redox state, apoptosis and endoplasmic reticulum stress in common carp (*Cyprinus carpio*). *Aquat. Toxicol.* 229:105657. doi: 10.1016/j.aquatox.2020.105657

Jia, R., Du, J., Cao, L., Feng, W., He, Q., Xu, P., et al. (2021). Application of transcriptome analysis to understand the adverse effects of hydrogen peroxide exposure on brain function in common carp (*Cyprinus carpio*). *Environ. Pollut.* 286:117240. doi: 10.1016/j.envpol.2021.117240

Karlsen, C., Bogevik, A. S., Krasnov, A., and Ytteborg, E. (2021). *In vivo* and *in vitro* assessment of Atlantic salmon skin exposed to hydrogen peroxide. *Aquaculture* 540:736660. doi: 10.1016/j.aquaculture.2021.736660

Kim, J. H., Jeong, E. H., Jeon, Y. H., Kim, S. K., and Hur, Y. B. (2021). Salinity-mediated changes in hematological parameters, stress, antioxidant responses, acetylcholinesterase of juvenile olive flounders (*Paralichthys olivaceus*). *Environ. Toxicol. Pharmacol.* 83:103597. doi: 10.1016/j.etap.2021.103597

Klein, R. D., Rosa, C. E., Colares, E. P., Robaldo, R. B., Martinez, P. E., and Bianchini, A. (2017). Antioxidant defense system and oxidative status in Antarctic fishes: the sluggish rockcod *Notothenia coriiceps* versus the active marbled notothen *Notothenia rossii*. *J. Therm. Biol.* 68, 119–127. doi: 10.1016/j.jtherbio.2017.02.013

Kocabas, A. M., Li, P., Cao, D., Karsi, A., He, C., Patterson, A., et al. (2002). Expression profile of the channel catfish spleen: analysis of genes involved in immune functions. *Mar. Biotechnol.* 4, 526–536. doi: 10.1007/s10126-002-0067-0

Kongsted, A. H., Tygesen, M. P., Husted, S. V., Oliver, M. H., Tolver, A., Christensen, V. G., et al. (2014). Programming of glucose-insulin homoeostasis: long-term consequences of pre-natal versus early post-natal nutrition insults. Evidence from a sheep model. *Acta Physiol.* 210, 84–98. doi: 10.1111/apha.12080

Kujawa, R., Lach, M., Pol, P., Ptaszkowski, M., and Kucharczyk, D. (2017). Influence of water salinity on the survival of embryos and growth of the sichel larvae *Pelecus cultratus* (L.) under controlled conditions. *Aquac. Res.* 48, 1302–1314. doi: 10.1111/are.12972

Kupriyanova, Y., Zaharia, O. P., Bobrov, P., Karusheva, Y., Burkart, V., Szendroedi, J., et al. (2021). Early changes in hepatic energy metabolism and lipid content in recent-onset type 1 and 2 diabetes mellitus. *J. Hepatol.* 74, 1028–1037. doi: 10.1016/j.jhep.2020.11.030

Kurien, B. T., and Scofield, R. H. (2003). Free radical mediated peroxidative damage in systemic lupus erythematosus. *Life Sci.* 73, 1655–1666. doi: 10.1016/S0024-3205(03)00475-2

Lacher, S. E., Levings, D. C., Freeman, S., and Slattery, M. (2018). Identification of a functional antioxidant response element at the HIF1A locus. *Redox Biol.* 19, 401–411. doi: 10.1016/j.redox.2018.08.014

Li, C., Zhang, Y., Wang, R., Lu, J., Nandi, S., Mohanty, S., et al. (2012). RNA-seq analysis of mucosal immune responses reveals signatures of intestinal barrier disruption and pathogen entry following Edwardsiella ictaluri infection in channel catfish, Ictalurus punctatus. *Fish Shellfish Immunol.* 32, 816–827. doi: 10.1016/j.fsi.2012.02.004

Lisboa, V., Barcarolli, I. F., Sampaio, L. A., and Bianchini, A. (2015). Acclimation of juvenile *Mugil liza* Valenciennes, 1836 (Mugiliformes: Mugilidae) to different environmental salinities. *Neotrop. Ichthyol.* 13, 591–598. doi: 10.1590/1982-0224-20140123

Liu, J., Plagnes-Juan, E., Geurden, I., Panserat, S., and Marandel, L. (2017a). Exposure to an acute hypoxic stimulus during early life affects the expression of glucose metabolism-related genes at first-feeding in trout. *Sci. Rep.* 7:363. doi: 10.1038/s41598-017-00458-4

Liu, J., Dias, K., Plagnes-Juan, E., Veron, V., Panserat, S., and Marandel, L. (2017b). Long-term programming effect of embryonic hypoxia exposure and high-carbohydrate diet at first feeding on glucose metabolism in juvenile rainbow trout. *J. Exp. Biol.* 220, 3686–3694. doi: 10.1242/jeb.161406

Liyanage, D. S., Omeka, W. K. M., Godahewa, G. I., Lee, S., Nam, B. H., and Lee, J. (2018). Membrane attack complex-associated molecules from redlip mullet (*Liza haematocheila*): molecular characterization and transcriptional evidence of C6, C7, C8β, and C9 in innate immunity. *Fish Shellfish Immunol.* 81, 1–9. doi: 10.1016/j.fsi.2018.07.006

Loro, V. L., Jorge, M. B., Silva, K. R., and Wood, C. M. (2012). Oxidative stress parameters and antioxidant response to sublethal waterborne zinc in a euryhaline teleost *Fundulus heteroclitus*: protective effects of salinity. *Aquat. Toxicol.* 110–111, 187–193. doi: 10.1016/j.aquatox.2012.01.012

Lucas, A. (1998). Programming by early nutrition: an experimental approach. *J. Nutr.* 128, 401s–406s.

Luo, W., Cao, X., Xu, X., Huang, S., Liu, C., and Tomljanovic, T. (2016). Developmental transcriptome analysis and identification of genes involved in formation of intestinal air-breathing function of Dojo loach, *Misgurnus anguillicaudatus*. *Sci. Rep.* 6:31845. doi: 10.1038/srep39108

Magondu, E. W., Rasowo, J., Oyoo-Okoth, E., and Charo-Karisa, H. (2011). Evaluation of sodium chloride (NaCl) for potential prophylactic treatment and its short-term toxicity to African catfish *Clarias gariepinus* (Burchell 1822) yolk-sac and swim-up fry. *Aquaculture* 319, 307–310. doi: 10.1016/j.aquaculture.2011.06.038

Mathieu, M., Tagliafierro, G., Angelini, C., and Vallarino, M. (2001). Organization of vasoactive intestinal peptide-like immunoreactive system in the brain, olfactory organ and retina of the zebrafish, *Danio rerio*, during development. *Brain Res.* 888, 235–247. doi: 10.1016/S0006-8993(00)03065-1

Menendez-Montes, I., Escobar, B., Gomez, M. J., Albendea-Gomez, T., Palacios, B., Bonzon-Kulichenko, E., et al. (2021). Activation of amino acid metabolic program in cardiac HIF1-alpha-deficient mice. *iScience* 24:102124. doi: 10.1016/j.isci.2021.102124

Metzger, D. C., Hemmer-Hansen, J., and Schulte, P. M. (2016). Conserved structure and expression of hsp70 paralogs in teleost fishes. *Comp. Biochem. Physiol. Part D Genomics Proteomics* 18, 10–20. doi: 10.1016/j.cbd.2016.01.007

Ministry of Agriculture and Rural Affairs of the People's Republic of China (2021). *China Fishery Statistical Yearbook*. Beijing: China Agriculture Press.

Mitra, T., Mahanty, A., Ganguly, S., Purohit, G. K., Mohanty, S., Parida, P. K., et al. (2018). Expression patterns of heat shock protein genes in *Rita rita* from natural riverine habitat as biomarker response against environmental pollution. *Chemosphere* 211, 535–546. doi: 10.1016/j.chemosphere.2018.07.093

Nakao, M., Tsujikura, M., Ichiki, S., Vo, T. K., and Somamoto, T. (2011). The complement system in teleost fish: progress of post-homolog-hunting researches. *Dev. Comp. Immunol.* 35, 1296–1308. doi: 10.1016/j.dci.2011.03.003

Ni, J., Wang, X., Stojanovic, A., Zhang, Q., Wincher, M., Bühler, L., et al. (2020). Single-cell RNA sequencing of tumor-infiltrating NK cells reveals that inhibition of transcription factor HIF-1α unleashes NK cell activity. *Immunity* 52, 1075–1087. doi: 10.1016/j.immuni.2020.05.001

Overton, K., Samsing, F., Oppedal, F., Dalvin, S., Stien, L. H., and Dempster, T. (2018). The use and effects of hydrogen peroxide on salmon lice and post-smolt Atlantic salmon. *Aquaculture* 486, 246–252. doi: 10.1016/j.aquaculture.2017.12.041

Peng, X. R., Feng, L., Jiang, W. D., Wu, P., Liu, Y., Jiang, J., et al. (2019). Supplementation exogenous bile acid improved growth and intestinal immune function associated with NF-κB and TOR signalling pathways in on-growing grass carp (*Ctenopharyngodon idella*): enhancement the effect of protein-sparing by dietary lipid. *Fish Shellfish Immunol.* 92, 552–569. doi: 10.1016/j.fsi.2019.06.047

Pérez-Jiménez, A., Abellán, E., Arizcun, M., Cardenete, G., Morales, A. E., and Hidalgo, M. C. (2017). Dietary carbohydrates improve oxidative status of common dentex (*Dentex dentex*) juveniles, a carnivorous fish species. *Comp. Biochem. Physiol. A Mol. Integr. Physiol.* 203, 17–23. doi: 10.1016/j.cbpa.2016.08.014

Phelps, R. P., and Walser, C. A. (1993). Effect of sea salt on the hatching of channel catfish eggs. *J. Aquat. Anim. Health* 5, 205–207. doi: 10.1577/1548-8667(1993)005<0205:EOSSOT>2.3.CO;2

Pisoschi, A. M., and Pop, A. (2015). The role of antioxidants in the chemistry of oxidative stress: a review. *Eur. J. Med. Chem.* 97, 55–74. doi: 10.1016/j.ejmech.2015.04.040

Pittman, K., Yúfera, M., Pavlidis, M., Geffen, A. J., Koven, W., Ribeiro, L., et al. (2013). Fantastically plastic: fish larvae equipped for a new world. *Rev. Aquac.* 5, S224–S267. doi: 10.1111/raq.12034

Post, G. (1987). *Textbook of Fish Health. Revised and Expanded Edition*. Neptune City, NJ: T.F.H. Publications.

Qin, C., Huang, K., and Xu, H. (2002). Protective effect of polysaccharide from the loach on the in vitro and in vivo peroxidative damage of hepatocyte. *J. Nutr. Biochem.* 13, 592–597. doi: 10.1016/S0955-2863(02)00193-6

Quoseena, M., Vuppaladadium, S., Hussain, S., Banu, S., Bharathi, S., and Idris, M. M. (2020). Functional role of annexins in zebrafish caudal fin regeneration – a gene knockdown approach in regenerating tissue. *Biochimie* 175, 125–131. doi: 10.1016/j.biochi.2020.05.014

Rach, J. J., Gaikowski, M. P., Howe, G. E., and Schreier, T. M. (1998). Evaluation of the toxicity and efficacy of hydrogen peroxide treatments on eggs of warm- and coolwater fishes. *Aquaculture* 165, 11–25. doi: 10.1016/S0044-8486(98)00248-8

Rach, J. J., Valentine, J. J., Schreier, T. M., Gaikowski, M. P., and Crawford, T. G. (2004). Efficacy of hydrogen peroxide to control saprolegniasis on channel catfish (*Ictalurus punctatus*) eggs. *Aquaculture* 238, 135–142. doi: 10.1016/j.aquaculture.2004.06.007

Rasowo, J., Okoth, O. E., and Ngugi, C. C. (2007). Effects of formaldehyde, sodium chloride, potassium permanganate and hydrogen peroxide on hatch rate of African catfish *Clarias gariepinus* eggs. *Aquaculture* 269, 271–277. doi: 10.1016/j.aquaculture.2007.04.087

Rojo-Cebreros, A. H., Ibarra-Castro, L., and Martínez-Brown, J. M. (2018). Immunostimulation and trained immunity in marine fish larvae. *Fish Shellfish Immunol.* 80, 15–21. doi: 10.1016/j.fsi.2018.05.044

Schelkle, B., Doetjes, R., and Cable, J. (2011). The salt myth revealed: treatment of gyrodactylid infections on ornamental guppies, *Poecilia reticulata*. *Aquaculture* 311, 74–79. doi: 10.1016/j.aquaculture.2010.11.036

Schnick, R. A. (1988). The impetus to register new therapeutants for aquaculture. *Prog. Fish Cult.* 50, 190–196. doi: 10.1577/1548-8640(1988)050<0190:TITRNT>2.3.CO;2

Schreier, T. M., Rach, J. J., and Howe, G. E. (1996). Efficacy of formalin, hydrogen peroxide, and sodium chloride on fungal-infected rainbow trout eggs. *Aquaculture* 140, 323–331. doi: 10.1016/0044-8486(95)01182-X

Shamsi, S., Steller, E., and Zhu, X. (2021). The occurrence and clinical importance of infectious stage of *Echinocephalus* (Nematoda: Gnathostomidae) larvae in selected Australian edible fish. *Parasitol. Int.* 83:102333. doi: 10.1016/j.parint.2021.102333

Shao, Y., Wang, Y., Yuan, Y., and Xie, Y. (2021). A systematic review on antibiotics misuse in livestock and aquaculture and regulation implications in China. *Sci. Total Environ.* 798:149205. doi: 10.1016/j.scitotenv.2021.149205

Sinha, A. K., Romano, N., Shrivastava, J., Monico, J., and Bishop, W. M. (2020). Oxidative stress, histopathological alterations and anti-oxidant capacity in different tissues of largemouth bass (*Micropterus salmoides*) exposed to a newly developed sodium carbonate peroxyhydrate granular algaecide formulated with hydrogen peroxide. *Aquat. Toxicol.* 218:105348. doi: 10.1016/j.aquatox.2019.105348

Small, B. C., and Wolters, W. R. (2003). Hydrogen peroxide treatment during egg incubation improves channel catfish hatching success. *N. Am. J. Aquac.* 65, 314–317. doi: 10.1577/C02-048

Subasinghe, R. P., Bueno, P. B., Phillips, M. J., Hough, C., McGladdery, S. E., and Arthur, J. (2000). "Aquaculture in the third millennium." in *Technical Proceedings of the Conference on Aquaculture in the Third Millennium*; February 20–25, 2000. NACA, Bangkok and FAO, 167–191.

Sunyer, J. O., Zarkadis, I. K., Sahu, A., and Lambris, J. D. (1996). Multiple forms of complement C3 in trout that differ in binding to complement activators. *Proc. Natl. Acad. Sci. U. S. A.* 93, 8546–8551.

Teresa Vega-Ramírez, M., Moreno-Lafont, M. C., Valenzuela, R., Cervantes-Olivares, R., Miguel Aller-Gancedo, J., Fregeneda-Grandes, J. M., et al. (2013). New records of *Saprolegniaceae* isolated from rainbow trout, from their eggs, and water in a fish farm from the state of México. *Rev. Mex. Biodivers.* 84, 637–649. doi: 10.7550/rmb.28627

Wang, H. S., Fang, Q. S., and Zheng, L. Y. (2002). Effects of salinity on hatching rates and survival activity index of the larvae of *Epinephelus akaara*. *J. Fish. China* 26, 344–350.

Wang, Q., Ji, W., and Xu, Z. (2020). Current use and development of fish vaccines in China. *Fish Shellfish Immunol.* 96, 223–234. doi: 10.1016/j.fsi.2019.12.010

Wang, Q., Yu, Y., Zhang, X., and Xu, Z. (2019). Immune responses of fish to *Ichthyophthirius multifiliis* (Ich): a model for understanding immunity against protozoan parasites. *Dev. Comp. Immunol.* 93, 93–102. doi: 10.1016/j.dci.2019.01.002

Webb, S., Mukhopadhyay, A. G., and Roberts, A. J. (2020). Intraflagellar transport trains and motors: insights from structure. *Semin. Cell Dev. Biol.* 107, 82–90. doi: 10.1016/j.semcdb.2020.05.021

Zambonino-Infante, J. L., Panserat, S., Servili, A., Mouchel, O., Madec, L., and Mazurais, D. (2019). Nutritional programming by dietary carbohydrates in European sea bass larvae: not always what expected at juvenile stage. *Aquaculture* 501, 441–447. doi: 10.1016/j.aquaculture.2018.11.056

Zhou, W., Rahimnejad, S., Lu, K., Wang, L., and Liu, W. (2019). Effects of berberine on growth, liver histology, and expression of lipid-related genes in blunt snout bream (*Megalobrama amblycephala*) fed high-fat diets. *Fish Physiol. Biochem.* 45, 83–91. doi: 10.1007/s10695-018-0536-7

Conflict of Interest: The authors declare that the research was conducted in the absence of any commercial or financial relationships that could be construed as a potential conflict of interest.

Publisher's Note: All claims expressed in this article are solely those of the authors and do not necessarily represent those of their affiliated organizations, or those of the publisher, the editors and the reviewers. Any product that may

be evaluated in this article, or claim that may be made by its manufacturer, is not guaranteed or endorsed by the publisher.

frontiers in Physiology

ORIGINAL RESEARCH
published: 28 January 2022
doi: 10.3389/fphys.2021.813451

Cold Acclimation for Enhancing the Cold Tolerance of Zebrafish Cells

Huamin Wang[1,2,3†], *Ying Wang*[1,2,3†], *Minghui Niu*[1,2,3], *Linghong Hu*[1,2,3] *and Liangbiao Chen*[1,2,3*]

[1] International Research Center for Marine Biosciences, Ministry of Science and Technology, Shanghai Ocean University, Shanghai, China, [2] Key Laboratory of Exploration and Utilization of Aquatic Genetic Resources, Ministry of Education, Shanghai Ocean University, Shanghai, China, [3] Shanghai Collaborative Innovation for Aquatic Animal Genetics and Breeding, Shanghai Ocean University, Shanghai, China

Cold stress is an important threat in the life history of fish. However, current research on the tolerance mechanisms of fish to cold stress is incomplete. To explore the relevant molecular mechanisms enabling cold stress tolerance in fish, here we studied ZF4 cells subjected to short-term (4 days) low temperature stress and long-term (3 months) low temperature acclimation. The results showed that cell viability decreased and the cytoskeleton shrank under short-term (4 days) low temperature stress, while the cell viability and the cytoskeleton became normal after cold acclimation at 18°C for 3 months. Further, when the cells were transferred to the lower temperature (13°C), the survival rate was higher in the acclimated than non-acclimated group. By investigating the oxidative stress pathway, we found that the ROS (reactive oxygen species) content increased under short-term (4 days) cold stress, coupled with changes in glutathione (GSH), catalase (CAT), superoxide dismutase (SOD) enzyme activity levels. In addition, overproduction of ROS disrupted physiological cellular homeostasis that generated apoptosis *via* the activation of the mitochondrial pathway. However, when compared with the non-domesticated group, both ROS levels and apoptosis were lowered in the long-term (3 months) domesticated cells. Taken together, these findings suggest that cold acclimation can improve the low temperature tolerance of the cells. This exploration of the mechanism by which zebrafish cells tolerate cold stress, thus contributes to laying the foundation for future study of the molecular mechanism of cold adaptation in fish.

Keywords: ZF4 cells, cold stress, cold acclimation, oxidative stress, apoptosis

OPEN ACCESS

Edited by:
Qingchao Wang,
Huazhong Agricultural University, China

Reviewed by:
Shenping Cao,
Changsha University, China
Yancui Zhao,
Ludong University, China
Guoxing Nie,
Henan Normal University, China

***Correspondence:**
Liangbiao Chen
lbchen@shou.edu.cn

† These authors have contributed equally to this work

Specialty section:
This article was submitted to Aquatic Physiology, a section of the journal Frontiers in Physiology

Received: *11 November 2021*
Accepted: *23 December 2021*
Published: *28 January 2022*

Citation:
Wang H, Wang Y, Niu M, Hu L and Chen L (2022) Cold Acclimation for Enhancing the Cold Tolerance of Zebrafish Cells. Front. Physiol. 12:813451. doi: 10.3389/fphys.2021.813451

INTRODUCTION

As the major component of aquatic fauna, fish species are often exposed to wide fluctuations of water temperature, which plays an essential role in their growth, survival, and reproduction (Vondracek et al., 1988; Schmidt and Starck, 2010; Shahjahan et al., 2017). Most vital activities decline or halt when fish are exposed to lower water temperatures, such as for zebrafish (*Danio rerio*), whose embryos' development slows down as the temperature drops (Kimmel et al., 1995; Schmidt and Starck, 2010). Furthermore, low temperature stress can cause gill apoptosis in both zebrafish and tilapia (Hu et al., 2016). Studies show that when exposed to low temperature, the metabolic rate decreased and energy homeostasis were disrupted in orange-spotted grouper (*Epinephelus coioides*) and coho salmon (*Oncorhynchus kisutch*) (Larsen et al., 2001; Sun et al., 2019). Even worse, in aquaculture and natural waters, a substantial temperature decline may trigger the death of various fish (Beitinger et al., 2000; Liang et al., 2015). Therefore, it is necessary to investigate how fish

physiologically respond to low temperature, and in recent years, many studies have examined fish responses to cold stress. For example, fish can tolerate cold stress by adjusting their metabolism, which includes increased energy demand and glycolysis and amino acid catabolism (Islam et al., 2021; Schleger et al., 2021). Furthermore, fish can also alter the rate of protein synthesis and the activity of enzymes under low temperature (Ren et al., 2021; Yilmaz et al., 2021). Nevertheless, those extensive research activities have focused on short-term stress responses to cold, leaving little known about the specific molecular mechanism by which fish improve their cold tolerance during the long-term process of acclimatization. Recently, many studies have shown that cold acclimation can enable the physiological activities of fish to adapt to a lower temperature (Johnson et al., 2014; Klaiman et al., 2014; Keen et al., 2017). However, research investigating the role of long-term temperature acclimation in specific mechanisms that enhance the low temperature tolerance of fish remains scarce.

Cold stress can cause oxidative stress by inducing the production of excess reactive oxygen species (ROS). When levels of active oxygen increases in an organism, the system of antioxidant enzymes that can eliminate ROS are activated in the body (Ali et al., 2010). For example, lipid and protein peroxidation products of the northern moray eel (*Zoarces viviparus*) increased markedly after its acute exposure to low temperature (Heise et al., 2006). The expression of antioxidant enzyme genes of tilapia (*Oreochromis niloticus*) and pufferfish (*Takifugu obscurus*) also increased considerably under low temperature stress (Cheng et al., 2017; Yilmaz et al., 2021). In pufferfish (*Takifugu obscurus*) and euryhaline milkfish (*Chanos chanos*), cold stress induced oxidative stress in their blood and hepatocytes, respectively (Cheng et al., 2018; Chang et al., 2021). However, excessive oxidative stress may trigger oxidative damage to organisms, which is likely to directly result in macromolecular damage and cell apoptosis (Xing et al., 2016; Zhuang et al., 2017). Recent reports have shown that many fish apoptosis-related genes are significantly induced by low temperature (Heise et al., 2006; Sun et al., 2019). Therefore, overcoming oxidative stress is also a great challenge for fish under conditions of hypothermic stress.

Zebrafish is a key model in zoology, being widely used in developmental biology, genetics, physiology, toxicology, and other fields of animal research (Grunwald and Eisen, 2002; Ruzicka et al., 2019). We should note that zebrafish is tropical bony fishes capable of tolerating water temperatures ranging from 10.6°C ± 0.5°C to 41.7°C ± 0.3°C (Cheryl and Beitinger, 2005). Hence, zebrafish is widely used in the study of fish temperature stress (López-Olmeda and Sánchez-Vázquez, 2011). Much like its individual fish, the embryonic fibroblast cell line of zebrafish (ZF4) has an optimum growth temperature of 28°C and exhibits a wide range of temperature tolerance. Accordingly, ZF4 cells are considered a suitable cell model for the low temperature stress research, and were selected for study here. To maintain cellular homeostasis, fish must activate a physiological cascade of acclimation strategies while under cold stress (Donaldson et al., 2008; Tseng et al., 2011). To better explore those responses, the effects of short-term cold stress and long-term cold acclimation on zebrafish cell physiology, oxidative stress, and apoptosis should be investigated. This study not only provides ideas toward low temperature stress but also deep insights into the theory that cold acclimation can improve low temperature tolerance.

MATERIALS AND METHODS

Cell Culture and Treatment

ZF4 cell lines were purchased from the American Type Culture Collection (ATCC, Cat No. CRL 2050). These cells were thawed, resuscitated, and passaged at 28°C, 5% CO_2, in Dulbecco's modified Eagle's medium/F12 nutrient mix (SH30023.01B, Hyclone, Thermo Scientific, MA, United States) with 10% fetal bovine serum (FBS) and 1% penicillin-streptomycin-glutamine solution (SV30082.01, Hyclone, Thermo Scientific, MA, United States). The temperature treatment for the cold stress experiment was selected to be consistent with previous reports on zebrafish (Wu et al., 2011; Han et al., 2016). For the short-term cold stress group, when adherent cells had reached 80–90% confluency, the cells were moved to 18 and 13°C incubators with 5% CO_2 for 4 days. For the cold acclimation group, the culture media was changed every 2–3 days and the cells were passaged regularly at 18°C, with 5% CO_2, for 3 months. After undergoing the cold acclimation treatment, the low temperature domesticated cells were divided into 13°C incubators with 5% CO_2 for a 5 day period. Meanwhile, the cells at 28°C were transferred into 13°C incubators, also for 5 days, to serve as the control group. The morphology of these treated cells was observed and photographed daily under a fluorescent inverted microscope.

Cell Viability Assay

Cell viability was detected using a CCK-8 assay kit (C0038, Beyotime Biotechnology, Shanghai China) and following the manufacturer's instructions. The ZF4 cells were seeded onto a 96-well plate, at a density of 5000 cells per well, with 100 μL of medium. After the cold temperature treatment, 10 μL of the CCK-8 reagent was added to each well at various time points, and then all cells were further incubated for 4 h. Their absorbance at 450 nm was quantified with an enzyme-linked immunosorbent assay reader.

Phalloidin Staining and Inverted Fluorescence Microscope

The cells that climbed onto the carry sheet glass (20 mm) were cultured in an incubator. At the start of the experiment, the cells were washed three times with 1 × PBS. Then, the cells were fixed with 4% paraformaldehyde for 15 min at room temperature, and then washed again with 1 × PBS. After fixation, cells were incubated in a 0.5% Triton X-100 solution for 5 min, and then washed again with 1 × PBS. The cytoskeleton was stained with TRITC-conjugated phalloidin (CA1610, Solarbio, Beijing, China) for 30 min, away from any light, at room temperature. Next, the cells were washed three times with 1 × PBS. Finally, DAPI (100 nM in PBS, Invitrogen, CA, United States) was used to counterstain the nuclei at room temperature for 40 s. Their

fluorescence images were captured under a confocal microscope (Leica, SP8 FALCON, Germany).

Antioxidant Enzyme Activity

ZF4 cells were seeded in 100-mm-diameter dishes (2×10^5 cells per dish) and cultured to 90% confluency. Their cold stress treatment was performed as described above. Then all the cells were collected and washed with 1 × PBS two times and centrifuged for a final collection. The respective activity of superoxide dismutase (SOD), catalase (CAT), and glutathione (GSH) enzymes was determined using commercial assay kits (Jiancheng Bioengineering Institute, Nanjing, China). The activities of SOD, CAT and GSH are expressed in U/mg protein.

Quantification of Reactive Oxygen Species

To monitor the intracellular generation of ROS, viable ZF4 cells were collected for staining. The generation of intracellular ROS was detected using 2′,7′-Dichlorodihydrofluorescein diacetate (DCFH-DA, D6883, Sigma, MO, United States) as the peroxide-sensitive fluorescent probe. The cell suspension (5×10^4 cells/mL) was incubated with 10 μM DCFH-DA for 30 min in the absence of any light. After being washed with 1 × PBS, the cell suspension was analyzed by flow cytometry within 30 min (BD FACS Accuri C6; BD Biosciences, CA, United States). Lastly, data analysis of intracellular ROS was conducted using FlowJo 10 software.

Mitochondrial Membrane Potential Assay

Two assays were used to evaluate the effects on cells' mitochondrial membrane potential. Mitochondrial membrane potential (MMP) was analyzed using JC-1 (T4069, Sigma, MO, United States) in both flow cytometric and cell fluorescence assays. All cells were washed with ice-cold 1 × PBS and stained with 5 mg/mL JC-1 for 30 min in the dark. Then, each cell suspension was quantified by flow cytometry (BD FACS Accuri C6; BD Biosciences, MO, United States). Fluorescence images were acquired using a confocal microscope (Leica, SP8 FALCON, Germany).

Apoptosis Assay

According to the manufacturer's instructions, cell apoptosis was detected by Annexin V-FITC/PI Apoptosis kit (CA1020, Solarbio, Beijing, China). The cells were dual-stained with Annexin V-FITC and PI at room temperature for 20 min in the dark. This method simultaneously determines the percentage of live and total apoptotic cells (early and late apoptotic). After incubation and washing, the cell suspension was analyzed by flow cytometry (BD FACS Accuri C6; BD Biosciences, MO, United States). Data analysis was performed using FlowJo 10 software.

Statistical Analysis

Results of each experiment were obtained three times ($n = 3$ replicates), with three biological replicates used in every experiment, unless noted otherwise. The experimental data are expressed here are the mean ± standard deviation (SD). All data analyses and graphing were done using IBM SPSS Statistics v20 and GraphPad Prism 8.0. The results were analyzed by single-factor analysis of variance (one-way ANOVA) and by the paired *t*-test. A result of $P < 0.05$ was considered significant (*); that of $P < 0.01$ was considered extremely significant (**); that of $P < 0.001$ was considered extremely significant (***).

RESULTS

Cold Acclimation Affected Cell Morphology and Viability

To investigate whether cold acclimation promotes cold tolerance, short-term cold stress (4 days) and long-term cold acclimation treatments (3 months) were applied to ZF4 cells. After being treated at 18°C for 4 days, the cells displayed a slight contraction and widening of the cell gaps. When the treatment temperature dropped from 18 to 13°C and was maintained for 4 days, the cells were observed to shrink and grow into strips, with the gaps between cells becoming larger and the boundary of cells unclear. In addition, some dead cells were observed floating in the culture medium. However, when we exposed the cells to 18°C for 3 months of cold acclimation, that contraction of cells and those cell gaps were not discernible. Next, we exposed the cold acclimation group (18°C for 3 months) and the non-acclimation group (28°C) to 13°C for 5 days, which revealed the shedding of cells was mild to moderate in the acclimation group but severe in the non-acclimation group.

Only a few cells were observed in the non-domesticated group, and the cell margin appeared fairly blurry (**Figure 1A**). In parallel, we used the CCK8 assay to detect cell viability in both the cold stress and cold acclimation groups. These results indicated no significant difference in the cell viability versus the control group (28°C) (**Figure 1B**). In stark contrast, the cell viability decreased dramatically in both cold stress groups ($P < 0.05$ vs. control). Further, after transferring the cells to a 13°C exposure, a significant difference was observed when comparing the cell viability of the cold acclimation group (18°C for 3 months) with the control group ($P < 0.05$) (**Figure 1C**). All these results suggested that cold acclimation enables the cell to remain intact and viable under lower temperatures. Given that cell viability was reduced by ∼50% in going from normal conditions (28°C) to 13°C exposure for 4 days, in subsequent experiments these variables were selected as the standard time points for the induction of ZF4 cell apoptosis.

Effects of Cold Stress on the Cytoskeleton Structure of ZF4

To observe the cell cytoskeleton under cold stress conditions, phalloidin-strained F-actin was used to stain the cytoskeleton. This F-actin cytoskeleton was then detected by rhodamine-phalloidin (red) staining, while the nuclei were visualized with DAPI (blue). As seen in **Figure 2**, the control group's (28°C) cells were arranged regularly and well clustered. However, the morphology of ZF4 cells underwent gradual shrinkage in the

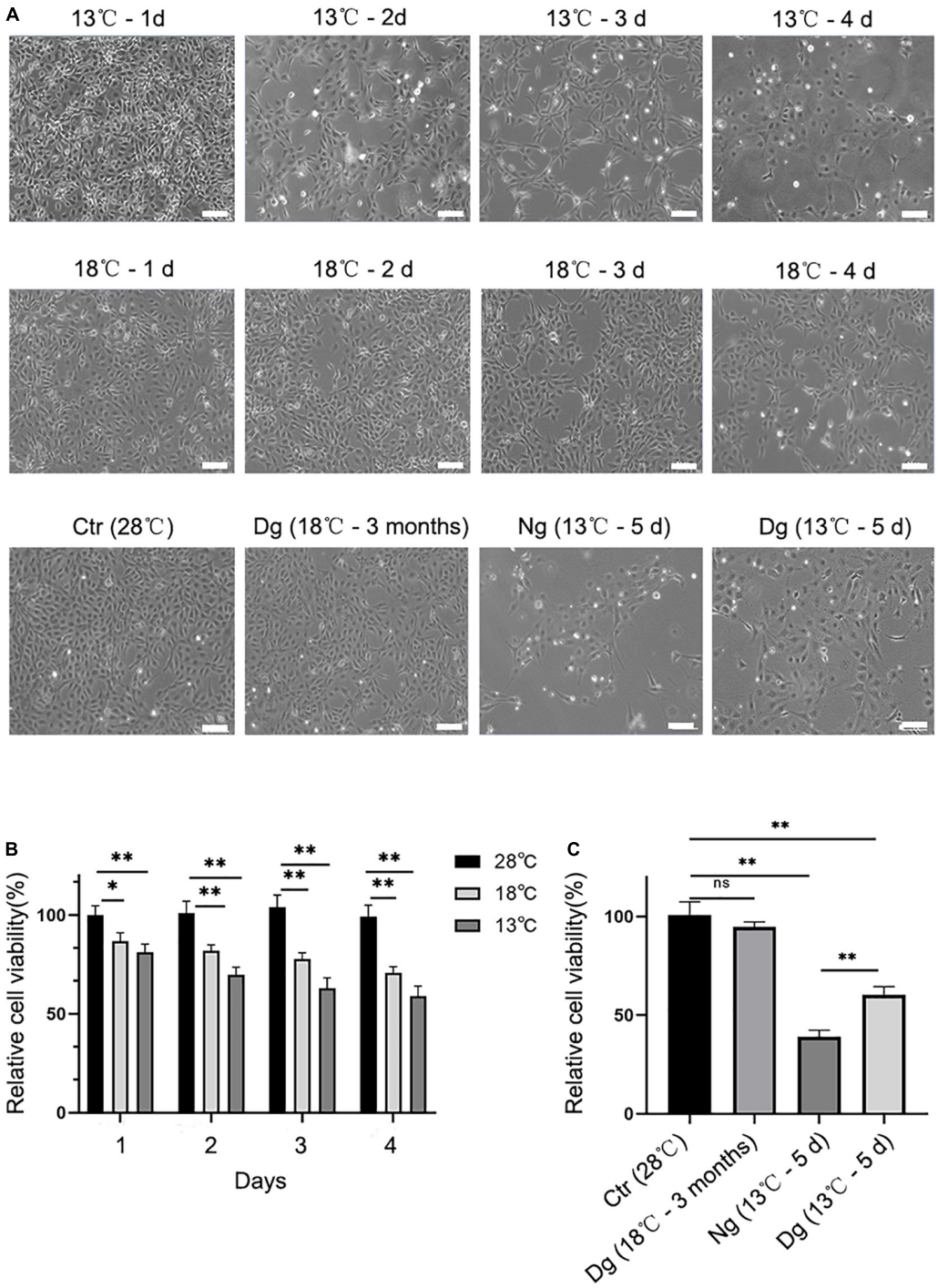

FIGURE 1 | Effect of cold stress on cell morphology and cell viability. Cells were allowed to grow in the incubator at 28°C in 5% CO2 and then treated with low temperature (13 and 18°C). Ctr, the control group; Dg, the domesticated group; Ng, the non-domesticated group. **(A)** Morphological pictures of ZF4 cells under normal or low temperature conditions. Cell morphology was examined under an inverted microscope at a 20 × magnification. Scale bar = 100 μm. **(B,C)** The CKK-8 assay was used to measure the viability of groups of short-term low temperature stress and long-term low temperature acclimation cells. The experiments were repeated three times. The results are presented as the mean ± SD ($n = 6$); $^{*}P < 0.05$, $^{**}P < 0.01$.

two cold stress groups, and became rounder with decreasing temperature. After a 3-month period of cold acclimation, the cell morphology gradually became regular in appearance. Yet, when we transferred the cells to the lower temperature without acclimation, the F-actin distribution lost its regularity. Furthermore, a large amount of granular fluorescence was found

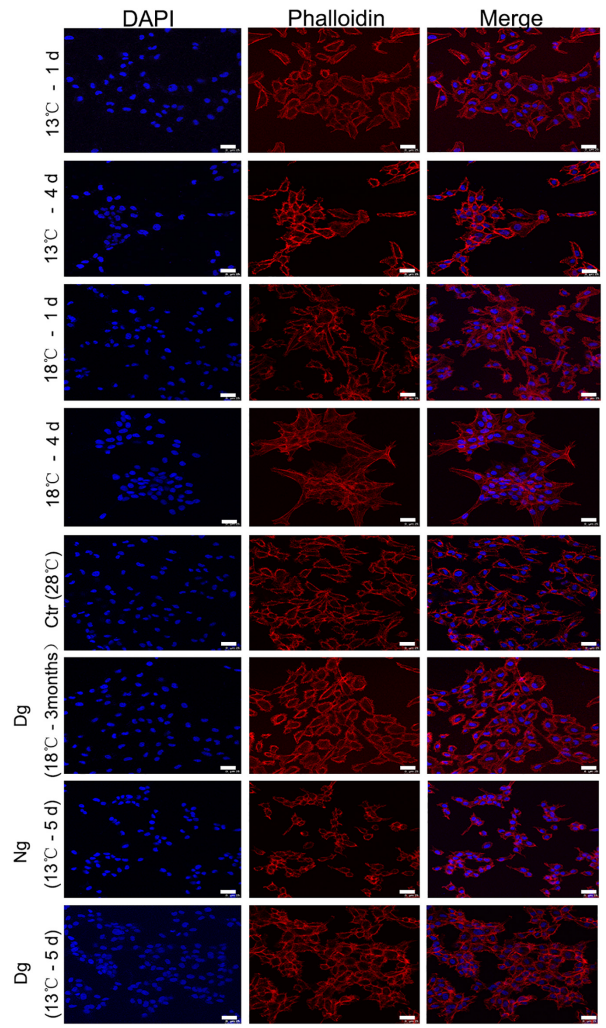

FIGURE 2 | Low temperature acclimation helps to maintain the ZF4 cell cytoskeleton. F-actin was labeled with rhodamin-phalloidin following exposure to low temperatures at different time points in ZF4 cells. The cell cytoskeletons were stained with phalloidin (red) and the staining of nuclei was performed with DAPI (blue). Laser scanning confocal microscopy was used to visualize the cytoskeleton of the cell. Scale bar = 25 μm. Ctr, the control group; Dg, the domesticated group; Ng, the non-domesticated group.

aggregating into clusters. Collectively, these results illustrated that cold stress significantly affected the cytoskeleton, but cold acclimation can protect the cells from death by stabilizing the cytoskeleton structure.

Cold Acclimation Inhibits Cold Stress-Induced Oxidant Stress in ZF4 Cells

To estimate the endogenous anti-oxidative capacity and oxidative stress status of ZF4 cells, we measured several antioxidant enzyme activities (SOD, CAT, and GSH) and ROS. Such antioxidant enzymes are considered the primary defense system against oxidative stress in cells. As **Figure 3** shows, SOD, CAT, and GSH activities were increased in a similar manner in both cold stress groups as the temperature decreased. CAT activity increased sharply on the 2nd day, while SOD and GSH activities peaked on the 3rd day ($P < 0.01$). After 3 months of acclimation, these cell enzyme activity levels had decreased substantially to below those of the control group (**Figures 3B,D,F**). At a lower temperature of 13°C, the antioxidant enzymes of the acclimated group were significantly higher ($P < 0.05$) in comparison with the non-acclimated group.

Reactive oxygen species is an important indicator of cellular oxidant stress induced by cold stress. As shown in **Figure 4**, ROS increased significantly in both cold stress groups at each time point vis-à-vis the control group ($P < 0.05$); however, the original ROS content was restored after cold acclimation ($P > 0.05$). When the cells were transferred to the lower temperature exposure, the ROS levels were lower in acclimated than non-acclimated group ($P < 0.01$). All these results indicated that cold acclimation protected the ZF4 cells against the oxidative stress induced by cold stress.

Effects of Cold Stress on Mitochondrial Membrane Potential in ZF4

Mitochondria have important roles in cellular aerobic respiration and oxidative phosphorylation, and their normal functioning is closely correlated with the level of intracellular ROS. JC-1 is a fluorescent probe for measuring mitochondrial membrane potential. When the mitochondrial membrane potential is normal, the JC-1 mitochondrial matrix aggregates to form polymers (J-aggregates) that emit red fluorescence. Conversely, when its mitochondrial membrane potential is low, JC-1 is a monomer in the mitochondrial matrix that produces green fluorescence. The shift of JC-1 from a red to green fluorescence state can be used to easily detect diminished cell membrane potential. Here, JC-1 staining and flow cytometry were both used to detect the changes in ZF4 cell mitochondrial membrane potential induced by low temperature stress. As evinced by **Figure 5A**, after JC-1 staining, the normal group cells showed red fluorescence, while the JC-1 in some cells changed from red fluorescence to green fluorescence under cold stress, indicating that mitochondrial membrane potential decreased under conditions of cold stress. Flow cytometry detected the mitochondrial membrane potential of ZF4 cells subjected to cold stress.

Compared with the control group (28°C), cold stress at 13 and 18°C for 4 days decreased the mean fluorescence intensity of the mitochondrial membrane potential by 55.28 and 65.51%, respectively ($P < 0.01$) (**Figure 5B**). In addition, the mitochondrial membrane potential of ZF4 cells decreased slightly after undergoing cold acclimation. Nevertheless, the differences in mitochondrial membrane potential between the cold acclimated group and control group were not pronounced ($P > 0.05$). Interestingly, when the acclimated group and the normal group were exposed to a lower temperature (13°C), statistically significant differences between these two groups were evident ($P < 0.01$). The mitochondrial membrane potential level was significantly lower in the normal group than the cold

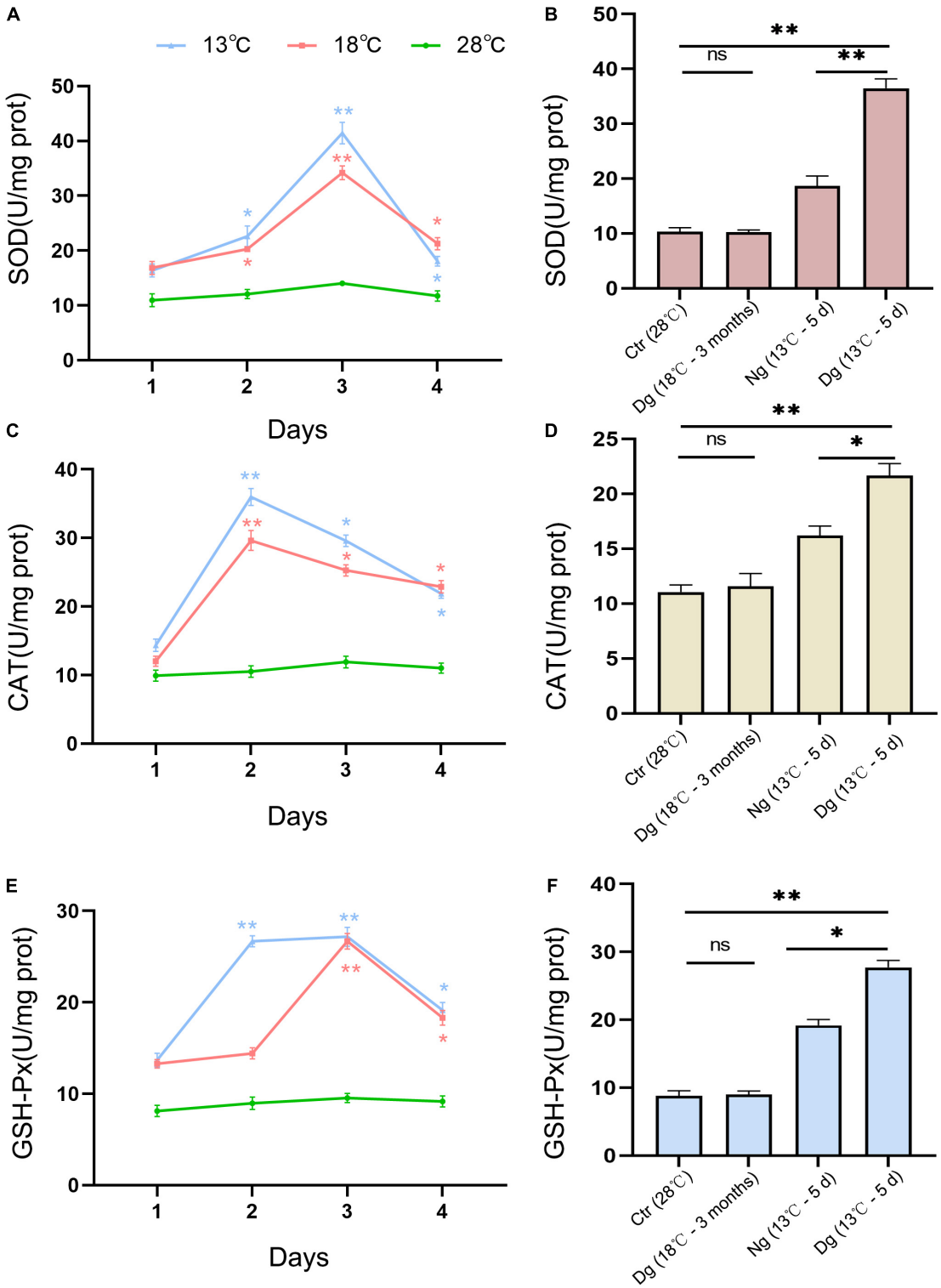

FIGURE 3 | Effects of cold stress on the antioxidant capacity of ZF4 cells. The effects of short-term low temperature stress and long-term cold acclimation on the antioxidant activities of SOD **(A,B)**, CAT **(C,D)**, and GSH-Px **(E,F)** in the ZF4 cells were measured using the corresponding detection kits. Ctr, the control group; Dg, the domesticated group; Ng, the non-domesticated group. The experiments were repeated three times. The results are presented as the mean ± SD ($n = 3$); $^{*}P < 0.05$, $^{**}P < 0.01$.

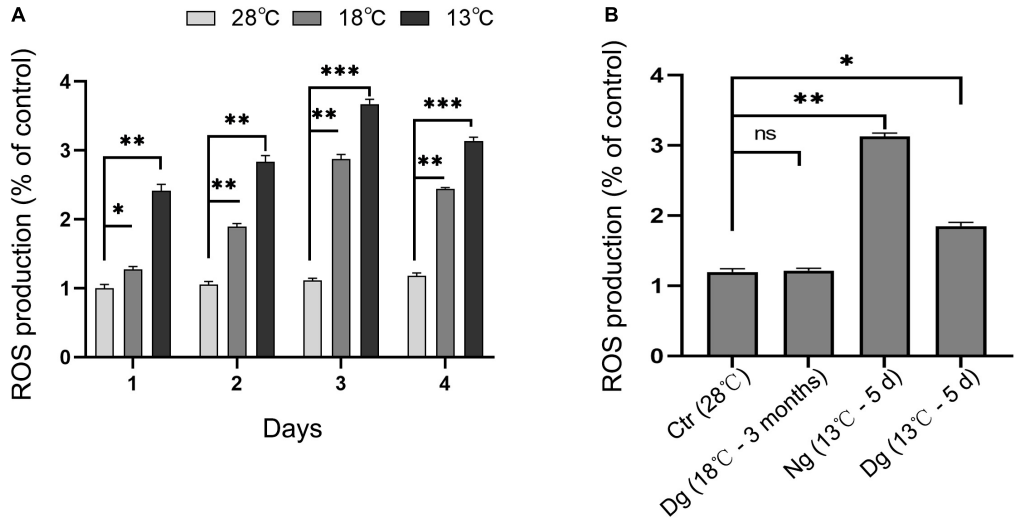

FIGURE 4 | Cold acclimation suppressed cold-induced oxidant stress in ZF4 cells. Ctr, the control group; Dg, the domesticated group; Ng, the non-domesticated group. **(A,B)** Cellular ROS production under cold stress. ROS was detected by flow cytometry and analyzed using FlowJo software. The results are presented as the mean ± SD ($n = 3$); $^{*}P < 0.05$, $^{**}P < 0.01$, $^{***}P < 0.001$.

acclimated group ($P < 0.05$) (**Figure 5C**). Altogether, these results suggested that cold acclimation significantly relieved mitochondrial dysfunction in ZF4 cells.

Cold Acclimation Reduces the Cold Stress-Induced Cellular Apoptosis of ZF4

It has been reported that increased ROS generation could lessen mitochondrial membrane potential ($\Delta\psi m$) and sequentially trigger mitochondria-dependent apoptosis. Therefore, we used Annexin V-FITC staining to detect the occurrence of ZF4 cell apoptosis induced by the cold stress. These results revealed the number of cell apoptosis increasing with a longer cold stress period relative to the control group. After 4 days of treatment at 13 and 18°C, the apoptosis rate of ZF4 cells was increased by 43.78 and 35.53%, respectively (both $P < 0.01$) (**Figures 6A,B**). However, the cold acclimation group only decreased the percentage of apoptosis by 10.97%. Similarly, we detected higher prevalence of apoptosis (54.24%) in the non-acclimation group than in the acclimation group (38.32%) after 5 days of cold treatment at 13°C (**Figure 6C**). These findings were consistent with the results of CCK-8 testing. Our results clearly showed that cold acclimation reduces the apoptosis induced by lower temperature stress.

DISCUSSION

As ectothermic animals, fish have particularly sensitive responses to changing temperatures in their aquatic environment. Over the past few decades, the major studies on the impact of climate change have focused on how high temperatures will affect fish biology. However, large-scale fish mortality and sublethal impacts caused by cold shock events also pose major challenges to fish survival (Viadero, 2005; O'Gorman et al., 2016). Generally, low temperature stress includes two aspects: cold acclimation and sudden temperature changes (Goos and Consten, 2002; Engelsma et al., 2003; Donaldson et al., 2008). Studies suggest that cold acclimation can improve the survival rate of fish under lethal low temperatures; for example, the survival rate of carp (*Cyprinus carpio*) at the lethal low temperatures of 8 and 10°C increased significantly after being cold-acclimated (Ge et al., 2020). Yet, our knowledge of the mechanisms through which low temperature domestication improves fish survival remains surprisingly limited. Therefore, here we studied zebrafish cells to explore the specific mechanism of cell survival after acute cold stress and cold acclimation. The present research contributes to a comprehensive understanding of cold tolerance in fish *via* novel insights into their cold acclimation-mediated physiology.

In this study, when facing acute cold stress, we found that cell viability decreased and the cytoskeleton shrank, whereas they remained normal after undergoing cold acclimation at 18°C for 3 months. These above findings indicate the successful establishment of a cold acclimation cell model. In addition, when the cells were exposed to a lower temperature (13°C), the cell viability of the acclimated group exceeded that of the non-acclimated group, indicating that the cells achieved cold tolerance ability and greater vigor after experiencing cold acclimation. Other studies have shown that acclimation generally fosters a corresponding compensation mechanism to maintain the homeostasis of the internal environment in fish (Goos and Consten, 2002; Engelsma et al., 2003). Also demonstrated in many animal studies, including those with zebrafish, is that cold acclimation affects the reduction in thickness of the compact myocardium and the changed collagen content when adjusting to a decrease in temperature (Johnson et al., 2014). In the process of cold acclimation, lipid catabolism and lipid oxidation were enhanced in milkfish (*Chanos chanos*) (Hsieh et al., 2003), and the actin cytoskeleton is known to be essential for maintaining

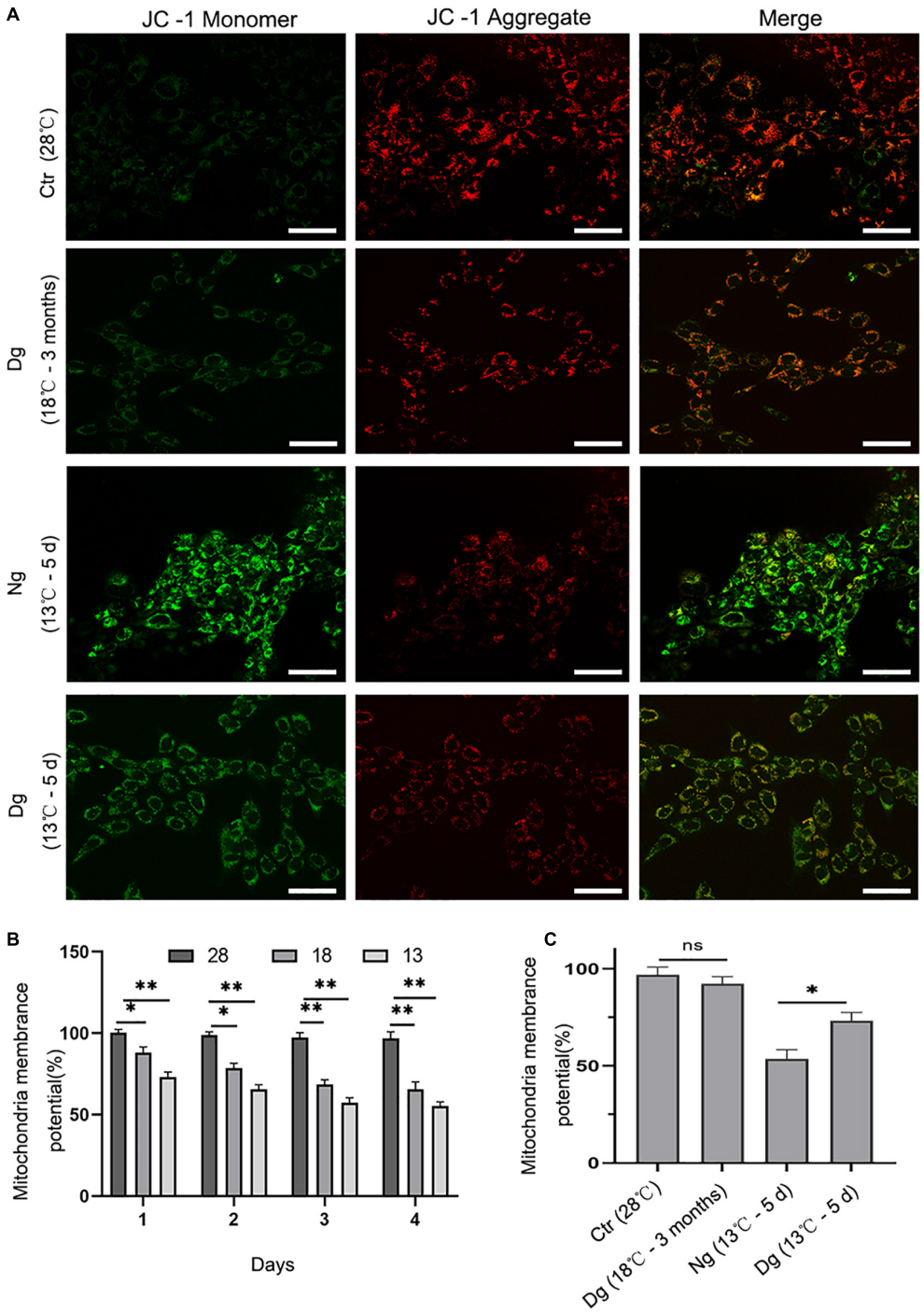

FIGURE 5 | The effect of cold stress on mitochondrial membrane potential. Ctr, the control group; Dg, the domesticated group; Ng, the non-domesticated group. **(A)** Representative images were scanned by a confocal microscope after staining with JC-1. The red fluorescence indicates high mitochondrial membrane potential, while the green indicates low mitochondrial membrane potential. Scale bar = 50 μm. **(B,C)** Quantitative results of mitochondrial membrane potential by flow cytometry. Each experiment was performed in triplicate. The results are presented as the mean ± SD ($n = 3$); $^{*}P < 0.05$, $^{**}P < 0.01$.

tissue architecture (Egge et al., 2019). In the present study, we found that those cells lacking cold acclimation had a significantly lessened F-actin cytoskeleton structure after being transferred to a 13°C exposure, whereas the acclimated cells retained a robust cytoskeleton. This fits with other research that has shown the cytoskeleton plays a key role in maintaining the structure and functioning of cells at low temperatures (Colinet et al., 2017; Marteaux et al., 2018). Our study suggests acclimated cells attain

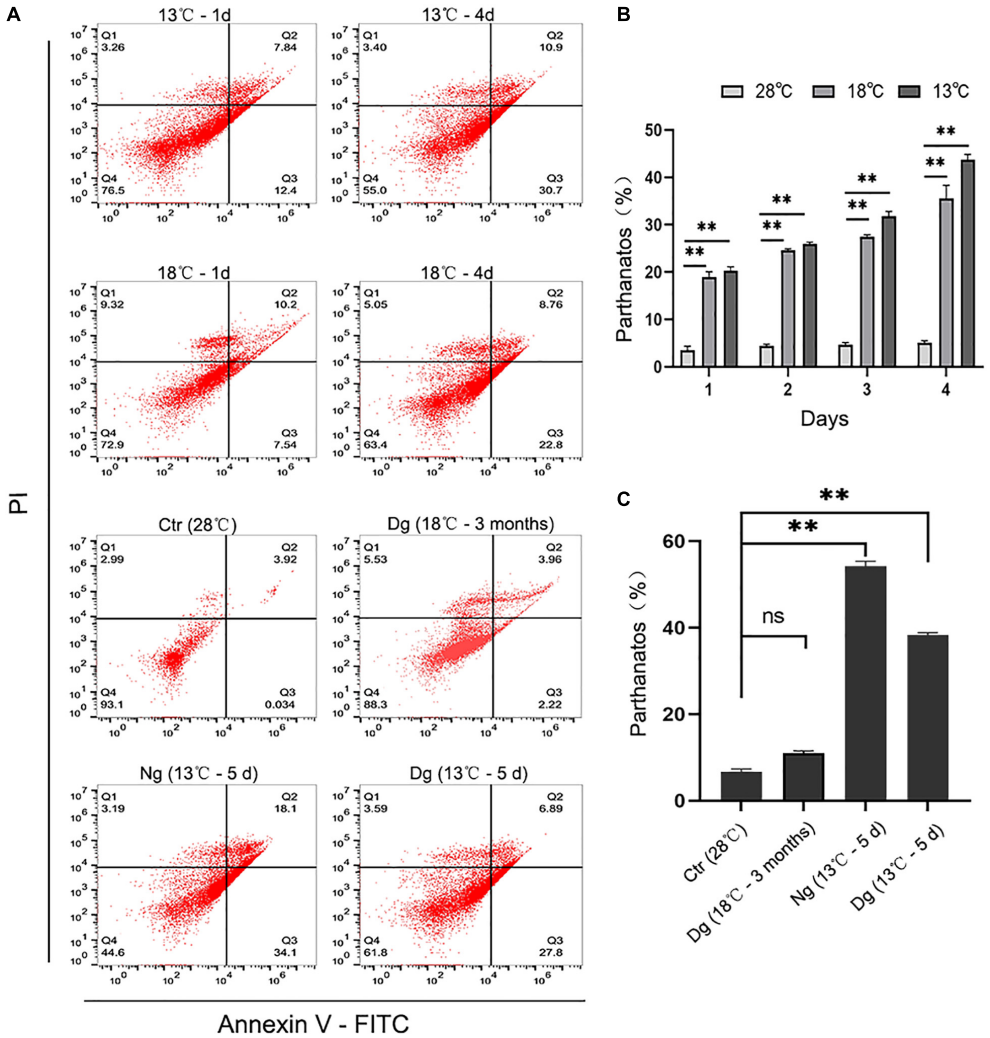

FIGURE 6 | Cold acclimation alleviated cold-induced cell apoptosis in ZF4 cells. Ctr, the control group; Dg, the domesticated group; Ng, the non-domesticated group. **(A)** Analysis of cell apoptosis by flow cytometry. Apoptosis was evaluated with AnnexinV-FITC/PI staining. **(B,C)** Apoptotic cells were calculated and graphed according to the flow cytometry results in GraphPad Prism 8 software. The results are presented as the mean ± SD (n = 3); $^{**}P < 0.01$.

better survival by improving their viability and modulating their cytoskeleton structures under cold stress conditions.

Cold stress can lead to an increase in endogenous ROS, such as hydroxyl radicals (-OH), superoxide free radicals (O_2-), and hydrogen peroxide free radicals (H_2O_2). However, the cell has an intracellular antioxidant defense system, including SOD, CAT, and GSH, which play pivotal roles in scavenging ROS. When the production of ROS exceeds the body's processing capacity, oxidative stress will occur (Lesser, 2006; An and Choi, 2010). In our study, antioxidant proteins and intracellular ROS were elevated at the onset of acute cold stress (13, 18°C). The upregulation of antioxidant enzymes protects the body from too much oxidative stress, and similar results have been reported in other fish studies (Cheng et al., 2017; Sánchez Nuño et al., 2018). Moreover, the level of mitochondrial membrane potential decrease and cell apoptosis increased with prolonged exposure to low temperature. Some researchers have pointed out that low temperature stress leads to the dysfunction of various biochemical reactions and physiological functions of fish. For example, acute cold stress affects the oxygen consumption rate and respiratory rate of fish (Maria Cristina and Paunescu, 2019), and a low temperature stress can alter the biochemical blood indexes and metabolism of large yellow croaker (*Pseudosciaena crocea*) (Liu et al., 2019). The intracellular ROS are mainly generated in mitochondria, and cold stress causes reduction the mitochondrial membrane potential and leads to enhanced ROS production (Morgan and Liu, 2011; Gerber et al., 2020; Xia et al., 2020). After a period of low temperature acclimation, the level of ROS and mitochondrial membrane potential in the cells returned to normal, and cell apoptosis decreased. This observation is consistent with previous findings that the apoptosis of zebrafish gill cells was decreased after undergoing cold acclimation (Chou et al., 2008).

Our study's results suggest the production and clearance of ROS is in a state of dynamic balance during cold acclimation, which was able to lessen oxidative damage and decrease cell apoptosis. In fact, low concentrations of ROS promote cell proliferation, but high concentrations of ROS lead the body to form oxidative stress damage, DNA breaks, mutations, and peptide chain breaks (Engelsma et al., 2003; Tang et al., 2015). For the non-domesticated group, enzyme activity level and survival rates decreased, and the ROS level of the cells dramatically increased at 13°C for 5 days. In recent years, many reports have demonstrated that ROS plays an indispensable role in the signal transduction related to apoptosis (Tang et al., 2017; Wang et al., 2017; Feng et al., 2021). Hence, it can be inferred that the non-domesticated group cells cannot remove excess ROS, leading to an imbalance of oxidative stress and subsequently inducing cell apoptosis. After being transferred to a lower temperature (13°C), the cold acclimation group featured higher levels of antioxidant enzyme activity and a decreased ROS content. While the mitochondrial membrane potential decreased, the ZF4 cells' rate of apoptosis rose in the non-domesticated group. Some reports have also suggested that low temperature acclimation improves mitochondrial function, including an increase in mitochondrial volume density and cristae surface area (Chung and Schulte, 2015; Yang et al., 2019). Accordingly, we could infer that cold acclimation results in enhanced mitochondrial function, which was able to reduce the accumulation of ROS and increase the mitochondrial membrane potential, and subsequently suppress the cell apoptosis caused by oxidative stress. In this way, the overall content of intracellular ROS would have been reduced, and mitochondrial functioning correspondingly changed to an enhanced state after domestication. These results explain why cold acclimation reduces oxidative stress to strengthen cold tolerance in ZF4 cells.

In conclusion, this study established a zebrafish ZF4 cell model for acute cold stress and long-term cold acclimation. It was determined that acute cold stress could induce oxidative stress in ZF4, and that low temperature acclimation could reduce oxidative damage and improve the low temperature tolerance of cells. These findings reveal the close connection between oxidative stress and the cold tolerance ability of fish, which should prove helpful for better understanding the cold tolerance mechanism of fish in general and finding ways to help them withstand low-temperature stress conditions in the future.

DATA AVAILABILITY STATEMENT

The raw data supporting the conclusions of this article will be made available by the authors, without undue reservation.

AUTHOR CONTRIBUTIONS

HW designed the experiment and wrote the manuscript. YW modified the original manuscript. MN and LH completed the data analysis. LC funding acquisition. All authors have read and agreed to the published version of the manuscript.

FUNDING

This work was supported by grants from the National Key Research and Development Program of China (2018YFD0900601), and the Natural Science Foundation of China (No. 41761134050) to LC.

ACKNOWLEDGMENTS

This is a short text to acknowledge the contributions of specific colleagues, institutions, or agencies that aided the efforts of the authors.

REFERENCES

Ali, S. S., Marcondes, M.-C. G., Bajova, H., Dugan, L. L., and Conti, B. (2010). Metabolic depression and increased reactive oxygen species production by isolated mitochondria at moderately lower temperatures. *J. Biol. Chem.* 285, 32522–32528. doi: 10.1074/jbc.M110.155432

An, M. I., and Choi, C. Y. (2010). Activity of antioxidant enzymes and physiological responses in ark shell, *Scapharca broughtonii*, exposed to thermal and osmotic stress: effects on hemolymph and biochemical parameters. *Comp. Biochem. Physiol. Part B Biochem. Mol. Biol.* 155, 34–42. doi: 10.1016/j.cbpb.2009.09.008

Beitinger, T. L., Bennett, W. A., and McCauley, R. W. (2000). Temperature tolerances of north american freshwater fishes exposed to dynamic changes in temperature. *Environ. Biol. Fishes* 58, 237–275.

Chang, C., Wang, Y., and Lee, T. (2021). Hypothermal stress-induced salinity-dependent oxidative stress and apoptosis in the livers of euryhaline milkfish, *Chanos chanos*. *Aquaculture* 534:736280.

Cheng, C., Liang, H., Luo, S., Wang, A., and Ye, C. (2018). The protective effects of vitamin C on apoptosis, DNA damage and proteome of pufferfish (*Takifugu obscurus*) under low temperature stress. *J. Therm. Biol.* 71, 128–135. doi: 10.1016/j.jtherbio.2017.11.004

Cheng, C., Ye, C., Guo, Z., and Wang, A. (2017). Immune and physiological responses of pufferfish (*Takifugu obscurus*) under cold stress. *Fish Shellfish Immunol.* 64, 137–145. doi: 10.1016/j.fsi.2017.03.003

Cheryl, C., and Beitinger, T. L. (2005). Temperature tolerances of wild-type and red transgenic zebra danios. *Trans. Am. Fish. Soc.* 134, 1431–1437.

Chou, M., Hsiao, C., Chen, S., Chen, I., Liu, S., and Hwang, P. (2008). Effects of hypothermia on gene expression in zebrafish gills: upregulation in differentiation and function of ionocytes as compensatory responses. *J. Exp. Biol.* 211, 3077–3084. doi: 10.1242/jeb.019950

Chung, D. J., and Schulte, P. M. (2015). Mechanisms and costs of mitochondrial thermal acclimation in a eurythermal killifish (*Fundulus heteroclitus*). *J. Exp. Biol.* 218, 1621–1631. doi: 10.1242/jeb.120444

Colinet, H., Pineau, C., and Com, E. (2017). Large scale phosphoprotein profiling to explore Drosophila cold acclimation regulatory mechanisms. *Sci. Rep.* 7:1713. doi: 10.1038/s41598-017-01974-z

Donaldson, M. R., Cooke, S. J., Patterson, D. A., and Macdonald, J. S. (2008). Cold shock and fish. *J. Fish Biol.* 73, 1491–1530.

Egge, N., Arneaud, S. L., Wales, P., Mihelakis, M., McClendon, J., Fonseca, R. S., et al. (2019). Age-onset phosphorylation of a minor actin variant promotes intestinal barrier dysfunction. *Dev. Cell* 51, 587–601. doi: 10.1016/j.devcel.2019.11.001

Engelsma, M. Y., Hougee, S., Nap, D., Hofenk, M., Rombout, J., Muiswinkel, W., et al. (2003). Multiple acute temperature stress affects leucocyte populations and antibody responses in common carp, *Cyprinus carpio L. Fish Shellfish Immunol.* 15, 397–410. doi: 10.1016/s1050-4648(03)00006-8

Feng, W., Han, X., Hu, H., Chang, M., Ding, L., Xiang, H., et al. (2021). 2D vanadium carbide MXenzyme to alleviate ROS-mediated inflammatory and neurodegenerative diseases. *Nat. Commun.* 12:2203. doi: 10.1038/s41467-021-22278-x

Ge, G., Long, Y., Shi, L., Ren, J., Yan, J., Li, C., et al. (2020). Transcriptomic profiling revealed key signaling pathways for cold tolerance and acclimation of two carp species. *BMC Genomics* 21:539. doi: 10.1186/s12864-020-06946-8

Gerber, L., Clow, K. A., Mark, F. C., and Gamperl, A. K. (2020). Improved mitochondrial function in salmon (*Salmo salar*) following high temperature acclimation suggests that there are cracks in the proverbial 'ceiling'. *Sci. Rep.* 10:21636. doi: 10.1038/s41598-020-78519-4

Goos, H. J., and Consten, D. (2002). Stress adaptation, cortisol and pubertal development in the male common carp, *Cyprinus carpio*. *Mol. Cell. Endocrinol.* 197, 105–116. doi: 10.1016/s0303-7207(02)00284-8

Grunwald, D. J., and Eisen, J. S. (2002). Timeline: headwaters of the zebrafish–emergence of a new model vertebrate. *Nat. Rev. Genet.* 3, 717–724. doi: 10.1038/nrg892

Han, B., Li, W., Chen, Z., Xu, Q., Luo, J., Shi, Y., et al. (2016). Variation of DNA methylome of zebrafish cells under cold pressure. *PLoS One* 11:e0160358. doi: 10.1371/journal.pone.0160358

Heise, K., Puntarulo, S., Nikinmaa, M., Lucassen, M., PöRtner, H. O., and Abele, D. (2006). Oxidative stress and HIF-1 DNA binding during stressful cold exposure and recovery in the North Sea eelpout (*Zoarces viviparus*). *Comp. Biochem. Physiol. Part A Mol. Integr. Physiol.* 143, 494–503. doi: 10.1016/j.cbpa.2006.01.014

Hsieh, S. L., Chen, Y. N., and Kuo, C. M. (2003). Physiological responses, desaturase activity, and fatty acid composition in milkfish (*Chanos chanos*) under cold acclimation. *Aquaculture* 220, 903–918.

Hu, P., Liu, M., Liu, Y., Wang, J., Zhang, D., Niu, H., et al. (2016). Transcriptome comparison reveals a genetic network regulating the lower temperature limit in fish. *Sci. Rep.* 6:28952. doi: 10.1038/srep28952

Islam, M. J., Kunzmann, A., and Slater, M. J. (2021). Extreme winter cold-induced osmoregulatory, metabolic, and physiological responses in European seabass (*Dicentrarchus labrax*) acclimatized at different salinities. *Sci. Total Environ.* 771:145202. doi: 10.1016/j.scitotenv.2021.145202

Johnson, A. C., Turko, A. J., Klaiman, J. M., Johnston, E. F., and Gillis, T. E. (2014). Cold acclimation alters the connective tissue content of the zebrafish (*Danio rerio*) heart. *J. Exp. Biol.* 217, 1868–1875. doi: 10.1242/jeb.101196

Keen, A. N., Klaiman, J. M., Shiels, H. A., and Gillis, T. E. (2017). Temperature-induced cardiac remodelling in fish. *J. Exp. Biol.* 220, 147–160. doi: 10.1242/jeb.128496

Kimmel, C. B., Ballard, W. W., Kimmel, S. R., Ullmann, B., and Schilling, T. F. (1995). Stages of embryonic-development of the zebrafish. *Dev. Dyn.* 203, 253–310.

Klaiman, J. M., Pyle, W. G., and Gillis, T. E. (2014). Cold acclimation increases cardiac myofilament function and ventricular pressure generation in trout. *J. Exp. Biol.* 217, 4132–4140. doi: 10.1242/jeb.109041

Larsen, D. A., Beckman, B. R., and Dickhoff, W. W. (2001). The effect of low temperature and fasting during the winter on metabolic stores and endocrine physiology (insulin, Insulin-like growth factor-I, and thyroxine) of coho salmon, *Oncorhynchus kisutch*. *Gen. Comp. Endocrinol.* 123, 308–323. doi: 10.1006/gcen.2001.7677

Lesser, M. P. (2006). Oxidative stress in marine environments: biochemistry and physiological ecology. *Annu. Rev. Physiol.* 68, 253–278. doi: 10.1146/annurev.physiol.68.040104.110001

Liang, L., Chang, Y., He, X., and Tang, R. (2015). Transcriptome analysis to identify cold-responsive genes in amur carp (*Cyprinus carpio haematopterus*). *PLoS One* 10:e0130526. doi: 10.1371/journal.pone.0130526

Liu, C., Shen, W., Hou, C., Gao, X., Wang, Q., Wu, X., et al. (2019). Low temperature-induced variation in plasma biochemical indices and aquaglyceroporin gene expression in the large yellow croaker *Larimichthys crocea*. *Sci. Rep.* 9:2717. doi: 10.1038/s41598-018-37274-3

López-Olmeda, J. F., and Sánchez-Vázquez, F. J. (2011). Thermal biology of zebrafish (*Danio rerio*). *J. Therm. Biol.* 36, 91–104.

Maria Cristina, P., and Paunescu, A. (2019). Research on the influence of temperature and water hardness on breathing in some fish species. *Trends Cogn. Sci.* 8, 140–146.

Marteaux, L. D., Stinziano, J. R., and Sinclair, B. J. (2018). Effects of cold acclimation on rectal macromorphology, ultrastructure, and cytoskeletal stability in *Gryllus pennsylvanicus crickets*. *J. Insect Physiol.* 104, 15–24. doi: 10.1016/j.jinsphys.2017.11.004

Morgan, M. J., and Liu, Z. (2011). Crosstalk of reactive oxygen species and NF-κB signaling. *Cell Res.* 21, 103–115.

O'Gorman, E. J., Ólafsson, ÓP., Demars, B. O. L., Friberg, N., Guðbergsson, G., Hannesdóttir, E. R., et al. (2016). Temperature effects on fish production across a natural thermal gradient. *Glob. Change Biol.* 22, 3206–3220. doi: 10.1111/gcb.13233

Ren, J., Long, Y., Liu, R., Song, G., Li, Q., and Cui, Z. (2021). Characterization of biological pathways regulating acute cold resistance of zebrafish. *Int. J. Mol. Sci.* 22:3208. doi: 10.3390/ijms22063028

Ruzicka, L., Howe, D. G., Ramachandran, S., Toro, S., Van Slyke, C. E., Bradford, Y. M., et al. (2019). The zebrafish Information network: new support for non-coding genes, richer gene ontology annotations and the alliance of genome resources. *Nucleic Acids Res.* 47, D867–D873. doi: 10.1093/nar/gky1090

Sánchez Nuño, S., Sanahuja, I., Fernández-Alacid, L., Ordóñez-Grande, B., Fontanillas, R., Fernández-Borràs, J., et al. (2018). Redox challenge in a cultured temperate marine species during low temperature and temperature recovery. *Front. Physiol.* 9:923. doi: 10.3389/fphys.2018.00923

Schleger, I. C., Pereira, D. M. C., Resende, A. C., Romão, S., Herrerias, T., Neundorf, A. K. A., et al. (2021). Cold and warm waters: energy metabolism and antioxidant defenses of the freshwater fish astyanax lacustris (*Characiformes: Characidae*) under thermal stress. *J. Comp. Physiol. B* [Epub Online ahead of print]. doi: 10.1007/s00360-021-01409-2

Schmidt, K., and Starck, J. M. (2010). Developmental plasticity, modularity, and heterochrony during the phylotypic stage of the zebra fish, *Danio rerio*. *J. Exp. Zool. B* 314, 166–178. doi: 10.1002/jez.b.21320

Shahjahan, M., Kitahashi, T., and Ando, H. (2017). Temperature affects sexual maturation through the control of kisspeptin, kisspeptin receptor, GnRH and GTH subunit gene expression in the grass puffer during the spawning season. *Gen. Comp. Endocrinol.* 243, 138–145. doi: 10.1016/j.ygcen.2016.11.012

Sun, Z., Tan, X., Liu, Q., Ye, H., Zou, C., and Ye, C. (2019). Physiological, immune responses and liver lipid metabolism of orange-spotted grouper (*Epinephelus coioides*) under cold stress. *Aquaculture* 498, 545–555.

Tang, L., Cheng, J., Long, Y., He, X., Liang, G., Tang, X., et al. (2017). PCB 118-induced endothelial cell apoptosis is partially mediated by excessive ROS production. *Toxicol. Methods* 27, 394–399. doi: 10.1080/15376516.2017.1296050

Tang, S., Hou, Y., Zhang, H., Tu, G., Yang, L., Sun, Y., et al. (2015). Oxidized ATM promotes abnormal proliferation of breast CAFs through maintaining intracellular redox homeostasis and activating the PI3K-AKT, MEK-ERK, and Wnt-β-catenin signaling pathways. *Cell Cycle* 14, 1908–1924.

Tseng, Y., Chen, R., Lucassen, M., Schmidt, M., Dringen, R., Abele, D., et al. (2011). Exploring uncoupling proteins and antioxidant mechanisms under acute cold exposure in brains of fish. *PLoS One* 6:e18180. doi: 10.1371/journal.pone.0018180

Viadero, R. C. (2005). Factors affecting fish growth and production. *Water Encycl.* 3, 129–133.

Vondracek, B., Wurtsbaugh, W., and Cech, J. (1988). Growth and reproduction of the mosquitofish,*Gambusia affinis*, in relation to temperature and ration level: consequences for life history. *Environ. Biol. Fishes* 21, 45–57.

Wang, X., Lu, X., Zhu, R., Zhang, K., Li, S., Chen, Z., et al. (2017). Betulinic acid induces apoptosis in differentiated PC12 cells via ROS-mediated mitochondrial pathway. *Neurochem. Res.* 42, 1130–1140. doi: 10.1007/s11064-016-2147-y

Wu, C., Lin, T., Chang, T., Sun, H., Hui, C., and Wu, J. (2011). Zebrafish HSC70 promoter to express carp muscle-specific creatine kinase for acclimation under cold condition. *Transgenic Res.* 20, 1217–1226. doi: 10.1007/s11248-011-9488-8

Xia, Y., Liu, S., Li, C., Ai, Z., Shen, W., Ren, W., et al. (2020). Discovery of a novel ferroptosis inducer-talaroconvolutin A—killing colorectal cancer cells in vitro and in vivo. *Cell Death Dis.* 11:998. doi: 10.1038/s41419-020-03194-2

Xing, X., Jiang, Z., Tang, X., Wang, P., Li, Y., Sun, Y., et al. (2016). Sodium butyrate protects against oxidative stress in HepG2 cells through modulating Nrf2 pathway and mitochondrial function. *J. Physiol.* 73, 405–414. doi: 10.1007/s13105-017-0568-y

Yang, M., Chen, P., Liu, J., Zhu, S., Kroemer, G., Klionsky, D. J., et al. (2019). Clockophagy is a novel selective autophagy process favoring ferroptosis. *Sci. Adv.* 5:eaaw2238. doi: 10.1126/sciadv.aaw2238

Yilmaz, S., Ergün, S., Çelik, E. Ş, Banni, M., Ahmadifar, E., and Dawood, M. A. O. (2021). The impact of acute cold water stress on blood parameters, mortality rate and stress-related genes in *Oreochromis niloticus*, *Oreochromis mossambicus* and their hybrids. *J. Therm. Biol.* 100:103049. doi: 10.1016/j.jtherbio.2021.103049

Zhuang, Y., Ma, Q., Guo, Y., and Sun, L. (2017). Protective effects of rambutan (*Nephelium lappaceum*) peel phenolics on H_2O_2-induced oxidative damages in HepG2 cells and d-galactose-induced aging mice. *Food Chem. Toxicol.* 108, 554–562. doi: 10.1016/j.fct.2017.01.022

Conflict of Interest: The authors declare that the research was conducted in the absence of any commercial or financial relationships that could be construed as a potential conflict of interest.

Publisher's Note: All claims expressed in this article are solely those of the authors and do not necessarily represent those of their affiliated organizations, or those of the publisher, the editors and the reviewers. Any product that may be evaluated in this article, or claim that may be made by its manufacturer, is not guaranteed or endorsed by the publisher.

frontiers | Frontiers in Physiology

DATA REPORT
published: 16 May 2022
doi: 10.3389/fphys.2022.910585

Identification of Neuropeptides Using Long-Read RNA-Seq in the Swimming Crab *Portunus trituberculatus*, and Their Expression Profile Under Acute Ammonia Stress

Daixia Wang[1,2], *Xiaochen Liu*[1,2], *Jingyan Zhang*[1,2], *Baoquan Gao*[2,3], *Ping Liu*[2,3], *Jian Li*[2,3] *and Xianliang Meng*[1,2]*

[1]Key Laboratory of Aquatic Genomics, Ministry of Agriculture and Rural Affairs, Yellow Sea Fisheries Research Institute, Chinese Academy of Fishery Sciences, Qingdao, China, [2]Laboratory for Marine Fisheries Science and Food Production Processes, Qingdao National Laboratory for Marine Science and Technology, Qingdao, China, [3]Key Laboratory of Sustainable Development of Marine Fisheries, Ministry of Agriculture and Rural Affairs, Yellow Sea Fisheries Research Institute, Chinese Academy of Fishery Sciences, Qingdao, China

OPEN ACCESS

Edited by:
Qingchao Wang,
Huazhong Agricultural University, China

Reviewed by:
Ce Shi,
Ningbo University, China
Wenfeng Li,
Xiamen University, China
Yunfei Sun,
Shanghai Ocean University, China

***Correspondence:**
Xianliang Meng
xlmeng@ysfri.ac.cn

Specialty section:
This article was submitted to Aquatic Physiology, a section of the journal Frontiers in Physiology

Received: 01 April 2022
Accepted: 29 April 2022
Published: 16 May 2022

Citation:
Wang D, Liu X, Zhang J, Gao B, Liu P, Li J and Meng X (2022) Identification of Neuropeptides Using Long-Read RNA-Seq in the Swimming Crab Portunus trituberculatus, and Their Expression Profile Under Acute Ammonia Stress. Front. Physiol. 13:910585. doi: 10.3389/fphys.2022.910585

Keywords: long-read transcriptome, *Portunus trituberculatus*, neuropeptide, ammonia, crab

INTRODUCTION

The swimming crab *Portunus trituberculatus* (*P.trituberculatus*) is widely distributed in estuary and coastal areas of temperate western Pacific Ocean (Dai et al., 1986), and comprises a large aquaculture industry in China with a production of 100,895 tons in 2020 (China Fishery Statistical Yearbook 2021). To satisfy the growing market demand, the crab aquaculture has been moving toward more intensive systems with higher feed inputs and stocking density. In intensive culture systems, ammonia (throughout this paper, the term "ammonia" refers to the sum of NH_3 and NH_4^+), mainly derives from the decomposition of leftover feeds and the excretion of cultured crabs, has been recognized the major limiting factor (Pan et al., 2018; Si et al., 2019; Zhang et al., 2021). Ammonia is a toxic molecule to aquatic animals, including the swimming crab (Liu et al., 2015; Pan et al., 2018). Recent studies have showed that ammonia exposure can disturb immune response (Romano and Zeng, 2013), which causes tissue injury (Si et al., 2019; Lu et al., 2022) and even death of *P. trituberculatus* (Liu et al., 2015; Zhao et al., 2020). Due to the increasing concerns on ammonia toxicity, several studies have been conducted on ammonia detoxification strategies in crustaceans. These studies found that the swimming crab can defend against environmental ammonia through several compensatory mechanisms, for example, ammonia excretion *via* its transporters in branchial epithelium, ammonia conversion into non-toxic or less toxic substances, and decreasing the rate of metabolic generated ammonia (Mykles et al., 2010; Henry et al., 2012; Liu et al., 2015; Pan et al., 2018; Zhang et al., 2021). In fact, strategies of ammonia detoxification have been identified, but the regulation mechanism still largely unknown.

Neuropeptides are a diverse set of endocrine signaling molecules in animals (Zhang et al., 2015; Egekwu et al., 2016; Wang et al., 2018; Li et al., 2020). Recently, many studies have focused on the identification of neuropeptides and their roles in physiology and behaviors of decapod crustaceans, such as in *Scylla paramamosain* (*S.paramamosain*) (Bao et al., 2018), *Carcinus maenas* (Jodi et al., 2018), *Chorismus antarcticus* (Toullec et al., 2017), and *Litopenaeus vannamei* (*L.vannamei*) (Zhang et al., 2020). Existing studies have demonstrated that neuropeptides play important roles in alleviating environmental stressors, such as ammonia (Si et al., 2019; Zhang et al., 2020), low salinity level (Barman et al., 2012; Li et al., 2014; Liu et al., 2014; Sun et al., 2020), hypoxia (Sun et al., 2020), and low pH value (Liu et al., 2019). However, there has been limited information regarding to

the neuropeptides and their regulatory roles in ammonia detoxification in swimming crab. The identification of neuropeptides represents the first and essential step to elucidate the functions of these molecules against ammonia stress.

In silico transcriptome mining is a powerful tool for identifying neuropeptide repertoire (Christie et al., 2008; Saowaros et al., 2015; Nguyen et al., 2018). In the past several years, many neuropeptides have been identified in crustaceans, using the second-generation RNA-seq technology (Veenstra 2015; Wang et al., 2018). With the rapid advancement in transcriptome sequencing, third-generation sequencing, including Oxford Nanopore Technologies (ONT) and Pacific Biosciences (PacBio), has been increasingly utilized in transcriptome analysis in crustaceans (Deamer et al., 2016). It has significant advantages in read length, accuracy, transcript identification, and genetic information richness, compared with the second-generation RNA-seq technology (Abdel-Ghany et al., 2016). In the present study, we explored the putative neuropeptides in *P. trituberculatus* using long-read ONT sequencing method, which analyzed the variation of genetic expressions of neuropeptides under the ammonia stress condition. To the best of our knowledge, this is the first report of nanopore transcriptome analysis in the swimming crab. The dataset of this study will lay the fundament for unraveling the regulatory roles of the neuropeptides in ammonia toxification process, and provide a valuable resource for genetic studies in this species.

MATERIALS AND METHODS

Animal and Sample Collection

A total of twenty female swimming crabs (202.6 ± 9.8 g) were obtained from Haifeng Company (Weifang, China), and acclimated to laboratory conditions for 14 days. During acclimation, the crabs were divided equally into two groups and they were cultured in different 3000-L tanks, water temperature was kept at 18.2°C ± 0.5°C, aeration was applied continuously, pH was 7.6 ± 0.2, the salinity was 30.3 ± 0.3, ammonia-N concentration was below 0.10 mg/L. The swimming crabs were fed *ad libitum* with live Manila clam *Ruditapes philippinarum* daily, and the feed residues were removed before the next feeding time. One-third of the rearing water was exchanged daily. After acclimation, three individuals were randomly chosen for both control and ammonia exposure groups. The control group was reared with low ammonia level (ammonia-N < 0.10 mg/L), while the exposure group was reared at high ammonia level (ammonia-N = 20 mg/L). The ammonia-N concentration for treatment group was realized by infusion of calculated amount ammonium chloride (NH_4Cl) stock solutions which was prepared with filtered seawater, and checked using salicylic acid method with spectrophotometer. Following 24-h exposure, the crabs in different groups were placed in an ice bath for anesthetization for 5min, and then sacrificed for eyestalk dissection and cerebral ganglia collection. The tissues were immediately frozen in liquid nitrogen and stored at −80°C.

ONT Transcriptome

Total RNA of the samples was extracted with *TRIzol* Reagent (Thermo Fisher Scientific, United States), and RNA integrity was evaluated using the RNA Nano 6000 Assay Kit with the Bioanalyzer 2100 system (Agilent Technologies, United States). An equal amount of total RNA from each sample of both groups were pooled together. Oxford PromethION 2D amplicon libraries were prepared according to the Nanopore community protocol using library preparation kit SQK-LSK109, and sequenced on R9 flowcells to generate fast5 files. All the generated fast5 reads were then basecalled in guppy v3.2.10 with the default options to produce fastq files. The clean reads were filtered using Nanofilt v2.5.0 with options of length = 300. The full-length transcripts were identified using the method of Pinfish pipeline, detected using Pychopper, and aligned to reference genome of *P. trituberculatus* with minimap2 v2.16 (Deamer et al., 2016). At present, there are two chromosome-level reference genome for P. trituberculatus, which are publicly available (Tang et al., 2020;Lv et al., 2021). In order to find more neuropeptide-encoding genes, we used the recent version with higher number of annotated genes (Lv et al., 2021). The consensus sequence was obtained by clustering according to the results of comparison, and known and novel transcripts were identified using Gffcompare v0.11.2.

Gene Annotation and Classification

The functional annotation of identified transcripts was performed using a Blast search against the NCBI non-redundant nucleotide sequences (Nt), NCBI non-redundant protein sequence (Nr), Gene Ontology (GO), Kyoto Encyclopedia of Genes and Genomes Ortholog database (KO), Orthologous Groups (KOG/COG), Protein family (Pfam), Clusters of a manually annotated and reviewed protein sequence database (Swiss-Prot) with a cutoff E-value of 10^{-10}.

Identification of Neuropeptides

To identify the neuropeptides in *P. trituberculatus*, we searched sequence annotation file for the keywords of known neuropeptides in other decapods. In addition, we carried out a local tblastn analysis with Bioedit 7.0.5.3 software, using the known crustacean neuropeptide precursors which were primarily from *Nephrops norvegicus* (Nguyen et al., 2018), *Lysmata vittata* (Bao et al., 2020), and *S. paramamosain* (Bao et al., 2018), as query sequences. All the identified neuropeptide sequences were validated with Blast in NCBI. The structure of the mature neuropeptides was predicted using a well-established workflow (Veenstra 2011; Nguyen et al., 2016; Bao et al., 2020). All the deduced precursors were analyzed for the presence of a signal peptide using the online program SignalP 5.0 (http://www.cbs.dtu.dk/services/SignalP/). Prohormone cleavage sites were identified based on the information presented in Veenstra (2000). Multiple sequence alignment of the predicted peptide sequences was conducted with ClustalX, and then the sequence alignment file was exported to LaTEX TexShade for conservation calculation.

A

Long-read transcriptome of *Portunus trituberculatus*						
Total bases (G)	Read number	Full-length reads	Min Length (bp)	Max Length (bp)	N50	Full-length Read Percentage
15.86	17743760	16346649	300	55950	1197	92.13%

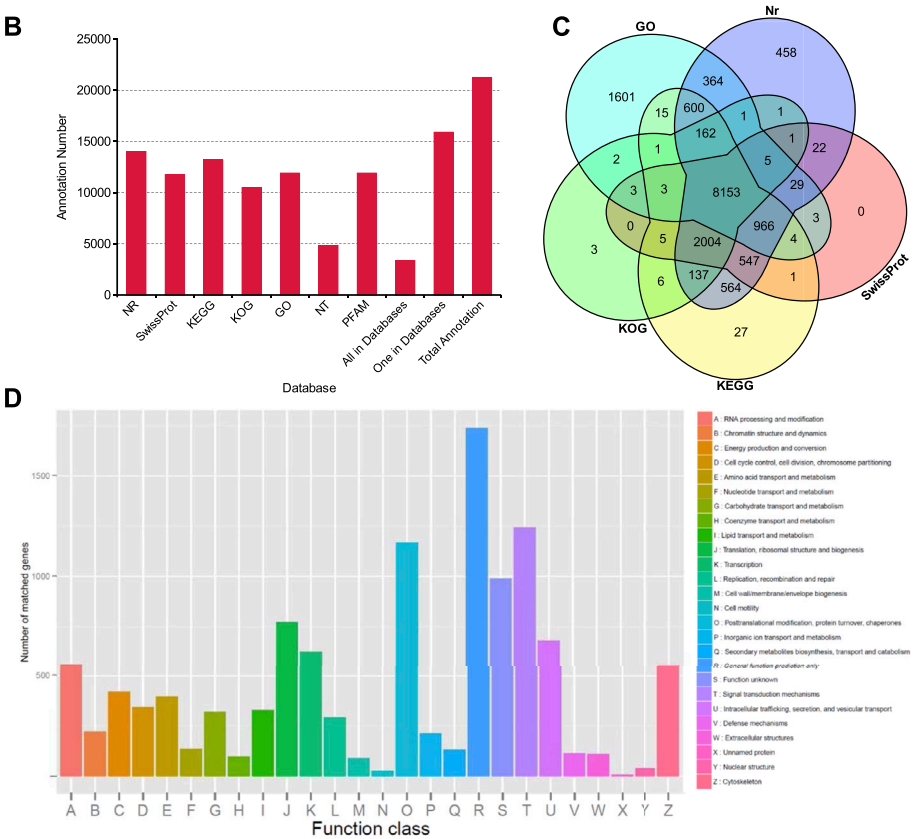

FIGURE 1 | *In silico* transcriptome analysis in *Portunus trituberculatus*. **(A)** Long-read transcriptome of *P. trituberculatus*. **(B)** The functional annotation of non-redundant sequences in seven databases. **(C)** Comparison of transcripts present in different datasets, including GO, Nr, KOG, SwissProt, KO and KOG. **(D)** Functional classification of assembled transcripts.

Expression Profile of the Neuropeptides Under Acute Ammonia Stress

Total RNA of the samples from the control and ammonia exposure groups were reverse-transcribed to cDNA using Evo M-MLV RT Kit with gDNA Clean for qPCR II (Accurate Biology, China) following the manufacturer's instruction. The PCR reaction was run on the ABI 7500 fast Real-Time PCR System (Applied Biosystems, United States) with SYBR Green Premix Pro Taq HS qPCR Kit II (Accurate Biology, China). The PCR reaction was carried out in a total volume of 20 μL, comprising of 10 μL of 2× SYBR Green Pro Taq HS Premix II, 0.8 μL each of 10 mM each primer, 2 μL of diluted cDNA, and 7.2 μL DNase-free water. The PCR program was set as followed: 95°C for 30 s; 40 cycles of 95°C for 5 s and 60°C for 30 s. *β-actin* was amplified as an internal control housekeeping gene which is commonly used in ammonia stress studies (Feng et al., 2010; Zhang et al., 2021), and the relative expression levels of the neuropeptides were calculated using the $2^{-\Delta\Delta ct}$ method (Livak and Schmittgen, 2002). Difference in expression level of a specific neuropeptide between the control and ammonia exposure groups was analyzed using independent-samples *t*-test with SPSS 24.0. Differences were considered significant if $p < 0.05$.

RESULTS AND DISCUSSION

ONT Sequencing and Annotation

In order to identify the neuropeptides in the swimming crab, a library was prepared from pooled RNA extracts of eyestalk and cerebral ganglia, and sequenced using the Oxford Nanopore PromethION platform. After removal of low quality reads and adaptors, a total of 15.86 GB clean reads were obtained (**Figure 1A**). After filtering rRNA, reads with the primers at both ends were considered as full-length reads. A total of 16,346,649 full-length reads were obtained, accounting for

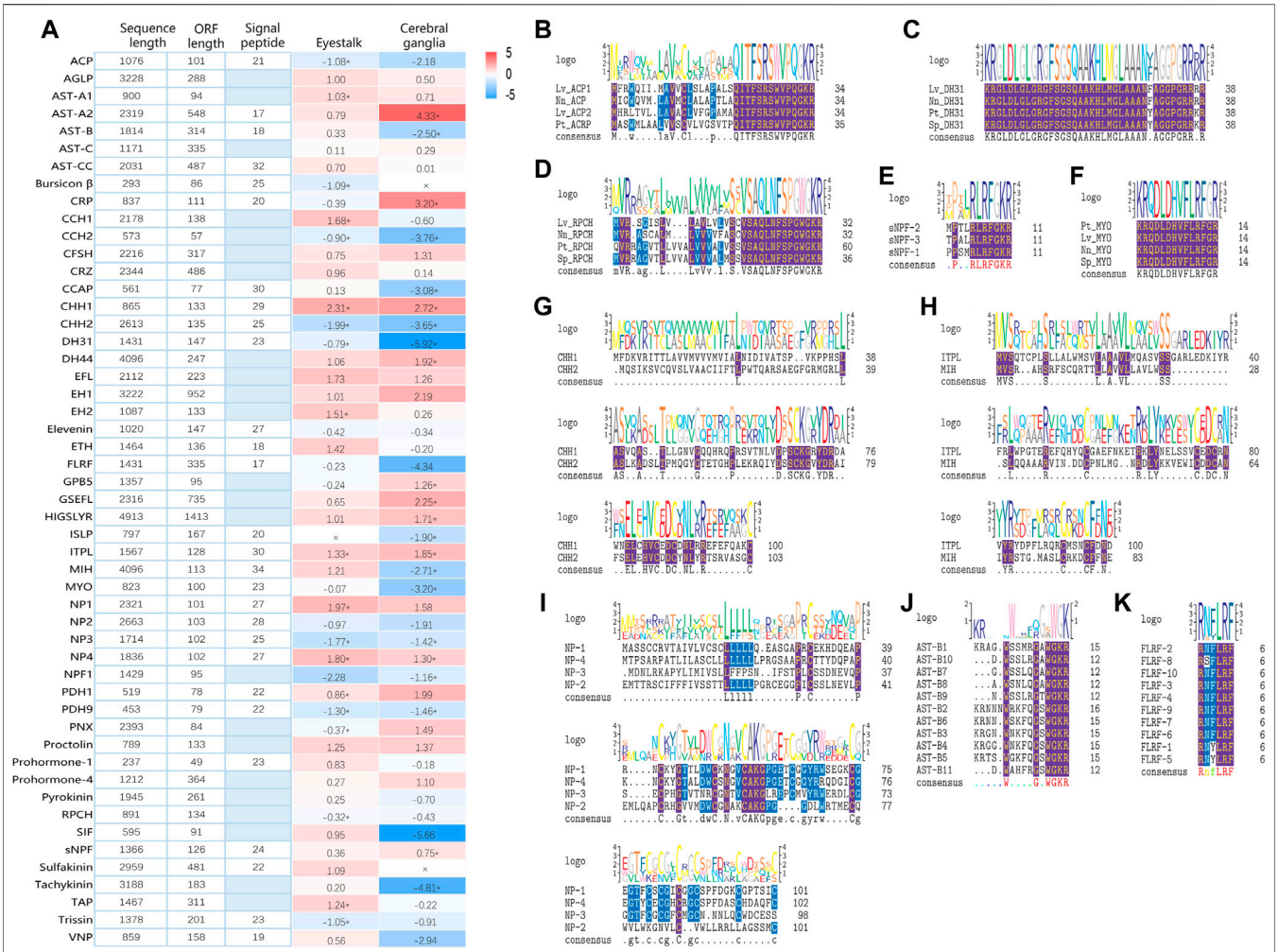

FIGURE 2 | Overview of putative neuropeptides identified in *Portunus trituberculatus*. **(A)**. Sequence length, ORF length, and signal peptide in each putative neuropeptide. Shades of blue indicate an absence of the signal peptide. Gene expression profile in eyestalk and cerebral ganglia are transformed into log2-fold changes (right) with color-coded as described in legend, and the asterisk indicates differentially expressed genes (DEGs) under ammonia stress. Sequence alignment of ACP **(B)**, DH31 **(C)**, RPCH **(D)**, sNPF **(E)**, MYO **(F)**, CHH-I **(G)**, CHH-II **(H)**, NP **(I)**, FLRF **(K)**, AST-B **(K)**, and AST-B **(J)**. Conserved amino acids are shown in purple shading while similar amino acids are shown with blue shading. Abbreviation: ACP, Adipokinetic hormone/Corazonin-related peptide; AGLP, Agatoxin-like peptide; AST-A, Allatostatin A-type; AST-B, Allatostatin B-type; AST-C/CC, Allatostatin C/CC-type; CRP, Calcitonin related peptide; CCH, CCHamide; CFSH, Crustacean female sex hormone; CRZ, Corazonin; CCAP, Crustacean cardioactive peptide; CHH, Crustacean hyperglycemic hormone; DH, Diuretic hormone; EFL, EFLamide; EH, Eclosion hormone; ETH, Ecdysis triggering hormone; FLRF, FLRFamide; GPB-5, Glycoprotein hormone beta-5; GSEFL, GSEFLamide; HIGSLYR, HYGSLYRamide; ISLP, Insulin-like peptide; ITPL, Ion transport peptide-like; MIH, Molt inhibiting hormone; MYO, Myosuppressin; NP, Neuroparsin; NPF1, Neuropeptide F1; PDH, Pigment dispersing hormone; PNX, Phoenixin; RPCH, Red pigment concentrating hormone; SIF, SIFamide; sNPF, short Neuropeptide; TAP, Terminal ampullae peptide; VNP, Vasotocin-neurophysin. Lv, *Lysmata vittata*; Nn, *Nephrops norvegicus*; Sp, *Scylla paramamosain*; Pt, *Portunus trituberculatus*.

92.13% of the clean reads (**Figure 1A**). Comparison of clean reads with the reference genome resulted in a mapped rate of 73.81%. The mapped reads were clustered to obtain consensus sequences, and the consensus sequences were aligned to reference genome of *P. trituberculatus* to eliminate redundant reads (Lv et al., 2021). After removing redundant reads, 25,054 non-redundant sequences were generated. The non-redundant sequences were functionally annotated in seven databases (**Figures 1B–D**). 14,014 (65.92%), 4,843 (22.78%), 11,912 (56.03%), 11,746 (55.26%), 11,912 (56.03%), 13,195 (62.06%), and 10,487 (49.32%) transcripts were annotated in Nr, Nt, Pfam, Swiss-prot, GO, KO, and KOG database, respectively. 3374 (15.87%) transcripts were annotated on all the seven databases. Generally, ONT sequencing generated a set of high-quality transcripts for identification of neuropeptides as well as other genetic studies in *P. trituberculatus*. All the reads of ONT sequencing were deposited in the Genome Sequence Archive (GSA) of the China National Center for Bioinformation (CNCB) with the accession number CRA006434.

In silico Mining of Putative Neuropeptides

Based on Nr-annotation and homology searches, a total of 51 putative neuropeptide precursor transcripts were identified in ONT transcriptome of *P. trituberculatus*, including isoforms of

Adipokinetic hormone/Corazonin-related peptide (ACP), Agatoxin-like peptide (AGLP), Allatostatin (AST), Bursicon β, Calcitonin related peptide (CRP), CCHamide (CCH), Crustacean female sex hormone (CFSH), Corazonin (CRZ), Crustacean cardioactive peptide (CCAP), Crustacean hyperglycemic hormone (CHH), Diuretic hormone (DH), EFLamide (EFL), Eclosion hormone (EH), Ecdysis triggering hormone (ETH), Elevenin, FLRFamide (FLRF), Glycoprotein hormone beta-5 (GPB-5), GSEFLamide (GSEFL), HYGSLYRamide (HIGSLYR), Insulin-like peptide (ISLP), Ion transport peptide-like (ITPL), Molt inhibiting hormone (MIH), Myosuppressin (MYO), Neuroparsin (NP), Neuropeptide F1 (NPF1), Pigment dispersing hormone (PDH), Phoenixin (PNX), Prohormone, proctolin, pyrokinin, Red pigment concentrating hormone (RPCH), SIFamide (SIF), short Neuropeptide (sNPF), Sulfakinin, Tachykinin, Terminal ampullae peptide (TAP), Trissin, and Vasotocin-neurophysin (VNP). These neuropeptides cover most of the previously identified neuropeptides in other decapods (Bao et al., 2015; Nguyen et al., 2018; Bao et al., 2020), and the majority of the neuropeptide transcripts (86.3%) contain the complete coding sequences, which indicate that ONT transcriptome sequencing is a powerful approach to mine the putative neuropeptides in the swimming crab.

As shown in **Figures 2B–K**, highly conserved motifs were identified in a number of neuropeptide families, such as AST-B (XWXGXWamide), FLRFamide (R/K-N/S-F/Y-LRFamide), MYO (QDLDHVFLRFamide), RPCH (pQLNFSPGWamide), sNPF (XPXXRLRFamide), and family of CHH and NP (conserved Cys) (Backing et al., 2002; Christie et al., 2010; Christie 2014; Nguyen et al., 2016; Liu et al., 2020; Qiao et al., 2020). In addition, the amino acid sequences of all the putative neuropeptide precursor and their structure information, including sites of bioactive mature peptides, location of cleavage sites, and precursor size were provided in **Supplementary File S1, S2**.

Expression Profile of the Neuropeptides Under Ammonia Stress

Although it is well-established that neuropeptides are critical in regulating stress responses in crustaceans, limited information is available on their roles in defending against ammonia stress (Si et al., 2019; Zhang et al., 2021). In the present study, we investigated the expression profile of neuropeptides in the swimming crab under ammonia exposure for the first time. As shown in **Figure 2A**, 19 and 22 neuropeptides exhibited differential expression in eyestalk and cerebral ganglia, respectively, after ammonia stress. In eyestalk, 9 neuropeptides showed upregulation under ammonia stress, while 10 exhibited downregulation. In cerebral ganglia, 10 and 12 neuropeptides were upregulated and downregulated, respectively. Among these differentially expressed neuropeptides, 6 including *CCH2*, *CHH2*, *DH31*, *ITPL*, *NP3*, and *PDH9*, showed the same expression pattern in eyestalk and cerebral ganglia.

It is well established that CHH regulates a diverse array of physiological processes in decapod crustaceans (Chen et al., 2020). A recent study demonstrated that CHH is crucial for regulating ammonia excretion in the white shrimp *L. vannamei*. *CHH* knockdown can significantly downregulate ammonia transporters in branchial epithelium, and result in ammonia accumulation in the hemolymph of white shrimp (Zhang et al., 2020). In addition to modulating ammonia excretion, CHH plays a major role in stimulation of glycolysis and lipolysis, which can result in higher levels of hemolymph glucose and ATP in decapods (Backing et al., 2002). In this study, a significant upregulation of *CHH1* in eyestalk was observed after ammonia stress. Given that ammonia excretion is highly energy-consuming, the result indicates that CHH1 may coordinate the processes of energy metabolism and ammonia excretion in the swimming crab, facilitating the defenses against ammonia stress. Interestingly, the other type of *CHH*, *CHH2*, was significantly downregulated. This result indicated that different types of CHH have distinct roles in regulating stress response to ammonia. Further studies are required to reveal the detailed functions of the different types of CHH under ammonia stress.

Our recent study found that ammonia exposure can result in a remarkable reduction in vitellogenesis in the swimming crab (Meng et al., 2021). In accordance with that result, expression of the key neuropeptides in vitellogenesis regulation, including *NP1* and *RPCH*, significantly changes after ammonia stress. *NP1*, functioning as inhibitory factor of vitellogenesis, has showed significant upregulation, whereas *RPCH* which promotes vitellogenesis was downregulated after ammonia exposure (Bao et al., 2015; Nguyen et al., 2016; Nguyen et al., 2018; Liu et al., 2020). Taken these results together, the neuropeptides *NP1* and *RPCH* may mediate the ammonia-induced inhibition of vitellogenesis in the swimming crab, which could represent a tradeoff between the allocation of energy to ammonia-defense and reproduction.

In summary, we identified putative neuropeptide-encoding transcripts from eyestalk and cerebral ganglia of *P. trituberculatus* using long-read ONT transcriptome sequences for the first time, which they were analyzed for their expression profiles under ammonia stress. This study provides a fundamental support for future research on the roles of neuropeptides in ammonia stress regulation process, and a valuable dataset for genetic studies in the swimming crab.

DATA AVAILABILITY STATEMENT

The datasets presented in this study can be found in online repositories. All the reads of ONT sequencing were deposited in the Genome Sequence Archive (GSA) of the China National Center for Bioinformation (CNCB) with the accession number CRA006434, PRJCA008798.

AUTHOR CONTRIBUTIONS

DW and XM: conceptualization. DW and JZ: methodology and investigation. XM, JZ, PL, and BG: software, validation, formal analysis, data curation, and original draft. DW and XM: writing,

review and editing. PL and JL: resources, supervision and project administration. XM: funding acquisition.

FUNDING

This research was funded by Chinese National Science Foundation (41976106), National Key R&D Program of China (2019YFD0900402-04), Central Public-interest Scientific Institution Basal Research Fund, CAFS (2020TD46), and China Agriculture Research System of MOF and MARA.

SUPPLEMENTARY MATERIAL

The Supplementary Material for this article can be found online at: https://www.frontiersin.org/articles/10.3389/fphys.2022.910585/full#supplementary-material

REFERENCES

Abdel-Ghany, S. E., Hamilton, M., Jacobi, J. L., Ngam, P., Devitt, N., Schilkey, F., et al. (2016). A Survey of the Sorghum Transcriptome Using Single-Molecule Long Reads. *Nat. Commun.* 7, 11706. doi:10.1038/ncomms11706

Backing, D., Dircksen, H., and Keller, R. (2002). *The Crustacean Neuropeptides of the CHH/MIH/GIH Family: Structures and Biological Activities*. Springer Berlin Heidelberg, 84

Bao, C., Liu, F., Yang, Y., Lin, Q., and Ye, H. (2020). Identification of Peptides and Their GPCRs in the Peppermint Shrimp *Lysmata Vittata*, a Protandric Simultaneous Hermaphrodite Species. *Front. Endocrinol.* 11, 226–240. doi:10.3389/fendo.2020.00226

Bao, C., Yang, Y., Huang, H., and Ye, H. (2015). Neuropeptides in the Cerebral Ganglia of the Mud Crab, *Scylla Paramamosain*: Transcriptomic Analysis and Expression Profiles during Vitellogenesis. *Sci. Rep.* 5 (1), 17055. doi:10.1038/srep17055

Bao, C., Yang, Y., Zeng, C., Huang, H., and Ye, H. (2018). Identifying Neuropeptide GPCRs in the Mud Crab, *Scylla Paramamosain*, by Combinatorial Bioinformatics Analysis. *General Comp. Endocrinol.* 269, 122–130. doi:10.1016/j.ygcen.2018.09.002

Barman, H. K., Patra, S. K., Das, V., Mohapatra, S. D., Jayasankar, P., Mohapatra, C., et al. (2012. Identification and Characterization of Differentially Expressed Transcripts in the Gills of Freshwater Prawn (*Macrobrachium Rosenbergii*) under Salt Stress. *Sci. World J.* 2012, 1–11. doi:10.1100/2012/149361

Chen, H.-Y., Toullec, J.-Y., and Lee, C.-Y. (2020). The Crustacean Hyperglycemic Hormone Superfamily: Progress Made in the Past Decade. *Front. Endocrinol.* 11, 578958. doi:10.3389/fendo.2020.578958

Christie, A. E., Cashman, C. R., Brennan, H. R., Ma, M., Sousa, G. L., Li, L., et al. (2008). Identification of Putative Crustacean Neuropeptides Using In Silico Analyses of Publicly Accessible Expressed Sequence Tags. *General Comp. Endocrinol.* 156 (2), 246–264. doi:10.1016/j.ygcen.2008.01.018

Christie, A. E. (2014). Identification of the First Neuropeptides from the Amphipoda (Arthropoda, Crustacea). *General Comp. Endocrinol.* 206, 96–110. doi:10.1016/j.ygcen.2014.07.010

Christie, A. E., Stemmler, E. A., and Dickinson, P. S. (2010). Crustacean Neuropeptides. *Cell. Mol. Life Sci.* 67 (24), 4135–4169. doi:10.1007/s00018-010-0482-8

Dai, A. Y., Yang, S. L., and Song, Y. Z. (1986). *Marine Crabs in China Sea*. Beijing: Marine Publishing Press. (in Chinese).

Deamer, D., Akeson, M., and Branton, D. (2016). Three Decades of Nanopore Sequencing. *Nat. Biotechnol.* 34, 518–524. doi:10.1038/nbt.3423

Egekwu, N., Sonenshine, D. E., Garman, H., Barshis, D. J., Cox, N., Bissinger, B. W., et al. (2016). Comparison of Synganglion Neuropeptides, Neuropeptide Receptors and Neurotransmitter Receptors and Their Gene Expression in Response to Feeding inIxodes scapularis(Ixodidae) vs.Ornithodoros turicata(Argasidae). *Insect Mol. Biol.* 25 (1), 72–92. doi:10.1111/imb.12202

Fishery Department of Ministry of Agriculture and Rural Affairs of China (2020). *China Fishery Statistical Yearbook 2020*. Beijing: China Agriculture Press. (In Chinese).

Henry, R. P., Lucu, C., Onken, H., and Weihrauch, D. (2012). Multiple Functions of the Crustacean Gill: Osmotic/ionic Regulation, Acid-Base Balance, Ammonia Excretion, and Bioaccumulation of Toxic Metals. *Front. Physiol.* 3, 431–433. doi:10.3389/fphys.2012.00431

Jodi, A., Andrew, O., Wilcockson, D. C., and Webster, S. G. (2018). Functional Identification and Characterization of the Diuretic Hormone 31 (DH31) Signaling System in the Green Shore Crab, *Carcinus maenas*. *Front. Neurosci.* 12, 454. doi:10.3389/fnins.2018.00454

Li, E., Wang, S., Li, C., Wang, X., Chen, K., and Chen, L. (2014). Transcriptome Sequencing Revealed the Genes and Pathways Involved in Salinity Stress of Chinese Mitten crab,Eriocheir Sinensis. *Physiol. Genomics* 46 (5), 177–190. doi:10.1152/physiolgenomics.00191.2013

Li, X., Du, L., Jiang, X.-J., Ju, Q., Qu, C.-J., Qu, M.-J., et al. (2020). Identification and Characterization of Neuropeptides and Their G Protein-Coupled Receptors (GPCRs) in the Cowpea Aphid *Aphis Craccivora*. *Front. Endocrinol.* 11, 640. doi:10.3389/fendo.2020.00640

Liu, J., Liu, A., Liu, F., Huang, H., and Ye, H. (2020). Role of Neuroparsin 1 in Vitellogenesis in the Mud Crab, *Scylla Paramamosain*. *General Comp. Endocrinol.* 285, 113248. doi:10.1016/j.ygcen.2019.113248

Liu, M., Pan, L., Li, L., and Zheng, D. (2014). Molecular Cloning, Characterization and Recombinant Expression of Crustacean Hyperglycemic Hormone in White Shrimp *Litopenaeus Vannamei*. *Peptides* 53, 115–124. doi:10.1016/j.peptides.2013.07.030

Liu, S., Pan, L., and Liu, M. (2015). Effects of Ammonia Exposure on Key Detoxification Metabolism Associated Genes Expression in Swimming Crab *Portunus Trituberculatus*. *Trans. Oceanol. Limnol.* 2, 97–104.

Liu, Y., Buchberger, A. R., DeLaney, K., Li, Z., and Li, L. (2019). Multifaceted Mass Spectrometric Investigation of Neuropeptide Changes in Atlantic Blue Crab, *Callinectes sapidus*, in Response to Low pH Stress. *J. Proteome Res.* 18 (7), 2759–2770. doi:10.1021/acs.jproteome.9b00026

Livak, K. J., and Schmittgen, T. D. (2002). Analysis of Relative Gene Expression Data Using Real-Time Quantitative PCR and the 2(-Delta Delta C(T)) Method. *Methods* 25, 402–408. doi:10.1006/meth.2001.1262

Lu, Y., Zhang, J., Cao, J., Liu, P., Li, J., and Meng, X. (2022). Long-term Ammonia Toxicity in the Hepatopancreas of Swimming Crab *Portunus Trituberculatus*: Cellular Stress Response and Tissue Damage. *Front. Mar. Sci.* 8, 757602. doi:10.3389/fmars.2021.757602

Lv, J., Li, R., Su, Z., Gao, B., Ti, X., Yan, D., et al. (2021). A Chromosome-level Genome of Portunus Trituberculatus Provides Insights into its Evolution, Salinity Adaptation and Sex Determination. *Mol. Ecol. Resour.* 22 (4), 1606–1625. doi:10.1111/1755-0998.13564

Meng, X., Jayasundara, N., Zhang, J., Ren, X., Gao, B., Li, J., et al. (2021). Integrated Physiological, Transcriptome and Metabolome Analyses of the Hepatopancreas of the Female Swimming Crab *Portunus Trituberculatus* under Ammonia Exposure. *Ecotoxicol. Environ. Saf.* 228, 113026. doi:10.1016/j.ecoenv.2021.113026

Mykles, D. L., Adams, M. E., Gäde, G., Lange, A. B., Marco, H. G., and Orchard, I. (2010). Neuropeptide Action in Insects and Crustaceans. *Physiological Biochem. Zoology* 83 (5), 836–846. doi:10.1086/648470

Nguyen, T. V., Cummins, S. F., Elizur, A., and Ventura, T. (2016). Transcriptomic Characterization and Curation of Candidate Neuropeptides Regulating Reproduction in the Eyestalk Ganglia of the Australian Crayfish, *Cherax Quadricarinatus*. *Sci. Rep.* 6 (1), 38658. doi:10.1038/srep38658

Nguyen, T. V., Rotllant, G. E., Cummins, S. F., Elizur, A., and Ventura, T. (2018). Insights into Sexual Maturation and Reproduction in the Norway Lobster (*Nephrops norvegicus*) via In Silico Prediction and Characterization of Neuropeptides and G Protein-Coupled Receptors. *Front. Endocrinol.* 9, 430. doi:10.3389/fendo.2018.00430

Pan, L., Si, L., Liu, S., Liu, M., and Wang, G. (2018). Levels of Metabolic Enzymes and Nitrogenous Compounds in the Swimming Crab *Portunus Trituberculatus* Exposed to Elevated Ambient Ammonia-N. *J. Ocean. Univ. China* 17 (4), 957–966. doi:10.1007/s11802-018-3574-y

Qiao, H., Xiong, Y., Jiang, S., Zhang, W., Xu, L., Jin, S., et al. (2020). Three Neuroparsin Genes from Oriental River Prawn, *Macrobrachium Nipponense*, Involved in Ovary Maturation. *3 Biotech.* 10 (12), 537–550. doi:10.1007/s13205-020-02531-8

Romano, N., and Zeng, C. (2013). Toxic Effects of Ammonia, Nitrite, and Nitrate to Decapod Crustaceans: A Review on Factors Influencing Their Toxicity, Physiological Consequences, and Coping Mechanisms. *Rev. Fish. Sci.* 21 (1), 1–21. doi:10.1080/10641262.2012.753404

Saowaros, S. A., Tipsuda, T., Tianfang, W., Min, Z., Abigail, E., Hanna, P. J., et al. (2015). In Silico Neuropeptidome of Female *Macrobrachium Rosenbergii* Based on Transcriptome and Peptide Mining of Eyestalk, Central Nervous System and Ovary. *Plos One* 10 (5), e0123848.

Serrano, L., Blanvillain, G., Soyez, D., Charmantier, G., Grousset, E., Aujoulat, F., et al. (2003). Putative Involvement of Crustacean Hyperglycemic Hormone Isoforms in the Neuroendocrine Mediation of Osmoregulation in the crayfishAstacus leptodactylus. *J. Exp. Biol.* 206, 979–988. doi:10.1242/jeb.00178

Si, L., Pan, L., Wang, H., and Zhang, X. (2019). Ammonia-N Exposure Alters Neurohormone Levels in the Hemolymph and mRNA Abundance of Neurohormone Receptors and Associated Downstream Factors in the Gills of *Litopenaeus Vannamei. J. Exp. Biol.* 222 (9), jeb200204. doi:10.1242/jeb.200204

Sun, S., Wu, Y., Jakovlić, I., Fu, H., Ge, X., Qiao, H., et al. (2020). Identification of Neuropeptides from Eyestalk Transcriptome Profiling Analysis of Female Oriental River Prawn (*Macrobrachium Nipponense*) under Hypoxia and Reoxygenation Conditions. *Comp. Biochem. Physiology Part B Biochem. Mol. Biol.* 241, 110392. doi:10.1016/j.cbpb.2019.110392

Sun, S., Zhu, M., Pan, F., Feng, J., and Li, J. (2020). Identifying Neuropeptide and G Protein-Coupled Receptors of Juvenile Oriental River Prawn (*Macrobrachium Nipponense*) in Response to Salinity Acclimation. *Front. Endocrinol.* 11, 623. doi:10.3389/fendo.2020.00623

Tang, B., Zhang, D., Li, H., Jiang, S., Zhang, H., Xuan, F., et al. (2020). Chromosome-level Genome Assembly Reveals the Unique Genome Evolution of the Swimming Crab (*Portunus Trituberculatus*). *GigaScience* 9 (1), giz161. doi:10.1093/gigascience/giz161

Toullec, J.-Y., Corre, E., Mandon, P., Gonzalez-Aravena, M., Ollivaux, C., and Lee, C.-Y. (2017). Characterization of the Neuropeptidome of a Southern Ocean Decapod, the Antarctic Shrimp *Chorismus Antarcticus*: Focusing on a New Decapod ITP-like Peptide Belonging to the CHH Peptide Family. *General Comp. Endocrinol.* 252, 60–78. doi:10.1016/j.ygcen.2017.07.015

Veenstra, J. A. (2000). Mono- and Dibasic Proteolytic Cleavage Sites in Insect Neuroendocrine Peptide Precursors. *Arch. Insect Biochem.* 43 (2), 49–63. doi:10.1002/(sici)1520-6327(200002)43:2<49::aid-arch1>3.0.co;2-m

Veenstra, J. A. (2011). Neuropeptide Evolution: Neurohormones and Neuropeptides Predicted from the Genomes of *Capitella Teleta* and *Helobdella Robusta*. *General Comp. Endocrinol.* 171 (2), 160–175. doi:10.1016/j.ygcen.2011.01.005

Veenstra, J. A. (2015). The Power of Next-Generation Sequencing as Illustrated by the Neuropeptidome of the Crayfish *Procambarus clarkii*. *General Comp. Endocrinol.* 224, 84–95. doi:10.1016/j.ygcen.2015.06.013

Wang, Z., Zhou, W., Hameed, M., Liu, J., and Zeng, X. (2018). Characterization and Expression Profiling of Neuropeptides and G-Protein-Coupled Receptors (GPCRs) for Neuropeptides in the Asian Citrus Psyllid, *Diaphorina Citri* (Hemiptera: Psyllidae). *Int. J. Mol. Sci.* 19 (12), 3912. doi:10.3390/ijms19123912

Yue, F., Pan, L., Xie, P., Zheng, D., and Li, J. (2010). Immune Responses and Expression of Immune-Related Genes in Swimming Crab *Portunus Trituberculatus* Exposed to Elevated Ambient Ammonia-N Stress. *Comp. Biochem. Physiol. A Mol. Integr. Physiol.* 157 (3), 246–251. doi:10.1016/j.cbpa.2010.07.013

Zhang, J., Zhang, M., Jayasundara, N., Ren, X., Gao, B., Liu, P., et al. (2021). Physiological and Molecular Responses in the Gill of the Swimming Crab *Portunus Trituberculatus* during Long-Term Ammonia Stress. *Front. Mar. Sci.* 8, 797241. doi:10.3389/fmars.2021.797241

Zhang, X., Pan, L., Wei, C., Tong, R., Li, Y., Ding, M., et al. (2020). Crustacean Hyperglycemic Hormone (CHH) Regulates the Ammonia Excretion and Metabolism in White Shrimp, *Litopenaeus Vannamei* under Ammonia-N Stress. *Sci. Total Environ.* 723, 138128. doi:10.1016/j.scitotenv.2020.138128

Zhang, Y., Buchberger, A., Muthuvel, G., and Li, L. (2015). Expression and Distribution of Neuropeptides in the Nervous System of the Crab *Carcinus maenas* and Their Roles in Environmental Stress. *Proteomics* 15 (23-24), 3969–3979. doi:10.1002/pmic.201500256

Zhao, M., Yao, D., Li, S., Zhang, Y., and Aweya, J. J. (2020). Effects of Ammonia on Shrimp Physiology and Immunity: a Review. *Rev. Aquacult.* 12 (4), 2194–2211. doi:10.1111/raq.12429

Conflict of Interest: The authors declare that the research was conducted in the absence of any commercial or financial relationships that could be construed as a potential conflict of interest.

Publisher's Note: All claims expressed in this article are solely those of the authors and do not necessarily represent those of their affiliated organizations, or those of the publisher, the editors and the reviewers. Any product that may be evaluated in this article, or claim that may be made by its manufacturer, is not guaranteed or endorsed by the publisher.

frontiers | Frontiers in Marine Science

ORIGINAL RESEARCH
published: 31 May 2022
doi: 10.3389/fmars.2022.891706

Cholesterol Accumulation in Livers of Indian Medaka, *Oryzias dancena*, Acclimated to Fresh Water and Seawater

Naveen Ranasinghe[1,2], *Chia-Hao Lin*[2,3]* *and Tsung-Han Lee*[1,2]*

[1] Department of Life Sciences, National Chung Hsing University, Taichung, Taiwan, [2] The integrative Evolutionary Galliform Genomics (iEGG) and Animal Biotechnology Center, National Chung Hsing University, Taichung, Taiwan, [3] Department of Marine Biotechnology, National Kaohsiung University of Science and Technology, Kaohsiung, Taiwan

Sterol regulatory-element binding proteins (SREBPs), sirtuin (SIRT1), and liver X receptor α (LXRα) play important roles in regulating cholesterol metabolism in mammals. However, little is known about the relationship between cholesterol metabolism and SIRT1, LXRα, and SREBP-1 in fish. In addition, knowledge of the effects of salinity on hepatic cholesterol metabolism in euryhaline teleosts is fragmented. This study revealed that hepatic cholesterol content was significantly different between fresh water (FW)- and seawater (SW)-acclimated Indian medaka. Gene expression analysis indicated *srebp-1*, *lxrα*, and *sirt1* transcripts were not affected by changes in ambient salinity. However, SREBP-1, but not LXRα and SIRT1 protein expression, was significantly induced in the liver of FW-acclimated medaka. When SREBP-1 Vivo-MO inhibited SREBP-1 translation, hepatic cholesterol content was predominantly downregulated in FW- and SW-acclimated medaka. This is the first study to show that SREBP-1 is involved in cholesterol biosynthesis in fish. Furthermore, SREBP-1 knockdown had different effects on the expression of *hmgcr* and *fdps*, which encode the key enzymes involved in cholesterol biosynthesis. This study further enhances our knowledge of cholesterol metabolism in the livers of euryhaline teleosts during salinity acclimation.

Keywords: SREBP-1, cholesterol, salinity, liver, medaka

OPEN ACCESS

Edited by:
Yu-Hung Lin,
National Pingtung University of Science and Technology, Taiwan

Reviewed by:
Zhen-Yu Du,
East China Normal University, China
Xiaodan Wang,
East China Normal University, China

***Correspondence:**
Chia-Hao Lin
ch123@nkust.edu.tw
Tsung-Han Lee
thlee@email.nchu.edu.tw

Specialty section:
This article was submitted to Aquatic Physiology, a section of the journal Frontiers in Marine Science

Received: *08 March 2022*
Accepted: *28 April 2022*
Published: *31 May 2022*

Citation:
Ranasinghe N, Lin C-H and Lee T-H (2022) Cholesterol Accumulation in Livers of Indian Medaka, Oryzias dancena, Acclimated to Fresh Water and Seawater. Front. Mar. Sci. 9:891706. doi: 10.3389/fmars.2022.891706

INTRODUCTION

Cholesterol is an essential component of all animal cell membranes and functions as a precursor to fat-soluble vitamins and steroid hormones (Lee, 2020). Mammalian physiology is usually influenced by the modification of cholesterol metabolism (Goedeke and Fernández-Hernando, 2012). Both mammals and fish acquire cholesterol from the diet (exogenous cholesterol) and *de novo* synthesis (endogenous cholesterol) (Babin and Vernier, 1989). Cholesterol is largely a product of metabolism in animals. The liver synthesizes more cholesterol than any other organ (Engelking, 2015). It could be absorbed by the intestine or released from the liver into the bloodstream (Khan, 2005). When cholesterol is supplemented in diets, it can significantly improve the growth of Atlantic salmon, catfish, rainbow trout, Nile tilapia, and turbot (Farrell et al., 1986; Twibell and Wilson, 2004; Yun et al., 2011; Yun et al.,

2012; Xu et al., 2018). Fish were found to grow well with exogenous cholesterol supplementation might because the energy used to synthesize cholesterol was saved for growth (Kemski et al., 2020).

The cholesterol contents in the tissues of aquatic animals varied with environmental factors including temperature (Hassett and Crockett, 2009), pollutants (Mohamed et al., 2019), and toxicity (Binukumari and Vasanthi, 2014). Environmental salinities were also reported to affect cholesterol levels in aquatic animals. Serum cholesterol levels were significantly higher in the 0 and 10 ‰ groups than the 20‰ group of pufferfish (*Takifugu fasciatus*, Wen et al., 2021). Cholesterol levels were also higher in hepatopancreases of the mud crab (*Scylla paramamosainduring*) of the 4 and 12 ‰ groups than the 25 ‰ group after overwintering. The adaptive significance of these changes in cholesterol contents may contribute to the building blocks necessary for modifying the membrane properties in response to an environmental challenge (Hazel and Williams, 1990). Cholesterol in excess of dietary requirements could facilitate lipid mobilization and storage in the hepatopancreas of the shrimp (*Litopenaeus vannamei*) to play important roles in increasing their adaptability to environments by improving osmoregulatory capacity, leading to better survival and growth under low salinity conditions (Roya et al., 2006). In addition, 0.4% dietary cholesterol was found to increase branchial Na^+, K^+-ATPase activity, and serum cortisol content of juvenile Nile tilapia to improve their ability for hyperosmotic adaptation (Xu et al., 2018).

In addition to dietary uptake, *de novo* synthesis is the other source of cholesterol. Cholesterol biosynthesis is tightly regulated by sterol regulatory element-binding proteins (SREBPs, Amemiya-Kudo et al., 2002; Horton et al., 2002). Mammalian cells produce three SREBP isoforms, SREBP-1a, SREBP-1c, and SREBP-2. Among them, SREBP-1c is the dominant isoform of SREBP-1 in the livers of adult mammals and is involved in the activation of genes related to the synthesis of fatty acids, but not cholesterol. No alternatively spliced isoforms of the *srebp-1* gene (e.g., *srebp-1a* and *1c* in mammals) were found in fish (Minghetti et al., 2011; Thomas et al., 2013; Dong et al., 2015). According to a comparison of the deduced amino acid sequences, fish SREBP-1 is more similar to human SREBP-1a than to human SREBP-1c (Dong et al., 2015). On the other hand, SREBP-2 was found to specifically transactivate cholesterol synthesis genes (Amemiya-Kudo et al., 2002; Horton et al., 2002). In mammals, SREBP-2 plays a vital role in the mevalonate pathway of cholesterol synthesis, involving the action of more than 20 enzymes (Horton et al., 2002; Xue et al., 2020). 3-hydroxy-3-methylglutaryl CoA reductase (HMGCR) and farnesyl diphosphate synthase (FDPS, also known as farnesyl pyrophosphate synthase; FPPS) among these enzymes are involved in highly synchronized sterol and cholesterol synthesis (Horton et al., 2002; Xue et al., 2020). HMGCR is a rate-limiting enzyme in cholesterol biosynthesis (Smith et al., 1988) and is induced by sterol depletion and repressed in response to sterol accumulation (Goldstein and Brown, 1990; Wang et al., 1994). In contrast, FDPS catalyzes the formation of farnesyl diphosphate, a key intermediate in the synthesis of cholesterol and isoprenylated cellular metabolites (Ishimoto et al., 2010). Feeding diets containing tuna fish oil for two weeks decreased the serum cholesterol concentration by 50% in mice, and the hepatic mRNA levels of *fdps* and *hmgcr* by 70% and 40%, respectively, in rats (Corcos et al., 2005).

In fish, Zhu et al. (2018) reported that the plasma cholesterol levels of rainbow trout decreased after being fed a plant-based diet. Meanwhile, the gene expression of *srebp-2* and *hmgcr* was significantly increased in livers of the rainbow trout. In addition, when cholesterol was supplemented in the plant-based diet to feed Atlantic salmon, the gene expression of *srebp-2* and *fdps* was suppressed, *hmgcr* was not altered, and *srebp-1* was induced in the liver (Kortner et al., 2014). Thus, *srebp-2* in trout and salmon was suggested to have similar roles in cholesterol metabolism in mammals. Cholesterol biosynthesis in fish may also be regulated by ambient salinity. The gene expression of *srebp-2*, *hmgcr*, and *fdps* was stimulated in livers of the tongue sole (*Cynoglossus semilaevis*) after transfer from 30 ‰ to 15 ‰ SW for 60 days (Si et al., 2018). In livers of the rabbitfish fed with the vegetable oil diet reared at 10 ‰ salt-water, *srebp-1* displayed higher expression levels and increased biosynthesis ability of long-chain polyunsaturated fatty acid, respectively, rather than those in the 32 ‰ seawater group (Zhang et al., 2016). Differential responses of SREBP-1 in fish could assist in adapting to different ambient salinity (Dong et al., 2017). Nevertheless, it remains unclear whether SREBP-1 is involved in cholesterol metabolism in fish.

When oxysterols increase because of cholesterol overload, the liver X receptors (LXRs) which are the oxysterol receptors could act as the cholesterol sensor to protect cells (Zhao and Dahlman-Wright, 2010). Two isoforms of LXR (Bertrand et al., 2004; Cruz-Garcia et al., 2009), LXRα (NR1H3) and LXRβ (NR1H2) were identified in this nuclear receptor superfamily (Peet et al., 1998). LXRα is abundantly expressed in the liver, intestine, adipose tissue, kidneys, and immune macrophages, whereas LXRβ is ubiquitously expressed in mice (Schultz et al., 2000). LXRs can promote hepatic lipogenesis by activating the transcriptional program of fatty acid synthesis, especially by increasing the transcription of *srebp-1c*, the key lipogenic activator, in mice (Repa et al., 2000). LXRα is vital for cholesterol metabolism through the increased expression of genes involved in bile acid synthesis and cholesterol excretion in mouse livers (Schultz et al., 2000). LXRs in fish is also involved in cholesterol metabolism (Kortner et al., 2014; Zhu et al., 2018). After feeding with a plant-based diet, hepatic *lxrα* expression as well as plasma cholesterol levels of rainbow trout decreased (Zhu et al., 2018). The expression of *lxr* was also induced when cholesterol was supplemented into the plant-based diet to feed Atlantic salmon (Kortner et al., 2014). On the other hand, transcriptome analysis revealed salinity effects on expression of genes related to lipid metabolism including *lxrα* and *srebp-1* in livers of the turbot (*Scophthalmus maximus*) and showed a significant downward trend under low salinity stress (Liu et al., 2021).

In addition to SREBP-1 and LXRα, sirtuin 1 (SIRT1) also plays a beneficial role in cholesterol metabolism by deacetylating both LXR and SREBP-1/2 (Walker et al., 2010). Sirtuins (SIRTs) are members of a protein family of NAD-dependent deacetylases (Grozinger et al., 2001; Albani et al., 2010; Vassilopoulos et al.,

2011). After deacetylation, SIRT1 destabilizes SREBP-1/2 (Ponugoti et al., 2010; Walker et al., 2010). Therefore, SIRT1 can modulate hepatic cholesterol metabolism by mediating LXR (Kemper et al., 2013) and SREBP-1/2 activities. In SIRT1 knockout mice, decreased expression of LXR downstream target genes involved in cholesterol metabolism and hepatic cholesterol accumulation was reported (Feige and Auwerx, 2007; Li et al., 2017). These results are consistent with the abnormal cholesterol accumulation observed in the liver-specific SIRT1 knockout mice (Li et al., 2007).

Upon salinity challenge, the euryhaline fish are able to survive well through efficient osmoregulatory mechanisms mainly exhibited on the membrane of epithelial cells in osmoregulatory tissues (Hwang and Lee, 2007). Previous studies have indicated that in some fish cholesterol contents which were pivotal for membrane structures and functions changed with environmental salinities (Xu et al., 2018; Wen et al., 2021). On the other hand, SREBP-1/2, LXRα, and SIRT1 were reported to be crucial for regulating cholesterol metabolism in mammals (Schultz et al., 2000; Horton et al., 2002; Li et al., 2007). Although in mammalian livers SIRT1 was known to control SREBP-1 gene expression through the mechanism involving the transcription factor LXR as described above, the mechanisms in cholesterol biosynthesis and accumulation in livers of euryhaline fish in response to ambient salinity changes were not clear.

The euryhaline Indian medaka (*Oryzias dancena*, the synonym of *Oryzias melastigma*, Yusof et al., 2011) is an ideal model species for osmoregulatory studies (Yang et al., 2013), of which the physiological, biochemical, and molecular responses after exposure to contaminants and other environmental stressors were commonly studied due to their characteristics, i.e., small in size, short in generation time, easy to handle, and strong intolerance to environmental stress (Dong et al., 2014). Therefore, this study used this model species to investigate whether changes in ambient salinity affected cholesterol accumulation in livers of the Indian medaka through the protein and gene expression of SREBP-1, LXRα, and SIRT1. SREBP-1 knockdown was further performed by Vivo-Morpholino to reveal its role in cholesterol biosynthesis in livers of this euryhaline fish. This study will enhance our understanding of the regulatory mechanisms of cholesterol metabolism of the euryhaline teleost during salinity acclimation.

MATERIAL AND METHODS

Experimental Fish and Treatments

Indian medaka with a total length of 3.5 ± 0.5 cm and weight of 8.0 ± 1.0 g) were purchased from an aquarium (Taichung, Taiwan) and kept in laboratory conditions in brackish water (15 ‰) prepared by adding appropriate amounts of Blue Treasure Sea Salts (New South Wales, Australia) to aerated tap water for at least two weeks before the experiments. The medaka were then transferred into fresh water (FW; 0 ‰) and seawater (SW; 35 ‰) tanks with re-circulatory filter units for at least four weeks and 50% of the water was changed every two days. The medaka were fed to satiation with a commercial diet (A045F; Hai Feng, Nantou, Taiwan) containing 45% crude protein, 6% crude lipid, 16% ash, and 8% water. Throughout the experimental period, a 12:12 h light: dark regime (08:00 to 20:00 h light period) was maintained using timed lighting. The water temperature of the control group was maintained at 28 ± 1°C (Juo et al., 2016), and 36 to 60 fish were kept in one tank. The experimental protocol was reviewed and approved by the Institutional Animal Care and Use Committee (IACUC) of the National Chung Hsing University, Taichung, Taiwan (IACUC Approval No. 106-054).

RNA Extraction and Reverse Transcription

Medaka acclimated to SW or FW were placed on ice under anesthesia, and the livers were immediately dissected. One sample (50–100 mg) from each group contained six livers collected from six individuals and was placed in an Eppendorf tube containing 200 μL of TriPure Isolation Reagent (Roche, Mannheim, Germany). The samples were frozen in liquid nitrogen and stored at -80 °C. The RNA extraction method used in this study was modified from that described by Hu et al. (2017). The RNA pellet was dissolved in sterilized diethyl pyrocarbonate (DEPC) water (20 μL). Extracted RNA integrity was verified on a 1% agarose gel (SeaKem® LE Agarose; Lonza, Basel, Switzerland) electrophoresed using SafeView™ Classic (ABM, San Jose, CA, USA). The concentration and purity of the total RNA were measured using a NanoDrop 2000 (Thermo, Wilmington, DE, USA). The purity of the RNA was evaluated by the ratio of absorbance A260/A280, with the accepted values between the ranges of 1.9–2.1.

To prepare genomic DNA-free RNA samples, purified RNA samples were further treated (10,000-25,000 units/mg) with DNase I (Thermo Fisher Scientific, Waltham, MA, USA). First-strand cDNA was synthesized using the iScript™ cDNA Synthesis Kit (Bio-Rad, Hercules, CA, USA) and 1 μg of genomic DNA-free total RNA, following the manufacturer's instructions. After the reverse transcription reaction, real-time PCR (qPCR) was used to determine the mRNA levels using FastStart™ Universal SYBR Green Master (04913850001; Roche).

Quantitative Real-Time PCR

Primers used for qPCR analyses were designed according to the sequences of *O. melastigma* (also named *O. dancena*) in the National Center for Biotechnology Information (NCBI) database (www.ncbi.nlm.nih.gov). Primer and thermal cycling conditions (Applied Biosystems® Veriti® 96-Well Thermal Cycler; Thermo Fisher Scientific) were analyzed using gradient temperatures ranging from 54–62°C. Thermal cycling is performed by mixing with 1.6 μL dNTP mixture (Takara, Shiga, Japan), 2 μL 10x Ex Taq reaction buffer (Takara), 0.1 μL Ex Taq polymerase (Takara), 1 μL of cDNA (20x dilution), 0.5 μL of each forward and reverse primer (250–400 nM), and adding nucleotide, DNase, and RNase-free water (Protech, Taipei, Taiwan) to the total volume of 20 μL. The PCR product was verified by 1–2% agarose gel electrophoresis (according to the length of the target sequence). The confirmed PCR product was sent to Tri-I Biotech

Company (Taipei, Taiwan) for sequence analysis. Sequencing results were confirmed against *O. melastigma* using the online database available in NCBI (https://www.ncbi.nlm.nih.gov).

The mRNA expression levels of *sirt1*, *lxrα*, and *srebp1* were measured using a Rotor-Gene Q Real-Time PCR System (QIAGEN, Hilden, Germany) in the reaction mixture for real-time PCR containing 1 μL cDNA (20x dilution), primers (0.5–1 μL) in the concentration range from 250–400 nM (according to the primer efficiency), and 10 μL KAPA SYBR FAST qPCR Master Mix (KAPA Biosystems, Cape Town, South Africa) to a total volume of 20 μL using nucleotide, DNase, and RNase-free water (Protech). Non-specific products were confirmed by melting curve analysis and gel electrophoresis of the primers. The primer efficiency was maintained within 95–105% to verify the primer specificity (**Table 1**). The corresponding values of the target genes were calculated using the relative Ct method (Livak and Schmittgen, 2001) using the following formula: Relative expression= 2^- [(Ct target gene, n – Ct β-actin, n) – (Ct target gene, c – Ct β-actin,c)]. Ct corresponded to the threshold cycle number, "n" indicated each sample, and "c" indicated the control mixed with cDNA samples of all experiments (Livak and Schmittgen, 2001). Actin was used as the normalization gene.

Preparation of the Nuclear Fraction

Livers were sampled from medaka as described in the previous paragraph. After sampling, 100 mg of liver samples were ground using disposable polypropylene pellet pestles in microtubes containing 1 ml of 1x phosphate-buffered saline (PBS) using a sonicator. The ground tissues were centrifuged at 1,300 × *g* at 4°C for 10 min, and the supernatants were discarded. After centrifugation, the pellets were used to extract nuclear and cytoplasmic proteins using the Nuclear/Cytosol Fractionation Kit (K266-25, BioVision, Milpitas, CA, USA) according to the manufacturer's instructions. Extracted cytoplasmic and nuclear protein samples were stored at -80°C. Protein concentration was determined using the Bradford assay (B6916, Sigma-Aldrich, St. Louis, MO, USA) and bovine serum albumin (Pierce, Hercules, CA, USA) as the standard.

Antibodies

Immunogens of the primary antibody were aligned with the medaka sequence to the most suitable primary antibody using multiple sequence alignments (Corpet, 1988). The primary antibodies used in this study included (1) SIRT1, a rabbit polyclonal antibody (13161-1-AP; Proteintech, Rosemont, IL, USA) raised against the residues AG3808 of human SIRT1; (2) LXRα, a mouse monoclonal antibody (sc-377260, Santa Cruz, Dallas, TX, USA) specific for epitope mapping between amino acid 433-461 of LXRα of human origin and (3) SREBP-1, a mouse monoclonal antibody (sc-13551, Santa Cruz, Dallas, Texas, USA) raised against amino acids 301–407-SREBP-1 of human origin. Primary antibodies were diluted 1:500 with antibody dilution buffer prior to immunoblotting. Secondary antibodies used in this study included the (1) goat anti-mouse IgG antibody (HRP) (GTX 213111-01, GeneTex, Irvine, CA, USA) for detecting the LXRα and SREBP-1a antibodies, and (2) goat anti-rabbit IgG antibody (HRP) (GTX 213110-01, GeneTex) for detecting the SIRT1 antibody. To test the specificity of the primary antibodies, negative controls were included using the antibody dilution buffer to replace the primary antibodies of SIRT1 (**Supplementary Figure 1**), LXR (**Supplementary Figure 2**), and SREBP-1 (**Supplementary Figure 3**). The antibody dilution buffer contained 1% bovine serum albumin and 0.01% sodium azide in 50 mL PBST.

Immunoblotting

Nuclear protein fractions with 6x sample loading buffer (12% SDS, 0.06% bromophenol blue, 30% glycerol, 0.6 M dithiothreitol, and 62.5 mM Tris at pH 6.8) added were incubated at 65°C for 15 min to denature the proteins. The protein ladder (PM2500, 3-color Regular Range Protein Marker, SMOBIO, Hsinchu, Taiwan; #26616, PageRuler™ Pre-stained Protein Ladder, Thermo Fisher Scientific) loaded for immunoblotting of SIRT1, LXR, SREBP-1 were 24, 50, and 50 μg of protein per lane, respectively, and PARP1 (sc8007, Santa Cruz Biotechnology, Dallas, TX, USA) was used as a positive control. Proteins were separated on 8–10% SDS-PAGE gels using a Mini-PROTEAN® II Electrophoresis Cell (Bio-Rad). The separated proteins were transferred to a PVDF membrane

TABLE 1 | Primer sequences used for the cDNA cloning (PCR) and expression detection (qPCR) of medaka livers.

Gene		Primer sequence (5′ to 3′)	Amplicon size (bp)	Reference number	Primer efficiency	Primer concentration
sirt1	F:	CTAAGAGACCTTCTGCCTGA G	138	XM_024297249.1	0.96	250 nM
	R:	AGACTGGTGTAGAAG TTGC				
lxrα	F:	CTCAGGTTTCCACTACAACG	117	XM_024295306.1	1.02	400 nM
	R:	TACAG GTAAA GTGTC GCC				
srebp-1	F:	CAGCA GTCTAACCAGAAACTC	103	XM_024272328.1	1.05	400 nM
	R:	ACGATACCTCCATCTACCTG				
srebp-2	F:	GAAATAGAGAATGGACGGAGG	171	XM_030794047.1	1.05	400 nM
	R:	ACTGACAAACTGAAGCATCTC				
hmgcr	F:	GGCTCTTCACCATCTTCTCC	117	XM_024260286.1	0.99	400nM
	R:	ACAGGTCTATGAGGAGCAGG				
fdps	F:	ACAGAGACCACATATCAGACGG	151	XM_024268301.1	1.03	400nM
	R:	CTCGTTCTACCTCCCAGTGG				
b-actin	F:	CCATTGAGCACGGTATTGTCA	102	XM_024296129.1	1.05	250nM
	R:	GCAACACGCAGCTCGTTGTA				

(Millipore, Bedford, MA, USA) by electrophoresis on ice. After blocking with 5% (w/v) skim milk for 1 h to minimize the non-specific binding, the blots were incubated overnight at 4°C with the primary antibody. The membranes were washed three times with PBST and incubated with the secondary antibody for 1 h at room temperature. Images were developed with Immobilon™ Western Chemiluminescent HRP Substrate (Millipore) using a cooling-charge-coupled device camera (ChemiDoc XRS+, Bio-Rad) and associated software (Quantity One v 4.6.8, Bio-Rad). The bands were converted to numerical values using ImageLab 3.0 (Bio-Rad) to quantify and compare the relative protein abundance of the immunoreactive bands.

Assay of Cholesterol Contents

After sampling, medaka livers (16 ± 1 mg) were placed in a microtube containing 200 µL of a mixture of chloroform (Merck, 14-650-505, Phillipsburg, NJ, USA), isopropanol (#SHBK4071, Sigma-Aldrich), and NP-40 (IGEPAL® CA-630, Sigma-Aldrich) in a ratio of 7:11:0.1, followed by grinding on ice. Samples were centrifuged for 10 min at 15,000 × *g* at 4°C. Subsequently, the supernatants were transferred to new and air-dried at 50°C to remove chloroform. The cholesterol content in the liver was assayed as described below using the Total Cholesterol Assay Kit (STA384-192 assays, Cell Biolabs, San Diego, CA, USA) according to the manufacturer's protocol. Cholesterol levels were measured at 570 nm using the colorimetric method with the cholesterol standard. Cholesterol standards were prepared before assays by diluting 10 mM stock solution in 1x Assay Diluent at a ratio of 1:40 to make a 250 µM working solution. The cholesterol standards were prepared promptly in serial dilutions from 0–250 µM, including 10 points, according to the manufacturer's protocol. The formula for calculating cholesterol content are:

$$\text{Total cholesterol (mg/g)} = \left[\frac{\text{Sample corrected absorbance}}{\text{Slope of standard curve}}\right] \text{x Sample dilution}$$

Vivo-Morpholino Design

The translational blocking of SREBP-1 Vivo-Morpholino (5'-GATAGGCGATTCATC TCTACGGTTG-3') was designed by Gene-Tools LLC (Philomath, OR, USA), reverse complementary to the SREBP-1 full-length sequence of the *O. melastigma* database (XM_024272328.1, https://www.ncbi.nlm.nih.gov/), and confirmed by the Vivo-MO sequence by BLAST search using the NCBI database. A standard Vivo-Morpholino (MO) control (5′-CCTCTTACC TCAGTTACAATTTATA-3′) was purchased from Gene-Tools.

FW- and SW-acclimated adult medaka were anesthetized with 4% MS222 made with aerated water and then injected with 0.5 mM SREBP-1 or control in 5 µL Vivo-MOs (either the original solution supplied by the vendor, 0.5 or 0.05 mM diluted with phosphate-buffered saline, pH 7.4 (PBS) using a BD insulin syringe and Ultra-Fine II needle (0.22 mm, 31G x 8 mm, Becton drive, Franklin lakes, NY, USA). Vivo-MO or control was gently injected into the region closer to the anal pore in the abdomen of the medaka. After injection, the fish were returned to their acclimated environments (i.e., FW or SW) and maintained for 24 h and 72 h. The effects of Vivo-MO were evaluated in a preliminary study using immunoblotting as previously described. The livers of the Vivo-MO and control groups were then sampled for cholesterol analysis.

Statistical Analyses

Statistical analyses were done in the statistical program Minitab (Minitab® 17 Minitab Inc., PA, USA). Normality and homogeneity of variance between the groups that were statistically compared were tested (the significance level was set at $P < 0.05$). For the mRNA and protein abundance and cholesterol level results, data between the FW- and SW-acclimated medaka of each temperature group were compared using Student's *t*-test ($P < 0.05$). The data of different temperature groups in FW or SW were compared using one-way analysis of variance (ANOVA) with Tukey's test ($P < 0.05$). Values are expressed as mean ± standard error of the mean (SEM).

RESULTS

Hepatic Cholesterol Content in FW- and SW-Acclimated Medaka

To explore the effects of ambient salinity on cholesterol accumulation in the livers of Indian medaka, fish were exposed to fresh water (FW) or seawater (SW) for two weeks. Subsequently, the livers were sampled to measure cholesterol content. **Figure 1** shows that the hepatic cholesterol content in the FW group was significantly higher than that in the SW group.

The Gene and Protein Expression of HMGCR, FDPS, and SREBP-1/2 in Livers of FW- and SW-Acclimated Medaka

Real-time PCR analyses revealed the mRNA expression of *hmgcr*, *fdps*, and *srebp-1/2* in the livers of FW- and SW-acclimated

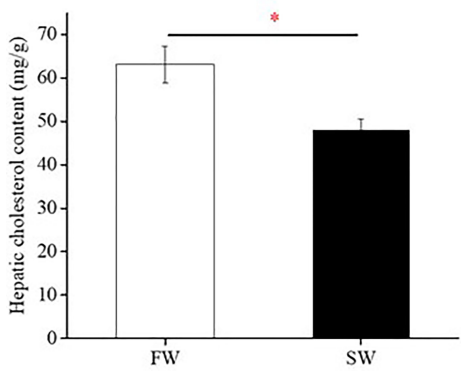

FIGURE 1 | Hepatic cholesterol content of fresh water (FW)- and seawater (SW)-acclimated Indian medaka. Values are mean ± S.E.M. (N = 6). Student's t-test, *p < 0.05.

medaka. Hepatic *hmgcr*, *fdps*, and *srebp-1/2* transcripts were not significantly different between FW- and SW-acclimated medaka (**Figure 2A**). In contrast, the relative protein abundance of SREBP-1 in the liver was significantly higher in FW- than in SW-acclimated medaka (**Figure 2B**). Cholesterol content was approximately 7-fold higher in FW-acclimated medaka than in SW-acclimated medaka (**Figure 2B**).

The Gene and Protein Expression of LXRα and SIRT1 in Livers of FW- and SW-Acclimated Medaka

Real-time PCR analyses revealed that the mRNA expression of *lxrα* and *sirt1* in the liver was similar in FW- and SW-acclimated medaka (**Figures 3A**, **4A**). Immunoblot analysis also revealed that the relative protein expression of LXRα and SIRT1 in the livers of FW- and SW-acclimated medaka was not significantly different (**Figures 3B**, **4B**).

The Effect of SREBP-1 Knockdown on Hepatic Cholesterol Content of Medaka

Vivo-morpholino (Vivo-MO) of SREBP-1 was used to inhibit SREBP-1 translation in Indian medaka. **Figure 5A** shows that SREBP-1 Vivo-MO could inhibit SREBP-1 protein expression predominantly in the livers of Indian medaka compared to the control Vivo-MO. In contrast, SREBP-1 knockdown in FW- or SW-acclimated Indian medaka significantly inhibited hepatic cholesterol content (**Figure 5B**).

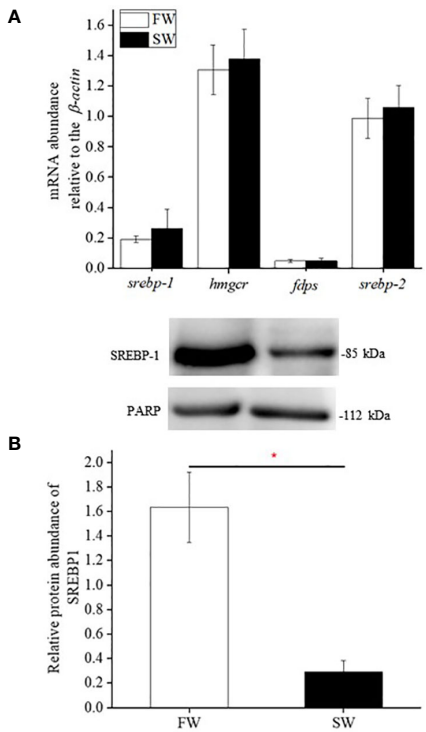

FIGURE 2 | Relative gene **(A)** and protein **(B)** expression of SREBP-1, HMGCR, FDPS, and SREBP-2 in livers of fresh water (FW)- and seawater (SW)-acclimated Indian medaka. mRNA expression was analyzed by real-time PCR. The immunoblots were used to detect SREBP-1 protein expression of in the nuclear fractions of livers. Values are mean ± S.E.M. (N = 6). Student's t-test, *p < 0.05.

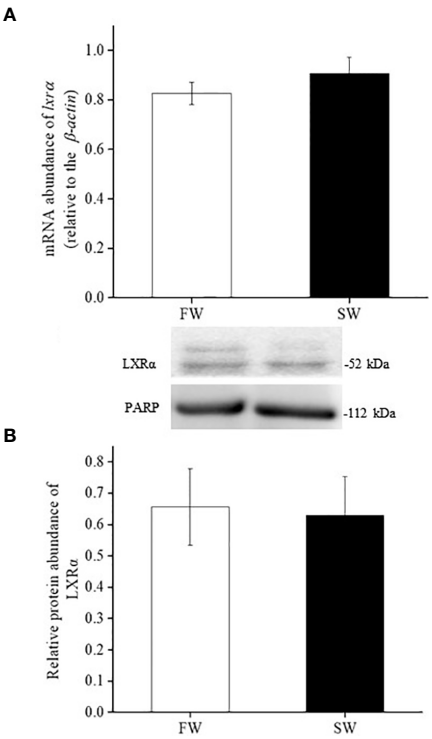

FIGURE 3 | Relative gene **(A)** and protein **(B)** expression of LXRα in livers of fresh water (FW) and seawater (SW)- acclimated Indian medaka. mRNA expression was analyzed by real-time PCR. The immunoblots were used to detect the protein expression. Values are mean ± S.E.M. (N = 6).

The Effect of SREBP-1 Knockdown on the mRNA Expression of Cholesterol Synthesis-Related Genes

In both FW- and SW-acclimated Indian medaka, SREBP-1 knockdown significantly decreased *hmgcr*, but increased *fdps* expression (**Figure 6**). However, hepatic *srebp-2* expression did not change in either FW- or SW-acclimated Indian medaka with SREBP-1 knockdown (**Figure 6**).

DISCUSSION

Steroid metabolism-related pathways, such as steroid and steroid hormone biosynthesis, are important for salinity adaptation in aquatic animals (Charmandari et al., 2005; Aruna et al., 2015). The expression of genes involved in lipid or steroid metabolism-related pathways in fish livers changes in response to ambient salinity (Si et al., 2018; Liu et al., 2021). Cholesterol is the sole precursor of steroids (Azhar et al., 2003).

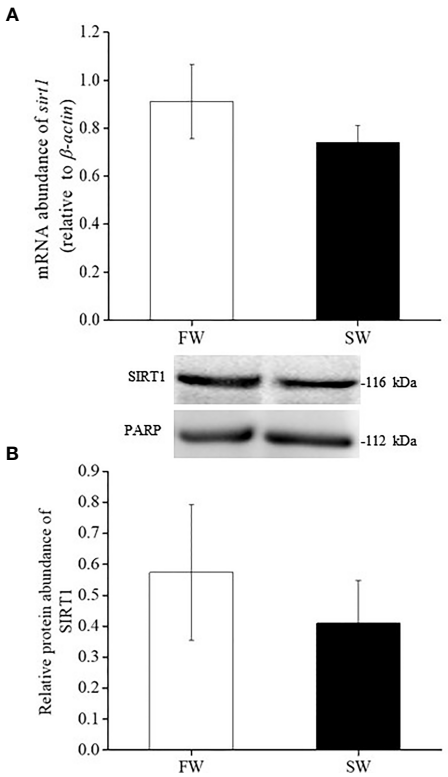

FIGURE 4 | Relative gene **(A)** and protein **(B)** expression of SIRT1 in livers of fresh water (FW) and seawater (SW)- acclimated Indian medaka. mRNA expression was analyzed by real-time PCR. The immunoblots were used to detect the protein expression. Values are mean ± S.E.M. (N = 6).

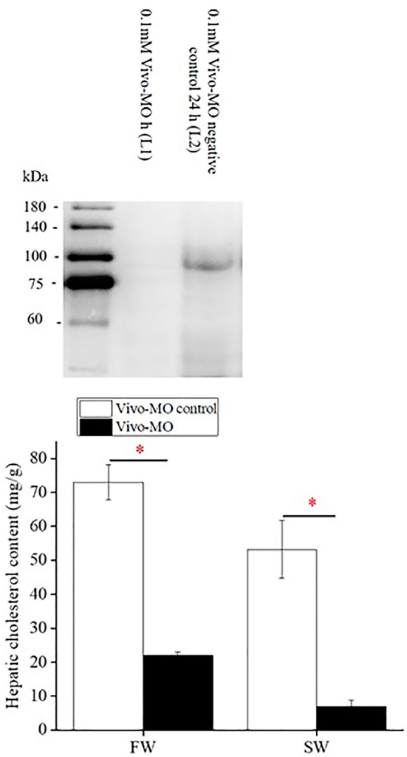

FIGURE 6 | The effect of SREBP-1 knockdown on mRNA expression of targeted genes in livers of fresh water (FW)- and seawater (SW)-acclimated Indian medaka. mRNA expression was analyzed by real-time PCR. Values are mean ± S.E.M. (N = 6). Student's t-test, *p < 0.05.

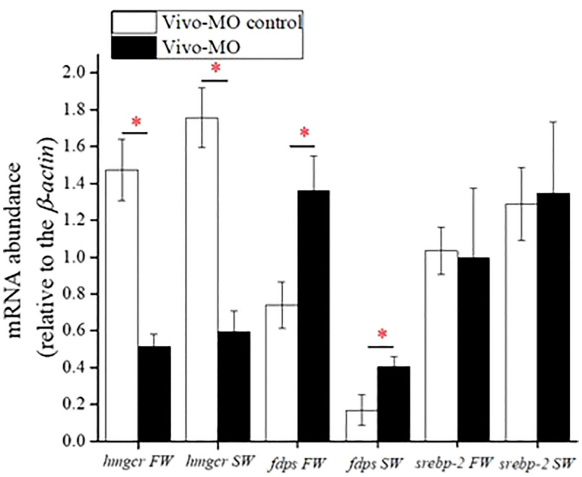

FIGURE 5 | The effect of SREBP-1 knockdown on hepatic cholesterol content in fresh water (FW)- and seawater (SW)-acclimated Indian medaka. **(A)** The specificity test of SREBP-1 Vivo-MO. **(B)** The measurement of hepatic cholesterol content in Indian medaka with/without SREBP-1 knockdown. Values are mean ± S.E.M. (N = 6). Student's t-test, *p < 0.05.

In this study, the cholesterol content of medaka liver, the central organ for cholesterol biosynthesis in vertebrates, was significantly higher in FW- than in SW-acclimated medaka. Cholesterol biosynthesis in the livers of Indian medaka may also be related to changes in ambient salinity, resulting in changes in hepatic cholesterol content. Kang et al. (2008) reported that plasma osmolality was significantly lower in Indian medaka under freshwater (FW) acclimation than in seawater (SW) acclimation. In contrast, the plasma osmolality was similar between the hypertonic SW and isotonic BW groups. The livers of FW-acclimated medaka may have experienced hypoosmotic stress. This is because osmotic stress can induce cell death; hence, maintenance of cell osmolality is a vital issue (Lang et al., 2000; Burg et al., 2007). Cholesterol biosynthesis in response to changes in ambient salinity is related to the physical properties of the cell membranes (Parasassi et al., 1995). The presence of cholesterol leads to a decrease in the permeability coefficients of phospholipid vesicles to Na^+, K^+, and Cl^- (Papahadjopoulosa et al., 1972). A previous study indicated that the erythrocytes of guinea pigs containing an increased amount of cholesterol showed a dominant decrease in membrane permeability to both the active and passive components of Na^+ efflux (Kroes and Ostwald, 1971). Therefore, the increased cholesterol

content in the livers of FW-acclimated medaka may help protect fish against extracellular hypoosmotic stress.

Under salinity stress, the gill is the predominant organ for osmoregulation in euryhaline teleosts. Na^+/K^+-ATPase (NKA) is expressed in mitochondria-rich cells (i.e., ionocytes) of the gill that actively transports Na^+ from and K^+ into cells and can provide a primary driving force to activate other ion transport systems involved in osmoregulation (Hwang et al., 2011; Lin C. H. et al., 2021). NKA comprises α- and β-subunits. The α-subunit is considered the catalytic center of NKA, with binding sites for cations and ATP (Scheiner-Bobis, 2002). Lipid rafts (LRs) are plasma membrane microdomains enriched in cholesterol. Previous mammalian studies have shown that LRs may play a crucial role in ion exchange. In milkfish and tilapia, the branchial NKA α-subunit was mainly expressed in LR (Lin Y. T. et al., 2021). In contrast, experiments on the mammalian kidney epithelial cell line (LLC-PK1) revealed that plasma membrane cholesterol positively affects NKA α1 expression (Chen et al., 2011; Lambropoulos et al., 2016; Zhang et al., 2020). A previous study indicated that FW-acclimated Indian medaka have higher branchial NKA α1 protein expression than SW-acclimated medaka (Kang et al., 2008). The liver is the central organ involved in vertebrate cholesterol biosynthesis. Therefore, the increased liver cholesterol content in FW-acclimated medaka may increase the delivery of cholesterol to the gill and increase membrane NKA α1 protein expression.

Sterol regulatory element-binding protein-1 and 2 (SREBP-1/2) are vital regulators of cholesterol metabolism, and 3-Hydroxy-3-Methylglutaryl CoA reductase (HMGCR) and farnesyl diphosphate synthase (FDPS) are key enzymes involved in cholesterol biosynthesis (Amemiya-Kudo et al., 2002; Horton et al., 2002; Xue et al., 2020). HMGCR is an important enzyme that controls the first rate-limiting step of the cholesterol synthesis pathway (Sharpe and Brown, 2013). In mammals, *hmgcr* is the transcriptional target of SREBP-1a and SREBP-2 (Horton et al., 2002; Sundqvist et al., 2005; Xue et al., 2020). Si et al. (2018) indicated that the gene expression of *srebp-2*, *hmgcr*, and *fdps* was upregulated in the livers of *Cynoglossus semilaevis* under long-term hypotonic stress. In this study, we found that the hepatic gene expression of *srebp-1/2*, *hmgcr*, and *fdps* was not different between FW- and SW-acclimated medaka. In contrast, in this study, we found that the nuclear protein expression of SREBP-1 was significantly upregulated in FW-acclimated medaka. When SREBP-1 translation was knocked down by intraperitoneal injection of SREBP-1 Vivo-MO, we found that SREBP-1 knockdown caused a dominant decrease in hepatic cholesterol content in both FW- and SW-acclimated medaka. The decreased percentage of hepatic cholesterol content was approximately 70-80% in SREBP-1 knockdown group compared to the control group. These results revealed that SREBP-1 is positively related to cholesterol biosynthesis in the liver of teleosts. Thus, higher SREBP-1 protein expression in the liver of FW-acclimated medaka may contribute to the upregulation of cholesterol content. In addition, we found that SREBP-1 knockdown caused a dominant downregulation in the transcription of *hmgcr* in the livers of FW- and SW-acclimated medaka. There are two SREBP-1 proteins in mammals, SREBP-1a and 1c, in mammals (Horton et al., 2002). SREBP-1a is universal for fatty acid and cholesterol biosynthesis, but SREBP-1c is restricted to fatty acid biosynthesis (Horton et al., 2002). In teleosts, several studies have indicated that only one SREBP-1 form was translated, and the analysis of amino acid sequences showed that teleostean SREBP-1 was close to mammalian SREBP-1a (Minghetti et al., 2011; Thomas et al., 2013; Dong et al., 2015). Dong et al. (2015) reported that the gene expression of SREBP-1 in the liver of Japanese seabass was decreased by dietary polyunsaturated fatty acids compared to dietary saturated or monounsaturated fatty acids. Hence, fish SREBP-1 may be involved in lipid metabolism. This study indicated that the knockdown of SREBP-1 caused a decrease in hepatic cholesterol content in Indian medaka. Taken together, teleost SREBP-1 may function universally in lipid metabolism, similar to mammalian SREBP-1a.

In zebrafish, aplexone treatment disturbs the transcription of enzymes in the HMGCR pathway and reduces cellular cholesterol levels. This causes a feedback loop to induce *fdps* gene expression (Choi et al., 2011). This study revealed that *fdps* gene expression was predominantly upregulated in SREBP-1 knockdown medaka. The decreased hepatic cholesterol content caused by SREBP-1 knockdown in Indian medaka may also cause a feedback effect that induces hepatic *fdps* gene expression. In mice, the target disruption of *the srebp-1* gene caused the upregulation of *the srebp-2* transcript and nuclear SREBP-2 protein expression, resulting in increased cholesterol synthesis in the liver (Shimano et al., 1997). In contrast, these results indicated that hepatic *srebp-2* gene expression was not changed in Indian medaka with SREBP-1 knockdown. Additionally, SREBP-1 knockdown did not positively affect hepatic cholesterol synthesis in Indian medaka. The regulatory mechanism for cholesterol homeostasis may have subtle differences between fish and mammals. Therefore, the impaired expression of SREBP-1 caused divergent SREBP-2 expression and cholesterol synthesis. SREBP-2 plays an essential role in regulating cholesterol synthesis in mammalian experiments (Amemiya-Kudo et al., 2002; Horton et al., 2002). Previous studies have indicated that dietary cholesterol depletion and supplementation induced a positive and negative feedback effect on hepatic *srebp-2* gene expression in fish (Kortner et al., 2014; Zhu et al., 2018). This study indicated that the gene expression level of *srebp-2* was approximately 5-fold higher than that of *srebp-1* in the livers of Indian medaka. Therefore, hepatic *srebp-2* gene expression was not significantly different between FW- and SW-acclimated medaka and SREBP-1 knockdown did not change SREBP-2 gene expression. The importance of SREBP-2 in cholesterol metabolism in fish cannot be neglected.

Liver X receptor α (LXRα) plays a key role in controlling cholesterol metabolism in mammalian livers (Zhao and Dahlman-Wright, 2010; Jakobsson et al., 2012). To maintain cholesterol homeostasis, LXRα induces the expression of a range of genes involved in cholesterol transport and catabolism in the target tissues (Zhao and Dahlman-Wright, 2010; Jakobsson et al., 2012). In turbot (*Scophthalmus maximus*), *lxrα* gene expression was significantly decreased 24 and 48 h post-transfer from SW to FW (Liu et al., 2021). On the contrary, our results indicated that

both gene and nuclear protein expression of LXRα were unchanged in the liver of Indian medaka acclimated to FW and SW for one week. Additionally, we found that sirtuin 1 (SIRT1) gene and nuclear protein expression in the liver of Indian medaka were not significantly different between FW and SW acclimation. SIRT1 is an NAD^+-dependent histone/protein deacetylase that can deacetylate LXRs and increase their activity. Increased activity of LXRs has a positive effect on cholesterol catabolism in target tissues (Li et al., 2007). According to these results, ambient salinity did not affect the nuclear protein expression of LXRα and STIR1. Cholesterol elimination in the liver may not change in Indian medaka after acclimation to FW and SW for one week. However, FW-acclimated medaka showed higher nuclear protein expression of SREBP-1, which may contribute to the elevation of hepatic cholesterol biosynthesis. Finally, these phenomena may result in elevated cholesterol levels in the liver of FW-acclimated medaka.

In conclusion, these results showed that the knockdown of SREBP-1 decreased the expression of cholesterol metabolism-related genes and cholesterol content in the liver of Indian medaka. This is the first study to show SREBP-1 may have a positive effect on hepatic cholesterol metabolism in teleosts. Thus, the SREBP-1 protein expression was upregulated in FW-acclimated medaka, which may contribute to the higher hepatic cholesterol content compared to that in SW-acclimated medaka. We found that the gene and protein expression of LXRα and SIRT1 did not differ between the FW and SW groups in Indian medaka, implying that cholesterol catabolism and other lipid metabolic reactions might not be regulated in Indian medaka under salinity stress. Further experiments will help verify these hypotheses in the future.

DATA AVAILABILITY STATEMENT

The original contributions presented in the study are included in the article/**Supplementary Material**. Further inquiries can be directed to the corresponding authors.

ETHICS STATEMENT

The animal study was reviewed and approved by Institutional Animal Care and Use Committee (IACUC). Written informed consent was obtained from the owners for the participation of their animals in this study.

AUTHOR CONTRIBUTIONS

NR, C-HL, and T-HL designed the experiments. NR performed the experiments and analyzed the data. NR, C-HL, and T-HL wrote the paper. All authors have read and approved the final manuscript.

FUNDING

This study was partly supported by research projects (108-2313-B-005-006-MY3) from the Ministry of Science and Technology (MOST), Taiwan, and in part by the iEGG and Animal Biotechnology Center from The Feature Area Research Center Program within the framework of the Higher Education Sprout Project by the Ministry of Education (MOE), Taiwan (MOE 109-S-0023-A) to T-HL.

SUPPLEMENTARY MATERIAL

The Supplementary Material for this article can be found online at: https://www.frontiersin.org/articles/10.3389/fmars.2022.891706/full#supplementary-material

Supplementary Figure 1 | Immunoblotting of SIRT1 in Indian medaka (*O. melastigma*) livers detected with a polyclonal antibody (Proteintech-13161-1-AP). **(A)** One immunoreactive band with a molecular mass of about 116 kDa was detected. **(B)** The negative control did not indicate an immunoreactive band with the secondary antibody. The arrow indicated the immunoreactive band. M, marker; N, nuclear fraction.

Supplementary Figure 2 | Immunoblotting of LXRα in Indian medaka (*O. melastigma*) livers detected with a monoclonal antibody (Santa Cruz sc-377260). **(A)** One immunoreactive band with a molecular mass of about 52 kDa was detected. **(B)** The negative control did not indicate an immunoreactive band with the secondary antibody. The arrow indicated the immunoreactive band. M, marker; N, nuclear fraction.

Supplementary Figure 3 | Immunoblotting of SREBP-1 in Indian medaka (*O. melastigma*) livers detected with a monoclonal antibody (Santa Cruz sc-13551). **(A)** The major immunoreactive band had a molecular mass of about 85 kDa. **(B)** Negative control did not indicate an immunoreactive band with the secondary antibody. The arrow indicated the immunoreactive band. M, marker; N, nuclear fraction.

REFERENCES

Albani, D., Polito, L., and Forloni, G. (2010). Sirtuins as Novel Targets for Alzheimer's Disease and Other Neurodegenerative Disorders: Experimental and Genetic Evidence. *J. Alzheimers Dis.* 19 (1), 11–26. doi: 10.3233/JAD-2010-1215

Amemiya-Kudo, M., Shimano, H., Hasty, A. H., Yahagi, N., Yoshikawa, T., Matsuzaka, T., et al. (2002). Transcriptional Activities of Nuclear SREBP-1a, -1c, and–2 to Different Target Promoters of Lipogenic and Cholesterogenic Genes. *J. Lipid Res.* 43 (8), 1220–1235. doi: 10.1194/jlr.M100417-JLR200

Aruna, A., Nagarajan, G., and Chang, C. F. (2015). The Acute Salinity Changes Activate the Dual Pathways of Endocrine Responses in the Brain and Pituitary of Tilapia. *Gen. Comp. Endocrinol.* 211, 154–164. doi: 10.1016/j.ygcen.2014.12.005

Azhar, S., Leers-Sucheta, S., and Reaven, E. (2003). Cholesterol Uptake in Adrenal and Gonadal Tissues: The SR-BI and 'Selective' Pathway Connection. *Rev. Front. Biosci.* 8, s998–1029. doi: 10.2741/1165

Babin, P. J., and Vernier, J. M. (1989). Plasma Lipoproteins in Fish. *J. Lipid Res.* 30 (4), 467–489. doi: 10.1016/S0022-2275(20)38342-5

Bertrand, S., Brunet, F. G., Escriva, H., Parmentier, G., Laudet, V., and Robinson-Rechavi, M. (2004). Evolutionary Genomics of Nuclear Receptors: From Twenty-Five Ancestral Genes to Derived Endocrine Systems. *Mol. Biol. Evol.* 21 (10), 1923–1937. doi: 10.1093/molbev/msh200

Binukumari, S., and Vasanthi, J. (2014). Changes in Cholesterol Content of the Freshwater Fish, Labeo Rohita Due to the Effect of an Insecticide 'Encounter' (Herbal Plant Extract). *Int. J. Pharm. Sci.* 5 (2), 397–399. doi: 10.13040/IJPSR.0975-8232

Burg, M. B., Ferraris, J. D., and Dmitrieva, N. I. (2007). Cellular Response to Hyperosmotic Stresses. *Physiol. Rev.* 87 (4), 1441–1474. doi: 10.1152/physrev.00056.2006

Charmandari, E., Tsigos, C., and Chrousos, G. (2005). Endocrinology of the Stress Response. *Annu. Rev. Physiol.* 67, 259–284. doi: 10.1146/annurev.physiol.67.040403.120816

Chen, Y., Li, X., Ye, Q., Tian, J., Jing, R., and Xie, Z. (2011). Regulation of Alpha1 Na/K-ATPase Expression by Cholesterol. *J. Biol. Chem.* 286 (17), 15517–15524. doi: 10.1074/jbc.M110.204396

Choi, J., Mouillesseaux, K., Wang, Z., Fiji, H. D., Kinderman, S. S., Otto, G. W., et al. (2011). Aplexone Targets the HMG-CoA Reductase Pathway and Differentially Regulates Arteriovenous Angiogenesis. *Development.* 138 (6), 1173–1181. doi: 10.1242/dev.054049

Corcos, C. L. J., Gonthier, C., Zaghini, I., Logette, E., Shechter, I., and Bournot, P. (2005). Hepatic Farnesyl Diphosphate Synthase Expression is Suppressed by Polyunsaturated Fatty Acids. *Biochem. J.* 385 (3), 787–794. doi: 10.1042/BJ20040933

Corpet, F. (1988). Multiple Sequence Alignment With Hierarchical Clustering. *Nucleic Acids Res.* 16 (22), 10881–10890. doi: 10.1093/nar/16.22.10881

Cruz-Garcia, L., Minghetti, M., Navarro, I., and Tocher, D. R. (2009). Molecular Cloning, Tissue Expression and Regulation of Liver X Receptor (LXR) Transcription Factors of Atlantic Salmon (*Salmo Salar*) and Rainbow Trout (*Oncorhynchus Mykiss*). *Comp. Biochem. Physiol.* 153 (1), 81–88. doi: 10.1016/j.cbpb.2009.02.001

Dong, S., Kang, M., Wu, X., and Ye, T. (2014). Development of a Promising Fish Model (*Oryzias Melastigma*) for Assessing Multiple Responses to Stresses in the Marine Environment. *BioMed. Res. Int.* 2014, 563131. doi: 10.1155/2014/563131

Dong, X., Tan, P., Cai, Z., Xu, H., Li, J., Ren, W., et al. (2017). Regulation of FADS2 Transcription by SREBP-1 and PPAR-α Influences LC-PUFA Biosynthesis in Fish. *Sci. Rep.* 7, 40024. doi: 10.1038/srep40024

Dong, X., Xu, H., Mai, K., Xu, W., Zhang, Y., and Ai, Q. (2015). Cloning and Characterization of SREBP-1 and PPAR-Alpha in Japanese Seabass *Lateolabrax Japonicus*, and Their Gene Expressions in Response to Different Dietary Fatty Acid Profiles. *Comp. Biochem. Physiol. B Biochem. Mol. Biol.* 180, 48–56. doi: 10.1016/j.cbpb.2014.10.001

Engelking, L. R. (2015). "In Textbook of Veterinary Physiological Chemistry," in *Cholesterol, 3rd ed.*, Waltham, MA, USA: Elsavier doi: 10.1016/C2010-0-66047-0

Farrell, A. P., Saunders, R. L., Freeman, H. C., and Mommsen, T. P. (1986). Arteriosclerosis in Atlantic Salmon: Effects of Dietary Cholesterol and Maturation. *J. Am. Heart Assoc.* 6 (4), 453–461. doi: 10.1161/01.ATV.6.4.453

Feige, N. J., and Auwerx, J. (2007). DisSIRTing on LXR and Cholesterol Metabolism. *Cell Metab.* 6 (5), 343–348. doi: 10.1016/j.cmet.2007.10.003

Goedeke, L., and Fernández-Hernando, C. (2012). Regulation of Cholesterol Homeostasis. *Cell Mol. Life Sci.* 69 (6), 915–930. doi: 10.1007/s00018-011-0857-5

Goldstein, J. L., and Brown, M. S. (1990). Regulation of the Mevalonate Pathway. *Nature.* 343 (6257), 425–430. doi: 10.1038/343425a

Grozinger, C. M., Chao, E. D., Blackwell, H. E., Moazed, D., and Schreiber, S. L. (2001). Identification of a Class of Small Molecule Inhibitors of the Sirtuin Family of NAD-Dependent Deacetylases by Phenotypic Screening. *J. Biol. Chem.* 276 (42), 38837–38843. doi: 10.1074/jbc.M106779200

Hassett, R. P., and Crockett, E. L. (2009). Habitat Temperature Is an Important Determinant of Cholesterol Contents in Copepods. *J. Exp. Biol.* 212 (1), 71–77. doi: 10.1242/jeb.020552

Hazel, J. R., and Williams, E. E. (1990). The Role of Alterations in Membrane Lipid-Composition in Enabling Physiological Adaptation of Organisms to Their Physical-Environment. *Prog. Lipid Res.* 29 (3), 167–227. doi: 10.1016/0163-7827(90)90002-3

Horton, J. D., Goldstein, J. L., and Brown, M. S. (2002). SREBPs: Activators of the Complete Program of Cholesterol and Fatty Acid Synthesis in the Liver. *J. Clin. Investig.* 109 (9), 1125–1131. doi: 10.1172/JCI200215593

Hu, Y. C., Chu, K. F., Yang, W. K., and Lee, T. H. (2017). Na^+, K^+-ATPase β1 Subunit Associates With α1 Subunit Modulating a "Higher-NKA-In-Hyposmotic Media" Response in Gills of Euryhaline Milkfish, *Chanos Chanos*. *J. Comp. Physiol.* 187 (7), 995–1007. doi: 10.1007/s00360-017-1066-9

Hwang, P. P., and Lee, T. H. (2007). New Insights Into Fish Ion Regulation and Mitochondrion-Rich Cells. *Comp. Biochem. physiol. Mol. A Integr. Physiol.* 148 (3), 479–497. doi: 10.1016/j.cbpa.2007.06.416

Hwang, P. P., Lee, T. H., and Lin, L. Y. (2011). Ion Regulation in Fish Gills: Recent Progress in the Cellular and Molecular Mechanisms. *Am. J. Physiol. Regul. Integr. Comp. Physiol.* 301 (1), R28–R47. doi: 10.1152/ajpregu.00047.2011

Ishimoto, K., Tachibana, K., Hanano, I., Yamasaki, D., Nakamura, H., Kawai, M., et al. (2010). Sterol-Regulatory-Element-Binding Protein 2 and Nuclear Factor Y Control Human Farnesyl Diphosphate Synthase Expression and Affect Cell Proliferation in Hepatoblastoma Cells. *Biochem.* 429 (2), 347–357. doi: 10.1042/BJ20091511

Jakobsson, T., Treuter, E., Gustafsson, J., and Steffensen, K. R. (2012). Liver X Receptor Biology and Pharmacology: New Pathways, Challenges and Opportunities. *Trends Pharmacol. Sci.* 33 (7), 394–404. doi: 10.1016/j.tips.2012.03.013

Juo, J. J., Kang, C. K., Yang, W. K., Yang, S. Y., and Lee, T. H. (2016). A Stenohaline Medaka, *Oryzias Woworae*, Increases Expression of Gill Na^+, K^+-ATPase and Na^+, K^+, $2Cl^-$ Cotransporter 1 to Tolerate Osmotic Stress. *Zool. Sci.* 33, 414–425. doi: 10.2108/zs150157

Kang, C. K., Tsai, S. C., Lee, T. H., and Hwang, P. P. (2008). Differential Expression of Branchial Na^+/K^+-ATPase of Two Medaka Species, *Oryzias Latipes* and *Oryzias Dancena*, With Different Salinity Tolerances Acclimated to Fresh Water, Brackish Water and Seawater. *CBP. A Mol. Integr. Physiol.* 151 (4), 566–575. doi: 10.1016/j.cbpa.2008.07.020

Kemper, J. K., Choi, S. E., and Kim, D. H. (2013). Sirtuin 1 Deacytylase: A Key Regulator of Hepatic Lipid Metabolism. *Vitam. Horm.* 91, 385–404. doi: 10.1016/B978-0-12-407766-9.00016-X

Kemski, M. M., Rappleye, C. A., Dabrowski, K., Bruno, R. S., and Wick, M. (2020). Transcriptomic Response to Soybean Meal-Based Diets as the First Formulated Feed in Juvenile Yellow Perch (Perca Flavescens). *Sci. Rep.* 10 (1), 3998. doi: 10.1038/s41598-020-59691-z

Khan, M. G. (2005). *Encyclopedia of Heart Diseases*, Waltham, MA, USA: Elsavier

Kortner, T. M., Björkhem, I., Krasnov, A., Timmerhaus, G., and Krogdahl, A. (2014). Dietary Cholesterol Supplementation to a Plant-Based Diet Suppresses the Complete Pathway of Cholesterol Synthesis and Induces Bile Acid Production in Atlantic Salmon (*Salmo Salar* L.). *Br. J. Nutr.* 111 (12), 2089–2103. doi: 10.1017/S0007114514000373

Kroes, J., and Ostwald, R. (1971). Erythrocyte Membranes–Effect of Increased Cholesterol Content on Permeability. *BBA.* 249 (2), 647–650. doi: 10.1016/0005-2736(71)90147-7

Lambropoulos, N., Garcia, A., and Clarke, R. ,. J. (2016). Stimulation of Na^+,K^+-ATPase Activity as a Possible Driving Force in Cholesterol Evolution. *J. Membr Biol.* 249 (3), 251–259. doi: 10.1007/s00232-015-9864-z

Lang, F., Ritter, M., Gamper, N., Huber, S., Fillon, S., Tanneur, V., et al. (2000). Cell Volume in the Regulation of Cell Proliferation and Apoptotic Cell Death. *Cell. Physiol. Biochem.* 10, 417–428. doi: 10.1159/000016367

Lee, G. M. D. (2020). *Disorders of Lipid Metabolism* (Goldman-Cecil Medicine), 1346. New York, USA: Elsavier

Li, S., Monroig, O., Wang, T., Yuan, Y., Navarro, J. C., Hontoria, F., et al. (2017). Functional Characterization and Differential Nutritional Regulation of Putative Elovl5 and Elovl4 Elongases in Large Yellow Croaker (*Larimichthys Crocea*). *Sci. Rep.* 7 (1), 3514–3528. doi: 10.1038/s41598-017-02646-8

Lin, Y. T., Hu, Y. C., Wang, Y. C., Hsiao, M. Y., Lorin-Nebel, C., and Lee, T. H. (2021). Differential Expression of Two ATPases Revealed by Lipid Raft Isolation From Gills of Euryhaline Teleosts With Different Salinity Preferences. *Comp. Biochem. Physiol. - B Biochem. Mol. Biol.* 253, 110562. doi: 10.1016/j.cbpb.2021.110562

Lin, C. H., Yeh, P. L., Wang, Y. C., and Lee, T. H. (2021). Dynamic Regulation of Ions and Amino Acids in Adult Asian Hard Clams *Meretrix Lusoria* Upon Hyperosmotic Salinity. *Front. Mar. Sci.* 8. doi: 10.3389/fmars.2021.749418

Liu, Z., Ma, A., Yuan, C., Zhao, T., Chang, H., and Zhang, J. (2021). Transcriptome Analysis of Liver Lipid Metabolism Disorders of the Turbot *Scophthalmus Maximus* in Response to Low Salinity Stress. *Aquaculture* 534, 736273. doi: 10.1016/j.aquaculture.2020.736273

Livak, K. J., and Schmittgen, T. D. (2001). Analysis of Relative Gene Expression Data Using Real Time Quantitative PCR and the 2-ΔΔct. *Method.* 25 (4), 402–408. doi: 10.1006/meth.2001.1262

Li, X., Zhang, S., Blander, G., Tse, J. G., Krieger, M., and Guarente, L. (2007). SIRT1 Deacetylates and Positively Regulates the Nuclear Receptor LXR. *Nat. Rev. Mol. Cell Biol.* 28 (1), 91–106. doi: 10.1016/j.molcel.2007.07.032

Minghetti, M., Leaver, M. J., and Tocher, D. R. (2011). Transcriptional Control Mechanisms of Genes of Lipid and Fatty Acid Metabolism in the Atlantic Salmon (*Salmo Salar* L.) Established Cell Line, SHK-1. *Int. J. Biochem.* 811 (3), 194–202. doi: 10.1016/j.bbalip.2010.12.008

Mohamed, A. S., Md, A. E., and Desoky, N. S. G. (2019). The Changes in Triglyceride and Total Cholesterol Concentrations in the Liver and Muscle of Two Fish Species From Qarun Lake, Egypt. *Fish. Oceanogr.* 9 (4), 86–90. doi: 10.19080/OFOAJ.2019.09.555770

Papahadjopoulosa, D., Nira, S., and Ohki, S. (1972). Permeability Properties of Phospholipid Membranes: Effect of Cholesterol and Temperature. *BBA.* 266 (3), 561–583. doi: 10.1016/0006-3002(72)90001-7

Parasassi, T., Giusti, A. M., Raimondi, M., Ravagnan, G., Sapora, O., and Gratton, E. (1995). Cholesterol Protects the Phospholipid Bilayer From Oxidative Damage. *Free Radic. Biol. Med.* 19 (4), 511–516. doi: 10.1016/0891-5849(95)00038-y

Peet, D. J., Janowski, B. A., and Mangelsdorf, D. J. (1998). The LXRs: A New Class of Oxysterol Receptors. *Curr. Opin. Genet. Dev.* 8 (5), 571–575. doi: 10.1016/S0959-437X(98)80013-0

Ponugoti, B., Kim, D. H., Xiao, Z., Smith, Z., Miao, J., Zang, M., et al. (2010). SIRT1 Deacetylates and Inhibits SREBP-1C Activity in Regulation of Hepatic Lipid Metabolism. *J. Biol. Chem.* 285 (44), 33959–33970. doi: 10.1074/jbc.M110.122978

Repa, J. J., Liang, G., Ou, J., Bashmakov, Y., and Lobaccaro, J. M. (2000). Regulation of Mouse Sterol Regulatory Element-Binding Protein-1c Gene (SREBP-1c) by Oxysterol Receptors, Lxrα and Lxrβ. *Genes Dev.* 14 (22), 2819–2830. doi: 10.1101/gad.844900

Roya, L. A., Davisa, D. A., and Saoud, A. P. (2006). Effects of Lecithin and Cholesterol Supplementation to Practical Diets for *Litopenaeus Vannamei* Reared in Low Salinity Waters. *Aquac.* 257, 446–452. doi: 10.1016/j.aquaculture.2006.02.059

Scheiner-Bobis, G. (2002). The Sodium Pump. Its Molecular Properties and Mechanics of Ion Transport. *Eur. J. Biochem.* 269, 2424–2433. doi: 10.1046/j.1432-1033.2002.02909.x

Schultz, J. R., Tu, H., Luk, A., Repa, J. J., Medina, J. C., Li, L., et al. (2000). Role of LXRs in Control of Lipogenesis. *Genes Dev.* 14 (22), 2831–2838. doi: 10.1101/gad.850400

Sharpe, L. J., and Brown, A. J. (2013). Controlling Cholesterol Synthesis Beyond 3-Hydroxy-3-Methylglutaryl-CoA Reductase (HMGCR). *J. Biol. Chem.* 288, 18707–18715. doi: 10.1074/jbc.R113.479808

Shimano, H., Shimomura, I., Hammer, R. E., Herz, J., Goldstein, J. L., Brown, M. S., et al. (1997). Elevated Levels of SREBP-2 and Cholesterol Synthesis in Livers of Mice Homozygous for a Targeted Disruption of the SREBP-1 Gene. *J. Clin. Invest.* 100 (8), 2115–2124. doi: 10.1172/JCI119746

Si, Y., Wen, H., Li, Y., He, F. H., Li, J., Li, S., et al. (2018). Liver Transcriptome Analysis Reveals Extensive Transcriptional Plasticity During Acclimation to Low Salinity in *Cynoglossus Semilaevis*. *BMC Genom.* 19 (1), 464. doi: 10.1186/s12864-018-4825-4

Smith, J. R., Osborne, T. F., Brown, M. S., Goldstein, J. L., and Gil, G. (1988). Multiple Sterol Regulatory Elements in Promoter for Hamster 3-Hydroxy-3-Methylglutaryl-Coenzyme A Synthase. *J. Biol. Chem.* 263 (34), 18480–18487. doi: 10.1016/S0021-9258(19)81383-2

Sundqvist, A., Bengoechea-Alonso, M. T., Ye, X., Lukiyanchuk, V., Jin, J., Harper, J. W., et al. (2005). Control of Lipid Metabolism by Phosphorylation-Dependent Degradation of the SREBP Family of Transcription Factors by SCF^{Fbw}. *Cell Metab.* 1 (6), 379–391. doi: 10.016/j.cmet.2005.04.010

Thomas, J. K., Wiseman, S., Giesy, J. P., and Janz, D. M. (2013). Effects of Chronic Dietary Selenomethionine Exposure on Repeat Swimming Performance, Aerobic Metabolism and Methionine Catabolism in Adult Zebrafish (*Danio Rerio*). *Aquat. Toxicol.* 130–131, 112–122. doi: 10.1016/j.aquatox.2013.01.009

Twibell, R. G., and Wilson, R. P. (2004). Preliminary Evidence That Cholesterol Improves Growth and Feed Intake of Soybean Meal-Based Diets Inaquaria Studies With Juvenile Channel Catfsh, *Ictalurus Punctatus*. *Aquat* 236 (1-4), 539–546. doi: 10.1016/j.aquaculture.2003.10.028

Vassilopoulos, A., Fritz, K. S., Petersen, D. R., and Gius, D. (2011). The Human Sirtuin Family: Evolutionary Divergences and Functions. *Hum. Genomics* 5 (5), 485–496. doi: 10.1186/1479-7364-5-5-485

Walker, A. K., Yang, F., Jiang, K., Ji, J. Y., Jennifer, L., Watts, J. L., et al. (2010). Conserved Role of SIRT1 Orthologs in Fasting-Dependent Inhibition of the Lipid/Cholesterol Regulator SREBP. *Genes Dev.* 24 (13), 1403–1417. doi: 10.1101/gad.1901210

Wang, X., Sato, R., Brown, M. S., Hua, X., and Goldstein, J. L. (1994). SREBP-1, a Membrane-Bound Transcription Factor Released by Sterol-Regulated Proteolysis. *Cell.* 77 (1), 53–62. doi: 10.1016/0092-8674(94)90234-8

Wen, X., Peng, C., Xu, J., Wei, X., Fu, D., Wang, T., et al. (2021). Combined Effects of Low Temperature and Salinity on the Immune Response, Antioxidant Capacity and Lipid Metabolism in the Pufferfish (*Takifugu Fasciatus*). *Aquac.* 531, 735866. doi: 10.1016/j.aquaculture.2020.735866

Xue, L., Qi, H., Zhang, H., Ding, L., Huang, Q., Zhao, D., et al. (2020). Targeting SREBP-2-Regulated Mevalonate Metabolism for Cancer Therapy. *Front. Oncol.* 21 (10). doi: 10.3389/fonc.2020.01510

Xu, C., Li, E., Xu, Z., Su, Y., Lu, M., Qin, J. G., et al. (2018). Growth and Stress Axis Responses to Dietary Cholesterol in Nile Tilapia (*Oreochromis Niloticus*) in Brackish Water. *Front. Physiol.* 26 (9), 254. doi: 10.3389/fphys.2018.00254

Yang, W. K., Kang, C. K., Chang, C. H., Hsu, A. D., Lee, T. H., and Hwang, P. P. (2013). Expression Profiles of Branchial FXYD Proteins in the Brackish Medaka *Oryzias Dancena*: A Potential Saltwater Fish Model for Studies of Osmoregulation. *PloS One* 8 (1), e55470. doi: 10.1371/journal.pone.0055470

Yun, B., Ai, Q., Mai, K., Xu, W., Qi, G., and Luo, Y. (2012). Synergistic Efects of Dietary Cholesterol and Taurine on Growth Performance and Cholesterol Metabolism in Juvenile Turbot (*Scophthalmus Maximus* L.) Fed High Plant Protein Diets. *Aquac.* 324 (325), 85–91. doi: 10.1016/j.aquaculture.2011.10.012

Yun, B., Mai, K., Zhang, W., and Xu, W. (2011). Effects of Dietary Cholesterol on Growth Performance, Feed Intake and Cholesterol Metabolism in Juvenile Turbot (*Scophthalmus Maximus* L.) Fed High Plant Protein Diets. *Aquac.* 495, 443–451. doi: 10.1016/j.aquaculture.2018.06.002

Yusof, S., Ismail, A., Koito, T., Kinoshita, M., and Inoue, K. (2011). Occurrence of Two Closely Related Ricefishes, Javanese Medaka (*Oryzias Javanicus*) and Indian Medaka (O. Dancena) at Sites With Different Salinity in Peninsular Malaysia. Environ. *Biol. Fishes.* 93 (1), 43–49. doi: 10.1007/s10641-011-9888-x

Zhang, J., Li, X., Yu, H., Larre, I., Dube, P. R., Kennedy, D., et al. (2020). Regulation of Na/K-ATPase Expression by Cholesterol: Isoform Specificity and the Molecular Mechanism. *Am. J. Physiol. Cell Physiol.* 319 (6), C1107–C1119. doi: 10.1152/ajpcell.00083.2020

Zhang, Q., You, C., Liu, F., Zhu, W., Wang, S., Xie, D., et al. (2016). Cloning and Characterization of Lxr and Srebp1, and Their Potential Roles in Regulation of LC-PUFA Biosynthesis in Rabbitfish *Siganus Canaliculatus*. *Lipids* 51, 1051–1063. doi: 10.1007/s11745-016-4176-3

Zhao, C., and Dahlman-Wright, K. (2010). Liver X Receptor in Cholesterol Metabolism. *J. Endocrinol.* 204 (3), 233–240. doi: 10.1677/JOE-09-0271

Zhu, T., Corraze, G., Juan, E. P., Quillet, E., Nivet, M. D., and Cassy, S. S. (2018). Regulation of Genes Related to Cholesterol Metabolism in Rainbow Trout (*Oncorhynchus Mykiss*) Fed a Plant-Based Diet. *Am. J. Physiol.* 314 (1), R58–R70. doi: 10.1152/ajpregu.00179

Conflict of Interest: The authors declare that the research was conducted in the absence of any commercial or financial relationships that could be construed as a potential conflict of interest.

Publisher's Note: All claims expressed in this article are solely those of the authors and do not necessarily represent those of their affiliated organizations, or those of the publisher, the editors and the reviewers. Any product that may be evaluated in

this article, or claim that may be made by its manufacturer, is not guaranteed or endorsed by the publisher.

frontiers | Frontiers in Physiology

ORIGINAL RESEARCH
published: 01 June 2022
doi: 10.3389/fphys.2022.913800

Dietary Supplementation With Hydroxyproline Enhances Growth Performance, Collagen Synthesis and Muscle Quality of *Carassius auratus* Triploid

*Shenping Cao[1], Yangbo Xiao[1], Rong Huang[1], Dafang Zhao[1], Wenqian Xu[1], Shitao Li[1], Jianzhou Tang[1], Fufa Qu[1], Junyan Jin[2], Shouqi Xie[2] and Zhen Liu[1]**

[1]Hunan Provincial Key Laboratory of Nutrition and Quality Control of Aquatic Animals, Department of Biological and Environmental Engineering, Changsha University, Changsha, China, [2]State Key Laboratory of Freshwater Ecology and Biotechnology, Institute of Hydrobiology, Chinese Academy of Sciences, Wuhan, China

OPEN ACCESS

Edited by:
Qingchao Wang,
Huazhong Agricultural University, China

Reviewed by:
Houguo Xu,
Chinese Academy of Fishery Sciences (CAFS), China
Shuyan Chi,
Guangdong Ocean University, China
Madison Powell,
University of Idaho, United States

***Correspondence:**
Zhen Liu
liuzhen_2015@sina.com

Specialty section:
This article was submitted to Aquatic Physiology, a section of the journal Frontiers in Physiology

Received: 06 April 2022
Accepted: 05 May 2022
Published: 01 June 2022

Citation:
Cao S, Xiao Y, Huang R, Zhao D, Xu W, Li S, Tang J, Qu F, Jin J, Xie S and Liu Z (2022) Dietary Supplementation With Hydroxyproline Enhances Growth Performance, Collagen Synthesis and Muscle Quality of Carassius auratus Triploid. Front. Physiol. 13:913800. doi: 10.3389/fphys.2022.913800

An eight-week experiment was undertaken to examine the effect of dietary hydroxyproline (Hyp) supplementation on growth performance, collagen synthesis, muscle quality of an improved triploid crucian carp (*Carassius auratus* Triploid) (ITCC). Six isonitrogenous (340 g/kg diet), isolipidic (60 g/kg diet) and isocaloric (17.80 MJ/kg diet) diets were formulated containing a certain amount of Hyp: 0.09% (the control group), 0.39, 0.76, 1.14, 1.53 and 1.90%. Each diet was randomly assigned to three tanks and each group was fed two times daily until apparent satiation. The results showed that growth performance and feed utilization of ITCC were significantly improved with the dietary Hyp level was increased from 0.09 to 0.76%. Crude protein, threonine and arginine content in the dorsal muscle in 0.76% hydroxyproline group were significantly higher than those in basic diet group ($p < 0.05$). The muscle textural characteristics increased remarkably with the amount of Hyp in the diet rising from 0.09 to 1.53% ($p < 0.05$). Meanwhile, the contents of type I collagen (Col I) and Pyridinium crosslink (PYD) in the muscle of fish were significantly increased by dietary Hyp ($p < 0.05$). The muscle fiber diameter and density of the fish were significantly increased when fed with 0.76% Hyp ($p < 0.05$). Furthermore, dietary supplementation with an appropriate concentration of Hyp substantially increased the expression of genes involved in collagen synthesis (*col1a1*, *col1a2*, *p4hα1*, *p4hβ*, *smad4*, *smad5*, *smad9,* and *tgf-β*) and muscle growth (*igf-1*, *tor*, *myod*, *myf5,* and *myhc*) ($p < 0.05$). In conclusion, dietary supplementation of Hyp can enhance fish growth performance, collagen production, muscle textural characteristics and muscle growth of ITCC. According to the SGR broken-line analysis, the recommended supplementation level of Hyp was 0.74% in the diet for ITCC, corresponding to 2.2% of dietary protein.

Keywords: hydroxyproline, growth performance, collagen synthesis, muscle texture, Carassius auratus triploid

INTRODUCTION

Fish meal has always been utilized as a preferred protein source due to its high protein content, excellent essential amino acid composition (EAA) and easy digestibility (Daniel, 2018). However, the limited supply of fish meal around the world has been unable to keep up with the fast development of global aquaculture, resulting in global rising of fish meal price year by year (Fawole et al., 2021). As a result, appropriate plant-derived alternative protein sources have received more and more attention. However, poor growth occurs when some farmed fish are fed diets that include high levels of plant ingredients (Chen et al., 2019b; Liu et al., 2020). Some researchers believed that the deficiency of some amino acids in plant protein feed is an important reason leading to the decrease of growth performance in fish, such as lysine, methionine and hydroxyproline (Hyp) (Hua et al., 2019; Clark et al., 2020).

Hydroxyproline (Hyp), extensively prevalent in marine and animal feedstuffs but mostly absent in plant-based source (Zhang et al., 2015). The hydroxylation of proline residues in protein (mainly collagen) results in the formation of Hyp via prolyl hydroxylase on the endoplasmic reticulum (Li and Wu, 2018). Always, Hyp is known to be a substrate for the production of glucose hydroxyproline, pyruvate and glycine (Li et al., 2009). And it is a conditionally-essential amino acid in aquatic organisms (Wu et al., 2011). So far, some studies in marine carnivorous fish have found that Hyp has different effects on the growth performance of cultured fish. For example, Rong et al. (2020b) discovered that supplementing Hyp in a high plant-protein diet substantially enhanced growth and vertebral development of chu's croaker (*Nibea coibor*). The growth-related indicators were substantially positively linked with the dietary Hyp levels for Atlantic salmon (*Salmo salar* L.) (Kousoulaki et al., 2009). However, a different result was found in Atlantic salmon that dietary supplementation of different contents of Hyp had no significant effect on growth performance and feed efficiency of fish (Zhang et al., 2013).

Skeletal muscle, composed of muscle fibers and intramuscular connective tissue, is the most palatable portion of fish flesh (Listrat et al., 2016). Collagen, the primary component of intramuscular connective tissue, helps maintain tissue stability and structural integrity and is directly related to muscle hardness and muscle quality (Palka, 1999). In vertebrates, roughly 99.8% of Hyp is located in collagen (Barbul, 2008). Hyp is key to forming triple-helical molecules, which helps to maintain the integrity of collagen fibrils and increases protein heat stability (Gelse et al., 2003; Li and Wu, 2018). Muscle texture is a conventional indicator used in the evaluation of fish flesh quality. Besides collagen concentration, the muscle texture of fish is also remarkably affected by collagen crosslink (Hansen et al., 2007). Research on Atlantic salmon revealed a strong positive correlation between pyridinium crosslink (PYD) content and muscle stiffness (Johnston et al., 2006). Also, the appropriate amount of Hyp can greatly improve the dorsal muscle textural characteristics, and collagen formation was found to be significantly correlated to the levels of PYD, prolyl 4-hydroxylase (P4H) and lysyl hydroxylase (LH) in the muscle of large yellow croaker (*Larimichthys crocea*) (Wei et al., 2016).

TABLE 1 | Formulation and chemical composition of the experimental diets for ITCC (% dry matter).

Ingredients	Dietary Hyp Level (%)					
	0.09	**0.39**	**0.76**	**1.14**	**1.53**	**1.90**
L-Hydroxyproline[1]	0.00	0.40	0.80	1.20	1.60	2.00
Fish meal[2]	0.50	0.50	0.50	0.50	0.50	0.50
Soybean meal[2]	22.00	22.00	22.00	22.00	22.00	22.00
Rapeseed meal[2]	19.00	19.00	19.00	19.00	19.00	19.00
Cottonseed meal[2]	16.00	16.00	16.00	16.00	16.00	16.00
Wheat flour	13.00	13.00	13.00	13.00	13.00	13.00
Soybean oil	3.70	3.70	3.70	3.70	3.70	3.70
α-starch	4.00	4.00	4.00	4.00	4.00	4.00
Corn starch	8.00	8.00	8.00	8.00	8.00	8.00
Choline chloride	0.50	0.50	0.50	0.50	0.50	0.50
Vitamin premix[3]	1.00	1.00	1.00	1.00	1.00	1.00
Mineral premix[4]	2.00	2.00	2.00	2.00	2.00	2.00
CMC	3.00	3.00	3.00	3.00	3.00	3.00
$Ca(H_2PO_4)_2$	1.00	1.00	1.00	1.00	1.00	1.00
Cellulose	4.30	4.30	4.30	4.30	4.30	4.30
Alanine[5]	2	1.60	1.20	0.80	0.40	0.00
Hydroxyproline	0.09	0.39	0.76	1.14	1.53	1.90
Crude protein	34.71	34.58	33.99	34.14	34.01	33.74
Crude lipid	5.87	5.82	5.79	6.00	5.96	6.10
Moisture	8.32	8.09	8.12	8.09	7.74	7.60
Ash	8.93	8.88	8.66	8.61	8.68	8.62
Total phosphorus	0.90	0.97	0.96	0.91	0.87	0.94
Total calcium	0.55	0.54	0.55	0.53	0.52	0.50
Gross energy (MJ/kg)	17.87	17.94	18.04	17.72	17.75	18.14

[1]L-Hydroxyproline: Purchased from Sigma-Aldrich Co. Ltd (United States).
[2]All of these ingredients were supplied by Hunan Zhenghong Science and Technology Develop Co., Ltd., China. Fish meal, crude protein: 68.87%, crude lipid: 10.47%; Soybean meal, crude protein: 48.57%, crude lipid: 1.40%; Rapeseed meal, crude protein: 44.37%, crude lipid: 2.63%; Cottonseed meal, crude protein: 54.60%, crude lipid: 2.02%.
[3]Vitamin premix (mg/kg diet): Vitamin B_1, 20; Vitamin B_2, 20; Vitamin B_6, 20; Vitamin B_{12}, 0.02; folic acid, 5; calcium pantothenate, 50; inositol, 100; niacin, 100; biotin, 0.1; Vitamin A, 11; Vitamin D, 2; Vitamin E, 50; Vitamin K, 10; Vitamin C, 100; cellulose, 3,412.
[4]Mineral premix (mg/kg diet): NaCl, 500.0; $MgSO_4{\cdot}7H_2O$, 8,155.6; $NaH_2PO_4{\cdot}2H_2O$, 12500.0; KH_2PO_4, 16000.0; $CaHPO_4{\cdot}2H_2O$, 7,650.6; $FeSO_4{\cdot}7H_2O$, 2286.2; $C_6H_{10}CaO_6{\cdot}5H_2O$, 1750.0; $ZnSO_4{\cdot}7H_2O$, 178.0; $MnSO_4{\cdot}H_2O$, 61.4; $CuSO_4{\cdot}5H_2O$, 15.5; $CoSO_4{\cdot}7H_2O$, 0.91; KI, 1.5; Na_2SeO_3, 0.60; Corn starch, 899.7.
[5]Alanine: Purchased from Sigma-Aldrich Co. Ltd (United States).

Furthermore, several investigations in mammals have indicated that the transforming growth factor-beta/SMAD family proteins (TGF-β/Smads) pathway is the primary signaling pathway controlling collagen production, especially the production of type I collagen (Yano et al., 2012; Xu et al., 2016). In contrast, the connection between the TGF-β/Smads pathway and type I collagen in fish is not entirely understood.

Muscle development is a complicated adaptive process that involves both developing new muscle fibers (hyperplasia) and expanding existing muscle fibers (hypertrophy), and it is regulated by a number of elements, including insulin-like growth factor I (IGF-1), myogenic regulators (MRFs) and myosin heavy chain (MyHC) (Rowlerson and Veggetti, 2001). Investigations *in vitro* and *in vivo* have shown that IGF-1, a major regulatory hormone governing vertebrate development, may increase the proliferation and differentiation of myoblasts and induce myotube hypertrophy (Zanou and Gailly, 2013). MRFs are muscle-specific basic helix-loop-helix transcription factors that govern the production of certain proteins throughout the cellular

TABLE 2 | Amino acid profile of the experimental diets for 8 weeks (% dry matter).

Ingredients	Dietary Hyp Level (%)					
	0.09	**0.39**	**0.76**	**1.14**	**1.53**	**1.90**
Essential amino acid						
Threonine	1.01	1.00	0.98	0.98	0.98	0.96
Phenylalanine	1.32	1.30	1.32	1.32	1.31	1.30
Valine	1.17	1.17	1.17	1.15	1.18	1.16
Isoleucine	1.16	1.17	1.16	1.15	1.17	1.16
Leucine	1.99	2.01	1.98	1.99	1.97	1.97
Methionine	0.29	0.29	0.30	0.28	0.29	0.28
Arginine	2.06	2.10	2.09	2.08	2.07	2.05
Lysine	1.46	1.48	1.48	1.45	1.43	1.40
Histidine	0.71	0.71	0.71	0.73	0.70	0.70
Tryptophan	ND[1]	ND	ND	ND	ND	ND
Non-essential amino acid						
Aspartic acid	2.38	2.39	2.39	2.38	2.37	2.37
Serine	1.30	1.33	1.30	1.32	1.30	1.29
Glutamic acid	5.23	5.24	5.26	5.22	5.22	5.20
Glycine	1.17	1.16	1.16	1.14	1.15	1.16
Alanine	2.69	2.30	1.87	1.50	1.12	0.84
Tyrosine	0.74	0.75	0.75	0.75	0.76	0.74
Proline	1.47	1.48	1.46	1.48	1.46	1.45

[1]*ND: not determined.*

differentiation and determination process (Hernández-Hernández et al., 2017). Myogenic factor 5 (Myf5) and myogenic differentiation antigen (MyoD) as representative transcription factors of MRFs are mainly involved in the initial proliferation process of myoblasts and the directional completion of myogenic cells (Zammit, 2017). Also, MyHC has essential regulatory effects on muscle fiber types and muscle specificity (Song et al., 2020). According to the recent research in turbot (*Scophthalmus maximus*), rich-Hyp fish meal hydrolysate can enhance muscle growth by modulating the expressions of genes related muscle growth, including *myod*, *myf5*, and *mrf4* (Wei et al., 2020). Nevertheless, the precise role of Hyp in regulating muscle development in fish remains unknown.

Carassius auratus Triploid is obtained from the crossing of red crucian carp (*Carassius auratus* red var.) × common carp (*Cyprinus carpio* L.) allotetraploid hybrids (♂) with the diploid Japanese crucian carp (♀) (*Carassius auratus cuvieri* T. et S.) (Chen et al., 2009). Because of its advantages of fast growth speed, strong stress tolerance and delicious flesh quality, ITCC is the preferred species of crucian carp in freshwater aquaculture in China (Fu et al., 2021). Up to now, some studies have reported that Hyp can promote growth and improve muscle quality in carnivorous marine fish, whereas Hyp's potential for the same effect on omnivorous freshwater fish remains unknown. Therefore, ITCC was used as a model in this study to evaluate the dietary requirements of Hyp and its effects on growth performance, collagen production, muscle texture and muscle fiber development.

MATERIALS AND METHODS

Experimental Diets

Table 1 shows the formulation and chemical composition of the experimental diets. Crystalline L-hydroxyproline (Hyp, >99% pure) was purchased from Sigma-Aldrich Co. Ltd. (United States). Six isonitrogenous (340 g/kg diet), isolipidic (60 g/kg diet) and isocaloric (17.80 MJ/kg diet) diets were formulated with graded levels of Hyp: 0% (control group), 0.4%, 0.8%, 1.2%, 1.6 and 2.0%, respectively. Using high-performance liquid chromatography (LC-6AD, Shimadzu Corporation, Japan), the amounts of Hyp in the diet contents were measured, and the final Hyp contents in each diet were 0.09%, 0.39%, 0.76%, 1.14%, 1.53% and 1.90%, respectively. Protein sources included fishmeal, rapeseed meal, cottonseed meal, soybean meal and wheat flour; soybean oil for a lipid source; corn starch and α-starch for the main carbohydrate sources. All feed components were passed through a 40-mesh sieve before thoroughly combined with 10% distilled water for 10 min, then the wet dough was extruded into 2 mm pellets using a laboratory granulator (SZLH200, Jiangsu Zhengchang Group Co. Ltd., China). The feed pellets were gradually dried in the air before being kept in separate sealed plastic bags at 4 C till usage. **Table 2** shows the amino acid composition of the experimental diets.

Fish and Feeding Trial

About 1,000 ITCC were purchased from the Fisheries Research Institute of Hunan Province (Changsha, Hunan, China). All the fish were soaked in 4% saline for 20 min before being transferred to the indoor recirculating aquaculture system. Two weeks prior to the formal experiment, all fish were cultured in two cylindrical fiberglass tanks (1,500 L) and fed the compound feed (a combination of six experimental diets) twice daily (9: 00 and 15: 00) to make fish adapt to the experimental feeds and feeding frequency.

Subsequently, all fish were fasted for 24 h before the feeding trial began. Four hundred and fourteen acclimatized fish with the similar size (initial body weight: 15.01 ± 0.05 g) and apparent health were weighed and randomly divided into 18 fiberglass tanks (100 L). With a density of 23 fish per tank, triplicate tanks were randomly assigned to each of the six experimental diets. Fish in all the groups were fed to apparent satiation, twice daily at 9: 00 and 15: 00 h for an 8-weeks feeding trial.

The water flowed into each tank at a constant rate of 1,200 ml min^{-1}. During the feeding study, dissolved oxygen and ammonia nitrogen in the experimental system and the experimental tank were determined once a week, the water temperature and pH were measured once a day. The dissolved oxygen was greater than 7.0 mg L^{-1}, and the ammonia nitrogen level was below 0.1 mg kg^{-1}. The water temperature was kept constant at 27.1 ± 2.9°C, while the pH ranged between 6.5 and 7.0. Furthermore, the photoperiod of this experiment was regularly controlled for a 12 h light-dark cycle (light from 8: 00 to 20: 00).

Sample Collection

Preceding the feeding trial, 30 fish were randomly selected and separated into three sample groups (10 fish per sample group) for the initial examination of body composition. All fish from each tank were starved for 24 h at the end of the feeding experiment, then netted out and sedated with 50 mg L^{-1} MS-222 (tricaine methane sulfonate, Sigma-Aldrich, United States). Four fish were

sampled in triplicate for final body composition analysis. Blood samples were drawn from the caudal vein with heparinized syringes, centrifuged at 3,000 g for 10 min, and kept at −80°C in a refrigerator. Following blood collection, the fish were dissected on ice to obtain the tissues of skin, liver and vertebrae for further detection of Hyp, and the muscle for detection of Hyp, biochemical composition, related enzymes as well as gene expressions analysis. Dorsal muscle of four fish from each tank were dissected on ice for texture analysis, also, dorsal muscle of another two fish were collected and fixed in a 4% paraformaldehyde solution for further histological analysis.

Biochemical Analysis

The Association of Official Analytical Chemists' technique was used to assess the approximate composition of the diets, dorsal muscle and whole fish samples (AOAC, 2005). The crude protein was measured using a Kjeltec 8,400 Analyzer Unit machine (FOSS Tecator, Haganas, Sweden), and the crude lipid was determined using the Soxtec ST 243 system (FOSS, Sweden). Moisture was determined by drying at 105°C in an oven to constant weight, and ash content was determined by burning for 3 h in a muffle furnace at 550°C. An automated adiabatic oxygen bomb calorimeter was used to measure the gross energy (Phillipson Microbomb Calorimeter, Gentry Instructions Inc., Aiken, United States), and the dietary and dorsal muscle total amino acid (TAA) was determined using high-performance liquid chromatography (LC-6AD, Shimadzu Corporation, Japan).

Hydroxyproline Determination

The muscle, skin, liver and vertebrae of ITCC were dissected and diluted in a solution of 0.67% physiological saline. The tissues were then crushed and homogenized using a high-speed tissue grinding device (KZ-II, Wuhan Servicebio technology, China) and centrifuged at 5,000 g for 10 min at 4 C. The Hyp content was determined using the isolated supernatant. The method used to calculate Hyp was modified somewhat from that used by Wei et al. (2016). Aliquots of 1 ml standard Hyp were prepared from a stock solution of Hyp (Sigma-Aldrich Corp., United States). 1 ml standard Hyp (1–50 μg/ml) or 1 ml of hydrolysed tissue sample (plasma, muscle and other tissues) were mixed with 2 ml buffered chloramines T reagent and incubated at room temperature for 30 min. Following incubation, 2 ml perchloric acid (dilute 27 ml 70% perchloric acid to a 100 ml solution) was added to the mixture and incubated for another 5 min at room temperature. The mixture was then heated at 60 C for 20 min with 2 ml of P-DMAB solution. Upon cooling, the absorbance was measured at 560 nm, and the concentration of Hyp was calculated using a standard curve.

The Type I Collagen, Pyridinium Crosslink, Prolyl 4-Hydroxylase and Lysyl Hydroxylase Assay

The type I collagen (Col I), pyridinium crosslink (PYD), prolyl 4-hydroxylase (P4H) and lysyl hydroxylase (LH) levels in dorsal muscle of ICTT were measured using a biotin double antibody sandwich ELISA kit (Nanjing Jiancheng Bioengineering Institute, Nanjing, Jiangsu, China) according to the manufacturer's instructions, respectively.

Muscle Texture Analysis

For the muscle texture examination, three fish from each tank were selected. From the dorsal muscles on both sides above the lateral line and below the dorsal fin of each fish, two pieces fillets was gently removed for texture analysis using a texture analyzer (TMS-PRO, Food Technology Corporation, America). The texture profile analyses (TPA) parameters were built using double compression. The compression ratio of the muscle sample was 60%, and the test speed was 1 mm/s. Each sample's textural characteristics such as chewiness, springiness, hardness, adhesiveness, cohesiveness and gumminess were calculated via the force-time curve produced using the computer software, Texture Lab Pro (1.18-408, FTC, America).

Histological Analysis

The histological examination of muscle samples was carried out in accordance with the previously reported technique (Cao et al., 2021). In brief, the muscle samples were cut into rectangular muscle blocks measuring 3 mm × 3 mm × 10 mm along the lateral line, fixed in 4% paraformaldehyde solution for 24 h, and then dried in 70% ethanol. The samples were embedded in paraffin wax after being dehydrated with varying amounts of ethanol and xylene. Sagittal sections with a thickness of 5 μm were taken from each sample, which were then dewaxed with xylene and stained with hematoxylin-eosin (H&E). The image analysis program Image-pro Plus was used to measure the muscle fiber diameter (DI) and density (DO) of sections. For each sample, eight microscopic fields were investigated at random. The contour of 150-250 muscle fibers in each microscopic field was digitized by Image Analysis System, and the diameter of muscle fibers was calculated. The number of fibers per mm^2 of muscle cross-sectional area was used to calculate fiber density.

Gene Expression Analysis

The sequences of the primers utilized in the measurement of transcriptional levels of prolyl 4-hydroxylase subunit α-1-like (*p4hα1*), prolyl 4-hydroxylase subunit β (*p4hβ*), collagen type I alpha 1 (*col1a1*), collagen type I alpha 2 (*col1a2*), *tgf-β*, SMAD family member 4 (*smad4*), *smad5*, *smad9*, *igf-1*, target of rapamycin (*tor*), *myod*, *myf5* and *myhc* are shown in **Table 3**. The PCR primers design used *Carassius auratus* sequences.

TRIzol reagent was used to extract total RNA from muscle tissues (Invitrogen Life Technologies). Next, 1.2% agarose gel electrophoresis was used to evaluate the integrity of the RNA, and spectrophotometry was used to determine the quantity of RNA (BioPhotometer, Eppendorf). The PrimeScrip RT kit was then used to reverse-transcribe total RNA into complementary DNA (cDNA) (Takara, Japan). The obtained cDNA was stored at −20°C. A CFX96 Real-time PCR Detection System (Bio-Rad,

TABLE 3 | Sequences of the primers used for qRT-PCR analysis.

Gene	Acronym	Primer Sequence	Accession No.	Amplicon Size (bp)	Annealing Temp. (°C)
Collagen type I alpha 1	*col1a1*	F: TGTCACTGAGGATGGTTGCAC R: GACGGGATGTTTTCGTTGTTT	AB275454	83	60
Collagen type I alpha 2	*col1a2*	F: TGAGGGCTAAGGATTATGAGG R: GGGCAGGGTTCTTCTTTGAGC	AB275455	99	60
Prolyl 4-hydroxylase subunit α-1-like	*p4hα1*	F: CGTCTTCCCTGGCATCGGAGTTG R: TTACCCAATAACACAGGGCATCC	XM_026207228	93	55
Prolyl 4-hydroxylase subunit β	*p4hβ*	F: AGGAGAGAAGGAGAACCCCAA R: AGCAATAAGAGACTCCGCCTG	XM_026213906	133	60
Transforming growth factor-β	*tgf-β*	F: CCTGGGCTGGAAGTGGATA R: GTAAAGGATGGGCAGTGGG	EU086521	190	60
SMAD family member 4	*smad4*	F: TGGCTGGTCGTAAAGGAT R: CTCGTAATGGTAAGGGTTCA	XM_026274091	152	60
SMAD family member 5	*smad5*	F: CGAGGTGTGCGAGTATCCGTT R: ATTGTGACTCAGGTTGCGAAA	XM_026281121	169	55
SMAD family member 9	*smad9*	F: GCACTCCACTACATCCATCAC R: TTTTCCTCCTCATCTCCTTGT	XM_026274041	93	55
Insulin-like growth factor 1	*igf-1*	F: AGCGTGTCTACAAGCTCCG R: GGATGTCTAGCGGTCATTTCT	KF813006	175	60
Target of rapamycin	*tor*	F: TTGATGGCACGGTGTTTCCTAA R: GCCCTGGTTCTGGTGCTTGTAG	KF772613	195	60
Myogenic differentiation antigen	*myod*	F: ACCAGAGGCTGCCCAAAG R: AGTCTCCGCTGTAATGTTCC	KP715154	123	60
Myogenic factor 5	*myf5*	F: GTTTGAGGCACTACGGCG R: CTTTCAGAACAGCTTGAGGAAG	KP715152	192	60
Myosin heavy chain	*myhc*	F: GTGCTTGACATTGCTGGGTT R: ATGCCTTCTTTCTTGTATTCCT	XM_026260328	143	60
β-actin	*β-actin*	F: TTGAGCAGGAGATGGGAACCG R: AGAGCCTCAGGGCAACGGAAA	AB039726.2	115	60

United States) was utilized to perform a quantitative real-time polymerase chain reaction (qRT-PCR). Then, 16 μl volume was used for the amplification, which included 8 μl 2 × SYBR Premix ExTaq polymerase (Takara), 1 μl cDNA, 0.64 μl forward and reverse primers, 0.32 μl ROX Reference Dye (20 μM) and 5.4 μl ddH_2O. The following were the cycling conditions for the qRT-PCR reaction: Pre-incubation at 95°C for 3 min, then 40 cycles of 95°C for 10 s, annealing temperature (about 60°C, **Table 3**) for 20 s, and 72°C for 10 s. In order to identify the relative expression levels of the target genes, *β-actin* was utilized as an internal reference. The comparative CT technique ($2^{-\Delta\Delta Ct}$ method) was used to do relative quantification of qRT-PCR (Livak and Schmittgen, 2001).

Calculations and Statistical Analysis

At the end of experiment, the growth parameters were calculated as follows:

Weight gain rate (WGR, %) = (total final body weight—total initial body weight)/total initial body weight × 100.

Specific growth rate (SGR, % day^{-1}) = [(ln FBW—ln IBW)/days] × 100.

Feed efficiency (FE, %) = (total final body weight—total initial body weight)/total dry feed intake × 100.

Feeding rate (FR, % body weight day^{-1}) = (total dry feed intake)/[days × (total final body weight + total initial body weight)/2] × 100.

Protein efficiency ratio (PER, %) = (total final body weight—total initial body weight)/total protein intake × 100.

Nitrogen retention efficiency (NRE, %) = (total final whole fish protein content—total initial whole fish protein content)/total protein intake × 100.

Total nitrogen waste output (TNW, g kg^{-1} weight gain) = (total protein intake × (100—NRE))/((total final body weight—total initial body weight) × 6.25) × 100.

Survival rate (SR, %) = (final fish number/initial fish number) × 100.

All data in Figures and Tables were performed as mean ± standard error (SE). SPSS 19.0 was used to conduct the statistical analysis (SPSS Inc., Chicago, IL, United States). Growth, biochemical composition, enzymatic activities, muscle texture, histological examination and gene expression underwent a one-way analysis of variance (ANOVA) followed by Duncan's multiple range test. When $p < 0.05$, differences were considered significant. The optimal supplemented level of Hyp in the diet on SGR was calculated via broken-line regression

TABLE 4 | Growth, feed utilization and survival rate of ITCC fed with the experimental diets containing different levels of Hyp for 8 weeks.

Items	Dietary Hyp Level (%)					
	0.09	0.39	0.76	1.14	1.53	1.90
IBW (g)	14.99 ± 0.04	15.01 ± 0.02	14.99 ± 0.05	15.05 ± 0.02	15.03 ± 0.02	15.00 ± 0.02
FBW (g)	41.94 ± 1.07^{a}	43.95 ± 1.32^{ab}	46.79 ± 0.62^{b}	46.58 ± 0.58^{b}	46.76 ± 0.72^{b}	46.68 ± 0.69^{b}
WGR (%)	179.76 ± 7.78^{a}	192.92 ± 9.22^{ab}	212.10 ± 3.54^{b}	209.49 ± 4.10^{b}	211.16 ± 4.88^{b}	211.12 ± 4.55^{b}
SGR (%/d)	1.84 ± 0.05^{a}	1.92 ± 0.06^{ab}	2.03 ± 0.02^{b}	2.02 ± 0.02^{b}	2.03 ± 0.03^{b}	2.03 ± 0.02^{b}
FE (%)	44.60 ± 1.73^{a}	47.21 ± 2.60^{a}	52.68 ± 0.86^{b}	52.43 ± 1.05^{b}	53.90 ± 1.22^{b}	52.62 ± 1.04^{b}
FR (%)	3.54 ± 0.06^{b}	3.43 ± 0.08^{b}	3.26 ± 0.03^{a}	3.25 ± 0.04^{a}	3.18 ± 0.04^{a}	3.25 ± 0.03^{a}
PER (%)	128.49 ± 4.97^{a}	141.04 ± 10.45^{ab}	154.97 ± 2.53^{bc}	153.57 ± 3.08^{bc}	158.47 ± 3.59^{c}	155.99 ± 3.08^{c}
NRE (%)	22.71 ± 0.85^{a}	23.40 ± 1.99^{a}	27.05 ± 1.09^{b}	25.63 ± 0.84^{ab}	25.67 ± 0.48^{ab}	25.35 ± 1.18^{ab}
TNW (g/kg WG)	45.57 ± 0.92^{b}	43.12 ± 2.65^{b}	38.77 ± 0.71^{a}	39.66 ± 0.87^{a}	38.56 ± 0.75^{a}	39.33 ± 0.97^{a}
SR (%)	100.00 ± 0.00	100.00 ± 0.00	100.00 ± 0.00	100.00 ± 0.00	100.00 ± 0.00	100.00 ± 0.00

Values are Means ± SE (n = 3); a, b, c mean values in the same row with different superscript letters are significantly different (p < 0.05); Absence of letters indicates no significant difference between treatments.

IBW: initial body weight. FBW: final body weight. WGR: weight gain rate. SGR: specific growth rate. FE: feed efficiency. FR: feeding rate. PER: protein efficiency ratio. NRE: nitrogen retention efficiency. TNW: total nitrogen waste output. SR: survival rate.

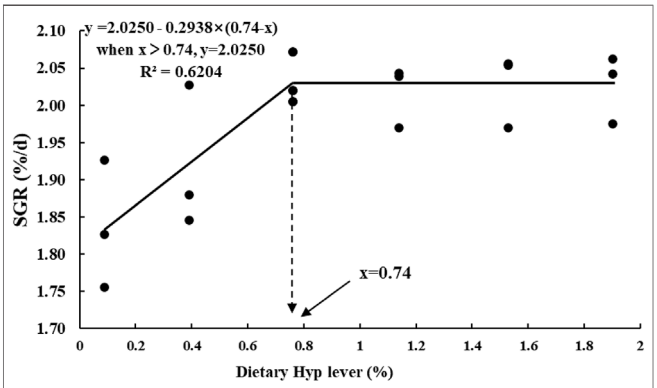

FIGURE 1 | Broken-line regression analysis between SGR and dietary Hyp level in ITCC fed with different experimental diets for 8 weeks. The breakpoint of the broken-line is 0.74% of dry diet.

analysis (y = L–U × (R–x)) in Origin 7.5 (Origin Software, CA, United States).

RESULTS

Growth Performance

Table 4 shows the growth performance and feed utilization of fish fed diets with different levels of Hyp. Final body weight (FBW), FE, WGR and SGR were significantly increased with increasing of dietary Hyp level from 0.09 to 0.76% ($p < 0.05$), however, with dietary Hyp supplemented levels further increased, FBW, FE, WGR and SGR remained largely unchanged. In contrast, FR exhibited an inverse relationship with SGR. According to the broken-line regression analysis, the association between SGR and dietary Hyp level was: y = 2.0250–0.2938 × (0.74–x) (R^2 = 0.6204, **Figure 1**). For the growth of ITCC, the optimal Hyp content in the diet was established at 0.74%. In terms of protein utilization, PER and NRE showed a similar trend to SGR with the gradual increase of Hyp in the diets. TNW was lowest in the group of fish that were fed the 0.76% Hyp supplemented diet, followed by 0.39, 1.14, 1.53, 1.90%, and highest in the control group.

Chemical Composition of Whole Fish and Dorsal Muscle

The ash level of whole fish samples treated with 0.39% Hyp was considerably higher than in the control group ($p < 0.05$) (**Table 5**). Initially, the content of crude protein was significantly enhanced when dietary Hyp increased from 0.09 to 0.76% but reduced as the Hyp level in the diet was further increased. Meanwhile, dietary Hyp level had no effect on crude protein, crude lipid and moisture content in whole fish samples ($p > 0.05$). No significant changes in moisture and ash were detected in dorsal muscle samples ($p > 0.05$). In addition, with the rising level of dietary Hyp supplementation, the content of most essential amino acids in dorsal muscle first increased and then decreased (**Table 6**). In particular, the levels of threonine and arginine increased significantly as the dietary Hyp supplemental level was raised from 0.09 to 0.76% but decreased gradually with additional Hyp supplemented in the diets ($p < 0.05$).

Muscle Texture

Table 7 displays the muscle texture results. Dietary Hyp inclusion substantially enhanced hardness, and the maximum value of hardness determined to be 4.30 in the 1.90% Hyp supplemented group ($p < 0.05$). Meanwhile, chewiness, springiness and gumminess were increased remarkably as the level of Hyp in the diets were raised from 0.09 to 1.53%, whereas these indices were decreased when the level of Hyp in the diet was 1.90%. And among the six treatments, there was no significant change in adhesiveness and cohesiveness ($p > 0.05$).

The Hydroxyproline Content in Different Tissues

Dietary Hyp levels had a significant effect on the amount of Hyp in different tissues of ITCC ($p < 0.05$) (**Table 8**). The Hyp

TABLE 5 | Whole body and dorsal muscle compositions of ITCC fed with different experimental diets for 8 weeks.

Items	Dietary Hyp Level (%)					
	0.09	**0.39**	**0.76**	**1.14**	**1.53**	**1.90**
Whole body composition (% fresh weight)						
Crude protein	15.72 ± 0.33	15.98 ± 0.11	16.35 ± 0.71	16.59 ± 0.59	16.01 ± 0.16	15.68 ± 0.06
Crude lipid	11.04 ± 0.5	11.18 ± 2.01	12.1 ± 0.55	12.17 ± 1.16	13.06 ± 0.91	13.57 ± 1.34
Ash	2.85 ± 0.16^{a}	2.47 ± 0.12^{b}	2.52 ± 0.07^{ab}	2.71 ± 0.08^{ab}	2.63 ± 0.05^{ab}	2.58 ± 0.08^{ab}
Moisture	69.85 ± 0.24	68.15 ± 0.46	68.22 ± 0.38	68.18 ± 0.79	67.94 ± 0.97	67.3 ± 1.22
Dorsal muscles composition (% fresh weight)						
Crude protein	17.06 ± 0.12^{a}	17.69 ± 0.11^{ab}	18.55 ± 0.73^{b}	17.79 ± 0.19^{ab}	17.57 ± 0.28^{ab}	17.26 ± 0.55^{ab}
Crude lipid	1.32 ± 0.07	1.24 ± 0.07	1.28 ± 0.06	1.30 ± 0.04	1.25 ± 0.08	1.20 ± 0.04
Ash	1.44 ± 0.06	1.38 ± 0.06	1.42 ± 0.04	1.38 ± 0.12	1.39 ± 0.04	1.51 ± 0.01
Moisture	75.65 ± 0.09	76.23 ± 0.42	76.00 ± 0.13	76.55 ± 0.57	75.92 ± 0.96	75.69 ± 0.75

Values are Means ± SE (n = 3); a, b, c mean values in the same row with different superscript letters are significantly different (p < 0.05); Absence of letters indicates no significant difference between treatments.

TABLE 6 | Amino acid profile in dorsal muscle of ITCC fed with different experimental diets for 8 weeks (% dry matter).

Amino Acids	Dietary Hyp Level (%)					
	0.09	**0.39**	**0.76**	**1.14**	**1.53**	**1.90**
Essential amino acid						
Threonine	2.62 ± 0.09^{a}	2.86 ± 0.15^{ab}	3.01 ± 0.08^{b}	2.87 ± 0.03^{ab}	2.89 ± 0.03^{ab}	2.65 ± 0.04^{a}
Phenylalanine	2.95 ± 0.11	3.16 ± 0.18	3.29 ± 0.12	3.24 ± 0.03	3.23 ± 0.09	2.95 ± 0.08
Valine	2.98 ± 0.11	3.13 ± 0.15	3.27 ± 0.10	3.19 ± 0.01	3.24 ± 0.05	2.97 ± 0.07
Isoleucine	3.03 ± 0.10	3.21 ± 0.16	3.37 ± 0.11	3.29 ± 0.02	3.31 ± 0.07	3.02 ± 0.08
Leucine	5.36 ± 0.18	5.68 ± 0.29	5.96 ± 0.18	5.80 ± 0.04	5.84 ± 0.11	5.34 ± 0.20
Methionine	1.72 ± 0.03	1.96 ± 0.11	2.05 ± 0.06	1.97 ± 0.02	1.97 ± 0.03	1.56 ± 0.27
Arginine	3.67 ± 0.13^{a}	3.94 ± 0.22^{ab}	4.12 ± 0.12^{b}	4.05 ± 0.04^{ab}	4.02 ± 0.09^{ab}	3.71 ± 0.06^{ab}
Lysine	6.01 ± 0.29	7.07 ± 0.43	7.19 ± 0.41	7.23 ± 0.10	6.95 ± 0.37	6.17 ± 0.41
Histidine	3.21 ± 0.14^{ab}	3.42 ± 0.16^{ab}	3.51 ± 0.10^{ab}	3.54 ± 0.08^{ab}	3.57 ± 0.09^{b}	3.16 ± 0.05^{a}
Tryptophan	ND[1]	ND	ND	ND	ND	ND
Non-essential amino acid						
Aspartic acid	6.84 ± 0.25	7.23 ± 0.40	7.58 ± 0.24	7.35 ± 0.07	7.40 ± 0.08	6.85 ± 0.32
Serine	2.74 ± 0.09	2.86 ± 0.15	3.00 ± 0.08	2.91 ± 0.02	2.95 ± 0.05	2.72 ± 0.04
Glutamic acid	9.74 ± 0.33	10.19 ± 0.58	10.75 ± 0.33	10.41 ± 0.10	10.54 ± 0.10	9.71 ± 0.48
Glycine	2.93 ± 0.06	2.95 ± 0.14	3.07 ± 0.05	3.05 ± 0.06	3.06 ± 0.03	2.93 ± 0.01
Alanine	3.27 ± 0.10	3.45 ± 0.20	3.63 ± 0.10	3.53 ± 0.04	3.53 ± 0.05	3.26 ± 0.08
Tyrosine	2.15 ± 0.08	2.27 ± 0.11	2.38 ± 0.07	2.31 ± 0.01	2.33 ± 0.05	2.16 ± 0.02
Proline	2.10 ± 0.05	2.09 ± 0.08	2.16 ± 0.04	2.15 ± 0.03	2.18 ± 0.03	2.06 ± 0.04

[1]*ND: not determined.*

Values are Means ± SE (n = 3); a, b, c mean values in the same row with different superscript letters are significantly different (p < 0.05); Absence of letters indicates no significant difference between treatments.

TABLE 7 | Muscle texture of ITCC fed with different experimental diets for 8 weeks.

Items	Dietary Hyp Level (%)					
	0.09	**0.39**	**0.76**	**1.14**	**1.53**	**1.9**
Hardness (N)	3.67 ± 0.17^{a}	4.11 ± 0.24^{ab}	3.89 ± 0.08^{ab}	4.12 ± 0.11^{ab}	4.16 ± 0.08^{b}	4.30 ± 0.11^{b}
Springiness (mm)	0.51 ± 0.04^{a}	0.54 ± 0.03^{ab}	0.63 ± 0.04^{b}	0.54 ± 0.02^{ab}	0.64 ± 0.05^{b}	0.60 ± 0.04^{ab}
Chewiness (mJ)	0.60 ± 0.07^{a}	0.60 ± 0.08^{a}	0.68 ± 0.09^{ab}	0.55 ± 0.06^{a}	0.93 ± 0.13^{b}	0.67 ± 0.10^{ab}
Adhesiveness (N*mm)	0.031 ± 0.004	0.032 ± 0.005	0.037 ± 0.004	0.031 ± 0.003	0.027 ± 0.003	0.031 ± 0.005
Cohesiveness (%)	0.38 ± 0.03	0.37 ± 0.03	0.39 ± 0.02	0.36 ± 0.02	0.43 ± 0.03	0.37 ± 0.03
Gumminess (g*mm)	1.04 ± 0.12^{a}	1.16 ± 0.14^{ab}	1.20 ± 0.11^{ab}	1.10 ± 0.10^{a}	1.54 ± 0.14^{b}	1.13 ± 0.16^{a}

Values are Means ± SE (n = 9); a, b mean values in the same row with different superscript letters are significantly different (p < 0.05); Absence of letters indicates no significant difference between treatments.

TABLE 8 | The hydroxyproline content in different tissues of ITCC fed with different experimental diets for 8 weeks.

Tissues	Dietary Hyp Level (%)					
	0.09	**0.39**	**0.76**	**1.14**	**1.53**	**1.90**
Muscle (mg/g)	0.91 ± 0.10^{a}	1.37 ± 0.01^{ab}	1.64 ± 0.19^{b}	1.41 ± 0.16^{ab}	1.46 ± 0.17^{ab}	1.44 ± 0.24^{ab}
Skin (mg/g)	8.77 ± 0.93^{a}	10.33 ± 0.31^{ab}	13.15 ± 1.10^{bc}	11.98 ± 0.94^{abc}	9.66 ± 0.94^{ab}	13.99 ± 1.52^{c}
Liver (μg/g)	256.88 ± 5.69^{a}	553.99 ± 72.59^{ab}	671.96 ± 103.44^{b}	567.93 ± 195.71^{ab}	430.59 ± 46.70^{ab}	456.84 ± 73.89^{ab}
Vertebra (mg/g)	7.39 ± 0.17^{a}	7.62 ± 0.49^{a}	8.45 ± 0.73^{ab}	9.47 ± 0.89^{ab}	9.04 ± 1.18^{ab}	10.5 ± 0.40^{b}
Plasma (mg/ml)	100.00 ± 9.62^{a}	119.84 ± 7.57^{ab}	124.60 ± 12.01^{ab}	141.27 ± 10.68^{bc}	142.86 ± 4.76^{bc}	170.63 ± 9.36^{c}

Values are Means ± SE (n = 6); a, b, c mean values in the same row with different superscript letters are significantly different (p < 0.05); Absence of letters indicates no significant difference between treatments.

TABLE 9 | The type I collagen (Col I) content, pyridinium crosslink (PYD) content, prolyl 4-hydroxylase (P4H) and lysyl hydroxylase (LH) activity in muscle of ITCC fed with different experimental diets for 8 weeks.

Items	Dietary Hyp Level (%)					
	0.09	**0.39**	**0.76**	**1.14**	**1.53**	**1.90**
Col I (ng/mg prot)	4.88 ± 0.02^{a}	5.53 ± 0.36^{ab}	5.34 ± 0.45^{ab}	5.13 ± 0.24^{ab}	6.02 ± 0.27^{b}	5.98 ± 0.27^{b}
PYD (ng/mg prot)	25.74 ± 1.06^{a}	28.76 ± 0.60^{ab}	26.91 ± 1.62^{ab}	26.73 ± 1.64^{ab}	30.37 ± 1.17^{b}	30.79 ± 1.18^{b}
P4H (ng/mg prot)	0.66 ± 0.03^{a}	0.74 ± 0.03^{ab}	0.75 ± 0.04^{ab}	0.83 ± 0.05^{b}	0.81 ± 0.07^{b}	0.84 ± 0.05^{b}
LH (ng/mg prot)	0.136 ± 0.005^{a}	0.142 ± 0.003^{ab}	0.157 ± 0.007^{ab}	0.154 ± 0.005^{ab}	0.154 ± 0.004^{ab}	0.161 ± 0.013^{b}

Values are Means ± SE (n = 6); a, b mean values in the same row with different superscript letters are significantly different (p < 0.05); Absence of letters indicates no significant difference between treatments.

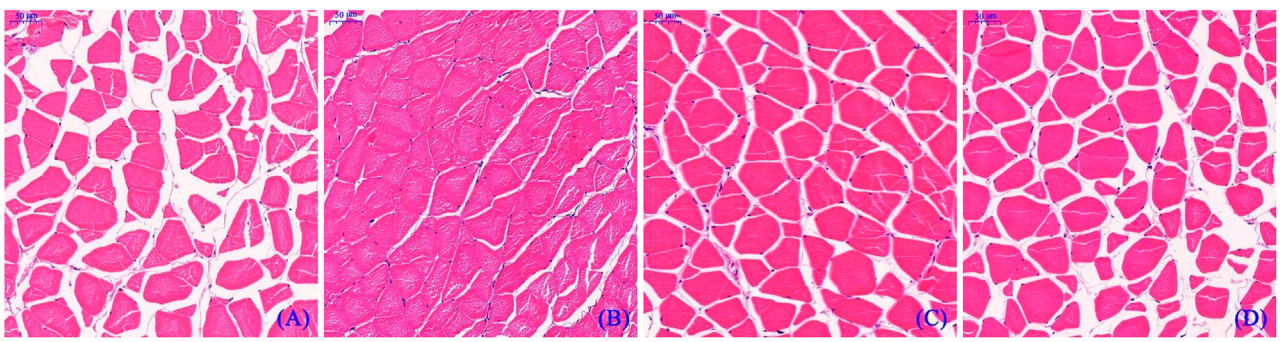

FIGURE 2 | Microstructure of dorsal muscle of ITCC in cross-section. Bars represent 50 μ; **(A–D)** represent different dorsal muscle from the 0.09, 0.76, 1.14 and 1.90% of Hyp supplemental groups, respectively.

TABLE 10 | The muscle fiber diameter (DI) and density (DE) of ITCC fed with different experimental diets for 8 weeks.

Items	Dietary Hyp Level (%)					
	0.09	**0.39**	**0.76**	**1.14**	**1.53**	**1.90**
DI (μm)	47.49 ± 1.94^{a}	55.84 ± 1.98^{b}	61.48 ± 1.36^{c}	58.12 ± 1.13^{bc}	56.39 ± 1.29^{b}	49.14 ± 1.79^{a}
DE (n/mm^{2})	158.67 ± 6.44^{a}	175.00 ± 7.09^{ab}	221.67 ± 18.00^{b}	218.00 ± 19.08^{b}	184.67 ± 19.38^{ab}	167.67 ± 6.06^{a}

Values are Means ± SE; a, b, c mean values in the same row with different superscript letters are significantly different (p < 0.05); Absence of letters indicates no significant difference between treatments.

contents in muscle and liver were substantially higher in the 0.76% Hyp supplemented group when compared to the non-Hyp group ($p < 0.05$). In addition, the levels of Hyp in the skin, vertebrae and plasma were all considerably higher following a gradient of increased Hyp level in feed, and the 1.90% group reached the maximum value ($p < 0.05$).

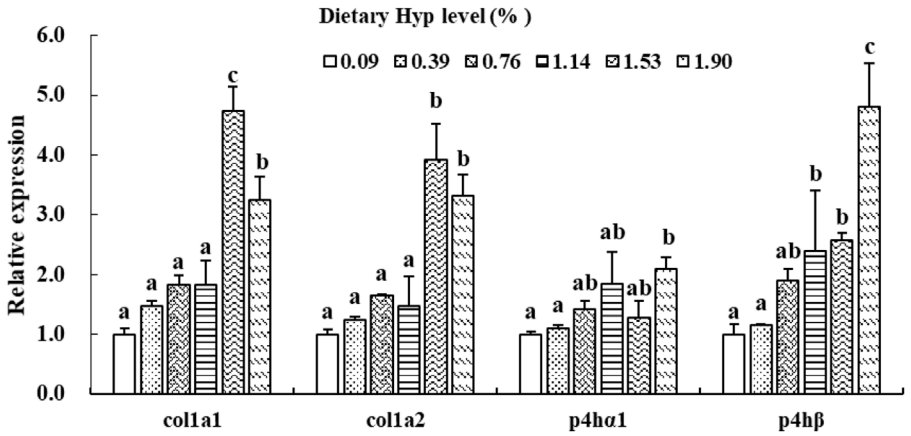

FIGURE 3 | Relative expressions of *col1a1*, *col1a2*, *p4hα1* and *p4hβ* in muscle of ITCC fed with different experimental diets for 8 weeks. Data are present as Means ± SE (n = 6). Different lowercase letters above the same group of bars represent significant difference between the corresponding groups ($p < 0.05$).

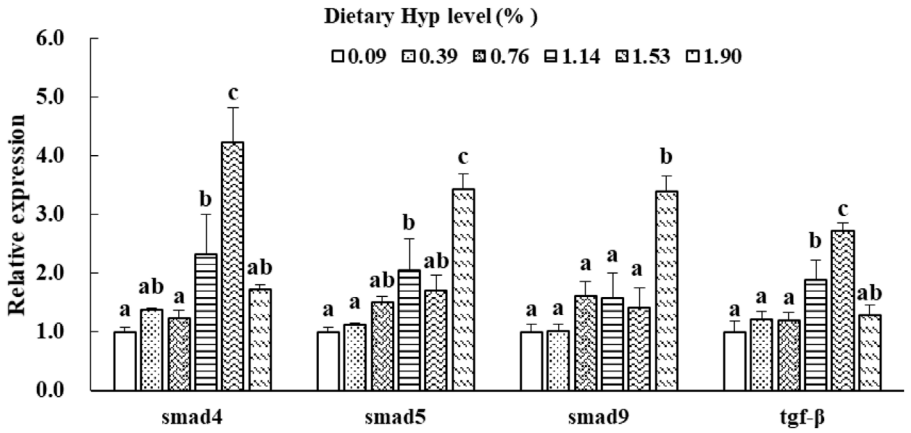

FIGURE 4 | Relative expressions of *smad4*, *smad5*, *smad9* and *tgf-β* in muscle of ITCC fed with different experimental diets for 8 weeks. Data are present as Means ± SE (n = 6). Different lowercase letters above the same group of bars represent significant difference between the corresponding groups ($p < 0.05$).

Col I, Pyridinium Crosslink and Relative Enzymatic Activities in Muscle

Dietary Hyp levels ranging from 1.53 to 1.90% substantially enhanced the contents of Col I and PYD in muscle ($p < 0.05$) (**Table 9**). Furthermore, the P4H activity of fish fed diets containing 1.14%, 1.53%, and 1.90% Hyp was substantially greater than the control group ($p < 0.05$). LH activity gradually increased with increasing dietary Hyp level, and the greatest value of LH was achieved in the 1.90% Hyp supplemented group ($p < 0.05$).

Histological Analysis

Figure 2 depicts the HE staining results of the dorsal muscle in a cross-section, and **Table 10** shows the effects of dietary Hyp on muscle fiber diameter (DI) and density (DE) in ITCC. The density of muscle fiber was greater in fish fed Hyp-supplemented diets than in the control group ($p < 0.05$). Furthermore, muscle fiber diameter rose progressively as the dietary Hyp supplemental level was raised from 0.09 to 0.76% but thereafter declined with dietary Hyp further increased.

Gene Expression

As shown in **Figures 3**, **4**, the *col1a1*, *col1a2*, *p4hα1*, *p4hβ*, *smad4*, *smad5*, *samd9* and *tgf-β* levels gradually increased with enhancing of Hyp levels in the diets ($p < 0.05$). The maximum expression levels of *col1a1*, *col1a2*, *smad4* and *tgf-β* appeared in the 1.53% Hyp supplemented group, and the maximum levels of *p4hα1*, *p4hβ*, *smad5* and *samd9* appeared in the 1.90% Hyp group. The expression levels of genes related to muscle growth and development are shown in **Figure 5**. Dietary Hyp levels substantially increased the transcriptional level of *igf-1* expression ($p < 0.05$). Muscle mRNA levels of *tor* were significantly higher in fish fed the 1.14% Hyp diet than fish fed the control diet, whereas *myod* mRNA levels were higher in fish fed the 1.53% Hyp diet. In addition, *myf5* and *myhc* mRNA expressions significantly rose with increasing Hyp level up to 0.76%, and decreased thereafter ($p < 0.05$).

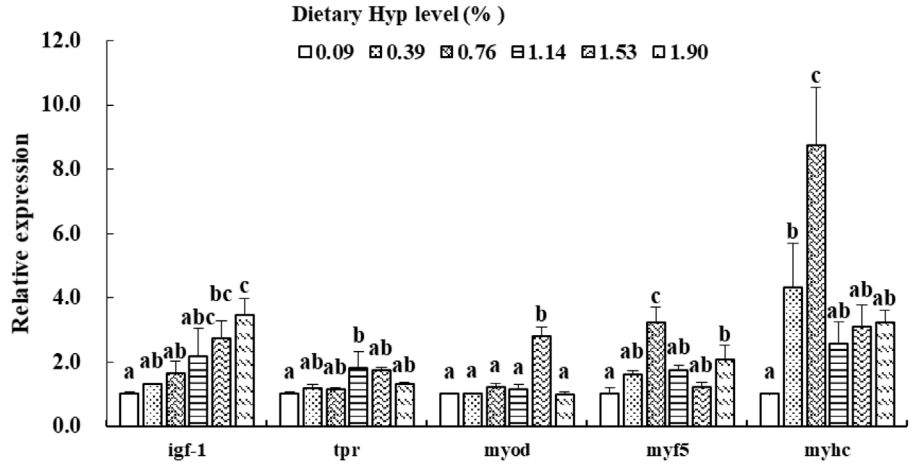

FIGURE 5 | Relative expressions of *igf-1*, *tor*, *myod*, *myf5* and *myhc* in muscle of ITCC fed with different experimental diets for 8 weeks. Data are present as Means ± SE (n = 6). Different lowercase letters above the same group of bars represent significant difference between the corresponding groups ($p < 0.05$).

DISCUSSION

Hydroxyproline (Hyp), as a conditionally necessary amino acid (Li et al., 2009), is plentiful in fish meal but lacking in plant protein sources commonly used in aquatic feed (Li et al., 2011). As a result, the possible negative consequences of Hyp deficiency should be addressed in diets high in plant-based feedstuff. Previous researches have shown that supplementation of Hyp in the diets can significantly increase the growth performance and feed utilization of some marine and carnivorous fish, including large yellow croaker (Wei et al., 2016), Atlantic salmon (Aksnes et al., 2008) and Chinese perch (*Siniperca chuatsi*) (Feng et al., 2022). In the present study, WGR, SGR and FE of ITCC were remarkably enhanced by increasing dietary Hyp level to 0.76%. These results agree with the finding that WG and SGR in the spotted drum (*Nibea diacanthus*) increased significantly when dietary Hyp content rose from 0 to 1%, but stayed stable when Hyp in the diet rose from 1 to 2.5% (Rong et al., 2020a). Rong et al. (2020a) revealed that enhancement of Hyp on growth and protein synthesis ability might be closely related to the significant upregulation of the TOR signaling pathway and upstream GH-IGF-1 axis. However, in some other studies, dietary addition of Hyp showed no significant influence on the growth performance of Atlantic salmon (Albrektsen et al., 2010) and turbot (Zhang et al., 2015). These findings showed that the effect of an Hyp-containing diet regimen on fish growth might be related to aquatic animal size and species, culture environment, and other feed nutrient content. Furthermore, when the dietary Hyp supplemented level was increased to more than 0.76% in the current study, fish growth did not further improve. The data indicates that the optimal requirement of Hyp in ITCC is about 0.76%, and the extra Hyp cannot be used for the growth of fish. The broken-line regression analysis of SGR and dietary Hyp level indicated that 0.74% dietary Hyp content was optimum for the growth of ITCC.

In general, the weight gain of fish is mainly due to muscular protein and lipid accretion (Tu et al., 2015). In this study, the utilization efficiency of feed protein (PER, NRE, and TNW) and the crude protein of dorsal muscle in the fish fed diet containing 0.76% Hyp was considerably greater than in fish provided a control diet. Crude protein of the whole body also showed a gradual upward trend with more Hyp in the diet ($p > 0.05$). The result was consistent with the previous researches in large yellow croaker and spotted drum, which found dietary protein utilization, crude protein in the whole body, dorsal muscle and swim bladder were all significantly elevated by dietary Hyp (Wei et al., 2016; Rong et al., 2020a). These phenomena indicated that dietary inclusion of appropriate Hyp might help with protein synthesis in the tissues of fish, contributing to the growth performance of fish. Protein deposition in fish is, in essence, amino acid deposition (Kaushik and Seiliez, 2010). In the current study, the contents of different amino acids in the dorsal muscle of ITCC exhibited a certain degree of increase under the influence of dietary Hyp, particularly threonine and arginine, which both reached maximum levels when 0.76% Hyp was supplemented. Nutrition research has found that the balance of dietary essential amino acids in vertebrates is key to the efficient absorption and utilization of amino acids (Heger and Frydrych, 2019). Some studies in fish have found that supplementation of amino acids lacking in diets can effectively improve the utilization efficiency of inferior diets and increase the deposition levels of protein and amino acids (Clark et al., 2020; Zhao et al., 2020). In this study, Hyp was the essential amino acid for fish fed diets high in plant-based ingredients. Dietary inclusion of appropriate amounts of Hyp improved dietary amino acid balance, promoting protein synthesis and growth of ITCC.

According to the study of Pinilla-Tenas et al. (2003), Hyp is likely to be absorbed and transported directly to tissues without dihydroxylation. In the current study, Hyp was significantly accumulated in the tissues (muscle, skin, liver, vertebrae and plasma) of ITCC with the increase of dietary Hyp. Similar findings were obtained in Chinese perch and Atlantic salmon, where dietary Hyp supplementation dramatically raised total Hyp content in plasma, liver, vertebrae and muscle (Aksnes et al.,

2008; Feng et al., 2022). Hyp content is always regarded as a significant indication of collagen concentration since it is nearly almost dense in collagen. In particular, as dietary Hyp increased, we saw a substantial rise in type I collagen (Col I) content in muscle, which was consistent with a progressive increase in muscular Hyp. The texture mechanical properties (hardness, springiness, chewiness, adhesiveness, cohesiveness and gumminess) are conventional indicators widely used to evaluate fish flesh quality (Hyldig and Nielsen, 2001; Moreno et al., 2012). In this study, the level of Hyp in the diet was increased from 0.09 to 1.53%, which resulted in substantial muscular improvement in hardness, springiness, chewiness and gumminess. Similarly, a sufficient amount of dietary Hyp supplementation has been shown to improve the muscle collagen content and texture of chu's croaker (Rong et al., 2020b), turbot (Liu et al., 2014) and Atlantic salmon (Albrektsen et al., 2010), suggesting that supplementation of Hyp aids in the improvement of ITCC muscle quality, most likely via raising the concentration of muscular collagen.

Collagen production involves several post-translational and co-translational modifications of polypeptide chains. P4H is the primary form of prolyl hydroxylase (PHD), an important collagen-specific enzyme that catalyzes the hydroxylation of proline residues to 4-Hyp (Gorres and Raines, 2010). *P4hα1* and *p4hβ*, two subunits of *p4h* gene identified in vertebrates, are the pivotal genes involved in regulating collagen maturation and secretion (Sekiya et al., 2005). We observed that P4H activity, *p4hα1* and *p4hβ* expression in fish muscle of specimens fed high-level Hyp were considerably higher than in control group fish. This result demonstrates that including adequate Hyp in the diet can stimulate collagen synthesis in fish muscle. Previous research has revealed that the muscle texture of fish is altered by both collagen crosslinking and concentration (Li et al., 2005). Hagen et al. (2007) discovered that the cross-linking process is critical for collagen hardness and strength and that PYD was the most essential parameter influencing fish muscle texture. Furthermore, the endogenous enzyme LH is known to be involved in the production of collagen crosslinks, which can catalyze lysine hydroxylation to hydroxylysine in collagen molecules (Yamauchi and Shiiba, 2002). In the present study, we observed significantly enhanced PYD content and LH activity in muscle with the inclusion of adequate dietary Hyp, which is similar with the results in large yellow croaker (Wei et al., 2016) and rainbow trout (*Oncorhynchus mykiss*) (Johnsen et al., 2011). These results showed evidence that dietary supplementation of Hyp improved the muscle texture properties of ITCC by promoting the biosynthesis of collagen in muscle and increasing the content of collagen crosslink.

Type 1 collagen (Col I), a primary constituent of collagen in fish muscle connective tissue, consists of one α2 (I) chain and two α1 (I) chains that undergo *col1a2* and *col1a1* gene regulation (Sato et al., 1997; Büttner et al., 2004). In this study, significant higher *col1a1* and *col1a2* genes expressions and Col I content in muscle were observed in the 1.53–1.90% Hyp supplemented groups. This result was consistent with a study of Chinese perch in which diets were supplemented with 1.92-2.37% of Hyp, the relative expression levels of *col1a1* and *col1a2* genes in muscle were significantly upregulated (Feng et al., 2022). Similarly, research on model mice suggests that Hyp content in the skin correlated positively with the expressions of connective tissue growth factor (*ctgf*) and *col1a1* mRNA (Liao et al., 2006). Moreover, *in vitro* research has showed that *tgf-β* significantly increased *col1a1* mRNA in mouse mesangial cells (Kato et al., 2007). TGF-β signal transduction occurs mainly through the activation of receptor substrate Smads protein pathway to achieve a signal from the cell membrane receptor into the nucleus (Moustakas et al., 2001). Smad4 is a critical regulator in the TGF-β/Smads signal pathway and is also key to the control of type I collagen expression in animals (Xia et al., 2021). Smad5 and Smad9 are two representative subtypes of receptor-activated Smad (R-Smad) (Kim and Kim, 2014). In the present study, the gene expressions of *smad4*, *smad5*, *smad9* and *tgf-β* were increased by dietary Hyp inclusion, especially in the high Hyp supplemented group. A similar result was found that feeding grass carp (*Ctenopharyngodon idella*) with faba bean significantly enhanced the mRNA and protein expressions of TGF-β and Smad4, as well as the expression of type I collagen (*col1a1* and *col1a2*) (Yu et al., 2019). These studies indicated that dietary supplementation of appropriate Hyp could increase substrates of collagen synthesis in tissues, thus up-regulating the expression of related genes and promoting Type 1 collagen biosynthesis and accumulation in fish. However, with the increase of Hyp in the diet, collagen content in fish muscle increased while *p4h* (*p4hα1*, *p4hα2,* and *p4hα3*), *col1a1*, and *col1a2* genes down-regulated in turbot (Zhang et al., 2013) and *Nibea diacanthus* (Rong et al., 2019). These investigators hypothesized that consuming Hyp supplements improves collagen levels in fish muscle by preventing collagen degradation rather than boosting collagen synthesis. Therefore, more research is needed to determine the mechanism of dietary Hyp on collagen production in fish muscle.

As it accounts for 40–60% of body weight, skeletal muscle is an integral part of the fish carcass. In fish, muscle fiber is the basic unit of skeletal muscle, representing the level of muscle development (Xu et al., 2019). Variations in dorsal muscle fiber diameter and density provide guidance for understanding of fish muscle growth and development. The current findings for the first time reveal that dietary supplemented Hyp dramatically enhanced fiber diameter and density in the dorsal muscle of fish, indicating that Hyp has positive effects on muscle growth. IGFs influence the development of fish skeletal muscle and can induce the proliferation and differentiation of myoblasts (Fuentes et al., 2013). As a crucial regulatory gene downstream of the GH-IGF-I growth axis, *tor* is required for promoting translation initiation and increasing muscle protein synthesis (Wullschleger et al., 2006). This study revealed that dietary supplementation with adequate Hyp dramatically up-regulated the relative expressions of *igf-1* and *tor* genes in muscle. Similarly, Rong et al. (2020a) demonstrated that optimal dietary Hyp significantly elevated the *tor* expression in the muscle, liver and swim bladder of the juvenile spotted drum. Zhao et al. (2020) suggested that leucine, another essential amino acid, improved muscle

protein synthesis in hybrid catfish (*Pelteobagrus vachelli* × *Leiocassis longirostris*) by up-regulating *igf-1* and *igf-1r* mRNA levels. Studies on mammals found that Hyp levels are highly consistent with *igf-1* relative expression (Chen et al., 2019a; Xiao et al., 2020). These results partially explain the mechanism of dietary Hyp increasing muscle growth of fish. Moreover, fish muscle fiber is formed by the proliferation and differentiation of activated satellite cells, a process that is also influenced by a number of myogenic regulatory elements (Rescan, 2005). *Myod* and *myf5* play an important regulatory role in the activation and proliferation of satellite cells (Zammit, 2017). *Myhc* affects fish muscle growth by promoting the proliferation and hypertrophy of muscle fibers (Song et al., 2020). The present studies showed that the appropriate level of dietary Hyp upregulated the gene expressions level of *myod*, *myf5* and *myhc* in fish muscle. This result was consistent with reports on turbot and Atlantic salmon that showed dietary Hyp-rich fish meal hydrolysate and fish bone hydrolysate improved muscle growth and upregulated the expressions of muscle *myod*, *myf5,* and *mrf4* (Albrektsen et al., 2018; Wei et al., 2020). These studies indicated that muscle growth and differentiation were at least partially positively regulated by intramuscular *myod*, *myf5* and *myhc* genes in ITCC. Recently, some growing evidences suggest that essential amino acids play a regulatory role in fish muscle development. For instance, methionine, histidine and lysine have been proved to affect muscle hyperplasia and up-regulate *myog* and *myod* gene expression in fish (Childress et al., 2016; Michelato et al., 2017; Alami-Durante et al., 2018). Hyp, as a conditionally essential amino acid, is presumed to have a similar regulating impact on fish muscle growth. Notwithstanding, additional research is needed to elucidate how dietary Hyp affects the expression of genes associated with muscle growth in fish.

CONCLUSION

This study demonstrates that dietary supplementation of 0.76% or more Hyp can significantly improve growth and feed utilization of ITCC. Dietary inclusion of Hyp improved Hyp accumulation in various tissues, muscle textural characteristics, collagen content in muscle and expressions of collagen synthesis-related genes. In addition, an appropriate level of Hyp in the diet significantly elevated protein synthesis in muscle by regulating muscle growth-related gene expression. According to the SGR broken-line analysis, the optimal level of Hyp in the diet for ITCC was estimated to be 0.74%.

DATA AVAILABILITY STATEMENT

The original contributions presented in the study are included in the article/supplementary material, further inquiries can be directed to the corresponding author.

ETHICS STATEMENT

The animal study was reviewed and approved by All the experimental procedures applied in this study did comply with the ARRIVE guidelines and carried out in accordance with United Kingdom. Animals (Scientific Procedures) Act, 1986 and associated guidelines, and were approved by the Institutional Animal Care and Use Committee of Changsha University (Changsha, China). Written informed consent was obtained from the owners for the participation of their animals in this study.

AUTHOR CONTRIBUTIONS

SC conducted data analysis and wrote the manuscript; YX performed the RT-PCR experiments; RH and DZ conducted biochemical analysis; JT and FQ provided technical assistance; SL and WX performed the feeding trial; SX provided experimental guidance; ZL and JJ designed the experiment. All authors have read and approved the final version of the manuscript.

FUNDING

This research was financially supported by the National Natural Science Foundation of China (Grant No. U19A2041 and 32102813), Hunan Provincial Natural Science Foundation of China (Grant No. 2021JJ40627), Changsha Municipal Natural Science Foundation (Grant No. kq2007083) and the Fund by the State Key Laboratory of Freshwater Ecology and Biotechnology (Grant No. 2022FB08).

REFERENCES

Aksnes, A., Mundheim, H., Toppe, J., and Albrektsen, S. (2008). The Effect of Dietary Hydroxyproline Supplementation on Salmon (*Salmo salar* L.) Fed High Plant Protein Diets. *Aquaculture* 275, 242–249. doi:10.1016/j.aquaculture.2007.12.031

Alami-Durante, H., Bazin, D., Cluzeaud, M., Fontagné-Dicharry, S., Kaushik, S., and Geurden, I. (2018). Effect of Dietary Methionine Level on Muscle Growth Mechanisms in Juvenile Rainbow Trout (*Oncorhynchus mykiss*). *Aquaculture* 483, 273–285. doi:10.1016/j.aquaculture.2017.10.030

Albrektsen, S., Østbye, T.-K., Pedersen, M., Ytteborg, E., Ruyter, B., and Ytrestøyl, T. (2018). Dietary Impacts of Sulphuric Acid Extracted Fish Bone Compounds on Astaxanthin Utilization and Muscle Quality in Atlantic Salmon (*Salmo salar*). *Aquaculture* 495, 255–266. doi:10.1016/j.aquaculture.2018.05.047

Albrektsen, S., Sirnes, E., Aksnes, A., and Hagen, Ø. (2010). Impacts of Dietary Hydroxyproline on Growth, Muscle Firmness, Collagen and PYD Cross-Links Formation in Atlantic Salmon (*Salmo salar*). *Program Abstr. 14th Int. Symposium Fish Nutr. Feed.*, 79. Qingdao, China.

Barbul, A. (2008). Proline Precursors to Sustain Mammalian Collagen Synthesis. *J. Nutr.* 138, 2021S–2024S. doi:10.1093/jn/138.10.2021s

Büttner, C., Skupin, A., and Rieber, E. P. (2004). Transcriptional Activation of the Type I Collagen Genes COL1A1 and COL1A2 in Fibroblasts by Interleukin-4: Analysis of the Functional Collagen Promoter Sequences. *J. Cell. Physiol.* 198, 248–258.

Cao, S., Zhao, D., Huang, R., Xiao, Y., Xu, W., Liu, X., et al. (2021). The Influence of Acute Ammonia Stress on Intestinal Oxidative Stress, Histology, Digestive

Enzymatic Activities and PepT1 Activity of Grass Carp (*Ctenopharyngodon Idella*). *Aquac. Rep.* 20, 100722. doi:10.1016/j.aqrep.2021.100722

Chen, S., Wang, J., Liu, S., Qin, Q., Xiao, J., Duan, W., et al. (2009). Biological Characteristics of an Improved Triploid Crucian Carp. *Sci. China Ser. C* 52, 733–738. doi:10.1007/s11427-009-0079-3

Chen, Y., Li, L., Wang, E., Zhang, L., and Zhao, Q. (2019a). Abnormal Expression of Pappa2 Gene May Indirectly Affect Mouse Hip Development through the IGF Signaling Pathway. *Endocrine* 65, 440–450. doi:10.1007/s12020-019-01975-0

Chen, Y., Ma, J., Huang, H., and Zhong, H. (2019b). Effects of the Replacement of Fishmeal by Soy Protein Concentrate on Growth Performance, Apparent Digestibility, and Retention of Protein and Amino Acid in Juvenile Pearl Gentian Grouper. *PLoS One* 14, e0222780. doi:10.1371/journal.pone.0222780

Childress, C. J., Fuller, S. A., Rawles, S. D., Beck, B. H., Gaylord, T. G., Barrows, F. T., et al. (2016). Lysine Supplementation of Commercial Fishmeal-free Diet in Hybrid Striped bassMorone Chrysops X M. Saxatilisaffects Expression of Growth-Related Genes. *Aquacult Nutr.* 22, 738–744. doi:10.1111/anu.12300

Clark, T. C., Tinsley, J., Sigholt, T., Macqueen, D. J., and Martin, S. A. M. (2020). Supplementation of Arginine, Ornithine and Citrulline in Rainbow Trout (*Oncorhynchus mykiss*): Effects on Growth, Amino Acid Levels in Plasma and Gene Expression Responses in Liver Tissue. *Comp. Biochem. Physiology Part A Mol. Integr. Physiology* 241, 110632. doi:10.1016/j.cbpa.2019.110632

Daniel, N. (2018). A Review on Replacing Fish Meal in Aqua Feeds Using Plant Protein Sources. *Int. J. Fish. Aquatic Stud.* 6, 164–179.

Fawole, F. J., Labh, S. N., Hossain, M. S., Overturf, K., Small, B. C., Welker, T. L., et al. (2021). Insect (Black Soldier Fly Larvae) Oil as a Potential Substitute for Fish or Soy Oil in the Fish Meal-Based Diet of Juvenile Rainbow Trout (*Oncorhynchus mykiss*). *Anim. Nutr.* 7 (4), 1360–1370. doi:10.1016/j.aninu.2021.07.008

Feng, H., Peng, D., Liang, X.-F., Chai, F., Tang, S., and Li, J. (2022). Effect of Dietary Hydroxyproline Supplementation on Chinese Perch (*Siniperca chuatsi*) Fed with Fish Meal Partially Replaced by Fermented Soybean Meal. *Aquaculture* 547, 737454. doi:10.1016/j.aquaculture.2021.737454

Fu, Y., Liang, X., Li, D., Gao, H., Wang, Y., Li, W., et al. (2021). Effect of Dietary Tryptophan on Growth, Intestinal Microbiota, and Intestinal Gene Expression in an Improved Triploid Crucian Carp. *Front. Nutr.* 8, 322. doi:10.3389/fnut.2021.676035

Fuentes, E. N., Valdés, J. A., Molina, A., and Björnsson, B. T. (2013). Regulation of Skeletal Muscle Growth in Fish by the Growth Hormone - Insulin-like Growth Factor System. *General Comp. Endocrinol.* 192, 136–148. doi:10.1016/j.ygcen.2013.06.009

Gelse, K., Pöschl, E., and Aigner, T. (2003). Collagens-structure, Function, and Biosynthesis. *Adv. Drug Deliv. Rev.* 55, 1531–1546. doi:10.1016/j.addr.2003.08.002

Gorres, K. L., and Raines, R. T. (2010). Prolyl 4-hydroxylase. *Crit. Rev. Biochem. Mol. Biol.* 45, 106–124. doi:10.3109/10409231003627991

Hagen, Ø., Solberg, C., Sirnes, E., and Johnston, I. A. (2007). Biochemical and Structural Factors Contributing to Seasonal Variation in the Texture of Farmed Atlantic Halibut (*Hippoglossus hippoglossus* L.) Flesh. *J. Agric. Food Chem.* 55, 5803–5808. doi:10.1021/jf063614h

Hansen, A. C., Rosenlund, G., Karlsen, O., Koppe, W., and Hemre, G. I. (2007). Total Replacement of Fish Meal with Plant Proteins in Diets for Atlantic Cod (*Gadus morhua* L.) I - Effects on Growth and Protein Retention. *Aquaculture* 272 (1–4), 599–611. doi:10.1016/j.aquaculture.2007.08.034

Heger, J., and Frydrych, Z. (2019). "Efficiency of Utilization of Amino Acids," in *Absorption and Utilization of Amino Acids* (Florida, US: CRC Press), 31–56. doi:10.1201/9780429487514-3

Hernández-Hernández, J. M., García-González, E. G., Brun, C. E., and Rudnicki, M. A. (2017). The Myogenic Regulatory Factors, Determinants of Muscle Development, Cell Identity and Regeneration. *Seminars Cell & Dev. Biol.* 72, 10–18.

Hua, K., Cobcroft, J. M., Cole, A., Condon, K., Jerry, D. R., Mangott, A., et al. (2019). The Future of Aquatic Protein: Implications for Protein Sources in Aquaculture Diets. *One Earth* 1, 316–329. doi:10.1016/j.oneear.2019.10.018

Hyldig, G., and Nielsen, D. (2001). A Review of Sensory and Instrumental Methods Used to Evaluate the Texture of Fish Muscle. *J. Texture Stud.* 32, 219–242. doi:10.1111/j.1745-4603.2001.tb01045.x

Johnsen, C. A., Hagen, Ø., Adler, M., Jönsson, E., Kling, P., Bickerdike, R., et al. (2011). Effects of Feed, Feeding Regime and Growth Rate on Flesh Quality, Connective Tissue and Plasma Hormones in Farmed Atlantic Salmon (*Salmo salar* L.). *Aquaculture* 318, 343–354. doi:10.1016/j.aquaculture.2011.05.040

Johnston, I. A., Li, X., Vieira, V. L. A., Nickell, D., Dingwall, A., Alderson, R., et al. (2006). Muscle and Flesh Quality Traits in Wild and Farmed Atlantic Salmon. *Aquaculture* 256, 323–336. doi:10.1016/j.aquaculture.2006.02.048

Kato, M., Zhang, J., Wang, M., Lanting, L., Yuan, H., Rossi, J. J., et al. (2007). MicroRNA-192 in Diabetic Kidney Glomeruli and its Function in TGF-β-Induced Collagen Expression via Inhibition of E-Box Repressors. *Proc. Natl. Acad. Sci. U.S.A.* 104, 3432–3437. doi:10.1073/pnas.0611192104

Kaushiak, R., and Seiliez, I. (2010). Protein and Amino Acid Nutrition and Metabolism in Fish: Current Knowledge and Future Needs. *Aquac. Res.* 104, 322–332. doi:10.1073/pnas.0611192104

Kim, J.-D., and Kim, J. (2014). Alk3/Alk3b and Smad5 Mediate BMP Signaling during Lymphatic Development in Zebrafish. *Mol. Cells.* 37, 270–274. doi:10.14348/molcells.2014.0005

Kousoulaki, K., Albrektsen, S., Langmyhr, E., Olsen, H. J., Campbell, P., and Aksnes, A. (2009). The Water Soluble Fraction in Fish Meal (Stickwater) Stimulates Growth in Atlantic Salmon (*Salmo salar* L.) Given High Plant Protein Diets. *Aquaculture* 289, 74–83. doi:10.1016/j.aquaculture.2008.12.034

Li, P., Mai, K., Trushenski, J., and Wu, G. (2009). New Developments in Fish Amino Acid Nutrition: towards Functional and Environmentally Oriented Aquafeeds. *Amino acids* 37, 43–53. doi:10.1007/s00726-008-0171-1

Li, P., and Wu, G. (2018). Roles of Dietary glycine, Proline, and Hydroxyproline in Collagen Synthesis and Animal Growth. *Amino acids* 50, 29–38. doi:10.1007/s00726-017-2490-6

Li, X., Bickerdike, R., Lindsay, E., Campbell, P., Nickell, D., Dingwall, A., et al. (2005). Hydroxylysyl Pyridinoline Cross-Link Concentration Affects the Textural Properties of Fresh and Smoked Atlantic Salmon (*Salmo salar* L.) Flesh. *J. Agric. Food Chem.* 53, 6844–6850. doi:10.1021/jf050743+

Li, X., Rezaei, R., Li, P., and Wu, G. (2011). Composition of Amino Acids in Feed Ingredients for Animal Diets. *Amino acids* 40, 1159–1168. doi:10.1007/s00726-010-0740-y

Liao, Z. H., Jian-Yun, L. U., Chen, J., Xiang, Y. P., and Zuo, C. X. (2006). Expression of CTGF mRNA in Sclerotic Skin of Mice with Bleomycin-Induced Scleroderma. *Chin. J. Dermatology* 39, 22–25.

Listrat, A., Lebret, B., Louveau, I., Astruc, T., Bonnet, M., Lefaucheur, L., et al. (2016). How Muscle Structure and Composition Influence Meat and Flesh Quality. *Sci. World J.* 2016, 1–14. doi:10.1155/2016/3182746

Liu, X., Han, B., Xu, J., Zhu, J., Hu, J., Wan, W., et al. (2020). Replacement of Fishmeal with Soybean Meal Affects the Growth Performance, Digestive Enzymes, Intestinal Microbiota and Immunity of *Carassius auratus* Gibelio♀ × *Cyprinus carpio*♂. *Aquac. Rep.* 18, 100472.doi:10.1016/j.aqrep.2020.100472

Liu, Y., He, G., Wang, Q., Mai, K., Xu, W., and Zhou, H. (2014). Hydroxyproline Supplementation on the Performances of High Plant Protein Source Based Diets in Turbot (*Scophthalmus maximus* L.). *Aquaculture* 433, 476–480. doi:10.1016/j.aquaculture.2014.07.002

Livak, K. J., and Schmittgen, T. D. (2001). Analysis of Relative Gene Expression Data Using Real-Time Quantitative PCR and the 2−ΔΔCT Method. *Methods* 25, 402–408. doi:10.1006/meth.2001.1262

Michelato, M., Zaminhan, M., Boscolo, W. R., Nogaroto, V., Vicari, M., Artoni, R. F., et al. (2017). Dietary Histidine Requirement of Nile tilapia Juveniles Based on Growth Performance, Expression of Muscle-Growth-Related Genes and Haematological Responses. *Aquaculture* 467, 63–70. doi:10.1016/j.aquaculture.2016.06.038

Moreno, H. M., Montero, M. P., Gómez-Guillén, M. C., Fernández-Martín, F., Mørkøre, T., and Borderías, J. (2012). Collagen Characteristics of Farmed Atlantic Salmon with Firm and Soft Fillet Texture. *Food Chem.* 134, 678–685. doi:10.1016/j.foodchem.2012.02.160

Moustakas, A., Souchelnytskyi, S., and Heldin, C.-H. (2001). Smad Regulation in TGF-β Signal Transduction. *J. Cell Sci.* 114, 4359–4369. doi:10.1242/jcs.114.24.4359

Palka, K. (1999). Changes in Intramuscular Connective Tissue and Collagen Solubility of Bovine m.Semitendinosus during Retorting. *Meat Sci.* 53, 189–194. doi:10.1016/s0309-1740(99)00047-9

Pinilla-Tenas, J., Barber, A., and Lostao, M. P. (2003). Transport of Proline and Hydroxyproline by the Neutral Amino-Acid Exchanger ASCT1. *J. Membr. Biol.* 195, 27–32. doi:10.1007/s00232-003-2041-9

Rescan, P. Y. (2005). Muscle Growth Patterns and Regulation during Fish Ontogeny. *General Comp. Endocrinol.* 142, 111–116. doi:10.1016/j.ygcen.2004.12.016

Rong, H., Lin, F., Zhang, Y., Bi, B., Dou, T., Wu, X., et al. (2020a). The TOR Pathway Participates in the Regulation of Growth Development in Juvenile Spotted Drum (*Nibea Diacanthus*) under Different Dietary Hydroxyproline Supplementation. *Fish. Physiol. Biochem.* 46, 2085–2099. doi:10.1007/s10695-020-00863-z

Rong, H., Zhang, Y., Hao, M., Lin, F., Zou, W., Zhang, H., et al. (2020b). Effect of Hydroxyproline Supplementation on Growth Performance, Body Composition, Amino Acid Profiles, Blood-biochemistry and Collagen Synthesis of Juvenile Chu's Croaker (Nibea Coibor). *Aquac. Res.* 51, 1264–1275. doi:10.1111/are.14477

Rong, H., Zhang, Y., Hao, M., Zou, W., Yu, J., Yu, C., et al. (2019). Effects of Dietary Hydroxyproline on Collagen Metabolism, Proline 4-hydroxylase Activity, and Expression of Related Gene in Swim Bladder of Juvenile *Nibea Diacanthus*. *Fish. Physiol. Biochem.* 45, 1779–1790. doi:10.1007/s10695-019-00676-9

Rowlerson, A., and Veggetti, A. (2001). "Cellular Mechanisms of Post-embryonic Muscle Growth in Aquaculture Species," in *Muscle Development and Growth* (Cambridge, Massachusetts, US: Academic Press), 103–140. doi:10.1016/s1546-5098(01)18006-4

Sato, K., Ando, M., Kubota, S., Origasa, K., Kawase, H., Toyohara, H., et al. (1997). Involvement of Type V Collagen in Softening of Fish Muscle during Short-Term Chilled Storage. *J. Agric. Food Chem.* 45 (2), 343–348. doi:10.1021/jf9606619

Sekiya, I., Larson, B. L., Vuoristo, J. T., Reger, R. L., and Prockop, D. J. (2005). Comparison of Effect of BMP-2, -4, and -6 on *In Vitro* Cartilage Formation of Human Adult Stem Cells from Bone Marrow Stroma. *Cell Tissue Res.* 320, 269–276. doi:10.1007/s00441-004-1075-3

Song, S., Ahn, C.-H., and Kim, G.-D. (2020). Muscle Fiber Typing in Bovine and Porcine Skeletal Muscles Using Immunofluorescence with Monoclonal Antibodies Specific to Myosin Heavy Chain Isoforms. *Food Sci. Anim. Resour.* 40, 132–144. doi:10.5851/kosfa.2019.e97

Tu, Y., Xie, S., Han, D., Yang, Y., Jin, J., Liu, H., et al. (2015). Growth Performance, Digestive Enzyme, Transaminase and GH-IGF-I axis Gene Responsiveness to Different Dietary Protein Levels in Broodstock Allogenogynetic Gibel Carp (*Carassius auratus Gibelio*) CAS III. *Aquaculture* 446, 290–297. doi:10.1016/j.aquaculture.2015.05.003

Wei, Y., Li, B., Xu, H., and Liang, M. (2020). Fish Protein Hydrolysate in Diets of Turbot Affects Muscle Fibre Morphometry, and the Expression of Muscle Growth-related Genes. *Aquacult. Nutr.* 26, 1780–1791. doi:10.1111/anu.13129

Wei, Z., Ma, J., Pan, X., Mu, H., Li, J., Shentu, J., et al. (2016). Dietary Hydroxyproline Improves the Growth and Muscle Quality of Large Yellow Croaker *Larimichthys Crocea*. *Aquaculture* 464, 497–504. doi:10.1016/j.aquaculture.2016.07.015

Wu, G., Bazer, F. W., Burghardt, R. C., Johnson, G. A., Kim, S. W., Knabe, D. A., et al. (2011). Proline and Hydroxyproline Metabolism: Implications for Animal and Human Nutrition. *Amino acids* 40, 1053–1063. doi:10.1007/s00726-010-0715-z

Wullschleger, S., Loewith, R., and Hall, M. N. (2006). TOR Signaling in Growth and Metabolism. *Cell* 124, 471–484. doi:10.1016/j.cell.2006.01.016

Xia, Y., Yu, E., Li, Z., Zhang, K., Tian, J., Wang, G., et al. (2021). Both TGF-β1 and Smad4 Regulate Type I Collagen Expression in the Muscle of Grass Carp, Ctenopharyngodon Idella. *Fish. Physiol. Biochem.* 47, 907–917. doi:10.1007/s10695-021-00941-w

Xiao, H., Huang, X., Wang, S., Liu, Z., Dong, R., Song, D., et al. (2020). Metformin Ameliorates Bleomycin-Induced Pulmonary Fibrosis in Mice by Suppressing IGF-1. *Am. J. Transl. Res.* 12 (3), 940–949.

Xu, F., Liu, C., Zhou, D., and Zhang, L. (2016). TGF-β/SMAD Pathway and its Regulation in Hepatic Fibrosis. *J. Histochem Cytochem.* 64, 157–167. doi:10.1369/0022155415627681

Xu, Y., Tan, Q., Kong, F., Yu, H., Zhu, Y., Yao, J., et al. (2019). Fish Growth in Response to Different Feeding Regimes and the Related Molecular Mechanism on the Changes in Skeletal Muscle Growth in Grass Carp (*Ctenopharyngodon idellus*). *Aquaculture* 512, 734295. doi:10.1016/j.aquaculture.2019.734295

Yamauchi, M., and Shiiba, M. (2002). "Lysine Hydroxylation and Crosslinking of Collagen," in *Posttranslational Modifications of Proteins* (Berlin, Germany: Springer), 277–290.

Yano, H., Hamanaka, R., Nakamura, M., Sumiyoshi, H., Matsuo, N., and Yoshioka, H. (2012). Smad, but Not MAPK, Pathway Mediates the Expression of Type I Collagen in Radiation Induced Fibrosis. *Biochem. Biophysical Res. Commun.* 418, 457–463. doi:10.1016/j.bbrc.2012.01.039

Yu, E.-m., Ma, L.-l., Ji, H., Li, Z.-f., Wang, G.-j., Xie, J., et al. (2019). Smad4-dependent Regulation of Type I Collagen Expression in the Muscle of Grass Carp Fed with Faba Bean. *Gene* 685, 32–41. doi:10.1016/j.gene.2018.10.074

Zammit, P. S. (2017). Function of the Myogenic Regulatory Factors Myf5, MyoD, Myogenin and MRF4 in Skeletal Muscle, Satellite Cells and Regenerative Myogenesis. *Seminars Cell & Dev. Biol.* 72, 19–32. doi:10.1016/j.semcdb.2017.11.011

Zanou, N., and Gailly, P. (2013). Skeletal Muscle Hypertrophy and Regeneration: Interplay between the Myogenic Regulatory Factors (MRFs) and Insulin-like Growth Factors (IGFs) Pathways. *Cell. Mol. Life Sci.* 70, 4117–4130. doi:10.1007/s00018-013-1330-4

Zhang, K., Ai, Q., Mai, K., Xu, W., Liufu, Z., Zhang, Y., et al. (2013). Effects of Dietary Hydroxyproline on Growth Performance, Body Composition, Hydroxyproline and Collagen Concentrations in Tissues in Relation to Prolyl 4-hydroxylase α(I) Gene Expression of Juvenile Turbot, *Scophthalmus maximus* L. Fed High Plant Protein Diets. *Aquaculture* 404-405, 77–84. doi:10.1016/j.aquaculture.2013.04.025

Zhang, K., Mai, K., Xu, W., Zhou, H., Liufu, Z., Zhang, Y., et al. (2015). Proline with or without Hydroxyproline Influences Collagen Concentration and Regulates Prolyl 4-hydroxylase α (I) Gene Expression in Juvenile Turbo (*Scophthalmus maximus* L.). *J. Ocean. Univ. China* 14, 541–548. doi:10.1007/s11802-015-2436-0

Zhao, Y., Li, J.-Y., Jiang, Q., Zhou, X.-Q., Feng, L., Liu, Y., et al. (2020). Leucine Improved Growth Performance, Muscle Growth, and Muscle Protein Deposition through AKT/TOR and AKT/FOXO3a Signaling Pathways in Hybrid Catfish Pelteobagrus Vachelli × Leiocassis Longirostris. *Cells* 9, 327. doi:10.3390/cells9020327

Conflict of Interest: The authors declare that the research was conducted in the absence of any commercial or financial relationships that could be construed as a potential conflict of interest.

Publisher's Note: All claims expressed in this article are solely those of the authors and do not necessarily represent those of their affiliated organizations, or those of the publisher, the editors and the reviewers. Any product that may be evaluated in this article, or claim that may be made by its manufacturer, is not guaranteed or endorsed by the publisher.

frontiers | Frontiers in Physiology

ORIGINAL RESEARCH
published: 24 June 2022
doi: 10.3389/fphys.2022.921709

Effects of Acute Hypoxic Stress on Physiological and Hepatic Metabolic Responses of Triploid Rainbow Trout (*Oncorhynchus mykiss*)

Buying Han[1,2†], Yuqiong Meng[2†], Haining Tian[2], Changzhong Li[2], Yaopeng Li[3], Caidan Gongbao[3], Wenyan Fan[3] and Rui Ma[1]*

[1]State Key Laboratory of Plateau Ecology and Agriculture, Qinghai University, Xining, China, [2]College of Eco-Environmental Engineering, Qinghai University, Xining, China, [3]Qinghai Minze Longyangxia Ecological Aquaculture Co., Ltd., Longyangxia, China

OPEN ACCESS

Edited by:
Jianlong Ge,
Chinese Academy of Fishery Sciences (CAFS), China

Reviewed by:
Mingchun Ren,
Chinese Academy of Fishery Sciences, China
Haokun Liu,
Institute of Hydrobiology (CAS), China
Hongyan Tian,
Yancheng Institute of Technology, China

***Correspondence:**
Rui Ma
myrui713@163.com

[†]These authors have contributed equally to this work

Specialty section:
This article was submitted to Aquatic Physiology, a section of the journal Frontiers in Physiology

Received: 16 April 2022
Accepted: 08 June 2022
Published: 24 June 2022

Citation:
Han B, Meng Y, Tian H, Li C, Li Y, Gongbao C, Fan W and Ma R (2022) Effects of Acute Hypoxic Stress on Physiological and Hepatic Metabolic Responses of Triploid Rainbow Trout (Oncorhynchus mykiss). Front. Physiol. 13:921709. doi: 10.3389/fphys.2022.921709

This experiment simulated the hypoxic environment caused by actual production operations in fish farming (i.e., catching, gathering, transferring, and weighting) to study the effects of acute hypoxic conditions on the physiological and metabolic responses of triploid rainbow trout (*O. mykiss*). Two groups of fish weighting 590 g were sampled in the normoxia group (dissolved oxygen above 7 mg/L) and hypoxia group (dissolved oxygen ranged from 2 to 5 mg/L for 10 min). The results showed that 1) regarding stress response, hypoxia increased plasma levels of cortisol, heat shock protein 70 (HSP-70), lysozyme, alanine aminotransferase (ALT), aspartate aminotransferase (AST) and creatine phosphokinase (CPK); induced the expression of hepatic genes encoding nuclear factor erythroid 2 related factor 2 (*Nrf2*), interferon γ (*IFN-γ*) and interleukin-1β (*IL-1β*). 2) Regarding metabolism response, hypoxia increased plasma levels of globulin (GLOB), glucose (GLU), triglyceride (TG) and lactate dehydrogenase (LDH); upregulated the hepatic gene expression of phosphoenolpyruvate carboxykinase, (*PEPCK*), pyruvate dehydrogenase kinase (*PDK1*), acetyl-CoA carboxylase (*ACC*) and acetyl-CoA oxidase (*ACO*); downregulated the hepatic gene expression of carnitine palmitoyl transferase 1 (*CPT1*); and unchanged the expression of hepatic genes in glycolysis and autophagy. 3) In response to hypoxia-inducible factors (HIFs), the hepatic *HIF-2α* gene was activated in the hypoxia group, but *HIF-1α* gene expression remained unchanged. Thus, during acute hypoxic stress, triploid rainbow trout were in a defensive state, with an enhanced immune response and altered antioxidant status. Additionally, the hepatic mitochondrial oxidation of glucose- and lipid-derived carbon in trout was suppressed, and hepatic gluconeogenesis and lipid synthesis were activated, which might be regulated by the HIF-2α pathway.

Keywords: triploid rainbow trout, acute hypoxia, physiology, metabolism, HIF-2α

INTRODUCTION

Rainbow trout (*O. mykiss*) is one of the most extensively farmed salmonid species, and in 2018, global production was over 848,000 tons (FAO, 2020). Because of its advantages of rapid growth, high meat quality and no gene pollution, triploid rainbow trout have become the main upmarket cold-water fish in China (Ma et al., 2019). Dissolved oxygen (DO) is one of the main restricted environmental factors in fish farming. Rainbow trout have been shown to be a hypoxia-sensitive fish species when the DO in water is below 7 mg/L (Abdel-Tawwab et al., 2019; Hou et al., 2020). Triploid salmonid fish appear to require higher oxygen for growth and feeding than diploid fish (Hansen et al., 2015). Therefore, hypoxic stress should be considered in triploid rainbow trout farming.

During the initial stage of hypoxia, some fish did not show any special activity and remained static at the bottom of the tank to conserve energy (Wu et al., 2007; Douxfils et al., 2012). With decreasing of DO levels, fish swam rapidly in a circular motion with a wide mouth opening, moved upward to the water surface, and began air breathing (Bowyer et al., 2015). A DO level consistently below 1–2 mg/L could lead to fish death (Abdel-Tawwab et al., 2019). Special production operations in fish farming, such as catching, gathering, transferring, or weighting, can cause local DO levels to decrease below 5 mg/L, or even 2 mg/L, within minutes. In land animals, the pulmonary vascular response was altered within 10 min of exposure to acute hypoxia in subjects developing high-altitude pulmonary edema (Dubowitz et al., 2009). In zebrafish, acute hypoxia (15 min at 10% or 5% air saturation) caused osmorespiratory compromise (Onukwufor and Wood, 2020). However, few studies have focused on the response of fish to short-term and intense hypoxic stress.

The effects of hypoxic stress on fish growth, physiological performance, immune responses and hypoxia signaling pathways have been reported (Zhu et al., 2013; Xiao, 2015; Abdel-Tawwab et al., 2019). When DO is insufficient for the oxygen demands of fish, blood biochemical indicators reflecting fish physiological function are changed, such as the number of red blood cells; the levels of cortisol, triglyceride (TG), and glucose (GLU); and the activities of lactic dehydrogenase and transaminase (Barcellos et al., 1999; Trenzado et al., 2006; Martos-Sitcha et al., 2019; Hou et al., 2020). Hypoxic stress can disturb the normal physiological function of fish by imposing oxidative stress on organisms by accelerating the generation of highly reactive oxygen species (ROS) (Lushchak, 2011). This causes oxidative damage and inflammatory reactions that seriously threaten the health of farmed fish. The aerobic metabolic pathway is converted into an anaerobic metabolic pathway to fulfill the high-energy requirements of fish during hypoxic stress (Abdel-Tawwab et al., 2019). Nutritional metabolism can be affected by hypoxia, but the results are controversial in different fish species and under different hypoxic conditions (acute or chronic stress) (Beck et al., 2016; Pillet et al., 2016; Li et al., 2018). Based on the data from the terrestrial animals, adaptive changes in physiological and metabolic conditions in fish may be mediated by a family of hypoxia-inducible factors (HIFs) (Majmundar et al., 2010; Mylonis et al., 2019). Several studies have reported a connection between HIFs and hypoxia in Atlantic croaker (*Micropogonias undulatus*) (Rahman and Thomas, 2007), Eurasian perch (*Perca fluviatilis*) (Rimoldi et al., 2012), whitefish (*Coregonus clupeaformis*) (Whitehouse and Manzon, 2019), largemouth bass (*Micropterus salmoides*) (Yang et al., 2019), and rainbow trout (Hou et al., 2020). However, the aforementioned information for triploid rainbow trout remains undefined.

Thus, this study simulated the hypoxic environment caused by actual production operations in fish farming to evaluate the effect of acute hypoxic stress on the physiological and metabolic responses of triploid rainbow trout by measuring plasma biochemical parameters, antioxidant capacity, immune responses, hypoxia-related gene expressions, and energy metabolism.

MATERIALS AND METHODS

Fish, Feeding, and Sampling

This study was performed in strict accordance with the Standard Operation Procedures of the Guide for the Use of Experimental Animals of Qinghai University. The research protocol was reviewed and approved by the Ethical Committee of Qinghai University.

Female triploid rainbow trout from the same population were obtained from the Qinghai Minze Longyangxia Ecological Aquaculture Co., Ltd., China. Before the sampling, the water temperature was 14°C, and DO remained higher than 7 mg/L. Eighteen fish were randomly selected from a cultured cage and then sampled directly as the normoxic group. For the simulation of the hypoxic environment caused by actual production operations of catching and gathering in fish farming, 30 fish were randomly picked from the same culture cage and gently placed in a sealed plastic 400 L tank. When the DO in the tank was reached 5 mg/L because of fish breathing, the time was started. After hypoxic treatment for 10 min, DO decreased to 2 mg/L because of oxygen depletion, and some fish bellied up and floated in the water. Six seemingly normal fish were then sampled directly. The other new fish were picked from the same cage to repeat the aforementioned procedure twice. Eighteen fish were in the hypoxic group. DO and water temperature were continuously monitored using a DO meter (OxyGuard Handy Polaris portable, Denmark).

Sample Collection

All sampled fish were anesthetized with eugenol (1:10,000) (Shanghai Reagent Corp, China) and then weighted (body weight, 592.89 ± 9.33 g; no difference was observed between the two groups). Blood was collected from the caudal vein by using heparinized syringes. Plasma was obtained by centrifugation at 3,000 rpm for 10 min. Plasma samples of similar volumes from three fish in the same group were pooled as one biological replicate. Liver tissue samples from the bled fish were subsequently dissected, and tissue samples of similar size were pooled according to the same procedure used for plasma. Six biological replicates ($n = 6$) from each group were analyzed. All samples were frozen in liquid nitrogen and then stored at −80°C for further biochemical and gene expression studies.

Liver samples were added to 0.9% cold physiological saline, and the ratio of tissue mass (g) to physiological saline (ml) was 1: 9. Tissue homogenates (10%) were prepared by grinding with a tissue homogenizer (XHF-D, Xinzhi, China) and then homogenized by centrifugation at 4°C and 3,000 rpm for 10 min to determine the total protein, malondialdehyde (MDA), and total antioxidant capacity (T-AOC) contents.

Biochemical Analysis

Plasma alanine aminotransferase (ALT), aspartate aminotransferase (AST), alkaline phosphatase (ALP), creatine phosphokinase (CPK), lactate dehydrogenase (LDH), total protein (TP), albumin (ALB), globulin (GLOB), glucose (GLU), triglyceride (TG), and total cholesterol (TC) levels were assayed in a certified hospital by using standard clinical methods in an automatic biochemical analyzer (ADVIA 2400; SIEMENS; Germany). Plasma cortisol, lysozyme, and heat shock protein 70 (HSP-70) levels were determined by enzyme-linked immunosorbent assay (ELISA), using commercial ELISA kits (Shanghai Enzyme Biotechnology Co., Ltd.).

The MDA and T-AOC contents in the plasma and liver were determined *via* a commercial kit (Nanjing Jiancheng Bioengineering Research Institute), using the TBA method and three FRAP methods, respectively. The protein content in the liver was determined by using a commercial kit (Nanjing Jiancheng Bioengineering Research Institute) and the Coomassie Brilliant Blue method.

Total RNA Extraction and cDNA Synthesis

Total RNA was extracted from the liver tissue of triploid rainbow trout by using a total RNA extraction kit (DP419, Tiangen, China). A cDNA template was obtained using the PrimeScriptTM II1st strand cDNA Synthesis Kit (6210A, TaKaRa, Japan).

Real-Time PCR Primer Design

According to the gene sequences of rainbow trout for nuclear factor erythroid 2 related factor 2 (*Nrf2*), superoxide dismutase (*SOD*), catalase (*CAT*), glutathione peroxidase (*GPx*), heme oxygenase 1 (*HO-1*), interferon γ (*IFN-γ*), tumor necrosis factor-α (*TNF-α*), heat shock protein 70 (*HSP-70*), interleukin-1β (*IL-1β*), interleukin-8 (*IL-8*), fatty acid synthase (*FAS*), acetyl-CoA carboxylase (*ACC*), acetyl-CoA oxidase (*ACO*), adipose differentiation-related protein (ADRP), carnitine palmitoyl transferase 1 (*CPT1*), pyruvate dehydrogenase kinase (*PDK1*), phosphoenolpyruvate carboxykinase, (*PEPCK*), glucose-6-phosphatase (*G6PASE*), glucokinase (*GK*), glucose transporter 2 (*GLUT2*), L-lactate dehydrogenase (*LDHA*), glycogen synthase (*GYS*), glycogen phosphorylase, liver form-like (*GYPL*), microtubule associated protein 1 light chain 3 beta (*LC3β*), autophagy-related 4β (*ATG4B*), autophagy-related 12 L (*ATG12L*), gamma aminobutyric acid receptor-associated protein (*GABARAPL1*), hypoxia-inducible factor 1α (*HIF-1α*), hypoxia-inducible factor 2α (*HIF-2α*), factor inhibiting hypoxia-inducible factor 1(*FIH1*), and egl nine 1-like protein (*EGLN1*/*PHD2*), real-time PCR primers were designed using Primer 6.0 software. The primer sequences are shown in **Table 1**.

Gene Expression Analysis

Real-time PCR was conducted using a PCR instrument (Light Cycler® 480, Roche, United States) in a final volume of 10 μl containing 5 μl SYBR® Premix Ex TaqTM II (2×), 0.3 μl forward primer, 0.3 μl reverse primer, 1 μl cDNA template, and 3.4 μl sterile water. The thermal cycling system reaction conditions were 95°C for 5 min; 95°C for 30 s, 60°C for 30 s, and 72°C for 30 s; and 40 cycles of 72°C, for 10 min. Each reaction was repeated three times. The relative abundance of the genes was normalized to that of *β-actin* and calculated using the $2^{-\Delta\Delta Ct}$ method.

Statistical Analysis

Statistical analysis of the experimental data was performed using SPSS 20 data analysis software, and the obtained data were expressed as the mean ± standard error. The effects of normoxia and hypoxia on individual indicators were analyzed using independent samples *t*-test. Compared with the normal group, $^{*}p < 0.05$; $^{**}p < 0.01$.

RESULTS

Effect of Acute Hypoxic Stress on the Plasma Biochemical Parameters of Triploid Rainbow Trout

As shown in **Table 2**, the ALT, AST, LDH, CPK, GLOB, GLU, and TG levels were significantly higher in the hypoxic group, but ALB level was lower than that in the normoxic group ($p < 0.05$). Particularly notable is that the maximal increase in LDH level was approximately 4.6-fold higher in the hypoxic group than in the normoxic group. No significant differences were observed in the plasma TP, TC, and ALP levels between the two groups ($p > 0.05$).

Under hypoxic conditions, plasma levels of lysozyme, cortisol, and HSP-70 increased significantly ($p < 0.01$; **Table 2**).

Effect of Acute Hypoxic Stress on the Hypoxia-Related Gene Expression in the Liver of Triploid Rainbow Trout

Changes in the expression of hypoxia-related genes are shown in **Figure 1**. The mRNA expression of *HIF-2α* was upregulated in the liver of triploid rainbow trout under acute hypoxic stress ($p < 0.05$; **Figure 1**). Particularly notable is that the maximal increase in *HIF-2α* was approximately 2.5-fold higher in the hypoxic group than in the normoxic group. However, the mRNA expression of *HIF-1α, FIH1, and PHD2* was not affected by acute hypoxic stress ($p > 0.05$).

Effect of Acute Hypoxic Stress on the Antioxidant Capacity and Antioxidant Related Genes Expressions in the Plasma or Liver of Triploid Rainbow Trout

As shown in **Figure 2**, the MDA contents of the plasma and liver in the hypoxic group were significantly higher than those in the normoxic group (**Figures 2A,B**; $p < 0.05$). T-AOC levels in the plasma and liver showed trends opposite those of MDA content (**Figures 2C,D**; $p < 0.05$).

TABLE 1 | Primers used for gene expression analysis in *Oncorhynchus mykiss*.

Primer	Primer sequence (5′to 3′)	Gene	Accession
Hypoxia-related genes			
RTHIF-1α-F1	TCTGAGGACGGGGACATGAT	*HIF-1α*	AF304864.1
RTHIF-1α-R1	GGTCTGAGCAGTGGAGAACC		
RTHIF-2α-F1	GGTTACATCAGACGGCGACA	*HIF-2α*	XM_021576379.1
RTHIF-2α-R1	CCTTCTTCCCAGTGCCATTTT		
RTFIH1-F1	ACAGCCCTATCTGGAACGACTC	*FIH1*	NM_001281328.1
RTFIH1-R1	CCACTGGTTGCTCGTTGTTTAT		
RTPHD2-F1	TGGAAAACCTGCTTAAATGTGGAC	*PHD2*	HQ615594.1
RTPHD2-R1	TTTGAACCGCTTGCCTTGC		
Antioxidant-related genes			
RTNrf2-F1	GCAGAGGTCTGCCCACCTGAAT	*Nrf2*	HQ916348.1
RTNrf2-R1	GCCACAAGGCAGGGTGACACTT		
RTSOD-F1	TGAAGGCTGTTTGCGTGCTGAC	*SOD*	NM_001160614.1
RTSOD-R1	CCGTTGGTGTTGTCTCCGAAGG		
RTCAT-F1	CCGTCCTTCGTCCACTCTCAGA	*CAT*	XM_021568213.1
RTCAT-R1	CTCGGCATCCTCAGGCTTCAAG		
RTGPx-F1	TCATCATGTGGAGCCCTGTCTG	*GPx*	AF281338.1
RTGPx-R1	TCTGCCTCAATGTCACTGGTCA		
RTHO-1-F1	CGCCTACACCCGTTACCTAG	*HO-1*	XM_021558210.1
RTHO-1-R1	CTCTCCGCTGCTTAACCCAA		
Immune-related genes			
RTIFN-γ-F1	TACCCTCACCTTCCCACCA	*IFN-γ*	NM_001124620.1
RTIFN-γ-R1	TTCCTGCGGTTGTCCTTCTT		
RTTNF-α-F1	GGCGAGCATACCACTCCTCTGA	*TNF-α*	AJ401377.1
RTTNF-α-R1	AGCTGGAACACTGCACCAAGGT		
RTHSP-70-F1	GGACGCAGCCAAGAACCAAGT	*HSP-70*	AB062281.1
RTHSP-70-R1	GGCCGTGTCGAGTCGTTGAT		
RTIL-1β-F1	ACGGTTCGCTTCCTCTTCTACA	*IL-1β*	AJ557021.2
RTIL-1β-R1	GCTCCAGTGAGGTGCTGATGAA		
RTIL-8-F1	GTCAGCCAGCCTTGTCGTTGT	*IL-8*	NM_001124362.1
RTIL-8-R1	CGTCTGCTTTCCGTCTCAATGC		
Glycometabolism genes			
RTGK-F1	AGATCACTGTGGGCATCGAC	*GK*	AF053331.2
RTGK-R1	GATGTCACAGTGAGGCGTCA		
RTLDHA-F1	GGCGTGAATGTTGCTGGTGT	*LDHA*	XM_021564046.1
RTLDHA-R1	TCCTCCTTGTCTGCGTCTGTG		
RTPEPCK-F1	CGGTGTGTTTGTAGGAGCCT	*PEPCK*	NM_001124275.1
RTPEPCK-R1	ACGTGGAAGATCTTGGGCAG		
RTG6PASE-F1	GCTGACCTGCATACCACCTT	*G6PASE*	XM_021575943.1
RTG6PASE-R1	CAGCCACCCAGATGAGCTTT		
RTPDK1-F1	CAGACCCCATCGTCAGCC	*PDK1*	XM_021597164.1
RTPDK1-R1	TACCCTCACCTTCCCACCA		
RTGLUT2-F1	GGACCAGCAACTTCATCATAGGC	*GLUT2*	AF321816.1
RTGLUT2-R1	CCAAACAACAGCACAGCAAACA		
RTGYS-F1	GACAGAGAGGCCAACGACTC	*GYS*	XM_021563420.1
RTGYS-R1	ACTCATGGAAATGGGCGAGG		
RTGYPL-F1	TGATTAACCTGGGGCTGCAG	*GYPL*	XM_021585435.1
RTGYPL-R1	GCCATCGAGTCCAGGAAACA		
Lipometabolism genes			
RTFAS-F1	TCTAGAGACGCCACCTTCGA	*FAS*	XM_021581290.1
RTFAS-R1	TGCAGTTTCTCCTCAGCCAG		
RTACC-F1	TCATCAATGCCAAGGACCCC	*ACC*	XM_021618451.1
RTACC-R1	CGTCAGAGTCCAGGTTTGCT		
RTCPT1-F1	TACAGCTGGCCCAATTCAGG	*CPT1*	AF327058.3
RTCPT1-R1	TCGCAGTGTTCTTGTCCTCC		
RTACO-F1	TTGGGCCTCATCATTGCAGT	*ACO*	XM_021613038.1
RTACO-R1	ACTGGGTCTGGTGCTCAATG		
RTADRP-F1	CAGATGGTCAGCAGCGGAATG	*ADRP*	XM_021615225.1
RTADRP-R1	GAGCCCAGACGGACATAGTAGC		
Autophagy-related genes			
RTLC3β-F1	CCCCAACAAGATTCCGGTCA	*LC3β*	KX845472.1
RTLC3β-R1	GGTTGGAGTTCAGCTGGAGG		
RTGBRAP-F1	TACCTTGTGCCCTCTGACCT	*GABARAPL1*	NM_001165091.1

(Continued on following page)

TABLE 1 | (*Continued*) Primers used for gene expression analysis in *Oncorhynchus mykiss*.

Primer	Primer sequence (5′to 3′)	Gene	Accession
RTGBRAP-R1	GCTGAGGTGGGAGGAATGAC		
RTATG4B-F1	TATGCGCTTCCGAAAGTTGTC	*ATG4B*	CA345181.1
RTATG4B-R1	CAGGATCGTTGGGGTTCTGC		
RTATG12L-F1	TGGAGGCCAATGAACAGCTG	*ATG12L*	XM_021623074.1
RTATG12L-R1	CTTCCCATCGCTGCCAAAAC		
Reference gene			
RTβ-actin-F1	TACAACGAGCTGAGGGTGGC	*β-actin*	AJ438158.1
RTβ-actin-R1	GGCAGGGGTGTTGAAGGTCT		

TABLE 2 | Effect of acute hypoxic stress on the plasma biochemical parameters of triploid rainbow trout (n = 6).

Biochemical parameters	Normoxic group	Hypoxic group	*t*-test
ALT[a] (U/L)	11.40 ± 0.40	21.80 ± 1.80	**
AST[b] (U/L)	276 ± 13.40	553 ± 42.00	**
ALP[c] (U/L)	186 ± 7.94	207 ± 16.50	ns
CPK[d] (U/L)	3414 ± 321	6688 ± 228	**
LDH[e] (U/L)	213 ± 13.60	982 ± 135.00	**
TP[f] (g/L)	42.90 ± 0.71	43.10 ± 0.95	ns
ALB[g] (g/L)	16.10 ± 0.25	15.10 ± 0.34	*
GLOB[h] (g/L)	26.70 ± 0.54	28.30 ± 0.56	*
GLU[i] (mg/dl)	91.08 ± 6.66	127.80 ± 3.60	**
TC[j] (mg/dl)	425.37 ± 11.99	444.71 ± 21.66	ns
TG[k] (mg/dl)	383.66 ± 8.84	472.94 ± 15.03	**
Cortisol (pg/ml)	325.75 ± 6.26	426.75 ± 11.64	**
HSP-70[l] (pg/ml)	115.41 ± 3.35	132.39 ± 3.97	**
Lysozyme (U/L)	1.69 ± 0.04	2.01 ± 0.05	**

*Note: mean ± standard error; ns, no significant difference (p > 0.05); *p < 0.05; **p < 0.01.*
[a]*ALT, alanine aminotransferase.*
[b]*AST, aspartate aminotransferase.*
[c]*ALP, alkaline phosphatase.*
[d]*CPK, creatine phosphokinase.*
[e]*LDH, lactic dehydrogenase.*
[f]*TP, total protein.*
[g]*ALB, albumin.*
[h]*GLOB, globulin.*
[i]*GLU, glucose.*
[j]*TC, total cholesterol.*
[k]*TG, triglyceride.*
[l]*HSP-70, heat shock protein 70.*

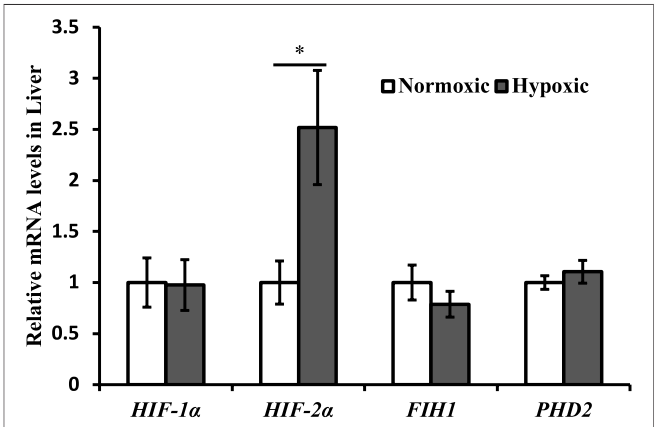

FIGURE 1 | Effect of acute hypoxic stress on the expression of the hypoxia-related genes in the liver of triploid rainbow trout (n = 6; *HIF-1α*, hypoxia-inducible factor 1α; *HIF-2α*, hypoxia-inducible factor 2α; *FIH1*, factor inhibiting hypoxia-inducible factor 1; *PHD2*, egl nine 1-like protein). Asterisks indicate the significant difference (*t*-test; *p < 0.05; **p < 0.01).

The effect of acute hypoxic stress on the antioxidant gene expression in the liver is shown in **Figure 3**. The expression of *Nrf2* mRNA was upregulated in the liver, and the mRNA expression of *SOD* and *HO-1* was downregulated (p < 0.05; **Figure 3**). Particularly notable is that the maximal increase in *Nrf2* was approximately 2.5-fold higher in the hypoxic group than in the normoxic group. No significant difference was observed in the mRNA expression of *CAT* and *GPx* in the liver of triploid rainbow trout (p > 0.05).

Effect of Acute Hypoxic Stress on the Immune-Related Genes Expressions in the Liver of Triploid Rainbow Trout

Changes in the expression of genes related to the immune system are shown in **Figure 4**. The mRNA expression of *IFN-γ* and *IL-1β* in the liver were upregulated under acute hypoxic stress (p < 0.05; **Figure 4**). Additionally, the maximal increase in *IFN-γ* was approximately 3.5-fold higher in the hypoxic group than in the normoxic group. However, the mRNA expression of *TNF-α* in the liver was downregulated (p < 0.05; **Figure 4**). No significant differences were observed in the mRNA expression levels of *HSP-70* and *IL-8* in the liver of triploid rainbow trout (p > 0.05; **Figure 4**).

Effect of Acute Hypoxic Stress on the Glycometabolic Genes Expressions in the Liver of Triploid Rainbow Trout

Data on the mRNA expression of the glycometabolic genes are shown in **Figure 5**. The mRNA expression of *PEPCK* and *PDK1* in liver tissue was upregulated under acute hypoxic stress (p < 0.05). Additionally, the maximal increase in *PEPCK* was approximately 4-fold higher in the hypoxic group than in the normoxic group. However, no significant differences were observed in the mRNA expression levels of *GLUT2*, *GYPL*, *GK*, *LDHA*, *G6Pase*, and *GYS* in the liver of triploid rainbow trout under acute hypoxic stress (p > 0.05).

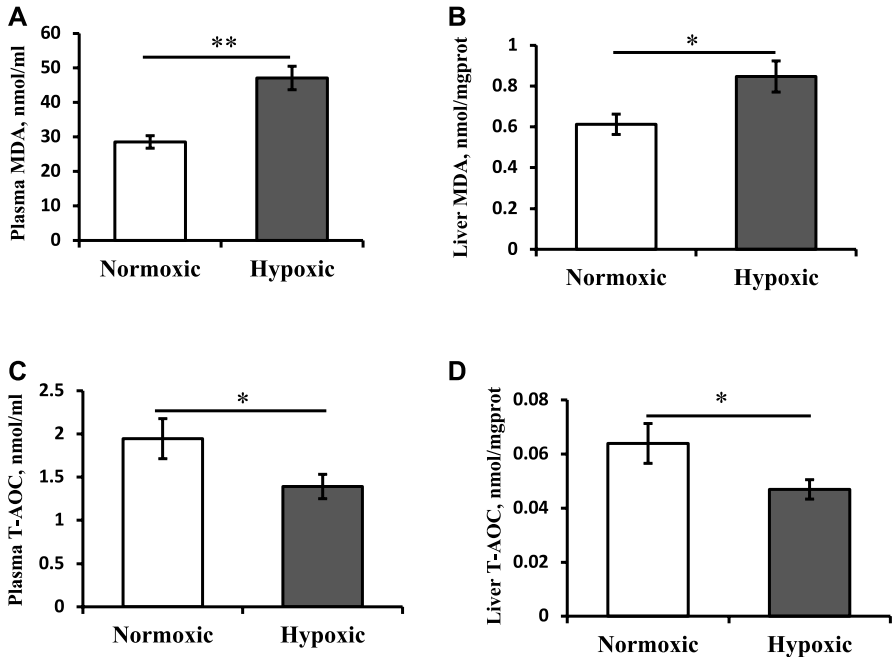

FIGURE 2 | Effect of acute hypoxic stress on the malondialdehyde (MDA) content in the plasma **(A)** and liver **(B)** as well as the total antioxidant capacity (T-AOC) level in the plasma **(C)** and liver **(D)** of triploid rainbow trout (n = 6). Asterisks indicate the significant differences (t-test; *p < 0.05; **p < 0.01).

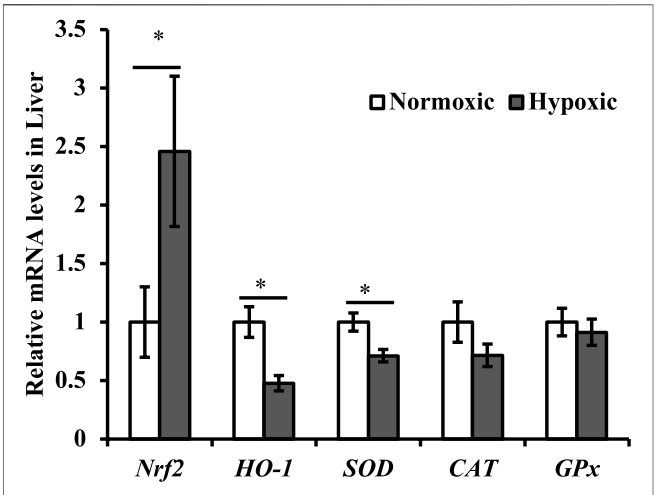

FIGURE 3 | Effect of acute hypoxic stress on the expression of the antioxidant-related genes in the liver of triploid rainbow trout (n = 6; Nrf2, nuclear factor erythroid 2 related factor 2; SOD, superoxide dismutase; CAT, catalase; GPx, glutathione peroxidase). Asterisks indicate significant differences (t-test; *p < 0.05; **p < 0.01).

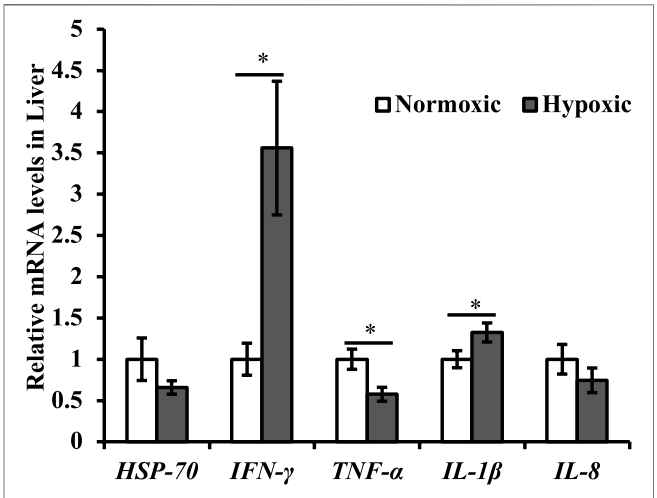

FIGURE 4 | Effect of acute hypoxic stress on the expression of the immune-related genes in the liver of triploid rainbow trout (n = 6; IFN-γ, interferon γ; TNF-α, tumor necrosis factor-α; HSP-70, heat shock protein 70; IL-1β, interleukin-1β; IL-8, interleukin-8). Asterisks indicate significant differences (t-test; *p < 0.05; **p < 0.01).

Effects of Acute Hypoxic Stress on the Lipometabolic Gene Expression in the Liver of Triploid Rainbow Trout

Data on the mRNA expression of the lipometabolic genes are shown in **Figure 6**. The mRNA expression levels of *ACC* and *ACO* were upregulated, but *CPT1* was downregulated in liver tissue under hypoxic stress (p < 0.05). Additionally, the maximal increase in *ACC* was approximately 8-fold higher in the hypoxic group than in the normoxic group. However, no significant differences were observed in the mRNA expression levels of *FAS* and *ADRP* in liver of triploid rainbow trout under hypoxic stress (p > 0.05).

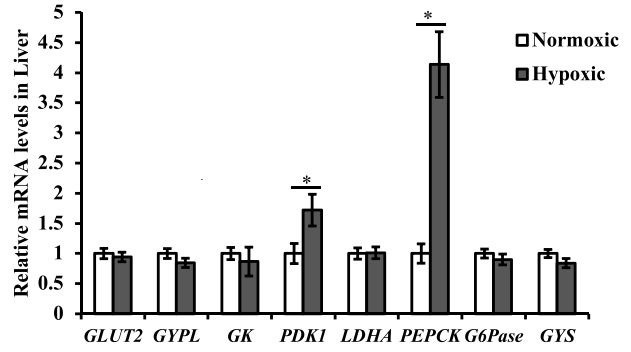

FIGURE 5 | Effect of acute hypoxic stress on the expression of the glycometabolic genes in the liver of triploid rainbow trout (n = 6; GLUT2, Glucose transporter 2; GYPL, Glycogen phosphorylase liver form-like; GK, Glucokinase; PDK1, Pyruvate dehydrogenase kinase; LDHA, L-lactate dehydrogenase; PEPCK, Phosphoenolpyruvate carboxykinase; G6Pase, Glucose-6-phosphatase; GYS, Glycogen synthase). Asterisks indicate significant differences (t-test; $^*p < 0.05$, $^{**}p < 0.01$).

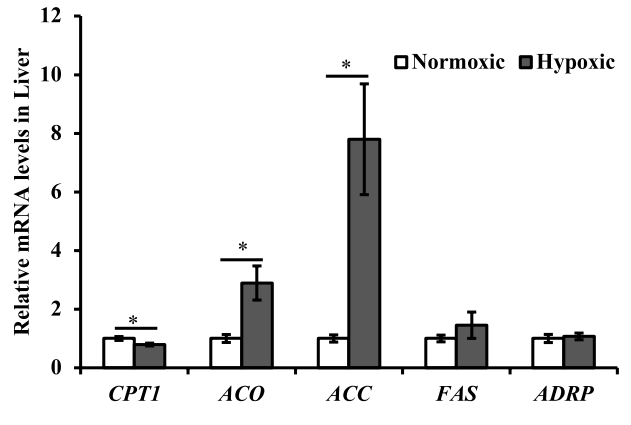

FIGURE 6 | Effect of acute hypoxic stress on the expression of the lipometabolic genes in the liver of triploid rainbow trout (n = 6; CPT1, carnitine palmitoyl transferase 1; ACO, acetyl-CoA oxidase; ACC, acetyl-CoA carboxylase; FAS, fatty acid synthase; ADRP, adipose differentiation-related protein). Asterisks indicate significant differences (t-test; $^*p < 0.05$, $^{**}p < 0.01$).

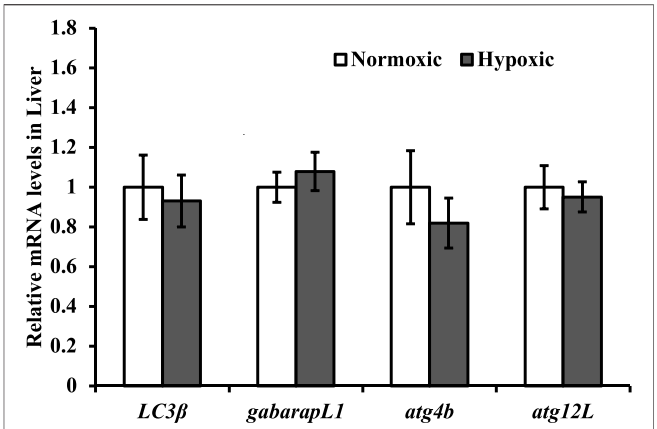

FIGURE 7 | Effect of acute hypoxic stress on the expression of the autophagy-related genes in the liver of triploid rainbow trout (n = 6; LC3β, microtubule associated protein 1 light chain 3 beta; gabarapL1, gamma aminobutyric acid receptor-associated protein; atg4b, autophagy-related 4β; atg12L, autophagy-related 12L). Asterisks indicate significant differences (t-test; $^*p < 0.05$; $^{**}p < 0.01$).

Effects of Acute Hypoxic Stress on Autophagy-Related Genes Expressions in the Liver of Triploid Rainbow Trout

No significant differences were observed in the mRNA expression levels of *LC3β*, *gabarapL1*, *atg4b*, and *atg12L* in the liver of triploid rainbow trout under hypoxic stress ($p > 0.05$; **Figure 7**).

DISCUSSION

The study simulated an acute hypoxic environment (2–5 mg/L for 10 min) caused by actual production operations of fish farming (i.e., catching, gathering, transferring, or weighting). During the hypoxic treatment, the fish firstly remained static at the bottom of the tank and then swam rapidly and moved upward to the water surface with a wide mouth opening. Finally, some fish bellied up and floated in the water. This treatment can lead to hypoxic stress in fish. When the fish body is stimulated by external adverse stress, a stress hormone, cortisol, is secreted, and its level increases in the blood (Bortoletti et al., 2021). In this study, the plasma cortisol content increased under acute hypoxic stress, which could be considered a sensitive signal of fish stress (Mommsen et al., 1999). A rapid, significant cortisol increase after an acute hypoxic disturbance was also found in other fish species (Abdel-Tawwab et al., 2019). Positive feedback potentiates the collaboration between cortisol and glucose in rainbow trout during stress (Conde-Sieira et al., 2012). A positive correlation between cortisol and glucose levels was observed in this study. In addition, plasma ALT and AST levels were increased in the hypoxic group in this study. Particularly notable is that the ALT activity (21.8 U/l) exceeded the normal reference range (4–19 U/L) of triploid rainbow trout reported in our previous study (Meng et al., 2019), reflecting the damage to the fish's liver. The MDA used as an indicator of lipid peroxidation and the T-AOC used as an indicator of the antioxidant capacity of the body were used in the analysis in this study. Based on the results of these indicators in the plasma and liver, the fish could experience oxidative stress under acute hypoxia.

The hypoxia-inducible factor-mediated signaling pathway has been recognized as a master regulator of cellular response to hypoxic stress (Xiao, 2015). Studies have found that acute hypoxic stress leads to upregulation of *HIF-1α* mRNA expression in the liver of fish, such as in zebrafish (*Danio rerio*) (Mandic et al., 2020), grouper (*Sebastes schlegelii*) (Jia et al., 2021), and big black mullet (*Dicentrarchus labrax*) (Vanderplancke et al., 2015). In this study, the expression

of *HIF-2α* in the liver increased, but not that of *HIF-1α* under acute hypoxia stress, suggesting that *HIF-2α* is a sensitive biomarker of acute hypoxic stress in triploid rainbow trout. In mammals, HIF-2α plays a critical role in stimulating the expression of genes encoding antioxidant enzymes to suppress the accumulation of ROS, inhibiting the mitochondrial consumption of glucose-derived carbon by PDK, regulating the lipid metabolism, and improving immune responses (Reviewed in Majmundar et al., 2010). Hence, the following studies aimed to evaluate the effect of the HIF-2α signaling pathway on the antioxidant, immune, and metabolic activties of triploid rainbow trout under acute hypoxic stress.

In the antioxidant system, an increase in the expression of *Nrf2* can activate the expression of Nrf2/ARE signaling pathway-related genes, leading to an increase in antioxidant enzyme activity (Balogun et al., 2003). In this study, the expression of the *Nrf2* gene in the liver was upregulated under acute hypoxic stress, and the expression of downstream genes such as *SOD*, *CAT*, and *GPx* was suppressed or unchanged. A study on *Schizothorax prenanti* found that the expression of *SOD*, *CAT*, and *GPX* was suppressed at the initial stage of acute hypoxic stress but increased at a later stage (Zhao et al., 2020). Only 10 min of hypoxic stress was used in this study, which was too short to stimulate the genes expression of antioxidant enzymes. HO-1 is a cytoprotective enzyme that could be involved in cytoprotection and antioxidant activity against hypoxic stress (Majmundar et al., 2010; Abdel-Tawwab et al., 2019). A study on rainbow trout showed that the expression of liver *HO-1* was downregulated by external adverse stress (Akdemir et al., 2016). The same result was also found in this study, whereas it was opposite to the result in mammals, that is, HIF2α could activate HO-1 (Majmundar et al., 2010). Therefore, further studies are required.

Regarding the immune response to hypoxia, this study found that plasma globulin, HSP-70, and lysozyme levels increased under acute hypoxic stress. The literature has speculated that fish can increase specific proteins such as lysozyme or HSP-70 to enhance immunity level and manage stress (Ortuno et al., 2001; Ming et al., 2012). In addition, HIFs can increase the production of inflammatory cytokines to participate in immunoreaction (Majmundar et al., 2010). The results of this study also showed that the expression of *IFN-γ* and *IL-1β* in the liver was upregulated after hypoxic stress. However, the expression of *TNF-α* decreased after hypoxia stress. Generally, the acute hypoxic stress made the fish body in a defensive state, thereby enhancing the immunity level in the study.

Under hypoxic stress, DO in water is insufficient to fulfill the oxygen demands for aerobic metabolism, and anaerobic metabolism is triggered (Abdel-Tawwab et al., 2019). Plasma LDH activity increased sharply under acute hypoxic stress in this study, reflecting an increase in anaerobic metabolism (Ma et al., 2019). Studies have shown that the HIF-1 pathway plays a vital role in the glycometabolic switch from aerobic to anaerobic processes by regulating downstream genes, such as *GLUT* and *LDH*, and the key enzyme of glycolysis (Richards, 2009; Rademakers et al., 2011; Goda and Kanai, 2014). However, the expression of *GLUT2*, *GK*, *and LDHA* in the liver did not change under acute hypoxic stress, which might be related to the lack of *HIF1a* in this study. PDK inhibits the pyruvate dehydrogenase complex and blocks the conversion of pyruvate (the glycolytic end-product) to acetyl-CoA (normally into the TCA cycle) (Mylonis et al., 2019). This study showed that the expression of *PDK1* in the liver was upregulated under acute hypoxic stress. The finding indicates that the flow of pyruvate into the mitochondria is decreased. Based on the result that the expression of *PEPCK* was upregulated in the hypoxic group, pyruvate participated in gluconeogenesis under acute hypoxic stress.

The liver is a critical site for lipid synthesis and export in fish (Tocher and Douglas, 2003). Lipids provide a rich source of energy *via* oxidative phosphorylation (Jungermann, 1988; Shohet and Garcia, 2007). Under hypoxic stress, lipid metabolism is reprogrammed to suppress lipid catabolism through β-oxidation and stimulate lipid storage and inhibition (Huss et al., 2001; Bostrom et al., 2006). The regulation of metabolism is more dependent on *HIF-2a* more than *HIF-1a* (Rankin et al., 2009). In this study, upregulation of the *HIF-2a* gene reduced *CPT-1* expression-mediated fatty acid mitochondrial β-oxidation and increased *ACC* expression-mediated fatty acid synthesis under acute hypoxic stress. This might explain why plasma TG levels increased in the hypoxic group. A notable result was found for *ACO*, which could control peroxisomal β-oxidation. The expression of *ACO* was upregulated under acute hypoxic stress, which might be related to the suppression of mitochondrial oxidation.

Under hypoxic conditions, autophagy is activated by ROS (Moore, 2008; Azad et al., 2009), and thus serves to reduce oxidative damage (Scherz-Shouval and Elazar, 2007; Gurusamy et al., 2009; Jain et al., 2015). However, the expression of autophagy-related genes (*LC3β*, *gabarapL1*, *atg4b*, and *atg12L*) in the liver was not induced by acute hypoxic stress. A possible reason for the results is that the fish body was in a defensive state after 10 min of hypoxic stress was applied.

CONCLUSION

This study simulated the hypoxic environment caused by actual production operations in fish farming (i.e., catching, gathering, transferring, or weighting), which could lead to acute hypoxic stress in fish. Under the hypoxic conditions, triploid rainbow trout are in a defensive state to manage stress by enhancing immunity levels, altering antioxidant status, suppressing hepatic mitochondrial oxidation of glucose- and lipid-derived carbon, and activating hepatic gluconeogenesis and lipid synthesis. These phenotypes might be regulated by the HIF-2α pathway.

DATA AVAILABILITY STATEMENT

The original contributions presented in the study are included in the article/Supplementary Materials, further inquiries can be directed to the corresponding author.

ETHICS STATEMENT

The animal study was reviewed and approved by The Ethical Committee of Qinghai University.

AUTHOR CONTRIBUTIONS

BH performed formal analysis, data curation, writing—original draft. YM performed methodology, supervision, writing—review and editing. HT and CL performed project administration. YL, CG, and WF performed investigation and resources. RM performed conceptualization, supervision, resources, and funding acquisition.

FUNDING

This research was financially supported by grants from the National Natural Science Foundation of China (No. 32060833) and the Provincial Important Science and Technology Specific Project of Qinghai, China (2019-NK-A2).

ACKNOWLEDGMENTS

We would like to thank Xiaohong Liu, Kangkang Qian, Xuemin Hu, Xiaoyan Su, Guocai Dong, Jianhua Hou, and Shuting Chen for their support and help during this study.

REFERENCES

Abdel-Tawwab, M., Monier, M. N., Hoseinifar, S. H., and Faggio, C. (2019). Fish Response to Hypoxia Stress: Growth, Physiological, and Immunological Biomarkers. *Fish. Physiol. Biochem.* 45, 997–1013. doi:10.1007/s10695-019-00614-9

Akdemir, F., Orhan, C., Tuzcu, M., Sahin, N., Juturu, V., and Sahin, K. (2016). The Efficacy of Dietary Curcumin on Growth Performance, Lipid Peroxidation and Hepatic Transcription Factors in Rainbow troutOncorhynchus Mykiss(Walbaum) Reared under Different Stocking Densities. *Aquac. Res.* 48, 4012–4021. doi:10.1111/are.13223

Azad, M. B., Chen, Y., and Gibson, S. B. (2009). Regulation of Autophagy by Reactive Oxygen Species (ROS): Implications for Cancer Progression and Treatment. *Antioxidants Redox Signal.* 11, 777–790. doi:10.1089/ars.2008.2270

Balogun, E., Hoque, M., Gong, P., Killeen, E., Green, C. J., Foresti, R., et al. (2003). Curcumin Activates the Haem Oxygenase-1 Gene via Regulation of Nrf2 and the Antioxidant-Responsive Element. *Biochem. J.* 371, 887–895. doi:10.1042/BJ20021619

Barcellos, L. J. G., Nicolaiewsky, S., De Souza, S. M. G., and Lulhier, F. (1999). The Effects of Stocking Density and Social Interaction on Acute Stress Response in Nile tilapia *Oreochromis niloticus* (L.) Fingerlings. *Aquac. Res.* 30, 887–892. doi:10.1046/j.1365-2109.1999.00419.x

Beck, B. H., Fuller, S. A., Li, C., Green, B. W., Zhao, H., Rawles, S. D., et al. (2016). Hepatic Transcriptomic and Metabolic Responses of Hybrid Striped Bass (*Morone saxatilis*×Morone Chrysops) to Acute and Chronic Hypoxic Insult. *Comp. Biochem. Physiology Part D Genomics Proteomics* 18, 1–9. doi:10.1016/j.cbd.2016.01.005

Bortoletti, M., Maccatrozzo, L., Radaelli, G., Caberlotto, S., and Bertotto, D. (2021). Muscle Cortisol Levels, Expression of Glucocorticoid Receptor and Oxidative Stress Markers in the Teleost Fish argyrosomus Regius Exposed to Transport Stress. *Animals* 11, 1160–1213. doi:10.3390/ani11041160

Boström, P., Magnusson, B., Svensson, P.-A., Wiklund, O., Bore´n, J., Carlsson, L. M. S., et al. (2006). Hypoxia Converts Human Macrophages into Triglyceride-Loaded Foam Cells. *Atvb* 26, 1871–1876. doi:10.1161/01.ATV.0000229665.78997.0b

Bowyer, J. N., Booth, M. A., Qin, J. G., D'Antignana, M. J. S., and Stone, D. A. J. (2014). Temperature and Dissolved Oxygen Influence Growth and Digestive Enzyme Activities of Yellowtail kingfishSeriola lalandi(Valenciennes, 1833). *Aquac. Res.* 45 (12), 2010–2020. doi:10.1111/are.12146

Conde-Sieira, M., Alvarez, R., López-Patiño, M. A., Míguez, J. M., Flik, G., and Soengas, J. L. (2012). ACTH-stimulated Cortisol Release from Head Kidney of Rainbow Trout Is Modulated by Glucose Concentration. *J. Exp. Biol.* 216, 554–567. doi:10.1242/jeb.076505

Douxfils, J., Deprez, M., Mandiki, S. N. M., Milla, S., Henrotte, E., Mathieu, C., et al. (2012). Physiological and Proteomic Responses to Single and Repeated Hypoxia in Juvenile Eurasian Perch under Domestication - Clues to Physiological Acclimation and Humoral Immune Modulations. *Fish Shellfish Immunol.* 33, 1112–1122. doi:10.1016/j.fsi.2012.08.013

Dubowitz, D. J., Dyer, E. A. W., Theilmann, R. J., Buxton, R. B., and Hopkins, S. R. (2009). Early Brain Swelling in Acute Hypoxia. *J. Appl. Physiology* 107 (1), 244–252. doi:10.1152/japplphysiol.90349.2008

FAO (2020). *The State of the World Fisheries and Aquaculture 2020,* Sustainability In Action. Rome, Italy: FAO.

Goda, N., and Kanai, M. (2012). Hypoxia-inducible Factors and Their Roles in Energy Metabolism. *Int. J. Hematol.* 95, 457–463. doi:10.1007/s12185-012-1069-y

Gurusamy, N., Lekli, I., Gorbunov, N. V., Gherghiceanu, M., Popescu, L. M., and Das, D. K. (2009). Cardioprotection by Adaptation to Ischaemia Augments Autophagy in Association with BAG-1 Protein. *J. Cell. Mol. Med.* 13, 373–387. doi:10.4161/auto.5.1.730310.1111/j.1582-4934.2008.00495.x

Hansen, T. J., Olsen, R. E., Stien, L., Oppedal, F., Torgersen, T., Breck, O., et al. (2015). Effect of Water Oxygen Level on Performance of Diploid and Triploid Atlantic Salmon Post-smolts Reared at High Temperature. *Aquaculture* 435, 354–360. doi:10.1016/j.aquaculture.2014.10.017

Hou, Z.-S., Wen, H.-S., Li, J.-F., He, F., Li, Y., and Qi, X. (2020). Environmental Hypoxia Causes Growth Retardation, Osteoclast Differentiation and Calcium Dyshomeostasis in Juvenile Rainbow Trout (*Oncorhynchus mykiss*). *Sci. Total Environ.* 705, 135272–135313. doi:10.1016/j.scitotenv.2019.135272

Huss, J. M., Levy, F. H., and Kelly, D. P. (2001). Hypoxia Inhibits the Peroxisome Proliferator-Activated Receptor α/ Retinoid X Receptor Gene Regulatory Pathway in Cardiac Myocytes. *J. Biol. Chem.* 276, 27605–27612. doi:10.1074/jbc.M100277200

Jain, A., Rusten, T. E., Katheder, N., Elvenes, J., Bruun, J.-A., Sjøttem, E., et al. (2015). p62/Sequestosome-1, Autophagy-Related Gene 8, and Autophagy in drosophila Are Regulated by Nuclear Factor Erythroid 2-related Factor 2 (NRF2), Independent of Transcription Factor TFEB. *J. Biol. Chem.* 290, 14945–14962. doi:10.1074/jbc.M115.656116

Jia, Y., Gao, Y., Wan, J., Gao, Y., Li, J., and Guan, C. (2021). Altered Physiological Response and Gill Histology in Black Rockfish, *sebastes Schlegelii*, during Progressive Hypoxia and Reoxygenation. *Fish. Physiol. Biochem.* 47, 1133–1147. doi:10.1007/s10695-021-00970-5

Jungermann, K. (1988). Metabolic Zonation of Liver Parenchyma. *Semin. Liver Dis.* 8, 329–341. doi:10.1055/s-2008-1040554

Li, M., Wang, X., Qi, C., Li, E., Du, Z., Qin, J. G., et al. (2018). Metabolic Response of Nile tilapia (*Oreochromis niloticus*) to Acute and Chronic Hypoxia Stress. *Aquaculture* 495, 187–195. doi:10.1016/j.aquaculture.2018.05.031

Lushchak, V. I. (2011). Environmentally Induced Oxidative Stress in Aquatic Animals. *Aquat. Toxicol.* 101, 13–30. doi:10.1016/j.aquatox.2010.10.006

Ma, R., Liu, X., Meng, Y., Wu, J., Zhang, L., Han, B., et al. (2019). Protein Nutrition on Sub-adult Triploid Rainbow Trout (1): Dietary Requirement and Effect on Anti-oxidative Capacity, Protein Digestion and Absorption. *Aquaculture* 507, 428–434. doi:10.1016/j.aquaculture.2019.03.069

Majmundar, A. J., Wong, W. J., and Simon, M. C. (2010). Hypoxia-inducible Factors and the Response to Hypoxic Stress. *Mol. Cell.* 40, 294–309. doi:10.1016/j.molcel.2010.09.022

Mandic, M., Best, C., and Perry, S. F. (2020). Loss of Hypoxia-Inducible Factor 1α Affects Hypoxia Tolerance in Larval and Adult Zebrafish (*Danio rerio*). *Proc. R. Soc. B* 287, 20200798. doi:10.1098/rspb.2020.0798

Martos-sitcha, J. A., Simó-Mirabet, P., de las Heras, V., Calduch-giner, J. À., and Pérez-Sánchez, J. (2019). Tissue-Specific Orchestration of Gilthead Sea Bream Resilience to Hypoxia and High Stocking Density. *Front. Physiol.* 10, 840. doi:10.3389/fphys.2019.00840

Meng, Y., Han, B., Li, C., Qian, K., Liu, X., Hu, X., et al. (2019). Digestive Characteristics and Blood Chemistry Profile of Triploid Rainbow Trout *Oncorhynchus mykiss*: Influence of Body Size and Seasonal Variation. *Fish. Sci.* 85, 1001–1010. doi:10.1007/s12562-019-01348-6

Ming, J., Xie, J., Xu, P., Ge, X., Liu, W., and Ye, J. (2012). Effects of Emodin and Vitamin C on Growth Performance, Biochemical Parameters and Two HSP70s mRNA Expression of Wuchang Bream (*Megalobrama amblycephala* Yih) under High Temperature Stress. *Fish Shellfish Immunol.* 32, 651–661. doi:10.1016fj.fsi.2012.01.00810.1016/j.fsi.2012.01.008

Mommsen, T. P., Vijayan, M. M., and Moon, T. W. (1999). Cortisol in Teleosts: Dynamics, Mechanisms of Action, and Metabolic Regulation. *Rev. Fish Biol. Fish.* 9, 211–268. doi:10.1023/A:1008924418720

Moore, M. N. (2008). Autophagy as a Second Level Protective Process in Conferring Resistance to Environmentally-Induced Oxidative Stress. *Autophagy* 4, 254–256. doi:10.4161/auto.5528

Mylonis, I., Simos, G., and Paraskeva, E. (2019). Hypoxia-inducible Factors and the Regulation of Lipid Metabolism. *Cells* 8, 214. doi:10.3390/cells8030214

Onukwufor, J. O., and Wood, C. M. (2020). Osmorespiratory Compromise in Zebrafish (danio Rerio): Effects of Hypoxia and Acute Thermal Stress on Oxygen Consumption, Diffusive Water Flux, and Sodium Net Loss Rates. *Zebrafish* 17 (6), 400–411. doi:10.1089/zeb.2020.1947

Ortuño, J., Esteban, M. A., and Meseguer, J. (2001). Effects of Short-Term Crowding Stress on the Gilthead Seabream (*Sparus aurata* L.) Innate Immune Response. *Fish Shellfish Immunol.* 11, 187–197. doi:10.1006/fsim.2000.0304

Pillet, M., Dupont-prinet, A., Chabot, D., Tremblay, R., and Audet, C. (2016). Effects of Exposure to Hypoxia on Metabolic Pathways in Northern Shrimp (*Pandalus Borealis*) and Greenland Halibut (*Reinhardtius hippoglossoides*). *J. Exp. Mar. Biol. Ecol.* 483, 88–96. doi:10.1016/j.jembe.2016.07.002

Rademakers, S. E., Lok, J., van der Kogel, A. J., Bussink, J., and Kaanders, J. H. (2011). Metabolic Markers in Relation to Hypoxia; Staining Patterns and Colocalization of Pimonidazole, HIF-1α, CAIX, LDH-5, GLUT-1, MCT1 and MCT4. *BMC Cancer* 11 (1), 167. doi:10.1186/1471-2407-11-167

Rahman, M. S., and Thomas, P. (2007). Molecular Cloning, Characterization and Expression of Two Hypoxia-Inducible Factor Alpha Subunits, HIF-1α and HIF-2α, in a Hypoxia-Tolerant Marine Teleost, Atlantic Croaker (*Micropogonias undulatus*). *Gene* 396, 273–282. doi:10.1016/j.gene.2007.03.009

Rankin, E. B., Rha, J., Selak, M. A., Unger, T. L., Keith, B., Liu, Q., et al. (2009). Hypoxia-inducible Factor 2 Regulates Hepatic Lipid Metabolism. *Mol. Cell. Biol.* 29, 4527–4538. doi:10.1128/MCB.00200-09

Richards, J. G. (2009). Chapter 10 Metabolic and Molecular Responses of Fish to Hypoxia. *Fish. Physiol.* 27, 443–485. doi:10.1016/S1546-5098(08)00010-1

Rimoldi, S., Terova, G., Ceccuzzi, P., Marelli, S., Antonini, M., and Saroglia, M. (2012). HIF-1α mRNA Levels in Eurasian Perch (*Perca fluviatilis*) Exposed to Acute and Chronic Hypoxia. *Mol. Biol. Rep.* 39, 4009–4015. doi:10.1007/s11033-011-1181-8

Scherz-shouval, R., and Elazar, Z. (2007). ROS, Mitochondria and the Regulation of Autophagy. *Trends Cell. Biol.* 17, 422–427. doi:10.1016/j.tcb.2007.07.009

Shohet, R. V., and Garcia, J. A. (2007). Keeping the Engine Primed: HIF Factors as Key Regulators of Cardiac Metabolism and Angiogenesis during Ischemia. *J. Mol. Med.* 85, 1309–1315. doi:10.1007/s00109-007-0279-x

Tocher, D. R., and Douglas, R. (2003). Metabolism and Functions of Lipids and Fatty Acids in Teleost Fish. *Rev. Fish. Sci.* 11, 107–184. doi:10.1080/713610925

Trenzado, C. E., Morales, A. E., and de la Higuera, M. (2006). Physiological Effects of Crowding in Rainbow Trout, *Oncorhynchus mykiss*, Selected for Low and High Stress Responsiveness. *Aquaculture* 258, 583–593. doi:10.1016/j.aquaculture.2006.03.045

Vanderplancke, G., Claireaux, G., Quazuguel, P., Madec, L., Ferraresso, S., Sévère, A., et al. (2015). Hypoxic Episode during the Larval Period Has Long-Term Effects on European Sea Bass Juveniles (*dicentrarchus Labrax*). *Mar. Biol.* 162 (2), 367–376. doi:10.1007/s00227-014-2601-9

Whitehouse, L. M., and Manzon, R. G. (2019). Hypoxia Alters the Expression of Hif-1a mRNA and Downstream HIF-1 Response Genes in Embryonic and Larval Lake Whitefish (*Coregonus clupeaformis*). *Comp. Biochem. Physiology Part A Mol. Integr. Physiology* 230, 81–90. doi:10.1016/j.cbpa.2019.01.005

Wu, Y., Zhong, H., Zhao, H. H., and Li, T. (2007). Effects of Different Dissolved Oxygen Concentration on Metabolic Level of Juvenile Rainbow Trout (*Oncorhynchus mykiss*) in the Recirculating Systems. *J. Shanghai Fish. Univ.* 16 (5), 438–442. doi:10.1360/yc-007-1071

Xiao, W. (2015). The Hypoxia Signaling Pathway and Hypoxic Adaptation in Fishes. *Sci. China Life Sci.* 58, 148–155. doi:10.1007/s11427-015-4801-z

Yang, S., Wu, H., He, K., Yan, T., Zhou, J., Zhao, L. L., et al. (2019). Response of AMP-Activated Protein Kinase and Lactate Metabolism of Largemouth Bass (*Micropterus salmoides*) under Acute Hypoxic Stress. *Sci. Total Environ.* 666, 1071–1079. doi:10.1016/j.scitotenv.2019.02.236

Zhao, L. L., Sun, J. L., Liang, J., Liu, Q., Luo, J., Li, Z. Q., et al. (2020). Enhancing Lipid Metabolism and Inducing Antioxidant and Immune Responses to Adapt to Acute Hypoxic Stress in Schizothorax Prenanti. *schizothorax prenantiAquaculture* 519, 734933. doi:10.1016/j.aquaculture.2020.734933

Zhu, C.-D., Wang, Z.-H., and Yan, B. (2013). Strategies for Hypoxia Adaptation in Fish Species: a Review. *J. Comp. Physiol. B* 183, 1005–1013. doi:10.1007/s00360-013-0762-3

Conflict of Interest: Authors YL, CG, and WF were employed by Qinghai Minze Longyangxia Ecological Aquaculture Co., Ltd.

The authors declare that the research was conducted in the absence of any commercial or financial relationships that could be construed as a potential conflict of interest.

Publisher's Note: All claims expressed in this article are solely those of the authors and do not necessarily represent those of their affiliated organizations, or those of the publisher, the editors and the reviewers. Any product that may be evaluated in this article, or claim that may be made by its manufacturer, is not guaranteed or endorsed by the publisher.

frontiers | Frontiers in Marine Science

ORIGINAL RESEARCH
published: 14 July 2022
doi: 10.3389/fmars.2022.835379

Metabolomic Profiling Reveals Changes in Amino Acid and Energy Metabolism Pathways in Liver, Intestine and Brain of Zebrafish Exposed to Different Thermal Conditions

Andrea Aguilar[1], *Humberto Mattos*[1], *Beatriz Carnicero*[1], *Nataly Sanhueza*[1], *David Muñoz*[1], *Mariana Teles*[2,3], *Lluis Tort*[2] *and Sebastian Boltaña*[1*]

[1]*Departamento de Oceanografía, Centro de Biotecnología, ThermoFish Lab, Universidad de Concepción, Concepción, Chile,* [2]*Department of Cell Biology, Physiology and Immunology, Universitat Autònoma de Barcelona, Barcelona, Spain,* [3]*Institute of Biotechnology and Biomedicine, Universitat Autònoma de Barcelona, Barcelona, Spain*

Global warming is predicted to increase prolonged thermal challenges for aquatic ectotherms, i.e. it causes metabolic performance declines, impacts food intake, and finally causes impaired growth. In this research work, we investigated whether a tropical fish, *Danio rerio* (zebrafish), could tolerate prolonged thermal challenges and whether the temperature increase has a significant impact on growth and metabolism. To answer our questions, we evaluate the metabolomic performance, a question that has received little attention so far, using differential chemical isotope labeling (CIL) liquid chromatography-mass spectrometry (LC-MS). Three groups of fish were exposed to various temperatures of 27.6 ± 2°C, 30.7 ± 2°C or 32.2 ± 2°C during 270 days post fecundation (dpf) to evaluate the impact of the temperature increase on the growth and metabolomic performance. The results obtained demonstrated different metabolomic changes in response to acclimation to the different temperatures. After 270 days, the fish maintained at the highest tested temperature (32°C) showed reduced growth, reduced condition factor, and elevated levels of metabolites associated with amino acid catabolism and lipid metabolism pathways in the liver and intestine compared with fish kept at lower temperatures (27.6 ± 2°C). These findings demonstrate an explicit redistribution of energy stores and protein catabolism in fish at the highest temperature, thus showing a preference for maintaining length growth during limited energy availability. Moreover, here we also screened out both the marker metabolites and the altered metabolic pathways to provide essential insights to ascertain the effects of the water temperature increase on the growth and development of tropical fish.

Keywords: metabolomics, climate change, ectotherm, fish, heat shock proteins

OPEN ACCESS

Edited by:
Yu-Hung Lin,
National Pingtung University of Science and Technology, Taiwan

Reviewed by:
Hsin-Wei Kuo,
National Pingtung University of Science and Technology, Taiwan
Wen-Jun Shi,
South China Normal University, China
Huan Wang,
Ningbo University, China

****Correspondence:***
Sebastian Boltaña
sboltana@udec.cl

Specialty section:
This article was submitted to Aquatic Physiology, a section of the journal Frontiers in Marine Science

Received: *14 December 2021*
Accepted: *14 June 2022*
Published: *14 July 2022*

Citation:
Aguilar A, Mattos H, Carnicero B, Sanhueza N, Muñoz D, Teles M, Tort L and Boltaña S (2022) Metabolomic Profiling Reveals Changes in Amino Acid and Energy Metabolism Pathways in Liver, Intestine and Brain of Zebrafish Exposed to Different Thermal Conditions. Front. Mar. Sci. 9:835379. doi: 10.3389/fmars.2022.835379

HIGHLIGHTS

- Metabolic response of zebrafish reared at different temperature were studied
- Brain, liver an intestine tissue reflects metabolic changes in physiology of fish
- Amino acid, protein catabolism and energy metabolism pathways are altered in all tissues by the temperature conditions
- The altered metabolome may be useful as a key indicator of adverse effect of the water warming

INTRODUCTION

Aquatic ecosystems worldwide are warm-up, and their average temperatures are progressively increasing due to climate change. Environmental temperature commands growth and metabolic performance in ectotherms, including most fish (Neuheimer et al., 2011). Metabolites (e.g., glucose, glycerol, and alanine) are products and intermediate metabolism compounds that respond to shifts in the environment (Bundy et al., 2009). Metabolite profiles play essential roles in the biochemical pathways that shape individual phenotypes (Wagner et al., 2013; Wagner et al., 2014). Metabolomics is a cutting-edge technology that offers considerable advantage over other omics techniques since metabolites are preserved among organisms, unlike genes or proteins. Gas chromatography-mass spectrometry, liquid chromatography-mass spectrometry (LC-MS), and nuclear magnetic resonance are the three most commonly used analytical technologies for metabolic analysis (Samuelsson et al., 2006; Samuelsson and Larsson, 2008; Samuelsson et al., 2011). In aquatic organisms, researchers have used metabolomic approaches to evaluate the impact of temperature increases on organisms such as molluscs (Ellis et al., 2014), crustaceans (Hammer et al., 2012) and marine coral communities (Coelho et al., 2015). However, despite their advantages, the evaluation of the impact of the water temperature increase on the metabolite composition in fish is still an underexplored area.

The survival of aquatic organisms underwater temperature increases depends on their capacity for physiological and cellular adaptation (Donelson et al., 2012; Miller et al., 2012). Most studies on thermal impacts on fish relate elevated temperatures with traits relevant to thermal stress resistance, including the induction of heat shock proteins (HSPs). HSPs are highly conserved, ubiquitously expressed families of stress response proteins induced in diverse organisms by different physiological and environmental stressors (Sørensen et al., 2003; Fabbri et al., 2008). In fish, prolonged exposure to high temperatures induces proteotoxic stress. Thus, the rise in the temperature leads to severe problems, such as the accumulation of misfolded proteins that involve an additional stress source on the proteostasis network, including protein translation, folding, trafficking, and turnover. Specifically, HSPs prevent and reduce the aggregation of other proteins damaged by heat and assist in the refolding or degradation of stress-damaged proteins (Wallace et al., 2015; Riback et al., 2017). In fish, the HSP protein expression increases when individuals are exposed to elevated temperature, and their sensitivity varies with species, developmental stage and season (Wallace et al., 2015), indicating a potential ecological relevance of HSPs in global warming. HSPs in fish have been studied extensively at the protein level and from the molecular aspect to quantifying the mRNA abundance. For example, the hsp70 mRNA has been identified in rainbow trout (Kothary et al., 1984), medaka (Arai et al., 1995), zebrafish (Lele et al., 1997), and tilapia (Molina et al., 2000), and well-increased mRNA levels have been registered due to heat stress. Recent studies in fish have shown that hsp90 and hsp47 increase due to heat stress in Puntius sophore and Channa striatus; the expression of several HSP proteins as hsp60, hsp70, hsp78, and hsp90 was up-regulated by the action of the increase on the temperature (Purohit et al., 2014; Mahanty et al., 2017).

In this research work, we report a method based on high-performance chemical isotope labelling (CIL) LC-MS platform (Su et al., 2016) that enables us to investigate the impact of the increase in water temperature on the metabolic performance of zebrafish a tropical species. Tropical fish species, in particular, are expected to have lower thermal adaptation capacity than temperate species because they have evolved in a more stable thermal environment (Wysocki, et al., 2009; Sinclair et al., 2016; Rezende and Bozinovic, 2019; Morgan et al., 2020). In particular, adult zebrafish is eurythermal and can occasionally tolerate warm temperatures in a short time (days), around 38°C (López-Olmeda and Sánchez-Vázquez, 2011). However, during the development, the zebrafish larvae and juvenile stage are highly susceptible to warm temperatures above 32°C (Pype et al., 2015). Therefore, for the fish that live within the limits of their thermal capacities, such as zebrafish, the prolonged exposure to warm temperatures (as projected by climate change) during their development can pleasantly impact their physiology and metabolic performance (Somero, 2010). Consequently, this study addresses questions regarding the mechanisms underlying the long time-scale impact of the water temperature increase during the development of zebrafish *Danio rerio*. Previous studies have shown variable effects on the growth of fish reared at >2°C and > 3–4°C above the current-day temperature water (Johansen and Jones, 2011). However, even if the increase in water temperature can impact fish growth, its effects on the animal's metabolic performance are unknown. The fish liver is an essential metabolic organ that controls metabolism, bile secretion, and glycogen storage and plays an essential role in environmental adaptation (Jiao et al., 2020). Additionally, the liver is vital to establishing energy balance to maintain general homeostasis and cope with environmental and physical disturbances. We use metabolomics to inspect changes in metabolites produced in a biological system (cell, tissue, or organism) in response to external stimuli, such as temperature in the liver. It can also be used to describe the observable chemical profiles of the metabolites (Ott et al., 2003). To inspect this metabolic profile, we also used the intestine, and brain tissue of fish reared for a long time at warm temperatures. Previous CL-based metabolomics studies on fish have revealed that the acute elevated temperature leads to changes in essential metabolites, including decreased liver glycogen and decreased

muscle phosphocreatine and ATP levels, indicating increased energetic costs at the higher temperature. However, to the date no studies have investigated the long-term response to temperature on the tissue metabolome in zebrafish while monitoring growth. Thus, this study aimed to clarify the effect of elevated temperature on the metabolome and dynamics concerning growth and food consumption in the water environment.

MATERIAL AND METHODS

Fish Husbandry and Experimental Conditions

All experiments were carried out at the ThermoFish Lab, Biotechnology Centre, University of Concepcion, Concepcion, Chile. Fish were handled in accordance with the "International Guiding Principles for Biomedical Research Involving Animals" established by the European Union Council (2010/63/EU). Zebrafish (*Danio rerio*) was used as a typical ectothermic animal. An advantage of these fishes is an enormous amount of scientific literature and a completely deciphered genome. Zebrafishes were maintained on a 14-h light/10-h dark cycle, and fertilized eggs were collected (Aquaneering zebrafish system). 540 embryos from the same parents were kept in 0.3× Danieau's solution [17.4 mM NaCl, 0.21 mM KCl, 0.12 mM $MgSO_4 \cdot 7H_2O$, 0.18 mM $Ca(NO_3)_2$, 1.5 mM HEPES (pH 7.6)] were obtained from JT Baker Chemical (Phillipsburg, NJ, USA). The larvae were maintained at 25°C with a 12 h light:12 h dark cycle in culture water (UV-sterilized and well-aerated water, pH 7.2 ± 0.5, dissolved oxygen: 6.6 ± 0.3 mg/L, electrical conductivity: 0.256 ± 0.005 mS/cm, water hardness: 185 ± 9 mg/L $CaCO_3$) and acclimated in 15 L glass tanks for 2 weeks before the experiment. At the start of the experiment, the temperature of three tanks was 27°C, then establishing experimental temperatures of 27.6 ± 0.9°C, 30.7 ± 1.2°C and 32.2 ± 0.8°C (**Figure 1**), in triplicate tanks for each temperature (3 thermal chambers per temperature). Each system had a flow rate of 5 m^3 h^{-1}, and water was U.V.-sterilized. The water temperature of each tank was measured twice per day. Dissolved oxygen was also measured daily and always remained above 6.6 ± 0.3 mg/L. Ammonia, nitrite, and pH were measured twice per week. Total ammonia and nitrite concentrations in each tank were kept under 0.05 and 0.01 mg L^{-1}, and pH remained at 8.0 ± 0.5. The thermal gradient was fixed through an outer water jacket system situated at unlike temperatures. The experimental set up was carried out as to correlate whether differences in the thermoregulation environment drive different metabolic traits and establish whether the growth parameters, heat-shock proteins expression and metabolic regulation is influenced by the water temperature. Fish were allowed to acclimate to the tanks and experimental temperatures for 7 days, and during this period the fish were not fed. On day 8, feeding was started. At month 1 (30 dpf) and month 9 (270 dpf) after the start of temperature acclimation, 9 fish/per condition were randomly sampled. We reared fish for a long time at unlike thermal conditions during 270 dpf. Our first sample time was at 30dpf after the first feeding. There were 60 fish in each replicate and thermal tank (N=180 by thermal group; n= 60 by replicate) and were fed a maintenance diet (Skretting, GEMMA Micro 300) twice daily for 270 dpf. Fish were sacrificed by over-anaesthesia with tricaine methanesulfonate (MS222, Sigma Aldrich). Body weight (BW) and length (L) was immediately determined and posteriorly used to calculate Fulton's K condition factor (100*(weight/length^3)). After 270 days of exposure, liver, intestine and brain were dissected and treated according to the metabolomic and gene expression approaches.

Homogenization and Metabolite Extraction

Liver, brain and intestine samples were collected from 9 individuals reared at three different temperatures. The individuals were randomly chosen. Milli-Q water was produced from a Millipore purification system (Waters-Millipore Corporation, Milford, MA, USA) Ceramic beads and 4:1 (v/v) pre-cooled LC-MS grade methanol:water (according to sample weight) were added into each of the individual sample tubes. Tissues were homogenized for one cycle of 15 seconds using a bead beater homogenizer (TissueLyser L, Qiagen). The tubes were centrifuged at 12,000 g for 10 min at 4°C. From each sample, all the supernatant was transferred into a new vial and dried down. The extracts were stored at -80°C until further analysis.

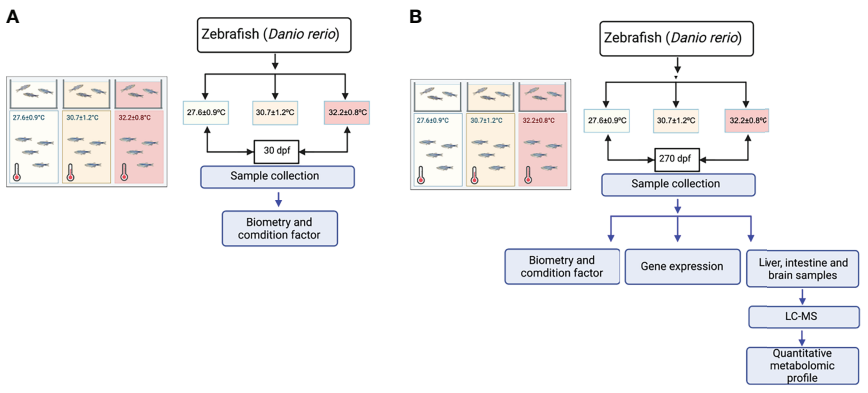

FIGURE 1 | Experimental setup. **(A)** Schematic diagram of the experimental setup 30 dpf. **(B)** Schematic diagram of the experimental setup 270 dpf.

Sample Quantification and Chemical Isotope Labelling

The dried extracts were taken from the -80°C freezer and re-dissolved in 30 µL of water. The total concentrations of samples were determined using the NovaMT Sample Normalization kit. For the samples having total concentration higher than 2 mM, water was added accordingly to adjust their concentrations to 2 mM. After concentration adjustment, supernatant was divided in 2 aliquots for labelling, backup and preparation of pooled sample. For the aliquot for amine-/phenol- labelling, 25 µL of samples was used. The individual samples were labelled separately using $^{12}C_2$-dansyl chloride and quantified by LC-UV based on absorption at 338 nm (Wu and Li, 2012). A pooled reference by tissue (i.e., liver-pool, intestine-pool and brain-pool) was prepared by mixing the same amount of aliquot from each of the 3 tissues. The reference-pool was taken and labeled by ^{13}C-dansylation ($^{13}C_2$-dansyl labeling). An aliquot of the ^{13}C-labeled pool was mixed with a ^{12}C-labeled individual sample in 1:1 molar ratio to produce a mixture for LC-MS analysis. ^{12}C-dansyl chloride (DnsCl) and amino acid standards were purchased from Sigma-Aldrich Canada (Markham, ON, Canada). The isotopic compound used to synthesize ^{13}C-dansyl chloride was purchased from Cambridge Isotope Laboratories (Cambridge, MA, USA).

LC-MS

An Agilent 1290 series binary UPLC system with a Waters ACQUITY UPLC BEH C18 column (2.1 mm 10 cm, 1.7 mm particle size, 130 Å pore size) connected to an Agilent electrospray ionization (ESI) time-of-flight mass spectrometer (Model 6230, Agilent, Palo Alto, CA, USA) was used for LC-MS analysis. For the TOF instrument, the ion source conditions were: nitrogen nebulizer gas: 1.38 Bar, dry gas flow: 5 L/min, dry temperature: 325 C, capillary voltage: 4000 V, end plate offset: 120 V, mass range: m/z up to 1700, and spectra rate: 1 Hz. The resolving power of the instrument was typically about 11,000 (FWHM) at m/z 622. All MS spectra were obtained in the positive ion mode. For LC-MS, LC solvent A was 0.1% (v/v) formic acid in water, and solvent B was 0.1% (v/v) formic acid in ACN. The gradient elution profile was as follows: t 1⁄4 0 min, 15% B; t 1⁄4 2 min, 15% B; t 1⁄4 15 min, 45% B; t 1⁄4 20 min, 65% B; t 1⁄4 26 min, 98% B; t 1⁄4 29 min, 98% B; t 1⁄4 29.1 min, 15% B. The flow rate was 250 mL/min. The sample injection volume varied, depending on the applications.

Data Processing

The MS data were internally mass-calibrated and then processed using a peak-pair picking software, IsoMS (Zhou et al., 2014). The level 1 peak pairs, along with their peak intensity ratios, were aligned from multiple runs by retention time within 20 s and accurate mass within 10 ppm using IsoMS-Align to generate the initial metabolite-intensity table. The Zero-fill program was used to find the missing ratios in the table from the raw LC-MS peak list and then fill in these values to produce the final table (Huan and Li, 2015a). Iso-Quant was finally applied to calculate the individual peak ratio based on chromatographic peak areas of the ^{12}C- and ^{13}C-labeled peaks with a peak pair in the table (Huan and Li, 2015b; Huan et al., 2015). The ratio values were used for statistical analysis (**Supplementary Tables S1–S6**).

RNA Extraction, cDNA Synthesis, and Transcript Quantification

9 random fish were sampled for each temperature (27.6 ± 2°C, 30.7 ± 2°C or 32.2 ± 2°C), and subsequently snap-frozen in liquid nitrogen and conserved at -80°C. Total RNA was extracted from the liver, intestine and brain of individual fish with the TRI Reagent® (0.5 ml; Sigma-Aldrich Missouri, United States) and quantified by absorbance at 260 nm. Only samples with an A260/280 ratio between 1.8 and 2.1, and an A260/230 ratio above 1.8 were used for reverse transcription. Purified RNA integrity was confirmed by agarose denaturing gel electrophoresis. cDNA was synthesized from 50 µl of total RNA (200 ng/µl) using the RevertAid H Minus First Strand cDNA Synthesis Kit (Fermentas, Waltham, MA, USA) according to the manufacturer's indications. RT-qPCR was performed using the StepOnePlus™ Real-Time PCR System (Applied Biosystems, Life Technologies, Carolina, USA), and each assay was run in triplicate using the Maxima SYBR Green qPCR Master Mix-2X (Bio-Rad, Carolina, USA). For qPCR assays, 5 µl of synthetized cDNA were diluted with 15 µl of nuclease-free water (Qiagen, Hilden, Germany). Each qPCR mixture contained the SYBR Green Master Mix, 2 µl of diluted cDNA, 500 nmol/l each primer, and RNase free water to a final volume of 10 µl. Amplification was performed in triplicate on 96-well plates with the following thermal cycling conditions: initial activation for 10 min at 95°C, followed by 40 cycles of 15 seconds (s) at 95°C, 30 s at 60°C, and 30 s at 72°C (primer table in **Supplementary Table S7**). An absolute quantification approach was used that involved calculating the number of gene copies in unknown "test" samples from comparison with a standard curve prepared using a dilution series of linearized plasmids with known concentrations. The PCR product for each gene was extracted from agarose gel using the Nucleospin Gel and PCR Clean-Up Kit (Macherey-Nagel, Dueren, Germany). The PCR amplicons were cloned the using pGEM-T Easy Vector and JM109 High-Efficiency Competent Cells (Promega, Madison, WI, USA). The Nucleospin Plasmid Quick Pure Kit (MACHEREY-NAGEL) was used to purify the plasmid DNA containing the PCR insert. Then, the plasmid was linearized using the HindIII restriction enzyme to prevent amplification efficiency problems that can arise from using supercoiled plasmids, and the amount of dsDNA was quantified using the Quant-iT PicoGreen dsDNA Assay Kit (Invitrogen, California, United States). The concentration of each plasmid was calculated by absorbance at 260 nm, and a five-fold dilution series produced for copy number calculations *via* qPCR and using Eq. (1).

$$Number\ of\ copies = \frac{amount * 6{,}022 \times 10^{23}}{length * 1 \times 10^{9} * 650}$$

where the amount of DNA (ng) was derived from absorbance at 260 nm and length (base pairs) was determined by adding the

PCR product length to the size of the plasmid. The use of these standard curves controlled for amplification efficiency differences between assays and permitted calculating the "absolute" number of mRNA transcripts, thereby facilitating gene comparisons.

Statistical Analysis

For statistical analysis of the organ samples, only the common peak-pairs shown up in at least 50% of the samples were retained for analysis. No outliers were found and all observations (n=27 for each of the temperature groups for each time point) were included in the data analyses. Orthogonal Partial Least Squares Discriminant Analysis (OPLS-DA) (Trygg and Wold, 2002; Nicholson et al., 2007) was conducted to find differences between temperature groups and different time points. Since only pairwise comparisons are possible in OPLS-DA we focused on effects of the highest temperature. Evaluation of the OPLS-DA models were conducted by assessing the model fit (R2) and prediction quality (Q2). Principle component analysis (PCA) and orthogonal partial least square discriminant analysis (OPLS-DA) were performed using SIMCA-Pþ 12.0 (Umetrics, Umeå, Sweden). The data were mean-centered and pareto-scaled (unit variance) prior to analysis. Condition factor (CF) was calculated as 100 × (BW × FL− 3) for initial and final average sizes of each group. Positive metabolite identification was performed based on mass and retention time match to the dansyl standard library containing 273 unique amines/phenols using DnsID (Huan et al., 2015). Putative identification was done based on accurate mass match to the metabolites in the human metabolome database (HMDB) (8021 known human endogenous metabolites) and the Evidence-based Metabolome Library (EML) (375,809 predicted metabolites with one reaction) using MyCompoundID (Li et al., 2013). The mass accuracy tolerance window was set at 10 ppm for database search.

RESULTS

Growth, Condition Factor and Molecular Regulation of Heat-Shock Proteins (*Hsps*)

The fish in each thermal tank were acclimatized to an artificial photoperiod of 12 h light:12 h dark 300 dpf. The cumulative mortality at different thermal gradients was 0.67%, 1.1%, and 2.7%, respectively. There were no significant differences in cumulative mortality in the treatment groups ($p > 0.05$). The fish grew in weight and length at all three temperatures, but the highest temperature tested significantly affected the growth (two-way ANOVA temperature * time $p = 0.0001$). A significant interaction between temperature and time on growth ($p = 0.0001$) was detected, while there was no difference in growth among the groups exposed to different temperatures during the first month (30 dpf). Fish at 32.2°C had a significantly lower BW (**Figure 2B**) and L (**Figure 2D**) than fish kept at the lower temperatures after 270 dpf ($p = 0.0001$ for both variables, **Figures 2A–D**). CF was affected by temperature and time ($p = 0.02$ and $p = 0.0001$, respectively), with a significant interaction between these variables ($p = 0.0001$). The fish at 30.7 and 32.2°C show a significant difference in CF just at 270 dpf in fish reared at 32.2°C with lower CF than fish at 27.6 and 30.7°C (p =0.002 and 0.0001, respectively, **Figures 2E, F**). A commonly used molecular marker of thermal stress is the molecular expression of cell chaperones, such as heat-shock proteins (HSPs). his represents a response rate where hsp mRNA levels were significantly altered in response to high temperatures. As shown in **Figure 3**, the expression of the hsp genes in the zebrafish was greatly enhanced upon exposure to 32°C heat stress mainly, in the liver and brain.

Metabolomic Analysis

Figure 1 shows the workflow for parallel organ metabolome profiling using CIL LC-MS. First, each organ is directly analysed. Next, the 12C-dansyl labelled individual samples are separately injected into LC-UV to measure each sample's total concentration of labelled metabolites for sample amount normalisation. Based on the total concentration, the volume of an individual sample (unlabelled) was mixed with an equal amount of other unlabelled samples to generate a pooled organ sample (i.e., liver-pool, brain pool, and intestine pool from 9 individuals in each thermal treatment). Then, the pooled sample labelled by 13C-dansylation served as a reference or internal standard for the 12C-labelled samples. Next, an equal amount of the 12C-labelled individual sample and the 13C-labeled pooled sample was mixed. Finally, a quality control (QC) sample was prepared by mixing an equal amount of the 12C-labeled and 13C- labelled pooled samples. LC-TOF-MS analysed the mixtures of 13C-pool (**Figure 4A**). A table of metabolite intensity was produced after peak pair extraction and peak ratio calculation. The peak ratio values (12C2-peak vs 13C2-peak) for a given metabolite peak pair in all individual samples reflected the relative concentration differences of the metabolite in these samples. The quantitative metabolome tables generated from all organs were used for data comparison and statistical analysis.

Liver Metabolome

The liver samples subjected to metabolic analysis by CIL-LC/MS were analysed posteriorly using the Metabolome Database (HMDB) and the Evidence-Based Metabolome Library (EML). A chart diagram (**Figure 4B**) was generated for the metabolites detected in the total sample after 270 dpf for each thermal treatment. Peak pairs that were presented in at least 89.4% of samples in any group were retained. Less commonly detected peak pairs were filtered out to ensure data quality (69.8%). The ratio of total proper signals was normalised for all data. The missing values of peak pairs in some samples due to low signal intensity (i.e., below the detection limit) were replaced with a rationally determined ratio by a unique zero-imputation program. 12 12C-/13C-mixtures were produced from triplicate experiments of 9 Liver samples using the workflow shown in **Figure 4A**. LC-MS individually analysed these mixtures, and three injections of the QC sample spaced evenly among the 9 sample injections were also performed (9 individual livers and three pools of the-liver samples, N=12). The QC data clustered together, indicating excellent analytical reproducibility in LC-MS data acquisition.

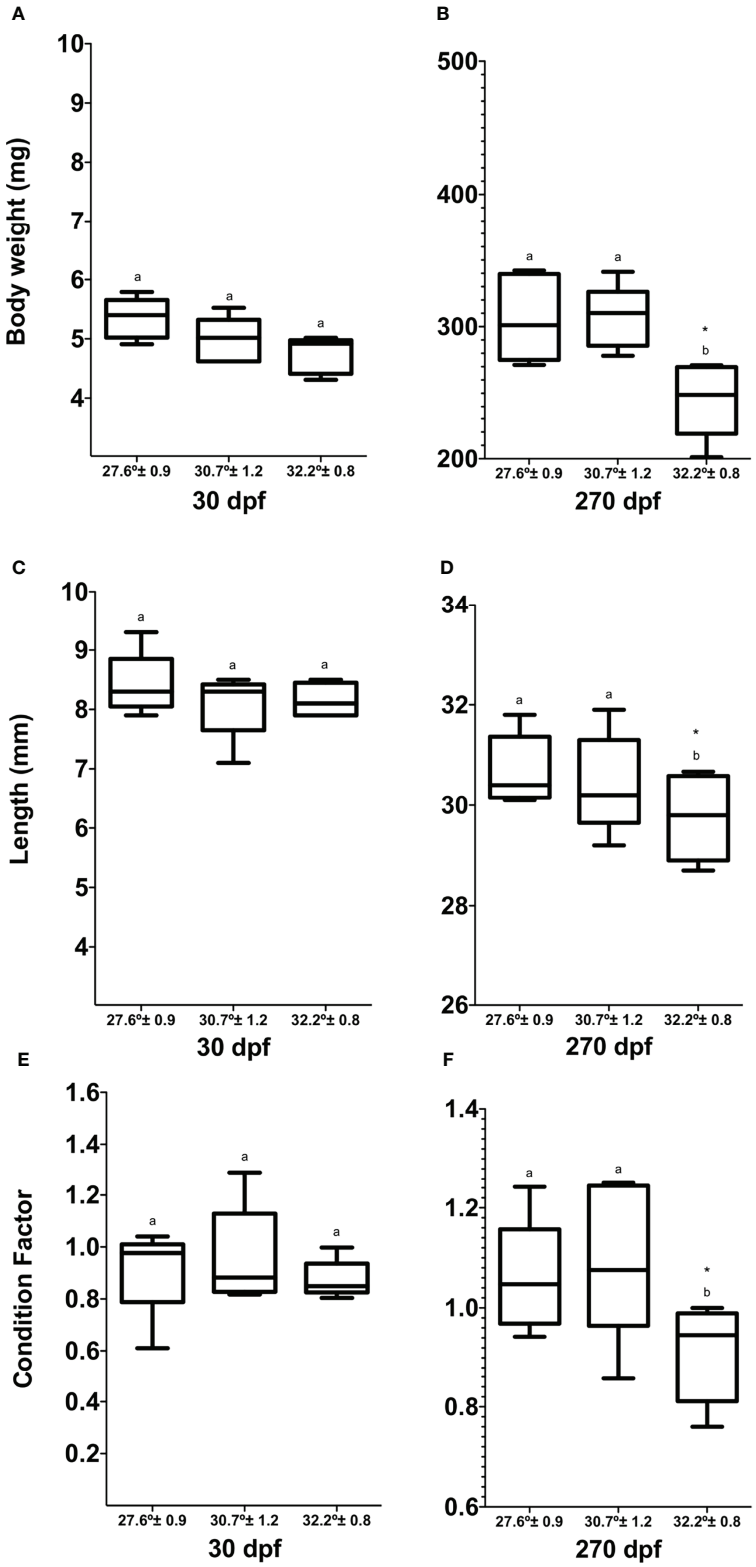

FIGURE 2 | Analysis of biometric parameters and condition factor of *Danio rerio* during the experimental period. **(A)** Body weight 30 dpf, **(B)** body weight 180 dpf, **(C)** length 30 dpf, **(D)** length 180 dpf, **(E)** condition factor 30 dpf, **(F)** condition factor 180 dpf. Different letters correspond to significant differences among temperature groups for each time point. Asterisk denotes significant change over time within each temperature group. Values are means ± SEM (n=27 for each experimental group).

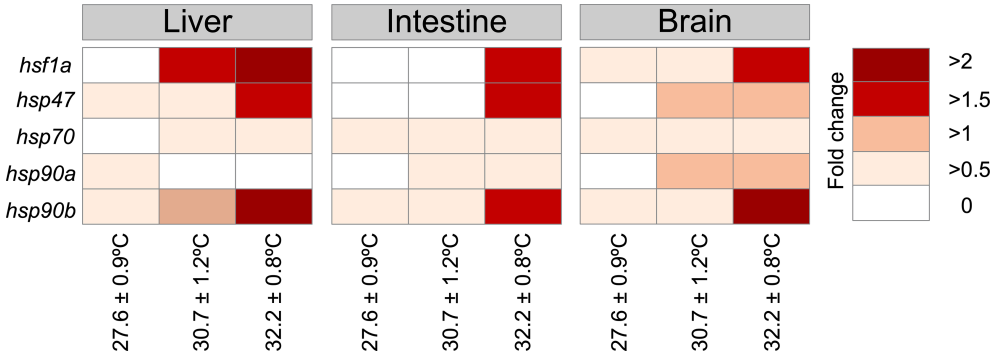

FIGURE 3 | Gene expression of heat-shock proteins (*hsp*). Heatmap of *hsp* expression from *Danio rerio* when comparing fish exposed to 30.7°C and 32.7°C with control fish (exposed to 27.6°C.

Some separations of the three thermal treatments were already visible. **Figure 5A** shows the PCA plot of the liver dataset according to three individuals by thermal treatment. 500 metabolites were detected positively (**Figure 4B**), including amino acids, nucleotides, carbohydrates, organic acids, and lipids (**Supplementary Tables S1, S2**).

PCA was used to show the impact of the temperature on the liver's metabolic functions. The PCA results revealed clear differences in metabolite profiles among the thermal treatments, indicating great differences in liver function after 270 days at different temperatures. OPLS-DA was used to identify differentially expressed metabolites in the liver of *D. rerio* in response to different temperatures during the development. The OPLS-DA results revealed notable differences in the metabolite profiles among treatments after 270 days of exposure to 30.7°C and 32.2°C. **Figure 5B** shows the OPLS-DA plot of the liver dataset according to the treatments. These three treatments are clearly separated (R2X = 0.369, R2Y = 0.952, and Q2 = 0.944). The R2Y metric describes the percentage of variation explained by the model, while the Q2 metric describes the model's predictive ability (27.6°C, **Figure 5B**).

Based on the OPLS-DA results, the differential metabolites among the groups were classified (**Supplementary Tables S1**, **S2**). The significant differences in the levels of differential metabolites among the groups were normalized, and clustered heat maps were generated (**Figure 5C**). Significant differences were registered in the liver metabolite profiles among the groups in response to different water temperatures, with most differences observed in the amino acid metabolism (20%), lipid metabolism (14.2%), protein and DNA methylation (13.9%, **Figures 6A, B**). Furthermore, a significant difference in the treatments were observed for the metabolites SCP-2 (sterol carrier protein 2), and HMG-CoA synthase (hydroxymethylglutaryl-CoA synthase), S-Adenosyl-L-homocysteine, N-acetyl-5-hydroxytryptamine, N-acetylserotonin, Serotonine, Alanine, Gamma-Glutamylglutamic acid, symmetric dimethylarginine, N(6)-Methyllysine, kanosamine, 7-Aminomethyl-7 carbaguanine and Very-low-density lipoprotein (VLDL), High-density lipoprotein (HDL). Interestingly, fish at normal thermal conditions also showed significantly lower concentrations of the metabolite annotated as Valyl-Aspartate than at higher temperatures. Valyl-Aspartate plays a critical role in the correct function of the fish liver. Significant treatment effects

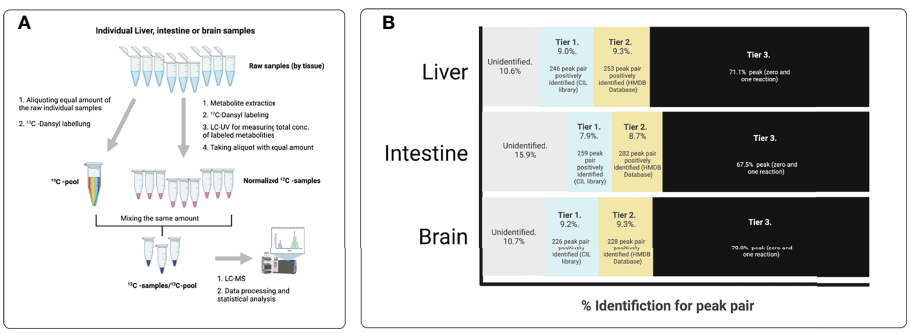

FIGURE 4 | Workflow of the differential chemical isotope labeling LC-MS method for tissue metabolomic profiling. **(A)** Procedure for analyzing individual samples within liver, intestine or brain. **(B)** Identification results for each peak pair in liver, intestine or brain in each thermal set-up. Metabolites identified in tier 1 and tier 2 correspond to high confidence identified results, and were used for pathway analysis the pathway analysis tools (CIL Library and Pathway Analysis module in MetaboAnalyst. Metabolites that were identified in tier 1 and tier 2 are shown in **Supplemental Tables 1–6**.

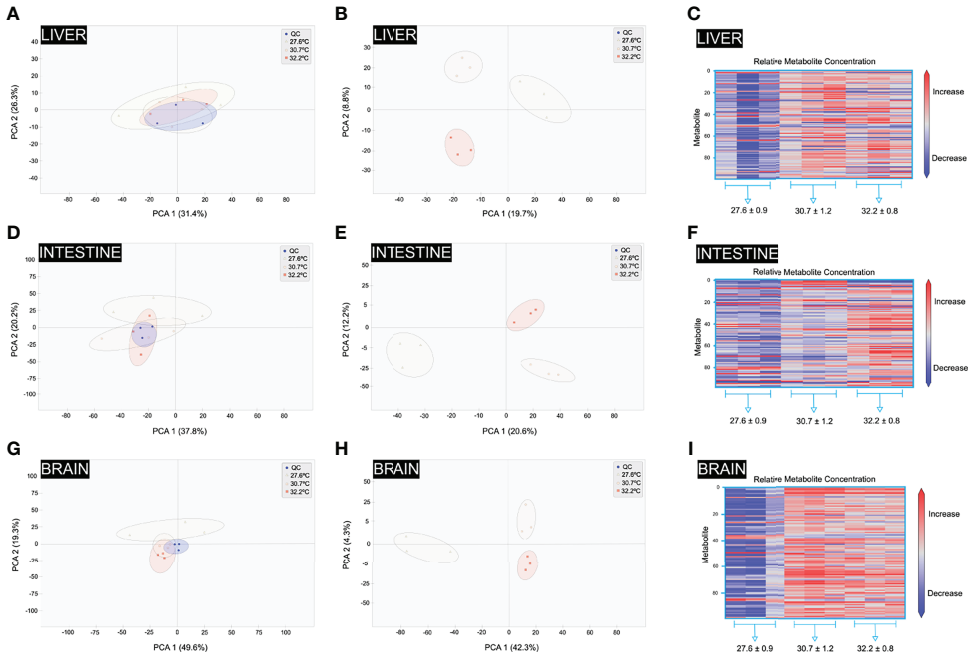

FIGURE 5 | Validation diagrams of metabolomics data and orthogonal partial least square discriminant analysis of liver, intestine and brain samples. **(A)** Liver principle component analysis (PCA) 2D scores plot (with QC). **(B)** Liver OPLS-DA score plots (without QC). **(C)** Liver OPLS-DA VIP Scores Heatmap. **(D)** Intestine principle component analysis (PCA) 2D scores plot (with QC). **(E)** Intestine OPLS-DA score plots (without QC). **(F)** Intestine OPLS-DA VIP Scores Heatmap. **(G)** Brain principle component analysis (PCA) 2D scores plot (with QC). **(H)** Brain OPLS-DA score plots (without QC). **(I)** Brain OPLS-DA VIP Scores Heatmap.

were observed for the metabolites annotated as α-ketoglutaric acid, which is an essential metabolite in the tricarboxylic acid cycle (TCA) and plays an important role in the synthesis and decomposition of glutamic acid. Glutamic acid is the precursor of arginine, proline, and glutathione. Therefore, variations in the amount of glutamic acid reflect changes in glutathione, arginine, and proline metabolism. Simultaneously, cysteamine was also identified as being differentially expressed between the groups. Cysteamine can directly or indirectly stimulate the release of growth hormones by inhibiting or weakening the effect of somatostatin, thereby promoting the growth differences observed in the fish reared at different temperatures. This observation highlights the impact of higher temperatures on the liver's metabolism.

Intestine Metabolome

In total, 12 ^{12}C-/^{13}C-mixtures were produced from triplicate experiments of 9 intestine samples by using the workflow shown in **Figure 4A**. These mixtures were analysed individually by LC-MS, and three injections of the QC sample spaced evenly among the 9 sample injections were also performed (9 individual intestines and three pool-intestine samples, N=12). The QC data were clustered together, indicating excellent analytical reproducibility in LC-MS data acquisition. Some separations of the three thermal treatments were already visible. **Figure 5D** shows the PCA plot of the intestine dataset according to three individuals by thermal treatment. A total of 541 metabolites were detected (**Figure 4B** and **Supplementary Tables S3**, **S4**). The PCA results revealed clear differences in the profiles of the metabolites among the different thermal treatments, showing higher differences in intestine function after 270 days of exposure to the different temperatures. The OPLS results also revealed notable differences in the metabolite profiles among treatments after 270 days of exposure to 27.6, 30.7 and 32.2°C. **Figure 5E** shows the OPLS-DA plot of the intestine dataset according to the treatments. These three treatments are clearly separated (R2X = 0.989, and Q2 = 0.193). Based on the OPLS-DA results, the differential metabolites among the groups were classified (**Supplementary Tables S3**, **S4**). The significant differences in the levels of differential metabolites among the groups were normalised, and clustered heat maps were generated (**Figure 5F**). The temperature-induced differences in the intestine metabolite profiles among the groups show the most differences in metabolites, such as nucleotide biosynthesis (46.4%), followed by D-amino acid metabolism and lipid metabolism-related metabolites (**Figures 6C, D**). A significant treatment effect was registered for the metabolites annotated as VLDL, HDL, 5-Guanidino-2-oxopentanoic acid, and Isomer 1 5-Guanidino-2-oxopentanoic acid, which display significantly higher concentrations than in the intestines of fish reared at higher temperatures (**Figure 6D**).

Interestingly, fish at normal thermal conditions also displayed significantly lower concentrations of the metabolite annotated as Aspartyl-Glycine and Valyl-Aspartate than the fish reared at the higher temperature. D-Amino acids

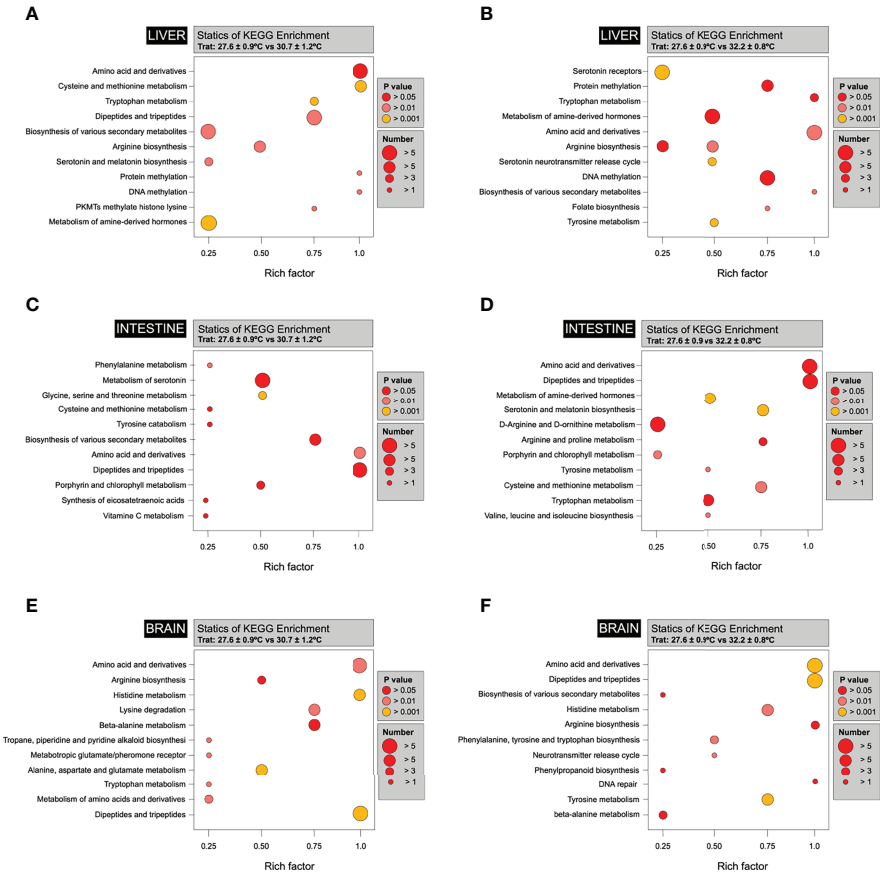

FIGURE 6 | Bubble diagrams of different metabolites between tissues. The abscissa in the bubble graphs represents the Rich factor (the ratio of the number of differentially expressed metabolites in the corresponding pathway to the total number of metabolites annotated by the pathway detection; the greater the value, the greater the degree of enrichment), while the ordinate is the name of the passage. A deeper red colour of the points indicates that the enrichment is more significant. The size of the spots represents the number of enriched differential metabolites. **(A)** A bubble diagram of the differential metabolites of Liver individuals at 27.6 ± 2°C and 30.7 ± 2°C. **(B)** A bubble diagram of the differential metabolites of Liver control individuals 27.6 ± 2°C and 32.7 ± 2°C. **(C)** A bubble diagram of the differential metabolites of Intestine individuals at 27.6 ± 2°C and 30.7 ± 2°C. **(D)** A bubble diagram of the differential metabolites of Intestine individuals at 27.6 ± 2°C and 32.7 ± 2°C. **(C)** A bubble diagram of the differential metabolites of Brain individuals at 27.6 ± 2°C and 30.7 ± 2°C. **(D)** A bubble diagram of the differential metabolites of Brain individuals at 27.6 ± 2°C and 32.7 ± 2°C.

play a significant role in relevant biological functions, such as D-Amino, which may have adverse effects as they can be found in some bacteria or form spontaneously in specific reactions for example, those induced by high temperatures. D-Amino acid oxidase (DAAO) is one of the main enzymes that metabolise D-Amino acids *via* deamination. DAAO is highly specific toward D-amino acids and favours free neutral D-amino acids or those with hydrophobic, polar, or aromatic groups (**Figure 6D**).

Brain Metabolome

454 metabolites were positively detected in the brain (**Figure 4B**), including amino acids, nucleotides, carbohydrates, organic acids, and lipids (**Supplementary Tables S5**, **S6**). The QC data were clustered together, indicating excellent analytical reproducibility in LC-MS data acquisition. Some separations of the three thermal treatments were already visible. **Figure 5G** shows the PCA plot of the intestinal dataset according to three individuals by thermal treatment. PCA was carried out to explore the effect of temperature on the metabolic functions of the brain. The PCA results revealed clear differences in metabolite profiles among the different thermal treatments, showing higher differences in brain function after 270 days of exposure to the different temperatures. The OPLS results revealed differences in the metabolite profiles among treatments after 270 days of exposure to 27.6, 30.7 and 32.2°C (**Figure 5H**). These three treatments were separated (R2Y = 0.999 and Q2 = 0.765). Significant differences in the levels of differential metabolites among the groups were normalized, and clustered heat maps were generated (**Figure 5I**). Notable differences were observed in the brain metabolite profiles among the groups in response to different water temperatures, with the most differences in lipid metabolism, arginine biosynthesis and phenylalanine, tyrosine and tryptophan biosynthesis (**Figures 6E, F**).

DISCUSSION

Climate change imposes various thermal challenges on organisms, mainly those inhabiting aquatic environments. It is projected that the mean temperature will increase by 1.5-5°C compared to early 1900 (IPCC, 2014), with heatwaves increasing frequency and severity (Perkins et al., 2012). Ectotherms, especially aquatic organisms, are vulnerable as their body temperature directly follows their environment (Angilletta, 2009). In this study, the growth and the metabolic performance are influenced in fish conditioned during the long term (270 dpf) at high temperatures (32°C). Specifically, we showed that fish reared at higher temperatures below the lethal (32.2°C) presented a reduced growth, reduced condition factor and significant increase in metabolites related to protein catabolism energy and lipid metabolism. These results agree with previous studies and show that specific zebrafish is sensitive to temperatures above 32°C (Åsheim et al., 2020) and showed that fish conditioned to long-term to supra-optimal temperatures drive reduced growth and fecundity (Pörtner et al., 2001; Pörtner and Knust, 2007; Gräns et al., 2014; Åsheim et al., 2020).

In this study, we demonstrated the utility of the CIL-LC/MS-based metabolomics method for assessing changes in the metabolome of *D. rerio* in the brain, intestine and liver of fish reared at high temperatures. In ectotherms, have been observed that the liver is the tissue impacted mainly by high temperatures. The physiological response of the liver to high temperatures remains consistent between different taxa, with significant metabolite performance; in contrast, the impact of the warm temperature on the metabolite composition in the fish intestine and other tissues is still limited. In mammals, high temperatures significantly increase hepatic lactate uptake through gluconeogenesis (Lucke, 1978; Hall et al., 1980). For example, mice exposed to high temperatures for a long time have been observed to alter the gluconeogenesis process, TCA cycle components (fumarate, malate, and 2-ketoglutarate) and the urea cycle (Araújo et al., 2019). Our results agree with mammal studies and show that the high temperature impacts the TCA cycle, gluconeogenesis, and fatty acid metabolism.

Additionally, we observed the up-regulation of SCP-2 (sterol carrierprotein2) and HMG-CoA synthase (hydroxymethylglutaryl-CoA synthase). Specific, SCP-2 binds and transports lipid ligands such as long-chain fatty acids and their CoA thioesters 4 (Hayashi et al., 2002) and phospholipids (Shimazu et al., 2013). HMG-CoA synthase catalyzes the condensation of acetyl-CoA with acetoacetyl-CoA to form 3-hydroxy-3-methylglutaryl-CoA (HMG-CoA), an intermediate in cholesterol synthesis and ketogenesis (Shimazu et al., 2010). HMG-CoA contributes to the synthesis of cholesterol, an essential component of membrane fluidity (Polymeropoulos et al., 2009). Fatty acids synthesized in the liver should be integrated into triacylglycerols and packaged into VLDL or HDL (Vitali et al., 2017), which drives the fatty acids to other tissues for use or storage (Xiao et al., 2020). We observed that changes in VLDL and HDL levels induced by the rise in the temperature indicate that lipids might be broken down into smaller, simple molecules, suggesting that the individuals are in a catabolic state. Thus, our results are in concordance with previous studies and show that the metabolic activity of the liver is highly susceptible to a catabolic state by external stressors, such as a rise in the water temperature (Surai et al., 2019; Xiao et al., 2020; Zhang et al., 2021).

Perhaps the most compelling finding is that heat treatment produced significant changes in the intestinal metabolites in the intestine, with most metabolites significantly reduced compared with the group reared at 27, 6°C, including oleic acid, palmitic acid, stearic acid, and mannose, myristic acid, and carbazole. These metabolites are involved in the fatty acid synthesis, mainly with energy and lipid metabolism (Savage et al., 2007; Loscalzo, 2011; Li et al., 2017). Previous reports have also shown that lengthy exposure to elevated temperature impacts the metabolism of the fatty acids in the intestine, including increased levels of VLDL and decreased HDL. As shown in **Figure 6**, the fatty acid pathway, VLDL, and HDL greatly impacted the intestine. This study also highlights those high temperatures induce a specific change in the amino-acid (AA) metabolism, mainly in the intestine and brain. The bubble diagram shows that the heat treatment inhibited fatty acid synthesis in the intestine and drove changes in the intestine's amino-acid (AAs) metabolism, linked explicitly with the AA turnover (Bouchama and Knochel, 2002; Kovats and Hajat, 2008; He et al., 2019). Our results indicate that fish reared at high temperatures reduce the phenylalanine and tyrosine pathways, suggesting an increased AA turnover (Boglione et al., 2013; Messineo et al., 2018). Several reports have shown that high temperature impacts the AAs' turnover (Kullgren et al., 2013; Sommer and Wolf, 2014; Salamanca et al., 2021), causing tyrosine and phenylalanine deficiency and reducing fish growth (Todgham et al., 2017; Valenzuela et al., 2018). These results are in concordance with our results that show that the warm temperature impacts AA turnover and reduces growth (**Figures 2**, **6**). However, the specific roles of AA deficiency by increased temperature and its relationship with reduced growth need further investigation.

One interesting finding is that AA deficiency is a process highly impacted in the three tissues. For example, in the liver and intestine, metabolites related to aminoacidic catabolism and some neuropeptides, both pathways linked to AA deficiency and feeding behaviour, were affected significantly in fish reared at high temperatures (Sanhueza et al., 2018), as observed in the brain. Our results are in concordance with the study in *Acipenser stellatus* and, in particular, show that warm temperature changes the turnover of L-glutamic acid, L-alanine, L-tryptophan, L-valine, and L-tryptophan, L-valine, L-valine L-leucine (Monselise et al., 2011; Mushtaq et al., 2014). We observed that other amino acids' synthesis also significantly impacted the three tissues, liver, intestine and brain, such as D -Serine or Alanine. D-Serine is related to the locomotor activity induced by environmental stressors and diseases (Fry, 1971; Reilly and Thompson, 2007; Hayes and Volkoff, 2014; Rosewarne et al., 2016; Speers-Roesch et al., 2018; Jutfelt, 2020; Le et al., 2020). In our study, D-Serine was highly expressed in fish reared at warm temperatures in all tissues. In fish, reports show that modifications on the D-Serine and the Alanine levels were triggered by heat stress.

CONCLUSION

The current research allowed the identification of significant changes in the metabolite performance of fish reared at high temperatures. Moreover, at high temperatures, fish show significant differences in the mean body weights. We identified vital metabolites and processes involved in thermal acclimation, including enhanced fatty acid oxidation, lipid and carbohydrate metabolism and amino acid catabolism such as α-ketoglutaric acid, SCP-2, HMG-CoA synthase, D-serine or alanine, serotonin, 5-hydroxytryptamine. Future research into genetic and epigenetic mechanisms and their effect on the metabolic pathways identified will help improve our understanding concerning the fish responses to climate change. This information may also be valuable for biomarker discovery research in untargeted metabolomics.

DATA AVAILABILITY STATEMENT

The original contributions presented in the study are included in the article/**Supplementary Material**. Further inquiries can be directed to the corresponding author.

ETHICS STATEMENT

All experiments with fish were carried out at the ThermoFish Lab, Biotechnology Centre, University of Concepcion, Concepcion, Chile. Fish were handled in accordance with the "International Guiding Principles for Biomedical Research Involving Animals" established by the European Union Council (2010/63/EU).

AUTHOR CONTRIBUTIONS

The study was conceived by SB. The behavioural experiments were performed by NS and AA. BC, HM, AA, and SB performed metabolomic analysis. MT and AA have performed the gene expression and provided extensive additional input. SB obtained the funding acquisition. SB, MT, and AA drafted the manuscript with substantial contributions from all other authors. All authors contributed to the article and approved the submitted version.

FUNDING

This work was supported by the following grants, FONDECYT 1190627 awarded by CONICYT Chile to SB and CONICYT-PCHA/Doctorado Nacional/2018-21181886 to NS, and CONICYT-PCHA/Doctorado Nacional/2019-21190538 to BC. MT acknowledge the support provided by the "Ministerio de Economía y Competitividad" from Spain ("Plan Nacional de Investigación", reference PID2020-113221RB-I00 and "Ramon y Cajal" contract, reference RYC2019-026841-I).

SUPPLEMENTARY MATERIAL

The Supplementary Material for this article can be found online at: https://www.frontiersin.org/articles/10.3389/fmars.2022.835379/full#supplementary-material

REFERENCES

Angilletta, M. J. (2009). "Thermal Adaptation: A Theoretical and Empirical Synthesis," in *Thermal Adaptation*, 1–302 p. doi:10.1093/acprof:oso/9780198570875.001.1

Arai, A., Naruse, K., Mitani, H. and Shima, A. (1995). Cloning and Characterization of cDNAs for 70-kDa Heat-Shock Proteins (Hsp70) From Two Fish Species of the Genus Oryzias. *Japanese J. Genet.* 70 (3), 423–433. doi: 10.1266/jjg.70.423

Araújo, A. M., Enea, M., Carvalho, F., Bastos M de, L., Carvalho, M. and de Pinho, P. G. (2019). Hepatic Metabolic Derangements Triggered by Hyperthermia: An *In Vitro* Metabolomic Study. *Metabolites* 9 (10), 228. doi: 10.3390/metabo9100228

Åsheim, E. R., Andreassen, A. H., Morgan, R. and Jutfelt, F. (2020). Rapid-Warming Tolerance Correlates With Tolerance to Slow Warming But Not Growth at non-Optimal Temperatures in Zebrafish. *J. Exp. Biol.* 223 (23), 1–7. doi: https://doi.org/10.1242/jeb.229195

Boglione, C., Gisbert, E., Gavaia, P., Witten, P. E., Moren, M., Fontagné, S., et al. (2013). Skeletal Anomalies in Reared European Fish Larvae and Juveniles. Part 2: Main Typologies, Occurrences and Causative Factors. *Rev. Aquac.* 5 (SUPPL.1) S121–S167. doi: https://doi.org/10.1111/raq.12016

Bouchama, A. and Knochel, J. P. (2002). Medical Progress: Heat Stroke. *N Engl. J. Med.* 346 (25), 1978–19788. doi: 10.1056/NEJMra011089

Bundy, J. G., Davey, M. P. and Viant, M. R. (2009). Environmental Metabolomics: A Critical Review and Future Perspectives. *Metabolomics* 5 (1), 3–21. doi: 10.1007/s11306-008-0152-0

Coelho, F. J. R. C., Cleary, D. F. R., Rocha, R. J. M., Calado, R., Castanheira, J. M., Rocha, S. M., et al. (2015). Unraveling the Interactive Effects of Climate Change and Oil Contamination on Laboratory-Simulated Estuarine Benthic Communities. *Glob. Chang. Biol.* 21 (5), 1871–1886. doi: 10.1111/gcb.12801

Donelson, J. M., Munday, P. L., McCormick, M. I. and Pitcher, C. R. (2012). Rapid Transgenerational Acclimation of a Tropical Reef Fish to Climate Change. *Nat. Clim. Chang.* 2 (1), 30–32. doi: 10.1038/nclimate1323

Ellis, R. P., Spicer, J. I., Byrne, J. J., Sommer, U., Viant, M. R., White, D. A., et al. (2014). 1h NMR Metabolomics Reveals Contrasting Response by Male and Female Mussels Exposed to Reduced Seawater Ph, Increased Temperature, and a Pathogen. *Environ. Sci. Technol.* 48 (12), 7044–7052. doi: 10.1021/es501601w

Fabbri, E., Valbonesi, P. and Franzellitti, S. (2008). HSP Expression in Bivalves. *Invertebr. Surviv. J.* 5 (2), 135–161.

Fry, F. E. J. (1971). The Effect of Environmental Factors on the Physiology of Fish. *Fish. Physiol.*, 6, 1–98. doi: 10.1016/S1546-5098(08)60146-6

Gräns, A., Jutfelt, F., Sandblom, E., Jönsson, E., Wiklander, K., Seth, H., et al. (2014). Aerobic Scope Fails to Explain the Detrimental Effects on Growth Resulting From Warming and Elevated CO2 in Atlantic Halibut. *J. Exp. Biol.* 217 (5), 711–717. doi: 10.1242/jeb.096743

Hall, G. M., Lucke, J. N., Lovell, R. and Lister, D. (1980). Porcine Malignant Hyperthermia. VII: Hepatic Metabolism. *Br. J. Anaesth.* 52 (1), 11–17.

Hammer, K. M., Pedersen, S. A. and Storseth, T. R. (2012). Elevated Seawater Levels of CO2 Change the Metabolic Fingerprint of Tissues and Hemolymph From the Green Shore Crab Carcinus Maenas. *Comp. Biochem. Physiol. - Part D Genomics Proteomics* 7 (3), 292–302. doi: 10.1016/j.cbd.2012.06.001

Hayashi, H., De Bellis, L., Hayashi, Y., Nito, K., Kato, A., Hayashi, M., et al. (2002). Molecular Characterization of an Arabidopsis Acyl-Coenzyme a Synthetase Localized on Glyoxysomal Membranes. *Plant Physiol.* 130 (4), 2019–2026. doi: 10.1104/pp.012955

Hayes, J. and Volkoff, H. (2014). Characterization of the Endocrine, Digestive and Morphological Adjustments of the Intestine in Response to Food Deprivation and Torpor in Cunner, Tautogolabrus Adspersus. *Comp. Biochem. Physiol. - A Mol. Integr. Physiol.* 170, 46–59. doi: 10.1016/j.cbpa.2014.01.014

He, J., Guo, H., Zheng, W., Xue, Y., Zhao, R. and Yao, W. (2019). Heat Stress Affects Fecal Microbial and Metabolic Alterations of Primiparous Sows During Late Gestation. *J. Anim. Sci. Biotechnol.* 10 (1), 84. doi: 10.1186/s40104-019-0391-0

Huan, T. and Li, L. (2015a). Counting Missing Values in a Metabolite-Intensity Data Set for Measuring the Analytical Performance of a Metabolomics Platform. *Anal. Chem.* 87 (2), 1306–1313. doi: 10.1021/ac5039994

Huan, T. and Li, L. (2015b). Quantitative Metabolome Analysis Based on Chromatographic Peak Reconstruction in Chemical Isotope Labeling Liquid Chromatography Mass Spectrometry. *Anal. Chem.* 87 (14), 7011–7016. doi: 10.1021/acs.analchem.5b01434

Huan, T., Wu, Y., Tang, C., Lin, G. and Li, L. (2015). DnsID in MyCompoundID for Rapid Identification of Dansylated Amine- and Phenol-Containing Metabolites in LC-MS-Based Metabolomics. *Anal. Chem.* 87 (19), 9838–9845. doi: 10.1021/acs.analchem.5b02282

IPCC (2014). *Climate Change 2014: Synthesis Report. Contribution of Working Groups I, II and III to the Fifth Assessment Report of the Intergovernmental Panel on Climate Change* (Ipcc), 151 p.

Jiao, S., Nie, M., Song, H., Xu, D. and engYou, F. (2020). Physiological Responses to Cold and Starvation Stresses in the Liver of Yellow Drum (Nibea Albiflora) Revealed by LC-MS Metabolomics. *Sci. Total Environ.* 715, 136940. doi: 10.1016/j.scitotenv.2020.136940

Johansen, J. L. and Jones, G. P. (2011). Increasing Ocean Temperature Reduces the Metabolic Performance and Swimming Ability of Coral Reef Damselfishes. *Glob. Chang. Biol.* 17 (9), 2971–2979. doi: 10.1111/j.1365-2486.2011.02436.x

Jutfelt, F. (2020). Metabolic Adaptation to Warm Water in Fish. *Funct. Ecol.* 34 (6), 1138–1141. doi: 10.1111/1365-2435.13558

Kothary, R. K., Burgess, E. A. and Candido, E. P. M. (1984). The Heat Shock Phenomenon in Cultured Cells of Rainbow Trout: Hsp70mrna Synthesis and Turnover. *Biochim. Biophys. Acta* 783, 137–143. doi: 10.1016/0167-4781(84)90005-8

Kovats, R. S. and Hajat, S. (2008). Heat Stress and Public Health: A Critical Review. *Annu. Rev. Public Health*, 29, 41–55. doi: 10.1146/annurev.publhealth.29.020907.090843

Kullgren, A., Jutfelt, F., Fontanillas, R., Sundell, K., Samuelsson, L., Wiklander, K., et al. (2013). The Impact of Temperature on the Metabolome and Endocrine Metabolic Signals in Atlantic Salmon (Salmo Salar). *Comp. Biochem. Physiol. - A Mol. Integr. Physiol.* 164 (1), 44–53. doi: 10.1016/j.cbpa.2012.10.005

Le, M. H., Dinh, K. V., Nguyen, M. V. and Rønnestad, I. (2020). Combined Effects of a Simulated Marine Heatwave and an Algal Toxin on a Tropical Marine Aquaculture Fish Cobia (Rachycentron Canadum). *Aquac. Res.* 51 (6), 2535–2544. doi: 10.1111/are.14596

Lele, Z., Engel, S. and Krone, P. H. (1997). Hsp47 and Hsp70 Gene Expression is Differentially Regulated in a Stress-and Tissue-Specific Manner in Zebrafish Embryos. *Dev. Genet.* 21 (2), 123–133. doi: 10.1002/(SICI)1520-6408(1997)21:2<123::AID-DVG2>3.0.CO;2-9

Li, L., Li, R., Zhou, J., Zuniga, A., Stanislaus, A. E., Wu, Y., et al. (2013). MyCompoundID: Using an Evidence-Based Metabolome Library for Metabolite Identification. *Anal. Chem.* 85 (6), 3401–3408. doi: 10.1021/ac400099b

Li, X., Yu, X., Sun, D., Li, J., Wang, Y., Cao, P., et al. (2017). Effects of Polar Compounds Generated From the Deep-Frying Process of Palm Oil on Lipid Metabolism and Glucose Tolerance in Kunming Mice. *J. Agric. Food Chem.* 65 (1), 208–215. doi: 10.1021/acs.jafc.6b04565

López-Olmeda, J. F. and Sánchez-Vázquez, F. J. (2011). Thermal Biology of Zebrafish (Danio Rerio). *J. Therm. Biol.* 36 (2), 91–104. doi: 10.1016/j.jtherbio.2010.12.005

Loscalzo, J. (2011). Lipid Metabolism by Gut Microbes and Atherosclerosis. *Circ. Res.* Vol. 109, 127–129. doi: 10.1161/RES.0b013e3182290620

Lucke, J. N. (1978). Liver Metabolism During Malignant Hyperthermia in the Pietrain Pig. *Vet. Anaesth. Analg.* 8 (1), 70–72. doi: 10.1111/j.1467-2995.1978.tb00445.x

Mahanty, A., Purohit, G. K., Yadav, R. P., Mohanty, S. and Mohanty, B. P. (2017). Hsp90 and Hsp47 Appear to Play an Important Role in Minnow Puntiussophore for Surviving in the Hot Spring Run-Off Aquatic Ecosystem. *Fish. Physiol. Biochem.* 43 (1), 89–102. doi: 10.1007/s10695-016-0270-y

Messineo, A. M., Gineste, C., Sztal, T. E., McNamara, E. L., Vilmen, C., Ogier, A. C., et al. (2018). L-Tyrosine Supplementation Does Not Ameliorate Skeletal Muscle Dysfunction in Zebrafish and Mouse Models of Dominant Skeletal Muscle α-Actin Nemaline Myopathy. *Sci. Rep.* 8 (1), 11490. doi: 10.1038/s41598-018-29437-z

Miller, G. M., Watson, S. A., Donelson, J. M., McCormick, M. I. and Munday, P. L. (2012). Parental Environment Mediates Impacts of Increased Carbon Dioxide on a Coral Reef Fish. *Nat. Clim. Chang.* 2 (12), 858–861. doi: 10.1038/nclimate1599

Molina, A., Biemar, F., Müller, F., Iyengar, A., Prunet, P., Maclean, N., et al. (2000). Cloning and Expression Analysis of an Inducible HSP70 Gene From Tilapia Fish. *FEBS Lett.* 474 (1), 5–10. doi: 10.1016/S0014-5793(00)01538-6

Monselise, E. B. I., Levkovitz, A., Gottlieb, H. E. and Kost, D. (2011). Bioassay for Assessing Cell Stress in the Vicinity of Radio-Frequency Irradiating Antennas. *J. Environ. Monit.* 13 (7), 1890–1896. doi: 10.1039/c1em10031a

Morgan, R., Finnøen, M. H., Jensen, H., Pélabon, C. and Jutfelt, F. (2020). Low Potential for Evolutionary Rescue From Climate Change in a Tropical Fish. *Proc. Natl. Acad. Sci. U. S. A.* 117 (52), 33365–33372. doi: 10.1073/pnas.2011419117

Mushtaq, M. Y., Marçal, R. M., Champagne, D. L., van der Kooy, F., Verpoorte, R. and Choi, Y. H. (2014). Effect of Acute Stresses on Zebra Fish (Danio Rerio) Metabolome Measured by Nmr-Based Metabolomics. *Planta. Med.* 80 (14), 1227–1233. doi: 10.1055/s-0034-1382878

Neuheimer, A. B., Thresher, R. E., Lyle, J. M. and Semmens, J. M. (2011). Tolerance Limit for Fish Growth Exceeded by Warming Waters. *Nat. Clim. Chang.* 1 (2), 110–113. doi: 10.1038/nclimate1084

Nicholson, J. K., Holmes, E. and Lindon, J. C. (2007). "Metabonomics and Metabolomics Techniques and Their Applications in Mammalian Systems," in *The Handbook of Metabonomics and Metabolomics*, 1–33. doi: 10.1016/B978-0- 444-52841-4.X5000-0

Ott, K., Aran, N., Singh, B. and Stockton, G. (2003). Metabonomics Classifies Pathways Affected by Bioactive Compounds. Artificial Neural Network Classification of NMR Spectra of Plant Extracts. *Phytochemistry* 62 (6), 971–985. doi: 10.1016/S0031-9422(02)00717-3

Perkins, S. E., Alexander, L. V. and Nairn, J. R. (2012). Increasing Frequency, Intensity and Duration of Observed Global Heatwaves and Warm Spells. *Geophys. Res. Lett.* 39 (20), L20714. doi: 10.1029/2012GL053361

Polymeropoulos, M. H., Licamele, L., Volpi, S., Mack, K., Mitkus, S. N., Carstea, E. D., et al. (2009). Common Effect of Antipsychotics on the Biosynthesis and Regulation of Fatty Acids and Cholesterol Supports a Key Role of Lipid Homeostasis in Schizophrenia. *Schizophr. Res.* 108 (1–3), 134–142. doi: 10.1016/j.schres.2008.11.025

Pörtner, H. O., Berdal, B., Blust, R., Brix, O., Colosimo, A., De Wachter, B., et al. (2001). Climate Induced Temperature Effects on Growth Performance, Fecundity and Recruitment in Marine Fish: Developing a Hypothesis for Cause and Effect Relationships in Atlantic Cod (Gadus Morhua) and Common Eelpout (Zoarces Viviparus). *Cont. Shelf. Res.* 21 (18–19), 1975–1997. doi: 10.1016/S0278-4343(01)00038-3

Pörtner, H. O. and Knust, R. (2007). Climate Change Affects Marine Fishes Through the Oxygen Limitation of Thermal Tolerance. *Science* 315 (5808), 95–97. doi: 10.1126/science.1135471

Purohit, G. K., Mahanty, A., Suar, M., Sharma, A. P., Mohanty, B. P. and Mohanty, S. (2014). Investigating Hsp Gene Expression in Liver of Channa Striatus Under Heat Stress for Understanding the Upper Thermal Acclimation. *BioMed. Res. Int.* 2014, 381719. doi: 10.1155/2014/381719

Pype, C., Verbueken, E., Saad, M. A., Casteleyn, C. R., Van Ginneken, C. J., Knapen, D., et al. (2015). Incubation at 32.5°C and Above Causes Malformations in the Zebrafish Embryo. *Reprod. Toxicol.* 56, 56–63. doi: 10.1016/j.reprotox.2015.05.006

Reilly, C. R. L. and Thompson, S. H. (2007). Temperature Effects on Low-Light Vision in Juvenile Rockfish (Genus Sebastes) and Consequences for Habitat Utilization. *J. Comp. Physiol. A Neuroethol. Sensory. Neural. Behav. Physiol.* 193 (9), 943–953. doi: 10.1007/s00359-007-0247-5

Rezende, E. L. and Bozinovic, F. (2019). Thermal Performance Across Levels of Biological Organization. *Philos. Trans. R Soc. B Biol. Sci.* 374 (1778), 20180549. doi: 10.1098/rstb.2018.0549

Riback, J. A., Katanski, C. D., Kear-Scott, J. L., Pilipenko, E. V., Rojek, A. E., Sosnick, T. R., et al. (2017). Stress-Triggered Phase Separation Is an Adaptive, Evolutionarily Tuned Response. *Cell* 168 (6), 1028–1040.e19. doi: 10.1016/j.cell.2017.02.027

Rosewarne, P. J., Wilson, J. M. and Svendsen, J. C. (2016). Measuring Maximum and Standard Metabolic Rates Using Intermittent-Flow Respirometry: A

Student Laboratory Investigation of Aerobic Metabolic Scope and Environmental Hypoxia in Aquatic Breathers. *J. Fish. Biol.* 88 (1), 265–283. doi: 10.1111/jfb.12795

Sørensen, J. G., Kristensen, T. N. and Loeschcke, V. (2003). The Evolutionary and Ecological Role of Heat Shock Proteins. *Ecol. Lett.* 6 (11), 1025–1037. doi: 10.1046/j.1461-0248.2003.00528.x

Salamanca, N., Giráldez, I., Morales, E., de la Rosa, I. and Herrera, M. (2021). Phenylalanine and Tyrosine as Feed Additives for Reducing Stress and Enhancing Welfare in Gilthead Seabream and Meagre. *Animals* 11 (1), 1–11. doi:10.3390/ani11010045

Samuelsson, L. M., Björlenius, B., Förlin, L. and Larsson, D. G. J. (2011). Reproducible 1h NMR-Based Metabolomic Responses in Fish Exposed to Different Sewage Effluents in Two Separate Studies. *Environ. Sci. Technol.* 45 (4), 1703–1710. doi: 10.1021/es104111x

Samuelsson, L. M., Förlin, L., Karlsson, G., Adolfsson-Erici, M. and Larsson, D. G. J. (2006). Using NMR Metabolomics to Identify Responses of an Environmental Estrogen in Blood Plasma of Fish. *Aquat. Toxicol.* 78 (4), 341–349. doi: 10.1016/j.aquatox.2006.04.008

Samuelsson, L. M. and Larsson, D. G. J. (2008). Contributions From Metabolomics to Fish Research. *Mol. Biosyst.* 4 (10), 974–979. doi: 10.1039/b804196b

Sanhueza, N., Donoso, A., Aguilar, A., Farlora, R., Carnicero, B., Míguez, J. M., et al. (2018). Thermal Modulation of Monoamine Levels Influence Fish Stress and Welfare. *Front. Endocrinol. (Lausanne)* 9. doi: 10.3389/fendo.2018.00717

Savage, D. B., Petersen, K. F. and Shulman, G. I. (2007). Disordered Lipid Metabolism and the Pathogenesis of Insulin Resistance. *Physiol. Rev.* Vol. 87, 507–520. doi: 10.1152/physrev.00024.2006

Shimazu, T., Hirschey, M. D., Hua, L., Dittenhafer-Reed, K. E., Schwer, B., Lombard, D. B., et al. (2010). SIRT3 Deacetylates Mitochondrial 3-Hydroxy-3-Methylglutaryl CoA Synthase 2 and Regulates Ketone Body Production. *Cell Metab.* 12 (6), 654–661. doi: 10.1016/j.cmet.2010.11.003

Shimazu, T., Hirschey, M. D., Newman, J., He, W., Shirakawa, K., Le Moan, N., et al. (2013). Suppression of Oxidative Stress by β-Hydroxybutyrate, an Endogenous Histone Deacetylase Inhibitor. *Science* 339 (6116), 211–214. doi: 10.1126/science.1227166

Sinclair, B. J., Marshall, K. E., Sewell, M. A., Levesque, D. L., Willett, C. S., Slotsbo, S., et al. (2016). Can We Predict Ectotherm Responses to Climate Change Using Thermal Performance Curves and Body Temperatures? *Ecol. Lett.* 19 (11), 1372–1385. doi: 10.1111/ele.12686

Somero, G. N. (2010). The Physiology of Climate Change: How Potentials for Acclimatization and Genetic Adaptation Will Determine "Winners" and "Losers". *J. Exp. Biol.* 213 (6), 912–920. doi: 10.1242/jeb.037473

Sommer, T. and Wolf, D. H. (2014). The Ubiquitin-Proteasome-System. *Biochim. Biophys. Acta - Mol. Cell Res.* 1843 (1), 1. doi: 10.1016/j.bbamcr.2013.09.009

Speers-Roesch, B., Norin, T. and Driedzic, W. R. (2018). The Benefit of Being Still: Energy Savings During Winter Dormancy in Fish Come From Inactivity and the Cold, Not From Metabolic Rate Depression. *Proc. R Soc. B Biol. Sci.* 285 (1886), 20181593. doi: 10.1098/rspb.2018.1593

Surai, P. F., Kochish, I. I., Fisinin, V. I. and Kidd, M. T. (2019). Antioxidant Defence Systems and Oxidative Stress in Poultry Biology: An Update. *Antioxidants* 8 (7), 235. doi: 10.3390/antiox8070235

Su, X., Wang, N., Chen, D., Li, Y., Lu, Y., Huan, T., et al. (2016). Dansylation Isotope Labeling Liquid Chromatography Mass Spectrometry for Parallel Profiling of Human Urinary and Fecal Submetabolomes. *Anal. Chim. Acta* 903, 100–109. doi: 10.1016/j.aca.2015.11.027

Todgham, A. E., Crombie, T. A. and Hofmann, G. E. (2017). The Effect of Temperature Adaptation on the Ubiquitin-Proteasome Pathway in Notothenioid Fishes. *J. Exp. Biol.* 220 (3), 369–378. doi: 10.1242/jeb.145946

Trygg, J. and Wold, S. (2002). Orthogonal Projections to Latent Structures (O-PLS). *J. Chemom.* 16 (3), 119–128. doi: 10.1002/cem.695

Valenzuela, C. A., Zuloaga, R., Mercado, L., Einarsdottir, I. E., Björnsson, B. T., Valdés, J. A., et al. (2018). Chronic Stress Inhibits Growth and Induces Proteolytic Mechanisms Through Two Different Nonoverlapping Pathways in the Skeletal Muscle of a Teleost Fish. *Am. J. Physiol. - Regul. Integr. Comp. Physiol.* 314 (1), R102–R113. doi: 10.1152/ajpregu.00009.2017

Vitali, C., Khetarpal, S. A. and Rader, D. J. (2017). HDL Cholesterol Metabolism and the Risk of CHD: New Insights From Human Genetics. *Curr. Cardiol. Rep.* 19 (12), 132. doi: 10.1007/s11886-017-0940-0

Wagner, N. D., Hillebrand, H., Wacker, A. and Frost, P. C. (2013). Nutritional Indicators and Their Uses in Ecology. *Ecol. Lett.* 16 (4), 535–544. doi: 10.1111/ele.12067

Wagner, L., Trattner, S., Pickova, J., Gómez-Requeni, P. and Moazzami, A. A. (2014). 1h NMR-Based Metabolomics Studies on the Effect of Sesamin in Atlantic Salmon (Salmo Salar). *Food Chem.* 147, 98–105. doi: 10.1016/j.foodchem.2013.09.128

Wallace, E. W. J., Kear-Scott, J. L., Pilipenko, E. V., Schwartz, M. H., Laskowski, P. R., Rojek, A. E., et al. (2015). Reversible, Specific, Active Aggregates of Endogenous Proteins Assemble Upon Heat Stress. *Cell* 162 (6), 1286–1298. doi: 10.1016/j.cell.2015.08.041

Wu, Y. and Li, L. (2012). Determination of Total Concentration of Chemically Labeled Metabolites as a Means of Metabolome Sample Normalization and Sample Loading Optimization in Mass Spectrometry-Based Metabolomics. *Anal. Chem.* 84 (24), 10723–10731. doi: 10.1021/ac3025625

Wysocki, L. E., Montey, K. and Popper, A. N. (2009). The Influence of Ambient Temperature and Thermal Acclimation on Hearing in a Eurythermal and a Stenothermal Otophysan Fish. *J. Exp. Biol.* 212 (19), 3091–3099. doi: 10.1242/jeb.033274

Xiao, W., Zou, Z., Li, D., Zhu, J., Yue, Y. and Yang, H. (2020). Effect of Dietary Phenylalanine Level on Growth Performance, Body Composition, and Biochemical Parameters in Plasma of Juvenile Hybrid Tilapia, Oreochromis Niloticus × Oreochromis Aureus. *J. World Aquac. Soc.* 51 (2), 437–451. doi: 10.1111/jwas.12641

Zhang, Z., Zhou, C., Fan, K., Zhang, L., Liu, Y. and Liu, P.f. (2021). Metabolomics Analysis of the Effects of Temperature on the Growth and Development of Juvenile European Seabass (Dicentrarchus Labrax). *Sci. Total Environ.* 769, 145155. doi: 10.1016/j.scitotenv.2021.145155

Zhou, R., Tseng, C. L., Huan, T. and Li, L. (2014). IsoMS: Automated Processing of LC-MS Data Generated by a Chemical Isotope Labeling Metabolomics Platform. *Anal. Chem.* 86 (10), 4675–4679. doi: 10.1021/ac5009089

Conflict of Interest: The authors declare that the research was conducted in the absence of any commercial or financial relationships that could be construed as a potential conflict of interest.

Publisher's Note: All claims expressed in this article are solely those of the authors and do not necessarily represent those of their affiliated organizations, or those of the publisher, the editors and the reviewers. Any product that may be evaluated in this article, or claim that may be made by its manufacturer, is not guaranteed or endorsed by the publisher.

frontiers | Frontiers in Marine Science

BRIEF RESEARCH REPORT
published: 20 July 2022
doi: 10.3389/fmars.2022.924130

Antimicrobial Resistance and Genotype Characteristics of *Vibrio scophthalmi* Isolated from Diseased Mariculture Fish Intestines With Typical Inter-Annual Variability

Yongxiang Yu[1,2†], Xiao Liu[3†], Yingeng Wang[1,2], Meijie Liao[1,2], Miaomiao Tang[1], Xiaojun Rong[1,2], Chunyuan Wang[1], Bin Li[1,2] and Zheng Zhang[1,2*]*

[1]Key Laboratory of Maricultural Organism Disease Control, Yellow Sea Fisheries Research Institute, Chinese Academic of Fishery Sciences, Qingdao, China, [2]Laboratory for Marine Fisheries Science and Food Production Processes, Qingdao National Laboratory for Marine Science and Technology, Qingdao, China, [3]Laboratory of Pathology and Immunology of Aquatic Animalscean, Fisheries College, Ocean University of China, Qingdao, China

OPEN ACCESS

Edited by:
Qingchao Wang,
Huazhong Agricultural University, China

Reviewed by:
Hao Wang,
Shanghai Ocean University, China
Yingli Gao,
Jiangsu Ocean Universiity, China

***Correspondence:**
Yingeng Wang
wangyg@ysfri.ac.cn
Zheng Zhang
zhangzheng@ysfri.ac.cn

†These authors have contributed equally to this work

Specialty section:
This article was submitted to Aquatic Physiology, a section of the journal Frontiers in Marine Science

Received: 20 April 2022
Accepted: 20 June 2022
Published: 20 July 2022

Citation:
Yu Y, Liu X, Wang Y, Liao M, Tang M, Rong X, Wang C, Li B and Zhang Z (2022) Antimicrobial Resistance and Genotype Characteristics of Vibrio scophthalmi Isolated From Diseased Mariculture Fish Intestines With Typical Inter-Annual Variability. Front. Mar. Sci. 9:924130. doi: 10.3389/fmars.2022.924130

As an intestinal organism settled long-term within the gut of marine fish, Vibrio scophthalmi is a potential object for the bacterium genetic variation and adaptation research. The genetic diversity, antimicrobial resistance phenotype, and genotype of 33 V. *scophthalmi* isolated from diseased marine fish intestines between 2002 and 2020 were evaluated. The results showed that all isolates were frequently resistant to penicillins, cephalosporins, aminoglycosides, and macrolides and displayed multidrug-resistant (MDR) phenotype *in vitro*. Thirty percent of isolates were resistant to more than 20 different drugs. The average insensitive (resistant and intermediate) rate of *V. scophthalmi* isolates was 49.5%~81.8% between 2002 and 2020, but the t-test revealed that there was no significant difference in the drug-resistance rate of *V. scophthalmi* isolates with typical interannual variability. Eleven antimicrobial resistance genes (*strB*, *strA*, *ant(3″)-I*, *mphA*, *blaPSE*, *qnrS*, *tetC*, *tetE*, *tetM*, *tetS*, and *int1*) were detected in these isolates, but the antimicrobial resistance phenotypes and genotypes of these isolates were not consistent. Enterobacterial repetitive intergenic consensus polymerase chain reaction (ERIC-PCR) analysis indicated that 33 isolates could be divided into two clusters (G1 and G3) and two single isolates (G2 and G4), and the G2 cluster was isolated from South Sea *C. undulates* with typical geographical species differences. There was no significant correlation between the drug susceptibility and the genetic types of *V. scophthalmi* isolates. The results reveal the mismatch phenomenon between antimicrobial resistance and genotype of inherent *V. scophthalmi* in the marine fish intestines, and the antimicrobial susceptibility isolates might be a potential risk source for storage and transmission of resistance genes.

Keywords: *Vibrio scophthalmi*, antimicrobial susceptibility, antimicrobial resistance genotype, genetic diversity, ERIC-PCR

INTRODUCTION

Vibrio scophthalmi was first isolated from the intestines of juvenile turbot and identified as a species of *Vibrio* genus based on phenotypic traits, G+C content, DNA-DNA hybridization, and 16*S* rDNA gene sequence in 1997 (Cerdag-cuellar et al., 1997). Previous studies have indicated that *V. scophthalmi* has pathogenicity to aquatic animals such as *Paralichthys olivaceus* (Qiao et al., 2012), *Dentex dentex* L. (Sitjà-bobadilla et al., 2010), and *Thunnus maccoyii* (Valdenegro-vega et al., 2013). Furthermore, *V. scophthalmi* was also the abundant *Vibrio* species in the healthy turbot intestinal microbiota and serves as an intestinal organism settled long term within the gut of marine fish (Cerdag-cuellar and Blanch, 2010).

As an intestinal bacterium in marine fish, the physiological and metabolic phenotype of *V. scophthalmi* was highly related to the breeding environment and food foundation of fish. Thus, *V. scophthalmi* could be a potential object for the bacterium genetic variation and adaptation research in fish culture. Identifying the types of microbial pathogens through various methods such as phenotyping and molecular typing to investigate the prevalence of hospitalized infections is a necessity (Healy et al., 2005). Antimicrobial resistance is an important concern in the public health systems that due to the rise in the resistant strains of bacteria (Nouri et al., 2020). And the enterobacterial repetitive intergenic consensus sequences polymerase chain reaction (ERIC-PCR) is a simple, fast, and affordable PCR-based methods for molecular typing analysis of different isolated bacteria, which were less dependent on effective and variable factors on bacterial growth (Sedighi et al., 2020).

In this study, we evaluated the antimicrobial resistance and genotype characteristics of *V. scophthalmi* from diseased fish intestines (85% strains isolated from diseased flatfish) from 2002–2020 and gained a better understanding of the relationship between antimicrobial-resistant phenotypes and resistance genotypes of those isolates. The results could provide an overview of the status of bacterial genetic diversity and antimicrobial sensitivity in intensive cultivation of fish and provide guidance on aquatic disease treatment.

MATERIALS AND METHODS

Strains Information and Growth Conditions

From Nov 2002 to Oct 2020, epidemiological and etiological investigations were performed which primarily aims at monitoring the prevalence of bacterial diseases among cultured marine fish in China. During this time, a total of 33 isolates were preliminarily identified to be *V. scophthalmi* with typical timeline differences. The isolates in our study were isolates from fish intestines with typical intestinal diseases. The detailed information of 33 V. *scophthalmi* isolates was shown in **Supplementary Table 1**. The isolate resources were resuspended in 20% glycerol and stored at −80°C in our laboratory for long-term preservation. For all the experiments, the *V. scophthalmi* isolates were grown in tryptic soy agar medium and incubated aerobically at 28°C for 24 h.

Antimicrobials Susceptibility Testing

A total of 33 agents were chosen for antimicrobials susceptibility test *in vitro* for scientific research. Some of the drugs were allowed in veterinary practices at different periods, and others were chosen for the drug resistance census in this study only. The types and concentrations of antimicrobials were listed in **Supplementary Table 2**. The testing was performed using the disc diffusion method as described in the Clinical and Laboratory Standards Institute M07 (CLSI-M07). *Escherichia coli* ATCC 25922 was used as the reference strain. The bacterial suspension was prepared and adjusted to approximately 1×10^8 cfu/ml. The disc contains antimicrobial agents that were affixed to the agar plate coated with 100 μl of bacterial suspension. Culture media were maintained in a normal atmosphere incubator for 24 h at 28°C. Each group was replicated twice, and the mean of the inhibition zone was used as the result. The bacterial sensitivity was calculated by referring to the aquatic bacterial susceptibility test standard issued by the CLSI.

Determination of ARGs

To determine the presence of antimicrobial resistance genes (ARGs), PCR detection assays were used to examine the presence or absence of 20 ARGs belonging to six categories (Versalovic et al., 1991; Yamamoto and Harayama, 1995; Byers et al., 1998; Speldooren et al., 1998; Jun et al., 2004; Kim et al., 2004; Chuanchuen and Padungtod, 2009; Nguyen et al., 2009; Colomer-lluch et al., 2011; Liu et al., 2013; Deng et al., 2014; Qiao et al., 2017; Moffat et al., 2020; Yuan et al., 2021; Yu et al., 2021). Primers of all target ARGs were based on the published literature and are shown in **Supplementary Table 3**. The PCR method employed to determine the presence of ARGs was based on the genomic DNA of *V. scophthalmi* isolates. The gene analyses used specific primers and PCR conditions modified according to primer Tm values. The PCR fragments were sequenced for both strands, and the sequence identities were conformed using the BLAST database.

ERIC-PCR Analysis

The optimized ERIC-PCR condition was employed for the genetic diversity analysis of *V. scophthalmi* isolates as Versalovic et al. (Versalovic et al., 1991) described with minor modification. The final optimized amplification conditions consisted of initial denaturation at 94°C for 5 min, followed by 30 cycles each of denaturation at 94°C for 30 s, annealing at 55°C for 1 min, extension at 72°C for 5 min, and an additional 10-min extension at 72°C. The amplification was repeated three times to confirm the reproducibility of the ERIC-PCR method. The zero-one manual method was used to analyze the patterns, and the dendrogram was drawn according to the clusters (Movahedi et al., 2021).

RESULTS

Antimicrobial Resistance Phenotypes of *V. scophthalmi*

All isolates *V. scophthalmi* were tested for antimicrobial susceptibilities to 33 selected antibiotics *in vitro*, and the antimicrobial resistance phenotypes were evaluated and summarized in **Figure 1**. Among the *V. scophthalmi* isolates, the resistance frequency to penicillins and aminoglycosides reached up to 48.48%–100% and 57.58%–93.94%, respectively. In contrast, there was a low resistance frequency to phenicols (9.09% for florfenicol and 15.15% for chloroamphenicol). When it comes to cephalosporins, tetracyclines, macrolides, and fluoroquinolones, there were significant differences in the antimicrobial resistance rates of *V. scophthalmi* isolates in different agents that belong to the same category. For cephalosporins, isolates were frequently resistant to cefradine and cefalexin with 75.76% and 72.73%, moderately resistant to cefazolin, ceftriaxone, ceftizoxime, ceftazidime, and cefotaxime with 33.33%–57.58%, and seldom resistant to sulbactam (18.18%). For tetracyclines, isolates were frequently resistant to tetracycline (36.36%) and doxycycline (30.30%) and infrequently resistant to minocycline (3.03%). For macrolides, isolates were frequently resistant to acetylspiramycin (90.91%) and moderately resistant to clarithromycin, erythromycin, and azithromycin (36.36%–42.42%). For fluoroquinolones, isolates were frequently resistant to pipemidic (90.91%), moderately resistant to lomefloxacin (42.42%), and infrequently resistant to ciprofloxacin, ofloxacin, fleroxacin, enrofloxacin, norfloxacin, and nalidixic with 3.03%–15.15%. Incidence of resistance to oxacillin (100%), neomycin (93.94%), acetylspiramycin (90.91%), and pipemidic acid (90.91%) was the highest among individual antimicrobials. Incidence of resistance to minocycline (3.03%), ciprofloxacin (3.03%), and norfloxacin (3.03%) was the least observed among the individual antimicrobials. Thirty percent of isolates were resistant to more than 20 different drugs. The most resistant isolate was VS11, which was resistant to 27 agents, and the least resistant isolate was VS19, which was resistant to 5 agents.

The proportion of drug-sensitive *V. scophthalmi* isolated reached the lowest in 2006 with 6.1% and the highest value in 2002 with 69.7%. Combining the resistance rate of *V. scophthalmi* with the isolation background indicated that there was no significant correlation between the resistance rate of *V. scophthalmi* and the host. Furthermore, the average insensitive (resistant and intermediate) rate was 49.5%~81.8% between 2002 and 2020, the insensitive rate was lowest in 2002, and the isolates in 2005 and 2019 recorded more than 75% insensitive rates, respectively. But based on the t-test statistical analysis, there was no significant difference in the drug-resistance rate of *V. scophthalmi* isolates with typical interannual variability.

Multidrug-Resistant Analysis

Isolates that were simultaneously non-susceptible to at least one agent in three or more antimicrobial categories were considered multidrug-resistant (MDR) (Magiorakos et al., 2012). As shown in **Figure 2**, there were six MDR profiles based on the *in vitro* susceptibility of 33 V. *scophthalmi* isolates to seven antimicrobial categories. All isolates were non-susceptible to at least one agent in penicillins (A), aminoglycosides (C), macrolides (E), and fluoroquinolones (G). This suggested that all *V. scophthalmi* displayed MDR *in vitro*. Furthermore, the MDR phenotype of *V. scophthalmi* isolates from 2002 to 2006 also with high growth rate equally. There was no significant correlation between the MDR phenotype of *V. scophthalmi* and the host.

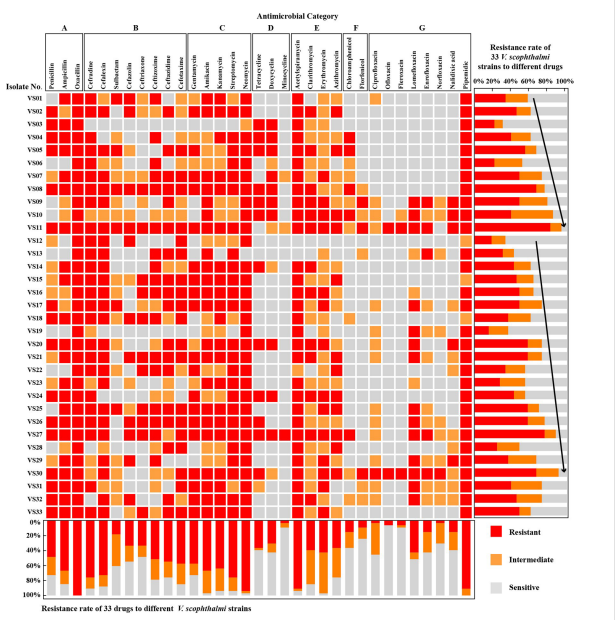

FIGURE 1 | Antimicrobial susceptibility tests of 33 *V. scophthalmi* isolates to different kinds of antimicrobials.

Antimicrobial Resistance Genotypes of *V. scophthalmi*

The distribution of ARGs was evaluated and summarized in **Figures 2**-**4**. Eleven of 38 resistance genes were detected in at least one isolates. Twenty-one isolates carried one or more ARGs evaluated. Among them, *tetM* was the most prevalent gene, with the detection frequencies of 48.5%, followed by *strA*, *strB*, *tetE*, *qnrS*, *int1*, *ant3″-I*, *mphA*, *blaPSE*, *tetC*, and *tetS*.

None of the isolates carry β-lactam and macrolides resistance genes except isolate VS17. Of all the tetracycline-resistant isolates, tetracycline- and doxycycline-resistant isolates VS24, VS27, and VS30 were found to be negative for any of the tetracycline resistance genes. Comparatively, tetracycline-resistant genes, *tetM*, *tetS*, or *tetC*, were present in isolates VS12, VS17, VS23, VS28, and VS33, which were susceptible to tetracycline antimicrobial agents. Among pipemidic acid–insensitive isolates (n = 33), only three isolates (VS30, VS31, and VS32) carry quinolone resistance genes *qnrS*. For aminoglycosides resistant genes, *strA*, *strB*, and *ant3″-I* were detected in 11 aminoglycoside-resistant isolates, but the other aminoglycoside-resistant isolates (n = 22) did not bear any aminoglycoside-resistant genes. Furthermore, integron factors *int1* occurred in isolates VS17, VS27, and VS28. The results showed that *V. scophthalmi* isolates were resistant to some antimicrobial agents but may present negative to relevant resistance genes.

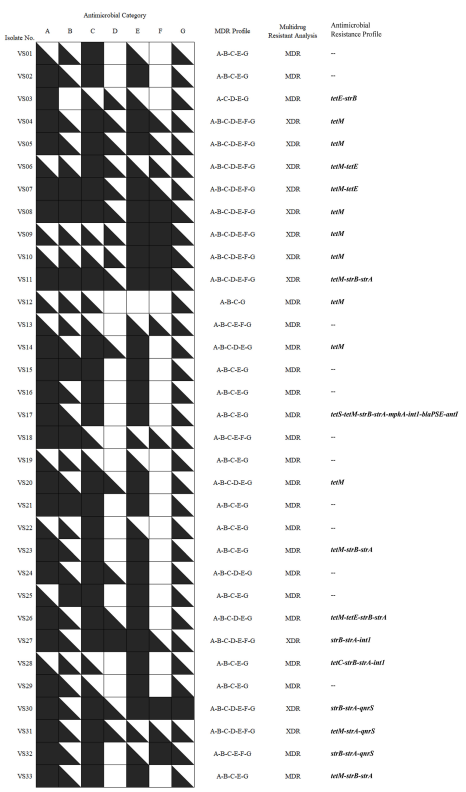

FIGURE 2 | Multidrug-resistant (MDR) profiles of 33 *V. scophthalmi* isolates to seven different antimicrobial categories. ■ is the isolate that is non-susceptible to all agents listed in category; ◣ is the isolate that is non-susceptible to some but not all agents listed in category; and □ is the isolate that is susceptible to all agents listed in the category.

ERIC-PCR Typing and Cluster Analysis

The DNA fingerprints gained by ERIC-PCR consisted of distinct bands ranging in size from 100 to 10,000 bp. The dendrogram was generated by using the software BioNumerics 7.0. All 33 isolates showed 25 ERIC-PCR patterns. As shown in **Figure 4**, when the relative similarity coefficient is 62%, 33 isolates could be divided into two clusters (G1 and G3) and two single isolates (G2 and G4). G1 and G3 were the dominant groups, in which G1 consisted of 12 (36.4%) isolates, whereas G3 contained 19 isolates (57.6%). Among them, fingerprints of isolate VS15 (G2) and isolates in G1 were quite similar, and the fingerprint of isolate VS04 presented a low similarity with other isolates.

Based on the epidemiological investigation information, VS15 (G2) was isolated from *Cheilinus undulates* only once, and 11 of 12 hosts in the G1 cluster and 16 of 19 hosts in the G3 cluster belonged to flatfish; in addition to that, VS21 (G1 cluster) was isolated from *Epinephelus septemfasciatus* and VS13/VS22/VS23 (G2 cluster) were isolated from *Sebastes schlegelii* and *Tetraodontidae*, respectively. The G2 and G4 clusters were isolated before 2009, and isolates in G2 and G4 clusters appeared alternately. There was no significant correlation between the ERIC-PCR genetic types, drug-resistant phenotype, and genotypes of *V. scophthalmi* isolates.

DISCUSSION

Vibrio spp. was identified as the common and serious pathogen in marine fish and shellfish worldwide, and the use of antimicrobials has greatly contributed to the development and spread of antimicrobial resistance among *Vibrio* sp. (Loo et al., 2020). To make the aquaculture industry more sustainable, surveillance of bacteria susceptibility and genetic variation was needed. As a native bacterium in the marine fish intestine, a high prevalence of *in vitro* resistance of *V. scophthalmi* to penicillins, cephalosporins, aminoglycosides, and macrolides was observed in this study. The ASEAN countries including Malaysia, Myanmar, and the Philippines permit the use of tetracycline and oxytetracyclines in their aquaculture sector (Weese et al., 2015). In European countries, oxytetracycline is approved for use in aquaculture (Rodgers and Furones, 2009). The *in vitro* resistance rate of *V. scophthalmi* to doxycycline was 58.33% during 2002–2006. In contrast, the resistance rate of *V. scophthalmi* to doxycycline was 14.29% during 2007–2020. Martineau et al. found that the

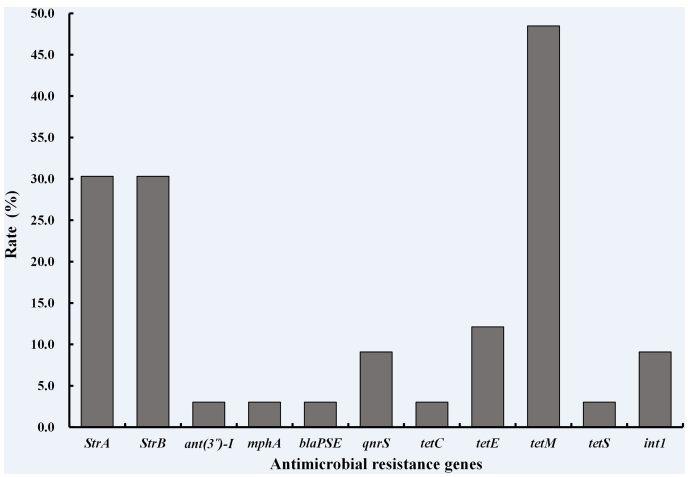

FIGURE 3 | Distribution of antimicrobial resistance genes in 33 *V. scophthalmi* isolates.

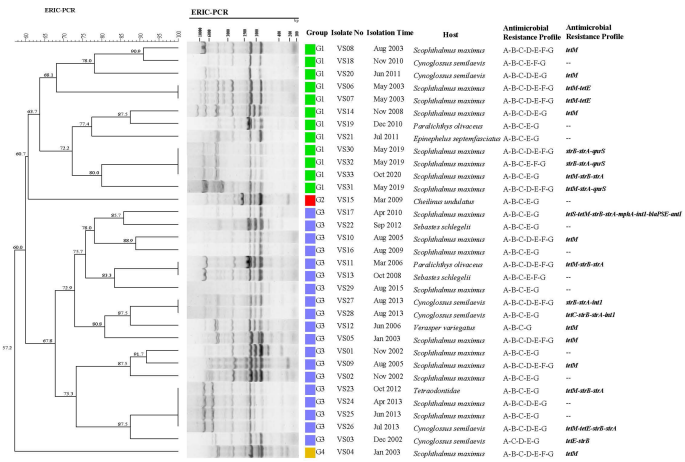

FIGURE 4 | Phylogenetic analysis of 33 *V. scophthalmi* isolates based on ERIC-PCR.

reduction of antimicrobial use could reduce the emergence of resistance (Martineau et al., 1996). The significant reduction in the resistance rate of *V. scophthalmi* to doxycycline, suggests that with the development of a standard and regulatory system of antimicrobials usage, as well as research and development of new techniques such as vaccination, microecologics, and Chinese herbal medicine, the consumption of doxycycline could be gradually reduced in aquaculture in China.

This study is the first large-scale survey on the ARGs of *V. scophthalmi* isolates. These findings showed that those *V. scophthalmi* isolates settled long term within the gut of marine fish carried a variety of ARGs, and the *V. scophthalmi* isolates might be considered as a potential vehicle for the transfer ARGs in species or seafood. Our findings also demonstrated an obvious mismatch between antimicrobial resistance phenotype and genotype in *V. scophthalmi* isolates, which were also found in other species, such as *V. parahaemolyticus*, *Lactobacillus pentosusand*, *Leuconostoc pseudomesenteroide*, *E. coli*, and *Listeria* sp. (Seung et al., 2012; Maria et al., 2014; Luo et al., 2016). The antimicrobial phenotype is mediated by membrane structure, antimicrobial resistance genes, or physiological metabolism. *V. scophthalmi* isolates in our study were resistant to some antimicrobial agents but may present negative to relevant resistance genes. The mechanism of drug resistance of *V. scophthalmi* isolates with diverse antimicrobial phenotypes should be investigated further. Furthermore, the antimicrobial resistance phenotype analysis reveals that there was no significant difference in the drug-resistance rate of *V. scophthalmi* isolated with typical interannual variability. But different kinds of ARGs were detected in *V. scophthalmi* isolated in recent years. Therefore, there is a great significance of surveillance of antimicrobial susceptibility of *V. scophthalmi*, which is highly relevant to food safety and public health.

ERIC-PCR is based on the targeting of repeated DNA sequences with oligonucleotide primers which has been broadly employed to perform the epidemiological typing of pathogenic bacteria such as *V. parahaemolyticus* (Sahilah et al., 2014), *Staphylococcus aureus* (Akindolire et al., 2018), and *Bacillus cereus* (Gao et al., 2018). In this study, the ERIC-PCR results suggested a low genetic diversity among *V. scophthalmi* isolates. In fact, the 33 isolates could only be divided into two clusters (G1 and G3) and two single isolates when the relative similarity coefficient was 62%. *V. scophthalmi* isolates shared a higher degree of similarity that usually came from close isolation time. What is surprising is that isolates VS30 and VS32, isolated during an outbreak in 2019, shared the same profiles with stain VS33, an isolate obtained in 2020. The same applies to isolates VS24, VS25, and VS26 that were isolated in 2013, and strain VS23 which was isolated in 2012. These findings showed evidence of epidemiological associations among *V. scophthalmi* isolates isolated at different times. The same ERIC profile was observed in isolates VS23, VS24, VS25, and VS26. However, the four isolates showed different hosts and antimicrobial resistance patterns. The phenomenon indicated that isolates sharing completely the same ERIC profile presented different antimicrobial resistance patterns or hosts, suggesting that the resistant phenotype of *V. scophthalmi* isolates may be associated with the antimicrobials distributed in the environment and was not associated with the genotype of isolates.

In conclusion, the antimicrobial susceptibility of *V. scophthalmi* isolated from diseased fish intestines with typical interannual differences in the costal mariculture area of China was highly prevalent and all of them were resistant to multiple antimicrobial agents. The distribution of ARGs reveals the mismatched phenomenon between the antimicrobial resistance phenotype and genotype of *V. scophthalmi* isolates. Furthermore, the ERIC-PCR analysis showed a low genetic diversity of *V. scophthalmi* isolates. Further, there was no significant correlation between the genetic types, drug resistance phenotype, and genotypes of *V. scophthalmi* isolates. The results will provide data support for further understanding the genetic variation of inherent strains in the fish breeding system and protection product development.

DATA AVAILABILITY STATEMENT

The original contributions presented in the study are included in the article/**Supplementary Material**. Further inquiries can be directed to the corresponding authors.

AUTHOR CONTRIBUTIONS

YY, YW, and ZZ contributed to conception and design of the research. YY, XL, and MT performed experiment. YY, BL, and CW performed data processing and statistical analysis. YY and XL drafted the manuscript. YW, XR, and ML contributed to revision of manuscript for important intellectual content. YW gave laboratory and project support. All authors read and approved the final manuscript.

FUNDING

This work was funded by the National Key R&D Program of China (2019YFD0900102), Basic Scientific Research Funds for Central Non-profit Institutes, Yellow Sea Fisheries Research Institutes (20603022021013), Central Public-interest Scientific Institution Basal Research Fund, CAFS (2022GH02) and Central Public-interest Scientific Institution Basal Research Fund, CAFS (2020TD40).

SUPPLEMENTARY MATERIAL

The Supplementary Material for this article can be found online at: https://www.frontiersin.org/articles/10.3389/fmars.2022.924130/full#supplementary-material

REFERENCES

Akindolire, M. A., Kumar, A. and Ateba, C. N. (2018). Genetic Characterization of Antibiotic-Resistant Staphylococcus Aureus From Milk in the North-West Province, South Africa. *Saudi J. Biol. Sci.* 25, 1348–1355. doi:10.1016/j.sjbs.2015.10.011

Byers, H. K., Stackebrandt, E., Hayward, C. and Blackall, L. L. (1998). Molecular Investigation of a Microbial Mat Associated With the Great Artesian Basin. *FEMS Microbiol. Ecol.* 25, 391–403. doi: 10.1111/j.1574-6941.1998.tb00491.x

Cerdag-cuellar, M. and Blanch, A. R. (2010). Detection and Identification of Vibrio Scophthalmi in the Intestinal Microbiota of Fish and Evaluation of Host Specificity. *J. Appl. Microbiol.* 93, 261–268. doi: 10.1046/j.1365-2672.2002.01697.x

Cerdag-cuellar, M., Rossello-mora, R. A., Lalucat, J., Jofre, J. and Blanch, A. (1997). Vibrio Scophthalmi Sp. Nov., a New Species From Turbot (Scophthalmus Maximus). *Int. J. System. Bacteriol.* 47, 58–61. doi: 10.1099/00207713-47-1-58

Chuanchuen, R. and Padungtod, P. (2009). Antimicrobial Resistance Genes in Salmonella Enterica Isolates From Poultry and Swine in Thailand. *J. Vet. Med. Sci.* 71, 1349–1355. doi: 10.1292/jvms.001349

Colomer-lluch, M., Jofre, J. and Muniesa, M. (2011). Antibiotic Resistance Genes in the Bacteriophage DNA Fraction of Environmental Samples. *PLoS One* 6, el7549. doi: 10.1371/journal.pone.0017549

Deng, Y. T., Wu, Y. L., Tan, A. P., Huang, Y. P., Jiang, L., Xue, H. J., et al. (2014). Analysis of Antimicrobial Resistance Genes in Aeromonas Spp. Isolated From Cultured Freshwater Animals in China. *Microbial. Drug Resist. (Larchmont N.Y.)* 20, 350–356. doi: 10.1089/mdr.2013.0068

Gao, T. T., Ding, Y., Wu, Q. P., Wang, J., Zhang, J., Yu, S. B., et al. (2018). Prevalence, Virulence Genes, Antimicrobial Susceptibility, and Genetic Diversity of Bacillus Cereus Isolated From Pasteurized Milk in China. *Front. Microbiol.* 9. doi: 10.3389/fmicb.2018.00533

Healy, M., Huong, J., Bittner, T., Lising, M., Frye, S., Raza, S., et al. (2005). Microbial DNA Typing by Automated Repetitive-Sequence-Based PCR. *J. Clin. Microbiol.* 43, 199–207. doi: 10.1128/JCM.43.1.199-207.2005

Jun, L. J., Jeong, J. B., Huh, M. D., Chung, J. K., Choi, D. I., Lee, C. H., et al. (2004). Detection of Tetracycline–Resistance Determinants by Multiplex Polymerase Chain Reaction in Edwardsiella Tarda Isolated From Fish Farms in Korea. *Aquaculture* 240, 89–100. doi: 10.1016/j.aquaculture.2004.07.025

Kim, S. R., Nonaka, L. and Suzuki, S. (2004). Occurrence of Tetracycline Resistance Genes Tet(M) and Tet(S) in Bacteria From Marine Aquaculture Sites. *FEMS Microbiol. Lett.* 237, 147–156. doi: 10.1016/j.femsle.2004.06.026

Liu, M., Wong, M. and Chen, S. (2013). Mechanisms of Fluoroquinolone Resistance in Vibrio Parahaemolyticus. *Int. J. Antimicrob. Agents* 42, 187–188. doi: 10.1016/j.ijantimicag.2013.04.024

Loo, K. Y., Letchumanan, V., Law, J. W., Pusparajah, P., Goh, B. H., Mutalib, N. S. A., et al. (2020). Incidence of Antibiotic Resistance in Vibrio Spp. *Rev. Aquacult.* 12, 2590–2608. doi: 10.1111/raq.12460

Lou, Y., Liu, H. Q., Zhang, Z. H., Pan, Y. J. and Zhao, Y. (2016). Mismatch Between Antimicrobial Resistance Phenotype and Genotype of Pathogenic Vibrio Parahaemolyticus Isolated From Seafood. *Food Control.* 59, 207–211. doi: 10.1016/j.foodcont.2015.04.039

Magiorakos, A. P., Srinivasan, A., Carey, R. B., Carmeli, Y., Falagas, M. E., Giske, C. G., et al. (2012). Multidrug-Resistant, Extensively Drug-Resistant and Pandrug-Resistant Bacteria: An International Expert Proposal for Interim Standard Definitions for Acquired Resistance. *Clin. Microbiol. Infect.* 18, 268–281. doi: 10.1111/j.1469-0691.2011.03570.x

Maria, D. C. C. M., Nabil, B., Leyre, L. L., Antonio, G. and Hikmate, A. (2014). Antibiotic Resistance of Lactobacillus Pentosus and Leuconostoc Pseudomesenteroides Isolated From Naturally-Fermented Alorena Table Olives Throughout Fermentation Process. *Int. J. Food Microbiol.* 172, 110–118. doi: 10.1016/j.ijfoodmicro.2013.11.025

Martineau, F., Picard, F. J., Roy, P. H., Ouellette, M. and Bergeron, M. G. (1996). Species-Specific and Ubiquitous-DNA-Based Assays for Rapid Identification of Staphylococcus Aureus. *J. Clin. Microbiol.* 34, 93–2888. doi: 10.1128/JCM.34.12.2888-2893.1996

Moffat, J., Chalmers, G., Reid-Smith, R., Mulvey, M. R. and Boerlin, P. (2020). Resistance to Extended-Spectrum Cephalosporins in Escherichia Coli and Other Enterobacterales From Canadian Turkeys. *PLoS One* 15, e0236442. doi: 10.1371/journal.pone.0236442

Movahedi, M., Zarei, O., Hazhirkamal, M., Karami, P., Shokoohizadeh, L. and Taheri, M. (2021). Molecular Typing of *Escherichia Coli* Strains Isolated From Urinary Tract Infection by ERIC-PCR. *Gene Rep.* 23, 101058. doi: 10.1016/j.genrep.2021.101058

Nguyen, M., Woerther, P. L., Bouvet, M., Andremont, A., Leclercq, R. and Canu, A. (2009). Escherichia Coli as Reservoir for Macrolide Resistance Genes. *Emerging. Infect. Dis.* 15, 1648–1650. doi: 10.3201/eid1510.090696

Nouri, F., Karami, P., Zarei, O., Kosari, F., Alikhani, M. Y., Zandkarimi, E., et al. (2020). Prevalence of Common Nosocomial Infections and Evaluation of Antibiotic Resistance Patterns in Patients With Secondary Infections in Hamadan, Iran. *Infect. Drug Resist.* 13, 2365. doi: 10.2147/idr.s259252

Qiao, G., Lee, D. C., Woo, S. H., Li, H., Xu, D. H. and Park, S. I. (2012). Microbiological Characteristics of Vibrio Scophthalmi Isolates From Diseased Olive Flounder Paralichthys Olivaceus. *Fish. Sci.* 78, 853–863. doi: 10.1007/s12562-012-0502-8

Qiao, J., Zhang, Q., Alali, W. Q., Wang, J., Meng, L., Xiao, Y., et al. (2017). Characterization of Extended-Spectrum β-Lactamases (Esbls)-Producing Salmonella in Retail Raw Chicken Carcasses. *Int. J. Food Microbiol.* 248, 72. doi: 10.1016/j.ijfoodmicro.2017.02.016

Rodgers, C. J. and Furones, M. (2009). "Antimicrobial Agents in Aquaculture: Practice, Needs and Issues," in *The Use of Veterinary Drugs and Vaccines in Mediterranean Aquaculture*, Zaragoza: CIHEAM, 41–59.

Sahilah, M. A., Laila, A. S. R., Azuhairi, A., Osman, H., Aminah, A. and Azuhairi, A. A. (2014). Antibiotic Resistance and Molecular Typing Among Cockle (Anadara Granosa) Strains of Vibrio Parahaemolyticus by Polymerase Chain Reaction (PCR)-Based Analysis. *World J. Microbiol. Biotechnol.* 30, 649–659. doi: 10.1007/s11274-013-1494-y

Sedighi, P., Zarei, O., Karimi, K., Taheri, M., Karami, P. and Shokoohizadeh, L. (2020). Molecular Typing of Klebsiella Pneumoniae Clinical Isolates by Enterobacterial Repetitive Intergenic Consensus Polymerase Chain Reaction. *Int. J. Microbiol.* 2020, 1–5. doi: 10.1155/2020/8894727

Seung, H. R., Seog, G. P., Sung, M. C., Young, O. H., Hee, J. H., Su, U. K., et al. (2012). Antimicrobial Resistance and Resistance Genes in *Escherichia Coli* Strains Isolated From Commercial Fish and Seafood. *Int. J. Food Microbiol.* 152, 14–18. doi: 10.1016/j.ijfoodmicro.2011.10.003

Sitjà-bobadilla, A., Pujalte, M. J., Bermejo, A., Garay, E., Alvarez-Pellitero, P. and Perez-Sanchez, J. (2010). Bacteria Associated With Winter Mortalities in Laboratory-Reared Common Dentex (Dentex Dentex L.). *Aquacult. Res.* 38, 733–739. doi: 10.1111/j.1365-2109.2007.01719.x

Speldooren, V., Heym, B., Labia, R. and Nicolaschanoine, M. H. (1998). Discriminatory Detection of Inhibitor-Resistant β-Lactamases in Escherichia Coli by Single-Strand Conformation Polymorphism-Pcr. *Antimicrob. Agents Chemother.* 42, 879–884. doi: 10.1097/0000113-199804000-00011

Valdenegro-vega, V., Naeem, S., Carson, J., Bowman, J. P., Tejedor del Real, J. L. and Nowak, B. (2013). Culturable Microbiota of Ranched Southern Bluefin Tuna (Thunnus Maccoyii Castelnau). *J. Appl. Microbiol.* 115, 923–932. doi: 10.1111/jam.12286

Versalovic, J., Koeuth, T. and Lupski, R. (1991). Distribution of Repetitive DNA Sequences in Eubacteria and Application to Fingerprinting of Bacterial Genomes. *Nucleic Acids Res.* 19, 6823–6831. doi: 10.1093/nar/19.24.6823

Weese, J. S., Giguère, S., Guardabassi, L., Morley, P. S., Papich, M., Ricciuto, D. R., et al. (2015). Acvim Consensus Statement on Therapeutic Antimicrobial Use in Animals and Antimicrobial Resistance. *J. Vet. Internal Med.* 29, 487–498. doi: 10.1111/jvim.12562

Yamamoto, S. and Harayama, S. (1995). PCR Amplification and Direct Sequencing of gyrB Genes With Universal Primers and Their Application to the Detection and Taxonomic Analysis of Pseudomonas Putida Strains. *Appl. Environ. Microbiol.* 61, 9–1104. doi: 10.1128/AEM.61.10.3768-3768.1995

Yuan, Y. Z., Zhang, Y. G., Qi, G. S., Ren, H., Gao, G. S., Jin, X. M., et al. (2021). Isolation, Identification, and Resistance Gene Detection of Vibrio Harveyi From Scophthalmus Maximus. *Aquacult. Int.* 29, 2357–2368. doi: 10.1007/s10499-021-00752-z

Yu, B., Zhang, Y., Yang, L., Xu, J. and Bu, S. (2021). Analysis of Antibiotic Resistance Phenotypes and Genes of *Escherichia Coli* From Healthy Swine in Guizhou, China. *Onderstepoort J. Vet. Res.* 88, 1–8. doi: 10.4102/ojvr.v88i1.1880

Conflict of Interest: The authors declare that the research was conducted in the absence of any commercial or financial relationships that could be construed as a potential conflict of interest.

Publisher's Note: All claims expressed in this article are solely those of the authors and do not necessarily represent those of their affiliated organizations, or those of the publisher, the editors and the reviewers. Any product that may be evaluated in this article, or claim that may be made by its manufacturer, is not guaranteed or endorsed by the publisher.

frontiers | Frontiers in Physiology

TYPE Original Research
PUBLISHED 21 July 2022
DOI 10.3389/fphys.2022.929094

OPEN ACCESS

EDITED BY
Qingchao Wang,
Huazhong Agricultural University, China

REVIEWED BY
Rantao Zuo,
Dalian Ocean University, China
Xuelin Zhao,
Ningbo University, China

*CORRESPONDENCE
Meijie Liao,
liaomj@ysfri.ac.cn
Xiaojun Rong,
rongxj@ysfri.ac.cn

†These authors have contributed equally to this work

SPECIALTY SECTION
This article was submitted to Aquatic Physiology, a section of the journal Frontiers in Physiology

RECEIVED 26 April 2022
ACCEPTED 27 June 2022
PUBLISHED 21 July 2022

CITATION
Chang M, Li B, Liao M, Rong X, Wang Y, Wang J, Yu Y, Zhang Z and Wang C (2022), Differential expression of miRNAs in the body wall of the sea cucumber Apostichopus japonicus under heat stress.
Front. Physiol. 13:929094.
doi: 10.3389/fphys.2022.929094

Differential expression of miRNAs in the body wall of the sea cucumber *Apostichopus japonicus* under heat stress

Mengyang Chang[1,2†], Bin Li[1,3†], Meijie Liao[1,3*], Xiaojun Rong[1,3*], Yingeng Wang[1,3], Jinjin Wang[1,3], Yongxiang Yu[1,3], Zheng Zhang[1,3] and Chunyuan Wang[1,3]

[1]Key Laboratory of Sustainable and Development of Marine Fisheries, Ministry of Agriculture and Rural Affairs, Yellow Sea Fisheries Research Institute, Chinese Academy of Fishery Sciences, Qingdao, China, [2]College of Fishers and Life Science, Shanghai Ocean University, Shanghai, China, [3]Laboratory for Marine Fisheries Science and Food Production Processes, Qingdao National Laboratory for Marine Science and Technology, Qingdao, China

MicroRNAs, as one of the post-transcriptional regulation of genes, play an important role in the development process, cell differentiation and immune defense. The sea cucumber *Apostichopus japonicus* is an important cold-water species, known for its excellent nutritional and economic value, which usually encounters heat stress that affects its growth and leads to significant economic losses. However, there are few studies about the effect of miRNAs on heat stress in sea cucumbers. In this study, high-throughput sequencing was used to analyze miRNA expression in the body wall of sea cucumber between the control group (CS) and the heat stress group (HS). A total of 403 known miRNAs and 75 novel miRNAs were identified, of which 13 miRNAs were identified as significantly differentially expressed miRNAs (DEMs) in response to heat stress. A total of 16,563 target genes of DEMs were predicted, and 101 inversely correlated target genes that were potentially regulated by miRNAs in response to heat stress of sea cucumbers were obtained. Based on these results, miRNA-mRNA regulatory networks were constructed. The expression results of high-throughput sequencing were validated in nine DEMs and four differentially expressed genes (DEGs) by quantitative real-time polymerase chain reaction (RT-qPCR). Moreover, pathway enrichment of target genes suggested that several important regulatory pathways may play an important role in the heat stress process of sea cucumber, including ubiquitin-mediated proteolysis, notch single pathway and endocytosis. These results will provide basic data for future studies in miRNA regulation and molecular adaptive mechanisms of sea cucumbers under heat stress.

KEYWORDS

***Apostichopus japonicus*, microRNA, heat stress, stress response, miRNA-mRNA network**

Introduction

The sea cucumber (*Apostichopus japonicus*) is widely distributed along the northwest Pacific coast at 35~44°N and has been utilized as an important marine economic resource for its nutritional and medicinal value (Chang and Loscalzo, 2010; Wang et al., 2015). The total amount of sea cucumber cultivation in China has continuously increased and the cultivation area has been expanding since 2003. In 2020, the annual production of sea cucumber cultivation reached 200,000 t with an increase of 14.48% over the previous year, and the production value reached 50 billion US dollars (Ministry of Agriculture and Rural Affairs, 2021). The sea cucumber aquaculture industry has suffered great loss, with the global warming and the frequent occurrence of high temperatures in summer. Heat stress was reported to impose many negative effects on the growth, metabolism, and reproduction of aquatic farmed animals. Therefore, understanding the molecular mechanism of miRNA under heat stress would help to reduce the damage caused by heat stress on sea cucumbers and breed new varieties with high temperature resistance.

As a typical temperate species, the sea cucumber was greatly affected by water temperature, not only on its physiological activities, but also on feeding and metabolism (Zhao et al., 2015; Li et al., 2016a). The high temperature was shown to reduce the activity and food intake of sea cucumber, disorder the metabolism of free radicals in the body and even lead to disease and death (Wang et al., 2011; Li et al., 2012). It was showed that the total number of coelomic cells, phagocytosis rate and lysozyme activity in the coelomic fluid of *A. japonicus* was decreased to a certain extent after entering summer dormancy (Shao et al., 2016). The research on the effects of temperature changes on the physiology, growth and gene expression of sea cucumbers has gotten a lot of attention. Zhang et al. (2015) found that increasing temperature can affect the DNA methylation level of *A. japonicus*, and then change the expression of the heat shock protein gene. The methylation sites of intestinal, respiratory tree and gonadal tissues in sea cucumber were mainly distributed in the gene functional regions, and the methylation sites were mainly of CG type (Li et al., 2018). Under heat stress at 26°C, the methylation level of intestinal genome in sea cucumber increased, while at 32°C, the methylation level decreased (Wen et al., 2021). At present, the research on the regulation mechanism of sea cucumber under heat stress focuses on the epigenetic and transcriptional regulation, but there are few studies on the post-transcriptional regulation.

MicroRNAs (miRNAs) are endogenous noncoding small RNAs with 22 nt, which regulate post-transcriptional gene expression by binding to the 3′ untranslated region (UTR) of target genes (Bartel, 2004; Pedersen et al., 2007). Numerous studies have reported that miRNAs can provide reversible gene silencing mechanisms during animal aestivation and hibernation, thus miRNAs can be involved in cellular adaptation to specific demands under stressful conditions (Jones-Rhoades and Bartel, 2004). It has been reported that miRNA played a key role in the response to heat stress of plants and animals (Jones-Rhoades and Bartel, 2004). In rainbow trout, some miRNAs, including ssa-miR-301a-3p, ssa-miR-30a-5p and ssa-miR-30a-5p, can regulate the key changes of cells under high temperature stress (Ma et al., 2019). In *Litopenaeus vannamei*, 41 differentially expressed miRNAs related to heat stress were selected, such as lva-miR-92b, lva-miR-317 and lva-miR-184 (Boonchuen et al., 2020). Recently, Li et al. (2016b) and Zhou et al. (2018) found that some miRNAs including miR-184 and miR-2004 played a key role in the coelomic fluid of sea cucumber in response to heat stress. However, it was largely unknown for the miRNA regulation in the body wall of diseased sea cucumber in response to heat stress.

The purpose of this study was to identify known miRNAs and novel miRNAs from the body wall of sea cucumber high-throughput sequencing analysis, as well as to investigate the regulation mechanism between miRNAs and their target genes in sea cucumber after heat treatment. Our findings will be useful in further studies of sea cucumber biomarkers and will provide basic data for future studies on miRNA regulation and sea cucumber molecular adaptive mechanisms under heat stress.

Materials and methods

Experimental design and tissue collection

Sea cucumbers (body weight 50.0 ± 2.0 g) of appr. 1 year old were collected from Qingdao Ruizi Group Co., Ltd., in Shandong Province, China. The sea cucumbers were transported to our lab in Qingdao and acclimated in aerated indoor tanks for 5 days. During the experiment, the temperature and salinity of sea water were around 15°C and 30‰, respectively. The sea cucumbers were fed with a regular compound feed, and one third of seawater was changed daily.

When acclimation finished, a total of 30 sea cucumbers were selected and randomly divided into two groups. For the control group (CS), the culture temperature was continued to maintain at 15°C. According to previous studies of our lab, the median lethal temperature (LT_{50}) to sea cucumber was 32°C (Zhang et al., 2022). Therefore, the temperature for the heat stress group (HS) was set to 32°C in the present study. Heaters were used to give thermal stress to the sea cucumbers. The temperature system was continuously increased at a heating rate of 2°C/24 h. The moment when the water temperature reached 32°C was regarded as the initial time. In the subsequent experiment, the water temperature was maintained at 32°C ± 0.5°C. On the third day of the experiment, three sea cucumbers in the CS group and three skin ulceration syndrome individuals in the HS group were randomly selected. The body wall of six sea cucumbers were

immediately sampled and frozen in liquid nitrogen, since the body wall was the target organ of skin ulceration syndrome. All the samples were stored at −80°C for miRNA sequencing analysis.

RNA extraction and processing

Total RNA was extracted from each sample using the Animal Tissue RNA Purification Kit (LC Sciences, Houston, TX, United States) according to the manufacturer's instructions. The quality of total RNA was checked in Bioanalyzer 2100 (Agilent, Santa Clara, CA, United States) with RNA integrity number >7.0.

Small RNA library was constructed according to the protocol of TruSeq Small RNA Sample Prep Kits (Illumina, San Diego, CA, United States). RNAs in the 16–30 nt size range were purified from a 15% polyacrylamide gel, then sequentially ligated to 5′ and 3′ adapters. Reverse transcription was subsequently performed by polymerase chain reaction (PCR) amplification. The purified PCR products were sequenced by Illumina Hiseq2500 (LC-BIO, Hangzhou, China).

Sequence data analysis

Raw reads were subjected to an in-house program, ACGT101-miR (LC Sciences, Houston, TX, United States) to remove adapter dimers, junk, low complexity, and clean reads ranging from 16 to 30 nt in length were obtained. Sequence matching non-coding RNAs, including rRNA, tRNA, small nuclear RNA (snRNA), and small nucleolus RNA (snoRNA), were mapped to Repbase database (http://www.girinst.org) and Rfam database (http://rfam.xfam.org). The unique small RNA sequences were aligned against the miRBase V22.0 (http://www.mirbase.org/blog) to select the known miRNAs and novel miRNAs and at most one mismatch inside of the sequence was allowed in the alignment. The Deuterostoma species in the miRBase were used as host species and the priority rank of these species in sequence alignment was listed in Supplementary Table S1. Then, the sequence was mapped to the sea cucumber genome (assembled by our lab, unpublished) by Bowtie 1 (Berthelot et al., 2014) to determine the genomic locations of known miRNAs and the flank sequences of novel miRNAs. The hairpin structures of the novel miRNAs were predicated from the flank 80 nt sequences using miRDeep2 (Friedlnder et al., 2012). Principal component analysis (PCA) was performed on the valid data using the vegan R package.

TPM (millions of transcripts) normalization was used for miRNA expression analysis. Differential expression of miRNAs was selected using DEGseq (http://www.bioconductor.org/packages/release/bioc/html/DEG-seq.html). Fold-change and *p*-values were calculated from the normalized expression referring to the methods in published studies (Song et al., 2017). $|\log_2(\text{Foldchange})| > 1$ and *p*-value lower than 0.05 was considered as significantly different expression miRNAs (DEMs).

TABLE 1 RT-qPCR primers used for validation of this study.

Gene ID	Primer sequences (5′–3′)
miR-210	TATACTTGTGCGTGCGACAGCG
miR-31ac	AGGCAAGATGTTGGCATAGCTGT
miR-10	CGCTACCCTGTAGATCCGAATTTGTG
miR-2004-5p	GGCTTTCTGTGGCTGTCGTGTTAAG
miR-92a-3p	CTATTGCACTTGTCCCGGCCTAT
miR-92a-5p	TATTGCACATGTCCCGGCCTG
miR-92c	TTATTGCACTCGTCCCGGCC
miR-193	TACTGGCCAGCACAATCCCAG
miR-4185	CGCGTTGTATTCGTACTGTCTGACC
BAG3 R	GTTATCGCCTCTCGGTTCAC
BAG3 F	GACTCTCAGCATCCATTCTTCA
WDR20 R	GGACTTGACCAGCCGAGAA
WDR20 F	AGCAGCAATTTAACACCAGAGA
TRAF7 R	ACAGCAGGAGTATGACAAGTGA
TRAF7 F	GGAATGGAATGAAGCGGTTGA
FUT4 R	CGGTCCACAAGTAGAAGTACG
FUT4 F	TGGCTTAGGTCGCTCTATGATA
ACTB R	GATGTCACGGACGATTTCACG
ACTB F	AAGGTTATGCTCTTCCTCACGCT
U6 R	TGGAACGCTTCACGAATTTGCG
U6 F	GGAACGATACAGAGAAGATTAGC

Target gene prediction and function analysis

MiRanda (http://www.microrna.org/) and TargetScan (http://www.targetscan.org/vert_80/) were used to predict the target genes of known miRNAs and novel miRNAs. Target genes with a context score percentile <50 were removed from the TargetScan, and target genes with maximum free energy (Max Energy) >−10 were removed from the miRanda. Finally, the intersection of these two websites was taken as the final target genes of different expression miRNA.

Gene ontology (GO) and kyoto encyclopedia of genes and genomes (KEGG) analyses were carried out to further understand genes biological functions. Target genes of differential expressed miRNAs were mapped to GO terms in the database (http://www.geneontology.org/) and KEGG database (http://www.genome.jp/kegg/) respectively. The GO terms and KEGG pathways with *p*-value < 0.05 through hypergeometric test were defined as significantly enriched terms.

Correlation analysis of miRNA and differentially expressed genes

In previous mRNA-seq studies, we have identified differentially expressed genes (DEGs) under heat stress using the same samples as the present study (Li, 2021). Therefore, correlation analysis of miRNA-mRNA were carried out in order to identify key miRNA-target pairs. $p < 0.05$ and fold change >2 were set as the threshold for screening miRNA-target pairs. Only inversely correlated miRNA-mRNA were identified. The identified miRNA-mRNA regulatory network was constructed by Cytoscape 2.8.3 software (Shannon et al., 2003).

Quantitative real-time PCR validation of miRNA and mRNA expression

Quantitative real-time PCR (RT-qPCR) was used to verify the expression level of nine DEMs and four DEGs that were selected from miRNA-mRNA regulatory network based on their potential functional importance. The remaining RNA samples from the small RNA-Seq library construction were used for RT-qPCR amplifications. β-Actin and *U6* were used as the internal control gene for DEGs and DEMs (Table 1). Total RNA after genome DNA removing was reverse-transcribed to cDNA using Evo M-MLV RT Kit (TaKaRa, Japan) following the manufacturer's instructions. The reaction was set for 25 min at 37°C and 5 s at 85°C. The cDNA was amplified using SYBR Green Premix Pro Taq HS qPCR Kit (TaKaRa, Japan) with miRNA and mRNA specific forward primers and universal reverse primers. The PCR amplification parameters were as follows: 95°C for 2 min, followed by 45 cycles of 95°C for 15 s, 60°C for 15 s, and 70°C for 25 s. Amplification specificity was verified by melting curve analysis. The relative expression levels of target gene transcripts were calculated according to the comparative cycle threshold (Ct) method ($2^{-\Delta\Delta CT}$), and GraphPad 6.0 was used for statistical analysis. All data are expressed as mean ± standard deviation (SD).

Results

Small RNA library construction

In total, six small RNA libraries (CS1, CS2, CS3, HS1, HS2, HS3) were constructed from the body wall of sea cucumbers in the present study. The raw data have been submitted to the National Center for Biotechnology Information under the accession number SRR18918495 ~ SRR18918500. A total of 11,929,100 and 10,107,557 raw reads were generated from the CS and HS, respectively. After removing low-quality reads, including repeat reads, junk reads, mRNA and other noncoding RNAs, a total of 5,902,588 and 5,053,528 valid reads were obtained from the CS and HS, respectively (Table 2). PCA analysis was performed on the data of six groups, and it was found that HS group and CS group had great repeatability, respectively (Supplementary Figure S1). From the valid reads length statistics, the distribution showed that 22 nt was the most common type (Supplementary Figure S2). A total of 403 known miRNAs were identified in six libraries (Supplementary Table S1). Among these known miRNAs, 281 miRNAs were grouped into 127 families, of which miR-25 was the largest family with 16 members, followed by let 7 family with 10 members, and the miR-1 with eight members (Supplementary Table S3). Among the 127 families, 61 families contained only one number, and 33 families contained two numbers. The information of top 20 families were displayed in a histogram (Supplementary Figure S3). The sequences nonmatched to miRBase database were compared with the genome to predict the novel miRNAs by miRDeep2 and 75 novel candidate miRNAs were predicted (Supplementary Table S4). Some novel miRNAs with the same mature sequence but different precursors were considered to belong to a novel miRNA family. These novel miRNA candidates were named in the form of "PC plus number" (Supplementary Table S4). The miRNA precursor sequences plus a sequence of 100 nt per site were presented in Supplementary Table S5.

Differential expression analysis of miRNAs

Compared with the control group, 144 miRNAs were upregulated including miR-92a and miR-210, while 334 miRNAs were downregulated including miR-152 and miR-22. The *t*-test was used for analysis and $p < 0.05$ was regarded as the criterion to identify the differential expressed miRNAs (DEMs). The result showed that 13 DEMs were identified between CS and HS, and the numbers of upregulated and downregulated DEMs were five and eight, respectively (Figure 1; Table 3). These miRNAs may play an important role in regulating sea cucumbers in response to heat stress. Besides, there was a novel miRNA (Novel-6338) that included in these DEMs. Among these DEMs, the expression of miR-92a-3p and miR-210 showed more than two-fold up regulation and miR-10 showed more than five-fold up regulation. Particularly, the expression levels of miR-31, miR-2004-5p and miR-1357-3p were downregulated over four fold.

Target gene prediction and functional analysis

In order to understand the biological processes and molecular functions of miRNAs during heat stress, Targetscan and miRanda were used to predict the target genes of the 13 DEMs. TargetScan algorithm removes the target gene whose context score percentile is less than 50, and miRanda algorithm removes the target gene whose maximum energy is greater than −10. Finally, the intersection of these two softwares is taken as the final target gene of DEMs. For the 13 DEMs, a total of 16,563 target genes were predicted, including

TABLE 2 Statistics of small RNA sequences from the six libraries in the body wall of *Apostichopus japonicas*.

Types	CS1	CS2	CS3	HS1	HS2	HS3
Raw reads	11,070,085	11,460,240	11,543,525	12,595,348	12,071,954	11,336,397
3ADT and length filter	5,147,178	3,551,267	4,822,194	4,836,882	3,588,507	4,170,684
Junk reads	15,992	7,360	7,356	7,965	5,557	6,489
rRNA	371,333	157,862	358,843	495,445	209,038	124,374
tRNA	47,955	53,999	122,106	93,783	51,361	56,706
snoRNA	3,600	9,253	8,105	3,609	11,341	4,357
snRNA	3,295	2,589	7,585	3,236	2,714	2,331
mRNA	1,759,941	1,867,237	1,034,122	1,238,688	2,096,006	2,023,885
Repeats	51,088	36,052	66,679	43,662	50,584	17,811
Valid reads	3,659,175	5,772,797	5,109,872	5,849,747	6,052,171	4,927,402
Known miRNA	266	244	280	147	168	249
Novel miRNA	55	23	17	17	20	14

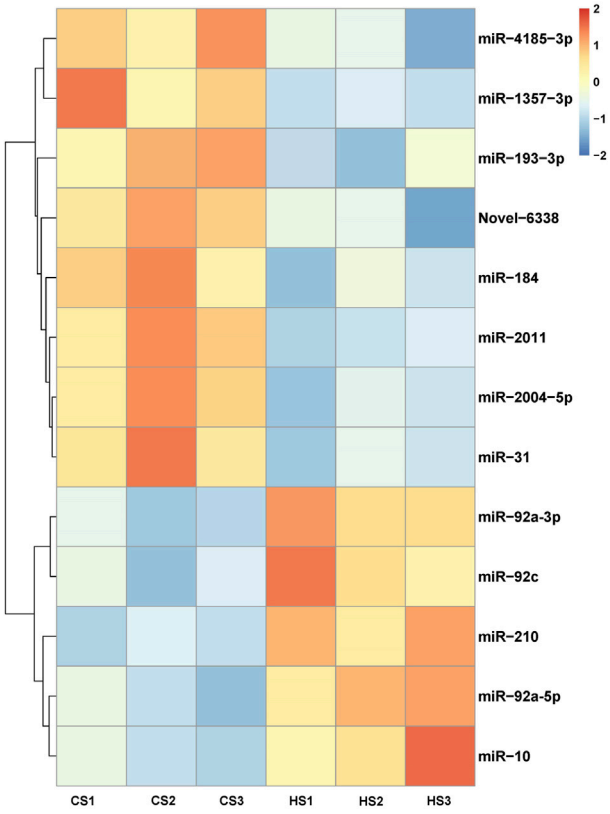

FIGURE 1
Cluster analysis heatmap of differentially expressed miRNAs.

5,153 target genes of five upregulated DEMs and 11,410 target genes of eight downregulated DEMs. The GO database annotation results showed that 11,001 target genes of 13 DEMs were annotated to 334 GO terms ($p < 0.05$), including 178 terms for biological processes, 65 terms for cellular components, and 91 terms for molecular functions. Of these GO terms, membrane, integral component of membrane and nucleus in cellular components are enriched with more genes, and we listed the top 10 terms with the most target genes number in each category (Figure 2). The result showed that 4,235 target genes were annotated into 25 KEGG pathways ($p < 0.05$), among which the endocytosis, ubiquitin mediated proteolysis, homologous recombination, axon guidance, notch signaling pathway interaction were the top five pathways with the most abundant target genes (Figure 3).

Correlation analysis of miRNA-mRNA

To reveal the roles of miRNAs, the DEMs were selected for association analysis with the DEGs obtained by previously transcriptome sequencing. Finally, we identified 101 inversely correlated target genes that potentially regulated by miRNAs in response to heat stress of sea cucumbers (Supplementary Table S6). Of these 101 inversely correlated target genes, 12 inversely correlated target genes were down regulated by four up regulated DEMs, and 89 inversely correlated target genes were up regulated by eight down regulated DEMs. Among them, miR-92c combined with the most DEGs in the upregulated DEMs, and miR-2004-5p combined with the most DEGs in the downregulated DEMs (Figures 4A,B). The DEGs in the regulation network, such as WD repeat-containing protein 20 (WD20), glycoprotein 3-alpha-L-fucosyltransferase A-like (FUT4), E3 ubiquitin-protein ligase (TRAF), Serine/threonine protein kinase TAO3-like isoform (PAK4), interleukin -17D-like (IN17) and BAG family molecular chaperone regulator 3 (BAG3) involved in ubiquitin-mediated proteolysis and notch signaling pathway. These results suggested that these negative regulatory genes might be involved in the response of *A. japonicus* to heat stress.

TABLE 3 Information of significantly differential expressed miRNAs in the body wall of *Apostichopus japonicas* under heat stress.

miRNA ID	Expression level of CS (mean ± SD)	Expression level of HS (mean ± SD)	log_2 (fold_change)	Up/down
miR-92a-5p	171,784.572 ± 0.03	326,057.996 ± 0.06	1.12	Up
miR-92a-3p	231.004 ± 0.05	504.888 ± 0.08	1.13	Up
miR-2004-5p	132.433 ± 0.07	23.616 ± 0.07	−2.49	Down
miR-2011	17,240.464 ± 0.05	7,210.385 ± 0.03	−1.26	Down
miR-210	407.597 ± 0.04	951.313 ± 0.04	1.22	Up
miR-184	257,392.996 ± 0.04	122,704.002 ± 0.06	−1.07	Down
miR-193-3p	770.017 ± 0.06	371.259 ± 0.13	−1.05	Down
miR-31	5,632.975 ± 0.08	1,503.164 ± 0.10	−1.91	Down
miR-4185-3p	26.704 ± 0.09	7.890 ± 0.06	−1.76	Down
miR-92c	6,493.253 ± 0.03	14,052.467 ± 0.08	1.11	Up
Novel-6338	20.839 ± 0.13	6.583 ± 0.01	−1.66	Down
miR-1357-3p	27.683 ± 0.10	1.259 ± 0.02	−4.46	Down
miR-10	15,749.221 ± 0.07	82,172.348 ± 0.09	2.38	Up

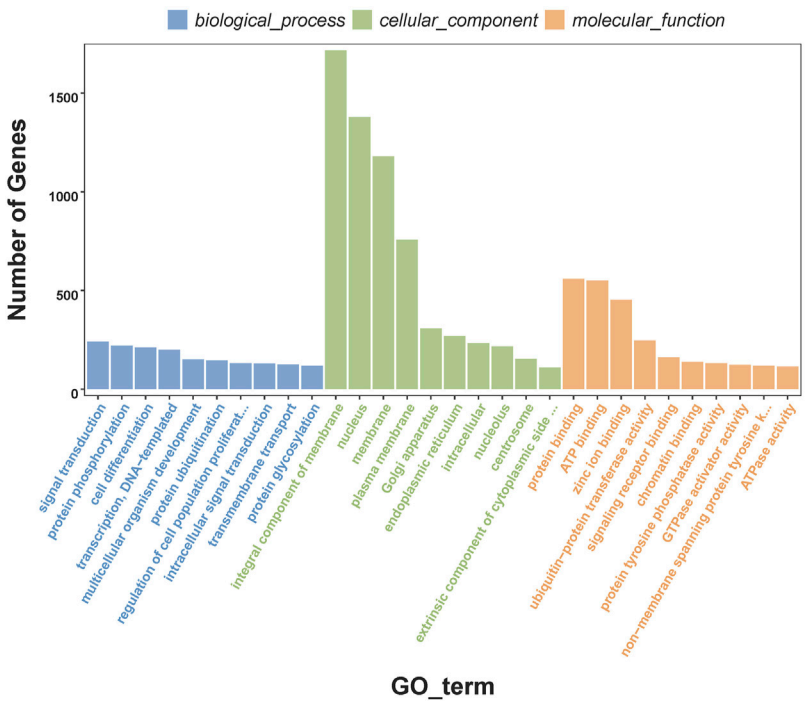

FIGURE 2
Top 10 enriched GO terms of the target genes of differentially expressed miRNAs.

Validation of differentially expressed miRNAs and their differentially expressed genes expression by real-time PCR

To verify the reliability of the sequencing expression profiles, nine miRNAs and four negative genes were applied to RT-qPCR. A peak was detected in the melting curve during the experiment, indicating that all PCR products were specifically amplified. The results of RT-qPCR showed that the expression trend of miRNA and negative genes were consistent with the high-throughput sequencing results. The expression of miR-210 and miR-10, miR-92a-3p, miR-92a-5p and miR-92c were significantly upregulated (Figure 5A), and miR-

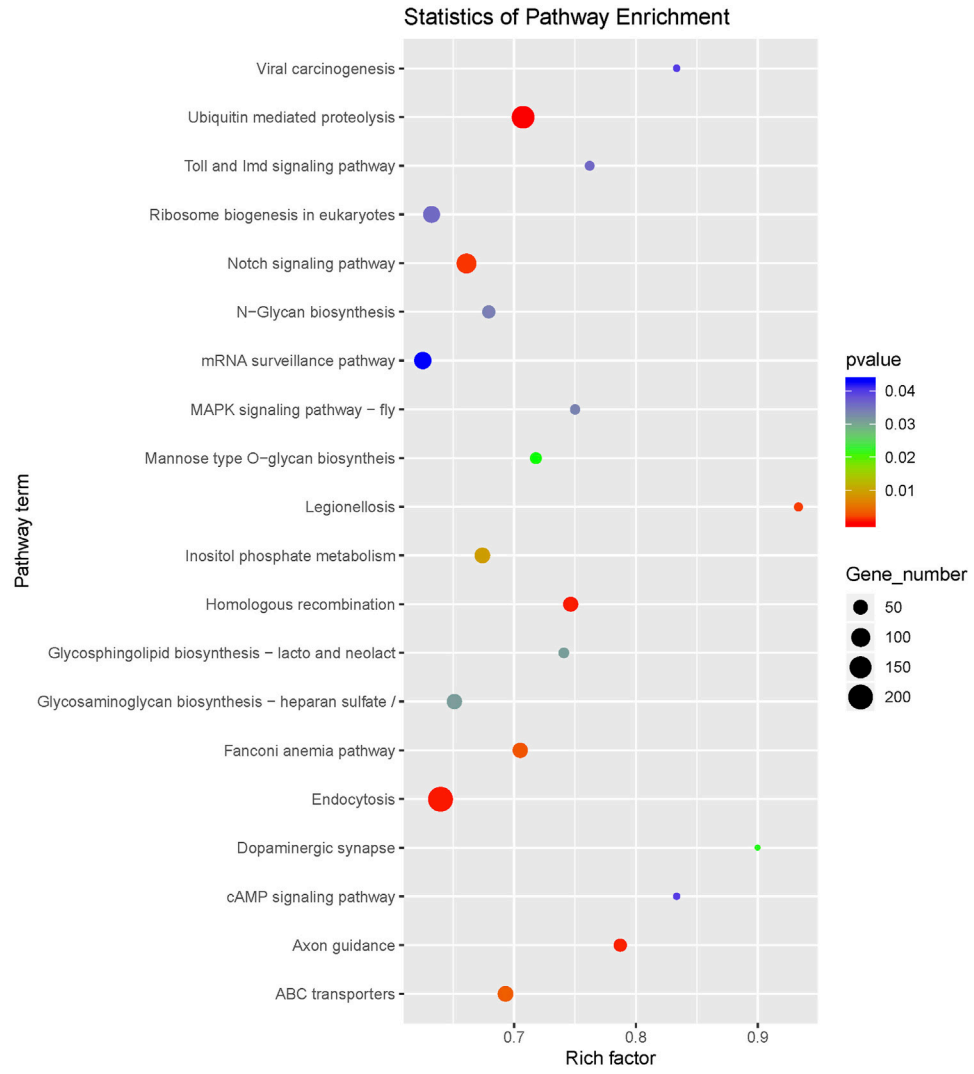

FIGURE 3
KEGG pathway enrichment of the target genes of differentially expressed miRNAs.

2004-5p, miR-31, miR-193 and miR-4185 were significantly downregulated (Figure 5B). The expression of BAG3 and TARF7 were significantly upregulated, and WDR20 and FUT4 were significantly downregulated (Figure 5C).

Discussion

In the present study, we performed a high-throughput miRNA sequencing and miRNA-mRNA correlation analysis to study the post-transcription regulation mechanism of *A. japonicus* in response to high-temperature stress. We obtained 13 significantly differentially expressed miRNAs and a list of negative regulator genes of these differentially expressed miRNAs in the body wall of *A. japonicus* during heat stress. These miRNAs, negative target genes and miRNAs-mRNA regulation networks may play important roles in regulating heat stress, which broadens our understanding of the molecular regulation mechanism of *A. japonicus* in response to heat stress.

Among the 13 identified differentially expressed miRNAs, some miRNAs (such as miR-184, miR-193, miR-2004, miR-31, miR-210 and miR-10) have been reported to be involved in stress responses or immune processes previously. MiR-184 has been reported to be related to the infection of *Procambarus clarkii* by *Spiroplasma eriocheiris* (Ou et al., 2013). Xu et al. (2019) found that miR-184 of *Sinopotamon henanense* was significantly upregulated in response to oxidative stress induced by cadmium (Cd). MiR-193 has been reported to be related to *Bos taurus* infection (Shi et al., 2014). The expression level of

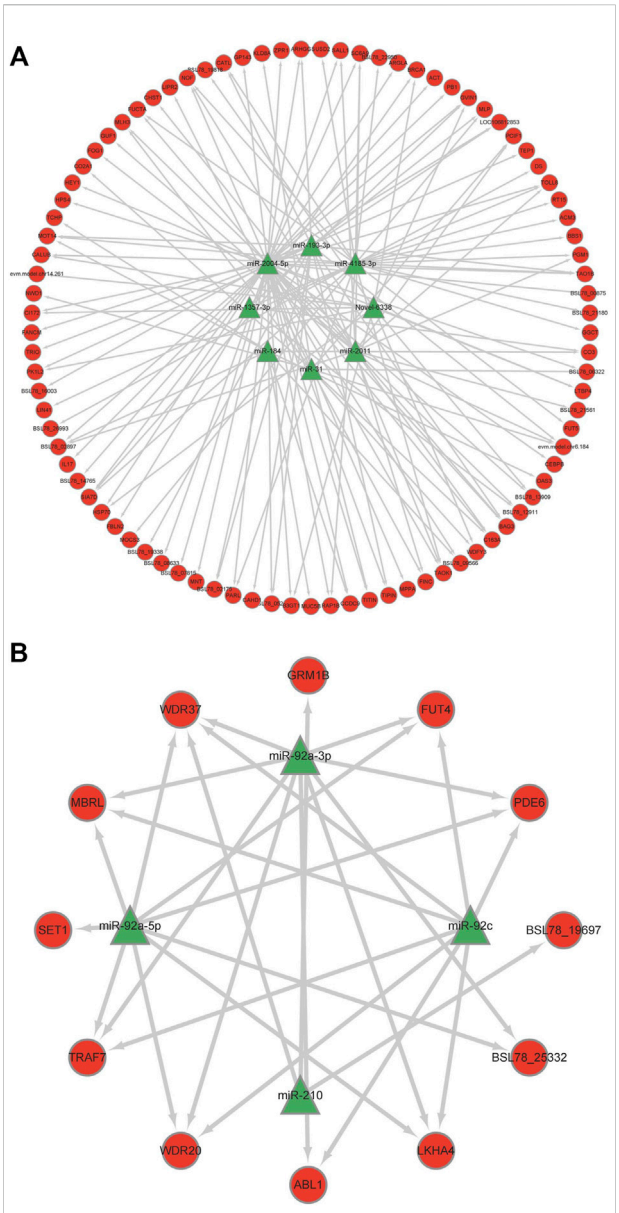

FIGURE 4
Regulation networks of miRNA-mRNA of key genes of correlation analysis. **(A)** Down-up mode; **(B)** Up-down mode.

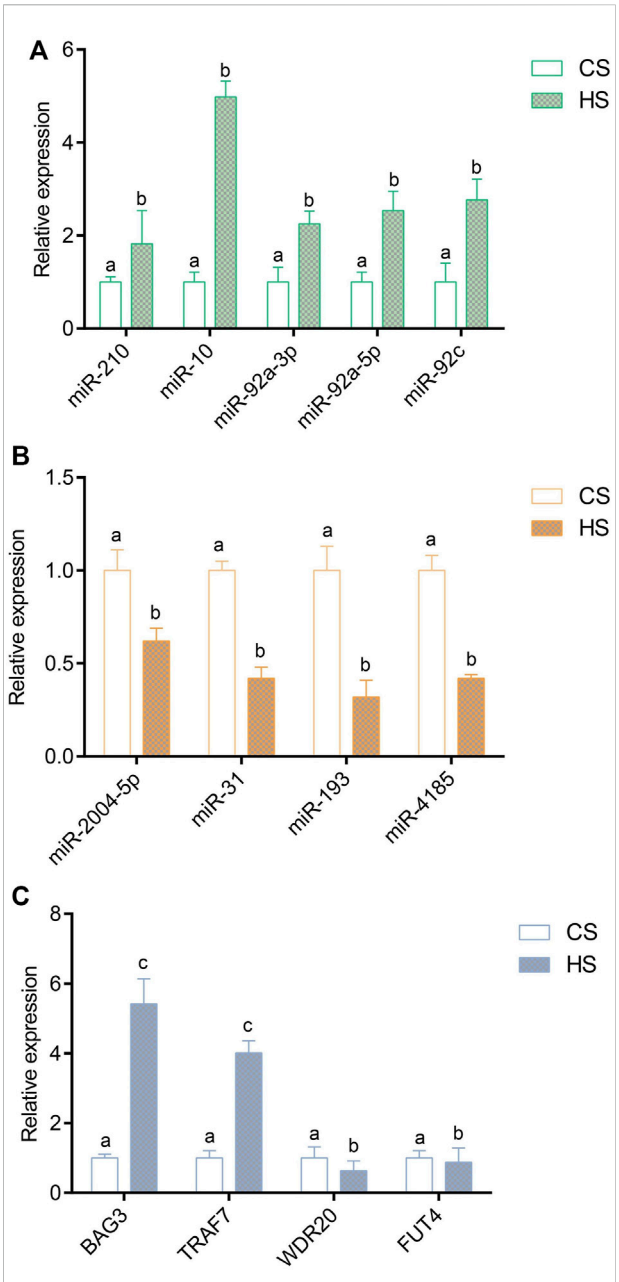

FIGURE 5
Validation of differentially expressed miRNAs and target genes *via* RT-qPCR method; **(A)** Validation of upregulated differentially expressed miRNAs; **(B)** Validation of downregulated differentially expressed target genes; **(C)** Validation of negative DEGs. Values indicate the mean ± SD (n = 3).

miR-2004 was increased with the increase of *A. japonicus* complement *AJC3* in the coelomic cells of *A. japonicus* in different periods after LPS stimulation (Zhong et al., 2015). The results of Zhou et al. (2018) showed that miR-2004 was regarded as a significantly expressed gene in the coelomic cells of *A. japonicus* under the infection of *V. splendidus*. MiR-31 has been proved to regulate the occurrence of inflammatory bowel disease by directly targeting the hypoxia-inducible factor (Olaru et al., 2015). Suzarez et al. (2010) confirmed that miR-31 could regulate the inflammatory response by negatively regulating the binding of e-selectin and neutrophils to endothelial cells. Kang et al. (2019) found that miR-31 was significantly upregulated in the liver after infecting grouper with *V. alginolyticus*, and the target genes were mainly concentrated in immune-related pathways. Therefore, we inferred that miRNA plays a complex regulatory role in various stress responses.

MiR-210 was known as a major hypoxia-inducible microRNA, which is evolutionarily conserved and

ubiquitously expressed in the hypoxic cell and tissue types, serving versatile functions (Chang and Loscalzo, 2010). It was found that miR-210 can negatively regulate the production of LPS-induced pro-inflammatory cytokines through NF-κB1 in mouse macrophages (Qi et al., 2012). Yu et al. (2021) found that miR-210 can activate PI3K/AKT pathway by regulating PI3K and p-AKT protein, promoting the proliferation, and inhibit the apoptosis of dental pulp stem cells. Recently, Li et al. (2016b) found that miR-210 regulated the host defense of *A. japonicus* through TLRs (Toll-like receptors) pathway. In the present study, the significantly upregulated expression indicates that miR-210 also play role in sea cucumber's body wall in response to heat stress. It was speculated that *A. japonicus* may reduce the expression of target genes by upregulating the expression level of miR-210 to cope with the harm of heat stress.

MiR-10 family members were highly conservative and closely associated with metabolizing response. MiR-10 can directly regulate the expression levels of FLT1 (vascular endothelial growth factor receptor 1) and sFLT1 (soluble vascular endothelial growth factor receptor 1), both of which are closely related to the growth of vascular endothelial cells (Livak and Schmittgen, 2013). Knock-out of miR-10 could lead to premature termination of the growth of blood vessels in the embryonic internodes of zebrafish larvae, while over-expression of miR-10 could accelerate the angiogenesis in zebrafish and the growth of human umbilical vein endothelial cells (Wienholds, 2005). Another study, found that miR-10 can regulate the growth of blood vessel endothelial cells by promoting new signal transmission (Naguibneva et al., 2006). Overexpression of miR-10 could promote virus-induced apoptosis, and researchers discovered that the expression of apoptosis protein caspase-3 increased in tandem with miR-10 expression (Zhang, 2014). Moreover, miR-10 was significantly upregulated in the process of infection by infecting porcine alveolar macrophages with PRRSV (Porcine Reproductive and Respiratory Syndrome Virus), and the transfection experiment demonstrated that the upregulated expression of miR-10 could significantly inhibit the replication of *HP-PRRSV* and *N-PRRSV* in porcine alveolar macrophages (Zhao et al., 2017). In the present study, we found that miR-10 was significantly upregulated 5-fold after heat stress. It indicates that miR-10 regulates the metabolism of *A. japonicus* during heat stress, but it is molecular function needs further to be studied.

In the process of *A. japonicus* in response to heat stress, ubiquitin-mediated proteolysis and notch signaling pathway were significantly enriched, indicating that they played important role in the process. Ubiquitin-mediated proteolysis is an important cellular immune pathway, which can control the basic life activities of cells by degrading key regulatory proteins and regulating the cellular stress response and immune response to pathogenic microorganisms (Chen et al., 2012). For example, when shrimp was infected by *V. cholerae*, ubiquitin proteins can mediate cellular immunity to cope with the infection (Li, 2020). The notch signaling pathway can regulate cell differentiation, proliferation and apoptosis, which is of great significance to cell growth and development. Abnormal expression of notch signaling can induce many kinds of cancers, such as breast cancer (Wang et al., 2017), lung cancer (Tian et al., 2017), and gastric cancer (Wang et al., 2018). We inferred that ubiquitin-mediated proteolysis and Notch signaling pathway could resist the effects of high temperature by regulating the expression of downstream immune genes in the process of heat stress.

Through the correlation analysis between the differentially expressed miRNAs and transcriptome data, it found that 12 DEMs can target 101 inversely correlated DEGs. TRAF7 has been partially studied in aquatic animals, and BAG3, WDR20 and FUT4 are mostly focused on wound tissue recovery and cancer treatment in medicine. BAG3 is a member of the BAG gene family, which plays an important role in regulating cell apoptosis, autophagy, movement and development, and mediating the adaptability of cells response to heat stress (Rosati et al., 2011). The results of GO enrichment analysis showed that BAG3 could inhibit cell apoptosis and promote tumor cell proliferation by binding to HSP70 (Manzerra and Brown, 1990). TRAF7 belongs to the TRAFs family, which involves a variety of biological functions including innate immunity, embryo development, stress response and inflammatory response (Reuss et al., 2013). In mammals, TRAF7 can regulate the signal activities by enhancing MEKK (mitogen-activated protein kinase), and then participate in the immune response of the body (Xu et al., 2004). *Cynoglossus semilaevis* has also been found to downregulate TRAF7 expression in all tissues infected with *V. harveyi*, particularly the liver (Wei et al., 2018). Studies have shown that WDR20 has a positive or negative correlation with the occurrence of lymphoma, prostate cancer and other diseases (Ohashi et al., 2015). At the same time, experiments have also proved that miR-3188 can target and inhibit the expression of WDR20 (Zhang et al., 2018). Screening of key genes of *A. japonicus* in response to heat stress provides basic data for elucidating its regulation mechanism. Further research will focus on the verification of the regulatory relationship between DEMs and DEGs.

Conclusion

In this study, we identified the expression profiles of miRNAs under heat stress in *A. japonicus* by using small RNA-seq. We highlighted 13 DEMs compared with the control group, which were involved of immunity response and cellular activity. In addition, we performed a correlation analysis of DEMs and differentially expressed genes in sea cucumber and 101 key negative regulator genes of DEMs were obtained, which may play important roles in regulating the process of *A. japonicus* under heat stress. Our study

provided an increasing understanding of miRNAs' roles in *A. japonicus* during heat stress. Through the discovery of their related targets, we have a deeper understanding of miRNAs and functional genes. In conclusion, our results provided new insights into the miRNA regulation and molecular adaptation mechanisms of *A. japonicus* under heat stress.

Data availability statement

The datasets presented in this study can be found in online repositories. The names of the repository/repositories and accession number(s) can be found below: Sequence read archive under the accession number SRR18918495 ~ SRR18918500.

Author contributions

MC, BL, ML, and XR contributed to conception and design of the research. MC and BL performed experiment. MC, BL, YW, XR, and JW performed data processing and statistical analysis. MC, ZZ, CW, and YY drafted the manuscript. XR and ML contributed to revision of manuscript for important intellectual content. ML and XR gave laboratory and project support. And all authors read and approved the final manuscript.

Funding

This work was funded by the National Key R&D Program of China (2018YFD0900305), Agriculture Seed Improvement Project of Shandong Province (2020LZGC015) and Key R&D Program of Qingdao (22-3-3-hygg-1-hy) and Central Public-Interest Scientific Institution Basal Research Fund, CAFS (2020TD40 and 2021GH05).

Conflict of interest

The authors declare that the research was conducted in the absence of any commercial or financial relationships that could be construed as a potential conflict of interest.

Publisher's note

Supplementary material

The Supplementary Material for this article can be found online at: https://www.frontiersin.org/articles/10.3389/fphys.2022.929094/full#supplementary-material

SUPPLEMENTARY FIGURE S1
PCA analysis of six body wall libraries in *Apostichopus japonicas*.

SUPPLEMENTARY FIGURE S2
Length distribution of valid reads in six libraries in the body wall of *Apostichopus japonicas*.

SUPPLEMENTARY FIGURE S3
Families and members distribution of known miRNAs.

References

Bartel, D. P. (2004). MicroRNAs. *Cell.* 116, 281–297. doi:10.1016/S0092-8674(04)00045-5

Berthelot, C., Brunet, F., Chalopin, D., Juanchich, A., Bernard, M., Noël, B., et al. (2014). The rainbow trout genome provides novel insights into evolution after whole-genome duplication in vertebrates. *Nat. Commun.* 5, 3657. doi:10.1038/ncomms4657

Boonchuen, P., Maralit, B. A., Jaree, P., Tassanakajon, A., and Somboonwiwat, K. (2020). MicroRNA and mRNA interactions coordinate the immune response in non-lethal heat stressed *Litopenaeus vannamei* against AHPND-causing *vibrio parahaemolyticus*. *Sci. Rep.* 10, 787. doi:10.1038/s41598-019-57409-4

Chan, S. Y., and Loscalzo, J. (2010). MicroRNA-210: A unique and pleiotropic hypoxamir. *Cell cycle.* 9, 1072–1083. doi:10.4161/cc.9.6.11006

Chen, K., Cheng, H.-H., and Zhou, R.-J. (2012). Molecular mechanisms and functions of autophagy and the ubiq-uitin-proteasome pathway. *Hered. (Beijing)* 34, 5–18. doi:10.3724/SP.J.1005.2012.00005

Friedländer, M. R., Mackowiak, S. D., Li, N., Chen, W., and Rajewsky, N. (2012). Mirdeep2 accurately identifies known and hundreds of novel microRNA genes in seven animal clades. *Nucleic Acids Res.* 40, 37–52. doi:10.1093/nar/gkr688

Jones-Rhoades, M. W., and Bartel, D. P. (2004). Computational identification of plant microRNAs and their targets, including a stress-induced miRNA. *Mol. Cell.* 14, 787–799. doi:10.1016/j.molcel.2004.05.027

Kang, H., Liang, Q.-J., Hu, R., Li, Z.-H., Liu, Y., and Wang, W.-N. (2019). Integrative mRNA-miRNA interaction analysis associated with the immune response of *Epinephelus coioddes* to *Vibrio alginolyticus* infection. *Fish Shellfish Immunol.* 90, 404–412. doi:10.1016/j.fsi.2019.05.006

Li, C., Feng, W., Qiu, L., Xia, C., Su, X., Jin, C., et al. (2012). Characterization of skin ulceration syndrome associated microRNAs in sea cucumber *Apostichopus japonicus* by deep sequencing. *Fish shellfish Immunol.* 33, 436–441. doi:10.1016/j.fsi.2012.04.013

Li, C., Zhao, M., Zhang, C., Zhang, W., Zhao, X., Duan, X., et al. (2016b). miR210 modulates respiratory burst in *Apostichopus japonicus* coelomocytes via targeting Toll-like receptor. *Dev. Comp. Immunol.* 65, 377–381. doi:10.1016/j.dci.2016.08.008

Li, G., Ren, L., Sun, G., Yang, J., and Wei, M. (2016a). Effects of hypoxic stress on oxidative stress indices in *Apostichopus japonicus*. *Prog. Fish. Sci.* 37, 133–139. doi:10.11758/yykxjz.20150708001

Li, X. (2021). Genomic DNA methylation level and transcriptome differences of sea cucumber under temperature and pathogen stress with their conjoint analysis. Shanghai: Shanghai Ocean University. [master's thesis].

Li, X. (2020). "Study on pathogenicity of non-01 Vibrio cholerae to Macrobrachium nipponensis, host immune response and probiotic effect of antagonistic bacteria. Yangzhou: Yangzhou University. [doctor's thesis].

Li, Y., Wang, R., Li, Y., Li, Y., Mou, C., Sun, H., et al. (2018). Genome-wide profiling of DNA methylation in *Apostichopus japonicus* based on methylRAD-Seq. *Periodical Ocean Univ. China Natural Sci.* 48, 41–50. doi:10.16441/j.cnki.hdxb.20170242

Livak, K. J., and Schmittgen, T. D. (2013). Analysis of relative gene expression data using real-time quantitative PCR and the 2(-Delta Delta C(T)) Method. *Methods.* 25, 402–408. doi:10.1006/meth.2001.1262

Ma, F., Liu, Z., Huang, J., Li, Y., Kang, Y., Liu, X., et al. (2019). High-throughput sequencing reveals microRNAs in response to heat stress in the head kidney of rainbow trout (*Oncorhynchus mykiss*). *Funct. Integr. Genomics.* 19, 775–786. doi:10.1007/s10142-019-00682-3

Manzerra, P., and Brown, I. R. (1990). Time course of induction of a heat shock gene (hsp70) in the rabbit cerebellum after LSD *in vivo*: Involvement of drug-induced hyperthermia. *Neurochem. Res.* 15, 53–59. doi:10.1007/bf00969184

Ministry of Agriculture and Rural Affairs (2021). *China fishery statistical yearbook*. Beijing: China Agriculture Press.

Naguibneva, I., Ameyar-Zazoua, M., Polesskaya, A., Ait-Si-Ali, S., Groisman, R., Souidi, M., et al. (2006). The microRNA miR-181 targets the homeobox protein hox-a11 during mammalian myoblast differentiation. *Nat. Cell Biol.* 8, 278–284. doi:10.1038/ncb1373

Ohashi, M., Holthaus, A. M., Calderwood, M. A., Lai, C.-Y., Krastins, B., Sarracino, D., et al. (2015). The EBNA3 family of epstein-barr virus nuclear proteins associates with the USP46/USP12 deubiquitination complexes to regulate lymphoblastoid cell line growth. *PLoS Pathog.* 11, e1004822. doi:10.1371/journal.ppat.1004822

Olaru, A. V., Selaru, F. M., Mori, Y., Vazquez, C., David, S., Paun, B., et al. (2011). Dynamic changes in the expression of microRNA-31 during inflammatory bowel disease-associated neoplastic transformation. *Inflamm. Bowel Dis.* 17, 221–231. doi:10.1002/ibd.21359

Ou, J., Li, Y., Ding, Z., Xiu, Y., Wu, T., Du, J., et al. (2013). Transcriptome-wide identification and characterization of the *Procambarus clarkii* microRNAs potentially related to immunity against *spiroplasma eriocheiris* infection. *Fish Shellfish Immunol.* 35, 607–617. doi:10.1016/j.fsi.2013.05.013

Pedersen, I. M., Cheng, G., Wieland, S., Volinia, S., Croce, C. M., Chisari, F. V., et al. (2007). Interferon modulation of cellular microRNAs as an antiviral mechanism. *Nature.* 449, 919–922. doi:10.1038/nature06205

Qi, J., Qiao, Y., Wang, P., Li, S., Zhao, W., and Gao, C. (2012). microRNA-210 negatively regulates LPS-induced production of proinflammatory cytokines by targeting NF-κB1 in murine macrophages. *FEBS Lett.* 586, 1201–1207. doi:10.1016/j.febslet.2012.03.011

Reuss, D. E., Piro, R. M., Jones, D. T. W., Simon, M., Ketter, R., Kool, M., et al. (2013). Secretory meningiomas are defined by combined klf4 k409q and traf7 mutations. *Acta Neuropathol.* 125 (3), 351–358. doi:10.1007/s00401-013-1093-x

Rosati, A., Graziano, V., De Laurenzi, V., Pascale, M., and Turco, M. C. (2011). BAG3: A multifaceted protein that regulates major cell pathways. *Cell Death Dis.* 2, e141. doi:10.1038/cddis.2011.24

Shannon, P., Markiel, A., Ozier, O., Baliga, N., Wang, J., Ramage, D., et al. (2003). Cytoscape: A Software Environment for Integrated Models of Biomolecular Interaction Networks. *Genome. Res.* 11, 2498–2504. doi:10.1101/gr.1239303

Shao, Y., Wang, Z., Lv, Z., Li, C., Zhang, W., Li, Y., et al. (2016). NF-κB/Rel, Not STAT5, Regulates Nitric Oxide Synthase Transcription in *Apostichopus japonicus*. *Dev. Comp. Immunol.* 61, 42–47. doi:10.1016/j.dci.2016.03.019

Shi, T., Meng, P., Qiang, F., Shi, H., Zhang, H., Ren, Y., et al. (20142014). Construction and preliminary identification of lentiviruses overexpressing and inhibiting *Bos taurus* miR-193a. *Biotechnology.* 24 52–57.

Song, H., Qi, L., Zhang, T., and Wang, H.-y. (2017). Understanding microRNA regulation involved in the metamorphosis of the veined rapa whelk (*Rapana venosa*). *G3 Genes| Genomes |Genetics.* 7, 3999–4008. doi:10.1534/g3.117.300210

Suárez, Y., Wang, C., Manes, T. D., and Pober, J. S. (2010). Cutting edge: TNF-induced microRNAs regulate TNF-induced expression of e-selectin and intercellular adhesion molecule-1 on human endothelial cells: Feedback control of inflammation. *J. I.* 184, 21–25. doi:10.4049/jimmunol.0902369

Tian, W., Wang, G., Liu, Y., Huang, Z., Zhang, C., Ning, K., et al. (2017). Retracted: The miR-599 promotes non-small cell lung cancer cell invasion via SATB2. *Biochem. Biophysical Res. Commun.* 485, 35–40. doi:10.1016/j.bbrc.2017.02.005

Wang, T., Yang, H., Zhao, H., Chen, M., and Wang, B. (2011). Transcriptional changes in epigenetic modifiers associated with gene silencing in the intestine of the sea cucumber, *Apostichopus japonicus* (Selenka), during aestivation. *Chin. J. Ocean. Limnol.* 29, 1267–1274. doi:10.1007/s00343-011-0143-2

Wang, X., Jin, Y., Zhang, H., Huang, X., Zhang, Y., and Zhu, J. (2018). MicroRNA-599 inhibits metastasis and epithelial-mesenchymal transition via targeting EIF5A2 in gastric cancer. *Biomed. Pharmacother.* 97, 473–480. doi:10.1016/j.biopha.2017.10.069

Wang, Y., Sui, Y., Zhu, Q., and Sui, X. (2017). Hsa-miR-599 suppresses the migration and invasion by targeting brd4 in breast cancer. *Oncol. Lett.* 14, 3455–3462. doi:10.3892/ol.2017.6651

Wei, M., Xu, W.-t., Li, K.-m., Chen, Y.-d., Wang, L., Meng, L., et al. (2018). Cloning, characterization and functional analysis of dctn5 in immune response of Chinese tongue sole (*Cynoglossus semilaevis*). *Fish Shellfish Immunol.* 77, 392–401. doi:10.1016/j.fsi.2018.04.007

Wen, Z., Zou, S., Chen, M., Zhou, H., Sun, G., Feng, Y., et al. (2021). DNA methylation level of genomic DNA of *Apostichopus japonicus* at different temperatures. *Prog. Fish. Sci.* 42, 46–54. doi:10.19663/j.issn2095-9869.20201204002

Wienholds, E., Kloosterman, W. P., Miska, E., Alvarez-Saavedra, E., Berezikov, E., de Bruijn, E., et al. (2005). MicroRNA expression in zebrafish embryonic development. *Science.* 309, 310–311. doi:10.1126/science.1114519

Xu, L.-G., Li, L.-Y., and Shu, H.-B. (2004). TRAF7 potentiates MEKK3-induced AP1 and CHOP activation and induces apoptosis. *J. Biol. Chem.* 279, 17278–17282. doi:10.1074/jbc.C400063200

Xu, P., Guo, H., Wang, H., Xie, Y., Lee, S. C., Liu, M., et al. (2019). Identification and profiling of microRNAs responsive to cadmium toxicity in hepatopancreas of the freshwater crab *Sinopotamon henanense*. *Hereditas.* 156, 34. doi:10.1186/s41065-019-0110-z

Yu, L., Yu, S., Xiong, Y., Dui, Y., Wang, D., and Huang, W. (2021). Effects of miR-210 on proliferation and Apoptosis of dental pulp stem cells based on PI3K/AKT Pathway. *Prog. Mod. Biomed.* 21, 1212–1216. doi:10.13241/j.cnki.pmb.2021.07.003

Zhang, L., Jia, D., Wei, M., Cao, Y., Jie, M., and Neurosurgery, D. (2018). The miR-3188 promotes proliferation and invasion of glioma cell by targeting WDR20. *J. Shanxi Med. Univ.* 49, 802–808. doi:10.13753/j.issn.1007-6611.2018.07.011

Zhang, Y., Yu, S., Liao, M., and Dong, Y. (2022). Evaluation and prediction of extreme high temperature on sea cucumber (*Apostichopus japonicus*) pond aquaculture in China. *J. Fish. Sci. China* 29, 408. doi:10.12264/JFSC2021-0376

Zhao, G., Hou, J., Xu, G., Xiang, A., Kang, Y., Yan, Y., et al. (2017). Cellular microRNA miR-10a-5p inhibits replication of porcine reproductive and respiratory syndrome virus by targeting the host factor signal recognition particle 14. *J. General Virology.* 98, 624–632. doi:10.1099/jgv.0.000708

Zhao, Y., Chen, M., Storey, K., Sun, L., and Yang, H. (2015). DNA Methylation Levels Analysis in Four Tissues of Sea Cucumber *Apostichopus Japonicus* Based on Fluorescence-Labeled Methylation-Sensitive Amplified Polymorphism (F-MSAP) During Aestivation. *Comp. Biochem. Phys. B.* 181, 26–32. doi:10.1016/j.cbpb.2014.11.001

Zhong, L., Zhang, F., Zhai, Y., Cao, Y., Zhang, S., and Chang, Y. (2015). Identification and comparative analysis of complement C3-associated microRNAs in immune response of *Apostichopus japonicus* by high-throughput sequencing. *Sci. Rep.* 5, 17763. doi:10.1038/srep17763

Zhou, Q. (2014). *The regulation of Bovine herpesvirus 5 encoded miR-10 on its target gene Us3*. Wuhan: Huazhong Agriculture University. [doctor's thesis].

Zhou, X., Chang, Y., Zhan, Y., Wang, X., and Lin, K. (2018). Integrative mRNA-miRNA interaction analysis associate with immune response of sea cucumber *Apostichopus japonicus* based on transcriptome database. *Fish Shellfish Immunol.* 72, 69–76. doi:10.1016/j.fsi.2017.10.031

frontiers | Frontiers in Marine Science

TYPE Original Research
PUBLISHED 22 August 2022
DOI 10.3389/fmars.2022.932255

OPEN ACCESS

EDITED BY
Qingchao Wang,
Huazhong Agricultural University, China

REVIEWED BY
Dao-Feng Zhang,
Hohai University, China
Qian Yang,
Faculty of Bioscience Engineering, Ghent University, Belgium
Yiqin Deng,
South China Sea Fisheries Research Institute (CAFS), China

*CORRESPONDENCE
Meijie Liao
liaomj@ysfri.ac.cn
Yingeng Wang
wangyg@ ysfri.ac.cn

†These authors have contributed equally to this work

SPECIALTY SECTION
This article was submitted to Aquatic Physiology, a section of the journal Frontiers in Marine Science

RECEIVED 29 April 2022
ACCEPTED 28 July 2022
PUBLISHED 22 August 2022

CITATION
Kang H, Yu Y, Liao M, Wang Y, Yang G, Zhang Z, Li B, Rong X and Wang C (2022) Physiology, metabolism, antibiotic resistance, and genetic diversity of Harveyi clade bacteria isolated from coastal mariculture system in China in the last two decades.
Front. Mar. Sci. 9:932255.
doi: 10.3389/fmars.2022.932255

Physiology, metabolism, antibiotic resistance, and genetic diversity of Harveyi clade bacteria isolated from coastal mariculture system in China in the last two decades

Hao Kang[1,2†], Yongxiang Yu[2,3†], Meijie Liao[2,3*], Yingeng Wang[2,3*], Guanpin Yang[1], Zheng Zhang[2,3], Bin Li[2,3], Xiaojun Rong[2,3] and Chunyuan Wang[2,3]

[1]College of Marine Life Sciences, Ocean University of China (OUC), Qingdao, China, [2]Key Laboratory of Maricultural Organism Disease Control, Yellow Sea Fisheries Research Institute, Chinese Academy of Fishery Sciences, Qingdao, China, [3]Laboratory for Marine Fisheries Science and Food Production Processes, Qingdao National Laboratory for Marine Science and Technology, Qingdao, China

Vibrio bacteria, particularly members of the Harveyi clade, are the most important pathogens of aquatic organisms that cause significant economic losses in the world. It is difficult to provide specific data on taxa of the Harveyi clade for biological research and prevention strategies. Therefore, we conducted an extensive phenotypic and antibiotic resistance study, as well as phylogenetic and molecular typing of 192 isolates of the Harveyi clade collection from 2000 to 2020 with a typical interannual difference from a coastal area in China. The isolates had a significant interspecific genetic and antibiotic resistance diversity. Based on the multilocus sequence analysis (MLSA) of housekeeping genes (*gyrB*, *pyrH*, *recA*, and *atpA*), 192 Harveyi clade isolates were rapidly and accurately classified into 10 species. The population of these isolates was composed of 95 sequence types (STs), of which 92 STs were newly identified, indicating a high degree of genetic diversity. ST327 ranked first, accounting for 11.5% of the total number of isolates (22 out of 192), followed by ST215 with 6.25%, while 63 STs included single isolates. At the metabolic level, the physiological and biochemical experiments revealed that all the Harveyi clade isolates were positive for oxidase and negative for melibiose. The isolates showed a varied tolerance to 11 antibiotics. No isolates were resistant to neomycin. The percentages of sulfadimidine-resistant strains (61 out of 192), sulfadiazine (44 out of 192), sulfamonomethoxine (44 out of 192), sulfamethoxazole (33 out of 192), thiamphenicol (34 out of 192), ciprofloxacin (52 out of 192), and enrofloxacin (31 out of 192) were 31.77%, 22.92%, 22.92%, 17.19%, 17.71%, 27.08%, and 16.15%, respectively. A proportion of 61.8% of the isolates presented a multiple antibiotic resistance index (MARI) lower than 0.1, indicating that the

risk of antibiotic resistance transmission of most of the Harveyi clade is low in mariculture systems in China. These results provide substantial data to support further studies on the identification and genetic and metabolic diversity of Harveyi clade isolates in mariculture systems in China.

KEYWORDS

vibrio, harveyi clade, phenotype, multi-locus sequence analysis (MLSA), multi-locus sequence typing (MLST), antibiotic resistance

Introduction

Vibrio spp. are curved rods of Gram-negative bacteria composed of halophile species with significant biodiversity and present naturally in marine, estuarine, and freshwater systems worldwide (Thompson et al., 2004; Baker-Austin et al., 2017; Baker-Austin et al., 2018; Hackbusch et al., 2020). A recent evolutionary event within the genus *Vibrio* occurred 39 million years ago (Sawabe et al., 2007). The genus *Vibrio* has over 100 species that have been classified into 14 clades (Ruwandeepika et al., 2012; Romalde et al., 2014). The colloquially "Harveyi clade" is considered as the most severely pathogenic *Vibrio* cluster of aquatic organisms, capable of causing more than 50 different types of aquatic animal diseases and potentially disrupting the aquaculture system due to its high mortality (Del Gigia-Aguirre et al., 2017; Wang et al., 2021). Multiple Harveyi clade species have been implicated in the aquatic diseases from different countries, causing mortalities up to 100% of some common economic aquatic animals such as *Litopenaeus vannamei* and tilapia, which are widely farmed around the world (Tran et al., 2013; Prithvisagar et al., 2021). Harveyi clade species were thought to be the major pathogens threatening the health development of the aquaculture industry globally.

The Harveyi clade consists of *V. harveyi* and 11 related species, i.e., *V. alginolyticus*, *V. parahaemolyticus*, *V. campbellii*, *V. rotiferianus*, *V. natriegens*, *V. azureus*, *V. mytili*, *V. owensii*, *V. jasicida*, *V. diabolicus*, and *V. sagamiensis* (Lin et al., 2010; Cano-Gomez et al., 2011; Ruwandeepika et al., 2012; Goudenège et al., 2014). These species share high phenotypic and genotypic homology, with 16S rDNA gene sequence similarities greater than 97% and DNA–DNA re-association values close to 70%, making it challenging to differentiate them (Sawabe et al., 2007; Cano-Gomez et al., 2009). Furthermore, because the maritime environment is complex and changing through time and space, marine microorganisms that live in it have adapted to this environment, and hence present a diverse range of species, metabolic types, functional gene composition, and ecological functions (Fraser et al., 2007). Traditional biochemical tests and single-gene sequencing led often to the misidentification of different species of the Harveyi clade (Gomez-Gil et al., 2004; Cano-Gomez et al., 2009).

The development in bacterial identification technology has been promoted by molecular identification techniques such as multilocus sequence analysis (MLSA), core genome tree, average nucleotide identity (ANI), DNA–DNA hybridization (DDH), and genomic characteristic dissimilarity (Richter and Rosselló-Móra (2009); Thompson et al., 2009; Fu et al., 2015). Meanwhile, bacterial typing systems are used to distinguish genera, species, and strains according to their phenotypic and genetic characteristics, e.g., restriction fragment length polymorphism (RFLP), amplified fragment length polymorphism (AFLP), pulsed-field gel electrophoresis (PFGE), multilocus sequence typing (MLST), core genome MLST (cgMLST), and enterobacterial repetitive intergenic consensus PCR (ERIC-PCR) (Botella et al., 2002; Yang et al., 2017; Alikhan et al., 2018; Yan et al., 2021). MLSA is rapid and robust in classifying all prokaryotes using a universal set of genes, and successful in establishing species-level taxonomy within the Harveyi clade based on different levels of genes (Gevers et al., 2005; Cano-Gomez et al., 2009). Pascual et al. (2010) reported that the concatenated sequences of *rpoD*, *rctB*, and *toxR* can be used to identify species of *Vibrio* strains appropriately. Coincidentally, the gene combination *topA-mreB* has also provided a practical yet accurate approach for routine identification of *V. harveyi*-related species (Cano-Gomez et al., 2011). Furthermore, MLST outperformed the other typing techniques in studies of evolutionary, phylogenetic, and population genetics, as it provided unambiguous data using a large international database (https://pubmlst.org/) (Maiden et al., 1998; Aanensen and Spratt, 2005; Harun et al., 2021). Typing can also be performed by directly identifying the nucleotide sequence and variation of multiple housekeeping genes of strains, which has been applied to numerous prokaryotes as well eukaryotic organisms, including the Harveyi clade species *V. parahaemolyticus* and the general database of *Vibrio* spp. (Han et al., 2015; Jelocnik et al., 2019).

Antibiotic resistance of Harveyi clade isolates is an important indicator of metabolic and phenotypic diversity. As the most important pathogen clade in aquatic organisms,

Harveyi clade strains caused more than 50 kinds of aquatic animal diseases and were considered to be a major economic threat to the aquaculture industry (Lin et al., 2010; Goudenège et al., 2014; Wang et al., 2021). Among them, *Vibrio harveyi* is one of the most serious *Vibrio* pathogenic, which can infect the most diverse range of aquatic animals in the world (Santhyia et al., 2015). Therefore, analyzing the antimicrobial resistance of pathogens in a particular area is crucial to the development of effective preventive measures.

China is the world's largest aquaculture producer. The total content of aquatic products exceeded 65 million tons in 2020, which guaranteed the national demand for high-quality protein (China Fisheries Yearbook, 2021). However, pathogens have become a restrictive factor for the development of aquaculture in China, resulting in annual losses of over 20 billion RMB, with *Vibrio* spp. proved as the most important pathogen of marine organisms (China Fisheries Yearbook, 2021). Moreover, the Chinese mariculture sector is characterized by rich and diversified breeding. In different aquaculture systems, a single bacterial species exhibits diverse metabolic phenotypes and ecological functions. During the past two decades, various species of the Harveyi clade have been isolated from infected animal in mariculture in China with dominance higher than 60% in our laboratory. In the present study, the genetic populations and evolutionary relationship of Harveyi clade strains isolated from coastal areas of a mariculture system in China were investigated based on different gene classes and levels. Following that, the prevalence, antibiotic resistance, and genetic diversity of all isolates were analyzed using phenotypic and molecular typing methods. The results of this study provide a theoretical foundation for understanding the differences in multivariate epigenetic mechanisms among species of the Harveyi clade from China with typical interannual variations, as well as basic data for prevention and treatment of aquatic animal diseases.

Materials and methods

Strains and culture conditions

We chose 192 isolates identified as Harveyi clade with typical temporal differences, isolated from animal parts of marine and mariculture environments infected with bacteria with prevalence and dominance of more than 60% in coastal areas of China from 2000 to 2020. Furthermore, 12 type strains served as process control, namely, *V. harveyi* ATCC 14348, *V. campbellii* ATCC 25920, *V. owensii* DSM 23055, *V. alginolyticus* ATCC 17749, *V. natriegens* ATCC 14048, *V. mytili* LMG 19157, *V. parahaemolyticus* ATCC 17802, *V. jasicida* DSM 21061, *V. rotiferianus* DSM 17186, *V. azureus* NBRC 104587, *V. sagamiensis* NBRC 104859, and *V. diabolicus* HE800.

All the strains were preserved in our laboratory in cryo-vials with 20% (v/v) glycerol at −80°C. Data on the isolates are depicted in Supplementary Table 1. The isolates were cultivated on trypticase soy broth (TSB) plates (TSB supplemented with 1.5% agar) at 28°C for 24 h until use.

DNA extraction

Genomic DNA was extracted from the cultivated isolates following the protocol described by Rahman et al. (2014) with minor modifications. A single colony was collected from a fresh culture and resuspended in 100 µl of nuclease-free water, vortexed for 5 s, and incubated at 99°C for 10 min. After that, the suspension was vortexed again and centrifuged at 12,000 relative centrifugal force (RCF) for 5 min. The supernatant was then transferred to a fresh tube and stored at −20°C. The concentration and purity of the extracted DNA were assessed using NanoDrop 2000. Solutions with a 260/280 ratio of 1.7 to 2.0 were used for PCR assays.

PCR amplification and sequencing

PCR amplification and sequencing of the 16S rDNA or 16S rRNA gene were performed according to Weisburg et al. (1991) using the primers 27F and 1492R. The four housekeeping genes *gyrB*, *pyrH*, *recA*, and *atpA* were amplified and sequenced using the primers and the amplification conditions described by Rahman et al. (2014). The complete list of genes analyzed in this study and all primers used for PCR amplification and sequencing are listed in Table 1. A PCR template of approximately 100 ng of DNA was used for amplification. PCR products were visualized on a 1.5% agarose gel. The qualified rate of the products was determined according to the molecular weight standard. Sequencing and purification of PCR products were performed by Shanghai Sangon Biological Engineering Technology and Services Co., Ltd. (Shanghai, China). The DNA sequences were analyzed using the BLAST tool of GenBank and optimized for highly similar sequences (Mega BLAST) (Kumari et al., 2020).

Phylogenetic analysis and genetic diversity

Sequences of the genes 16S rDNA, *gyrB*, *pyrH*, *recA*, and *atpA* were aligned using ClustalX (Tamura et al., 2013). Phylogenetic analysis based on the genes 16S rDNA (1298 bp), *gyrB*, *pyrH*, *recA*, and *atpA*, as well as various concatenations of four protein-coding loci (*gyrB*, *pyrH*, *recA*, and *atpA*), were conducted using the neighbor-joining (NJ) approach. Bootstrap (BT) support for individual nodes was calculated with the Kimura 2-parameter model using 1000 BT replications. The trees were constructed using MEGA 6.0 software. A fully

TABLE 1 Primers used for amplification and sequencing of Harveyi clade isolates.

Primer name	sequence (5'-3')	Tm (°C)	product size	Reference
VigyrBF	GAAGGTGGTATTCAAGCGTT	55	570	(Rahman et al., 2014)
VigyrBR	CGGTCATGATGATGATGTTGT	55		
VipyrHdgF	CCCTAAACCAGCGTATCAACGTATTC	55	501	(Rahman et al., 2014)
VipyrHdgR	CGGATWGGCATTTTGTGGTCACGWGC	55		
VirecAF	TGCGCTAGGTCAAATTGAAA	55	462	(Rahman et al., 2014)
VirecAdgR	GTTTCWGGGTTACCRAACATYACACC	55		
ViatpA-01-F	CTDAATTCHACNGAAATYAGYG	57	489	(Rahman et al., 2014)
ViatpA-04-R	TTACCARGWYTGGGTTGC	57		
27F	AGAGTTTGATCCTGGCTCAG	56	1298	(Weisburg et al., 1991)
1492R	TACGGCTACCTTGTTACGACTT	56		

resolved and highly harmonious tree topology was obtained, depicting individual strain relationships.

Morphological, physiological, and biochemical analyses

Single colonies of the Harveyi clade isolates were picked up and inoculated on thiosulfate-citrate–bile salts–sucrose (TCBS) agar, TSB, and HB7011-5 Vibrio chromogenic medium (hopebio Biotechnology Co., Ltd, China) plates and incubated at 28°C for 24 h, after which colony morphology was observed. Twenty-three biochemical tests were evaluated by the following tests: gram staining, o-Nitrophenyl β-D-galactopyranoside (ONPG), urease, xylose, sucrose, Simmons citrate agar, lysine decarboxylase, gelatin, amygdalin, melibiose, α-L-rhamnopyranose monohydrate, hydrogen sulfide (H_2S), malonic acid disodium salt, mannitol, D-glucose, methyl red and Voges-Proskauer tests (MR-VP), inositol, ornithine decarboxylase, DL-arabinose, sorbitol, lactose, arginine double hydrolase, tryptone water, and glucose oxidase. All the selected biochemical tests were determined with the Bacterial biochemical identification kit (hopebio Biotechnology Co., Ltd, China), according to the manufacturer's instructions.

Antimicrobial susceptibility testing

The antibiotic susceptibility of the Harveyi clade isolates was tested on TSB following the Kirby–Bauer disc diffusion method (K-B method) and the Clinical and Laboratory Standards Institute [CLSI], (2017) guidelines. Eleven antimicrobial agents were tested, namely, aminoinositols: florfenicol (FFC, 30 μg/disk) and thiamphenicol (THI, 30 μg/disk); tetracycline: neomycin (NEO, 30 μg/disk) and doxycycline (DOX, 30 μg/disk); quinolones: ciprofloxacin (CIP, 5 μg/disk), enrofloxacin (ENR, 10 μg/disk), and flumequine (FLU, 30 μg/disk); and sulfonamides: trimethoprim/sulfamethoxazole (SMZ, 1.25 μg/disk and 25 μg/disk, respectively), sulfamonomethoxine (SMM, 250 μg/disk), sulfadiazine (SDI, 250 μg/disk), and sulfadimidine (SDM, 250 μg/disk). The isolates were inoculated in TSB with 1.5% NaCl solution and adjusted to an optical density (OD) 0.5 McFarland standard after a 24-h incubation period at 28°C. The antibacterial discs were then applied after 100 μl of the bacterial solution was equally spread over the agar plates. The inhibition zones were measured using the SCAN 4000 automatic image analysis colony counter (Interscience, France) after 20 h of incubation at 28°C. The reference strain *Escherichia coli* ATCC 25922 was used for quality control. All the experiments were performed in triplicates. Each strain was classified as resistant, intermediate, or susceptible, according to Clinical and Laboratory Standards Institute [CLSI] (2017). The multiple antibiotic resistance index (MARI) was calculated based on the formula described by Krumperman (1983).

MLST and UPGMA analysis

PCR primers, amplification conditions, and housekeeping gene sequencing methods were carried out following the methods of Rahman et al., (2014). The *Vibrio* spp. Pubmlst database (http://pubmlst.org/Vibrio.spp) was used to obtain the allele number and define the sequence type (ST). If STs or alleles other than the database are identified, submit the new allele to the database administrator to obtain a serial number of the newly identified allele or STs (Jiang et al., 2019). Using goeBURST (http://goeBURST.phyloviz.net) and the MLST classification data, we created a minimal spanning tree based on PHYLOViZ 2.0 (Ribeiro-Gonçalves et al., 2016) and assigned STs to clonal complexes (CC). The nucleotide diversity was determined using the software DNA Sequence Polymorphism DnaSP version 6.12.03 (Rozas et al., 2017). The number of polymorphic sites, GC content, and the ratio of nonsynonymous to synonymous substitutions (d_N/d_S) were calculated by START v 2.0 (Jolley et al., 2001).

Results

Epidemiological investigation of the Harveyi clade isolates

A total number of 192 isolates were identified, of which 101 isolates were isolated from fish (52.7%), 60 in flatfish (31.3%), 22 in grouper (11.6%), 19 in other species (9.8%), 64 in shrimp (*L. vannamei*) (33.3%), 23 in sea cucumber (12%), and 4 in crab (2%) (Figure 1). In addition, 63 of the total strains (33.2%) were from 2010 and earlier, while 129 strains (66.8%) were collected from 2011 to 2020. Based on the BLASTn search of the 16S rDNA gene, *V. harveyi* (79 isolates), *V. alginolyticus* (63 isolates), *V. owensii* (19 isolates), *V. rotiferianus* (11 isolates), *V. natriegens* (9 isolates), *V. azureus* (3 isolates), *V. parahaemolyticus* (2 isolates), *V. campbellii* (2 isolates), *V. jasicida* (2 isolates), and *V. sagamiensis* (2 isolates) were identified.

Taxonomic evolution of the Harveyi clade based on MLSA

As shown in Figure 2, the phylogenetic tree cluster analysis based on the concatenated sequences of the genes *gyrB*, *pyrH*, *recA*, and *atpA* divided the 192 isolates together with 12 reference strains into 10 distinct clades (representing 10 gene species) and three outgroups. The numbers of the 10 gene species were distributed as follows: 77 V. *harveyi*, 41 V. *alginolyticus*, 19 V. *parahaemolyticus*, 17 V. *owensii*, 17 V. *natriegens*, 12 V. *rotiferianus*, 3 V. *campbellii*, 3 V. *diabolicus*, 2 V. *jasicida*, and 1 V. *mytili*. Two subgroups emerged from all the strains of *V. alginolyticus* and *V. diabolicus*. When we compared the phylogenetic tree constructed using only 16S rDNA sequencing, we could not identify the strains of *V. harveyi*, *V. campbellii*, *V. rotiferianus*, *V. parahaemolyticus*, and *V. owensii* within the *Harveyi* clade (99% to 100% sequence identities) (Supplementary Figure 1).

Furthermore, the phylogenetic analysis based on different gene combination levels indicated that it was possible to accurately classify *Vibrio* species within the Harveyi clade based on the phylogenetic tree constructed using the concatenated sequences of the four genes. After analyzing all the concatenated genes, the three-locus phylogeny (*gyrB*, *pyrH*, and *atpA*) was consistent with the four-locus phylogeny and the *Harveyi* clade was identified (Supplementary Figure 2). As for the two-locus concatenated sequences, the genes *gyrB* and *atpA* identified *V. owensii*, *V. parahaemolyticus*, and *V. rotiferianus*, while the genes *gyrB* and *pyrH* identified *V. owensii* (Supplementary Figure 3). A slightly more complicated grouping emerged from all the single-gene trees of the nucleotide sequences (Supplementary Figure 4). Nonetheless, *atpA* was the only gene with the highest discriminatory power. The aforementioned results indicate that the MLSA scheme based on the concatenated sequences of four protein-coding genes can offer a robust phylogenetic reconstruction to resolve unitary relationships of the Harveyi clade isolates. Meanwhile, the three-gene scheme based on *gyrB*, *pyrH*, and *atpA* is suitable for Harveyi clade identification to some extent.

The 16S rDNA gene, *gyrB*, *pyrH*, *atpA*, and *recA* sequences determined in this study have been deposited in the GenBank of

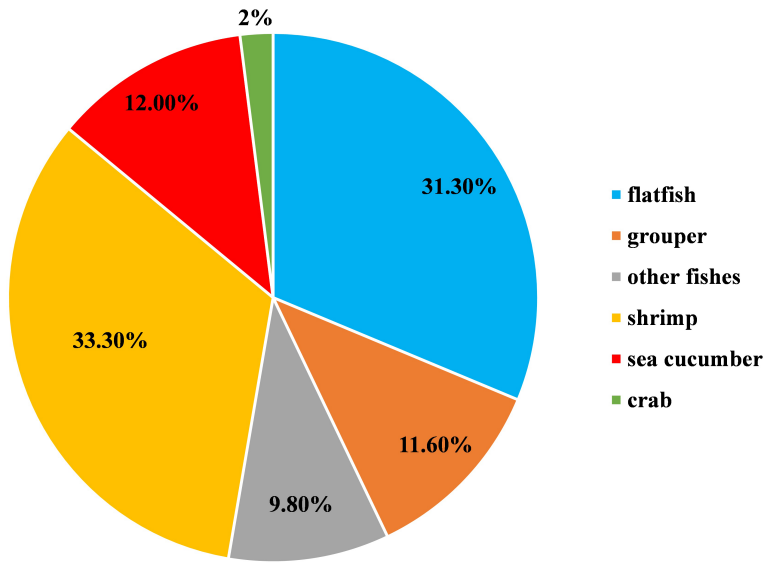

FIGURE 1
Host composition of the 192 Harveyi clade isolates (100%).

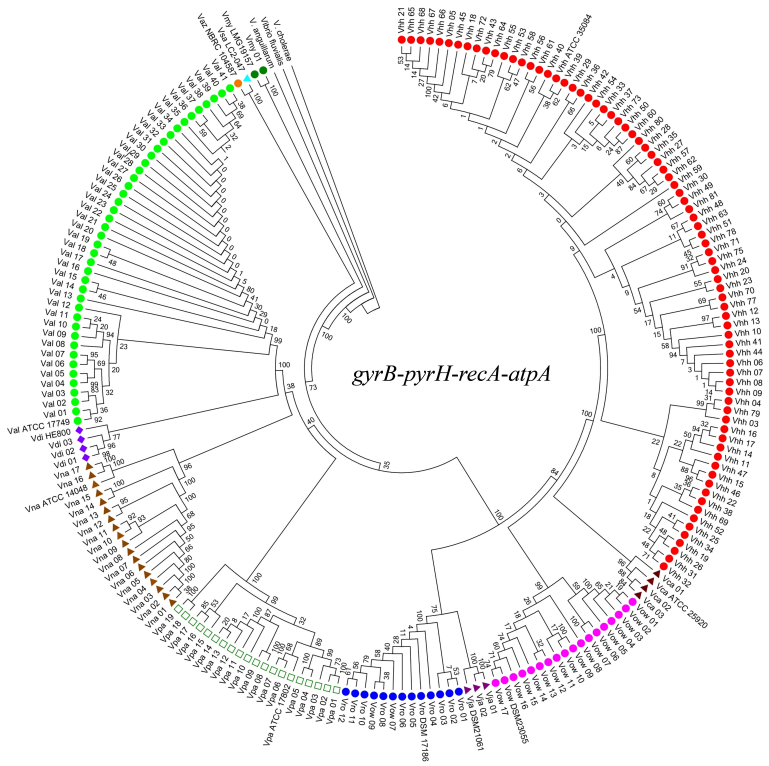

FIGURE 2
Neighbor-joining phylogenetic analysis based on concatenated gene sequences of four protein-coding loci (i.e., *gyrB-pyrH-recA-atpA*). Vhh, *V. harveyi*; Val, *V. alginolyticus*; Vro, *V. rotiferianus*; Vca, *V. campbellii*; Vpa, *V. parahaemolyticus*; Vow, *V. owensii*; Vna, *V. natriegens*; Vdi, *V. diabolicus*; Vsa, *V. sagamiensis*; Vaz, *V. azureus*; Vja, *V. jasicida*; Vmy, *V. mytili*. Bootstrap values based on 1,000 resamplings are shown as percentages at the branch nodes.

NCBI under the accession numbers ON437347-ON437538, ON469581-ON469772, ON778048-ON778239, ON778240-ON778431, and ON4491819-ON492010, respectively.

Phenotypic and physiological characterization of Harveyi clade bacteria

The phenotypic analysis of the Harveyi clade isolates in this study was in accordance with Bergey's manual of determinative bacteriology (Holt et al., 1994). All the Harveyi clade isolates growing on TCBS agar were yellowish or greenish colonies, Gram-negative, oxidase-positive, and glucose-fermenting bacteria. Macroscopic observation showed that the upper surface of the colonies of the Harveyi clade isolates on the solid medium was raised, smooth, and wet (Supplementary Figure 5). These characteristics can be first attributed to the genus *Vibrio*. The biochemical features indicated that the Harveyi clade isolates had a positive oxidase and were unable to ferment melibiose, rhamnose, and amygdalin. In addition, 153 isolates were able to ferment sucrose and showed negative MR-VP and positive inositol reactions, 85 isolates had a positive ONPG reaction, 106 isolates produced a positive urease reaction, 175 isolates showed a positive lysine decarboxylase test, 55 isolates had a positive gelatin test, and 107 isolates showed a positive arginine double hydrolase test and were unable to decompose hydrogen sulfide (Table 2). On the other hand, all the isolates of *V. harveyi*, *V. alginolyticus*, *V. campbellii*, *V. owensii*, and *V. diabolicus* tested positive for lysine decarboxylase. *V. rotiferianus*, *V. campbellii*, and *V. diabolicus* were all citrate and urease positive (Table 2). The results indicated that these biochemical markers may be employed for the early screening of these *Harveyi* clade species.

In addition to MLSA, all members of the *V. campbellii*, *V. jasicida*, and *V. parahaemolyticus* group showed green colonies on TCBS agar, indicating that they were unable to ferment sucrose. Nevertheless, *V. diabolicus* and *V. owellii* were sucrose positive. The other groups showed yellow and green colonies on TCBS, and thus were either sucrose positive or negative. The colonies of *V. harveyi*, *V. campbellii*, *V. sagamiensis*, and *V. aliginolyticus* appeared translucence on TSB, while the colonies of the other strains were transparent. On the modified Vibrio chromogenic medium, *V. parahaemolyticus* and *V. jasicida*

TABLE 2 Results of Harveyi clade isolates based on biochemical tests.

Biochemical kit	Number of positive isolates										
	Total(n=192)	Vhh (n=77)	Vow(n=17)	Vro(n=12)	Val(n=41)	Vca(n=3)	Vpa(n=19)	Vja(n=2)	Vmy(n=1)	Vna(n=17)	Vdi(n=3)
ONPG	85	35	15	1	3	3	10	0	1	15	2
Urease	106	56	6	12	16	3	6	2	0	2	3
Xylose fermentation kit	4	2	0	0	0	0	0	1	1	0	0
Sucrose	153	68	16	5	35	3	5	1	1	17	2
Simon's Citrate	147	60	16	12	38	3	13	0	1	1	3
Lysine decarboxylase	175	77	17	11	41	3	18	1		4	3
Gelatin	55	21	10	9	5	0	0	0	1	16	2
Amygdalin	20	1	0	0	0	0	0	0	0	0	0
Melibiose	0	0	0	0	0	0	0	0	0	0	0
α-L-Rhamnopyranose monohydrate	3	2	0	0	1	0	0	0	0	0	0
H_2S biochemical kit	11	2	0	2	0	0	2	1	0	1	3
Malonic acid disodium salt	162	75	13	8	31		14	1	1	16	3
Mannitol	174	74	15	6	37	3	19	1	1	15	3
D (+)-Glucose	179	73	17	11	36	3	19	0	1	16	2
3% NaCl MR-VP	4	3	0	0	1	0	0	0	0	0	0
Inositol	8	5	0	0	3	0	0	0	0	0	0
Ornithine decarboxylase	125	51	12	9	29	3/3	11	1	0	6	3
DL-Arabinose	46	0	1	1	11	0	17	0	1	15	0
Sorbitol	12	5	0	2	2	0	1	0	0	1	1
Lactose	18	0	4	2	6	0	1	0	1	2	2
Arginine double hydrolase	107	55	7	8	16	3	4	2	1	8	3
Tryptone water	22	0	0	0	5	3	7	0	0	6	1
Glucose oxidase	192	77	17	12	41	3	19	2	1	17	3

10.3389/fmars.2022.932255

showed large colonies of blue-green color and the colonies of *V. alginolyticus* were pale yellow or beige, while the other species were inhibited.

Diversity and clustering analysis of sequence types

The nucleotide sequence variations of the four gene fragments are summarized in Table 3. The GC contents of every locus were similar and varied per locus from 47.31% (*atpA*) to 48.53% (*pyrH*). The number of alleles of each locus in the 192 Harveyi clade isolates was distributed as follows: 53 *pyrH*, 56 *atpA*, 79 *gyrB*, and *recA*. The number of polymorphic sites ranged per locus from 137 (*atpA*) to 170 (*recA*). The nucleotide diversity varied from 0. 0.02643 (*atpA*) to 0.08482 (*pyrH*), indicating that allele loci had a low mutation rate. The value of d_N/d_S of each locus was lower than 0.25, suggesting a purifying selection of the four housekeeping genes for the 192 Harveyi clade isolates.

A total of 95 STs were identified, of which 92 were newly identified STs (Supplementary Table 1). The MLST analysis revealed high molecular diversity among the Harveyi clade isolates, with most strains forming unique sequence types in the Chinese mariculture system of this study. ST327 was the most common among the newly identified STs, accounting for 11.5% of the total number of isolates (22 out of 192), with all of them being *V. alginolyticus*. ST215, represented by *V. harveyi*, was the second most common STs and accounted for 6.25% of the total number of isolates (12 out of 192). Sixty-three STs had single isolates. Twenty-seven were identified in 77 isolates of *V. harveyi*, with each ST comprising 1 to 12 isolates. Fifteen STs were found in 41 isolates of *V. alginolyticus*, with each ST having 1 to 22 isolates. Eleven STs were identified in 19 V. *parahaemolyticus* isolates, with each ST containing 1 to 5 isolates, followed by *V. natriegens* (15 out of 17), *V. owensii* (11 out of 17), *V. rotiferianus* (9 out of 12), *V. campbellii* (3 out of 3), *V. diabolicus* (3 out of 3), *V. jasicida* (2 out of 2), and *V. mytili* (1 out of 1). Furthermore, the statistical classification of the ST strains according to their host origin showed that 42 STs were present in 101 isolates from fish, 26 STs in 64 isolates from shrimp, 4 STs in 4 isolates from crab, and 23 STs in 23 isolates from sea cucumber.

The identification of the CC clustering patterns indicated that 95 STs were separated into 7 CCs (CC0, CC1, CC2, CC3, CC4, CC5, and CC6) and 4 doublets (D1–D5) (Figure 3), while the remaining 36 STs were singletons. The most common CC was CC0, which included 78 isolates with 5 STs, all of which were identified as *V. harveyi*. Based on UPGMA analysis, the STs that belong to the same CCs and doublets were also clustered together in the UPGMA tree (Figure 4). CC0 was composed of *V. harveyi* and represented the core group, which was divided into two major branches. One branch included *V. campbellii*, *V. rotiferianus*, *V. owensii*, *V. mytili*, and *V. jasicida*, while the other branch included *V. parahaemolyticus*, *V. diabolicus*, *V. alginolyticus*, and *V. natriegens*. Among them, *V. parahaemolyticus* and *V. campbellii* had the closest genetic distance to *V. harveyi*. *V. jasicida* (composed of D2) and *V. natriegens* (composed of CC1 and CC5) were the most genetically distant species from CC0.

Antimicrobial susceptibility characteristics of the Harveyi clade isolates

The antibiotic resistance profiles of each Harveyi clade isolate are illustrated in Figure 5. The results showed that 93.8% of the Harveyi clade isolates were resistant to NEO. SDM resistance was found in 31.9% of the isolates. SDI and SMM resistance were observed in 22.9% of the isolates. Resistance to SMZ, THI, and ENR was recorded in 17.3%, 14.6%, and 8.3% of the isolates, respectively. On the other hand, Harveyi clade isolates were highly sensitive to certain antibiotics. Susceptibility to FFC, THI, FLU, ENR, CIP, SMZ, SMM, and SDI was recorded in 92.8%, 82.3%, 89%, 84%, 73%, 78%, 72%, and 61% of the isolates, respectively (Figure 6).

Multiple antibiotic resistance analysis indicated that the multiple antibiotic resistance index (MARI) of all the isolates ranged from 0 to 0.82 (Figure 7 and Supplementary Table S1), which revealed that 97.9% of the isolates (188 out of 192) were resistant to at least one antibiotic. A MARI value higher than 0.2 was observed in 30.7% of the resistant isolates (59 out of 192). These isolates have a transmission potential since the MARI was higher than 0.2, indicating a high antibiotic exposure risk. The isolates Vhh 50, Vhh 60, Val 14, and Vna 09 had the highest

TABLE 3 Nucleotide sequence variations of each MLST locus for 192 Harveyi clade isolates.

Locus	Fragment size (bp)	Alleles number	GC content (100%)	Nucleotide diversity	Polymorphic site number	d_N/d_S ratio
gyrB	570	79	48.01	0.07722	160	0.10715
pyrH	501	53	48.53	0.08482	145	0.06443
recA	462	79	47.99	0.06461	170	0.04899
atpA	489	56	47.31	0.02643	137	0.16802

The ratio of nonsynonymous to synonymous substitutions (d_N/d_S).

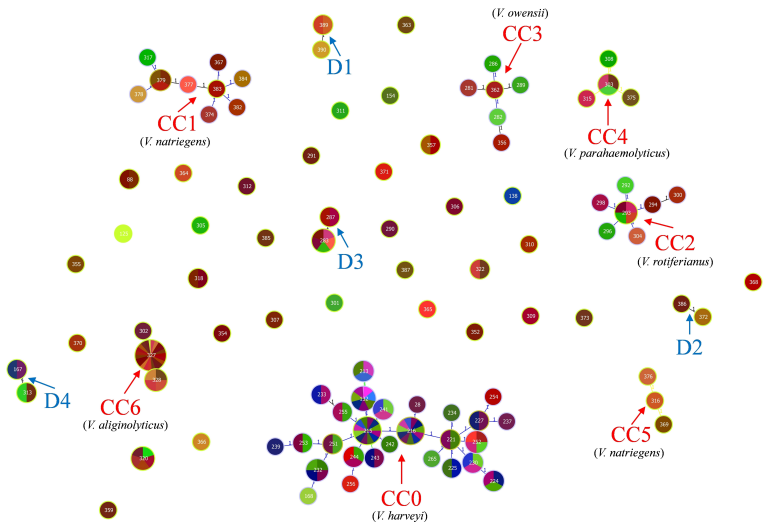

FIGURE 3
goeBURST minimum spanning tree for all the 95 sequence types obtained from the combination of all allele types of the four MLST loci *gyrB*, *pyrH*, *recA*, and *atpA* using the PHYLOViZ 2.0 analysis software. The genetic relationships between all the analyzed Chinese Harvey*i* clade isolates are indicated. Note: The different numbers in the circles represent different STs.

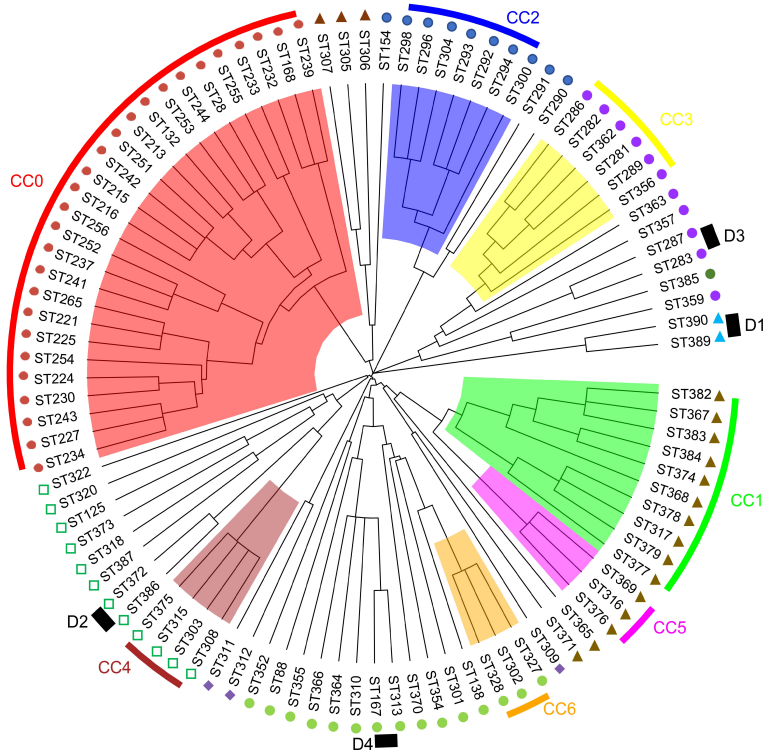

FIGURE 4
MLST hierarchical clustering phylogenetic map of the *Harveyi* clade. ●: *V. harveyi*; □: *V. parahaemolyticus*; ◆: *V. diabolicus*; ●: *V. alginolyticus*; ▲: *V. natriegens*; ▲: *V. jasicida*; ●: *V. owensii*; ●*V. mytili*; ●: *V. rotiferianus*.

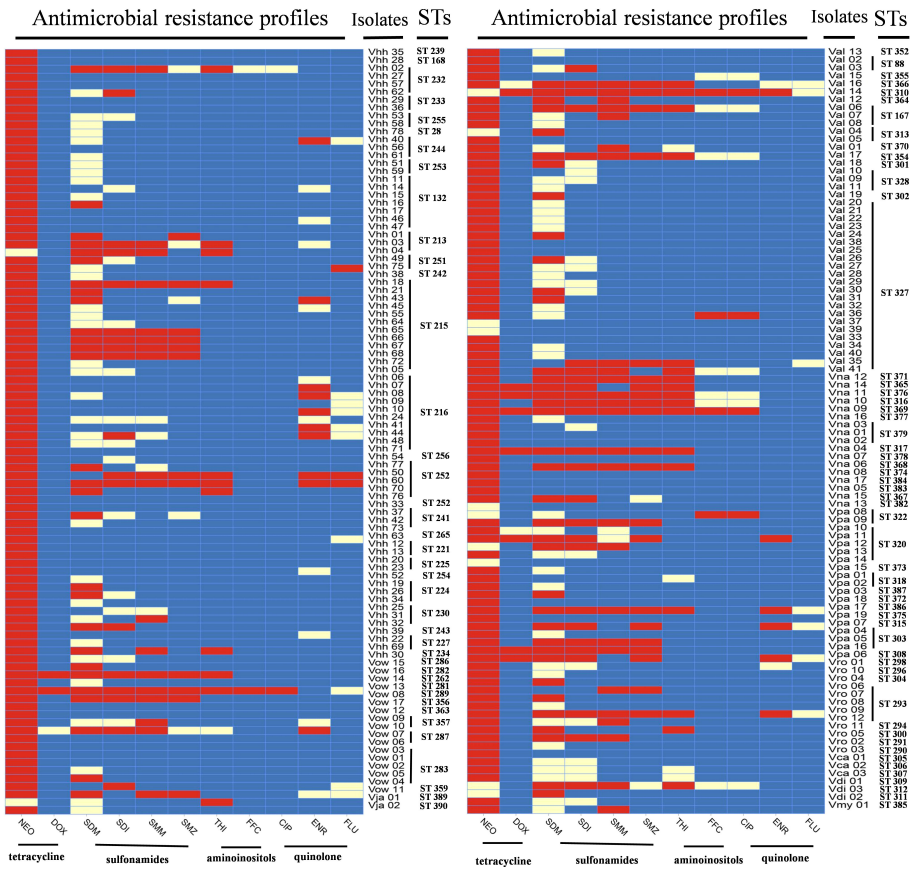

FIGURE 5
Levels of antibiotic resistance profiles of 11 tested antibiotics. The black bar, the gray bar, and the light gray bar represent the proportion of resistant strains, intermediate strains, and sensitive strains, respectively. The gray striped bar represents the proportion of the multiple antibiotic resistance index of the strains.

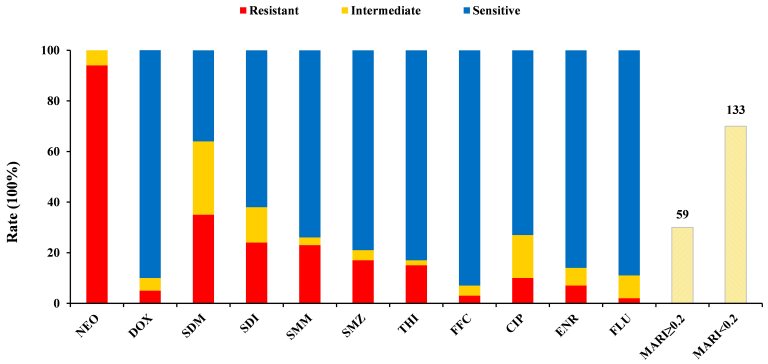

FIGURE 6
Antibiotic resistance profiles of the Harveyi clade isolates. The colors represent different levels of resistance. ■: resistance, ■: intermediate, ■: susceptibility. Note: MAR index is calculated by dividing the total numbers of the tested antibiotics into the numbers of antibiotics, to which the isolate was resistant.

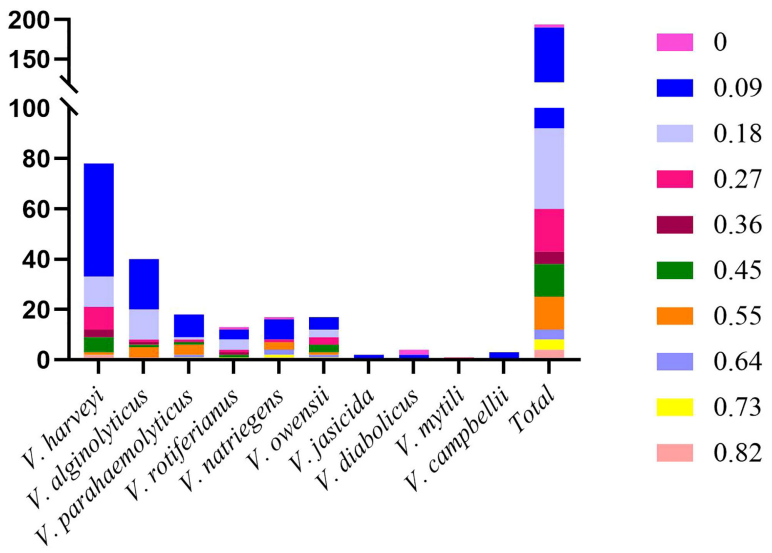

FIGURE 7
Distribution of multi-antibiotic resistance strains.

MARI value (0.82) and were resistant to nine antibiotics. The remaining 55 isolates showed multidrug resistance to at least three tested antibiotics (Figure 6).

Association analysis of antimicrobial resistance with the genetic population of the isolates is shown in Figure 5. ST132 consisted of seven isolates of *V. harveyi*, all of which were resistant to neomycin, while the other STs had sensitive phenotypes. The resistance profiles of the other isolates of the same ST showed different profiles. Moreover, 59 strains were resistant to the three antibiotics mentioned above, including 40 non-repetitive STs scattered in different years. Due to the large number of various STs and the significantly varying ST numbers, the relationship between the different STs and antimicrobial resistance was difficult to determine.

Discussion

We analyzed a total of 192 isolates of the Harveyi clade from infected parts of animals from marine and mariculture environments in coastal areas of China from 2000 to 2020. The phenotypic, metabiotic, and genotypic properties of these isolates were investigated thoroughly in this study. Many researchers confirmed that the phenotypic traits do not affect the differentiation of Harveyi clade isolates (Gauger and Gómez-Chiarri, 2002; Thompson, 2003). Lukjancenko et al. (2012) showed that the traditional phenotypes were unable to distinguish sister species due to large conserved regions in the proteome prediction. Gomez-Gil et al. (2004) demonstrated that *V. harveyi*, *V. campbellii*, and *V. rotiferianus* had similar phenotypes and were misidentified. The results of this study also revealed that the phenotypic methods have a limited ability to discriminate Harveyi clade members. Although 16S rDNA gene sequencing is considered as a gold standard method for bacterial taxonomy, it does not have sufficient resolution to correctly identify Harveyi clade species (Gomez-Gil et al., 2004; Janda and Abbott, 2007; Chatterjee and Haldar, 2012). The low discriminating ability of the 16S rDNA gene in identifying the 192 isolates in the present research was consistent with previous studies. In recent years, studies have shown that MLSA can accurately identify Harveyi clade strains with high resolution and reproducibility (Thompson et al., 2005; Xie et al., 2020). Rahman et al. (2014) found that most *Vibrio* species could be easily identified using population and phylogenetic analyses based on the combination of the genes *gyrB-pyrH-atpA-recA*. Using five housekeeping genes (i.e., *rpoA*, *pyrH*, *topA*, *ftsZ*, and *mreB*), Cano-Gomez et al. (2011) identified 36 *Vibrio harveyi*-related isolates as *V. harveyi*, *V. campbellii*, *V. rotiferianus*, and *V. owensii*. Furthermore, Pascual et al. (2010) identified rapidly and accurately 44 *Vibrio* core groups as *V. harveyi*, *V. campbellii*, *V. rotiferianus*, and *V. parahaemolyticus* using seven concatenated genes (i.e., 16S rDNA, *recA*, *pyrH*, *rpoD*, *gyrB*, *rctB*, and *toxR*). Xie et al. (2020) have recently demonstrated that the two pathogenic bacteria HM-12 and HM-14 were confirmed as *V. harveyi* and *V. alginolyticus*, respectively, using the five housekeeping genes *ftsZ*, *gapA*, *gyrB*, *mreB*, and *topA*. Furthermore, the NJ tree analysis of the species *V. alginolyticus* and *V. diabolicus* revealed two subgroups, which

supports the reports stating that the two species were originally one species (Rahman et al., 2014). In the present study, 192 *Harveyi* clade isolates were accurately identified to 10 species using the four concatenated genes *gyrB*, *pyrH*, *atpA*, and *recA*. Likewise, *V. rotiferianus* and *V. jasicida* revealed two subgroups, which led us to speculate that these two species may also have originated from one species. These studies clearly show that MLSA can effectively resolve phylogenetic relationships at the genus and species level; however, there are no general criteria for selecting the genes and their number for MLSA. Therefore, the use of MLSA needs to be improved to make its application more viable and ubiquitous.

Molecular subtyping is widely used for epidemiological and population genetic analysis of pathogenic bacteria. MLST was first introduced in the epidemiology of pathogenic *Neisseria meningitidis* strains (Maiden et al., 1998). MLST has been widely employed in recent years for *V. parahaemolyticus*. Han et al. (2015) found that 218 V. *parahaemolyticus* clinical isolates in China produced 137 STs, indicating that *V. parahaemolyticus* from China has a high genetic diversity. Using MLST, Jiang et al. (2019) found that 90 V. *parahaemolyticus* strains from Bohai and Yellow Seas of China were composed of 68 sequence types, displaying a high level of genetic diversity. Rahman et al. (2014) reported that 182 *Vibrio* strains obtained from the Venice Lagoon and a marine environment were classified into 162 STs and were processed as distinct species/taxa. We analyzed in the present study the extent of genetic diversity on nucleotide variations among the Harveyi clade isolates. Han et al. (2015) and Turner et al. (2013) reported the same phenomena in *V. parahaemolyticus* strains. The observed alleles, polymorphic site numbers, and nucleotide diversity reveal the richness and uniqueness of the Harveyi clade isolates from coastal areas of China.

In this study, we identified 95 STs among 192 Harveyi clade isolates. In comparison to the pubMLST database, 92 STs were newly discovered, demonstrating that our research contributed substantially to the diversity of *Vibrio* spp. in the MLST database. ST28, ST88, and ST132 were found to be identical to the sequence types of isolates recovered from the Venice Lagoon (Rahman et al., 2014). When examining the three STs with the largest number, no significant relationship between the STs and the annual change was observed. The analysis of the STs and their origin (host and collection data) shows that the isolates with the same ST may have originated from the same host (e.g., ST327). Nevertheless, the majority of the STs consisted of isolates from different regions and sampling years (e.g., ST215 and ST216). However, cgMLST correlates with time and regions of bacterial isolates well (Alikhan et al., 2018). As a bacterial typing system, it has become an innovative tracing tool in recent years (Monte et al., 2021). Gonzalez-Escalona et al. (2017) demonstrated that cgMLST clearly showed higher resolution than traditional MLST for *V. parahaemolytics*. With the development of whole genome sequencing technology, we will use comparative genomics and cgMLST scheme for higher-resolution analysis of Harvey clade isolates.

Antibiotic resistance of Harveyi clade isolates is an important indicator of metabolic and phenotypic diversity. In the current investigation, antibiotic susceptibility tests showed that all the Harveyi clade isolates were resistant to neomycin, but showed low resistance to other antibiotics. Similarly, Obaidat et al. (2017) reported that all *V. parahaemolyticus* isolates in the Harveyi clade were neomycin resistant. In the Indian subcontinent, *Vibrio* spp. exhibited high neomycin resistance (Guardiola et al., 2012). Ciprofloxacin was the most active quinolone antibiotic against the Harveyi clade in this study, which is consistent with the results of Zanetti et al. (2001). The increased resistance to quinolones in *Vibrio* spp., with spatial and temporal differences, may be related to various antibiotic resistance mechanisms (Blair et al., 2015; Blanco et al., 2016; Deng et al., 2020). In this study area, compared with other areas, we found the uniqueness and diversity of Harveyi clade isolates between the coastal areas of China and other countries. For instance, the MARI values of the Harveyi clade isolates ranged from 0 to 0.82. The MARI reflects the degree of the environmental pollution caused by antibiotics that may be dangerous to human health (Tanil et al., 2005; Páll et al., 2021). A value higher than 0.2 indicates a high antibiotic exposure risk, while a value lower than 0.2 indicates a low antibiotic exposure risk (Mohamad et al., 2019). According to our findings, 61.8% of the Harveyi clade isolated from coastal areas in the past 20 years have a MARI value less than 0.1, indicating that the risk of antibiotic resistance transmission of most Harveyi clade is low in mariculture systems in China. However, the resistance to the 11 antibiotics was found in various combinations, showing that this resistance was not concentrated in a single ST. Thus, the Harveyi clade isolates analyzed by MLST are multidrug-resistant bacteria. New non-antibiotic bacteriostatic medications and alternatives should be developed to reduce the impact of the extensive use of antibiotics on the environment and ecological health (Tan et al., 2016). In recent years, antibiotic drugs have been made into dietary microspheres by scholars to achieve high availability, attractiveness and digestibility to fish, which will promote the source of antibiotics, reduce antibiotic contamination in fisheries, and ease the control of antibiotic resistance (Zhang et al., 2021). Therefore, analyzing the drug resistance of pathogens in different regions of the eastern coast of China in the past 20 years is of great significance for formulating antibacterial drug reduction policies and effective antibacterial drug use programs.

Conclusions

Our analyses showed that the strains have significant interspecific genetic and antibiotic resistance diversity. The Harveyi clade isolates were classified rapidly and robustly using the MLSA approach. The MLST analysis showed high genetic diversity and uniqueness of the Harveyi clade isolates from China with multiple sequence types. Furthermore, our study confirmed the presence of multiple antibiotic resistance in the Harveyi clade from the coastal areas of China collected in the last two decades. Although the MARI demonstrated that most Harveyi clade isolates from marine and mariculture environments in coastal areas of China had a low probability of antibiotic resistance transmission, they were still highly resistant to various antibiotics, emphasizing the need to increase the development of non-antibiotic drugs and antibiotic alternatives. These results will provide a basis for further studies on the genetic and metabolic diversity of Harveyi clade isolates in mariculture systems in China.

Data availability statement

The 16S rDNA gene, gyrB, pyrH, atpA, recA sequences determined in this study have been deposited in the GenBank of NCBI under the accession numbers: ON437347-ON437538, ON469581-ON469772, ON778048-ON778239, ON778240-ON778431, ON4491819-ON492010.

Author contributions

The research was conceived and designed by YW, ML, and YY. The experiments were executed by HK, YY, and CW. ZZ assisted in statistical analysis. YY and BL analyzed the data. HK and YY drafted the manuscript. ML, XR, and GY reviewed the manuscript. All authors approved the final manuscript.

Funding

This work was supported by the National Key R&D Program of China (2019YFD0900102), Central Public-interest Scientific Institution Basal Research Fund, CAFS (2022GH02), Basic Scientific Research Funds for Central Non-profit Institutes, Yellow Sea Fisheries Research Institutes (20603022021013), and Central Public-interest Scientific Institution Basal Research Fund, CAFS (2020TD40).

Conflict of interest

The authors declare that the research was conducted in the absence of any commercial or financial relationships that could be construed as a potential conflict of interest.

Publisher's note

All claims expressed in this article are solely those of the authors and do not necessarily represent those of their affiliated organizations, or those of the publisher, the editors and the reviewers. Any product that may be evaluated in this article, or claim that may be made by its manufacturer, is not guaranteed or endorsed by the publisher.

Supplementary material

The Supplementary Material for this article can be found online at: https://www.frontiersin.org/articles/10.3389/fmars.2022.932255/full#supplementary-material

SUPPLEMENTARY TABLE 1
Allele profiles, sequence types, multiple antibiotic resistance index values (MARI), antimicrobial resistance profiles' identification based on multilocus sequence analysis (MLSA), and sources of 192 Harveyi clade isolates.

SUPPLEMENTARY FIGURE 1
Neighbor-joining (NJ) phylogenetic analysis based on 16S rDNA gene sequences of Harveyi clade isolates and reference strains used in this study. Numbers at nodes represent the bootstrap (BT) values based on 1000 resamplings.

SUPPLEMENTARY FIGURE 2
NJ phylogenetic analysis based on all three-locus concatenated sequences of Harveyi clade isolates and reference strains used in this study. Numbers at nodes represent the BT values based on 1000 resamplings.

SUPPLEMENTARY FIGURE 3
NJ phylogenetic analysis based on two-locus concatenated sequences of Harveyi clade isolates and reference strains used in this study. Numbers at nodes represent the BT values based on 1000 resamplings.

SUPPLEMENTARY FIGURE 4
Phylogenetic reconstructions based on individual analyses of *gyrB*, *pyrH*, *recA*, and *atpA* using the NJ method. Numbers at nodes represent the BT values base on 1000 resamplings.

SUPPLEMENTARY FIGURE 5
Morphology of Harveyi clade type strains. **(A)** growth of Harveyi clade type strains on TCBS agar; **(B)** microscopy Harveyi clade type strains on TCBS agar.

References

Aanensen, D. M., and Spratt, B. G. (2005). The multilocus sequence typing network: mlst.net. *Nucleic Acids Res.* 33, 728–733. doi: 10.1093/nar/gki415

Alikhan, N. F., Zhou, Z., Sergeant, M. J., and Achtman, M. (2018). A genomic overview of the population structure of salmonella. *PloS Genet.* 14, e1007261. doi: 10.1371/journal.pgen.1007261

Baker-Austin, C., Oliver, J. D., Alam, M., Ali, A., Waldor, M. K., Qadri, F., et al. (2018). *Vibrio* spp. infections. *Nat. Rev. Dis. Primers.* 4, 8. doi: 10.1038/s41572-018-0005-8

Baker-Austin, C., Trinanes, J., Gonzalez-Escalona, N., and Martinez-Urtaza, J. (2017). Non-cholera *Vibrios*: The microbial barometer of climate change. *Trends Microbiol.* 25, 76–84. doi: 10.1016/j.tim.2016.09.008

Blair, J. M., Webber, M. A., Baylay, A. J., Ogbolu, D. O., and Piddock, L. J. (2015). Molecular mechanisms of antibiotic resistance. *Nat. Rev. Microbiol.* 13, 42–51. doi: 10.1038/nrmicro3380

Blanco, P., Hernando-Amado, S., Reales-Calderon, J. A., Corona, F., Lira, F., Alcalde-Rico, M., et al. (2016). Bacterial multidrug efflux pumps: Much more than antibiotic resistance determinants. *Microorganisms* 4, 14. doi: 10.3390/microorganisms4010014

Botella, S., Pujalte, M. J., Macián, M. C., Ferrús, M. A., Hernández, J., and Garay, E. (2002). Amplified fragment length polymorphism (AFLP) and biochemical typing of photobacterium damselae subsp. damselae. *J. Appl. Microbiol.* 93, 681–688. doi: 10.1046/j.1365-2672.2002.01748.x

Cano-Gomez, A., Bourne, D. G., Hall, M. R., Owens, L., and Hoj, L. (2009). Molecular identification, typing and tracking of vibrio harveyi in aquaculture systems: current methods and future prospects. *Aquaculture* 287, 1–10. doi: 10.1016/j.aquaculture.2008.10.058

Cano-Gomez, A., Høj, L., Owens, L., and Andreakis, N. (2011). Multilocus sequence analysis provides basis for fast and reliable identification of *Vibrio harveyi*-related species and reveals previous misidentification of important marine pathogens. *Syst. Appl. Microbiol.* 34, 561–565. doi: 10.1016/j.syapm.2011.09.001

Chatterjee, S., and Haldar, S. (2012). *Vibrio* related diseases in aquaculture and development of rapid and accurate identification methods. *J. Mar. Sci. Res. Dev.* 1, 1–7. doi: 10.4172/2155-9910.S1-002

China Fisheries Yearbook (2021). *Fisheries department of agriculture ministry of China* (Beijing: China Agriculture Press).

Clinical and Laboratory Standards Institute [CLSI] (2017). *Performance standards for antimicrobial susceptibility testing. 27th Edn* (Wayne, PA: Clinical and Laboratory Standards Institute).

Del Gigia-Aguirre, L., Sánchez-Yebra-Romera, W., García-Muñoz, S., and Rodríguez-Maresca, M. (2017). First description of wound infection with *Vibrio harveyi* in Spain. *New Microbes New Infect.* 19, 15–16. doi: 10.1016/j.nmni.2017.05.004

Deng, Y., Xu, L., Chen, H., Liu, S., Guo, Z., Cheng, C., et al. (2020). Prevalence, virulence genes, and antimicrobial resistance of *Vibrio* species isolated from diseased marine fish in south China. *Sci. Rep.* 10, 14329. doi: 10.1038/s41598-020-71288-0

Fraser, C., Hanage, W. P., and Spratt, B. G. (2007). Recombination and the nature of bacterial speciation. *Science* 315, 476–480. doi: 10.1126/science.1127573

Fu, S., Octavia, S., Tanaka, M. M., Sintchenko, V., and Lan, R. (2015). Defining the core genome of salmonella enterica serovar typhimurium for genomic surveillance and epidemiological typing. *J. Clin. Microbiol.* 53, 2530–2538. doi: 10.1128/JCM.03407-14

Gauger, E. J., and Gómez-Chiarri, M. (2002). 16S ribosomal DNA sequencing confirms the synonymy of *Vibrio harveyi* and *Vibrio carchariae*. *Dis. Aquat Organ* 52, 39–46. doi: 10.3354/dao052039

Gevers, D., Cohan, F. M., Lawrence, J. G., Spratt, B. G., Coenye, T., Feil, E. J., et al. (2005). Re-evaluating prokaryotic species. *Nat. Rev. Microbiol.* 3, 733–739. doi: 10.1038/nrmicro1236

Gomez-Gil, B., Soto-Rodríguez., S., García-Gasca, A., Roque, A., and Swings, J. (2004). Molecular identification of *Vibrio harveyi*-related isolates associated with diseased aquatic organisms. *Microbiology* 150, 1769–1777. doi: 10.1099/mic.0.26797-0

Gonzalez-Escalona, N., Jolley, K. A., Reed, E., and Martinez-Urtaza, J. (2017). Defining a core genome multilocus sequence typing scheme for the global epidemiology of vibrio parahaemolyticus. *J. Clin. Microbiol.* 55, 1682–1697. doi: 10.1128/JCM.00227-17

Goudenège, D., Boursicot, V., Versigny, T., Bonnetot, S., Ratiskol, J., Sinquin, C., et al. (2014). Genome sequence of *Vibrio diabolicus* and identification of the exopolysaccharide HE800 biosynthesis locus. *Appl. Microbiol. Biotechnol.* 98, 10165–10176. doi: 10.1007/s00253-014-6202-9

Guardiola, F. A., Cuesta, A., Meseguer, J., and Esteban, M. A. (2012). Risks of using antifouling biocides in aquaculture. *Int. J. Mol. Sci.* 13, 1541–1560. doi: 10.3390/ijms13021541

Hackbusch, S., Wichels, A., Gimenez, L., Döpke, H., and Gerdts, G. (2020). Potentially human pathogenic *Vibrio* spp. in a coastal transect: Occurrence and multiple virulence factors. *Sci. Total Environ.* 707, 136113. doi: 10.1016/j.scitotenv.2019.136113

Han, D., Tang, H., Ren., C., Wang, G., Zhou, L., and Han., C. (2015). Prevalence and genetic diversity of clinical *Vibrio parahaemolyticus* isolates from China, revealed by multilocus sequence typing scheme. *Front. Microbiol.* 6. doi: 10.3389/fmicb.2015.00291

Harun, A., Kan, A., Schwabenbauer, K., Gilgado, F., Perdomo, H., Firacative, C., et al. (2021). Multilocus sequence typing reveals extensive genetic diversity of the emerging fungal pathogen *Scedosporium aurantiacum*. *Front. Cell Infect. Microbiol.* 11. doi: 10.3389/fcimb.2021.761596

Holt, J. G., Krieg, N. R., Sneath, P. H. A., Staley, J. T., and Williams, S. T. (1994). *Bergey's manual of determinative bacteriology. 9th edn* (Baltimore: Williams & Wilkins).

Janda, J. M., and Abbott, S. L. (2007). 16S rRNA gene sequencing for bacterial identification in the diagnostic laboratory: pluses, perils, and pitfalls. *J. Clin. Microbiol.* 45, 2761–2764. doi: 10.1128/JCM.01228-07

Jelocnik, M., Polkinghorne, A., and Pannekoek, Y. (2019). Multilocus sequence typing (MLST) of chlamydiales. *Methods Mol. Biol.* 2042, 69–86. doi: 10.1007/978-1-4939-9694-0-7

Jiang, Y., Chu, Y., Xie, G., Li, F., Wang, L., Huang, J., et al. (2019). Antimicrobial resistance, virulence and genetic relationship of *Vibrio parahaemolyticus* in seafood from coasts of bohai Sea and yellow Sea, China. *Int. J. Food Microbiol.* 290, 116–124. doi: 10.1016/j.ijfoodmicro.2018.10.005

Jolley, K. A., Feil, E. J., Chan, M. S., and Maiden, M. C. (2001). Sequence type analysis and recombinational tests (START). *Bioinformatics* 17, 1230–1231. doi: 10.1093/bioinformatics/17.12.1230

Krumperman, P. H. (1983). Multiple antibiotic indexing of *Escherichia coli* to identify high-risk sources of fecal contamination of foods. *Appl. Environ. Microbiol.* 46, 165–170. doi: 10.1128/AEM.46.1.165-170.1983

Kumari, P., Poddar, A., and Das, S. K. (2020). Characterization of multidrug resistance in *Vibrio* species isolated from marine invertebrates from Andaman Sea. *3 Biotech.* 10, 456. doi: 10.1007/s13205-020-02445-5

Lin, B., Wang, Z., Malanoski, A. P., O'Grady, E. A., Wimpee, C. F., Vuddhakul, V., et al. (2010). Comparative genomic analyses identify the *Vibrio harveyi* genome sequenced strains BAA-1116 and HY01 as *Vibrio campbellii*. *Environ. Microbiol. Rep.* 2, 81–89. doi: 10.1111/j.1758-2229.2009.00100.x

Lukjancenko, O., Ussery, D. W., and Wassenaar, T. M. (2012). Comparative genomics of bifidobacterium, lactobacillus and related probiotic genera. *Microb. Ecol.* 63, 651–673. doi: 10.1007/s00248-011-9948-y

Maiden, M. C., Bygraves, J. A., Feil, E., Morelli, G., Russel, J. E., Urwin, R., et al. (1998). Multilocus sequence typing: A portable approach to the identification of clones within populations of pathogenic microorganisms. *Proc. Natl. Acad. Sci. U. S. A.* 95, 3140–3145. doi: 10.1073/pnas.95.6.3140

Mohamad, N., Amal, M., Saad, M. Z., Yasin, I., Zulkiply, N. A., Mustafa, M., et al. (2019). Virulence-associated genes and antibiotic resistance patterns of vibrio spp. isolated from cultured marine fishes in Malaysia. *BMC Vet. Res.* 15, 176. doi: 10.1186/s12917-019-1907-8

Monte, D. F. M., Nethery, M. A., Barrangou, R., Landgraf, M., and Fedorka-Cray, P. J. (2021). Whole-genome sequencing analysis and CRISPR genotyping of rare antibiotic-resistant salmonella enterica serovars isolated from food and related sources. *Food Microbiol.* 93, 103601. doi: 10.1016/j.fm.2020.103601

Obaidat, M. M., Salman, A. E. B., and Roess, A. A. (2017). Virulence and antibiotic resistance of vibrio parahaemolyticus isolates from seafood from three developing countries and of worldwide environmental, seafood, and clinical isolates from 2000 to 2017. *J. Food Prot.* 80, 2060–2067. doi: 10.4315/0362-028X.JFP-17-156

Páll, E., Niculae, M., Brudașcă, G. F., Ravilov, R. K., Șandru, C. D., Cerbu, C., et al. (2021). Assessment and antibiotic resistance profiling in *Vibrio* species isolated from wild birds captured in Danube delta biosphere reserve, Romania. *Antibiot (Basel)* 10, 333. doi: 10.3390/antibiotics10030333

Pascual, J., Macian, M. C., Arahal, D. R., Garay, E., and Pujalte, M. J. (2010). Multilocus sequence analysis of the central clade of the genus *Vibrio* by using the 16S rRNA, recA, pyrH, rpoD, gyrB, rctB and toxR genes. *Int. J. Syst. Evol. Microbiol.* 60, 154–165. doi: 10.1099/ijs.0.010702-0

Prithvisagar, K. S., Krishna Kumar, B., Kodama, T., Rai, P., Iida, T., Karunasagar, I., et al. (2021). Whole genome analysis unveils genetic diversity and potential

virulence determinants in *Vibrio parahaemolyticus* associated with disease outbreak among cultured *Litopenaeus vannamei* (Pacific white shrimp) in India. *Virulence* 12, 1936–1949. doi: 10.1080/21505594.2021.1947448

Rahman, M. S., Martino, M. E., Cardazzo, B., Facco, P., Bordin, P., Mioni, R., et al. (2014). *Vibrio* trends in the ecology of the Venice lagoon. *Appl. Environ. Microbiol.* 80, 2372–2380. doi: 10.1128/AEM.04133-13

Ribeiro-Gonçalves, B., Francisco, A. P., Vaz, C., Ramirez, M., and Carriço, J. A. (2016). PHYLOViZ online: web-based tool for visualization, phylogenetic inference, analysis and sharing of minimum spanning trees. *Nucleic Acids Res.* 44, 246–251. doi: 10.1093/nar/gkw359

Richter, M., and Rosselló-Móra, R. (2009). Shifting the genomic gold standard for the prokaryotic species definition. *Proc. Natl. Acad. Sci. U. S. A.* 106, 19126–19131. doi: 10.1073/pnas.0906412106

Romalde, J. L., Dieguez, A. L., Lasa, A., and Balboa, S. (2014). New *Vibrio* species associated to molluscan microbiota: a review. *Front. Microbiol.* 4. doi: 10.3389/fmicb.2013.00413

Rozas, J., Ferrer-Mata, A., Saínchez-DelBarrio, J. C., Guirao-Rico, S., Librado, P., Ramos-Onsins, S. E., et al. (2017). DnaSP 6: DNA sequence polymorphism analysis of Large data sets. *Mol. Biol. Evol.* 34, 3299–3302. doi: 10.1093/molbev/msx248

Ruwandeepika, H., Jayaweera, T., Bhowmick, P. P., Karunasagar, I., Bossier, P., and Defoirdt, T. (2012). Pathogenesis, virulence factors and virulence regulation of *Vibrios* belonging to the harveyi clade. *Rev. Aquacult.* 4, 59–74. doi: 10.1111/j.1753-5131.2012.01061.x

Santhyia, A. V., Mulloorpeedikayil, R. G., Kollanoor, R. J., and Jeyaseelan, P. M. (2015). Molecular variations in vibrio alginolyticus and v. harveyi in shrimp-farming systems upon stress. *Braz. J. Microbiol.* 46, 1001–1008. doi: 10.1590/S1517-838246420140410

Sawabe, T., Kita-Tsukamoto, K., and Thompson, F. L. (2007). Inferring the evolutionary history of vibrios by means of multilocus sequence analysis. *J. Bacteriol.* 189, 7932–7936. doi: 10.1128/JB.00693-07

Tamura, K., Stecher, G., Peterson, D., Filipski, A., and Kumar, S. (2013). MEGA6: Molecular evolutionary genetics analysis version 6.0. *Mol. Biol. Evol.* 30, 2725–2729. doi: 10.1093/molbev/mst197

Tan, L. T., Chan, K. G., Lee, L. H., and Goh, B. H. (2016). Streptomyces bacteria as potential probiotics in aquaculture. *Front. Microbiol.* 7. doi: 10.3389/fmicb.2016.00079

Tanil, G. B., Radu, S., Nishibuchi, M., Rahim, R. A., Napis, S., Maurice, L., et al. (2005). Characterization of *Vibrio parahaemolyticus* isolated from coastal seawater in peninsular Malaysia. *Southeast Asian J. Trop. Med. Public Health* 36, 940–945. doi: 10.1109/43.31533

Thompson, F. L. (2003). *Improved taxonomy of the family vibrionaceae. ph. d. thesis* (Ghent, Belgium: Ghent University).

Thompson, F. L., Gevers, D., Thompson, C. C., Dawyndt, P., Naser, S., Hoste, B., et al. (2005). Phylogeny and molecular identification of vibrios on the basis of multilocus sequence analysis. *Appl. Environ. Microbiol.* 71, 5107–5115. doi: 10.1128/AEM.71.9.5107-5115.2005

Thompson, F. L., Iida, T., and Swings, J. (2004). Biodiversity of *Vibrios*. *Mol. Biol. Rev.* 68, 403–431. doi: 10.1128/MMBR.68.3.403-431.2004

Thompson, C. C., Vicente, A. C., Souza, R. C., Vasconcelos, A. T., Vesth, T., Alves, N.Jr., et al. (2009). Genomic taxonomy of vibrios. *BMC Evol. Biol.* 9, 258. doi: 10.1186/1471-2148-9-258

Tran, L., Nunan, L., Redman, R. M., Mohney, L. L., Pantoja, C. R., Fitzsimmons, K., et al. (2013). Determination of the infectious nature of the agent of acute hepatopancreatic necrosis syndrome affecting penaeid shrimp. *Dis. Aquat Organ* 105, 45–55. doi: 10.3354/dao02621

Turner, J. W., Paranjpye, R. N., Landis, E. D., Biryukov, S. V., Gonzalez-Escalona, N., Nilsson, W. B., et al. (2013). Population structure of clinical and environmental *Vibrio parahaemolyticus* from the pacific northwest coast of the united states. *PloS One* 8, e55726. doi: 10.1371/journal.pone.0055726

Wang, W., Liu, J., Guo, S., Liu, L., Yuan, Q., Guo, L., et al. (2021). Identification of *Vibrio parahaemolyticus* and *Vibrio* spp. specific outer membrane proteins by reverse vaccinology and surface proteome. *Front. Microbiol.* 11. doi: 10.3389/fmicb.2020.625315

Weisburg, W. G., Barns, S. M., Pelletier, D. A., and Lane, D. J. (1991). 16S ribosomal DNA amplification for phylogenetic study. *J. Bacteriol.* 173, 697–703. doi: 10.1128/jb.173.2.697-703.1991

Xie, J., Bu, L., Jin, S., Wang, X., and Xu, Y. (2020). Outbreak of vibriosis caused by *Vibrio harveyi* and *Vibrio alginolyticus* in farmed seahorse hippocampus kuda in China. *Aquaculture* 523, 735168. doi: 10.1016/j.aquaculture.2020.735168

Yang, Y., Xie, J., Li, H., Tan, S., Chen, Y., and Yu, H. (2017). Prevalence, antibiotic susceptibility and diversity of *Vibrio parahaemolyticus* isolates in seafood from south China. *Front. Microbiol.* 8. doi: 10.3389/fmicb.2017.02566

Yan, S., Zhang, W., Li, C., Liu, X., Zhu, L., Chen, L., et al. (2021). Serotyping, MLST, and core genome MLST analysis of *Salmonella enterica* from different sources in China during 2004-2019. *Front. Microbiol.* 12. doi: 10.3389/fmicb.2021.688614

Zanetti, S., Spanu, T., Deriu, A., Romano, L., Sechi, L. A., and Fadda, G. (2001). *In vitro* susceptibility of *Vibrio* spp. isolated from the environment. *Int. J. Antimicrob. Agents* 17, 407–409. doi: 10.1016/s0924-8579(01)00307-7

Zhang, M., Cai, Z., Zhang, G., Zhang, Y., Xue, N., Zhang, D., et al. (2021). Effectively reducing antibiotic contamination and resistance in fishery by efficient gastrointestine-blood delivering dietary millispheres. *J. Hazard Mater.* 409, 125012. doi: 10.1016/j.jhazmat.2020.125012

frontiers | Frontiers in Physiology

TYPE Original Research
PUBLISHED 26 August 2022
DOI 10.3389/fphys.2022.925752

OPEN ACCESS

EDITED BY
Jianlong Ge,
Yellow Sea Fisheries Research Institute (CAFS), China

REVIEWED BY
Daniel Carneiro Moreira,
University of Brasilia, Brazil
Song Yang,
Sichuan Agricultural University, China

*CORRESPONDENCE
Liangbiao Chen,
lbchen@shou.edu.cn

SPECIALTY SECTION
This article was submitted to Aquatic Physiology, a section of the journal Frontiers in Physiology

RECEIVED 21 April 2022
ACCEPTED 27 July 2022
PUBLISHED 26 August 2022

CITATION
Hu R, Li G, Xu Q and Chen L (2022), Iron supplementation inhibits hypoxia-induced mitochondrial damage and protects zebrafish liver cells from death. *Front. Physiol.* 13:925752. doi: 10.3389/fphys.2022.925752

Iron supplementation inhibits hypoxia-induced mitochondrial damage and protects zebrafish liver cells from death

Ruiqin Hu[1,2], Genfang Li[1,2], Qianghua Xu[1,2,3] and Liangbiao Chen[1,2]*

[1]International Joint Research Centre for Marine Biosciences (Ministry of Science and Technology), College of Fisheries and Life Science, Shanghai Ocean University, Shanghai, China, [2]Key Laboratory of Exploration and Utilization of Aquatic Genetic Resources (Ministry of Education) and International Research Centre for Marine Biosciences, College of Fisheries and Life Science, Shanghai Ocean University, Shanghai, China, [3]Key Laboratory of Sustainable Exploitation of Oceanic Fisheries Resources, College of Marine Science, Shanghai Ocean University, Shanghai, China

Acute hypoxia in water has always been a thorny problem in aquaculture. Oxygen and iron play important roles and are interdependent in fish. Iron is essential for oxygen transport and its concentration tightly controlled to maintain the cellular redox homeostasis. However, it is still unclear the role and mechanism of iron in hypoxic stress of fish. In this study, we investigated the role of iron in hypoxic responses of two zebrafish-derived cell lines. We found hypoxia exposed zebrafish liver cells (ZFL) demonstrated reduced expression of Ferritin and the gene *fth31* for mitochondrial iron storage, corresponding to reduction of both intracellular and mitochondrial free iron and significant decrease of ROS levels in multiple cellular components, including mitochondrial ROS and lipid peroxidation level. In parallel, the mitochondrial integrity was severely damaged. Addition of exogenous iron restored the iron and ROS levels in cellular and mitochondria, reduced mitochondrial damage through enhancing mitophagy leading to higher cell viability, while treated the cells with iron chelator (DFO) or ferroptosis inhibitor (Fer-1) showed no improvements of the cellular conditions. In contrast, in hypoxia insensitive zebrafish embryonic fibroblasts cells (ZF4), the expression of genes related to iron metabolism showed opposite trends of change and higher mitochondrial ROS level compared with the ZFL cells. These results suggest that iron homeostasis is important for zebrafish cells to maintain mitochondrial integrity in hypoxic stress, which is cell type dependent. Our study enriched the hypoxia regulation mechanism of fish, which helped to reduce the hypoxia loss in fish farming.

KEYWORDS

hypoxia, iron, ROS, mitochondria, mitophagy

Introduction

Dissolved oxygen is one of the key physical and chemical factors in aquatic ecological environment, and also is an important limiting factor in fish culture (Valavanidis et al., 2006). Aquatic habitats often experience extreme fluctuations in O_2 content ranging from near anoxia (<1% O_2) to hyperoxia (300–500% O_2) reflecting the local dynamics of the photosynthesis, respiration and atmospheric gas exchange (Diaz and Rosenberg, 2008). Although terrestrial amphibians and reptiles encounter hypoxic burrow environments, the degree of hypoxia that experienced by aquatic species is more serious (Bickler and Buck, 2007). Low dissolved oxygen, or hypoxia, can negatively affect fish behavior, physiology, immunology, and growth (Abdel-Tawwab et al., 2019; Qiang et al., 2019). Mild hypoxic conditions do not cause fish death, although it can cause behavior and feeding abnormalities, but severe hypoxic conditions or anoxia (0.1% O_2) can be fatal to fish (Richards, 2011). Studies found that red blood cells (RBC), hemoglobin and/or blood cells in fish increased rapidly under hypoxia stress (Affonso et al., 2002; Boggs et al., 2022). Hemoglobin is an important protein that carries oxygen in red blood cells. Thus, more hemoglobin needs to be synthesized to increase oxygen supply under hypoxic conditions.

Iron is essential for oxygen transport and is a component of proteins that carry oxygen molecules, such as hemoglobin and myoglobin, which iron deficiency causes anemia, limits mitochondrial respiration and result in mitochondrial DNA damage (Walter et al., 2002; Rouault 2006; Salahudeen and Bruick, 2009). At the physiological level, cellular iron is necessary for maintenance of metabolism, and excessive free iron may lead to oxidative damage and/or cell death (Mittler 2017). Therefore, the homeostasis of iron must be strictly controlled. Many studies have shown that hypoxia stress causes iron metabolism dysfunction, and hypoxia can also protect cells from damage caused by the disrupted iron metabolism (Fuhrmann et al., 2020; Duarte et al., 2021; Ni et al., 2021). It is very important to coordinate the physiological hypoxia response with the effective control of iron. However, it is still unclear the role and mechanism of iron in hypoxic stress of fish.

Superoxide and other reactive oxygen species (ROS) have been recognized harmful and toxic byproducts of aerobic metabolism, but they are also important signaling molecules in a variety of physiological and pathophysiological conditions (Sena and Chandel, 2012; Mittler 2017). Low level of ROS is utilized for signal transduction, but prolonged elevations of ROS result in the oxidation of nucleic acid, protein, lipid and leading to cell dysfunction or death (Zhang et al., 2008). ROS and ROS-dependent signaling pathways seem to be linked in different ways to those that adapt to low oxygen conditions (Schieber and Chandel, 2014). As one of the significant source of cellular ROS, mitochondria play central roles in hypoxic responses (Lenaz 2001; Murphy 2009; Zhang and Wong, 2021). On one hand, mitochondria themselves are especially vulnerable to ROS-mediated oxidative damage (Sena and Chandel, 2012). On the other hand, ROS production from the mitochondria is temporarily increased in response to acute hypoxia (Hernansanz-Agustín et al., 2014). However, localization and speciation of the paradoxical increase in reactive oxygen species production in hypoxia remain debatable. Therefore, the cell types and the time frame of hypoxic should be considered.

Mitochondria have been viewed as pluripotent organelles, controlling cellular life, stress and death (Galluzzi et al., 2012). Thus, maintaining a functional mitochondrial network is the basis of cellular homeostasis in response to conditioned stress and physiological adaptation. Mitochondrial autophagy is one of the major mechanisms of mitochondrial quality control (Ashrafi and Schwarz, 2013; Ni et al., 2015). Autophagosomes selectively engulf dysfunctional or redundant mitochondria and degrade them in lysosomes (Kroemer and Jaattela, 2005). Mitophagy is highly sensitive to dynamic changes in endogenous metabolites, including iron-, glycolysis-TCA-, NAD + -, amino acids-, and fatty acid-related metabolites (Ting Zhang et al., 2021). In addition, disturbances of iron homeostasis (including iron deposition and iron deficiency) and abnormal iron metabolism have been widely reported to be closely associated with mitochondrial dysfunction (Bogdan et al., 2016; Wei et al., 2020). Mitochondria provide a place for iron metabolism in cells, and iron deprivation triggers mitophagy (Palikaras et al., 2018).

Fish liver is one of the earliest and most sensitive tissues to external stimuli, and is also the earliest tissue to appear damage (Kietzmann 2019). Meanwhile, liver plays an important role in iron homeostasis (Rishi and Subramaniam, 2017). Oxygen is the basic element to maintain cell life activities, and hypoxia will cause different effects on different cells (Michiels 2004). Therefore, we used zebrafish liver cells (ZFL) and zebrafish embryonic fibroblasts cells (ZF4), a kind of cell that is insensitive to both hypoxia and iron, to explore the role and mechanism of iron in fish cells respond to hypoxia stress. Hypoxia (3–0.1% O_2) is capable of rapidly inducing, via the hypoxia-inducible factor (HIF-1), a cell survival response engaging autophagy. This process is a HIF-1dependent autophagic response which also mediate mitophagy, a metabolic adaptation for survival that is able to control reactive oxygen species (ROS) production. In contrast, severe hypoxic condition or anoxia (0.1% O_2), where the latter is often confused with physiological hypoxia, are capable of inducing a HIF independent autophagic response. (Mazure and Pouysségur, 2010). Many studies focus on oxygen concentration above 1%, but there are few studies on lower oxygen concentration. Therefore, 0.1% oxygen concentration was selected as hypoxic stress for study. In this study, we demonstrated that hypoxic stress caused iron loss in the cytoplasm and mitochondria of ZFL cells, resulting in mitochondrial damage and ultimately cell death. The cell death due to hypoxia is a non-ferroptosis form of death, although iron supplementation can reverse the course. However, iron has different roles in ZF4 cells to respond to hypoxia stress. This study established the role of iron in maintaining mitochondrial integrity in hypoxic response,

which help to understand the regulatory mechanism of fish response to hypoxia stress to reduce the hypoxia loss in fish farming.

Material and method

Cell culture and treatment

ZFL and ZF4 cells were provided by the Cell Bank of the Chinese Academy of Sciences. Cells were cultured in DMEM F12 medium containing 10% fetal bovine serum (FBS) and 100 U/mL penicillin/streptomycin in cell culture incubator (Eppendorf, Germany). The cells were seeded 24 h before to ensure attachment, then were cultured under normoxic (21% O_2) and hypoxic (0.1% O_2, balanced nitrogen) environment with 5% CO_2 at 28°C when the cellular confluency reached 70%.

Biological reagents ferric ammonium citrate (FAC) (Sigma, United States), Deferoxamine (DFO) (MedChemExpress, United States) and Ferrostatin-1 (Fer-1) (MedChemExpress, United States) have been used to rescue cells under hypoxia stress. FAC, DFO and Fer-1 were dissolved and stored according to the manufacturers' protocol, and then diluted to the appropriate concentration in cell culture medium for cell treatment. In detail, the final concentrations of FAC were 0, 0.1, 0.25, 0.5, 0.75, 1.0 and 2.0mM; the final concentrations of DFO were 0, 10, 30, 50, 70, 90 and 100μM; the final concentrations of Fer-1 were 0, 1, 2, 4, 6, 8 and 10 μM. Cells were pretreated with FAC, DFO and Fer-1 for 1 h before hypoxia stress.

The determination of cell morphology

Cells were seeded onto 6 cm culture dishes with the cell confluency reached 70%. The cells were treated with or without FAC, DFO or Fer-1 for 1 h prior hypoxic incubations. Upon incubated with or without treatment for corresponding time under normoxia or hypoxia, the morphological features of cells were captured using Zeiss microscope directly.

Cell vitality assay

To analyze the viability of the cells, cells were plated in 96-well plate with 90 μl medium 24 h before to ensure attachment and were cultured under normoxic (21% O_2) environment with 5% CO_2 at 28°C. When the cellular confluency reached 70%, cells in the control group were directly analyzed for cell activity, and cells in the experimental group were pretreated with FAC, DFO and Fer-1 for 1 h under normoxic (21% O_2). Then the experimental group cells were transferred to hypoxic (0.1% O_2, balanced nitrogen) environment with 5% CO_2 at 28 °C for 1, 2, 3 and 4 d.

PrestoBlue™ HS Cell Viability Regent (Invitrogen, United States) were used to analyze the viability of the cells. Briefly, add 10 μl of cell viability regent directly to cells in culture medium, and incubate for 3 h under normoxic (21% O_2) environment with 5% CO_2 at 28 °C. Afterwards, absorbance was measured on a plate reader (Biotek, United States) at 570 nm, using 600 nm as a reference wavelength.

Western blotting

Total protein was extracted using RIPA (sigma, Germany) lysis buffer containing protease inhibitor PMSF (Invitrogen, United States). Protein concentration was detected by BCA protein assay kit (Invitrogen, United States). Total of 20 μg protein was electrophoresed in 10% SDS-PAGE gels and transferred onto PVDF membranes (Merk, Germany). The membranes were blocked with TBST solution containing 5% milk for 2.5 h at room temperature, then probed with the primary antibody overnight and the secondary antibody for 1 h. Wash the membranes with TBST solution three times for 5 min each before and after incubation of secondary antibodies. Finally, the blots were captured by Amersham imager 600 (GE, United States) and the quantitative results were analyzed by ImageJ analysis software. The list of antibodies is as follows: Ferritin (Huabio, China), Hif1α (Boster, China), LC3 (Cell Signaling Technology, United States), P62 (Cell Signaling Technology, United States), Actin (Huabio, China) and the secondary antibody (Huabio, China).

Real-time quantitative PCR analysis

RNA was isolated using Trizol according to the manufacturer's protocol (Invitrogen, United States) and measured using a Nanodrop spectrophotometer (ThermoFisher, United States). Reverse transcription was performed with the Maxima First Strand cDNA Synthesis Kit for RT-PCR (Takara, Japan). RNA expression of *tfa*, *tfr2*, *fth27*, *fth28* and *fth31* was analyzed using SYBR Green Master Mix (Roche, Switzerland) on a Roche 480 System (Roche, Switzerland) and normalized to Actin. Primers are listed in Table 1.

Intracellular ROS measurement

Intracellular ROS production was detected by 2,7-dichlorodihydrofluorescein diacetate (CM-H2DCFDA) (Invitrogen, United States) according to the manufacturer's introduction. Briefly, ZFL and ZF4 cells were seed in 6 cm plates and harvested after treatment for 3 days. Firstly, cells were washed twice with DPBS solution (Sangon, China). Then cells were labeled with 5 μM CM-H2DCFDA for 30 min at 28°C and washed for two times. The fluorescence was quantified using

TABLE 1 Primer information.

Gene name	Forward primer	Reverse primer
tfa	AGCAGCAGACATTGAGTGTC	TTTGCTCCATCTACTGTAAC
tfr2	AGCAGTTTACCTCACACTGAC	AGGAATGTTGTCCGGCTCG
fthl27	TGCGAGGCTTTGATCAACAAG	TGGCAAATCCAGGAAGAGCC
fthl28	AAGATGATCAATCTGGAGC	TTGAAGAACTTGGCAAATCC
fthl31	AGGCTGCGATCAACAAGATG	AGGAAGAGCCACATCGTC
actin	TGTCCCTGTATGCCTCTGGT	AAGTCCAGACGGAGGATG

Biosciences AccuriC6 flow cytometry (Becton Dickinson, United States) with an excitation wavelength of 488 nm and emission at 525 nm.

Detection of lipid peroxidation level

Lipid peroxidation was quantified by incubating with C11-BODIPY™ superoxide indicator (Invitrogen, United States). This fluorophore is readily incorporated into cellular membranes and is about twice as sensitive to oxidation as arachidonic acid, thereby losing its bright red fluorescence with a shift to green. The green fluorescence was selectively detected using the excitation and emission bandpass filters of 488 and 510 nm, respectively. Therefore, the increase of oxidative stress was accompanied with a linear increase in green fluorescence intensity.

In brief, cells were washed twice with DPBS solution firstly, then incubated with C11-BODIPY reagent solution (5 μM) at 28°C for 15 min. Removed the remaining C11-BODIPY reagent and washed cells two times with DPBS solution. The fluorescence was quantified using Biosciences AccuriC6 flow cytometry (Becton Dickinson, United States) at the fluorescence intensity (488/510 nm).

Mitochondria-derived ROS determination

The level of mitochondria-derived ROS is determined with the MitoSOX™ Red mitochondrial superoxide indicator (Invitrogen, United States). Briefly, cells were washed twice with DPBS solution firstly, then incubated with MitoSOX reagent solution (5 μM) at 28°C for 15 min. Removed the remaining MitoSOX reagent and washed cells two times with DPBS solution. The fluorescence was quantified using Biosciences AccuriC6 flow cytometry (Becton Dickinson, United States) at the fluorescence intensity (510/580 nm).

Mitochondrial iron determination

Mitochondrial iron concentration was determined by RPA (rhodamine B-[(1,10-phenanthrolin-5-yl)aminocarbonyl] benzyl ester) (Squarix biotechnology, Germany). Deprotonated rhodamine B (rhodamine B base) was chosen for mitochondrial targeting and as a fluorophore, and was coupled with 4-(bromomethyl)-N-(1,10- phenanthrolin-5-yl) benzamide for iron chelation, which is the specific indicator allowing selective determination of mitochondrial chelatable iron in viable cells (Bapat et al., 2002; Gordan et al., 2020).

In brief, ZFL cells were washed with DPBS solution for two times and incubated with RPA dye solution (10 μM) at 28°C for 15 min. Cells were removed remaining RPA reagent and washed for two times with DPBS solution. Then photographed with Zeiss fluorescence confocal microscope (Zeiss, Germany) at proper fluorescence intensity (564/601 nm) and the density of fluorescence was analyzed by ImageJ analysis software (Tang et al., 2019).

Intracellular iron determination

Intracellular iron concentration was determined by PGSK fluorescence probe (Phen Green™ SK, Diacetate) (Invitrogen, United States). PGSK fluorescence is quenched upon binding chelatable iron and fluorescence intensity can be used to quantify the amount of chelatable iron when the remaining probe is removed (Petrat et al., 1999; Ramachandran et al., 2004; Siri-Angkul et al., 2021).

Briefly, ZFL cells were washed with DPBS solution for two times and incubated with PGSK dye solution (10 μM) at 28°C for 15 min. Cells were removed remaining PGSK reagent and washed for two times with DPBS solution. Ferrous ion in cytoplasm could quench the green fluorescence of cell. Then photographed with Zeiss fluorescence confocal microscope at proper fluorescence intensity (507/532 nm) and the density of fluorescence was analyzed by ImageJ analysis software.

RNA sequencing and analysis

Total RNA of ZFL cell was extracted using TRIzol Reagent according to the manufacturer's protocol (Invitrogen, United States). The concentration of total RNA was determined with a Qubit fluorometer (Life Technologies, United States). A microgram of RNA from each sample was used to prepare the mRNA-Seq library with the TruSeq RNA Sample Prep Kit (Illumina, United States) following the manufacturer's instructions and then sequenced with Illumina HiSeq 2,500 system.

RNA-seq reads were trimmed using Trimmomatic (Ver. 0.33 AVGQUAL:20 TRAILING:20 MINLEN:50). The clean Illumina paired-end reads of each sample were mapped to the annotated zebrafish genome (GRCz11) using HISAT2 aligner (Ver. 2.0.4). Cufflinks was used to count the reads for each gene and transformed to FPKM. Differentially expressed genes (DEGs) were determined using the edgeR package developed in R. Genes with log2FC > 1 and *p*_value <0.05 were up-regulated. Genes with log2FC < -1 and *p*_value <0.05 were down-regulated, GO enrichment and KEGG enrichment analysis for the DEGs were performed using ClusterProfiler package (cutoff, *p*-value < 0.05). Volcanic maps were generated using R.

Analysis of mitochondrial membrane potential

Mitochondrial membrane potential of ZFL cells were measured by JC-1 fluorescent probe (Beyotime, China). After treatment, cells were incubated with JC-1 working solution at 28°C for 30 min. Subsequently, cells were washed with JC-1 buffer solution for two times. Then photographed with Zeiss fluorescence confocal microscope at proper fluorescence intensity (485 and 590 nm). Results were expressed as the ratio of the red/green fluorescence intensity, which represented the degree of mitochondrial damage.

Mitochondrial tracking

Cells were plated on coverslips. After treatment, remove the medium from the dish and add the prewarmed MitoTracker probe-containing medium (Invitrogen, United States). Incubate the cells for 30 min at 28°C. Then replace the loading solution with fresh 4% PFA (Sangon, China) for 15 min. Washed cells two times with DPBS solution and photographed with Zeiss fluorescence confocal microscope at proper fluorescence intensity (644/665 nm).

Lysosomal tracking

Cells were plated on coverslips. After treatment, remove the medium from the dish and add the prewarmed LysoTracker™ Red DND-99 probe-containing medium (Invitrogen, United States). Incubate the cells for 1 h at 28°C. Then replace the loading solution with fresh 4% PFA for 15 min. Washed cells two times with DPBS solution and photographed with Zeiss fluorescence confocal microscope at proper fluorescence intensity (577/590 nm).

Statistical analysis

All data was performed at least three times. Bar graphs were plotted, and error bars were calculated using GraphPad Prism seven software (San Diego, United States). Statistical analysis was conducted using the Student's t-test or one-way ANOVA with Tukey's post hoc test. All values are shown as mean ± s.d., $p < 0.05$ were considered statistically significant. One asterisk, two asterisks and three asterisks indicate $p < 0.05$, $p < 0.01$ and $p < 0.001$, respectively.

Results

Hypoxia inhibits cell growth and ROS production, leading to iron deficiency in cytoplasm and mitochondria

We first investigated the effects of hypoxia on ZFL cells. At 21% O_2 (normoxia), ZFL cells grew well. When grew at 0.1% O_2 (hypoxia), however, cells grew poorly and began to die severely from the third day, with only a small fraction of the cells (about 20%) survived to the fourth day (Figures 1A,B). We then investigated the effect of hypoxia on ROS levels, since the main effect of hypoxia is oxidative damage. We examined the total ROS level by CM-H2DCFDA probe and found that ROS level was down-regulated under hypoxia stress (Figure 1C). Further investigation revealed that both mitochondrial-derived ROS and lipid peroxidation levels were reduced (Figures 1D,E). These results revealed that hypoxia is harmful to ZFL cells that can inhibit cell growth and ROS production.

Iron is the main driving force of REDOX reaction (Jomova and Valko, 2011). Western blotting showed that the expression of Ferritin, a cytoplasmic iron storage protein, was significantly reduced, suggesting loss of iron in the cytoplasm (Figure 1F). The same observation is also confirmed by chelatable Fe^{2+} sensitive probe PGSK, showing a significant reduction in chelatable iron (Figure 1G). Mitochondrial iron is required to trigger the ROS-oxidative stress via Fenton action (Levi and Rovida, 2009). The results revealed the expression of mitochondrial iron storage gene *fth31* was significantly reduced (Figure 1H), which was consistent with the results of specific probing of mitochondrial Fe^{2+} using RPA (Figure 1I). Collectively, hypoxia in the ZFL cells caused cytoplasmic and mitochondrial iron loss.

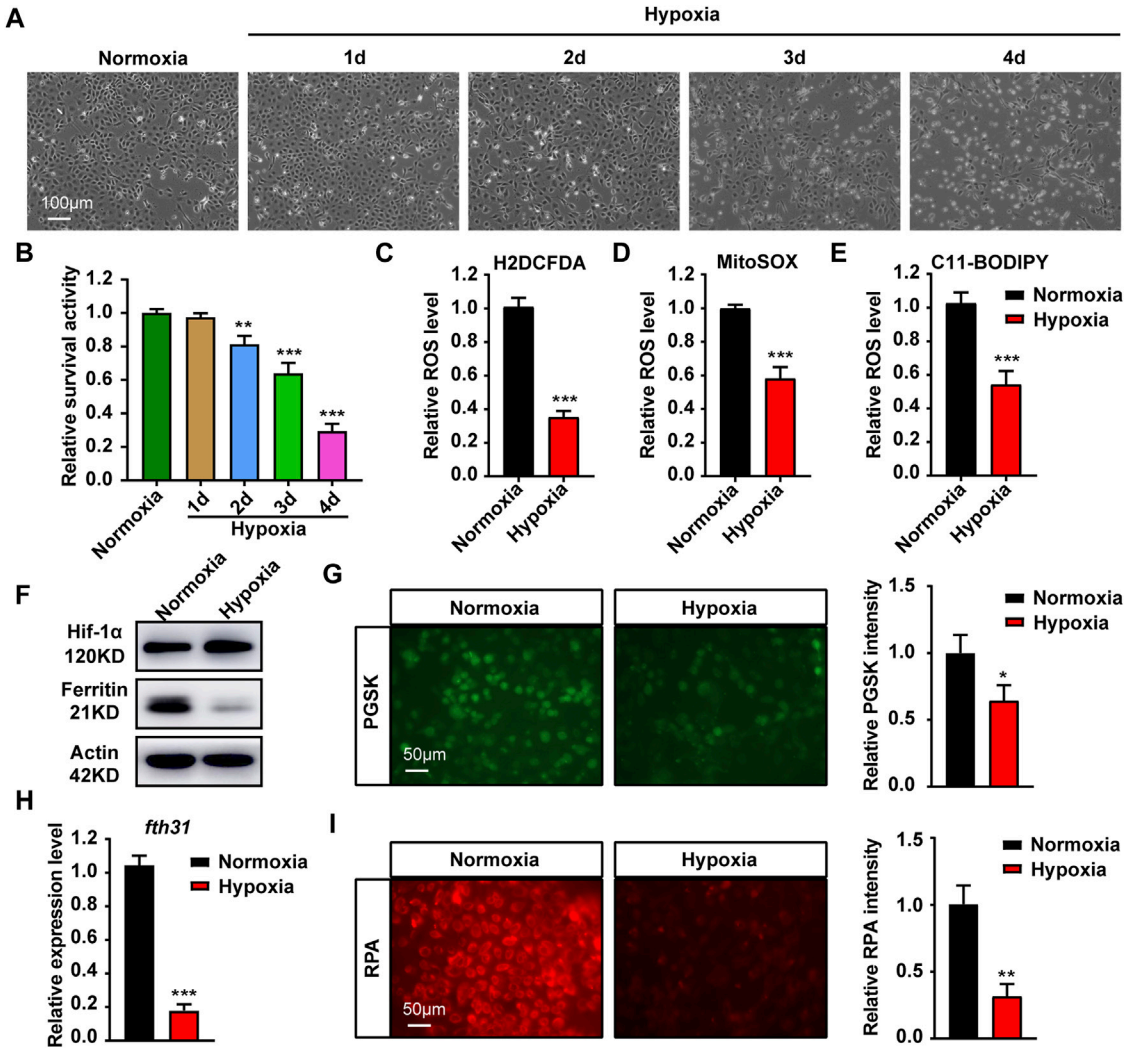

FIGURE 1
Hypoxia stress affects cell growth, ROS production and iron metabolism in cytoplasma and mitochondria. **(A)** Microscopic analysis of morphological changes of ZFL cells under normoxia or hypoxia for 1, 2, 3 and 4 d. **(B)** Cell Viability analyzed with PrestoBlue™ HS Cell Viability Regent under normoxia or hypoxia for 1, 2, 3 and 4 d. **(C–E)** Analysis of changes in total ROS **(C)**, mitochondrial-derived ROS **(D)** and lipid peroxidation **(E)** levels in cells with CM-H2DCFDA, MitoSOX and C11-BODIPY probe under normoxia and hypoxia for 3 days. **(F)** Western blot analysis of Ferritin expression in ZFL cells cultured under normoxia and hypoxia for 3 days. **(G)** Phen Green™ SK (PGSK) probe analysis and quantification of cytoplasmic free iron content in ZFL cells after treated under normoxia and hypoxia for 3 days. **(H)** The mRNA expression of mitochondrial iron storage gene *fth31* in ZFL cells quantified by real-time RT–PCR under normoxia and hypoxia for 3 days. **(I)** Fluorescence microscope with RPA red indicator analysis and quantification of mitochondrial iron content in ZFL cells treated under normoxia and hypoxia for 3 days. Normoxia was used as a control group for significance analysis. Error bars, mean ± s.d., $n = 3$ (biological replicates).

Iron homeostasis is important for ZFL cells to respond to hypoxic stress, which is independent of ferroptosis

To explore the effect of iron concentration on ZFL cell viability under hypoxia stress, FAC and DFO were used to supplement and chelate iron in ZFL cells respectively. The results showed that the proliferation capacity and survival rate of ZFL cells without FAC (0 mM) under hypoxia decreased gradually compared with the normoxia group (con group) (Figure 2A). However, the proliferation and survival rate of the hypoxic treated cells supplemented with proper amounts of FAC were significantly higher than that without exogenous iron supplementation (0 mM). Moreover, the proliferation and survival rate of FAC group (0.1, 0.25, 0.5 mM) were even higher than that of normoxia group after 2 days of hypoxia stress (Figure 2A).

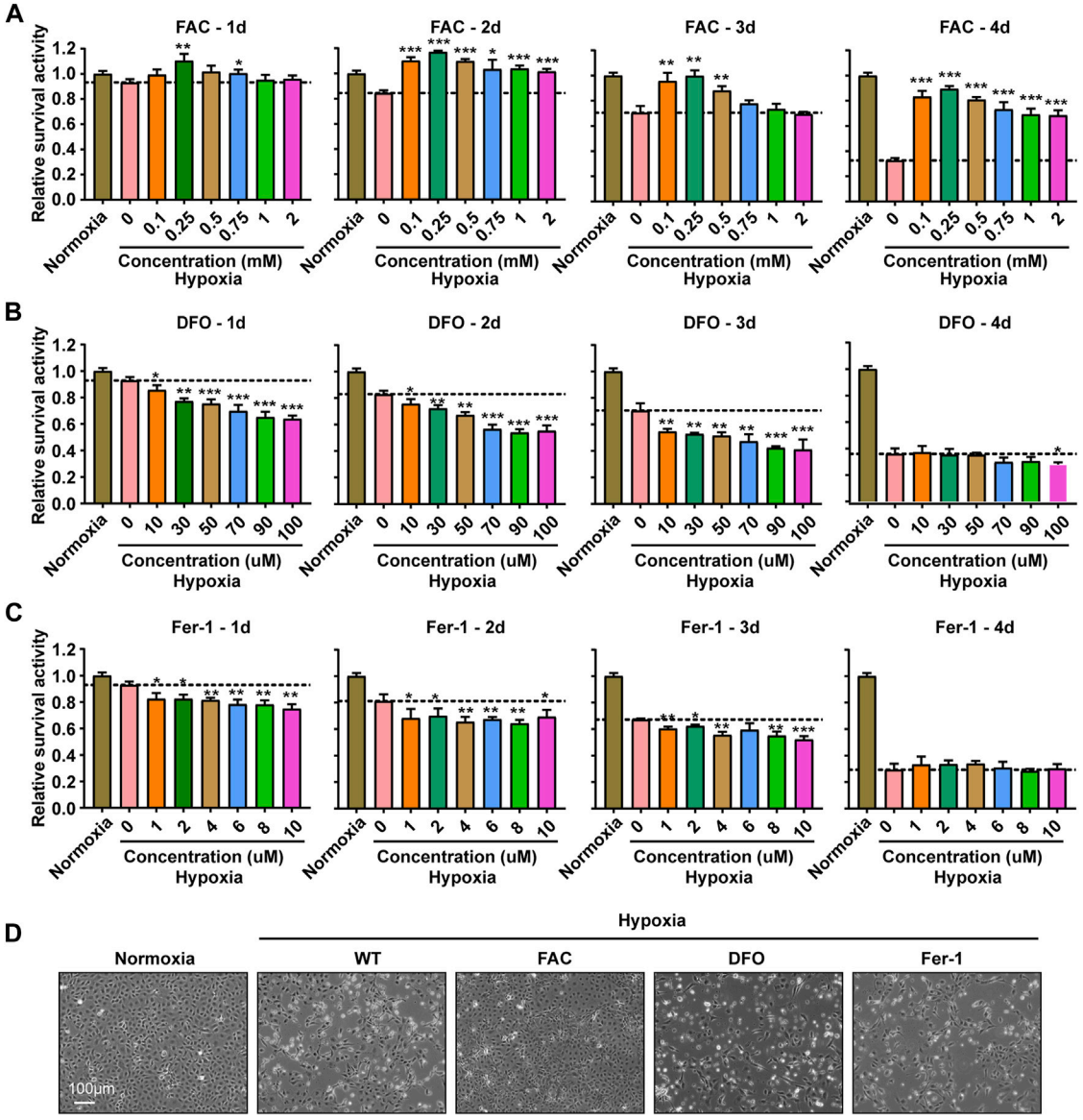

FIGURE 2
Iron supplementation could improve the survival activity of ZFL cells under hypoxia stress, but iron chelation and inhibition of ferroptosis could not. **(A–C)** Survival rate of ZFL cells analyzed with PrestoBlue™ HS Cell Viability Regent after treated with a series of concentrations of FAC **(A)**, DFO **(B)** and Fer-1 **(C)** under hypoxic stress from one to 4 days. Hypoxia 0 mM or hypoxia 0 μM was used as a control group for significance analysis. **(D)** The microscope analysis of morphology changes of ZFL cells under normoxia or treated with FAC (2.5 mM), DFO (10 μM) and Fer-1 (2.5 μM) under hypoxic stress for 3 days. Error bars, mean ± s.d., n = 3 (biological replicates).

Evenly, the survival rate of ZFL cells in the FAC group was about 2–3 times higher on the fourth day of the treatment compared with the hypoxic group without FAC treatment (0 mM) (Figure 2A). Conversely, DFO treatment resulted in non-proliferation and significantly reduced cell survival compared with the normoxia group and the hypoxia control group (0 μM) in the first 3 days (Figure 2B), indicating iron chelation exacerbate ZFL death under hypoxic stress. At the fourth day, both DFO treated and untreated cells exhibited poor survival rates under hypoxia (Figure 2B).

Ferroptosis is an iron- and ROS-dependent form of regulated cell death (RCD) (Xie et al., 2016). To investigate whether the cell damage under hypoxia is related to ferroptosis, we tried to rescue the damage with Fer-1 (Ferrostatin-1), an inhibitor of ferroptosis by inhibiting lipid peroxidation. The results

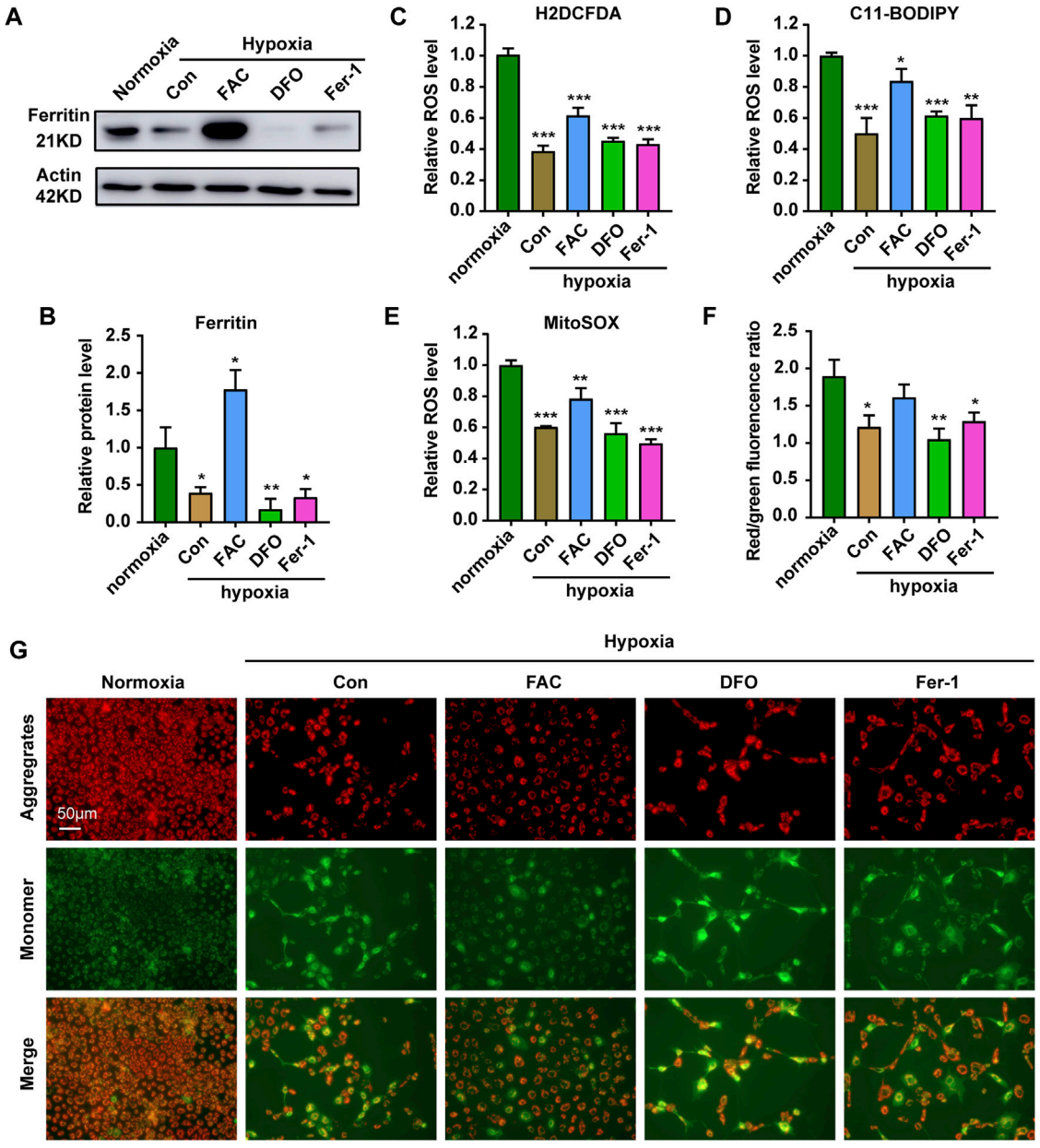

FIGURE 3
Iron supplementation can increase ROS level and reduce mitochondrial damage in cells under hypoxia stress. **(A,B)** Western blot analysis and quantification of Ferritin expression in ZFL cells cultured under normoxia and hypoxia treated with FAC, DFO and Fer-1 for 3 days. Actin as a loading control. **(C–E)** Analysis of changes in total ROS **(C)**, lipid peroxidation level **(D)** and mitochondrial-derived ROS **(E)** levels in cells with H2DCFDA, C11-BODIPY and MitoSOX probe under normoxia and hypoxia for 3 days. Cells under hypoxic stress were rescued with FAC (2.5 mM), DFO (10 μM) and Fer-1 (2.5 μM). **(F,G)** Quantitative results and representative images of cellular JC-1 fluorescence in normoxic cell and hypoxic cells treated with FAC (2.5 mM), DFO (10 μM) and Fer-1 (2.5 μM) under hypoxia stress. Normoxia was used as a control group for significance analysis. Error bars, mean ± s.d., n = 3 (biological replicates).

revealed that Fer-1 failed to rescue the hypoxia induced cell death, suggesting a ferroptosis independent death (Figure 2C). This observation was consistent with the decreased lipid peroxidation level (Figure 1E). Further morphological observation of cells showed that exogenous iron supplementation could prevent cell death and improve cell viability under hypoxia stress, while DFO and Fer-1 could not (Figure 2D).

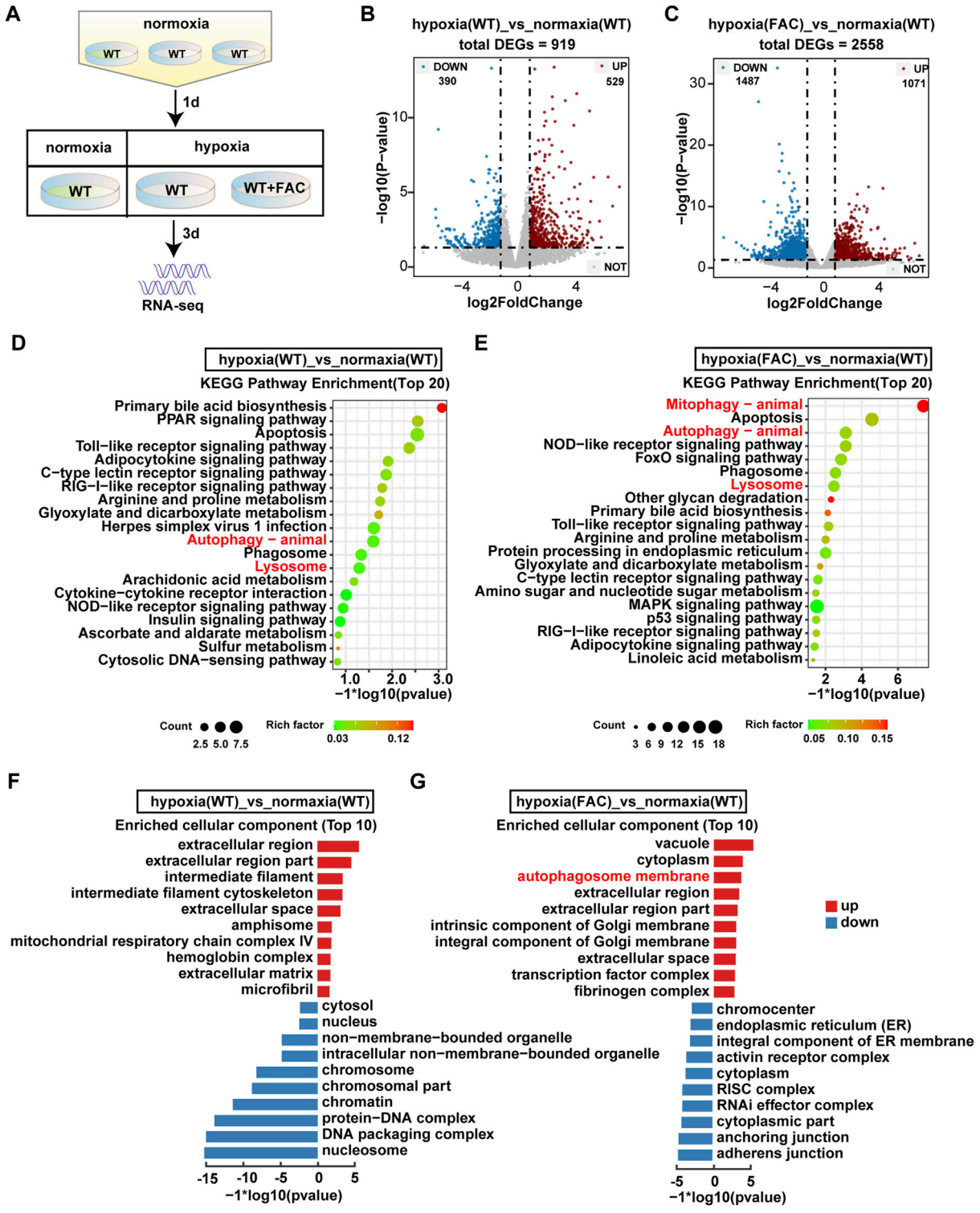

FIGURE 4
RNA-seq analysis revealed significant transecriptomic changes in hypoxia ZFL cell. **(A)** Flow chart of sampl processing for RNA-seq. WT: ZFL cell. WT + FAC: ZFL cell treated with FAC. **(B,C)** Volcanic map analysis of gene expression. UP: up-regulated differentially expressed gene; DOWN: down-regulated differentially expressed gene; NOT: non-differentially expressed gene. **(D,E)** The enriched KEGG pathways identified from up-regulated DEGs of hypoxia (WT) cell and hypoxia (FAC) cell compared with normoxia (WT) cell. **(F,G)** GO enrichment test on the DEGs of hypoxia (WT) cell and hypoxia (FAC) cell compared with normoxia (WT) cell.

Iron supplementation restored ROS levels and reduced mitochondrial damage of ZFL cells under hypoxia

To explore the role of iron in the ZFL cells response to hypoxic stress, we carried out further exploration. Firstly, WB showed that exogenous iron supplementation increased the expression level of iron-storing protein Ferritin, while iron chelation reduced Ferritin level, whereas addition of the ferroptosis inhibitor had no significant effect (Figures 3A,B). Accordingly, further examination of ROS levels showed that only exogenous iron supplementation partially restored the total ROS levels (Figure 3C). As iron is the cofactor of lipoxygenase, iron supplementation significantly increased the level of lipid peroxidation (Figure 3D). In addition, mitochondria are important source of reactive oxygen species (ROS) (Lenaz 2001). Iron supplementations increase mitochondrial-derived ROS level (Figure 3E). Indeed, iron supplementation restored the membrane potential of mitochondria and reduced the damage, which did not occur in DFO nor Fer-1 treatment (Figures 3F,G). These results indicated the importance of iron in maintaining the mitochondrial integrity and a certain amount of ROS level to sustain the physiological function of mitochondria and cell under hypoxic stress.

RNA-seq analysis revealed iron supplementation improved mitophagy

In order to explore how the FAC protect ZFL cells from death under hypoxia stress, we performed RNA-seq analysis (Figure 4A). There were totally 919 and 2,558 genes that were differentially expressed in WT and FAC cells under hypoxia compared with WT cells under normoxia (Figures 4B,C). KEGG enrichment analysis revealed that the pathway of autophagy and lysosome were significantly up-regulated in WT hypoxia cells compared with WT normoxia cells (Figure 4D). However, the enrichment analysis of hypoxic cells treated by FAC found that mitophagy pathway was the most significantly up-regulated pathway except autophagy and Lysosome pathways (Figure 4E). Furthermore, GO enrichment analysis showed that autophagosome membrane components were significantly upregulated in FAC treated hypoxia cell (Figures 4F,G). Taken together, these analyses suggest that maintaining mitochondrial normality is essential for ZFL cells to survive the hypoxia stress.

Iron supplementation restores mitochondrial function under hypoxia stress

Mitochondrial quality is controlled by the selective removal of damaged mitochondria through mitophagy (Ashrafi and Schwarz, 2013). Results indicated the expression of autophagy-related proteins LC3 and P62 were significantly up-regulated under hypoxia stress (Figures 5A–D). In combination, the expressions of LC3 and P62 after iron supplementation were weaker than those of chelated iron and inhibited ferroptosis (Figures 5A–D). Further exploration found that mitochondria were evenly distributed in the cytoplasm under hypoxia supplemented with iron, while the density of mitochondria decreased and clustered around the nucleus treated with DFO and Fer-1 (Figure 5E). The tracking of lysosomes revealed that the level of acid lysosomes increased and showed a large amount of aggregation in the control group (Figure 5F), indicating that hypoxia caused mitochondrial damage (Figures 5E,F). However, iron supplementation could improve mitochondrial damage caused by hypoxic stress, while DFO and Fer-1 did not.

ZF4 cells showed different patterns of iron responses under hypoxic condition

Given that the liver is an important organ for iron metabolism (Rishi and Subramaniam, 2017), we next sought to test whether other cell types had similar responses. Results showed that compared with ZFL cells, ZF4 cells had a better survival rate under hypoxia stress, with about 80% cells being alive on the fourth day (Figure 6A). The mRNA expression of genes related to iron metabolism showed completely opposite trends in ZF4 cells (Figure 6B), and also the protein levels of Hif1a and Ferritin (Figure 6C), indicating cytoplasmic and mitochondrial iron contents was increased in this cell line. Consistent with this, iron supplementation reduced the cell survival rate under hypoxia, while iron chelation or inhibition of ferroptosis showed no significant changes (Figures 6D,E). Further ROS level detection of cells showed that hypoxia stress reduced the general ROS level (Figure 6F), mitochondrial-derived ROS and lipid peroxidation levels (Figures 6G,H). In addition, iron supplementation can significantly increase ROS level, and even mitochondrial ROS and general ROS level exceed those of normoxic group (Figures 6F,H), which caused cell damage (Figures 6D,E). Chelation of iron or inhibition of ferroptosis slightly lowers ROS level. These results suggest that ZF4 cells have a different hypoxic stress response in terms of iron regulation compared with ZFL cells, indicating iron regulation under hypoxic response is cell type dependent.

Discussion

In this study, we revealed hypoxia causes iron loss in cytoplasm and mitochondria of the ZFL cells, which leads to mitochondrial damage and ultimately cell death. Iron supplementation inhibits hypoxia-induced cell death, increase ROS levels, reduce mitochondrial damage and restore mitochondrial function. Therefore, iron plays essential roles in mitochondrial responses to hypoxic stress in ZFL cells. The

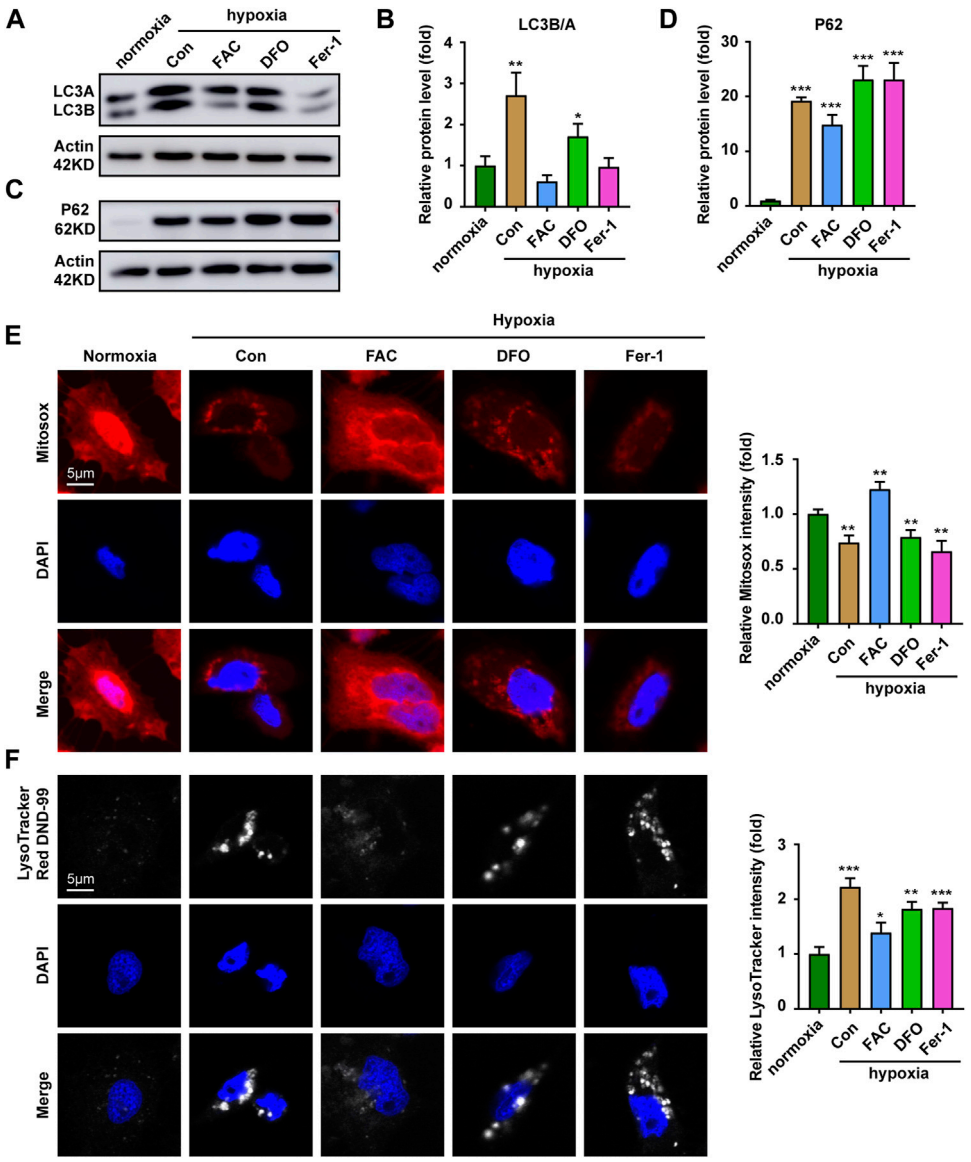

FIGURE 5
Iron supplementation increases the proportion of functioning mitochondria. **(A,B)** Western blot analysis and quantitative results of LC3 expression in ZFL cells cultured under normoxia and hypoxia treated with or without FAC (2.5 mM), DFO (10 μM) and Fer-1 (2.5 μM) for 3 days. Actin as a loading control. **(C,D)** Western blot analysis and quantitative results of P62 expression in ZFL cells cultured under normoxia and hypoxia treated with or without FAC (2.5 mM), DFO (10 μM) and Fer-1 (2.5 μM) for 3 days. Actin as a loading control. **(E)** Representative images and quantitative results of Mitotraker red Dye to visualize mitochondrial mass in normoxia cell and cell treated with or without FAC (2.5 mM), DFO (10 μM) and Fer-1 (2.5 μM) under hypoxia stress for 3 days. **(F)** Representative images and quantitative results of Lysotraker red DND-99 Dye to visualize acid lysosomal in normoxia cell and cell treated with or without FAC (2.5 mM), DFO (10 μM) and Fer-1 (2.5 μM) under hypoxia stress for 3 days. Normoxia was used as a control group for significance analysis. Error bars, mean ± s.d., n = 3 (biological replicates).

involvement of iron in hypoxia responses is also demonstrated by ZF4 cells in which higher cell survival rate is sustained with the elevation of expression of the iron storage proteins.

Oxygen and iron are important for the health of living organisms. Hypoxia imposes stress to cells and organisms, which occurs under both pathological and non-pathological conditions (Fuhrmann and Brune, 2017). Cells in living organisms adapt to hypoxia by changing metabolism, which is facilitated by changes in protein expression, mRNA or protein stability that occur at the level of transcription or translation (Solaini et al., 2010; Zhang et al., 2021). Multiple studies have clearly shown that oxygen homeostasis and iron metabolism are interlinked, such as the target of HIF, which play an important role in cell adaptation to low oxygen levels in normal and

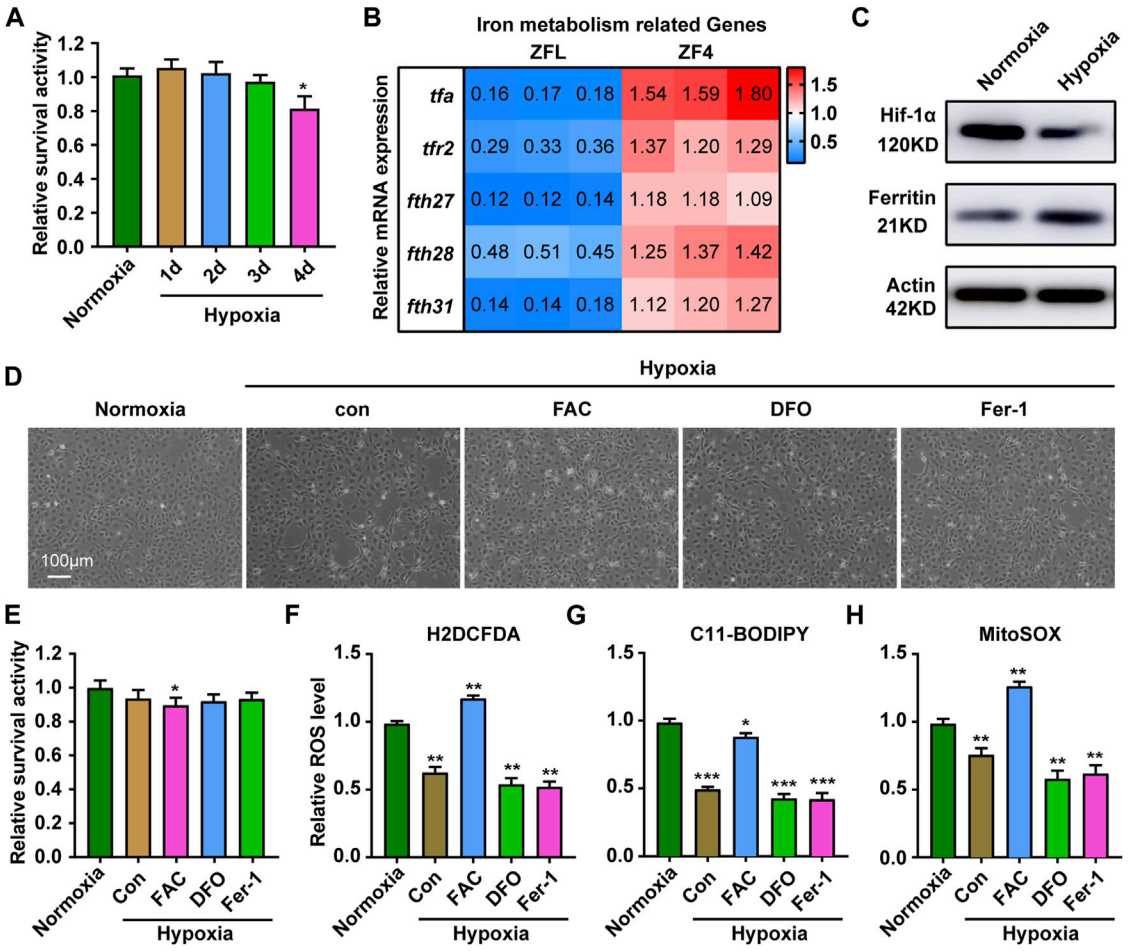

FIGURE 6
Response of ZF4 cells to hypoxic stress. **(A)** Cell Viability was analyzed with PrestoBlue™ HS Cell Viability Regent under normoxia or hypoxia treated for 1, 2, 3 and 4 d. **(B)** The mRNA expression of iron absorption and storage gene in ZFL cells was quantified by real-time RT–PCR under normoxia and hypoxia for 3 days. **(C)** Western blot analysis of Hif-1α and Ferritin expression in ZF4 cells cultured under normoxia and hypoxia for 3 days. **(D)** The microscope analysis of morphology changes in ZF4 cells under normoxia or hypoxia treated with or without FAC (2.5 mM), DFO (10 μM) and Fer-1 (2.5 μM) for 3 days. **(E)** Cell Viability was analyzed with PrestoBlue™ HS Cell Viability Regent under normoxia or hypoxia treated with or without FAC (2.5 mM), DFO (10 μM) and Fer-1 (2.5 μM). **(F–H)** Analysis of changes in general ROS **(F)**, mitochondrial-derived ROS **(G)** and lipid peroxidation **(H)** levels in cells with H2DCFDA, MitoSOX and C11-BODIPY probe under normoxia and hypoxia for 3 days. Cells under hypoxic stress were rescued with FAC (2.5 mM), DFO (10 μM) and Fer-1 (2.5 μM). Normoxia was used as a control group for significance analysis. Error bars, mean ± s.d., n = 3 (biological replicates).

damaged tissues, are involved in iron homeostasis (Shah and Xie, 2014; Xu et al., 2017; Yang et al., 2018; Han et al., 2022). The regulation between hypoxia and iron is complexed. On the one hand, hypoxia stress can cause iron homeostasis disorder (Aral et al., 2020; Hu et al., 2022); on the other hand, hypoxia is beneficial and can protect cells from death caused by abnormal iron metabolism (Ast et al., 2019; Fuhrmann et al., 2020; Ni et al., 2021). Our study also confirms that maintaining iron homeostasis is critical to respond to hypoxia stress. The expression of genes related to iron absorption and storage was significantly decreased in ZFL cells under hypoxia stress, which directly correlated hypoxia with iron metabolism.

Mitochondria are the main consumers of oxygen in cells and are severely affected by reduced oxygen utilization (Hamanaka and Chandel, 2009; Dan Dunn et al., 2015). Mitochondria require large amounts of iron for heme synthesis and iron-sulfur cluster maturation to form the electron transfer chain essential for oxidative phosphorylation (Hirota 2019). Thus, iron metabolism is essential for mitochondrial function and cell survival. Controlling the balance between iron availability and physiological hypoxia response is important to maintain intracellular homeostasis (Lakhal-Littleton and Robbins, 2017). ROS produced by the OXPHOS complex not only manifests as an unexpected escape of electrons from ETC and transfer to

molecular oxygen, but also recognized as an important medium of cellular physiological signaling to cope with hypoxia (Zhang et al., 2022). As we found, hypoxic stress reduced the free iron content of cytoplasmic and mitochondrial, thereby reducing the ROS levels of cytoplasmic and mitochondrial, which can be restored by iron supplementation. This suggests that the homeostasis of free iron and ROS levels is important to respond to hypoxia stress.

Mitochondrial ROS (mtROS) considered as an essential component of physiological cell communication (Shadel and Horvath, 2015). Large amounts of mtROS directly destroy proteins, lipids, and nucleic acids, while low levels of mtROS act as signaling molecules to adapt to stress (Sena and Chandel, 2012; Fuhrmann and Brune, 2017). Even lower levels of mtROS are required for normal cell homeostasis (Sena and Chandel, 2012). Therefore, mtROS are not categorically harmful (Kalogeris et al., 2014). In a hypoxic environment, mitochondrial biology is altered (Fuhrmann and Brune, 2017). Presumably, mitochondria try to reduce ROS formation to reduce the risk of macromolecular damage during hypoxia (Fuhrmann and Brune, 2017). Excessive mtROS promote mitochondrial dysfunction and inflammation leading to mitochondrial damage (Zhao et al., 2021). Mitophagy is an essential mitochondrial quality control mechanism that eliminates damaged mitochondria and the production of ROS (Su et al., 2022). Our study found that iron supplementation can reduce mitochondrial damage and restore ROS levels produced by mitochondria, thereby enhancing the ability of cells to respond to hypoxic stress. There is certainly a need to learn more about the communicating ability and distinct targets of ROS under hypoxia and explore how a gradual and time-dependent decrease of oxygen affects mitochondrial biology.

Several studies of different groups, including marine gastropods, fish, frog and turtles, have reported increases in antioxidants during hypoxia (Hermes-Lima and Zenteno-Savin, 2002). This response to increased antioxidant levels in low oxygen conditions is called preparation for oxidative stress (Oliveira et al., 2018). This adaptive mechanism refers to the increased expression and/or activity of antioxidant enzymes during hypoxia, which may attenuate the effects of increased ROS formation during hypoxia (Estrada-Cárdenas et al., 2021). However, it has been suggested that increased mitochondrial ROS formation induced by hypoxia may trigger the activation of antioxidant defenses during hypoxia limitation (Welker et al., 2013). Our study found that hypoxia stress for 3 days led to a decrease in mitochondrial ROS levels in ZFL cells. Therefore, further investigations should be directed to study the interplay between hypoxia, ROS production, antioxidant and tolerance to hypoxia.

In recent years, research on aquaculture shows that iron plays an important role in hypoxic response. The comparative transcriptomic analysis revealed abundant hypoxia response-related genes and their differential regulation mechanism in muscle and liver of different common carp strains under acute hypoxia, including HIFs (hypoxia-inducible factors), MAP kinase, iron ion binding, and heme binding (Suo et al., 2022). Morphological observation on three tilapia exhibited widespread hepatic and splenic inflammation with marked hemosiderin accumulations which is caused by direct tissue hypoxia and polycythemia-related iron deposition (Edwards et al., 2020). Gene ontology enrichment analyses revealed that genes up-regulated by hypoxia are primarily involved in cellular iron homeostasis in zebrafish larvae (Long et al., 2015). Therefore, targeting iron homeostasis is a potential strategy to protect aquaculture against environmental hypoxia. Our findings show that iron supplementation improves the ability of ZFL cells to resist hypoxic stress, which will facilitate future investigation on the hypoxia response mechanism and provide a solid theoretical basis for breeding projects in aquaculture.

Data availability statement

The raw data supporting the conclusions of this article will be made available by the authors, without undue reservation. All of the Illumina RNA sequencing data of this project have been deposited at NCBI under the accession no. BioProject PRJNA848069 (http://www.ncbi.nlm.nih.gov/sra/).

Author contributions

RH designed and performed the experiments. GL helped culture the cell. QX provided hypoxic equipment. LC conceived, designed, supervised the study, and with RH wrote the manuscript.

Funding

The work is supported by grants from the National Key Research and Development Program of China 2018YFD0900601 and the Natural Science Foundation of China (32130109).

Conflict of interest

The authors declare that the research was conducted in the absence of any commercial or financial relationships that could be construed as a potential conflict of interest.

Publisher's note

References

Abdel-Tawwab, M., Monier, M. N., Hoseinifar, S. H., and Faggio, C. (2019). Fish response to hypoxia stress: Growth, physiological, and immunological biomarkers. *Fish. Physiol. Biochem.* 45 (3), 997–1013. doi:10.1007/s10695-019-00614-9

Affonso, E. G., Polez, V. L., Corrêa, C. F., Mazon, A. F., Araújo, M. R., Moraes, G., et al. (2002). Blood parameters and metabolites in the teleost fish *Colossoma macropomum* exposed to sulfide or hypoxia. *Comp. Biochem. Physiol. C. Toxicol. Pharmacol.* 133 (3), 375–382. doi:10.1016/s1532-0456(02)00127-8

Aral, L. A., Ergün, M. A., Engin, A. B., Börcek, A., and Belen, H. B. (2020). Iron homeostasis is altered in response to hypoxia and hypothermic preconditioning in brain glial cells. *Turk. J. Med. Sci.* 50 (8), 2005–2016. doi:10.3906/sag-2003-41

Ashrafi, G., and Schwarz, T. L. (2013). The pathways of mitophagy for quality control and clearance of mitochondria. *Cell Death Differ.* 20 (1), 31–42. doi:10.1038/cdd.2012.81

Ast, T., Meisel, J. D., Patra, S., Wang, H., Grange, R. M. H., Kim, S. H., et al. (2019). Hypoxia rescues frataxin loss by restoring iron sulfur cluster biogenesis. *Cell* 177 (6), 1507–1521. e1516. doi:10.1016/j.cell.2019.03.045

Bapat, S., Post, J. A., Braam, B., Goldschmeding, R., Koomans, H. A., Verkleij, A. J., et al. (2002). Visualizing tubular lipid peroxidation in intact renal tissue in hypertensive rats. *J. Am. Soc. Nephrol.* 13 (12), 2990–2996. doi:10.1097/01.asn.0000036870.58561.81

Bickler, P. E., and Buck, L. T. (2007). Hypoxia tolerance in reptiles, amphibians, and fishes: life with variable oxygen availability. *Annu. Rev. Physiol.* 69, 145–170. doi:10.1146/annurev.physiol.69.031905.162529

Bogdan, A. R., Miyazawa, M., Hashimoto, K., and Tsuji, Y. (2016). Regulators of iron homeostasis: New players in metabolism, cell death, and disease. *Trends biochem. Sci.* 41 (3), 274–286. doi:10.1016/j.tibs.2015.11.012

Boggs, T. E., Friedman, J. S., and Gross, J. B. (2022). Alterations to cavefish red blood cells provide evidence of adaptation to reduced subterranean oxygen. *Sci. Rep.* 12 (1), 3735. doi:10.1038/s41598-022-07619-0

Dan Dunn, J., Alvarez, L. A., Zhang, X., and Soldati, T. (2015). Reactive oxygen species and mitochondria: A nexus of cellular homeostasis. *Redox Biol.* 6, 472–485. doi:10.1016/j.redox.2015.09.005

Diaz, R. J., and Rosenberg, R. (2008). Spreading dead zones and consequences for marine ecosystems. *Science* 321 (5891), 926–929. doi:10.1126/science.1156401

Duarte, T. L., Talbot, N. P., and Drakesmith, H. (2021). NRF2 and hypoxia-inducible factors: Key players in the redox control of systemic iron homeostasis. *Antioxid. Redox Signal.* 35 (6), 433–452. doi:10.1089/ars.2020.8148

Edwards, T. M., Mosie, I. J., Moore, B. C., Lobjoit, G., Schiavone, K., Bachman, R. E., et al. (2020). Low oxygen: A (tough) way of life for okavango fishes. *PLoS One* 15 (7), e0235667. doi:10.1371/journal.pone.0235667

Estrada-Cárdenas, P., Cruz-Moreno, D. G., González-Ruiz, R., Peregrino-Uriarte, A. B., Leyva-Carrillo, L., Camacho-Jiménez, L., et al. (2021). Combined hypoxia and high temperature affect differentially the response of antioxidant enzymes, glutathione and hydrogen peroxide in the white shrimp Litopenaeus vannamei. *Comp. Biochem. Physiol. A Mol. Integr. Physiol.* 254, 110909. doi:10.1016/j.cbpa.2021.110909

Fuhrmann, D. C., and Brüne, B. (2017). Mitochondrial composition and function under the control of hypoxia. *Redox Biol.* 12, 208–215. doi:10.1016/j.redox.2017.02.012

Fuhrmann, D. C., Mondorf, A., Beifuß, J., Jung, M., and Brüne, B. (2020). Hypoxia inhibits ferritinophagy, increases mitochondrial ferritin, and protects from ferroptosis. *Redox Biol.* 36, 101670. doi:10.1016/j.redox.2020.101670

Galluzzi, L., Kepp, O., Trojel-Hansen, C., and Kroemer, G. (2012). Mitochondrial control of cellular life, stress, and death. *Circ. Res.* 111 (9), 1198–1207. doi:10.1161/circresaha.112.268946

Gordan, R., Fefelova, N., Gwathmey, J. K., and Xie, L. H. (2020). Iron overload, oxidative stress and calcium mishandling in cardiomyocytes: Role of the mitochondrial permeability transition pore. *Antioxidants (Basel)* 9 (8), E758. doi:10.3390/antiox9080758

Hamanaka, R. B., and Chandel, N. S. (2009). Mitochondrial reactive oxygen species regulate hypoxic signaling. *Curr. Opin. Cell Biol.* 21 (6), 894–899. doi:10.1016/j.ceb.2009.08.005

Han, B., Meng, Y., Tian, H., Li, C., Li, Y., Gongbao, C., et al. (2022). Effects of acute hypoxic stress on physiological and hepatic metabolic responses of triploid rainbow trout (*Oncorhynchus mykiss*). *Front. Physiol.* 13, 921709. doi:10.3389/fphys.2022.921709

Hermes-Lima, M., and Zenteno-Savín, T. (2002). Animal response to drastic changes in oxygen availability and physiological oxidative stress. *Comp. Biochem. Physiol. C. Toxicol. Pharmacol.* 133 (4), 537–556. doi:10.1016/s1532-0456(02)00080-7

Hernansanz-Agustín, P., Izquierdo-Álvarez, A., Sánchez-Gómez, F. J., Ramos, E., Villa-Piña, T., Lamas, S., et al. (2014). Acute hypoxia produces a superoxide burst in cells. *Free Radic. Biol. Med.* 71, 146–156. doi:10.1016/j.freeradbiomed.2014.03.011

Hirota, K. (2019). An intimate crosstalk between iron homeostasis and oxygen metabolism regulated by the hypoxia-inducible factors (HIFs). *Free Radic. Biol. Med.* 133, 118–129. doi:10.1016/j.freeradbiomed.2018.07.018

Hu, D. W., Zhang, G., Lin, L., Yu, X. J., Wang, F., and Lin, Q. (2022). Dynamic changes in brain iron metabolism in neonatal rats after hypoxia-ischemia. *J. Stroke Cerebrovasc. Dis.* 31 (4), 106352. doi:10.1016/j.jstrokecerebrovasdis.2022.106352

Jomova, K., and Valko, M. (2011). Advances in metal-induced oxidative stress and human disease. *Toxicology* 283 (2-3), 65–87. doi:10.1016/j.tox.2011.03.001

Kalogeris, T., Bao, Y., and Korthuis, R. J. (2014). Mitochondrial reactive oxygen species: A double edged sword in ischemia/reperfusion vs preconditioning. *Redox Biol.* 2, 702–714. doi:10.1016/j.redox.2014.05.006

Kietzmann, T. (2019). Liver zonation in health and disease: Hypoxia and hypoxia-inducible transcription factors as concert masters. *Int. J. Mol. Sci.* 20 (9), E2347. doi:10.3390/ijms20092347

Kroemer, G., and Jäättelä, M. (2005). Lysosomes and autophagy in cell death control. *Nat. Rev. Cancer* 5 (11), 886–897. doi:10.1038/nrc1738

Lakhal-Littleton, S., and Robbins, P. A. (2017). The interplay between iron and oxygen homeostasis with a particular focus on the heart. *J. Appl. Physiol. (1985)* 123 (4), 967–973. doi:10.1152/japplphysiol.00237.2017

Lenaz, G. (2001). The mitochondrial production of reactive oxygen species: Mechanisms and implications in human pathology. *IUBMB Life* 52 (3-5), 159–164. doi:10.1080/15216540152845957

Levi, S., and Rovida, E. (2009). The role of iron in mitochondrial function. *Biochim. Biophys. Acta* 1790 (7), 629–636. doi:10.1016/j.bbagen.2008.09.008

Long, Y., Yan, J., Song, G., Li, X., Li, X., Li, Q., et al. (2015). Transcriptional events co-regulated by hypoxia and cold stresses in Zebrafish larvae. *BMC Genomics* 16 (1), 385. doi:10.1186/s12864-015-1560-y

Mazure, N. M., and Pouysségur, J. (2010). Hypoxia-induced autophagy: cell death or cell survival? *Curr. Opin. Cell Biol.* 22 (2), 177–180. doi:10.1016/j.ceb.2009.11.015

Michiels, C. (2004). Physiological and pathological responses to hypoxia. *Am. J. Pathol.* 164 (6), 1875–1882. doi:10.1016/s0002-9440(10)63747-9

Mittler, R. (2017). ROS are good. *Trends Plant Sci.* 22 (1), 11–19. doi:10.1016/j.tplants.2016.08.002

Murphy, M. P. (2009). How mitochondria produce reactive oxygen species. *Biochem. J.* 417 (1), 1–13. doi:10.1042/bj20081386

Ni, H. M., Williams, J. A., and Ding, W. X. (2015). Mitochondrial dynamics and mitochondrial quality control. *Redox Biol.* 4, 6–13. doi:10.1016/j.redox.2014.11.006

Ni, S., Yuan, Y., Qian, Z., Zhong, Z., Lv, T., Kuang, Y., et al. (2021). Hypoxia inhibits RANKL-induced ferritinophagy and protects osteoclasts from ferroptosis. *Free Radic. Biol. Med.* 169, 271–282. doi:10.1016/j.freeradbiomed.2021.04.027

Oliveira, M. F., Geihs, M. A., França, T. F. A., Moreira, D. C., and Hermes-Lima, M. (2018). Is "preparation for oxidative stress" a case of physiological conditioning hormesis? *Front. Physiol.* 9, 945. doi:10.3389/fphys.2018.00945

Palikaras, K., Lionaki, E., and Tavernarakis, N. (2018). Mechanisms of mitophagy in cellular homeostasis, physiology and pathology. *Nat. Cell Biol.* 20 (9), 1013–1022. doi:10.1038/s41556-018-0176-2

Petrat, F., Rauen, U., and de Groot, H. (1999). Determination of the chelatable iron pool of isolated rat hepatocytes by digital fluorescence microscopy using the fluorescent probe, phen green SK. *Hepatology* 29 (4), 1171–1179. doi:10.1002/hep.510290435

Qiang, J., Zhong, C. Y., Bao, J. W., Liang, M., Liang, C., Li, H. X., et al. (2019). The effects of temperature and dissolved oxygen on the growth, survival and oxidative capacity of newly hatched hybrid yellow catfish larvae (Tachysurus fulvidraco♀ × Pseudobagrus vachelliii♂). *J. Therm. Biol.* 86, 102436. doi:10.1016/j.jtherbio.2019.102436

Ramachandran, A., Ceaser, E., and Darley-Usmar, V. M. (2004). Chronic exposure to nitric oxide alters the free iron pool in endothelial cells: Role of mitochondrial respiratory complexes and heat shock proteins. *Proc. Natl. Acad. Sci. U. S. A.* 101 (1), 384–389. doi:10.1073/pnas.0304653101

Richards, J. G. (2011). Physiological, behavioral and biochemical adaptations of intertidal fishes to hypoxia. *J. Exp. Biol.* 214 (Pt 2), 191–199. doi:10.1242/jeb.047951

Rishi, G., and Subramaniam, V. N. (2017). The liver in regulation of iron homeostasis. *Am. J. Physiol. Gastrointest. Liver Physiol.* 313 (3), G157–G165. doi:10.1152/ajpgi.00004.2017

Rouault, T. A. (2006). The role of iron regulatory proteins in mammalian iron homeostasis and disease. *Nat. Chem. Biol.* 2 (8), 406–414. doi:10.1038/nchembio807

Salahudeen, A. A., and Bruick, R. K. (2009). Maintaining mammalian iron and oxygen homeostasis: Sensors, regulation, and cross-talk. *Ann. N. Y. Acad. Sci.* 1177, 30–38. doi:10.1111/j.1749-6632.2009.05038.x

Schieber, M., and Chandel, N. S. (2014). ROS function in redox signaling and oxidative stress. *Curr. Biol.* 24 (10), R453–R462. doi:10.1016/j.cub.2014.03.034

Sena, L. A., and Chandel, N. S. (2012). Physiological roles of mitochondrial reactive oxygen species. *Mol. Cell* 48 (2), 158–167. doi:10.1016/j.molcel.2012.09.025

Shadel, G. S., and Horvath, T. L. (2015). Mitochondrial ROS signaling in organismal homeostasis. *Cell* 163 (3), 560–569. doi:10.1016/j.cell.2015.10.001

Shah, Y. M., and Xie, L. (2014). Hypoxia-inducible factors link iron homeostasis and erythropoiesis. *Gastroenterology* 146 (3), 630–642. doi:10.1053/j.gastro.2013.12.031

Siri-Angkul, N., Song, Z., Fefelova, N., Gwathmey, J. K., Chattipakorn, S. C., Qu, Z., et al. (2021). Activation of TRPC (transient receptor potential canonical) channel currents in iron overloaded cardiac myocytes. *Circ. Arrhythm. Electrophysiol.* 14 (2), e009291. doi:10.1161/circep.120.009291

Solaini, G., Baracca, A., Lenaz, G., and Sgarbi, G. (2010). Hypoxia and mitochondrial oxidative metabolism. *Biochim. Biophys. Acta* 1797 (6-7), 1171–1177. doi:10.1016/j.bbabio.2010.02.011

Su, L., Zhang, J., Gomez, H., Kellum, J. A., and Peng, Z. (2022). Mitochondria ROS and mitophagy in acute kidney injury. *Autophagy* 19, 1–14. doi:10.1080/15548627.2022.2084862

Suo, N., Zhou, Z. X., Xu, J., Cao, D. C., Wu, B. Y., Zhang, H. Y., et al. (2022). Transcriptome analysis reveals molecular underpinnings of common carp (*Cyprinus carpio*) under hypoxia stress. *Front. Genet.* 13, 907944. doi:10.3389/fgene.2022.907944

Tang, M., Huang, Z., Luo, X., Liu, M., Wang, L., Qi, Z., et al. (2019). Ferritinophagy activation and sideroflexin1-dependent mitochondria iron overload is involved in apelin-13-induced cardiomyocytes hypertrophy. *Free Radic. Biol. Med.* 134, 445–457. doi:10.1016/j.freeradbiomed.2019.01.052

Ting Zhang, T., Liu, Q., Gao, W., Sehgal, S. A., and Wu, H. (2021). The multifaceted regulation of mitophagy by endogenous metabolites. *Autophagy* 18, 1216–1239. doi:10.1080/15548627.2021.1975914

Valavanidis, A., Vlahogianni, T., Dassenakis, M., and Scoullos, M. (2006). Molecular biomarkers of oxidative stress in aquatic organisms in relation to toxic environmental pollutants. *Ecotoxicol. Environ. Saf.* 64 (2), 178–189. doi:10.1016/j.ecoenv.2005.03.013

Walter, P. B., Knutson, M. D., Paler-Martinez, A., Lee, S., Xu, Y., Viteri, F. E., et al. (2002). Iron deficiency and iron excess damage mitochondria and mitochondrial DNA in rats. *Proc. Natl. Acad. Sci. U. S. A.* 99 (4), 2264–2269. doi:10.1073/pnas.261708798

Wei, S., Qiu, T., Yao, X., Wang, N., Jiang, L., Jia, X., et al. (2020). Arsenic induces pancreatic dysfunction and ferroptosis via mitochondrial ROS-autophagy-lysosomal pathway. *J. Hazard. Mat.* 384, 121390. doi:10.1016/j.jhazmat.2019.121390

Welker, A. F., Moreira, D. C., Campos É, G., and Hermes-Lima, M. (2013). Role of redox metabolism for adaptation of aquatic animals to drastic changes in oxygen availability. *Comp. Biochem. Physiol. A Mol. Integr. Physiol.* 165 (4), 384–404. doi:10.1016/j.cbpa.2013.04.003

Xie, Y., Hou, W., Song, X., Yu, Y., Huang, J., Sun, X., et al. (2016). Ferroptosis: Process and function. *Cell Death Differ.* 23 (3), 369–379. doi:10.1038/cdd.2015.158

Xu, M. M., Wang, J., and Xie, J. X. (2017). Regulation of iron metabolism by hypoxia-inducible factors. *Sheng Li Xue Bao* 69 (5), 598–610.

Yang, L., Wang, D., Wang, X. T., Lu, Y. P., and Zhu, L. (2018). The roles of hypoxia-inducible Factor-1 and iron regulatory protein 1 in iron uptake induced by acute hypoxia. *Biochem. Biophys. Res. Commun.* 507 (1-4), 128–135. doi:10.1016/j.bbrc.2018.10.185

Zhang, H., Bosch-Marce, M., Shimoda, L. A., Tan, Y. S., Baek, J. H., Wesley, J. B., et al. (2008). Mitochondrial autophagy is an HIF-1-dependent adaptive metabolic response to hypoxia. *J. Biol. Chem.* 283 (16), 10892–10903. doi:10.1074/jbc.M800102200

Zhang, H., Zhao, X., Guo, Y., Chen, R., He, J., Li, L., et al. (2021). Hypoxia regulates overall mRNA homeostasis by inducing Met(1)-linked linear ubiquitination of AGO2 in cancer cells. *Nat. Commun.* 12 (1), 5416. doi:10.1038/s41467-021-25739-5

Zhang, B., Pan, C., Feng, C., Yan, C., Yu, Y., Chen, Z., et al. (2022). Role of mitochondrial reactive oxygen species in homeostasis regulation. *Redox Rep.* 27 (1), 45–52. doi:10.1080/13510002.2022.2046423

Zhang, Y., and Wong, H. S. (2021). Are mitochondria the main contributor of reactive oxygen species in cells? *J. Exp. Biol.* 224 (5), jeb221606. doi:10.1242/jeb.221606

Zhao, M., Wang, Y., Li, L., Liu, S., Wang, C., Yuan, Y., et al. (2021). Mitochondrial ROS promote mitochondrial dysfunction and inflammation in ischemic acute kidney injury by disrupting TFAM-mediated mtDNA maintenance. *Theranostics* 11 (4), 1845–1863. doi:10.7150/thno.50905

frontiers | Frontiers in Physiology

TYPE Original Research
PUBLISHED 13 October 2022
DOI 10.3389/fphys.2022.991366

OPEN ACCESS

EDITED BY
Yu-Hung Lin,
National Pingtung University of Science and Technology, Taiwan

REVIEWED BY
Sandra Imbrogno,
University of Calabria, Italy
Neeraj Kumar,
National Institute of Abiotic Stress Management (ICAR), India

*CORRESPONDENCE
Amrutlal K. Patel,
jd2@gbrc.res.in
Chaitanya G. Joshi,
director@gbrc.res.in

SPECIALTY SECTION
This article was submitted to Aquatic Physiology, a section of the journal Frontiers in Physiology

RECEIVED 11 July 2022
ACCEPTED 28 September 2022
PUBLISHED 13 October 2022

CITATION
Harshini V, Shukla N, Raval I, Kumar S, Shrivastava V, Patel AK and Joshi CG (2022), Kidney transcriptome response to salinity adaptation in Labeo rohita. *Front. Physiol.* 13:991366. doi: 10.3389/fphys.2022.991366

Kidney transcriptome response to salinity adaptation in *Labeo rohita*

Vemula Harshini[1], Nitin Shukla[1], Ishan Raval[1], Sujit Kumar[2], Vivek Shrivastava[2], Amrutlal K. Patel[1]* and Chaitanya G. Joshi[1]*

[1]Gujarat Biotechnology Research Centre, Gandhinagar, Gujarat, India, [2]Postgraduate Institute of Fisheries Education and Research, Kamdhenu University, Himmatnagar, Gujarat, India

The increasing salinization of freshwater resources, owing to global warming, has caused concern to freshwater aquaculturists. In this regard, the present study is aimed at economically important freshwater fish, *L. rohita* (rohu) adapting to varying degrees of salinity concentrations. The RNA-seq analysis of kidney tissue samples of *L. rohita* maintained at 2, 4, 6, and 8 ppt salinity was performed, and differentially expressed genes involved in various pathways were studied. A total of 755, 834, 738, and 716 transcripts were downregulated and 660, 926, 576, and 908 transcripts were up-regulated in 2, 4, 6, and 8 ppt salinity treatment groups, respectively, with reference to the control. Gene ontology enrichment analysis categorized the differentially expressed genes into 69, 154, 92, and 157 numbers of biological processes with the p value < 0.05 for 2, 4, 6, and 8 ppt salinity groups, respectively, based on gene functions. The present study found 26 differentially expressed solute carrier family genes involved in ion transportation and glucose transportation which play a significant role in osmoregulation. In addition, the upregulation of inositol-3-phosphate synthase 1A (INO1) enzyme indicated the role of osmolytes in salinity acclimatization of *L. rohita*. Apart from this, the study has also found a significant number of genes involved in the pathways related to salinity adaptation including energy metabolism, calcium ion regulation, immune response, structural reorganization, and apoptosis. The kidney transcriptome analysis elucidates a step forward in understanding the osmoregulatory process in *L. rohita* and their adaptation to salinity changes.

KEYWORDS

***L. rohita*, salinity adaptation, transcriptome, kidney, differential gene expression**

Introduction

One of the main environmental factors affecting the spatial distribution of aquatic life and a significant selective force for local adaptation is salinity (Lemaire et al., 2002; Thiyagarajan et al., 2003; Aktas and Cavdar, 2012). Fish tolerance to variation in salinity depends on their osmoregulatory mechanism, which plays a key role in the maintenance of body fluid homeostasis for survival and efficiency (Rubio et al., 2005; Hwang and Lee, 2007). The kidney is one of the most important osmoregulatory organs, which counterbalances the

diffusive loss of major mono and divalent ions through the gills and skin. In freshwater fishes, the kidney produces large volumes of diluted urine by re-absorption of major ions in proximal, distal, convoluted tubules and collecting ducts (Takvam et al., 2021). In recent times, the impact of climate change has resulted in increased salinity levels in fresh water resources (Chong-Robles et al., 2014; Yang et al., 2016; Haque et al., 2020), causing serious effects on the aquatic ecosystem *via* osmotic and ionic stresses on aquatic life.

L. rohita (rohu), a local freshwater fish, is distributed throughout South Asia, Southeast Asia, Sri Lanka, Japan, China, the Philippines, Malaysia, and Nepal. Rohu has significantly higher muscle protein content than other major carps (Shakir et al., 2013), the species commands a good market price, and consumer demand makes it an economically important fish. Previous studies in *L. rohita* have investigated the effects of salinity variations on growth performance, hematological and histological changes, and survival (Baliarsingh et al., 2018; Hoque et al., 2020; Murmu et al., 2020); however, the molecular mechanisms involved in salinity adaptation are not well understood.

Studies on the identification of candidate genes involved in adaptation to salinity changes (Zhang et al., 2017) and transcriptome of osmoregulatory organs in fresh and marine water fishes on salinity variations as environmental stressors have been undertaken. The studies highlighted candidate genes of the kidney involved in several pathways such as oxidative phosphorylation, metabolic process, inflammatory response (Chen et al., 2021), energy metabolism, immune-related pathways, and signaling pathways (Xu et al., 2015). In addition, several differentially expressed solute carrier family (SLC) genes as candidate genes in osmotic regulation under salinity stress (Nguyen et al., 2016; Zhang et al., 2017; Zhao et al., 2021) and the myosin and keratin family genes involved in cytoskeletal reorganization (Nguyen et al., 2016; Zhang et al., 2017) have been reported. These studies indicated that fish have differential regulatory mechanisms toward salinity adaptation. Therefore, the present study was conducted to explore the underlying mechanisms of *L. rohita* during salinity tolerance using RNA-seq technology.

The current study is focused on transcriptomic characterization of the *L. rohita* kidney to gradually increased salinity conditions. The aim was to compare the differential expression patterns of genes among varying salt concentrations and identify the genes that play a key role in salinity tolerance. The findings of this study provide a better understanding of how *L. rohita* regulates the genes and pathways to adapt to elevated salinity concentrations.

Materials and methods

Salinity stress experimental design

The experiment was conducted at the Postgraduate Institute of Fisheries Education and Research, Kamdhenu University, Himmatnagar, Gujarat. Healthy *L. rohita* fingerlings (>10 g) were acquired and acclimatized to laboratory conditions in 150 L tanks (15 fingerlings/tank) for 7 days with continuous aeration at 27°C ± 5°C. A constant stocking density of 1 gm/L was maintained throughout the experiment, and the water level was maintained accordingly. Feeding was carried out three times a day at the rate of 5% of the body weight. Unused feed and fecal matter were siphoned out, and 25% of water was replaced daily. Later, the fingerlings were randomly divided into control and salinity treatment groups. The experiment was performed in triplicate.

The control group was maintained at 0 ppt throughout the experiment, while in the treatment group, it was gradually increased (1 ppt/day) to the specified salinity (2, 4, 6, and 8 ppt) and thereafter maintained at the particular salinity for 6 days, and on the sixth day, three fish were randomly sampled from the control and treatment groups. Then, the salinity was increased to the next level, and the process was repeated until the last set of samples was collected at 8 ppt on the 32nd day from the start of the experiment. Survival of the fingerlings was observed in the control and treated groups. During experimentation, three fishes from each replicate were randomly selected in respective time intervals according to the salt concentrations and sampled immediately. The collected kidney tissue samples were stored at −80°C in RNA until further RNA extraction. Samples from the control group were also collected simultaneously during sampling at specific salinity. Among the collected samples, one sample each in the control (K1C2, K1C4, K1C6, and K1C8) and treatment (K1T2, K1T4, K1T6, and K1T8) groups at 2, 4, 6, and 8 ppt were processed for the transcriptomic analysis.

RNA extraction, library construction, and RNA sequencing

Total RNA isolation was carried out using the RNeasy Plus Mini Kit (QIAGEN, Germany), according to the manufacturer's protocol, and the purity of the isolated RNA was checked with the QIAxpert instrument (QIAGEN, Germany). The quantity and integrity of the RNA were assessed with the Qubit 4 Fluorometer (Thermo Fisher Scientific, United States) and Agilent 2100 Bioanalyzer system (Agilent technologies, California, United States), respectively. Depletion of rRNA was carried out using Low Input RiboMinus Eukaryote System v2 (Thermo Fisher, Massachusetts, United States). Eight sequencing libraries were generated from K1C2, K1C4, K1C6, K1C8, K1T2, K1T4, K1T6, and K1T8 using the TruSeq Stranded Total RNA Library Prep Kit (Illumina, California, United States), following the manufacturer's instructions, and index codes were added to attribute the sequences of each sample. After purification of enriched DNA fragments, high-throughput sequencing (Miseq/NovaSeq 6000) was performed using

TABLE 1 Details of the biosample and short-read archive (SRA) submission of the *L. rohita* kidney transcriptome to the NCBI along with the mapping percentage against the reference genome.

Bioproject accession no.	Sample name	Biosample accession no.	Study	Accession no.	Mapping %
PRJNA853878	K1C2	SAMN29416598	SRP384125	SRR19895145	95.51
	K1C4	SAMN29416599	SRP384125	SRR19895144	87.41
	K1C6	SAMN29416600	SRP384125	SRR19895143	83.91
	K1C8	SAMN29416601	SRP384125	SRR19895142	92.89
	K1T2	SAMN29416602	SRP384125	SRR19895141	95.51
	K1T4	SAMN29416603	SRP384125	SRR19895140	85.92
	K1T6	SAMN29416604	SRP384125	SRR19895139	85.89
	K1T8	SAMN29416605	SRP384125	SRR19895138	90.2

paired-end chemistry. The raw sequences were submitted to NCBI Short Read Archive (SRA; Table 1).

Assembly and differential gene expression analysis

Quality check of data was performed by FastQC (v0.11.9). After quality control, reads were aligned against the reference genome *L. rohita* (Jayanti) breed (GenBank assembly accession: GCA_004120215.1) with segemehl (v0.2.0-418). The reference genome and gene model annotation files (GCA_004120215.1_ASM412021v1) were downloaded from the NCBI, and an index of the reference genome was generated. The read numbers mapped to each gene were counted by featureCounts (v2.0.1). The gene expression levels of each gene were estimated by reads per kilobase of exon per million mapped reads (RPKM). The count data were simulated using the seqgendiff v1.2.3 R package (Gerard, 2020), the analysis of differentially expressed genes between control and salinity-challenged groups was performed with the DESeq R package (v1.34.0), and the genes with the significant *p*-value (<0.05) applied as the threshold were considered as differentially expressed genes (DEGs).

Enrichment and network analysis

To assess the biological significance of up- and downregulated genes, GO enrichment was performed using ClueGO in Cytoscape (v3.9.1). ClueGO performs functional enrichment in terms of biological processes or pathways which are visualized and grouped to form a network. This highlights the relationship between the enriched genes and their ontology. The default parameters used for ontology were two-sided hypergeometric tests for both enrichment and depletion. Network specificity was set to detail with a kappa score (0.4). Benjamini–Hochberg methodology was applied for statistical pV correction. The DEGs having log2FC < −0.5 OR log2FC > 0.5 and *p*-value <0.05 were considered for network analysis, and in order to increase the readability of the text, the networks were manually arranged.

Results

Survivability of *L. rohita* under different salinity concentrations

The survival rate of the fingerlings was found to be 100% up to 8 ppt salinity concentration. This might be due to the slow and gradual increase of the salinity, which helped the fingerlings to adapt to the increased salinity concentrations.

Data preprocessing and identification of differentially expressed genes

Alignment of reads against the *L. rohita* (Jayanti) reference genome revealed mapping percentages that varied from 83.91% to 95.51% for the control and salinity-challenged groups, respectively (Table 1). A total of 37,462 transcripts were obtained in both the control and treatment groups. The total number of differentially expressed genes (DEGs) (up and down) is presented in Figure 1 with the threshold of a *p*-value < 0.05 and log2 fold change > ± 0.5. The entire list of the DEGs is given in Supplementary Tables S1–S4. The volcano plots representing the differentially expressed genes for 2, 4, 6, and 8 ppt are presented in Figures 2–5, respectively. The hierarchical clustering properly divided the control samples from the salinity-challenged samples representing the differential regulation of genes at 2, 4, 6, and 8 ppt based on normalized counts for differentially expressed mRNA libraries of differentially expressed genes (Supplementary Figures S1–S4).

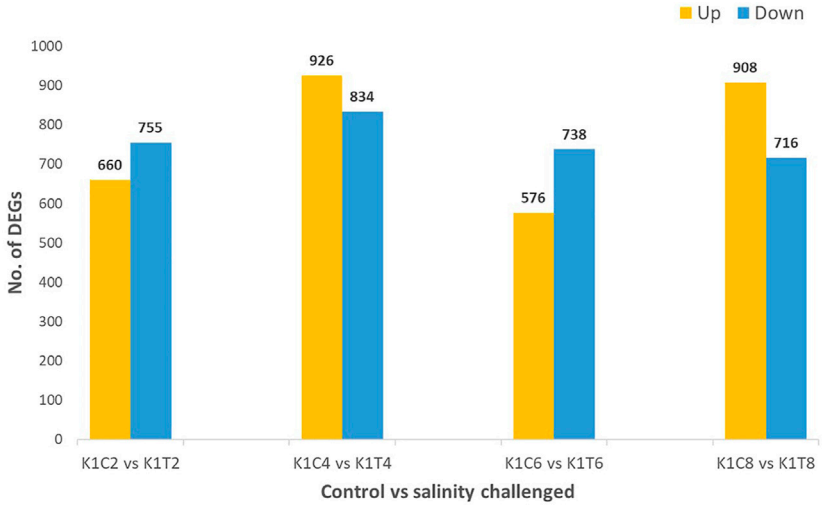

FIGURE 1
Differentially expressed (up- and downregulated) genes of the *L. rohita* kidney transcriptome at 2, 4, 6, and 8 ppt salinity concentrations (K1C2, K1C4, K1C6, and K1C8; and K1T2, K1T4, K1T6, and K1T8 are the control and salinity treatment groups at 2, 4, 6, and 8 ppt salt concentrations, respectively).

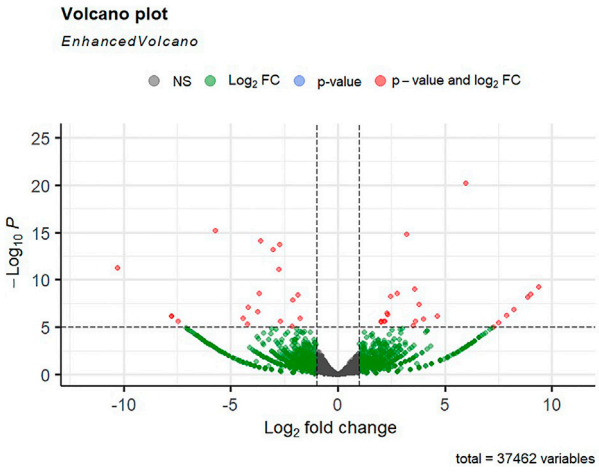

FIGURE 2
Volcano plot of differentially expressed genes identified between control and 2-ppt salinity group rohu fish. The *X*-axis signifies the Log2 fold change value, and the *Y*-axis indicates the –Log10 *p* value. The ash color dots indicate no significant difference between the two groups. The green dots indicate moderately significant and red dots highly significant differential genes.

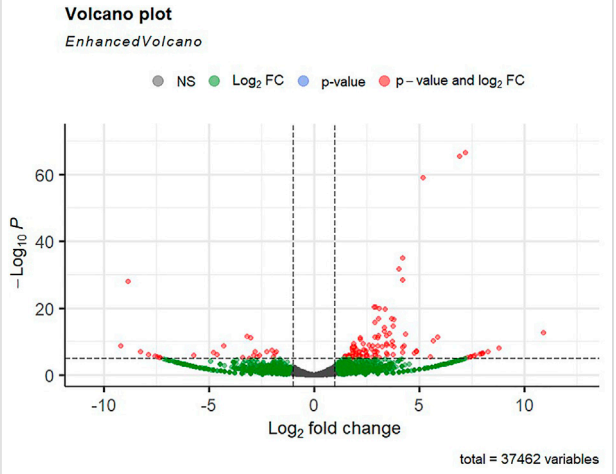

FIGURE 3
Volcano plot of differentially expressed genes identified between control and the 4-ppt salinity group rohu fish. The *X*-axis signifies the Log2 fold change value, and the *Y*-axis indicates the –Log10 *p* value. The ash color dots indicate no significant difference between the two groups. The green dots indicate moderately significant and red dots highly significant differential genes.

Network and gene ontology analysis

The differential gene expression analysis provided information regarding the genes functionally related to the salinity stress in *L. rohita*. However, in the differential expression analysis, each gene is considered independently, while in reality, the expressions of gene and gene products are interconnected and function in networks. Hence, to discover the

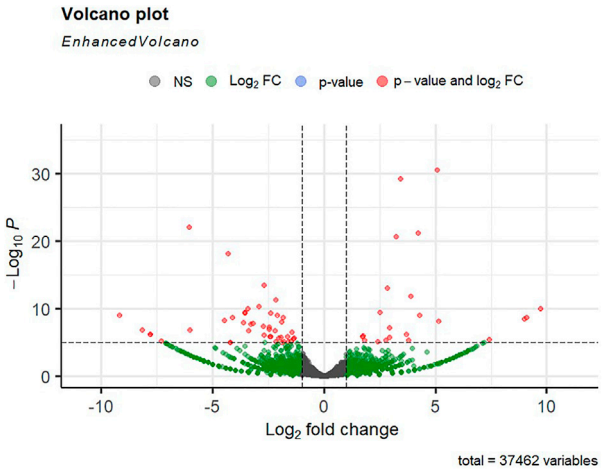

FIGURE 4
Volcano plot of differentially expressed genes identified between control and the 60-ppt salinity group rohu fish. The *X*-axis signifies the Log2 fold change value, and the *Y*-axis indicates the –Log10 *p* value. The ash color dots indicate no significant difference between the two groups. The green dots indicate moderately significant and red dots highly significant differential genes.

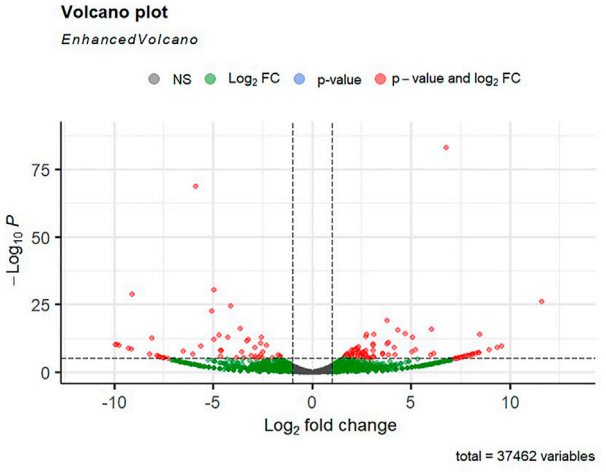

FIGURE 5
Volcano plot of differentially expressed genes identified between control and the 8-ppt salinity group rohu fish. The *X*-axis signifies the Log2 fold change value, and the *Y*-axis indicates the –Log10 *p* value. The ash color dots indicate no significant difference between the two groups. The green dots indicate moderately significant and red dots highly significant differential genes.

genes which are co-expressed, GO enrichment analysis was conducted using ClueGO, which has also generated the visualization of interactions between different biological pathways (Figures 6–9) and thus grouped into biological processes based upon the similarity in the functionality of the genes. In 2, 4, 6, and 8 ppt salinity concentrations, the most enriched biological processes are given in Table 2 (Supplementary Figures S5–S8). A complete list of all enriched biological processes along with GO ids and associated genes is reported in Supplementary Tables S5–S8.

The overall GO enrichment analysis of 2, 4, 6, and 8 ppt salinity concentrations revealed many specific modified pathways in relation to salinity stress. The biological processes predominantly enriched are involved in osmoregulation (GO: 0005246, GO:0015114, GO:0008331, GO:1901841, GO:1901842, GO:0034766, GO:0032413, GO:1904063, GO:2001258, GO: 0015114, and GO:0045162), osmolyte production (GO: 0014066, GO:0005368, GO:0005369, GO:0046934, GO: 0052812, GO:0052813, GO:0004430, and GO:0015734), energy metabolism (GO:0006850, GO:0019427, GO:0006083, GO: 1902001, GO:0005324, GO:0050996, GO:0090207, GO: 0090208, GO:0010896, and GO:0010898), calcium ion regulation (GO:0005246, GO:0002115, GO:2001256, GO: 0008331, GO:1901841, GO:1901842, GO:0051926, GO: 1903170, and GO:1901020), immune response (GO:0002369, GO:0002709, GO:0001959, GO:0034341, GO:0060330, GO: 0071346, GO:0060333, GO:0032480, and GO:0060334), and apoptosis (GO:0008630, GO:0030262, GO:0006309, and GO: 0043523).

The GO enrichment analysis is restricted to *L. rohita*, not a model species, and thus, rohu-specific annotations are not readily recognized. Therefore, we further explored the differentially expressed genes individually and observed genes involved in hypersalinity stress, viz., genes involved in the activation of hypoxia-related pathways, endoplasmic reticulum-associated protein degradation, cell cycle arrest, FOXO signaling pathway, and the genes involved in the structural reorganization and detoxification under environmental shift (migration from freshwater to saltwater).

Discussion

A significant number of genes were differentially expressed upon salinity adaptation in *L. rohita*. We have discussed key components of categories and their potential functions in response to salinity variations.

Earlier, it has been reported that 20%–62% of the total energy of a fish is spent on osmoregulation under elevated salinity levels (Bœuf and Payan, 2001). In our study, there was upregulation of acyl-CoA synthetase (ACS), polyketide synthase (PKS), and malonyl acyl carrier mitochondrial (MCAT) key enzymes utilized in the energy metabolism. ACS plays an important role in the production of acetyl-CoA, which involves fatty acid synthesis and the tricarboxylic acid (TCA) cycle (Fujino et al., 2001). MCAT is an important metabolic enzyme in the saturated

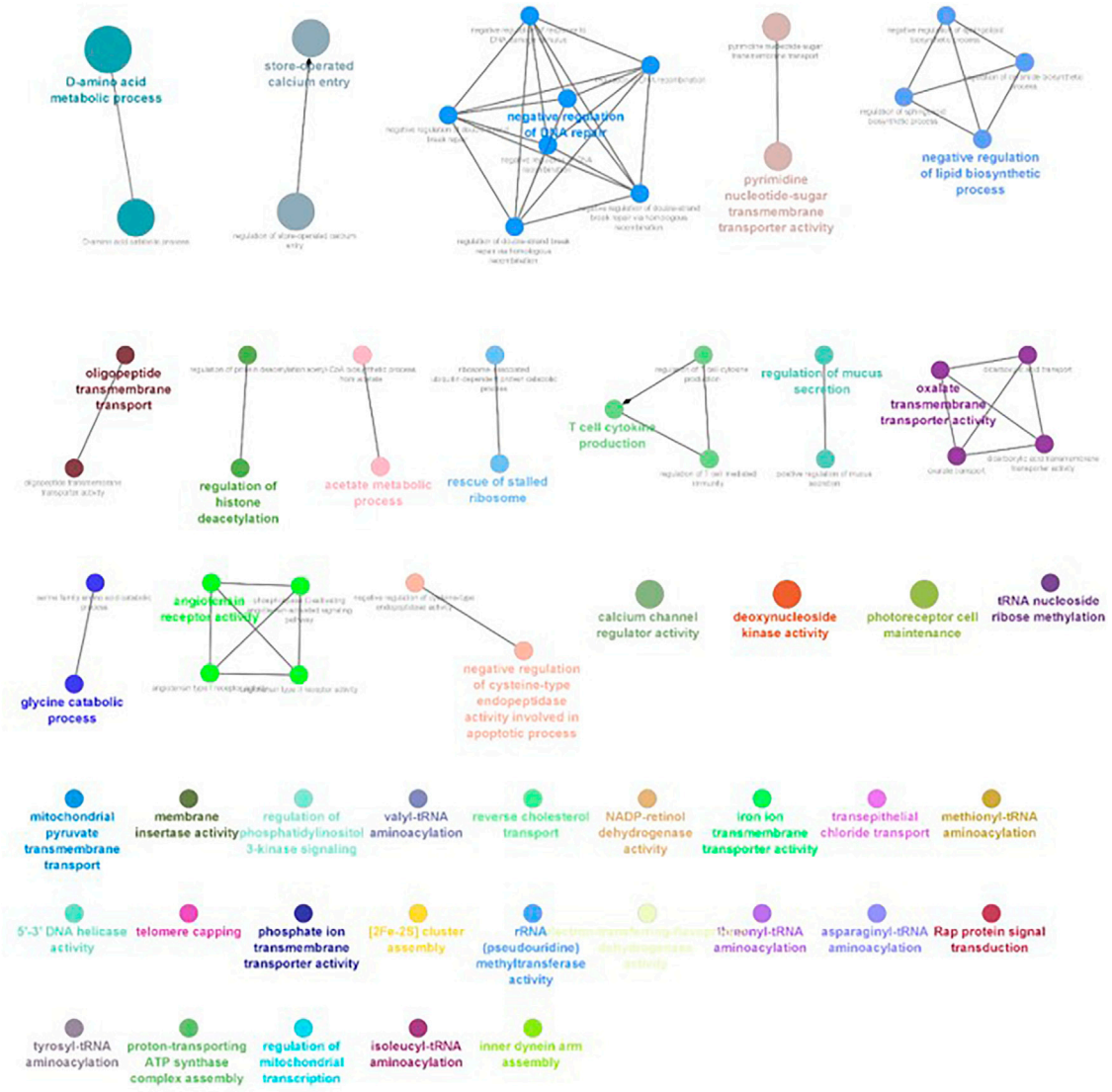

FIGURE 6
ClueGO enrichment network of the 2-ppt salinity-challenged treatment group DEGs of *L. rohita*, with the *p*-value cut-off <0.05, the interactions of the GO term network determined by functional nodes, and edges shared between differentially expressed genes with a kappa score of 0.4. The generated network has 121 nodes and 164 edges. Each node represents an individual biological process, and the color refers to the GO group. In total, 41 GO groups are present in the network, and edges represent the relationship between the GO terms based on the similarity of their associated genes. The bold font indicates an important GO term that defines the name of the biological process of each group.

fatty acid synthesis pathway, and its upregulation has a positive effect on the accumulation of C16 and C18 fatty acids (Simon and Slabas, 1998). Polyunsaturated fatty acids (PUFA), produced through the PKS pathway, are catalyzed by polyketide synthase (PKS) (Metz et al., 2001). The upregulated PKS indicated the increased production of PUFA as the salinity tolerance of *L. rohita*, as concluded by Sui et al. (2007) in Chinese mitten crab larvae. Along with the genes involved in the energy metabolism, several genes with functions of transporting molecules were differentially expressed. Corresponding to the overexpression of lipid metabolic enzymes, lipid transporters such as apolipoproteins (*APOL6*, *APOB*, *APOE*, *APOA1*, and *APOL3*) and *SLC22A5* were upregulated. *APOE* and *APOB* act as ligands for the lipoprotein receptors and are involved in the transportation of lipids. Similar results were reported in spotted sea bass under salinity stress-responsive transcriptomic analysis (Zhang et al., 2017). This inferred that the lipid metabolism plays an important role in energy production to maintain osmoregulation under salinity stress in *L. rohita*. The differential expression of several

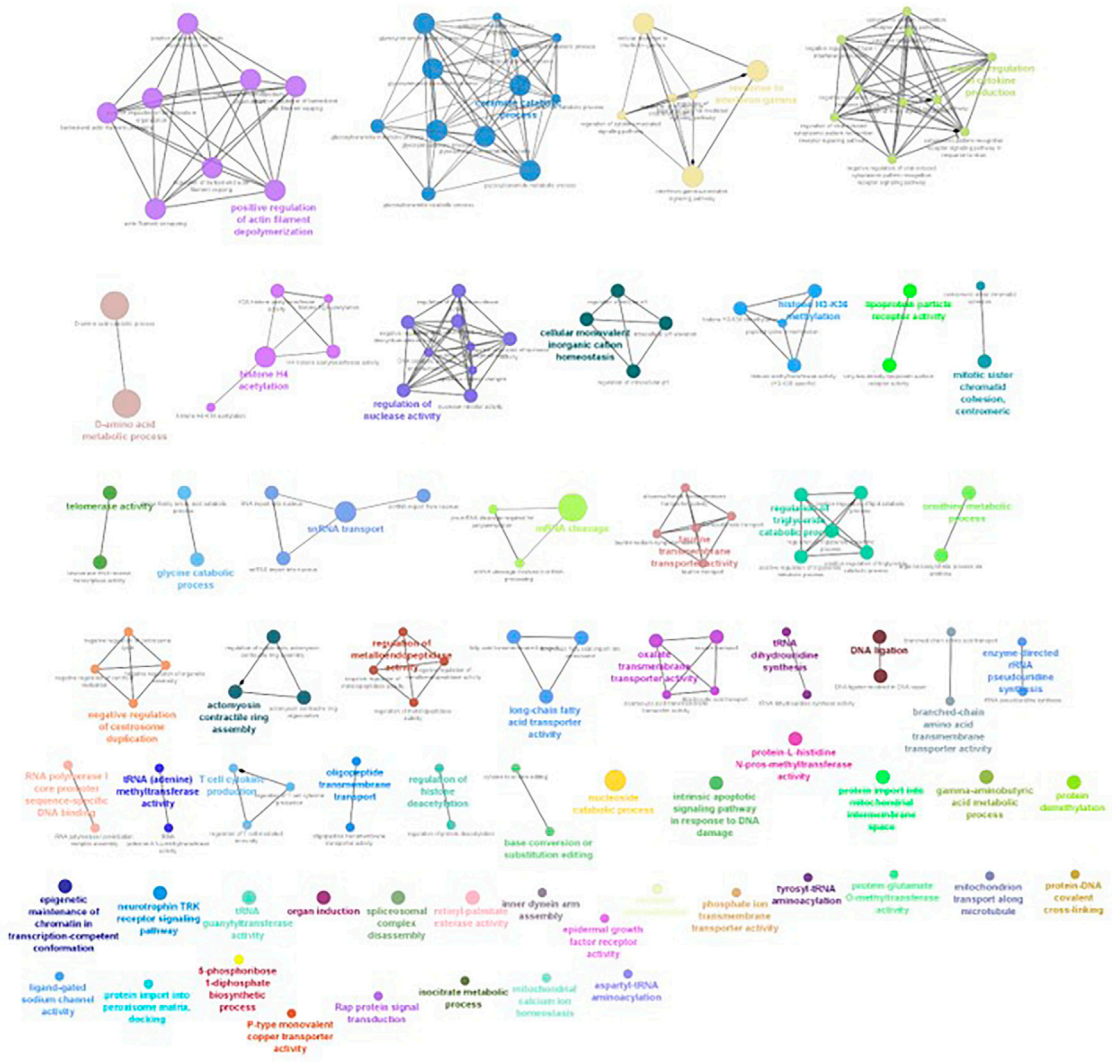

FIGURE 7
ClueGO enrichment network of the 4-ppt salinity-challenged treatment group DEGs of *L. rohita*, with a *p*-value cut-off <0.05, the interactions of the GO terms network determined by functional nodes, and edges shared between differentially expressed genes with a kappa score of 0.4. The generated network has 227 nodes and 554 edges. Each node represents an individual biological process, and the color refers to the GO group. In total, 60 GO groups are present in the network, and edges represent the relationship between the GO terms based on the similarity of their associated genes. The bold font indicates an important GO term that defines the name of the biological process of each group.

solute carrier family genes that participate in glucose transportation, i.e., *SLC2A2*, *SLC2A1*, *SLC2A9*, *SLC2A11*, and *SLC5A1* and in amino acid transportation, *SLC7A3*, was observed in *L. rohita*. During high salinity conditions, the free amino acids can be metabolized in order to provide the ATP necessary for the metabolic process (Nguyen et al., 2016) and can also be potentially involved in the regulation of intracellular osmotic pressure (Venkatachari, 1974; Tseng and Hwang, 2008).

In addition to this, there was differential expression of other SLC family genes (*SLC13A1*, *SLC41A1*, *SLC26A6*, *SLC4A4*, *SLC12A1*, *SLC12A3*, *SLC12A4*, *SLC20A1*, and *SLC34A1*) which indicated the reduced re-absorption levels of the major ions in the kidney as the fish were adapting to the salt water. This finding coincides with that of Watanabe and Takei (2011) for euryhaline fish, where migration from freshwater to saltwater caused a drastic change in ion regulation in the opposite direction, from absorption to excretion in osmoregulatory organs such as the gills, kidney, and intestines. Interestingly, there was also an enrichment of the calcium channel regulatory activity, regulation of store-operated calcium entry biological processes, and also differential regulation of *phospholipase C beta 4 (PLCB4)* and *inositol 1,4,5 trisphosphate receptor (IP3R)* type II genes, causing the release of calcium from the endoplasmic reticulum (Vervloessem et al., 2014). Calcium has been known to be

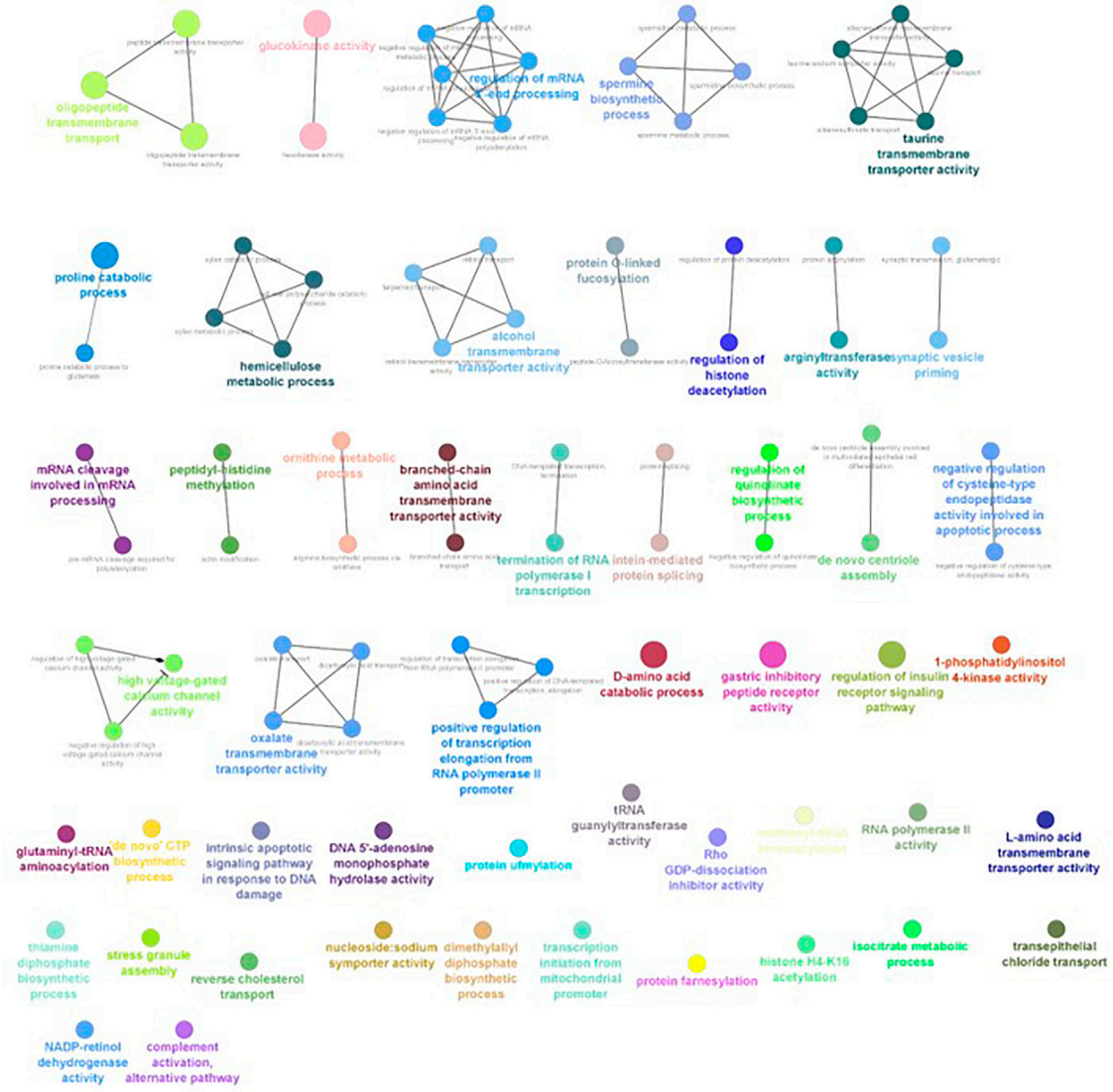

FIGURE 8
ClueGO enrichment network of the 6-ppt salinity-challenged treatment group DEGs of *L. rohita*, with the *p*-value cut-off <0.05, the interactions of the GO terms network determined by functional nodes, and edges shared between differentially expressed genes with a kappa score of 0.4. The generated network has 148 nodes and 217 edges. Each node represents an individual biological process, and the color refers to the GO group. In total, 49 GO groups are present in the network, and edges represent the relationship between the GO terms based on the similarity of their associated genes. The bold font indicates an important GO term that defines the name of the biological process of each group.

involved in many biological pathways including the apoptotic process (Jiang et al., 1994) and also cell survival through cAMP-responsive element binding (CREB), a Ca^{2+}-activated transcription factor (Bito and Takemoto-Kimura, 2003; Persengiev and Green, 2003). The differential expression of CREB-regulated transcription co-activators and protein kinases (phosphorylation of serine, which is related to CREB activity) (PK, 1992) demonstrates that Ca^{2+} activates the CREB as a pro-survival transcription factor under hyperosmotic environmental conditions.

Likewise, *L. rohita* also showed various interesting mechanisms involved in osmolyte production to counterbalance the osmotic pressure induced due to hypersalinity. The upregulation of the inositol-3-phosphate synthase 1A (*INO1*) enzyme, *SLC6A6*, and *SLC6A18* was noticed. The *INO1* gene converts glucose-6-phosphate to 1D myo-inositol-3-phosphate, eventually converting to myo-inositol (Sacchi et al., 2013). The enzymatic action of phosphatidylinositol 4-kinase alpha and phosphatidylinositol 5-phosphate-4-kinase through a series of events leads to the

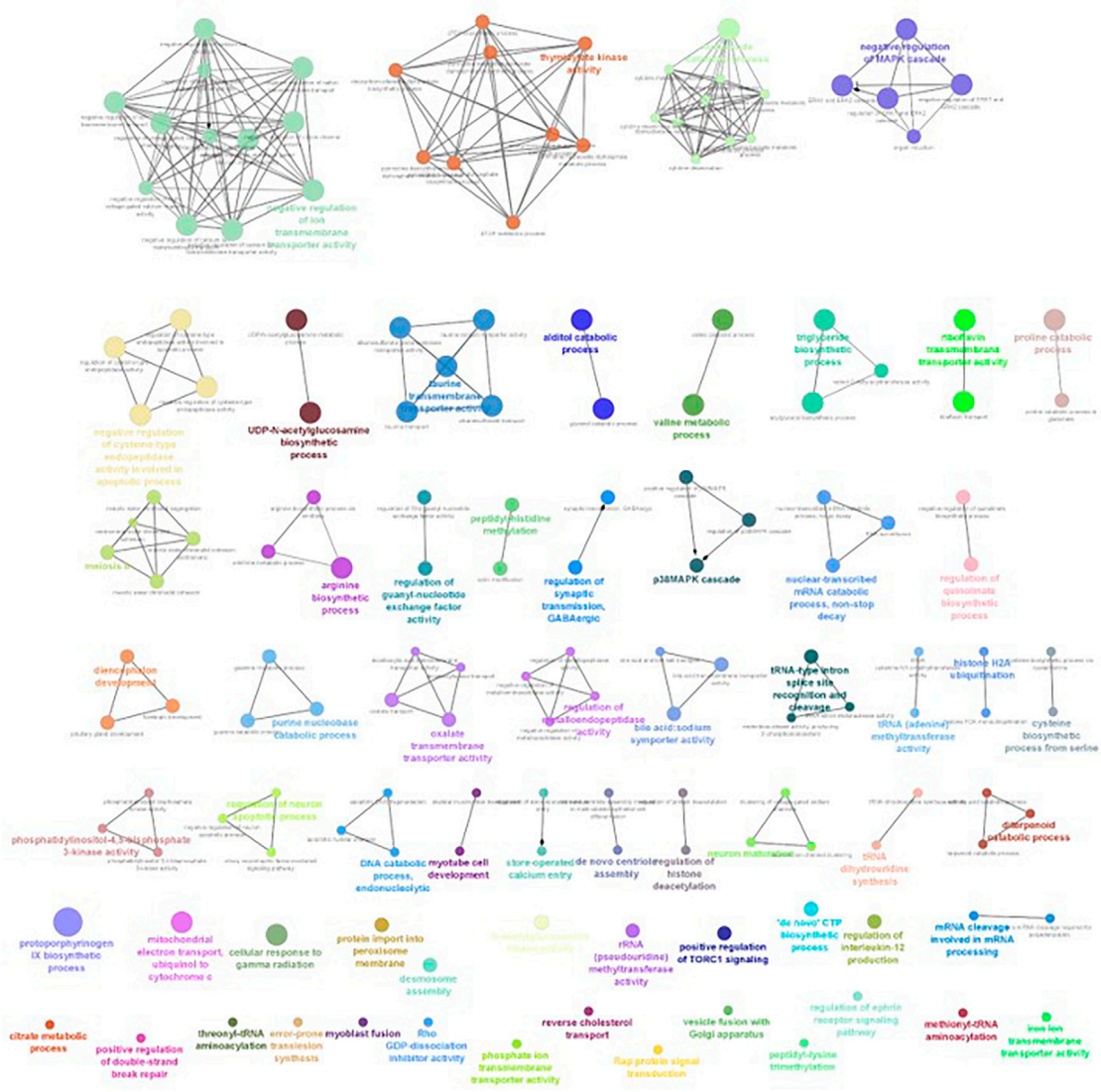

FIGURE 9
ClueGO enrichment network of the 8-ppt salinity-challenged treatment group DEGs of *L. rohita*, with the *p*-value cut off <0.05, the interactions of the GO terms network determined by functional nodes, and edges shared between differentially expressed genes with a kappa score of 0.4. The generated network has 238 nodes and 550 edges. Each node represents an individual biological process, and the color refers to the GO group. In total, 63 GO groups are present in the network, and edges represent the relationship between the GO terms based on the similarity of their associated genes. The bold font indicates an important GO term that defines the name of the biological process of each group.

myo-inositol synthesis (KEGG pathway id: 00562) (Figure 10). *SLC6A6* and *SLC6A18* genes involved in the sodium and chloride-dependent taurine transport determine the role of taurine as an osmolyte in the acclimatization of *L. rohita* to hypersalinity conditions. Similar conclusions were also made by Gonçalves et al. (2011) in Nile tilapia.

The significant differential expression of the myosin gene family members (*MYO1H*, *MYO6*, *MYO3B*, *MYO5B*, *MYO28A*, *MYH9*, *MYO9A*, *MYO7A*, and *MYLK*), keratin (KRT-8), and collagen family genes in rohu under a high salt concentration was observed. The genes encoding the structural components of the cytoskeleton induced at hypersalinity conditions might be to adjust the elements for cell reorganization during cell volume regulation (Nguyen et al., 2016) under osmotic stress to maintain the equilibrium. The increased expression of myosin light chain genes was also found in *Pangasianodon hypophthalmus* (Nguyen et al., 2016) and *L. maculatus* (Zhang et al., 2017) under salinity stress, whereas the expression of keratin-related genes was observed in catfish under heat stress (Liu et al., 2013). In rohu, under high salt concentration, the gradual upregulation of several cytochrome *P450* genes and several isoforms of glutathione-S-transferase (GST) (Supplementary Tables S1–S4) was observed among the

TABLE 2 List of predominantly enriched GO terms with their biological processes (based on the number of genes involved) of the *L. rohita* kidney transcriptome under increased salinity concentrations obtained from the ClueGO network analysis of DEGs.

Salinity concentration (ppt)	GO ids	Biological process
2	0046416	D-amino acid metabolic process
	0090481	Pyrimidine nucleotide-sugar transmembrane transporter activity
	0005246	Calcium channel regulator activity
	0002115	Store-operated calcium entry
	0045494	Photoreceptor cell maintenance
	0019136	Deoxynucleoside kinase activity
4	0046416	D-amino acid metabolic process
	0046514	Ceramide catabolic process
	0006379	mRNA cleavage
	0030836	Positive regulation of actin filament depolymerization
	0034341	Response to interferon-gamma
	0051030	snRNA transport
	0009164	Nucleoside catabolic process
6	0019478	D-amino acid catabolic process
	0016519	Gastric inhibitory peptide receptor activity
	0046626	Regulation of the insulin receptor signaling pathway
	0035672	Oligopeptide transmembrane transport
	0004340	Glucokinase activity
	0006562	Proline catabolic process
8	0032413	Negative regulation of the ion transmembrane transporter activity
	0009164	Nucleoside catabolic process
	0005368	Taurine transmembrane transporter activity
	0043409	Negative regulation of MAPK cascade
	0043154	Negative regulation of the cysteine-type endopeptidase activity involved in the apoptotic process
	0019432	Triglyceride biosynthetic process
	0006526	Arginine biosynthetic process
	0032217	Riboflavin transmembrane transporter activity
	0019405	Alditol catabolic process
	0071480	Cellular response to gamma radiation
	0006122	Mitochondrial electron transport, ubiquinol to cytochrome c
	0006782	Protoporphyrinogen IX biosynthetic process
	0006048	UDP-N-acetylglucosamine biosynthetic process
	0006573	Valine metabolic process

four salinity treatment groups. *CYP1A* is believed to be important in acclimatization of freshwater fishes to a higher salt concentration, and increased expression was also reported in *Oncorhynchus mykiss* (Leguen et al., 2010), *Geophagus mirabilis* (Evans and Somero, 2008), and *Oncorhynchus kisutch* (Lavado et al., 2014) gill transcriptome studies. Glutathione-S-transferase (GST) quenches reactive molecules and catalyzes glutathione conjugation to hydrophobic and electrophilic substrates, thus protecting the cells against an oxidative burst (Kumar and Trivedi, 2018). The results coincided with transcriptomic findings of *Anguilla anguilla* (Kalujnaia et al., 2007) and *P. hypophthalmus* (Nguyen et al., 2016).

Furthermore, the exploration of significantly expressed genes manifested an ER-associated degradation (ERAD) of misfolded proteins (KEGG term ID: 04141) (Supplementary Figure S9) as a consequence of the unfolded protein response. The overexpressed mannosyl-oligosaccharide alpha-1,2-

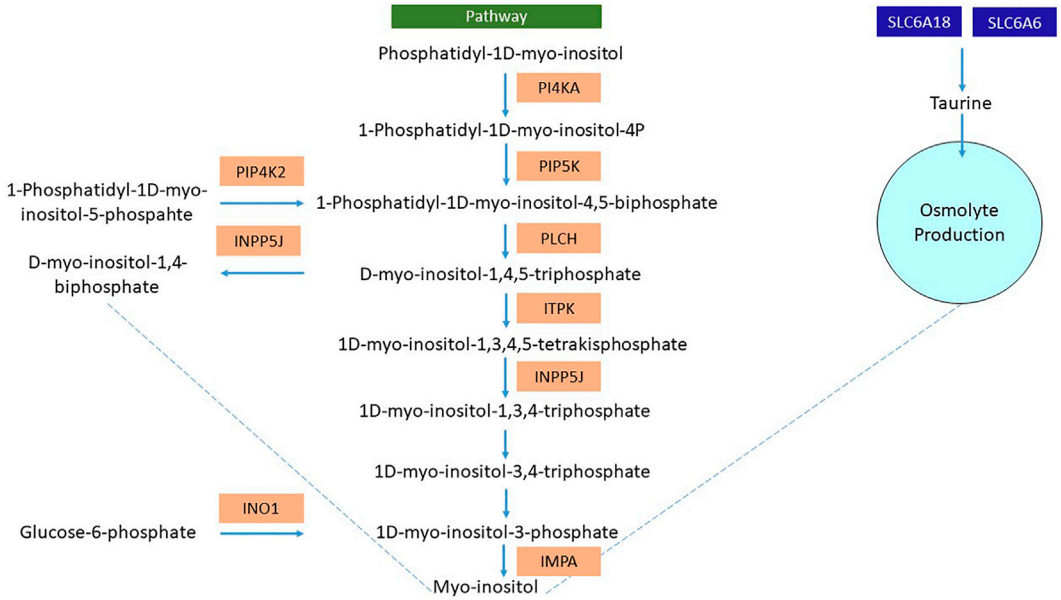

FIGURE 10
Representative flowchart of differentially expressed genes (highlighted in orange) involved in the osmolyte production (myo-inositol and taurine) of the *L. rohita* kidney after transferring to a high salt concentration. PI4KA, phosphatidylinositol 4-kinase alpha; PIP5K, phosphatidylinositol-4-phosphate 5-kinase; PLCH, phospholipase C-like protein; ITPK, inositol trisphosphate 3-kinase; INPP5J, phosphatidylinositol 4,5-bisphosphate-5-phosphatase; PIP4K2, phosphatidylinositol 5 phosphate-4-kinase; INO1, inositol-3-phosphate synthase; SLC6A6, solute carrier family 6 member 6; SLC6A18, solute carrier family 6 member 18.

mannosidase (*MAN1A1*) gene accelerated the ER-associated degradation of misfolded proteins (Hosokawa et al., 2007; Ogen-Shtern et al., 2016). The conceptual hypothesis from the differentially expressed genes is that terminally misfolded proteins were recognized by ERAD substrate recognizers, BiP (*HSPA5*), a molecular chaperon, and endoplasmic reticulum lectin 1 (*ERLEC1*) gene (Nakatsukasa and Brodsky, 2008) and translocated to the cytoplasm called retrotranslocation. Then, ERAD substrates interacted with the E3 ubiquitin ligase complex (*DNAJB2*, *HSPA1*, and *UBE2D*) in the cytoplasm, and the ubiquitinated substrates were delivered to the proteasome by the p97 complex (VCP), an ATP-requiring hexameric AAA ATPase (Ye et al., 2001; Jarosch et al., 2002; Rabinovich et al., 2002). There was an upregulation of *HERPUD1* gene, which also acted as a shuttle factor for delivering the ubiquitinated ERAD substrates to the proteasome (Okuda-Shimizu and Hendershot, 2007; Huang et al., 2014). There was also a differential expression of several proteasomal subunits (*PSMD2*, *PSMD6*, *PSMD10*, *PSMD11*, *PSMD12*, *PSMB2*, *PSMB6*, *PSMB7*, *PSMG4*, and *PSME3*) which explains the proteasomal degradation of ubiquitinated proteins through an ATP-dependent mechanism (Motosugi and Murata, 2019). Corresponding to this, there was also the upregulation of NEK5, polyubiquitin B, C, and cathepsins involved in removal or degradation of misfolded proteins (Pratt et al., 2010; Kaminskyy and Zhivotovsky, 2012; Lin and Qin, 2013; Bianchi et al., 2019).

In addition, an elevated salt concentration also had an influence on the immune response in *L. rohita*. There was a differential expression of genes involved in the phagosome pathway (KEGG term id: 04145) (Supplementary Figure S10). Manifestation of the phagocytic process under salinity stress was also reported in *Oreochromis mossambicus* (Jiang et al., 2008) and *P. hypophthalmus* (Schmitz et al., 2017). Maturation of phagosomes leads to the antigen presentation by MHC complex I/II and causes the activation of T cells (Krogsgaard et al., 2005). Moreover, there was an enrichment of biological processes such as the regulation of T-cell-mediated immunity and regulation of T-cell cytokine production. Continuous downregulation of the lysozyme G activity was found across the four salinity-challenged groups, which might be due to the increased complement activity, as also observed in *O. mossambicus* after transferring to saltwater (Jiang et al., 2008).

Transfer of *L. rohita* from freshwater to saltwater stimulated the pathways involved in prolonging the lifespan of the species. Among them, the FOXO signaling pathway (KEGG term ID: 04068) (Supplementary Figure S11) either induced or inhibited apoptosis, depending on the level of stress. In case of prolonged stress, apoptosis of the abnormal cells prolonged the longevity of the organism (Carter and Brunet, 2007). The cellular senescence pathway (KEGG term ID: 04218) (Supplementary Figure S12) caused cell cycle arrest and can be triggered in response to different kinds of stress. Under hypersalinity stress, cellular senescence may be an alarming response to prevent the

multiplication of abnormal cells and protect the animal (Kumari and Jat, 2021). There was also enrichment of the apoptotic pathway (KEGG term ID: 04210) (Supplementary Figure S13). Under the salinity effect, these three pathways might balance cell proliferation and survival to maintain cellular homeostasis in *L. rohita*.

Conclusion

The current experiment investigated the transcriptomic response of the *L. rohita* kidney treated under four different salt concentrations (2, 4, 6, and 8 ppt). From the molecular aspect, during adaptation to high salinity levels, *L. rohita* produced significant changes in osmoregulation, energy metabolism, hypoxia, protein processing, immune response, structural reorganization, and detoxification, suggesting the importance of core components of the kidney in salinity acclimatization. The differential gene expression patterns and their pathways give insights into the molecular mechanisms involved in the salinity adaptation in rohu. Our findings also support the earlier studies on *L. rohita* for the plasticity of salinity tolerance and the maintenance of individuals at low-to-moderate salt concentrations without affecting their performance. The transcriptomic information also suggests the scientific basis of response to climate change, causing increased salinity levels in freshwater resources and is also helpful to scientists involved in research on freshwater fishes.

Data availability statement

The datasets presented in this study can be found in online repositories. The names of the repository/repositories and accession number(s) can be found at: https://www.ncbi.nlm.nih.gov/, SRR19895145; https://www.ncbi.nlm.nih.gov/, SRR19895144; https://www.ncbi.nlm.nih.gov/, SRR19895143; https://www.ncbi.nlm.nih.gov/, SRR19895142; https://www.ncbi.nlm.nih.gov/, SRR19895141; https://www.ncbi.nlm.nih.gov/, SRR19895140; https://www.ncbi.nlm.nih.gov/, SRR19895139; and https://www.ncbi.nlm.nih.gov/, SRR19895138.

Ethics statement

The animal study was reviewed and approved by Kamdhenu University, Gandhinagar, Gujarat.

Author contributions

VH–wet laboratory work, literature review, and manuscript writing; NS–assistance in the wet laboratory work, transcriptomic data analysis, and drafting the bioinformatics pipeline in materials and methods; IR–troubleshooting in the wet laboratory work, guidance in manuscript writing, and review; SK–maintenance of fishes under salinity conditions and sample collection; VS–experimental setup and maintenance of fishes under salinity stress; AP–experimental design, troubleshooting in the wet laboratory work, and manuscript proof-reading; CJ–experimental design, guidance in the data analysis, and manuscript proof-reading.

Funding

The project was funded by the Government of Gujarat-Department of Science and Technology (GOG-DST), project reference no: MB-18.

Conflict of interest

The authors declare that the research was conducted in the absence of any commercial or financial relationships that could be construed as a potential conflict of interest.

Publisher's note

All claims expressed in this article are solely those of the authors and do not necessarily represent those of their affiliated organizations, or those of the publisher, the editors, and the reviewers. Any product that may be evaluated in this article, or claim that may be made by its manufacturer, is not guaranteed or endorsed by the publisher.

Supplementary material

The Supplementary Material for this article can be found online at: https://www.frontiersin.org/articles/10.3389/fphys.2022.991366/full#supplementary-material

References

Aktas, M., and Cavdar, N. (2012). The combined effects of salinity and temperature on the egg hatching rate, incubation time, and survival until protozoal stages of *Metapenaeus monoceros* (Fabricius) (Decapoda: Penaeidae). *Turk. J. Zool.* 36, 249–253.

Baliarsingh, M. M., Panigrahi, J. K., and Patra, A. K. (2018). Effect of salinity on growth and survivality of *Labeo rohita* in captivity. *Int. J. Sci. Res.* 7, 28–30.

Bœuf, G., and Payan, P. (2001). How should salinity influence fish growth? *Comp. Biochem. Physiol. C. Toxicol. Pharmacol.* 130, 411–423. doi:10.1016/s1532-0456(01)00268-x

Bianchi, M., Crinelli, R., Giacomini, E., Carloni, E., Radici, L., Scarpa, E. S., et al. (2019). A negative feedback mechanism links UBC gene expression to ubiquitin levels by affecting RNA splicing rather than transcription. *Sci. Rep.* 9, 18556. doi:10.1038/s41598-019-54973-7

Bito, H., and Takemoto-Kimura, S. (2003). Ca2+/CREB/CBP-dependent gene regulation: A shared mechanism critical in long-term synaptic plasticity and neuronal survival. *Cell Calcium* 34, 425–430. doi:10.1016/s0143-4160(03)00140-4

Carter, M. E., and Brunet, A. (2007). FOXO transcription factors. *Curr. Biol.* 17, 113–114. doi:10.1016/j.cub.2007.01.008

Chen, X., Gong, H., Chi, H., Xu, B., Zheng, Z., and Bai, Y. (2021). Gill transcriptome analysis revealed the difference in gene expression between freshwater and seawater acclimated guppy (*Poecilia reticulata*). *Mar. Biotechnol.* 23, 615–627. doi:10.1007/s10126-021-10053-4

Chong-Robles, J., Charmantier, G., Boulo, V., Lizárraga-Valdéz, J., Enriquez-Paredes, L. M., and Giffard-Mena, I. (2014). Osmoregulation pattern and salinity tolerance of the white shrimp *Litopenaeus vannamei* (Boone, 1931) during post-embryonic development. *Aquaculture* 422, 261–267. doi:10.1016/j.aquaculture.2013.11.034

Evans, T. G., and Somero, G. N. (2008). A microarray-based transcriptomic time-course of hyper-and hypo-osmotic stress signaling events in the euryhaline fish *Gillichthys mirabilis*: Osmosensors to effectors. *J. Exp. Biol.* 211, 3636–3649. doi:10.1242/jeb.022160

Fujino, T., Kondo, J., Ishikawa, M., Morikawa, K., and Yamamoto, T. T. (2001). Acetyl-CoA synthetase 2, a mitochondrial matrix enzyme involved in the oxidation of acetate. *J. Biol. Chem.* 276, 11420–11426. doi:10.1074/jbc.M008782200

Gerard, D. (2020). Data-based RNA-seq simulations by binomial thinning. *BMC Bioinforma.* 21, 206–214. doi:10.1186/s12859-020-3450-9

Gonçalves, G. S., Ribeiro, M. J. P., Vidotti, R. M., and Sussel, F. R. (2011). Taurine supplementation in diets for Nile tilapia (*Oreochromis niloticus*). *World Aquac.* 2011, 6.

Haque, R., Parr, N., and Muhidin, S. (2020). Climate-related displacement, impoverishment and health care accessibility in mainland Bangladesh. *Asian Popul. Stud.* 16, 220–239. doi:10.1080/17441730.2020.1764187

Hoque, F., Adhikari, S., Hussan, A., Mahanty, D., Pal, K., and Pillai, B. R. (2020). Effect of water salinity levels on growth performance and survival of *Catla catla*, genetically improved *Labeo rohita* (Jayanti Rohu) and *Cirrhinus mrigala*. *Int. J. Oceanogr. Aquac.* 4, 190. doi:10.23880/ijoac-16000190

Hosokawa, N., You, Z., Tremblay, L. O., Nagata, K., and Herscovics, A. (2007). Stimulation of ERAD of misfolded null Hong Kong alpha1-antitrypsin by Golgi alpha1, 2-mannosidases. *Biochem. Biophys. Res. Commun.* 362, 626–632. doi:10.1016/j.bbrc.2007.08.057

Huang, C.-H., Chu, Y.-R., Ye, Y., and Chen, X. (2014). Role of HERP and a HERP-related protein in HRD1-dependent protein degradation at the endoplasmic reticulum. *J. Biol. Chem.* 289, 4444–4454. doi:10.1074/jbc.M113.519561

Hwang, P. P., and Lee, T. H. (2007). New insights into fish ion regulation and mitochondrion-rich cells. *Comp. Biochem. Physiol. A Mol. Integr. Physiol.* 148, 479–497. doi:10.1016/j.cbpa.2007.06.416

Jarosch, E., Taxis, C., Volkwein, C., Bordallo, J., Finley, D., Wolf, D. H., et al. (2002). Protein dislocation from the ER requires polyubiquitination and the AAA-ATPase Cdc48. *Nat. Cell Biol.* 4, 134–139. doi:10.1038/ncb746

Jiang, I., Kumar, V. B., Lee, D., and Weng, C. (2008). Fish & Shellfish Immunology Acute osmotic stress affects Tilapia (*Oreochromis mossambicus*) innate immune responses. *Fish. Shellfish Immunol.* 25, 841–846. doi:10.1016/j.fsi.2008.09.006

Jiang, S., Chow, S. C., Nicotera, P., and Orrenius, S. (1994). Intracellular Ca2+ signals activate apoptosis in thymocytes: Studies using the Ca2+-ATPase inhibitor thapsigargin. *Exp. Cell Res.* 212, 84–92. doi:10.1006/excr.1994.1121

Kalujnaia, S., McWilliam, I. S., Zaguinaiko, V. A., Feilen, A. L., Nicholson, J., Hazon, N., et al. (2007). Transcriptomic approach to the study of osmoregulation in the European eel *Anguilla anguilla*. *Physiol. Genomics* 31, 385–401. doi:10.1152/physiolgenomics.00059.2007

Kaminskyy, V., and Zhivotovsky, B. (2012). Proteases in autophagy. *Biochim. Biophys. Acta* 1824, 44–50. doi:10.1016/j.bbapap.2011.05.013

Krogsgaard, M., Li, Q., Sumen, C., Huppa, J. B., Huse, M., and Davis, M. M. (2005). Agonist/endogenous peptide--MHC heterodimers drive T cell activation and sensitivity. *Nature* 434, 238–243. doi:10.1038/nature03391

Kumar, S., and Trivedi, P. K. (2018). Glutathione S-transferases: Role in combating abiotic stresses including arsenic detoxification in plants. *Front. Plant Sci.* 9, 751. doi:10.3389/fpls.2018.00751

Kumari, R., and Jat, P. (2021). Mechanisms of cellular senescence: Cell cycle arrest and senescence associated secretory phenotype. *Front. Cell Dev. Biol.* 9, 1–24. doi:10.3389/fcell.2021.645593

Lavado, R., Aparicio-Fabre, R., and Schlenk, D. (2014). Effects of salinity acclimation on the expression and activity of Phase I enzymes (CYP450 and FMOs) in coho salmon (*Oncorhynchus kisutch*). *Fish. Physiol. Biochem.* 40, 267–278. doi:10.1007/s10695-013-9842-2

Leguen, I., Odjo, N., Le Bras, Y., Luthringer, B., Baron, D., Monod, G., et al. (2010). Effect of seawater transfer on CYP1A gene expression in rainbow trout gills. *Comp. Biochem. Physiol. A Mol. Integr. Physiol.* 156, 211–217. doi:10.1016/j.cbpa.2010.02.002

Lemaire, P., Bernard, E., Martinez-Paz, J. A., and Chim, L. (2002). Combined effect of temperature and salinity on osmoregulation of juvenile and sub adult *Penaeus stylirostris*. *Aquaculture* 209, 307–317. doi:10.1016/s0044-8486(01)00756-6

Lin, F., and Qin, Z.-H. (2013). Degradation of misfolded proteins by autophagy: Is it a strategy for huntington's disease treatment? *J. Huntingt. Dis.* 2, 149–157. doi:10.3233/JHD-130052

Liu, S., Wang, X., Sun, F., Zhang, J., Feng, J., Liu, H., et al. (2013). RNA-Seq reveals expression signatures of genes involved in oxygen transport, protein synthesis, folding, and degradation in response to heat stress in catfish. *Physiol. Genomics* 45, 462–476. doi:10.1152/physiolgenomics.00026.2013

Metz, J. G., Roessler, P., Facciotti, D., Levering, C., Dittrich, F., Lassner, M., et al. (2001). Production of polyunsaturated fatty acids by polyketide synthases in both prokaryotes and eukaryotes. *Sci. (80)* 293, 290–293. doi:10.1126/science.1059593

Motosugi, R., and Murata, S. (2019). Dynamic regulation of proteasome expression. *Front. Mol. Biosci.* 6, 30. doi:10.3389/fmolb.2019.00030

Murmu, K., Rasal, K. D., Rasal, A., Sahoo, L., Nandanpawar, P. C., Udit, U. K., et al. (2020). Effect of salinity on survival, hematological and histological changes in genetically improved rohu (Jayanti), *Labeo rohita* (Hamilton, 1822). *Indian J. Anim. Res.* 54, 673–678. doi:10.18805/ijar.B-3801

Nakatsukasa, K., and Brodsky, J. L. (2008). The recognition and retrotranslocation of misfolded proteins from the endoplasmic reticulum. *Traffic* 9, 861–870. doi:10.1111/j.1600-0854.2008.00729.x

Nguyen, T. V., Jung, H., Nguyen, T. M., Hurwood, D., and Mather, P. (2016). Evaluation of potential candidate genes involved in salinity tolerance in striped catfish (*Pangasianodon hypophthalmus*) using an RNA-Seq approach. *Mar. Genomics* 25, 75–88. doi:10.1016/j.margen.2015.11.010

Ogen-Shtern, N., Avezov, E., Shenkman, M., Benyair, R., and Lederkremer, G. Z. (2016). Mannosidase IA is in quality control vesicles and participates in glycoprotein targeting to ERAD. *J. Mol. Biol.* 428, 3194–3205. doi:10.1016/j.jmb.2016.04.020

Okuda-Shimizu, Y., and Hendershot, L. M. (2007). Characterization of an ERAD pathway for nonglycosylated BiP substrates, which require Herp. *Mol. Cell* 28, 544–554. doi:10.1016/j.molcel.2007.09.012

Persengiev, S. P., and Green, M. R. (2003). The role of ATF/CREB family members in cell growth, survival and apoptosis. *Apoptosis* 8, 225–228. doi:10.1023/a:1023633704132

Pk, B. (1992). Montminy MR. The CREB family of transcription activators. *Curr. Opin. Genet. Dev.* 2, 199–204.

Pratt, W. B., Morishima, Y., Peng, H. M., and Osawa, Y. (2010). Proposal for a role of the Hsp90/Hsp70-based chaperone machinery in making triage decisions when proteins undergo oxidative and toxic damage. *Exp. Biol. Med.* 235, 278–289. doi:10.1258/ebm.2009.009250

Rabinovich, E., Kerem, A., Fröhlich, K. U., Diamant, N., and Bar-Nun, S. (2002). AAA-ATPase p97/Cdc48p, a cytosolic chaperone required for endoplasmic reticulum-associated protein degradation. *Mol. Cell. Biol.* 22, 626–634. doi:10.1128/mcb.22.2.626-634.2002

Rubio, V. C., Sánchez-Vázquez, F. J., and Madrid, J. A. (2005). Effects of salinity on food intake and macronutrient selection in European sea bass. *Physiol. Behav.* 85, 333–339. doi:10.1016/j.physbeh.2005.04.022

Sacchi, R., Li, J., Villarreal, F., Gardell, A. M., and Kültz, D. (2013). Salinity-induced regulation of the myo-inositol biosynthesis pathway in tilapia gill epithelium. *J. Exp. Biol.* 216, 4626–4638. doi:10.1242/jeb.093823

Schmitz, M., Ziv, T., Admon, A., Baekelandt, S., Mandiki, S. N. M., L'Hoir, M., et al. (2017). Salinity stress, enhancing basal and induced immune responses in striped catfish *Pangasianodon hypophthalmus* (Sauvage). *J. Proteomics* 167, 12–24. doi:10.1016/j.jprot.2017.08.005

Shakir, H. A., Quazi, J. I., Chaudhary, A. S., Hussain, A., and Ali, A. (2013). Nutritional comparison of three fish species co-cultured in an earthen pond. *Biol. Bratisl.* 59, 353–356.

Simon, J. W., and Slabas, A. R. (1998). cDNA cloning of Brassica napus malonyl-CoA: ACP transacylase (MCAT) (fab D) and complementation of an *E. coli* MCAT mutant. *FEBS Lett.* 435, 204–206. doi:10.1016/s0014-5793(98)01055-2

Sui, L., Wille, M., Cheng, Y., and Sorgeloos, P. (2007). The effect of dietary n-3 HUFA levels and DHA/EPA ratios on growth, survival and osmotic stress tolerance of Chinese mitten crab *Eriocheir sinensis* larvae. *Aquaculture* 273, 139–150. doi:10.1016/j.aquaculture.2007.09.016

Takvam, M., Wood, C. M., Kryvi, H., and Nilsen, T. O. (2021). Ion transporters and osmoregulation in the kidney of teleost fishes as a function of salinity. *Front. Physiol.* 12, 664588–664625. doi:10.3389/fphys.2021.664588

Thiyagarajan, V., Harder, T., and Qian, P.-Y. (2003). Combined effects of temperature and salinity on larval development and attachment of the subtidal barnacle *Balanus trigonus* Darwin. *J. Exp. Mar. Biol. Ecol.* 287, 223–236. doi:10.1016/s0022-0981(02)00570-1

Tseng, Y.-C., and Hwang, P.-P. (2008). Some insights into energy metabolism for osmoregulation in fish. *Comp. Biochem. Physiol. C. Toxicol. Pharmacol.* 148, 419–429. doi:10.1016/j.cbpc.2008.04.009

Venkatachari, S. A. T. (1974). Effect of salinity adaptation on nitrogen metabolism in the freshwater fish *Tilapia mossambica*. I. Tissue protein and amino acid levels. *Mar. Biol.* 24, 57–63. doi:10.1007/bf00402847

Vervloessem, T., Yule, D. I., Bultynck, G., and Parys, J. B. (2014). The type 2 inositol 1, 4, 5-trisphosphate receptor, emerging functions for an intriguing Ca^{2+}-release channel. *Biochim. Biophys. Acta* 1853, 1992–2005. doi:10.1016/j.bbamcr.2014.12.006

Watanabe, T., and Takei, Y. (2011). Molecular physiology and functional morphology of SO_4^{2-} excretion by the kidney of seawater-adapted eels. *J. Exp. Biol.* 214, 1783–1790. doi:10.1242/jeb.051789

Xu, Z., Gan, L., Li, T., Xu, C., Chen, K., Wang, X., et al. (2015). Transcriptome profiling and molecular pathway analysis of genes in association with salinity adaptation in Nile tilapia *Oreochromis niloticus*. *PLoS One* 10, e0136506–e0136525. doi:10.1371/journal.pone.0136506

Yang, W.-K., Chung, C.-H., Cheng, H. C., Tang, C.-H., and Lee, T.-H. (2016). Different expression patterns of renal Na+/K+-ATPase α-isoform-like proteins between tilapia and milkfish following salinity challenges. *Comp. Biochem. Physiol. B Biochem. Mol. Biol.* 202, 23–30. doi:10.1016/j.cbpb.2016.07.008

Ye, Y., Meyer, H. H., and Rapoport, T. A. (2001). The AAA ATPase Cdc48/p97 and its partners transport proteins from the ER into the cytosol. *Nature* 414, 652–656. doi:10.1038/414652a

Zhang, X., Wen, H., Wang, H., Ren, Y., Zhao, J., and Li, Y. (2017). RNA-Seq analysis of salinity stress-responsive transcriptome in the liver of spotted sea bass (*Lateolabrax maculatus*). *PLoS One* 12, 01732388–e173318. doi:10.1371/journal.pone.0173238

Zhao, X., Sun, Z., Gao, T., and Song, N. (2021). Transcriptome profiling reveals a divergent adaptive response to hyper-and hypo-salinity in the yellow drum, *Nibea albiflora*. *Animals.* 11 (8), 2201. doi:10.3390/ani11082201

Frontiers in Physiology

Understanding how an organism's components work together to maintain a healthy state

The second most-cited physiology journal, promoting a multidisciplinary approach to the physiology of living systems - from the subcellular and molecular domains to the intact organism and its interaction with the environment.

Discover the latest Research Topics

See more →

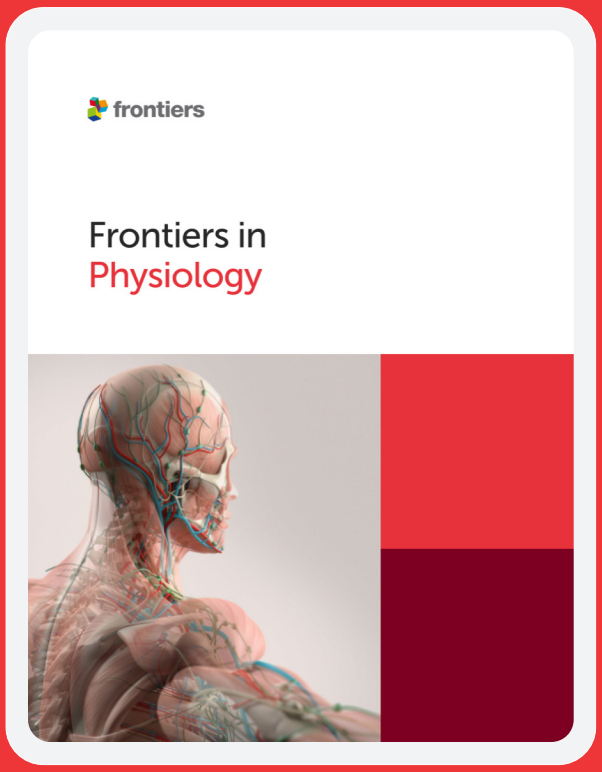

Frontiers

Avenue du Tribunal-Fédéral 34
1005 Lausanne, Switzerland
frontiersin.org

Contact us

+41 (0)21 510 17 00
frontiersin.org/about/contact